Mechanisms and Machine Science 51

Veniamin Goldfarb
Evgenii Trubachev
Natalya Barmina *Editors*

Advanced Gear Engineering

Springer

Mechanisms and Machine Science

Volume 51

Series editor

Marco Ceccarelli
LARM: Laboratory of Robotics and Mechatronics
DICeM: University of Cassino and South Latium
Via Di Biasio 43, 03043 Cassino (Fr), Italy
e-mail: ceccarelli@unicas.it

More information about this series at http://www.springer.com/series/8779

Veniamin Goldfarb · Evgenii Trubachev
Natalya Barmina
Editors

Advanced Gear Engineering

Springer

Editors
Veniamin Goldfarb
Institute of Mechanics
Kalashnikov Izhevsk State
Technical University
Izhevsk
Russia

Natalya Barmina
Institute of Mechanics
Kalashnikov Izhevsk State
Technical University
Izhevsk
Russia

Evgenii Trubachev
Institute of Mechanics
Kalashnikov Izhevsk State
Technical University
Izhevsk
Russia

ISSN 2211-0984 ISSN 2211-0992 (electronic)
Mechanisms and Machine Science
ISBN 978-3-319-60398-8 ISBN 978-3-319-60399-5 (eBook)
DOI 10.1007/978-3-319-60399-5

Library of Congress Control Number: 2017943219

Manuscripts 3, 6, 7, 9, 11, 16, 17, 19, 20, 21, 22, 23 were translated from Russian into English by Natalya Barmina, Ph.D., the other manuscripts were written in English by their authors.

Printed on acid-free paper

This Springer imprint is published by Springer Nature
The registered company is Springer International Publishing AG
The registered company address is: Gewerbestrasse 11, 6330 Cham, Switzerland

Series Editor's Preface

This book deals with the technology of gearing systems by looking at theory, research and practice with recent updates and results. Gearing is an important area of MMS (Mechanism and Machine Science) both in the design and performance of machines, even in the most sophisticated solutions.

This second volume is organized as a continuation and enlargement of the first book, also coming from experts within the IFToMM community from all over the world. Therefore, I am sure that readers will find interesting discussions and current research results that can reinforce and indeed stimulate their own work in the field of both research and applications.

I congratulate the editors on the successful result of their efforts and thank them for the time they have spent in coordinating and preparing this volume. I thank the authors for their valuable contributions that show clearly that gearing systems are of fundamental importance in further developing mechanical and mechatronic systems. This volume can also be considered as a source of inspiration to promote work in gearing systems within the challenges of modern developments of science and technology.

Cassino, Italy

Marco Ceccarelli
IFToMM President 2016–19

Contents

Introduction

Dear readers,

We are pleased to offer the next issue-related volume of contributions, carrying on the tradition of the previously published books in this series [1, 2].

Again and, I suppose, not for the last time, we turn to the theme of improving the theoretical scientific fundamentals of the design, production and operation of gears and transmissions that determine the level of quality of a variety of modern mechanisms and machines, both in the present day and long into the future.

The development of equipment and techniques and the appearance of new trends and areas of gear application require increased transmission loads, wider ranges of operating temperatures, higher operating speeds, and improved technical and economic parameters of gearbox systems. At the same time, requirements are also increased in regard to the accuracy of motion transfer, as well as to minimization of the overall sizes of gears while enhancing their strength and rigidity. Along with a number of specific requirements within certain branches of industry, this leads to the necessity of solving multiple theoretical design and manufacturing tasks when developing the new generation of advanced gears and transmissions.

The investigations presented in this compiled volume cover spur and helical, worm, spiroid, planetary gears and a relatively new type of gear—rod-toothed gears with approximated transmission ratio. The following issues are considered:

- computer-aided simulation of manufacturing errors of spur and helical gears and their compensation; basic relations of quality indices for operating and machine-tool meshings; development and application of geometrical certificates for gear-machining tools; optimization of requirements for the accuracy of basic surfaces within tooth cutting;
- development of new manufacturing schemes and methods of efficient gear machining for worm and spiroid gears and the grinding of helical surfaces;
- creation of a computer-aided system for gearbox system design;
- simulation of load distribution in planetary and spiroid gears, and for two interacting misaligned cylinders;

- improvement of gear quality and load capacity by applying advanced laser techniques;
- design and manufacture of kinematic pairs made of polymer materials by prototyping;
- investigation of new types of gear—rod-toothed gears and a new variety of planetary pumps, and methods for the highly efficient machining of impellers;
- general issues related to the education of advanced experts in the field of mechanism and machine science, focusing on gears and the development of a competent terminology for gears.

No doubt, many issues remained uncovered. We propose publishing further issue-related compiled volumes, dedicated to the dynamics of gears and gearboxes, their geometrical synthesis, advanced techniques of gear-machining, etc. The relevant information will be distributed by the editors and the Springer publishing house.

We hope that this book will be of great interest and use to experts in design, production and the investigation of gears and transmissions, including for young researchers and students.

The editors and authors of the present volume are grateful to the Springer publishers, especially to the chief editor of the MMS series, Prof. Marco Ceccarelli, for their support and assistance in publication of the previous, present and, we hope, future compiled volumes.

We also want to express our deep gratitude to Dr. Eng. Sergey Lagutin for his sustained efforts, assistance and advice in converting Russian gear terminology into English.

[1] Proceedings of the International Symposium “Theory and practice of gearing”, January 21–23 2014, Izhevsk, Russia. 578 p. ISBN: 978-5-7526-0629-8.

[2] Theory and Practice of Gearing and Transmissions: In Honor of Prof. Faydor L. Litvin. Springer International Publishing AG Switzerland, 2016, 450 p. 279 illus., ISBN: 978-3-3 19-19739-5, DOI 10.1007/978-3-319-19740-1.

Veniamin Goldfarb,

D.Sc. in Engineering, Professor

Honored Scientist of Russian Federation and Udmurt Republic

Director of Scientific Department “Institute of Mechanics”

Vice-president of International Federation for the Promotion of Mechanism and Machine Science (IFToMM) in 2011–2015.

Computerized Simulation of Manufacturing Errors in Cylindrical Spur Gears and Their Compensation Through Flank Modifications

Alfonso Fuentes-Aznar, Scott Eisele and Ignacio Gonzalez-Perez

Abstract AGMA and ISO standards consider different types of deviation of gear geometry caused during manufacturing processes of cylindrical gears through a system of accuracy grades, in which each grade corresponds to deviations within a certain range. The gear drive behavior is affected by the level and type of deviation, causing transmission errors, shifts in the bearing contact, increase of contact and bending stresses, and vibration and noise. The main goal of this paper is the investigation of the influence of manufacturing errors on transmission errors and contact and bending stresses, and the determination of the corresponding flank modifications required for their compensation. The contact pattern and the unloaded function of transmission errors are obtained through application of tooth contact analysis (TCA). Application of finite element analysis (FEA) allows for contact and bending stresses to be determined along one or two cycles of meshing. Surface deformations are used for determination of the loaded function of transmission errors in which its peak-to-peak value is related to the vibration and noise response in operating conditions. Several numerical examples considering different levels and types of manufacturing error and their compensation through predefined flank modifications are presented.

Keywords Gear geometry · Spur gears · Manufacturing errors · Tooth contact analysis · Finite element analysis

A. Fuentes-Aznar (✉) · S. Eisele
Department of Mechanical Engineering, Rochester Institute of Technology (RIT), Rochester, NY, USA
e-mail: afeme@rit.edu

I. Gonzalez-Perez
Department of Mechanical Engineering, Polytechnic University of Cartagena (UPCT), Cartagena, Spain
e-mail: ignacio.gonzalez@upct.es

V. Goldfarb et al. (eds.), *Advanced Gear Engineering*,
Mechanisms and Machine Science 51, DOI 10.1007/978-3-319-60399-5_1

1 Introduction

Manufacturing errors play a fundamental role in gear drive performance. Manufacturing errors cause transmission errors and influence the appearance of dynamic loads, noise and vibration, not only in the gear drive, but in all elements along the power transmission path. In order to ensure the quality of the gears and to limit the maximum magnitudes of manufacturing errors along with it, the AGMA (American Gear Manufacturers Association) and the ISO (International Organization for Standardization) have proposed a system of accuracy grades. The ISO system of gear accuracy comprises 13 accuracy grades (Q = 0, 1, 2 … 12) of which grade 0 is the highest and grade 12 the lowest degree of accuracy [1]. The AGMA system [2] comprises 10 accuracy grades numbered A2 through A11, of which A2 is the highest and A11 is the lowest degree of accuracy. The achievement of higher quality gears implies a higher cost of production, so that a trade-off has to be found between the required performance in terms of noise, vibration, and strength and the cost of production by selecting the required accuracy grade.

Application of manufacturing errors such as time-varying mesh stiffness and tooth separations have been considered in dynamic models to predict a vibrational response in cylindrical and planetary gear sets [3]. However, a static model in which predefined deviations are provided within the gear geometry would be very useful for predicting transmission errors and contact and bending stresses, and judging the appropriateness of flank modifications for compensation of manufacturing errors as well. In this regard, the effect of a number of manufacturing and assembly-related carrier and gear errors on the load sharing among the planets was presented in [4]. In [5], the results of an experimental study to describe the impact of certain types of manufacturing errorson gear stresses and the individual planet loads in planetary gear sets were presented.

Using purely analytical methods, in [6], the results of a study on how accuracy grades affect the calculation of stresses were presented. The design of experiments and Monte Carlo simulation techniques were used to quantify the effects of different manufacturing and assembly errors on root and contact stresses. In that study, it was shown that the increment in stresses due to profile and lead deviations are certainly significant, being as high as 26% for the root stresses of an example with accuracy grade 8. In [7], a comparative investigation of the effect of helix slope and form deviation tolerances as specified by grades 5 and 7 of the ISO 1328-1 was presented. In that work, the consequences of longitudinal flank crowning and radial tip relief modifications were investigated. It was concluded that reducing or increasing the quality class of a gear pair will proportionally influence the gear's performance as well as its life [7]. In this paper, the influence of manufacturing errors on transmission errors and contact and bending stresses, and the determination of flank modifications required for their compensation, will be investigated. The influence of pitch deviation, profile deviation, and helix deviation errors on the contact and bending stresses of cylindrical gears are studied. The direction of profile deviation

is also considered in this study, because, apparently, it may have an important effect on contact stresses. Micro-geometry modifications comprising the required tip relief, and longitudinal and profile crowning are proposed to reduce the effect of those mentioned manufacturing errors on the mechanical behavior of the gear drive.

2 Geometry Deviations Due to Manufacturing Errors

The ISO and AGMA classify geometry deviations due to manufacturing errors into three main categories. These categories are pitch deviations, profile deviations, and helix deviations [1, 2]. Each of these categories contains multiple parameters which determine the grade of the gear. The equations relating these parameters to ISO grade are outlined in the ISO's "Cylindrical Gears—ISO System of Flank Tolerance Classification—Part 1" [1]. Also worthy of note, the factor between each consecutive ISO grade is $\sqrt{2}$, meaning that moving up two ISO grades equates to tolerance levels twice as large.

2.1 Pitch Deviations

The single pitch deviation is the algebraic difference between the actual pitch and the corresponding theoretical pitch in the transverse plane, defined on a circle concentric with the gear axis at approximately the mid-depth of the tooth [1]. The cumulative pitch deviation is the algebraic difference over a sector of several pitches between the actual length and the theoretical length of the relevant arc [1]. It is equal to the algebraic sum of the single pitch deviations of the same considered pitches. In this work, pitch deviations are modeled through superimposition of two sinusoidal functions that takes into account the total cumulative pitch deviation F_p and the single pitch deviation f_{pt}.

The cumulative pitch deviation $F_{pk}^{(1)}$ of the first function is defined as

$$F_{pk}^{(1)} = A_1 \sin\left(k\frac{2\pi}{N_g}\right) \qquad k = (0, 1, 2, \ldots, N_{g-1}). \tag{1}$$

Here, A_1 is the amplitude of the sinusoidal function and N_g is the gear tooth number.

The cumulative pitch deviation $F_{pk}^{(2)}$ of the second function is defined as

$$F_{pk}^{(2)} = A_2 \sin\left(k\frac{\pi}{2}\right) \qquad k = (0, 1, 2, \ldots, N_{g-1}), \tag{2}$$

where A_2 is the amplitude of the sinusoidal function.

The maximum increment of the single pitch deviation occurs at $k = 0$, and can be obtained as

$$\Delta f_{pt,max} = (F_{p1}^{(1)} + F_{p1}^{(2)}) - (F_{p0}^{(1)} + F_{p0}^{(2)}) = A_1 \sin\frac{2\pi}{N_g} + A_2. \tag{3}$$

Amplitudes A_1 and A_2 can be derived as a function of f_{pt} and F_p by imposing the conditions

$$F_p = 2(A_1 + A_2) \tag{4}$$

$$(F_{p1}^{(1)} + F_{p1}^{(2)}) - (F_{p0}^{(1)} + F_{p0}^{(2)}) = f_{pt} - 0. \tag{5}$$

The necessity of the two sinusoidal functions is due to the two values, f_{pt} and F_p, that each accuracy grade provides. The sinusoidal functions are used for the location of each single tooth on the reference circle, and this means that each tooth has to be generated individually for the modelling of the pitch deviation. Since the maximum increment of the single pitch deviation occurs from $k = 0$ to $k = 1$ (or from $k = N_g - 1$ to $k = 0$), the finite element model will consider those teeth with indexes $k = (N_g - 2, N_g - 1, 0, 1, 2)$ (see Sect. 4).

2.2 Profile Deviations

Profile deviation is the amount by which a measured profile deviates from the design profile [2]. As shown in Fig. 1, the total profile deviation F_α is the superposition of the profile form deviation $f_{f\alpha}$ and the profile slope deviation $f_{H\alpha}$. The profile evaluation range, L_α, according to [1], is considered equal to 92% of the active length, which is defined as the difference between two base tangents, one corresponding to the tip tooth limit T, and the other one corresponding to the endpoint E of the effective contact with the mating gear

$$L_\alpha = 0.92\left(\sqrt{r_T^2 - r_b^2} - \sqrt{r_E^2 - r_b^2}\right). \tag{6}$$

Here, r_b is the base radius of the gear.

In this work, profile deviations are modelled by variation of the pressure angle of the gear. We will assume here that the profile form deviation $f_{f\alpha}$, mainly caused by the roughness or small undulations along the profile direction, is zero, and therefore the profile slope deviation $f_{H\alpha}$ is the only deviation affecting the considered value of the profile deviation. In relation to profile deviation, the influence of positive or negative profile slope deviations will be considered. The profile slope deviation direction is positive when the profile line shows an increase in the

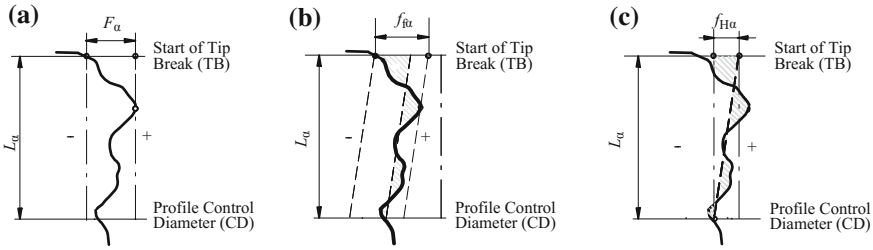

Fig. 1 Schematic representation of the components of the total profile deviation: **a** profile deviation F_α, **b** profile form deviation $f_{f\alpha}$, and **c** profile slope deviation $f_{H\alpha}$

material towards the tooth tip, relative to the design profile, corresponding to a negative pressure angle deviation.

The total profile deviation for an accuracy grade of 5 is obtained by considering the following equation [1]:

$$F_\alpha = 3.2\sqrt{m} + 0.22\sqrt{d} + 0.7, \tag{7}$$

where m is the module and d the pitch radius of the gear. Once the profile deviation and the profile evaluation distance are known, the variation of the pressure angle to simulate the profile deviation $\Delta\alpha$ is determined as

$$\Delta\alpha = \arctan\left(\frac{F_\alpha}{L_\alpha \tan\alpha}\right), \tag{8}$$

where α is the pressure angle.

2.3 Helix Deviations

Helix deviation is the amount by which a measured helix deviates from the design helix [2]. As shown in Fig. 2, the total helix deviation F_β is the superposition of the helix form deviation $f_{f\beta}$ and the helix slope deviation $f_{H\beta}$. In Fig. 2, L_β is the helix evaluation range, which is given by the face width shortened at both sides by the smaller value of the 5% of the face width or a length equal to one module.

In this work, helix deviations are modeled by variation of the helix angle of the gear. For that, we assume that the helix form deviation $f_{f\beta}$, mainly caused by the roughness of the surface, is zero, so that the helix slope deviation $f_{H\beta}$ is the only deviation affecting the helix deviation. In order to consider the most unfavorable scenario for simulations, the value of the total helix deviation F_β according to the ISO will be considered for determination of the effective variation of the helix angle $\Delta\beta$, and therefore,

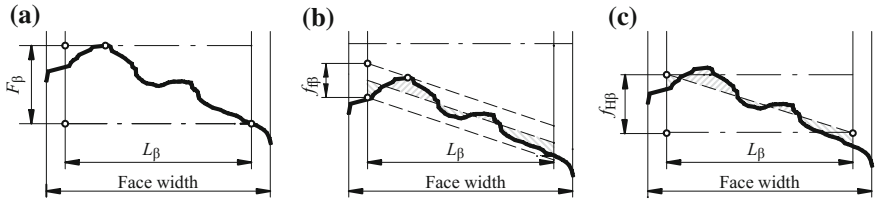

Fig. 2 Schematic representation of the components of the total helix deviation: **a** total helix deviation F_β, **b** helix form deviation $f_{f\beta}$, and **c** helix slope deviation $f_{H\beta}$

$$\Delta\beta = \arctan\left(\frac{F_\beta}{L_\beta}\right). \tag{9}$$

The total helix deviation for an accuracy grade of 5 is obtained by considering the following equation [1]:

$$F_\beta = 0.1\sqrt{d} + 0.63\sqrt{b} + 4.2. \tag{10}$$

Here, d is the pitch radius of the gear and b is the face width.

3 Geometry Modifications

The application of intended micro-geometry modifications is investigated to determine if they are effective in absorbing the effect of manufacturing errors on transmission errors, and contact and bending stresses for different accuracy grades. The following typologies of gear tooth surface micro-geometry modifications are considered.

3.1 Tip Relief

AGMA [8] defines tip relief as "a modification of a tooth profile whereby a small amount of material is removed near the tip of the gear tooth." It is used to avoid premature contact between contacting teeth due to the elastic deformation of gear tooth surfaces and pitch or profile errors. Tip relief can be defined for cylindrical gears with involute profiles by defining the amount of tip relief at the addendum radius, δ, the shape of the tip relief (linear or parabolic) and the starting point on the involute profile. For definition of the starting point, the following three definition methods can be considered: (i) the datum length for tip relief, L, (ii) the rolling length, r_L, or (iii) the rolling angle, ε. As shown in Fig. 3, the relation between the rolling length and the corresponding rolling angle is

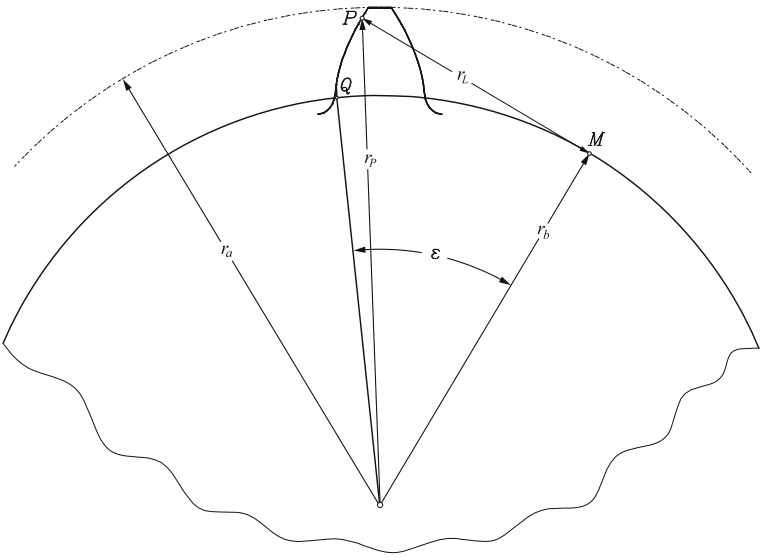

Fig. 3 Towards definition of rolling length and rolling angle

$$r_L = r_b \varepsilon, \tag{11}$$

where r_b is the base radius of the gear. Given one of the following tip relief definition factors, the radius r_P of the starting point for tip relief can be obtained as follows:

- Datum length, L:

$$r_P = r_a - L; \tag{12}$$

- Rolling length, r_L:

$$r_P = \sqrt{r_b^2 + r_L^2}; \tag{13}$$

- Rolling angle, ϵ:

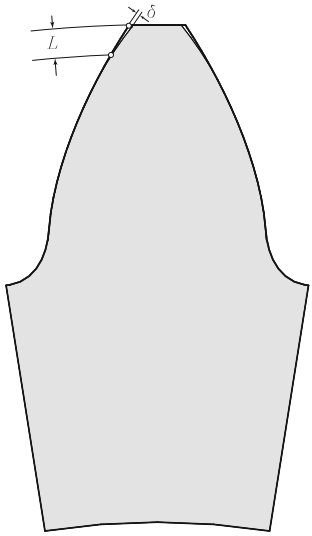

Fig. 4 Representation of tip relief with parabolic shape in a spur gear drive

$$r_P = \sqrt{r_b^2 + (r_b\varepsilon)^2} = r_b\sqrt{1+\varepsilon^2}. \tag{14}$$

The starting point for tip relief, r_P, being known, the profile of the gear tooth surfaces will be modified from this radius to the addendum radius, r_a, according to the shape of the tip relief (linear or parabolic) in order to reach the maximum modification at the addendum radius. Figure 4 shows the tip relief with parabolic shape on a spur gear drive as a function of the datum length L and the amount of tip relief at the addendum radius δ.

3.2 Longitudinal Crowning

AGMA [8] defines longitudinal crowning as "teeth which have surfaces modified in the length-wise direction to produce localized contact or to prevent contact at their ends." It is known that at high torques, crowning can benefit gear performance by localizing contact stresses in the center of the gear tooth, away from the edges [9]. In that study, it was also shown that there exist optimal crowning parameters. Longitudinal crowning has also been analytically demonstrated to contribute to reduction of the stress distribution factor [10]. A visual representation of longitudinal crowning with a parabolic shape applied to the tooth surfaces of a spur gear is shown in Fig. 5.

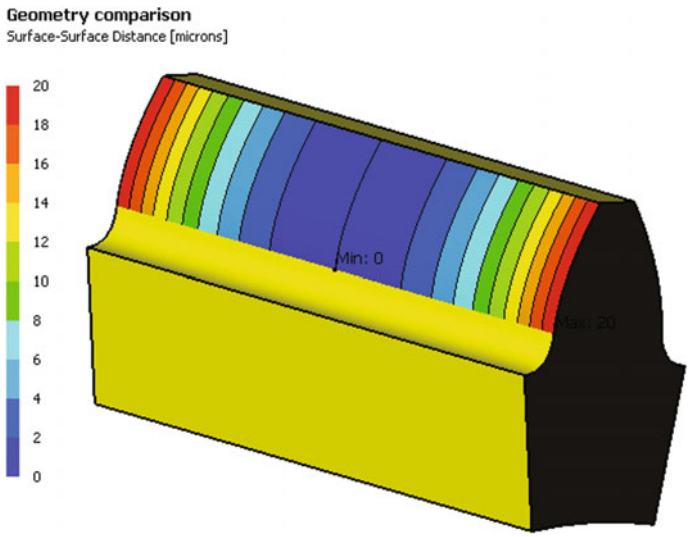

Fig. 5 Longitudinal crowning of 20 μm applied to the active tooth surfaces of a spur gear

3.3 Profile Crowning

Profile crowning is considered in which a constantly increasing amount of material is removed from the transverse section of the gear tooth in the direction of the tip and root circle, starting at the middle of the calculated tooth flank length. It can be achieved through the selection of a generating profile that deviates from a straight profile. It can be considered parabolic or circular, and therefore the parabola coefficient of the profile for the first case, or the radius of the circular profile for the second one, are design parameters to be determined. For spur cylindrical gears, the profile crowning is responsible for the predesign of a parabolic function of transmission errors that will absorb the linear or quasi-linear functions of transmission errors caused by errors of alignment or manufacturing errors [11].

4 Methodology

The geometry of spur gears with manufacturing errors is generated and simulated by a custom-made software. This software allows for gear geometry to be modified to reflect manufacturing errors and intentional profile modifications. Manufacturing errors will only be applied to the pinion of the gear drive. The gear will always be considered to be free of any manufacturing error, and therefore it will always have the expected targeted geometry.

The finite element method is used to determine the contact and bending stresses for gears under different limits of manufacturing errors. Figure 6 shows an example of the sort of finite element model with five pairs of contacting teeth that has been considered in this work. It is assumed that all nodes at the cutoff rim surface remained perfectly rigid. Considering five pairs of teeth keeps the cutoff rim surface away from the teeth in contact and avoids influence on the contact and bending stresses to be obtained. The model size consists of 106,000 elements and 131,922 nodes. The contacting surfaces are made of 1200 elements corresponding to 20 elements in the longitudinal direction and 60 elements in the profile direction. Gear active tooth surfaces have been defined as master surfaces, while pinion active tooth surfaces have been defined as slave surfaces. Three-dimensional solid elements of type C3D8I [12] have been used, being hexahedral first order elements enhanced by

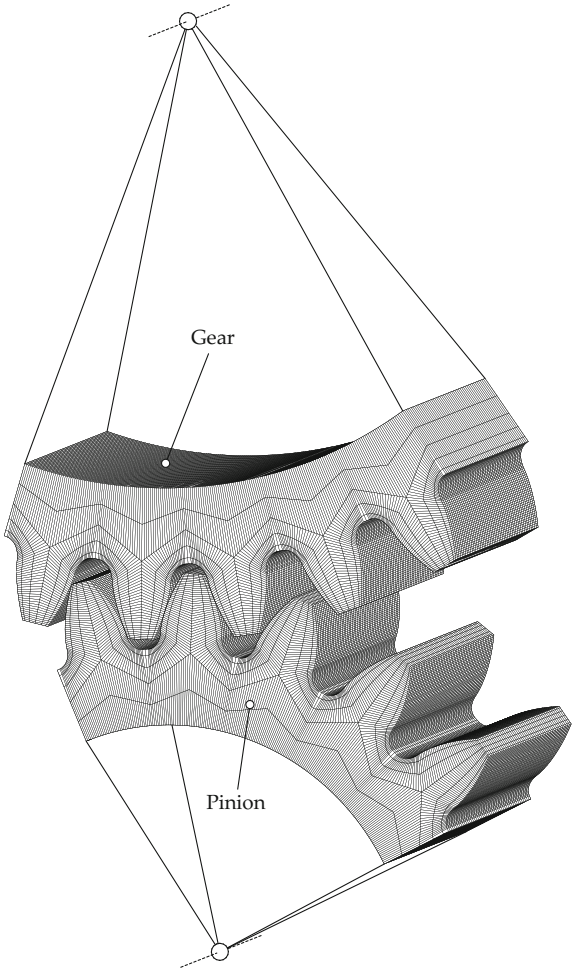

Fig. 6 Finite element mesh applied for determination of contact and bending stresses

incompatible deformation modes in order to improve their bending behavior. Pinion and gear material is steel defined with an elastic modulus of 210 GPa and a Poisson ratio of 0.3.

An advanced freeform design tool is used to modify the active part of the gear tooth surface according to the typology of the intentional geometry modifications to be applied. Three possible geometry modifications will be investigated in this paper. Firstly, a parabolic tip relief will be considered to smooth the transition between the active part of the gear tooth surface and the tip relief area. This type of parabolic relief does not increase the Hertzian contact stresses in the way that linear relief does [13]. No bottom relief will be considered for the pinion and gear tooth surfaces, because the tip relief applied to both members of the gear drive plays the same role. Secondly, a longitudinal parabolic crowning will be considered, and finally, a parabolic profile crowning will be applied.

The design of experiments (DOE) methodology is used to evaluate the influence of the different types of manufacturing error on contact and bending stresses, using a two-level full factorial numerical experiment. Design of experiments (DOE) is a well-known technique extensively applied in many fields of engineering to evaluate which design variables or process inputs have the largest impact on different outputs. The tested cases will be organized according to the selected full factorial design, and in this way, with a limited series of tested cases, a general analysis of the different factors and their combined effects on the selected output will be performed.

5 Numerical Examples

Table 1 shows the macro-geometry design parameters of two spur gear drives with pressure angles of 20° and 25° applied for investigation of the compensation of manufacturing errors by the application of flank modifications. Table 2 shows the derived geometrical data of the tested gears.

Firstly, the influence of the magnitude of pitch deviations, profile deviations, helix deviations, and direction of the profile slope deviation (positive or negative) on contact and bending stresses is investigated for gears with and without profile modifications. The considered parameters for the designed experiment can be seen in Table 3. The limits of the considered deviations or input parameters will be the same for both geometries 1 and 2 described in Table 1. The selected minimum and maximum values represent the maximum tolerances expected for gears having an ISO accuracy grade of 2 and 6, with the additional parameter of profile slope deviation direction as positive or negative. For the pitch deviation, the values provided correspond to the cumulative pitch deviation and the single pitch deviation in parentheses.

A full factorial experiment set up with the parameters shown in Table 3 yields sixteen runs, with the details of each run shown in Table 4.

Table 1 Macro-geometry parameters of tested gears

	Geometry 1		Geometry 2	
	Pinion	Gear	Pinion	Gear
Number of teeth	21	37	21	37
Module [mm]	4.0		4.0	
Normal pressure angle [°]	20		25.0	
Addendum coefficient [–]	1.00	1.00	1.00	1.00
Dedendum coefficient [–]	1.25	1.25	1.25	1.25
Root radius coefficient [–]	0.38	0.38	0.25	0.25
Profile shift coefficient [–]	0.2060	−0.2060	0.1416	−0.1416
Generating shift coefficient [–]	0.1802	−0.2317	0.1215	−0.1617
Face width [mm]	40		40	
Center distance [mm]	116.0		116.0	

Table 2 Derived data of tested gears

	Geometry 1		Geometry 2	
	Pinion	Gear	Pinion	Gear
Pitch [mm]	12.5664		12.5664	
Base pitch [mm]	11.8085		11.3890	
Transverse contact ratio [–]	1.6089		1.4491	
Circumferential backlash [mm]	0.150		0.150	
Normal backlash [mm]	0.141		0.1359	
Reference diameter [mm]	84.0000	148.0000	84.0000	148.0000
Tip diameter [mm]	93.6477	154.3523	93.1325	154.8675
Root diameter [mm]	75.4417	136.1462	74.9717	136.7066
Base diameter [mm]	78.9342	139.0745	76.1299	134.1336
Root form diameter [mm]	79.5104	140.7741	77.9765	139.5654
Addendum [mm]	4.8239	3.1761	4.5663	3.4337
Dedendum [mm]	4.2792	5.9269	4.5141	5.6467
Tooth depth [mm]	9.1030	9.1030	9.0804	9.0804
Tooth thickness [mm]	6.8079	5.6085	6.7363	5.6801
Space width [mm]	5.7585	6.9579	5.8301	6.8863

Table 3 Parameters of designed experiment

Parameter	Units	Min. value	Max. value
Pitch deviation, $F_p\left(f_{pt}\right)$	[μm]	7.0 (2.3)	28.0 (9.3)
Profile deviation, $F_{H\alpha}\left(f_{f\alpha}\right)$	[μm]	3.4 (0.0)	13.0 (0.0)
Helix deviation, $F_{H\beta}\left(f_{f\beta}\right)$	[μm]	3.0 (0.0)	12.0 (0.0)
Profile (slope) deviation direction	[–]	Positive	Negative

Table 4 Details of the configuration of each run for the experiment

Case #	Pitch deviation $F_p(f_{pt})$	Profile deviaton $F_{H\alpha}$	Helix deviation $F_{H\beta}$	Profile slope deviation direction
1	7.0 (2.3)	3.4	3.0	Positive
2	28.0 (9.0)	3.4	3.0	Positive
3	7.0 (2.3)	13.0	3.0	Positive
4	28.0 (9.0)	13.0	3.0	Positive
5	7.0 (2.3)	3.4	12.0	Positive
6	28.0 (9.0)	3.4	12.0	Positive
7	7.0 (2.3)	13.0	12.0	Positive
8	28.0 (9.0)	13.0	12.0	Positive
9	7.0 (2.3)	3.4	3.0	Negative
10	28.0 (9.0)	3.4	3.0	Negative
11	7.0 (2.3)	13.0	3.0	Negative
12	28.0 (9.0)	13.0	3.0	Negative
13	7.0 (2.3)	3.4	12.0	Negative
14	28.0 (9.0)	3.4	12.0	Negative
15	7.0 (2.3)	13.0	12.0	Negative
16	28.0 (9.0)	13.0	12.0	Negative

Values given in μm

The minimum principal stress at the integration points of the finite element mesh forming the contacting surfaces is considered to be contact stress and the values will be represented in MPa. The maximum principal stress at the integration points of the elements forming the fillets of the contacting sides of pinion and gear tooth surfaces is considered to be the bending stress and will also be represented in MPa.

Results of the influence of manufacturing errors on contact and bending stresses have been obtained for the two considered geometries depicted in Table 1. Results will be presented in separate sections for Geometry 1 having a pressure angle of 20° and Geometry 2 having a pressure angle of 25°.

5.1 Geometry 1 with Pressure Angle of 20°

Figure 7 shows the Pareto chart of the standardized effect of manufacturing errors on the pinion contact and bending stresses for a spur gear drive with macro-geometry represented as Geometry 1 in Table 1 and no micro-geometry modifications. A Pareto chart is a bar diagram in which the length of each of the bars represents the influence of the factors represented on the left on the considered objective variable. Here, the Pareto chart is arranged with bars distributed horizontally, with the longest bars (high influence) at the top and the shortest bars (lower influence) at the bottom of the diagram. In this way, the Pareto chart gives

visual information on the most important factors of influence on the considered objective variable, ranking those factors after the analysis of the considered factorial design (as shown in Table 4). The represented dashed line is shown for all analyses as a reference. Any effect which extends beyond that mentioned dashed reference line is considered significant for the investigated objective. Therefore, according to the results shown in Fig. 7-left, the main factors affecting the maximum contact stresses on the pinion tooth surfaces are the profile slope deviation direction and the helix deviation. The pitch deviation and the combined effect of profile deviation with the profile slope deviation direction are also of relevant influence on contact stresses on the pinion tooth surfaces. Regarding the maximum bending stress (Fig. 7-right), the main factor of influence is the helix deviation. The profile deviation direction, although its influence is not as relevant as the helix deviation, is also considered to be an influence factor on bending stresses for the pinion.

Figure 8 shows the Pareto chart of the standardized effect of manufacturing errors on gear contact and bending stresses for the gear drive with Geometry 1. For contact stresses (Fig. 8-left), the two main factors of influence are, similarly as for the pinion, the profile slope deviation direction and the helix deviation applied as manufacturing errors to the pinion. Regarding the bending stresses (Fig. 8-right), the main factors of influence are the helix deviation and the profile slope deviation direction.

The results show that, in general, for a spur gear drive without any flank modifications, the most sensitive factor for the maximum contact stress is the profile deviation direction. The profile deviation direction dictates whether the gear or the pinion receives increased loading due to this deviation. For positive profile deviations, representing an increase of material towards the tooth tip, and corresponding to a negative variation of the pressure angle, the contact stresses will increase considerably. The second most significant manufacturing error affecting the maximum contact stress is the helix deviation, followed by pitch deviations. For bending stresses, the most sensitive tolerance is the helix deviation.

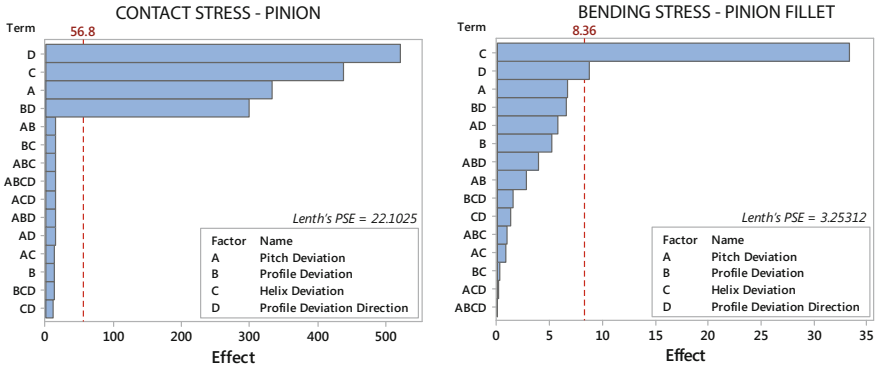

Fig. 7 Pareto chart of the standardized effect of manufacturing errors on pinion tooth contact stress (*left*) and bending stress (*right*) for Geometry 1 without micro-geometry modifications

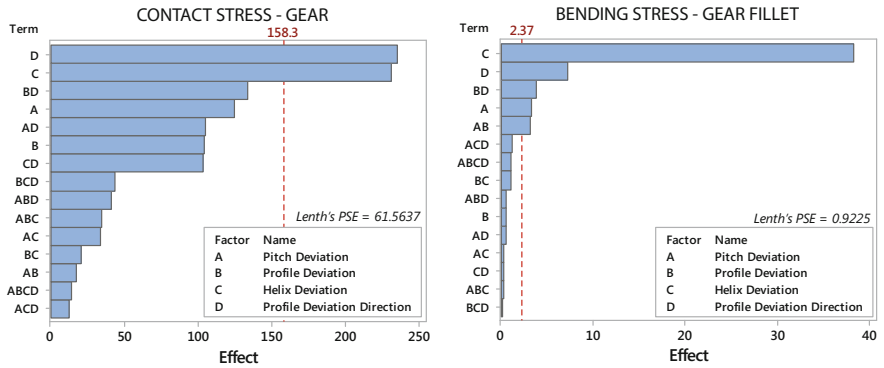

Fig. 8 Pareto chart of the standardized effect of manufacturing errors on gear tooth contact stress (*left*) and bending stress (*right*) for Geometry 1 without micro-geometry modifications

Table 5 Micro-geometry parameters of tested gears

	Geometry 1		Geometry 2	
	Pinion	Gear	Pinion	Gear
Number of teeth	21	37	21	37
Tip relief datum length [mm]	1.0	1.0	1.0	1.0
Tip relief modification [μm]	12.0	12.0	18.0	12.0
Tip relief shape [–]	Parabolic	Parabolic	Parabolic	Parabolic
Lead crowning zeroed at mid-face [μm]	6.0	–	6.0	–
Lead crowning shape [–]	Parabolic	–	Parabolic	–
Profile crowning zeroed at pitch radius [μm]	16.0	–	16.0	–
Profile crowning shape [–]	Parabolic	–	Parabolic	–

In order to reduce the increase of contact and bending stresses due to manufacturing errors, the application of a tip-relief for the pinion and gear tooth surfaces is first investigated. The same sixteen runs listed in Table 4 will be performed for a gear drive with pinion and gear designed with tip relief, as defined in Table 5. No lead or profile crowning is applied at this time. The selected tip relief geometric parameters were chosen based on values which were previously calculated to provide a smooth evolution of contact stresses all over the cycle of meshing without the appearance of edge contacts when a torque of 1000 Nm is applied to the pinion. This process of determination of the best design of tip relief is performed without the consideration of manufacturing errors.

Figure 9 shows the Pareto chart of standardized effect of manufacturing errors on pinion tooth contact stress (left) and bending stress (right) for Geometry 1 with pinion and gear geometry modified with tip relief. Now, after application of tip relief as a micro-geometry modification, the only relevant factor that affects the contact and bending stresses on the pinion is the helix deviation. The designed tip

relief helps significantly to reduce the sensitivity of the maximum contact stresses and the maximum bending stresses with respect to all manufacturing errors except the helix deviation.

Figure 10 shows the Pareto chart of the standardized effect of manufacturing errors on the gear tooth contact stress (left) and bending stress (right) for Geometry 1 with pinion and gear geometry modified with tip relief. Helix deviation is again the most relevant effect on contact and bending stresses.

In an effort to reduce this sensitivity of contact and bending stresses with the helix deviation error, the same tip relief that was previously applied will be considered now, together with a parabolic longitudinal crowning (or lead crowning) of six microns of maximum deviation at the front and back sections of the pinion.

Figure 11 shows the Pareto chart of the standardized effect of manufacturing errors on pinion tooth contact stress (left) and bending stress (right) for Geometry 1 with pinion and gear geometry modified with tip relief and longitudinal crowning according to the data shown in Table 5 applied to the pinion member of the gear set. The sensitivity of contact and bending stresses on the pinion tooth surfaces with respect to the helix deviation after consideration of longitudinal crowning is reduced by a factor of almost four, showing that the application of a longitudinal crowning is an effective way to absorb the helix deviation and minimize its effect on contact and bending stresses. The same results are obtained for the gear (see Fig. 12).

Figure 13 shows the Pareto chart of the standardized effect of manufacturing errors on the peak-to-peak level of loaded transmission errors for Geometry 1 with pinion and gear geometry without flank modifications (left) and with tip relief (right). The peak-to-peak level of loaded transmission errors when the geometry has no intentional modifications (Fig. 13-left) strongly depends on the profile deviation, followed, in order of importance, by the profile slope deviation direction, the

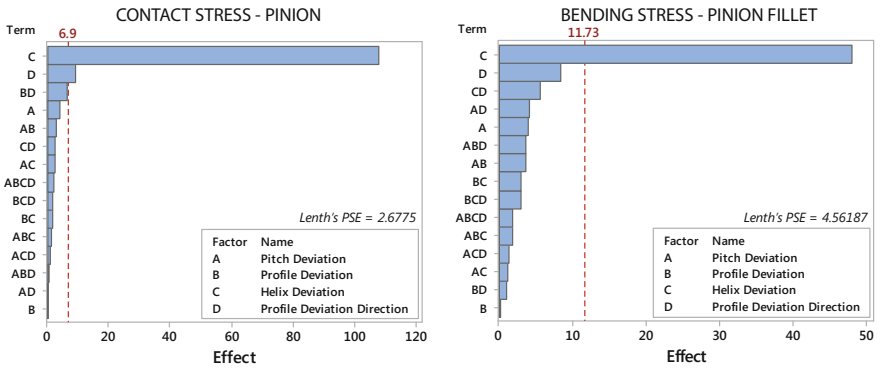

Fig. 9 Pareto chart of the standardized effect of manufacturing errors on pinion tooth contact stress (*left*) and bending stress (*right*) for Geometry 1 with pinion and gear geometry modified with tip relief

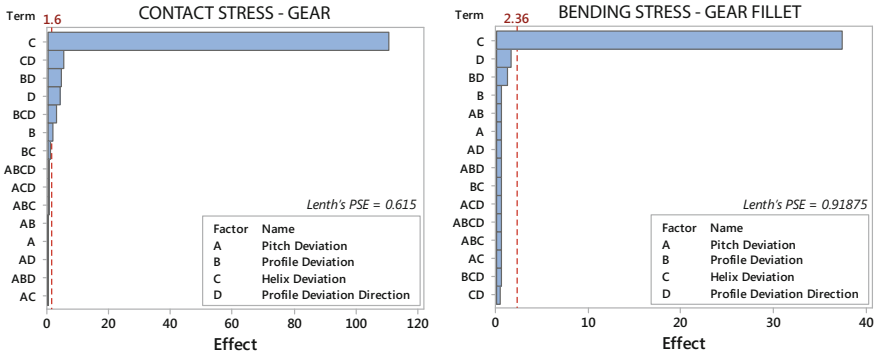

Fig. 10 Pareto chart of the standardized effect of manufacturing errors on gear tooth contact stress (*left*) and bending stress (*right*) for Geometry 1 with pinion and gear geometry modified with the optimum tip relief

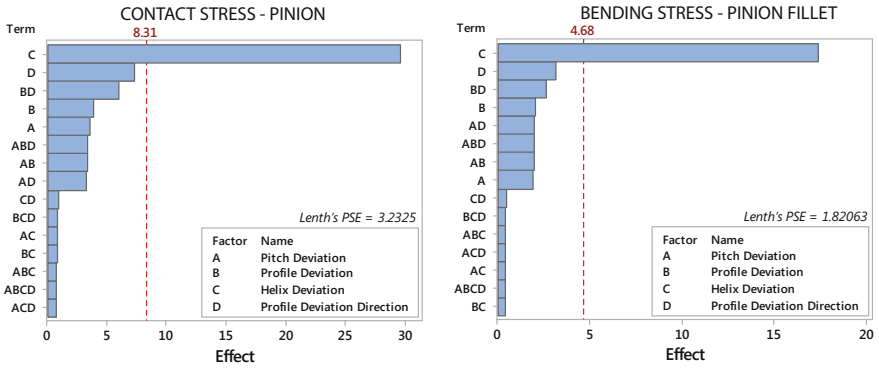

Fig. 11 Pareto chart of the standardized effect of manufacturing errors on pinion tooth contact stress (*left*) and bending stress (*right*) for Geometry 1 with pinion and gear geometry modified with the optimum tip relief and longitudinal parabolic crowning

interaction between the pitch deviation and the profile slope deviation direction, and finally, the pitch deviation.

The application of tip relief (Fig. 13-right) for the modification of the pinion and gear contacting surfaces allows us to reduce the sensitivity of the peak-to-peak level of transmission errors with the pitch deviation and its interaction with the profile slope deviation direction. However, the dependency with the magnitude of the profile deviation and the profile deviation direction still remains. Application of a longitudinal crowning showed no improvement on the effect of manufacturing errors on the peak-to-peak level of loaded transmission errors with respect to that shown in Fig. 13-right corresponding to the consideration of tip relief.

The next step in this investigation has been the consideration of a 16 μm profile crowning of parabolic shape applied to the pinion tooth surfaces. The application of

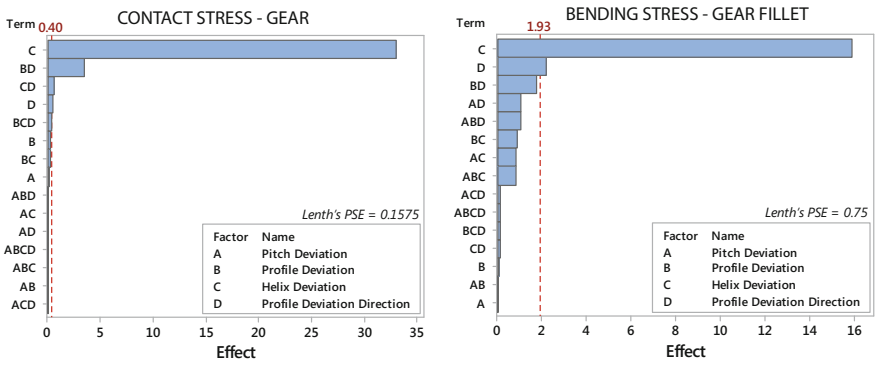

Fig. 12 Pareto chart of the standardized effect of manufacturing errors on gear tooth contact stress (*left*) and bending stress (*right*) for Geometry 1 with pinion and gear geometry modified with the optimum tip relief and longitudinal parabolic crowning

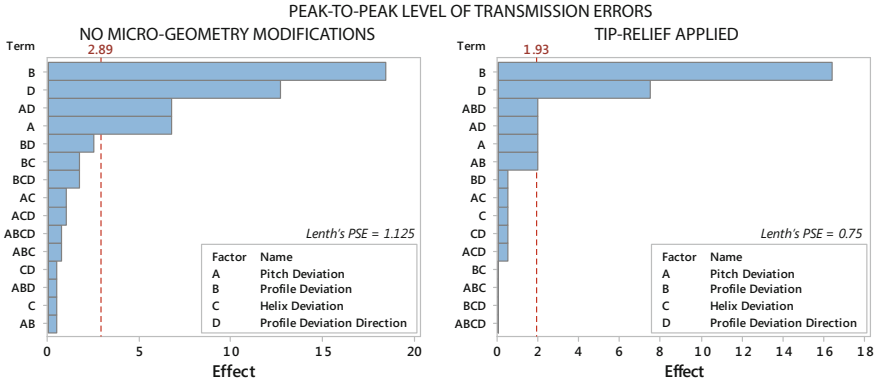

Fig. 13 Pareto chart of the standardized effect of manufacturing errors on the peak-to-peak level of transmission errors for Geometry 1 with pinion and gear geometry without flank modification (*left*) and with tip relief (*right*)

a profile parabolic crowning yielded the same results regarding the effect of manufacturing errors on the contact and bending stresses as those shown for the application of tip relief and longitudinal crowning. However, in terms of the peak-to-peak level of loaded transmission errors, the application of profile crowning effectively absorb the profile deviation error, as shown in Fig. 14. The effect of the profile slope deviation direction and its interaction with the profile deviation are the factors of influence on the peak-to-peak level of loaded transmission errors after all intended modification has been applied.

Figure 15 shows the evolution of contact stresses on the pinion tooth surfaces of the gear set with Geometry 1 and no flank modifications for the 16 runs of the first experiment. The effect of the negative profile slope deviation direction on the

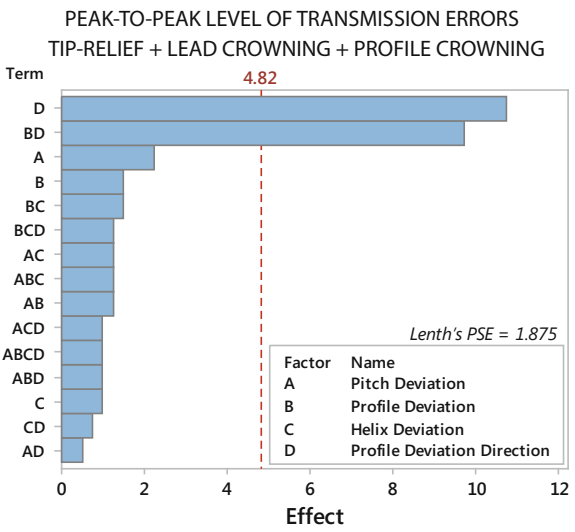

Fig. 14 Pareto chart of the standardized effect of manufacturing errors on the peak-to-peak level of transmission errors for Geometry 1 with pinion and gear geometry with tip relief and pinion modified with profile and lead crowning

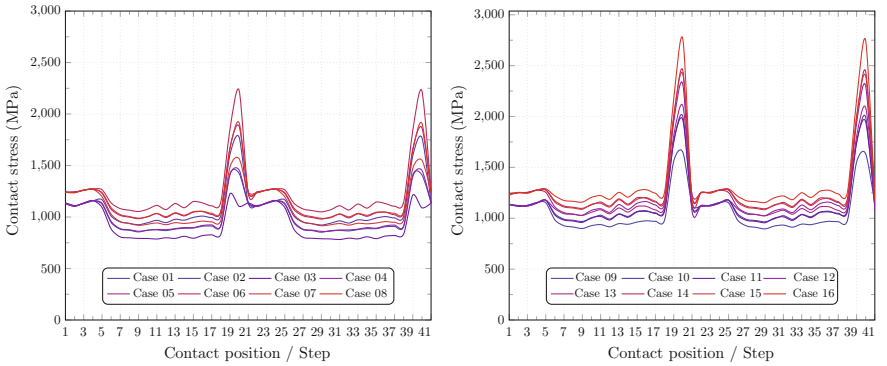

Fig. 15 Evolution of contact stresses for Geometry 1 with manufacturing errors and no flank modifications

increment of the maximum contact stresses (runs 9–16) when no flank modifications are applied is clearly seen in Fig. 15-right. In this case, a negative profile slope deviation direction increases the effect of edge contacts on contact stresses. Application of tip relief is directed mainly towards removing those peaks on contact stresses. Figure 16 shows how the application of the right-chosen tip relief indeed removes any increment on contact stresses due to edge contacts and leaves naked the effect of the different manufacturing errors on contact stresses. It is also observed how Cases 1–4 (with a helix deviation of 3.0 μm) yield lower maximum contact stresses than Cases 5–8 (with a helix deviation of 12.0 μm). The same behavior is found for Cases 9–12 with respect to Cases 13–16. Finally, Fig. 17

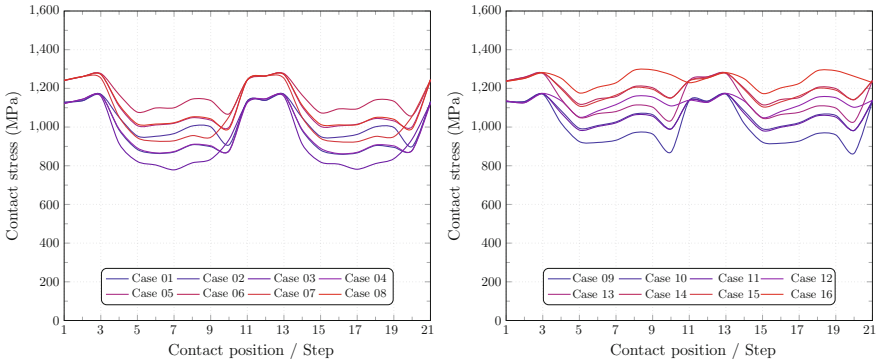

Fig. 16 Evolution of contact stresses for Geometry 1 with manufacturing errors and tip relief as surface modification

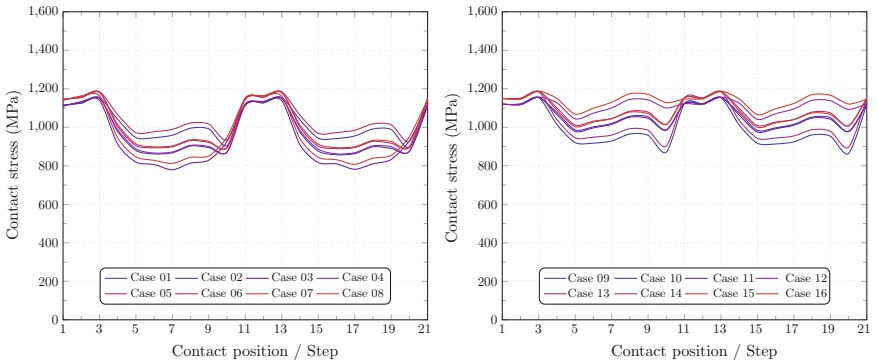

Fig. 17 Evolution of contact stresses for Geometry 1 with manufacturing errors, and tip relief and longitudinal crowning as surface modifications

shows how the application of tip relief and longitudinal crowning reduce the difference in the maximum contact stresses with respect to the different manufacturing errors.

5.2 Geometry 2 with Pressure Angle of 25°

For the sake of brevity, the content of this section will only show the results of the effect of manufacturing errors on contact and bending stresses for the pinion member of the gear set with Geometry 2, having a pressure angle of 25°. The goal here is to observe whether there is any influence of the pressure angle on the individual effect of the different manufacturing errors on contact and bending

stresses or if the intended geometry modifications are effectively absorbing the effect of manufacturing errors. Although the results for the gear member of the gear set are not shown here, it was observed that the effect of the manufacturing errors are similar to that shown for the pinion, following a similar pattern as that for Geometry 1.

Figure 18 shows the Pareto chart of the standardized effect of manufacturing errors on pinion tooth contact stress (left) and bending stress (right) for Geometry 2, wherein no micro-geometry modifications are applied to the pinion member of the gear drive. Similarly as for the pinion of Geometry 1, the main factors affecting the maximum contact stresses on the pinion tooth surfaces of Geometry 2 (Fig. 18-left) are the profile slope deviation direction and the helix deviation. The combined effect of profile deviation with the profile slope deviation direction and the pitch deviation also shows a relevant influence on contact stresses for the pinion tooth

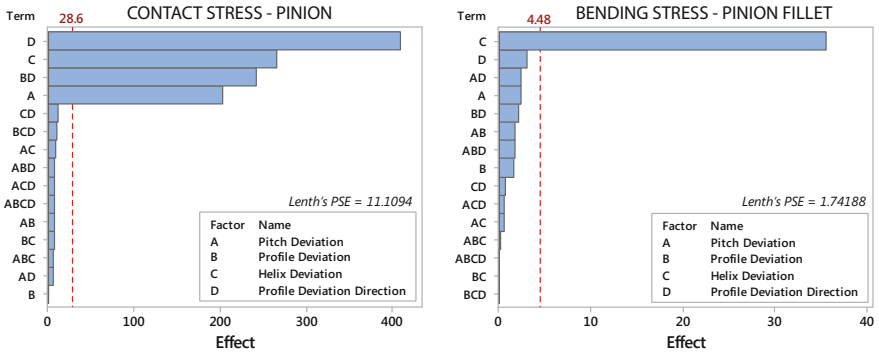

Fig. 18 Pareto chart of the standardized effect of manufacturing errors on pinion tooth contact stress (*left*) and bending stress (*right*) for Geometry 2

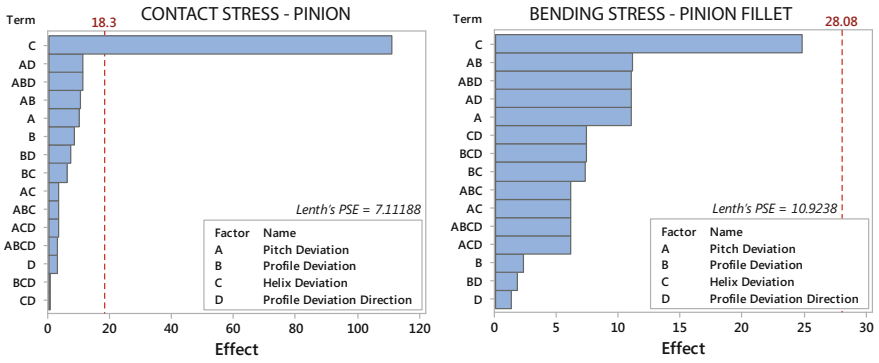

Fig. 19 Pareto chart of the standardized effect of manufacturing errors on pinion tooth contact stress (*left*) and bending stress (*right*) for Geometry 2 with pinion and gear modified with tip relief

surfaces. The maximum bending stress (Fig. 18-right), depends mainly on the helix deviation.

A higher value of tip relief was needed for the pinion of Geometry 2 in order to avoid the influence of edge contacts on contact stresses (see Table 5). The sensitivity of contact stresses to errors of manufacturing was reduced with application of tip relief to the pinion and gear to the helix deviation alone (Fig. 19-left). For bending stresses, Geometry 2 has better behaviour, and the design of experiment technique shows that there is no influence of manufacturing errors, although the most relevant factor affecting the maximum value of bending stresses remains the helix deviation (Fig. 19-right).

Figure 20 shows the Pareto chart of the standardized effect of manufacturing errors on pinion tooth contact stress (left) and bending stress (right) for Geometry 2 with pinion and gear modified with tip relief and pinion modified with longitudinal crowning. As expected, the application of a longitudinal crowning reduces the effect of the helix deviation on contact and bending stresses.

5.3 *Optimal Longitudinal Crowning Versus Magnitude of Helix Deviation*

With the knowledge that tip relief can compensate for manufacturing defects other than helix deviation, and that longitudinal crowning contributes effectively to reducing the effect of helix deviation, the next step is to find, if it exists, an optimal longitudinal crowning for different values of helix deviations. The criterion for optimization is the minimization of the absolute value of the minimum principal stress (largest compression stress) on the pinion tooth flanks. Simulations were run for gears of varying helix deviations and magnitudes of longitudinal crowning. Helix deviation was varied to reflect the maximum magnitudes of different ISO

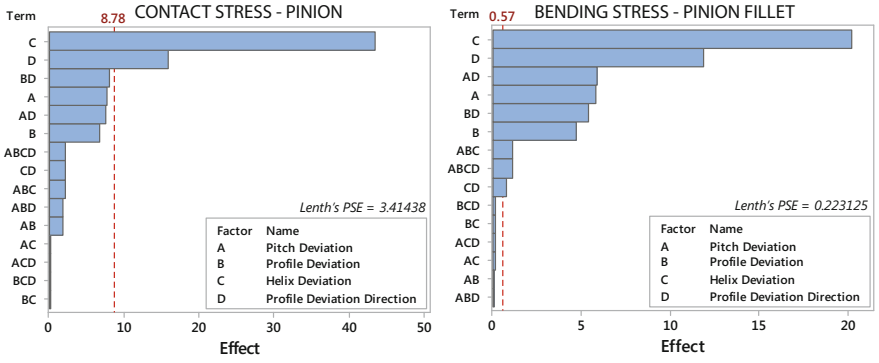

Fig. 20 Pareto chart of the standardized effect of manufacturing errors on pinion tooth contact stress (*left*) and bending stress (*right*) for Geometry 2 with pinion and gear modified with tip relief and pinion modified with longitudinal crowning

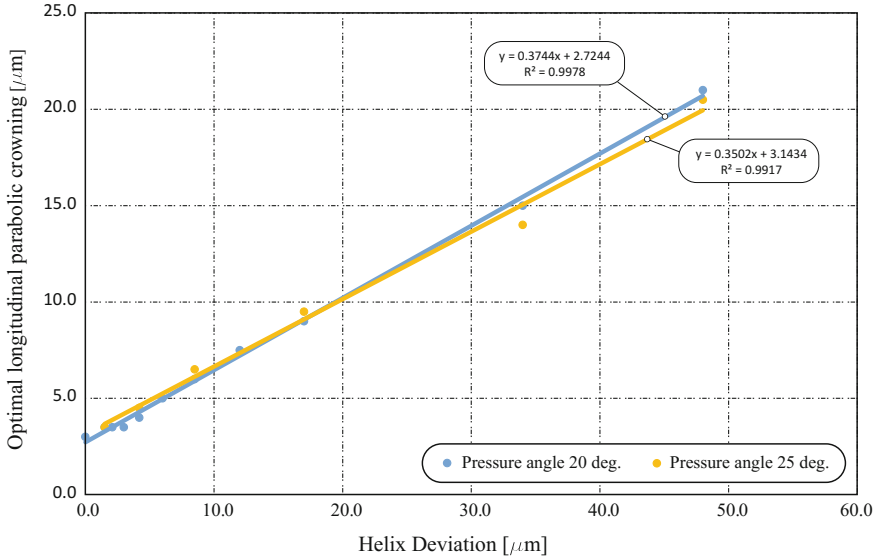

Fig. 21 Optimal longitudinal crowning for different values of helix deviation

grades, whereas crowning magnitudes were incremented by 0.5 μm until an optimal was found. The results obtained are shown in Fig. 21 for both Geometries 1 and 2. As seen in the plot, optimal longitudinal crowning and helix deviation are linearly related. A regression analysis yielded the trend lines shown in Fig. 21, which are described by Eqs. (15) and (16) for Geometries 1 and 2, respectively. Both trend lines feature an R^2 value higher than 0.99.

$$\text{Optimal longitudinal crowning} = 2.7244 + 0.3744\, F_\beta \tag{15}$$

$$\text{Optimal longitudinal crowning} = 3.1434 + 0.3502\, F_\beta \tag{16}$$

6 Conclusions

Based on the performed research, the following general conclusions can be drawn:

- Gear drives with no flank modifications applied to any of the gear members show a very sensitive tolerance for contact stresses with the profile slope deviation direction and the magnitude of the helix deviation. The effect of the profile slope deviation direction on contact stresses is amplified for higher values of profile deviation due to the effect of an interaction between those two factors.
- Maximum bending stress is mainly affected by the value of the helix deviation.

- Consideration of the optimal tip relief micro-geometry modification to the pinion and the gear causes sensitivity of contact stresses with respect to all parameters to decrease substantially. After application of tip relief, the only parameter which has a significant effect on contact stresses is the helix deviation. The application of tip relief does not improve the sensitivity of maximum bending stresses to helix deviation.
- Application of longitudinal crowning reduces the sensitivity of contact stresses with respect to the helix deviation to very low levels. The sensitivity of bending stresses to helix deviation is also reduced with the application of a longitudinal crowning.
- Application of profile crowning has no effect on contact or bending stresses, but it is able to reduce the sensitivity of the peak-to-peak level of loaded transmission errors with respect to pitch, profile, and helix deviations. The main effect that remains in regard to the maximum peak-to-peak level of the function of transmission errors after intended flank modifications is the profile slope deviation direction and its interaction with the profile deviation.
- The optimal longitudinal crowning and the value of maximum helix deviation are linearly related. Equations that give the optimal longitudinal crowning as a function of the helix deviation have been proposed.

Acknowledgements The authors express their deep gratitude to the Spanish Ministry of Economy and Competitiveness (MINECO), for the financial support of research project ref. DPI2013-47702-C2-1-P (financed jointly by FEDER funds), and the Kate Gleason College of Engineering of the Rochester Institute of Technology for the support obtained under the summer undergraduate research program.

References

1. ISO 1328-1: Cylindrical gears—ISO System of Flank Tolerance Classification—Part 1: Definitions and Allowable Values of Deviations Relevant to Flanks of Gear Teeth. International Organization for Standardization, Switzerland (1995)
2. ANSI/AGMA 2015-1-A01: Accuracy Classification System—Tangential Measurements for Cylindrical Gears. American Gear Manufacturers Association, Alexandria, Virginia (2002)
3. Chaari, F., Fakhfakh, T., Hbaieb, R., Louati, J., Haddar, M.: Influence of manufacturing errors on the dynamic behavior of planetary gears. Int. J. Adv. Manuf. Technol. **27**, 738–746 (2006)
4. Bodas, A., Kahraman, A.: Influence of carrier and gear manufacturing errors on the static load sharing behavior of planetary gear sets. JSME Int. J. Ser. C Mech. Syst. Mach. Elem. Manuf. **47**, 908–915 (2004)
5. Ligata, H., Kahraman, A., Singh, A.: An experimental study of the influence of manufacturing errors on the planetary gear stresses and planet load sharing. J. Mech. Des. Trans. ASME. **130**, 041701 (2008)
6. Houser, D.R.: The effect of manufacturing microgeometry variations on the load distribution factor and on gear contact and root stresses. Gear Technol. **6**, 51–60 (2009)
7. Guilbault, R., Gosselin, C., Cloutier, L.: Helical gears, effects of tooth deviations and tooth modifications on load sharing and fillet stresses. J. Mech. Design **128**(2), 444 (2006)

8. ANSI/AGMA 1012-F90: Gear Nomenclature. Definitions of Terms with Symbols, 05 (March) (1990)
9. Xu, L., Li, L., Liu, Y.: Stress analysis and optimization of gear teeth. In: International Conference on Measuring Technology and Mechatronics Automation, pp. 895–898 (2009)
10. Simon, V.: Optimal tooth modifications for spur and helical gears. J Mech Trans Autom Design, **111** (1989)
11. Litvin, F.L., Fuentes, A.: Gear Geometry and Applied Theory, 2nd edn. Cambridge University Press, New York (2004)
12. ABAQUS/Standard User's Manual, Providence, Rhode Island 02909-2499 US (2016)
13. Markovic, K., Franulovi, M.: Contact stresses in gear teeth due to tip relief profile modification. Eng. Rev. **31–1**, 19–26 (2011)

Gear Geometry as a Function of the Production Method

Proposal of Invo-Planar bevel gears for good productivity with 5X-machine

A. Kubo and A. Ueda

Abstract In the frame of the activity of the JSME RC-268 committee, a new bevel gear, i.e., the Invo-Planar bevel gear, is developed, the tooth flank of the wheel of which is a plane or whose transverse tooth profile is a straight line. The cutting/grinding time for this bevel wheel can be more than 10 times shorter than the working time for a conventional bevel gear wheel, when it is cut with a 5-axis machining center, because it cuts or grinds the tooth flank through one path of tool movement. The finished tooth flank is far smoother than the curved tooth flank manufactured through many paths of the cutting blades of the tool. The production rate of the mating pinion with a 5-axis machining center is the same as that of a conventional bevel pinion. Some experiences in the production and quality assessment of product gears, and a performance survey of this new bevel gear, are introduced to promote discussion.

Keywords Bevel gear · Face gear · Design · Manufacturing · Induced stress · Surface integrity

1 Introduction

When we look at the history of gearing, we see that it began with pin or lantern gears. Initially, in cylindrical gears, the theory of the conjugate action of gear meshing was investigated and it was found that a good transverse tooth form was the main point of interest. Subsequently, the cycloid tooth form took up the primary position in the practical field of usage, but now, the involute profile prevails. The main factor driving this change is the fact that the involute gear system has

A. Kubo (✉)
Research Institute for Applied Sciences, Kyoto 606-8202, Japan
e-mail: aizokubo@hera.eonet.ne.jp

A. Ueda
AMTEC Inc., Prio Tower 4305, Osaka 552-0007, Japan
e-mail: ueda@amtecinc.co.jp

V. Goldfarb et al. (eds.), *Advanced Gear Engineering*,
Mechanisms and Machine Science 51, DOI 10.1007/978-3-319-60399-5_2

(1) a high efficiency production system using a basic rack form, (2) tools for high accuracy quality inspection and (3) the permissible strength and toughness of the product gears in practical usage.

There is now a major trend towards a change in the production method of big gears, especially big bevel gears: Until recently, all gears were produced with a specialized gear cutting and/or grinding machine, but now, a multipurpose 5-axis machine is often used for the production of big bevel gears with a sufficient accuracy grade. When we consider the history of gear technology as mentioned above, the production method decides the kind of gear that prevails in the field of practical usage. We can see this history in cylindrical involute gears, in worm gears, and in bevel gears. In addition, the gear production system using a 5-axis machine can be more flexible than the system consisting of specialized gear production machines alone. As a result, this trend of utilizing 5-axis machines for gear production will continue to prevail in the near future. The detail of the 3D dimension of the traditional bevel gear is the result of the Gleason and Klingelnberg machines and their production systems. Thus, the following question arises here: "Is today's bevel gear optimal for production with a 5-axis machine?" This report details a trial designed to find the optimal bevel gear for 5-axis machine production.

One of the problems of gear production with a 5-axis machine is the efficiency of gear tooth cutting or grinding, i.e., the time needed to produce the curved and twisted 3D surface of tooth flanks is too long. For gear manufacturing, many paths of the movement of a cutting/grinding tool are necessary to realize the conjugate 3D curved surface of the tooth flanks, and long manufacturing time means greater production cost. Another problem is the surface integrity of tooth flanks finished with a 5-axis machine: the surface roughness is especially insufficiently smooth in comparison with a tooth flank finished with conventional specialized gear production machinery. The task we have to solve is how such demerits of gear production with a 5-axis machine can be improved so as to draw out the merits of this new production method for realizing better big gears.

2 Way of Thinking

First, we consider an involute rack and pinion in mesh. Then, we bend the rack in the horizontal plane to make a circle, as shown in Fig. 1. Such a system consisting of a pinion and a horizontal circular wheel is known as a Face Gearing system. The mechanical action of the bevel gears can be replaced with face gears. This is the reason why we take face gears as the starting point for developing new bevel gears that can be better produced with a 5-axis machine. The pinion of face gearing is, e.g., of a cylindrical involute gear, and there is no difficulty in producing it. The wheel, however, is a tough problem: The pressure angle at the heel becomes small and the greater part of the dedendum is covered with an unworkable, big tooth fillet curved surface. The pressure angle at the toe becomes very large, making tooth crest into a sharp point (see Fig. 2). When we want to take a reasonable amount of

the tooth width for gear performance, or when we want to take the small tooth number of a wheel to create a somewhat smaller gear ratio, the wheel tooth can no longer exist in a reasonable form.

For this reason, it is not easy to design face gears whose ratio is less than ca. 4. This brings up a common difficulty in designing a power transmission gear box with face gears. In addition, the transverse tooth form of the wheel is almost a straight line, like the rack tooth form, but it is slightly convex, and by an amount that is not negligible. This condition brings up a big problem in producing the face gear wheel economically. These are the reasons why we cannot utilize face gears well in practical fields of usage.

The solution to this problem, however, is not difficult: When we use a conical involute pinion that has somewhat of the same cone angle as that of normal bevel gears (see Fig. 3), the pressure angle at the toe and the heel approaches a reasonable value. The tooth profile of the wheel is almost a straight line, but it is still a little bit convex, because the teeth number is not infinity. When we replace this curved transverse tooth form of the wheel with a straight line and give the corresponding amount of 3D tooth form modification to the tooth flank form of the mating pinion, we have a gear set that does not lose the conjugate action of gear meshing. We call this gear set "Invo-Planar bevel gears of the 2nd kind." The amount of 3D form modification of the pinion tooth flank from the tooth flank of the involute conical gear is not significant. It can then be ground with a grinding machine for cylindrical involute gears, when adequate software for NC control and a corresponding grinding tool is developed.

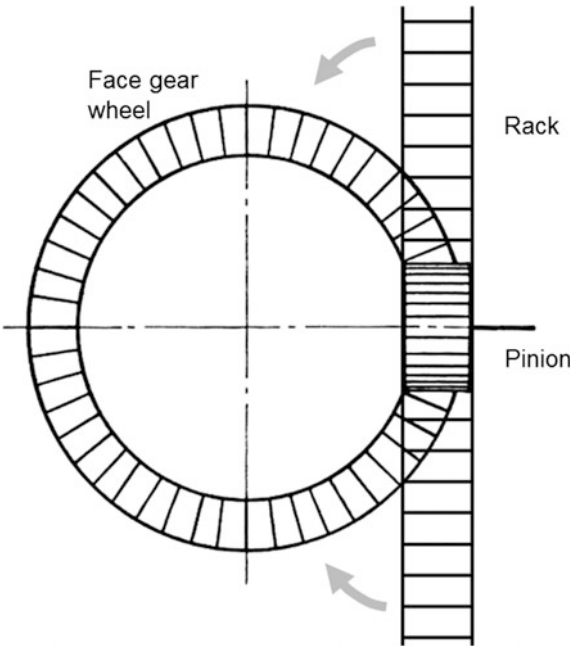

Fig. 1 Transformation of rack and pinion to a face gear set

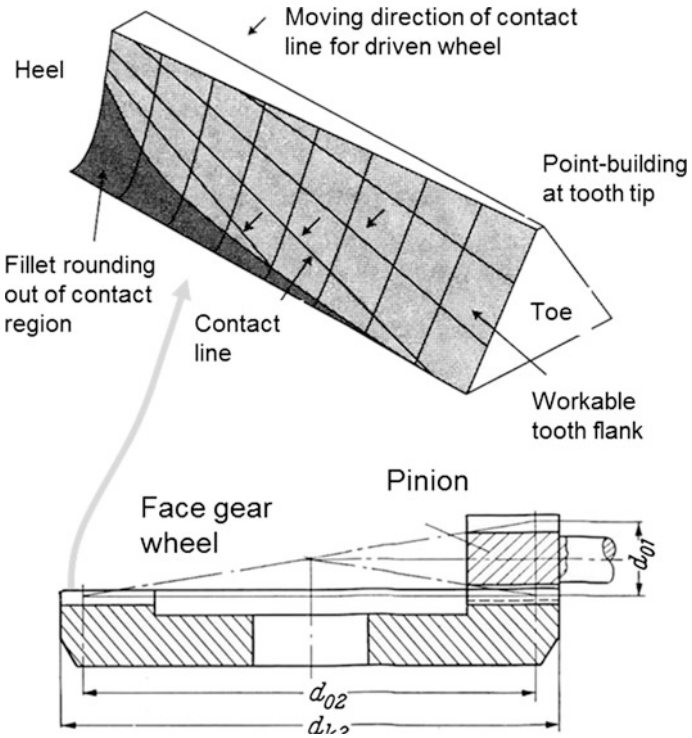

Fig. 2 Face gear set and tooth form of the wheel

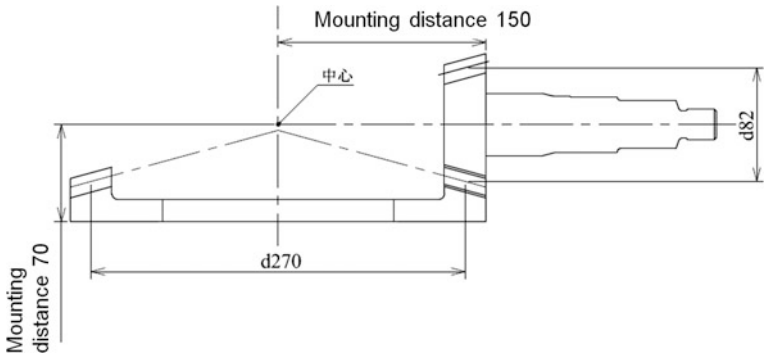

Fig. 3 Conical pinion and mating face gear wheel

The small difference in the pressure angle at the toe and the heel of this bevel wheel then suggests an idea: that we can replace the whole tooth flank of the wheel with a pure plane. Of course, the 3D tooth flank form correction of the mating tooth flank of the pinion must be changed to realize the conjugate action. We call this

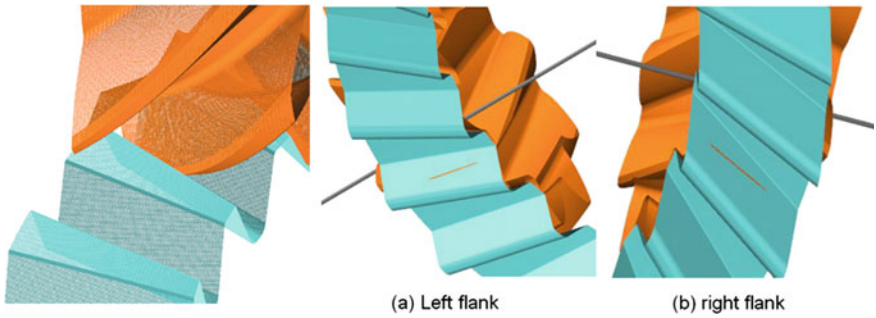

Fig. 4 Tooth meshing of IPB gears and the contact line

gear set with a very simple plane tooth flank form "Invo-Planar bevel gears of the 1st kind," referring to "IP-bevel gears" or "IPB gears." The tooth flank of the IPB wheel can be manufactured by one path of the cutting/grinding tool. The production rate of the wheel is then drastically accelerated by reducing and minimizing the number of cutting/grinding tool paths for forming the tooth flank. The production rate of the IPB pinion with a 5-axis machine, however, remains the same as the working time for conventional bevel pinion production.

3 Invo-Planar Bevel Gear

The leftmost picture in Fig. 4 shows how the IPB gears mesh to transmit motion and power. The center and rightmost figures in Fig. 4 show the contact line on the plane tooth flank of the wheel.[1] The simulation was carried out to visualize the contact line by bringing a very small amount of interpenetration of the pinon tooth flank into the wheel tooth flank by using a CAD model. The figure sees this state from inside the wheel. It is well-recognized that line contact is realized: this is quite a natural matter, of course, because the IPB gear is a strong modification of the involute rack and pinion, as explained above.

The two uppermost pictures in Fig. 5 are the tooth contact pattern obtained by moving the contact line shown in Fig. 4 under the constant rotational speed of both the pinion and the wheel. You can see that the amount of interpenetration between the tooth flanks of the pinion and the mating wheel stays constant during gear rotation. This comes from the fact that this motion is a conjugate action of the rotational angle transmission of the IPB gearing. The lowermost two pictures in Fig. 5 show the distribution of relative slipping velocity between the mating tooth flanks of the pinion and the wheel. The constant slip-velocity line on the pinion

[1]In this CAD model, the tooth flank form of the IPB wheel at the tooth edges is gradually and smoothly modified from the plane, so as not to cause edge contact at the gear mesh.

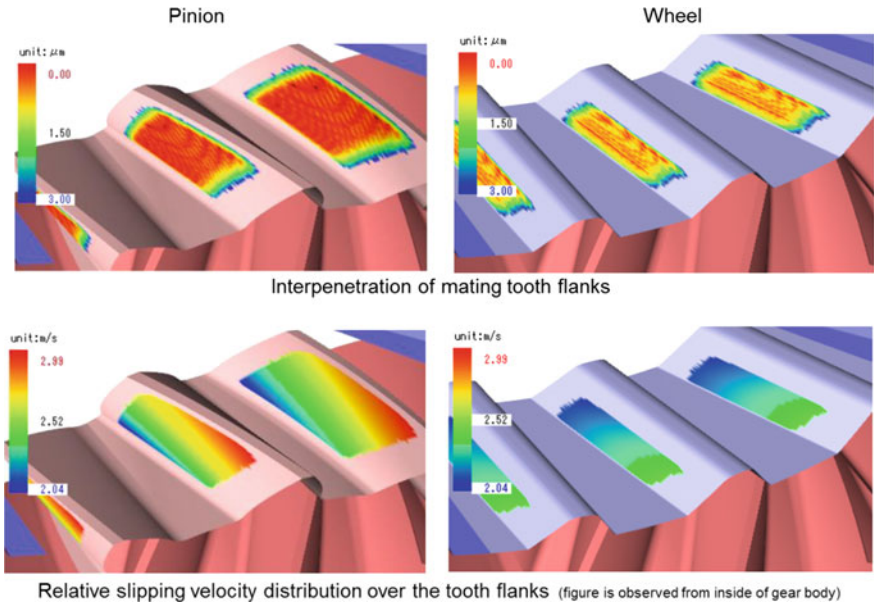

Fig. 5 State of tooth flank contact and slipping velocity distribution

tooth flank is somewhat inclined in the same manner as a common face gear meshing. In this gear design, the pitch line (the rolling contact line) looks to be lower than the dedendum of the pinion tooth flank. The slipping velocity on the wheel tooth flank is changing longitudinally in the tooth width direction. The slipping velocity increases in the direction of the near heel, but the difference is not much at the toe and heel.

4 Production

For this investigation, gear material JIS SCM420H is taken, and both the wheel and pinion are roughly cut with a flat end mill, as shown on the left sides of Figs. 6 and 10. Then, they are case carburized and hardened, and their tooth flanks are finished with a CBN electro-deposited disk grinding tool. The operation is shown on the right sides of Figs. 6 and 10. The final finishing touch of the wheel tooth flank is worked out by one path of tool movement in the lead direction, with a grinding speed of 2034 m/min, a feed of 0.012 mm/rev, and a grinding depth of 5 μm. The pinion tooth flank is ground by many paths of tool movement in the lead direction, with step 0.4 mm in the tooth form direction, a grinding speed of 2034 m/min, a feed of 0.012 mm/rev, and a grinding depth of 5 μm.

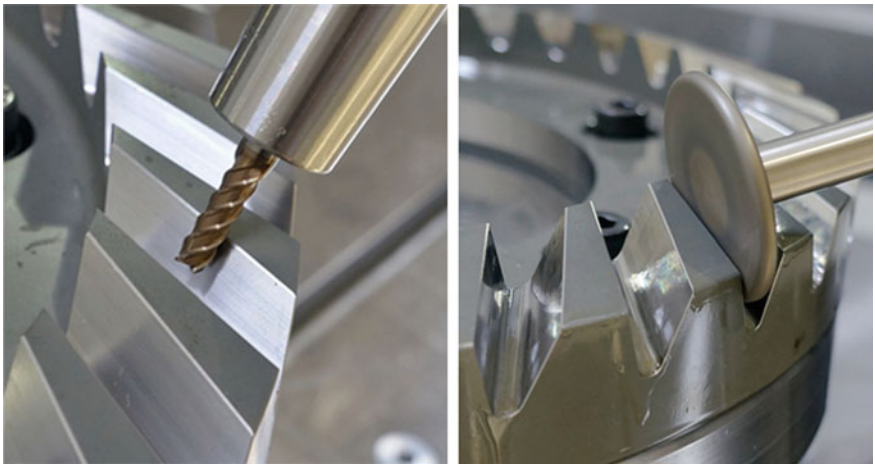

Fig. 6 Rough-cutting and finish-grinding of IPB wheel teeth

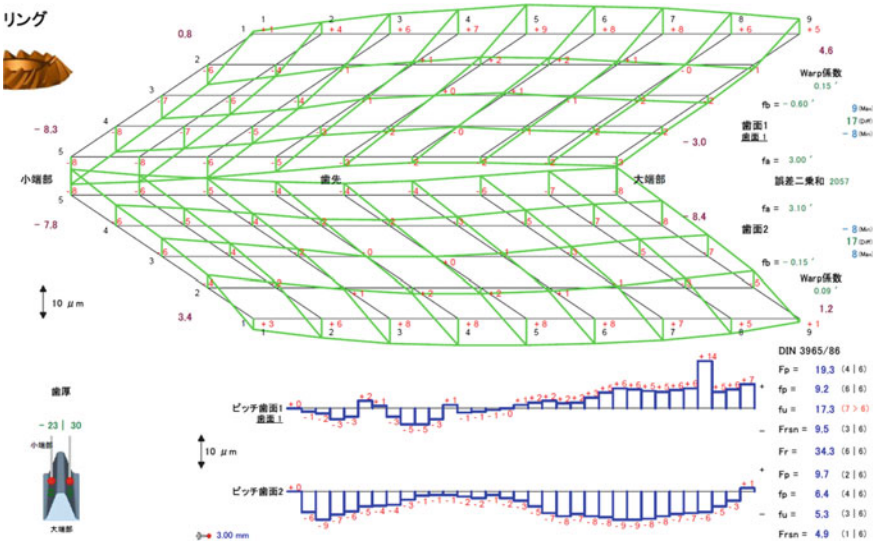

Fig. 7 Pitch and tooth flank form accuracy of an IPB wheel

The completed gears are examined in the 3D form accuracy of the tooth flank. Figure 7 shows the results measured with a high precision CMM. The definition of the form accuracy is the form deviation between the actual tooth flank and the CAD data of the IPB wheel. The gear accuracy is better than ca. 7 µm. Figure 8 is the detailed 3D form deviation of one whole tooth flank measured with a high

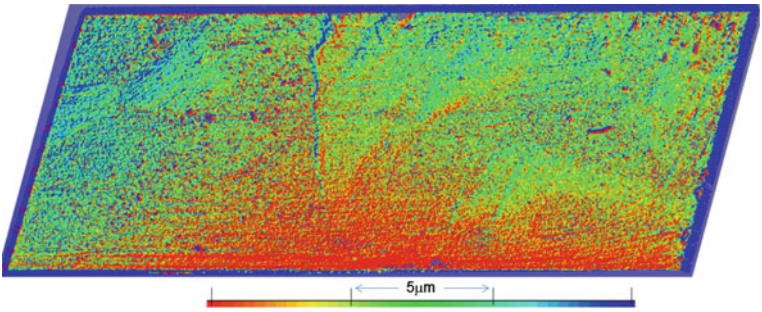

Fig. 8 3D form accuracy of a whole tooth flank

precision, contact-free 3D form-checker using the light beam cutting method. The peak to valley amplitude of the grinding mark on the tooth flank is ca. 0.3–0.4 μm, but they are well-measured. Figure 9 shows the form accuracy of the whole wheel teeth measured with the same contact-free form inspection machine. The geometrical form of all tooth flanks is well-manufactured (Fig. 10).

Figure 11 shows the measured tooth flank form deviation of the pinion. The form deviation of the pinion tooth flank is about 2 times worse than that of the wheel. This result, perhaps, from (1) the polygon effect of the grinding paths needed to form the 3D tooth flank and (2) the difficulty of simultaneous 5-axes NC control during the grinding operation in comparison with the grinding of a plane.

5 Estimated Performance

The induced tooth fillet stress is examined by using FEM analysis. The same analysis was carried out with a spherical involute bevel gear of the same size. The tooth root and fillet form of the spherical involute bevel gear is optimized to minimize the induced stress. Much of our analysis shows that the induced fillet stress of such a spherical involute bevel gear is somewhat lower than that of conventional bevel gears after a normal Gleason or Klingelnberg system. This is the reason why we take spherical involute bevel gears as the object for comparison in induced tooth root stress to evaluate the IPB gears.

Figures 12 and 14 show the form of gear teeth of these two kinds of bevel gear, incorporated for comparison. The load is applied to the FEM nodes at the tooth tip, in the normal direction of the tooth flank, and the total amount of loading is 10 kN. Figures 13 and 15 show the state of induced tooth fillet stress and their maximum value. The induced stress of the IPB wheel is somewhat smaller than that of the spherical involute bevel wheel. When we see Fig. 12, we note that the tooth thickness of the IPB wheel looks too large: this is because the design for sharing tooth thickness between wheel and pinion is still not well done; that is the task of development to come. This means that the width of this wheel tooth should be

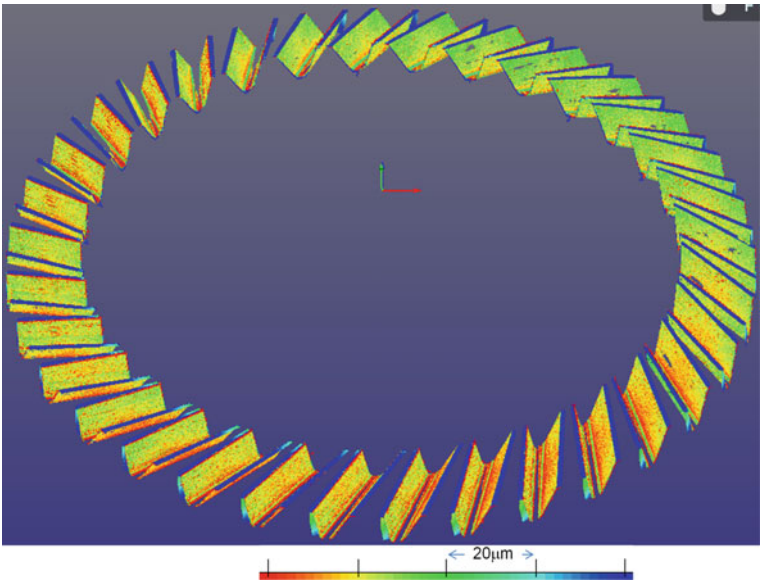

Fig. 9 Accuracy of all the teeth of an IPB wheel

Fig. 10 Rough-cutting and finish-grinding of IPB pinion teeth

reduced to some extent, and the pinion tooth thickness should correspondingly increase. It is really remarkable that the induced stress of the IPB pinion, though its tooth thickness is not yet optimized, is somewhat smaller than that of the spherical involute bevel pinion. This fact indicates that the induced stress in IPB gears is surely considerably lower than that of the conventional bevel gears used today. There must exist some additional rooms beyond the results of this simulation to increase reliability, to make the gear box smaller and its weight lighter by incorporating IPB gears. This is the additional advantage of IPB gears, besides the efficient productivity. The potential for improved IPB gears is high.

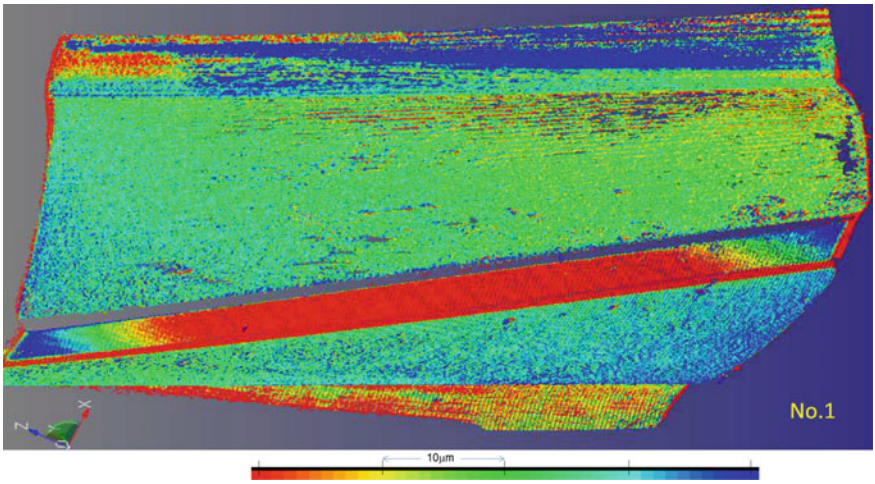

Fig. 11 3D tooth flank form deviation of an IPB pinion

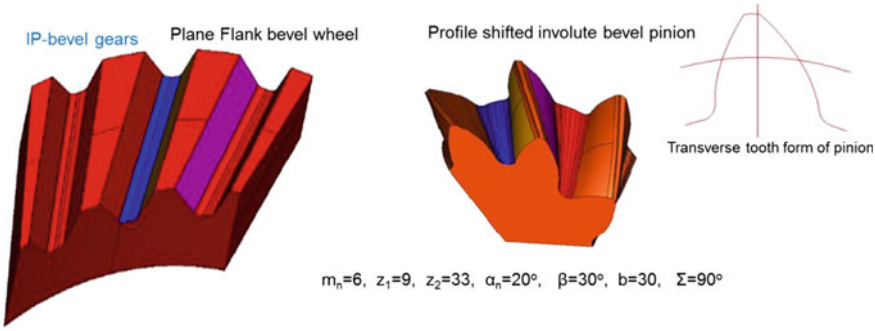

Fig. 12 Sample of IPB gears

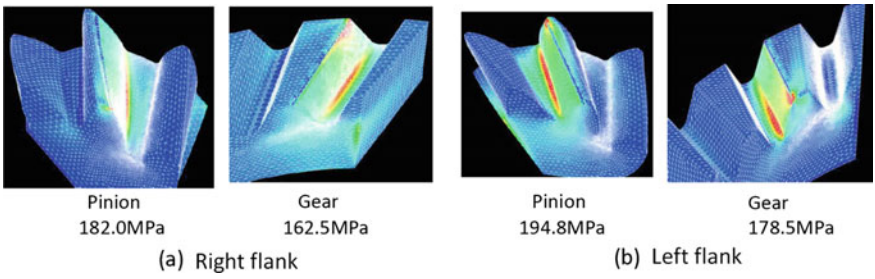

Fig. 13 Bending stress induced in an IPB gear

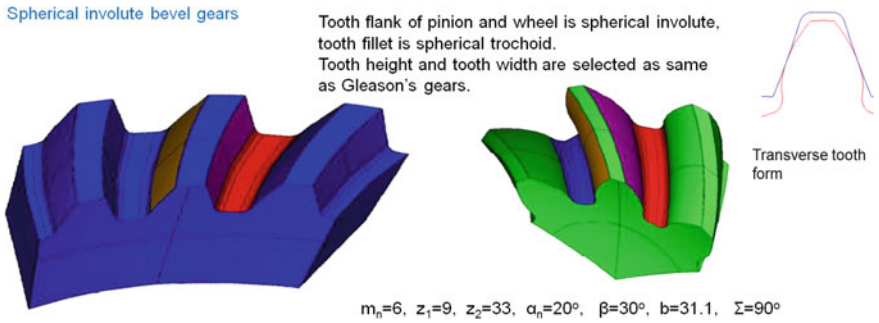

Fig. 14 Sample of *spherical* involute bevel gears

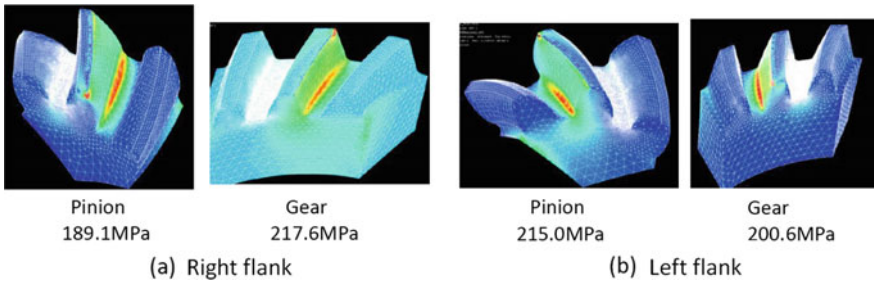

Fig. 15 Bending stress induced on *spherical* involute bevel gears

6 Surface Integrity of the Tooth Flank

Induced Hertzian stress as the index for surface durability is a function of the relative radii of contacting surfaces. The relative radii of the tooth flanks of IPB gears are somewhat larger than those of conventional bevel gears. We are therefore not anxious about the calculated magnitude of the contact stress. The problem could be the surface roughness of the finished tooth flank of IPB gears, when we deal with the surface durability of those same gears. Figure 16 shows the typical look of a tooth flank of an IPB wheel finished by one path of cutting with a ϕ8 mm flat end mill.

The horizontal stripes in the lead direction come from the different cutting capability of the milling tool blades in its axial direction. The magnitude between these stripes in the tooth form direction is not large, about 0.7 μm, as shown in Fig. 17. The rippling figure of surface micro-geometry in the tooth lead direction comes from the eccentricity of the milling tool on the 5-axis machine. The magnitude of that ripple is about 0.8 μm, but the mounting eccentricity of the milling tool must be considerably larger than this value. Such an amount of tool mounting eccentricity cannot be avoided. Figure 18 shows the enlarged figure of

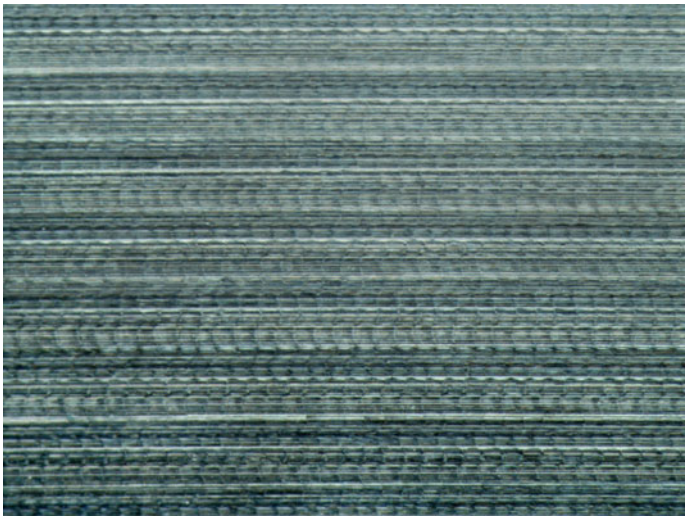

Fig. 16 Typical plane tooth flank of an IPB wheel finished by one path of cutting with a ø8 mm flat end mill

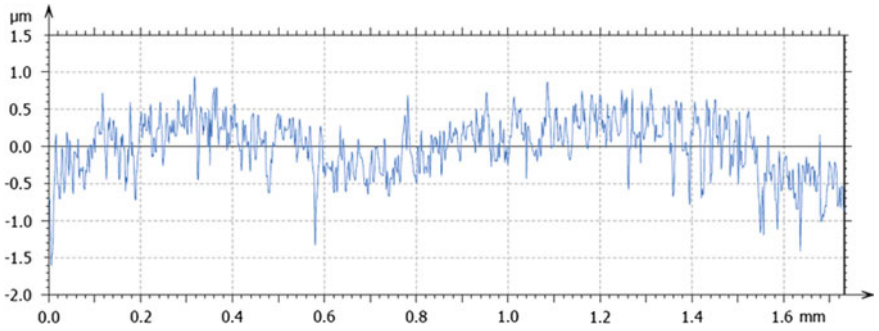

Fig. 17 Surface form of an IPB wheel tooth flank in the tooth form cross-section (figure sampled by 1 μm pitch, with no filtering)

that surface. It is very interesting to find that cutting induces a small amount of very local melting of the cut surface. In certain places in the picture, you can see small black balls: those are the result of the melting of very local surface material by cutting. Melted material congeals. The diameter of the congealed steel ball is ca. 10–40 μm.

Figure 19 shows the tooth flank of an IPB wheel ground by one path of a CBN disk tool. Perhaps we have chosen too fine a CBN grain size of #400–500 for the grinding tool. The ground surface is almost mirror-like, but many very thin scratching traces can be observed, along with some regional, loose, mirror-like glare. We observe the surface as reflecting many colors, due to the diffraction of

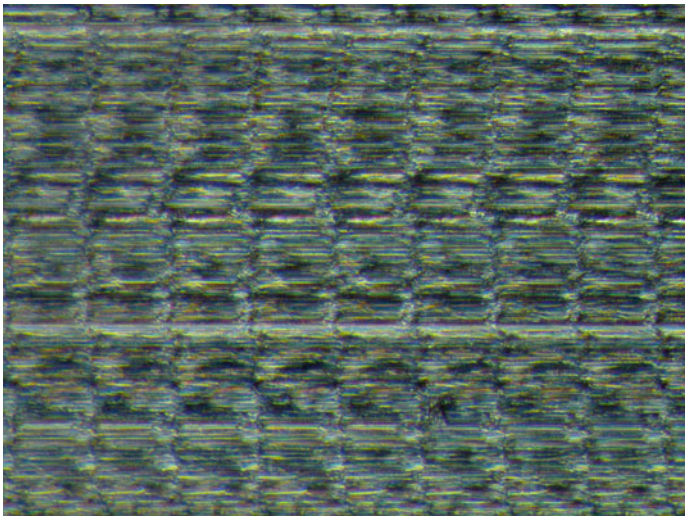

Fig. 18 Rippling due to eccentricity of tool, and small black balls as the evidence of local tooth flank melting at cutting

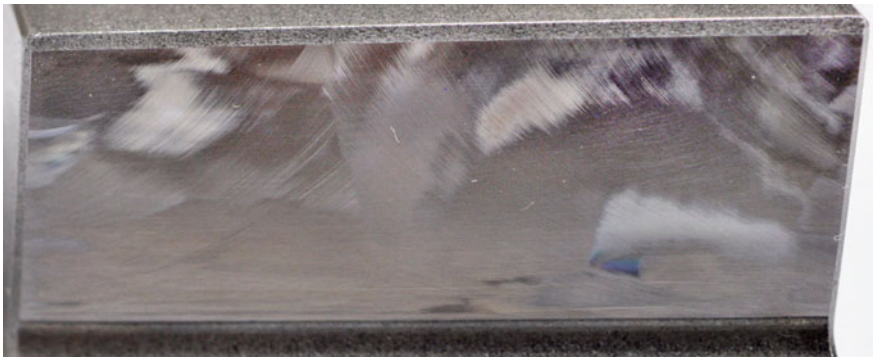

Fig. 19 Plane tooth flank of an IPB wheel finished by one path with a CBN disk tool

light. Figure 20 is the enlarged figure of the surface. It looks as if CBN grains have caused some deep scratching on the ground surface. Figure 21 shows a greatly enlarged picture of the surface, where the lighting is adjusted into a very soft, i.e., into a strongly scattered, light state. Thus, it is confirmed that the CBN grains have caused quite a number of groups of very shallow scratched grooves, the magic of light causing people to get the impression of deep grooves or ridges. The measured surface roughness is indicated in Table 1, and it is very fine. The grinding surface of the CBN tool cannot be set in a perfect, flat contacting state against the objective surface to be ground: the grinding surface of the tool can vibrate in sub-micrometer amplitude at grinding. The resulting ground surface features a stripe-like grouping

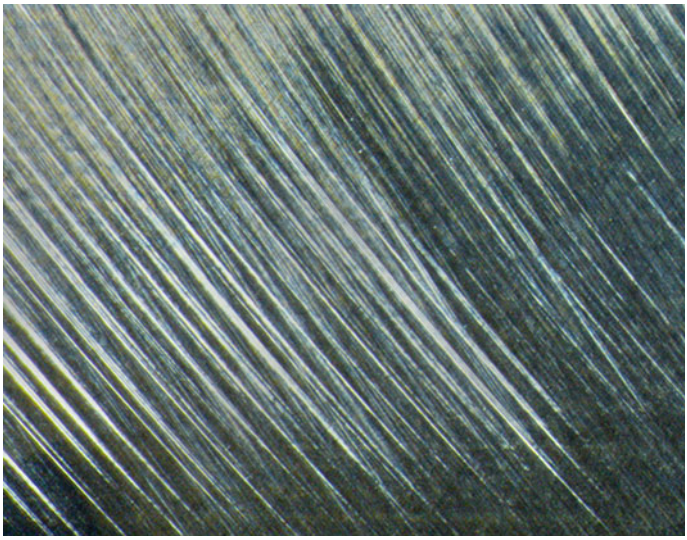

Fig. 20 Nominal ridges on the wheel flank

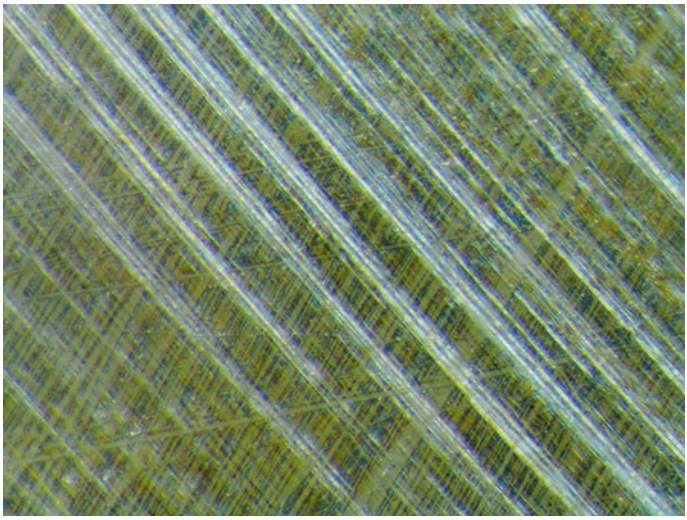

Fig. 21 Shallow groups of scratching on the wheel flank

of ground traces, i.e., like micro scratching, and the resulting distance between these stripes is almost equal.

Figure 22 shows an example of a detailed 3D figure of the tooth flank of the IPB wheel in Fig. 19. CBN grains have ground against the objective flank, causing fine grooves of 0.3–0.4 μm in depth. By the side of those grooves, slightly projected

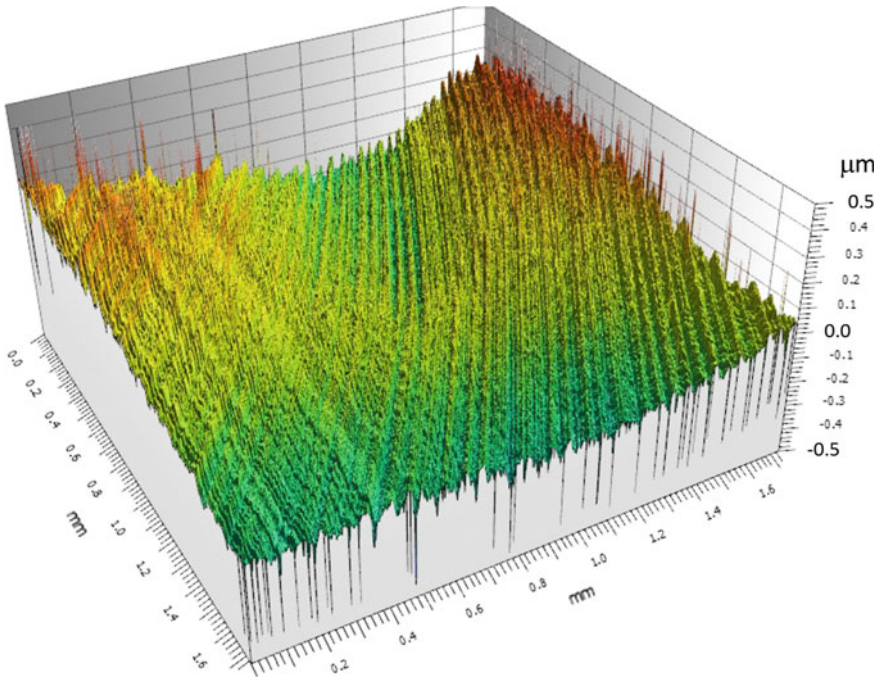

Fig. 22 3D figure of the ground flank of an IPB wheel (distance figure from the optical flat, sampled by 1 µm pitch mesh, with no filtering)

banks of plastically deformed surface material of less than 0.05 µm in height are generated.[2] Aside or on those banks, many small, ball-like objects of 0.1–0.3 µm in diameter adhere. Perhaps very local tooth flank material became plastically deformed and melted during grinding of the grain scratches into the objective tooth flank, and the melted surface material then congealed to become small ball-like objects adhering to the flank. In Fig. 22, they are expressed as a group of needles that exists by the side of the scratching grooves made with the grinding grains. This needle form, however, is the result of the big magnification difference in the z-direction, in comparison with the x- and y-directions in the figure configuration. The part of the tooth flank with the majority of such adhering chips or ball-like objects allows the glare outlook of the surface to look frosted.

Due to repeated contact of the grinding tool surface against the objective surface to be ground, or to a different state of lubrication between the grinding surface of the CBN grinder and the objective tooth flank, or to a slight imperfection in the tool mounting, or to tool vibration, the grinding disk makes contact with some parts of the tooth flank multiple times. That part of the objective tooth flank surface is ground slightly deeper, by 0.3 µm.

[2]The resolution of the measuring apparatus is 0.1 nm.

Fig. 23 Tooth flank of an IPB pinion finished by many paths with a CBN disk tool

Figure 23 shows the tooth flank of an IPB pinion finished by many paths of grinding with a CBN disk tool. The nominal grinding depth is 5 μm and the step pitch of the tool path in the direction of the tooth form is 0.4 mm. Under such a grinding condition, the CBN grinding tool disk is not rigid enough, which means that the micrometer-order deformation of the tool disk is very easy. As a result, the stripe mark in the tooth lead direction due to tool feeding takes on a very obscure form. From the state of the scratching traces on the tooth flank, it is recognized that a considerably wide part of the disk flat of the grinding tool is making contact with the objective tooth flank of the pinion.

Tables 1 and 2 sum up the results of the residual stress of the surface material of the tooth flank and surface roughness to determine the nature of the finished tooth flank of IPB gears manufactured with a 5-axis machine. The residual stress, or to be exact, the residual lattice strain of the ferrite crystal of the tooth flank material, is investigated by using X-ray diffraction. The amount of compressive/tensile residual deformation and shearing deformation of the ferrite lattice is modified so as to obtain the stress dimension by multiplying the nominal elastic modulus. The full width at half maximum (FWHM) of the diffracted X-ray beam corresponds well to the Vickers hardness value at a depth of ca. 7 μm from the surface. In the case of this material, 100 times the FWHM-degree value corresponds well to the micro-Vickers hardness, e.g., 6.03°. FWHM corresponds to ca. 600Hv.

The tooth flank ground by the CBN disk grinder is covered with traces of micro scratching due to the grinding grain movement and results in very smooth surface roughness. The surface hardness, however, looks to turn out a little lower than that of the milled tooth flank. It suggests the surface temperature at grinding with a CBN disk has the tendency to increase. The grinding tool, perhaps, rubs the target surface strongly. The residual compressive stress has some orientation concerning the direction of the grinding grain movement. Those results come from the fact that we

Table 1 Residual stress or ferrite crystal lattice deformation

		Cutting direction			Normal direction to cutting		
		σ_x (MPa)	T_{xy} (MPa)	FWHM	σ_x (MPa)	T_{xy} (MPa)	FWHM
CBN disc grain size #400–500	Wheel	−978	−93	6.03	−711	50	5.84
	Pinion	−901	128	5.89	−1044	−87	5.81
ø8 mm flat end mill	Wheel	−791	−148	6.38	−696	175	6.27
	Pinion	−548	−76	6.55	−731	192	6.24

Table 2 3D and 2D surface roughness

		Sz	Sa	Rz	Ra
CBN disc grain size #400–500	Wheel	1.7	0.06	0.46, 0.38	0.06, 0.04
	Pinion	2.76	0.07	0.56, 0.18	0.05, 0.03
ø8 mm flat end mill	Wheel	5	0.32	1.91, 0.88	0.21, 0.14
	Pinion	4.64	028	2.3, 1.31	0.36, 0.24
				Values max to min	

have chosen too fine a CBN grain size for the grinding tool. When we use grains of a somewhat rougher size, then the surface roughness becomes a little bit more pronounced, but deterioration of the ground surface concerning residual stress and hardness must be improved.

The milled tooth flank looks very rough, at least according to the impression given by such photos as those shown in Figs. 16 and 18, but the measured roughness value is not nearly as bad as one might suppose from the look of the photos. A 5-axis machine can produce gears comparable to those made with a hobber, a shaper, etc., for machining involute gears.

7 Bevel Gears to Come

Our development work shows that the performance of IPB gears can surely be a little bit better than that of conventional bevel gears. The number of tool paths needed to generate the tooth flank form of an IPB wheel decreases by more than 10 times that needed for conventional bevel wheel production, when a 5-axis machine produces it. We can surely produce an IPB wheel far more efficiently than a conventional bevel wheel. However, the problem remains for the production of an IPB pinion. When we produce an IPB pinion with a 5-axis machine, we need the same working time as for the production of a conventional bevel pinion. The basic tooth flank form of an IPB pinion is that of a conical involute gear with 3D micro-geometry correction. The amount of this tooth flank correction is usually less than 130 μm. One other problem will be the interference of the back side of the

Fig. 24 IPB gears in good mesh and smooth working

grinding wheel against the back flank of the pinion to be ground. That problem can be solved by the design of a proper grinding disk tool. It must therefore be possible to grind the tooth flank of a conical involute gear with a 3D flank form correction with today's better gear grinders, if a clever disk tool design is created and adequate numerical control software is supplied. Then, the production rate of the IPB pinion is improved to the level of cylindrical involute gears. The total production rate of IPB gears then becomes far better than that of the conventional bevel gear. Of course, there already exists a great amount of production machinery and facilities for conventional bevel gear production today, and it would cost too much to discard them to incorporate IPB gears. Perhaps in the field of bevel gear usage in which the amount of such already existing production facilities, and their accompanying inheritance, is comparatively small, IPB gears will be gradually incorporated (Fig. 24).

Acknowledgements The intention of this publication is that the technology concerning IPB gears should not be patented, for the benefit of the public throughout the world. The authors appreciate the agreement of the JSME RC268 committee members on this matter. The IPB gear is free to be used!

Model of Loaded Contact in Multi-pair Gears

E. Trubachev, A. Kuznetsov and A. Sannikov

Abstract The paper describes the problem of LTCA of a heavy-loaded multi-pair spiroid gear. The algorithm for analysis of load distribution, accounting for elastic and elastic-and-plastic contact in general and micro-roughnesses of contact surfaces in particular, is proposed. Agreement of the algorithm at various accelerating procedures is studied. Numerical examples that illustrate the efficiency of the algorithm are given.

Keywords LTCA · Multi-pair heavy-loaded gear · Elastic and plastic contact

1 Introduction

It became common in both the theory and practice of gearing [4, 5, 8] to solve the problems of assessing the load state and strength with account for the elastic character of contact interaction. The traditional means of solution of this problem is the finite element method (FEM) and the corresponding software. The following inter-related problems of FEM application for analysis of loaded gears should be mentioned:

- increase in error of computations for cases of assessing the stresses at tooth roots for relatively non-smooth conjugations between tooth flanks and their roots;
- abrupt increase in the computational complexity (requirements for computational resources, accumulation of computational error because of rounding at numerous operations, provision of convergence) for the case of a multi-pair contact.

The assessment of stresses at tooth roots of multi-pair spiroid gears should be related to these exact cases. As for gears of heavy-loaded, low-speed gearboxes, the calculation values reach 1500–2000 MPa, even for maximum contact stresses that

E. Trubachev (✉) · A. Kuznetsov · A. Sannikov
Kalashnikov Izhevsk State Technical University, Izhevsk, Russia
e-mail: truba@istu.ru

V. Goldfarb et al. (eds.), *Advanced Gear Engineering*,
Mechanisms and Machine Science 51, DOI 10.1007/978-3-319-60399-5_3

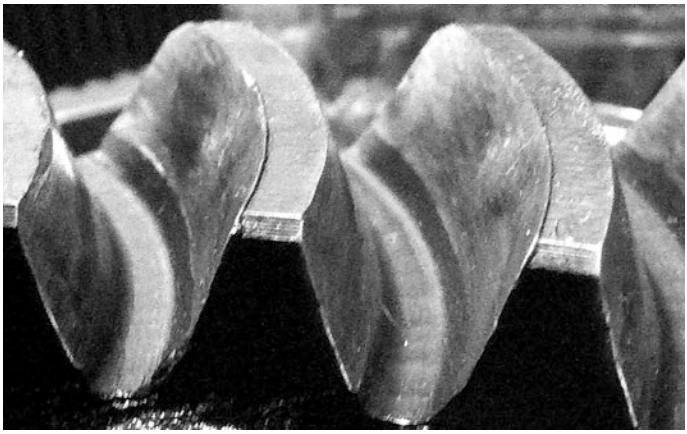

Fig. 1 Crumbling of apexes of spiroid gearwheel teeth after heavy loading

are uniformly distributed along lines of the conjugated contact. Concern over loss of contact and/or the bending strength of teeth at stress concentration in these or those areas due to the action of errors and deformations is natural. However, these gears do successfully operate. Evidently, this is due to the rapid equalizing of loads acting on teeth and to the reduction of corresponding stresses. The practice of testing and operation proves this assumption: even after the first cycles of heavy loading, one can observe plastically deformed areas of teeth (Fig. 1). Therefore, consideration of this factor is very urgent for assessment of the strength of multi-pair heavy-loaded spiroid gears.

As for the elastic-and-plastic statement of the problem, the above-mentioned issues of FME application are revealed to an even greater extent. For this reason, we developed the original iterative algorithm of analysis of the elastic and elastic-and-plastic loaded contact in the spatial multi-pair gear; the present paper considers its basic aspects.

2 Model of the Elastic Loaded Contact

As usual, let us consider that such an initial position of gear elements (accounting for errors) is determined before the analysis, at which time the clearance between teeth at a certain point or points is equal to zero (the presence or absence of the common normal at this point is insignificant). At the remaining points of the flanks, there is a clearance S_0 that is greater than zero.

As is known, the loaded gear is a multiply statically indeterminable system with unilateral links. As for the discretized representation of this system, the following conditions should be fulfilled for cells of tooth flanks that participate in the load transmission:

$$\begin{cases} \sum\limits_{D} F_{k'm'} \nu_{km\,k'm'} + S_{0km} - \Delta_{\varphi 2km} = 0; \\ \sum\limits_{D} F_{k'm'} \breve{r}_{2k'm'} - T_2 = 0; \end{cases} \tag{1}$$

where S_{0km} is the initial (prior to load application) clearance between the kmth cells of surfaces for the position of links when the clearance at one of the cells is equal to zero, $\nu_{km\,k'm'}$ is the value of the influence function determining the transmission of surfaces at the kmth cells when applying the unit loads at the $k'm'$th cells, $\Delta_{\varphi 2km}$ is the relative transmission of the kmth cells as a result of the close approach of elements at gear loading, and $\breve{r}_{2k'm'}$ is the arm of action of the force $F_{k'm'}$ applied at the $k'm'$th knot with respect to the gearwheel axis. The first km equations of system (1) are the conditions of compatibility for the displacement of points of contacting areas of teeth (in the model, they are the cells of the contact area), the latter equation is the equation of equilibrium of torques developed by forces applied at cells and the external torque T_2 applied to the gearwheel.

The cells at which forces are applied are unknown prior to analysis; therefore, neither the number of the first km equations of system (1), nor their specific form are known either. That is why iterative algorithms of calculation [1, 2, 11, 12] were given development implying the consequent specification of: the approaching of elements, the contact area, and the values of discretely applied forces. The latter for the elastic statement linearly influence the displacement of tooth points (by the factors $\nu_{km\,k'm'}$).

Our developed algorithm for solving system (1) originated in works by Zablonsky [13] and Sheveleva [11]; and it implied the following steps (see also Fig. 2):

(1) *The value of the initial approach of elements is assigned as* $\Delta\varphi_2^{(n)} = \Delta\varphi_2^{(1)}$ (here and further within description of the algorithm, n is the number of the iteration). The result is the formation of the area $D^{(1)}$ with the penetration of teeth into each other.

(2) *For the pointed area, the zero approach of discretely applied forces is determined as* $F_{km}{}^{(n)} = F_{km}{}^{(1)}$ with account for the condition of force equilibrium proportional to the formed penetrations $S_{0km} - \Delta_{\varphi 2km}{}^{(1)}$ as follows:

$$f_{km}{}^{(1)} = S_{0\,km} - \mathrm{D}_{\varphi 2km}{}^{(1)}, \tag{2}$$

$$F_{\mathrm{km}}{}^{(1)} = T_2 f_{\mathrm{km}}{}^{(1)} / \sum_{D} f_{\mathrm{km}}{}^{(1)} \breve{r}_{2km} \tag{3}$$

The following steps of the algorithm are related to both the first and all the subsequent nth iterations.

(3) *Displacement of points due to application of forces and corresponding discrepancies* ξ_{km} *of the first km equations of system* (1) *are determined*:

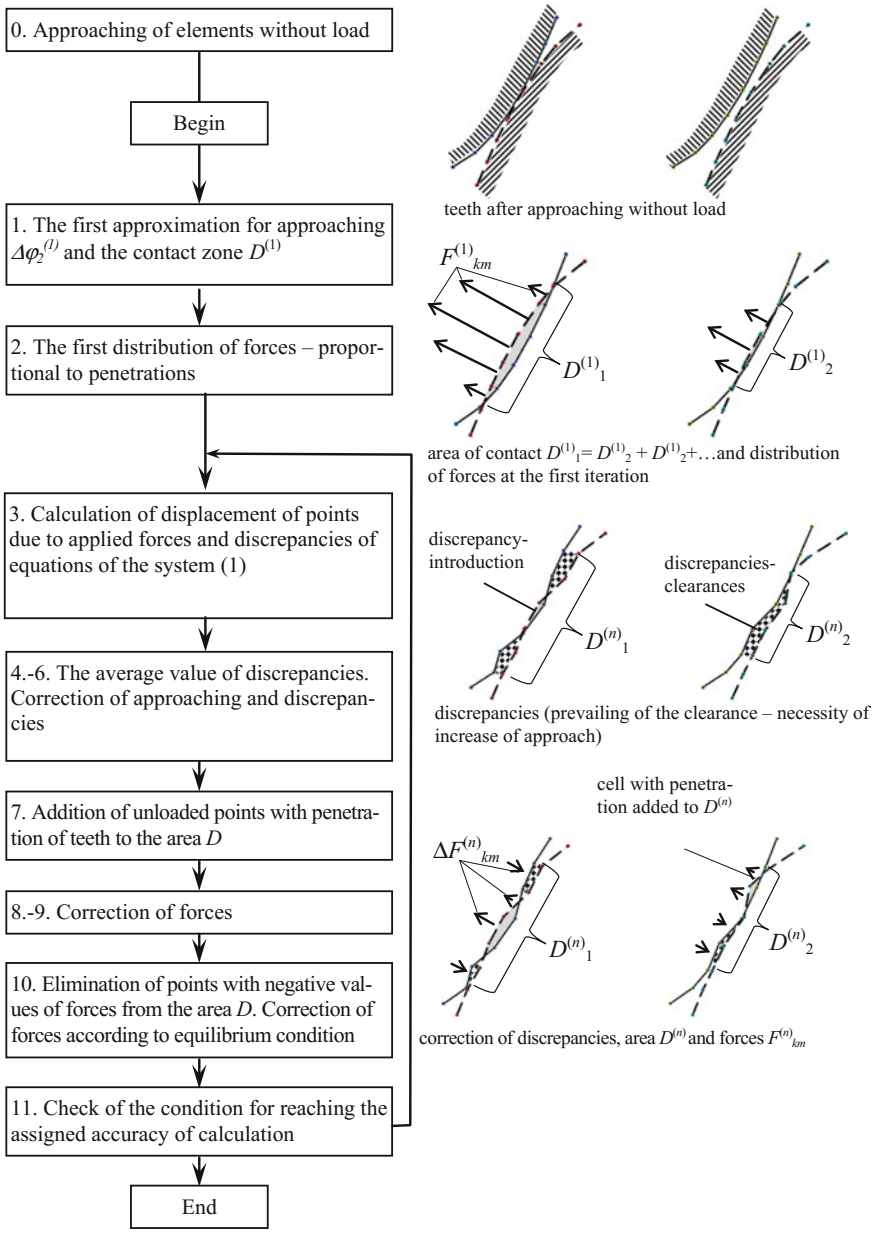

Fig. 2 Scheme of analysis of a multi-pair elastic loaded gear

$$w_{km} = \sum_{D} F_{k'm'}(v_{1km\,k'm'} + v_{2km\,k'm'}) = \sum_{D} F_{k'm'} v_{km\,k'm'}, \tag{4}$$

$$\xi_{km}{}^{(n)} = w_{km}{}^{(n)} + S_{0\,km} - \Delta_{\varphi 2\,km}{}^{(n)}. \tag{5}$$

(4) *The average value of discrepancies within the area D reduced to the angle of the gearwheel rotation is determined*:

$$\xi_{av}{}^{(n)} = \frac{1}{I} \sum_{D} \xi_{km}^{(n)} / r_{2km}. \tag{6}$$

(5) *The chosen value of approaching* $\Delta\varphi_2^{(n)}$ *for the next* (*n* + 1)th *iteration is corrected by the value of the average discrepancy:*

$$\Delta\varphi_2^{(n+1)} = \Delta\varphi_2^{(n)} + \xi^{(n)}{}_{av}. \tag{7}$$

(6) *Discrepancies* ξ_{km} *are corrected for the new value of approaching* $\Delta\varphi_2^{(n+1)}$:

$$\tilde{\xi}_{km}{}^{(n)} = S_{0\,km} + w_{km}^{(n)} - \Delta_{\varphi 2 km}{}^{(n+1)} = \xi_{km}{}^{(n)} - \xi^{(n)}{}_{av} r_{2\,km}. \tag{8}$$

(7) *The area D* [*the number km of equations of system* (1)] *is corrected.*
After correction of the value of approaching (7), those cells (unloaded at the *n*th iteration) should be added to area *D,* for which $\tilde{\xi}_{km}{}^{(n)} < 0$.

(8) *Corrections* $\Delta F_{km}{}^{(n+1)}$ *to discretely applied forces are determined.*
This is the crucial step of the algorithm. The manner of changing the values of forces determines the convergence of iteration to the solution. In our opinion, in order to correct the forces, it is reasonable to use the moments of discrepancies available at the moment. This issue will be considered in detail below.

(9) *Values of forces are determined at the following iteration:*

$$f_{km}{}^{(n+1)} = F_{km}{}^{(n)} + \Delta F_{km}{}^{(n+1)}. \tag{9}$$

(10) *The area D is corrected again* [*the number km of equations of system* (1)].
Cells with negative values of $f_{km}{}^{(n+1)}$ are excluded from it, while for the rest of the cells, the values of forces are corrected in accordance with the condition of their equilibrium:

$$F_{\mathrm{km}}{}^{(n+1)} = T_2 f_{\mathrm{km}}{}^{(n+1)} / \sum_D f_{\mathrm{km}}{}^{(n+1)} \breve{r}_{2km}. \tag{10}$$

(11) *The condition of reaching the value of correction of forces* (*step* 8) *of the assigned allowable low value is checked.* In the case of a negative result, we return to step 3.

The end of the algorithm.

Let us consider the issue of the rational variation of values of discretely applied forces within iterations. In particular, we study the classical method for a simple iteration applied for solution of traditional large systems of linear equations (note that the "peculiarity" of our case is that the number of equations in (1) can, in general, be varied during analysis). Let us further assume conditionally that the first I equations of system (1) will be solved at each iteration, having represented it as

$$\mathbf{N} \cdot \mathbf{F} = \mathbf{b}, \tag{11}$$

where $\mathbf{N}$ is the matrix of the influence factors, $\mathbf{F}$ is the column vector of the sought-after, discretely applied forces, and $\mathbf{b}$ is the column vector of free members of the system, its coordinates being the values $\Delta_{\varphi 2km} - S_{0km}$ (therefore, the value $\Delta_{\varphi 2km}$ is temporarily considered to be constant). Discrepancies in equations of system (11) should be reduced to a minimum. It should be accounted for that, in general, the matrix $\mathbf{N}$ is unsymmetrical, since the compliance of various areas of teeth is different, for example, it is increased when approaching the edges (faces or apexes) of teeth and it is decreased closer to the recess (tooth root) [1, 2, 6], thus imposing limitations for choosing certain efficient methods of solution of such large systems of equations.

The method of simple iteration for solving system (11) implies its reduction to the form

$$\mathbf{F} = \mathbf{B} \cdot \mathbf{F} + \mathbf{c}. \tag{12}$$

In this case, the solution is found to be the limit of the sequence

$$\mathbf{F}^{(n+1)} = \mathbf{B} \cdot \mathbf{F}^{(n)} + \mathbf{c}. \tag{13}$$

In the simplest case, the basis for correction of $\boldsymbol{F}$ can be the column vector $\boldsymbol{\xi}$ of discrepancies of Eq. (11) obtained at the previous iteration

$$\mathbf{F}^{(n+1)} = \mathbf{F}^{(n)} - t^{(n+1)} \boldsymbol{\xi}^{(n)} = \mathbf{F}^{(n)} - t^{(n+1)} (\mathbf{N} \cdot \mathbf{F}^{(n)} - \mathbf{b}). \tag{14}$$

Equation (14) is reduced to the form (13) if we accept that

$$\mathbf{B} = \mathbf{E} - t^{(n)}\mathbf{N}, \tag{15}$$

where $\mathbf{E}$ is the unit matrix. In the general case, the scalar parameter $t^{(n)}$ can be replaced by the matrix $\mathbf{T}^{(n)}$ with the diagonal consisting of factors $t_{km}^{(n)}$ that are suitably chosen for the kmth components of $\mathbf{F}$ and the remaining cells are zero:

$$\mathbf{F}^{(n+1)} = \mathbf{F}^{(n)} - \mathbf{T}^{(n)} \cdot \boldsymbol{\xi}^{(n)}. \tag{16}$$

Let us call the iteration process in which $t^{(n)}$ ($\mathbf{T}^{(n)}$) does not change at iteration a stationary one; otherwise, we deal with a non-stationary process.

The iteration process (14) can be given a reasonable physical essence: for the cells in which $\xi_{km}^{(n)} > 0$ (a clearance appeared at iteration), the increment of the force at the following iteration must be negative (the current value of the force causes too large a deformation, which is why a clearance appears); otherwise (if there is a penetration, that is, $\xi_{km}^{(n)} < 0$), the increment of the force must be positive. The iteration relations for the correction of forces proposed in [2, 11] can be reduced to the following form at the next iteration:

$$F_{km}^{(n+1)} = F_{km}^{(n)} - \frac{\tau_I}{\left(w_{km}^{(n)} + S_{0km}\right)} \tilde{\xi}_{km}^{(n)}, \tag{17}$$

$$F_{km}^{(n+1)} = F_{km}^{(n)} - \frac{\tau_{II}}{\sum\limits_{k'm' \in D} \nu_{kmk'm'}} \tilde{\xi}_{km}^{(n)}. \tag{18}$$

We proposed the following, more simple and, as will be shown below, rather efficient iteration relation for the correction of forces:

$$F_{km}^{(n+1)} = F_{km}^{(n)} - \frac{\tau_{III}}{\nu_{km}} \tilde{\xi}_{km}^{(n)}, \tag{19}$$

factors τ/ν_{km} of which are components of the vector of parameters $\mathbf{T}^{(n)}$. Another non-crucial correction that considers the feature of the algorithm stated above is introduced here: having defined the method for correcting the value of approaching $\Delta\varphi_2$ and the area D at the next iteration in steps 6, 7 and 8, it is better that we use the column vector $\tilde{\boldsymbol{\xi}}$ of the corrected discrepancies (8).

The physical meaning of relation (19) can be explained as: the $(n + 1)$th increment of the force for compensation of "penetration" or "clearance" (appearing within the calculation at the nth iteration) depends on the elastic properties of the loaded system, that is, the more the system reacts to the change of load at this step (the factors of influence are greater at the denominator), the less the increment of the force must be.

We considered the convergence of the above given iteration algorithm for different parameters τ by the example of the conjugated spiroid gear of a heavy-loaded

low-speed gearbox with a loading torque of 2000 Nm. The basic parameters of the test gear are given in Table 1.

Figure 3 shows the diagrams of variation of numerical parameters of the analysis when applying relations (17)–(19) within the iteration cycle. As can be seen, the parameters can be arranged as follows with regard to the velocity of specification: approaching, discrepancies, discretely applied forces.

We considered the behavior of a stationary iteration process for different values of parameters τ. The main results are shown in Fig. 4. As was expected, when decreasing the values $\tau_{I,II,III}$, the velocity of convergence is decreased; and when the above given values are increased, the algorithm begins diverging—first locally and then, as a rule, globally.

As can be seen, the optimal parameter τ can have a very wide range of values. In this context, it is desirable to have a more versatile parameter that regulates the velocity of convergence. In order to get it, let us consider the possibilities of a non-stationary iteration process for which we will use information on the variation of discrepancies at the last iteration; namely, let us assume that:

– this variation depends on the parameter τ linearly:

$$\frac{\Delta\xi^{(n)}_{\text{mean sq.}}}{\tau^{(n)}} = \frac{\Delta\xi^{(n+1)}_{\text{mean sq.}}}{\tau^{(n+1)}}, \tag{20}$$

where $\Delta\xi^{(n,n+1)}_{\text{mean sq.}} = \sqrt{\sum_{D^{(n)}} \left(\xi^{(n-1,n)}_{km} - \xi^{(n,n+1)}_{km}\right)^2 / N^{(n)}_D}$ is the mean square variation of discrepancies at the nth ((n + 1)th) iteration;

– there is a certain desired value of V of the relation. At first sight, it is desirable to assign a big relation, however, as the results shown in Fig. 5 prove, there is a certain improvement of system (1) that is limited for solution of the elastic system; and it is obtained at two neighboring iterations:

$$\xi_{km}{}^{(n+1)} = \xi_{km}{}^{(n)}/V. \tag{21}$$

Table 1 Basic parameters of the test gear

Center distance (mm)	60
Axial module of the worm (mm)	2.75
Gear ratio	46:1
External diameter of the spiroid worm (mm)	42
External/internal diameters of the spiroid gearwheel (mm)	175/138
Factors of the addendum/dedendum	1/1.2
Profile angles of the right/left flanks	10°/30°

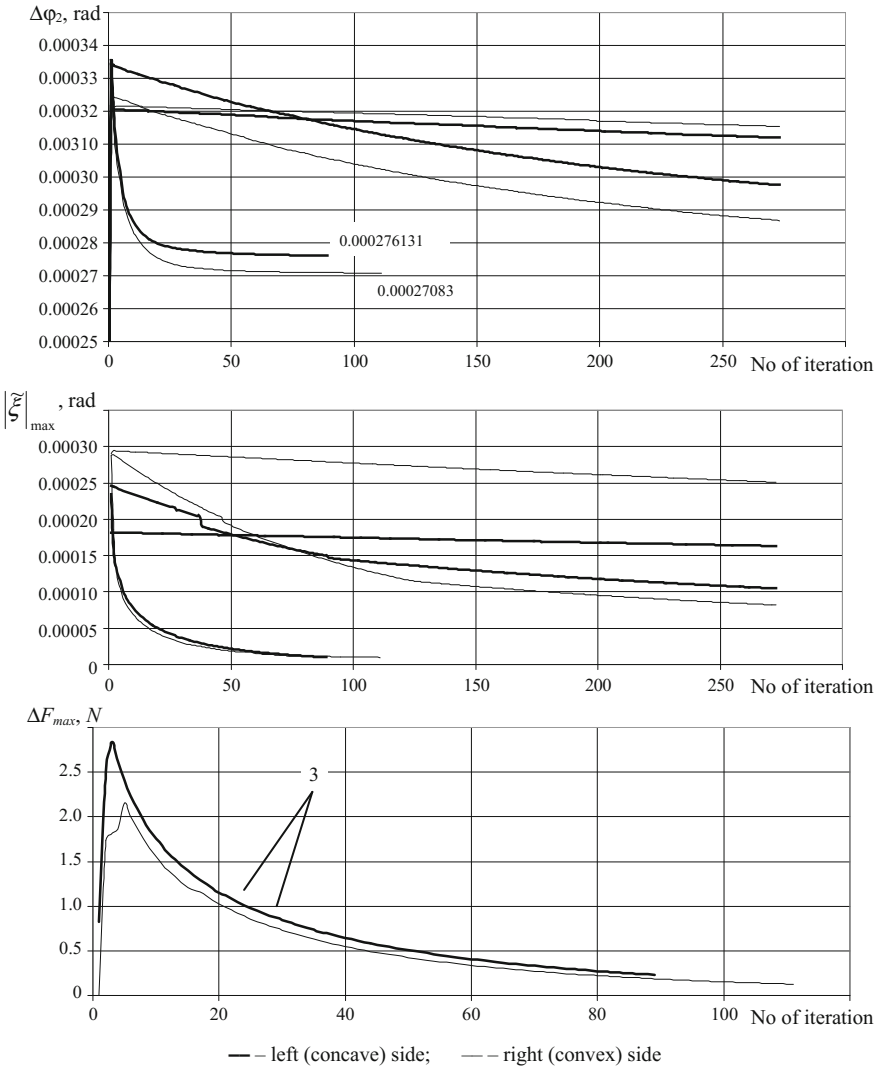

Fig. 3 Convergence of the algorithm for different iteration relations: *1*, *2*, *3* correction of forces with regard to (17–19), respectively

One can obtain, as a result,

$$\tau^{(n+1)} = \tau^{(n)} \left(1 - \frac{1}{V}\right) \frac{\xi^{(n)}_{\text{mean sq.}}}{\Delta\xi^{(n)}_{\text{meansq.}}}. \tag{22}$$

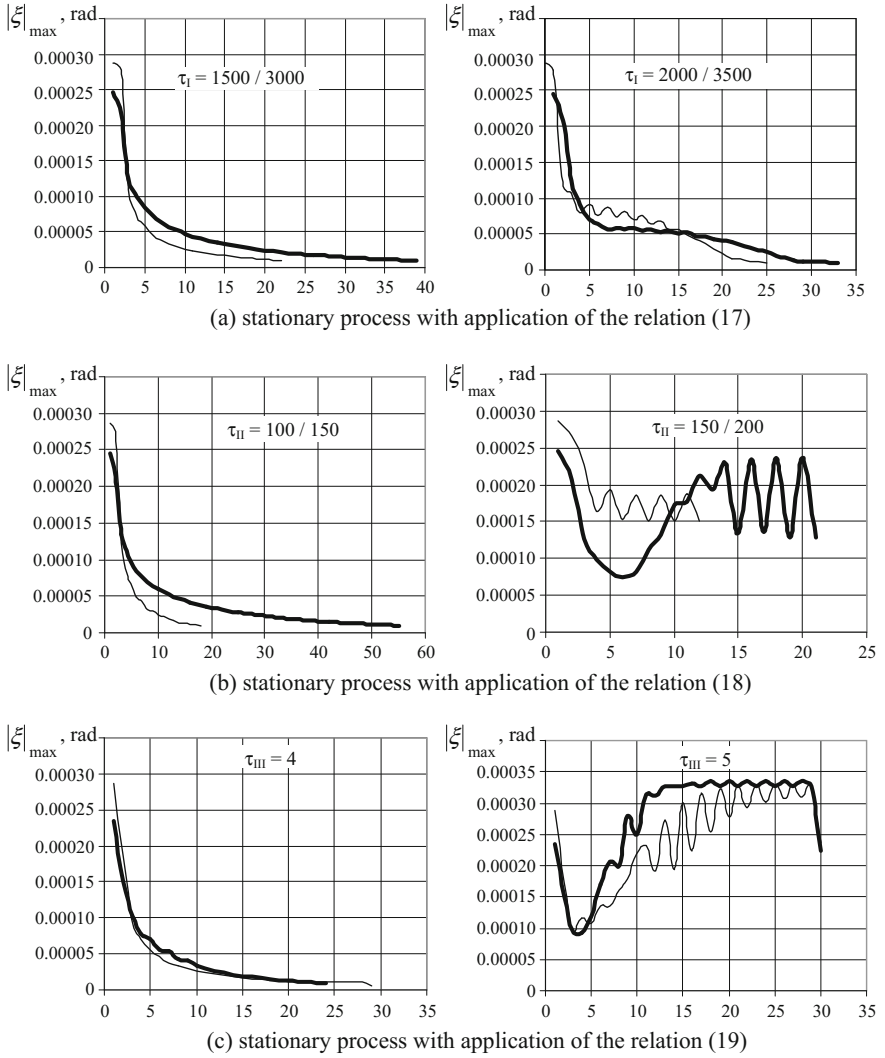

Fig. 4 Convergence of the algorithm for different parameters of τ (the nominator of the value is for the *left flank*, the denominator is for the *right flank*)

The efficiency of the applied procedure is illustrated by the results of the test calculations shown in Fig. 5. As can be seen, comparatively close optimal values of the parameter V are obtained: 1.6–1.8, providing, in this case and as a rule, better convergence than that for the stationary process.

Specific extrapolation (20) of the behavior of discrepancies at the nth iteration to the future behavior of discrepancies obtained at the (n + 1)th iteration is a rather contradictory procedure. The greater the specification obtained at a certain iteration

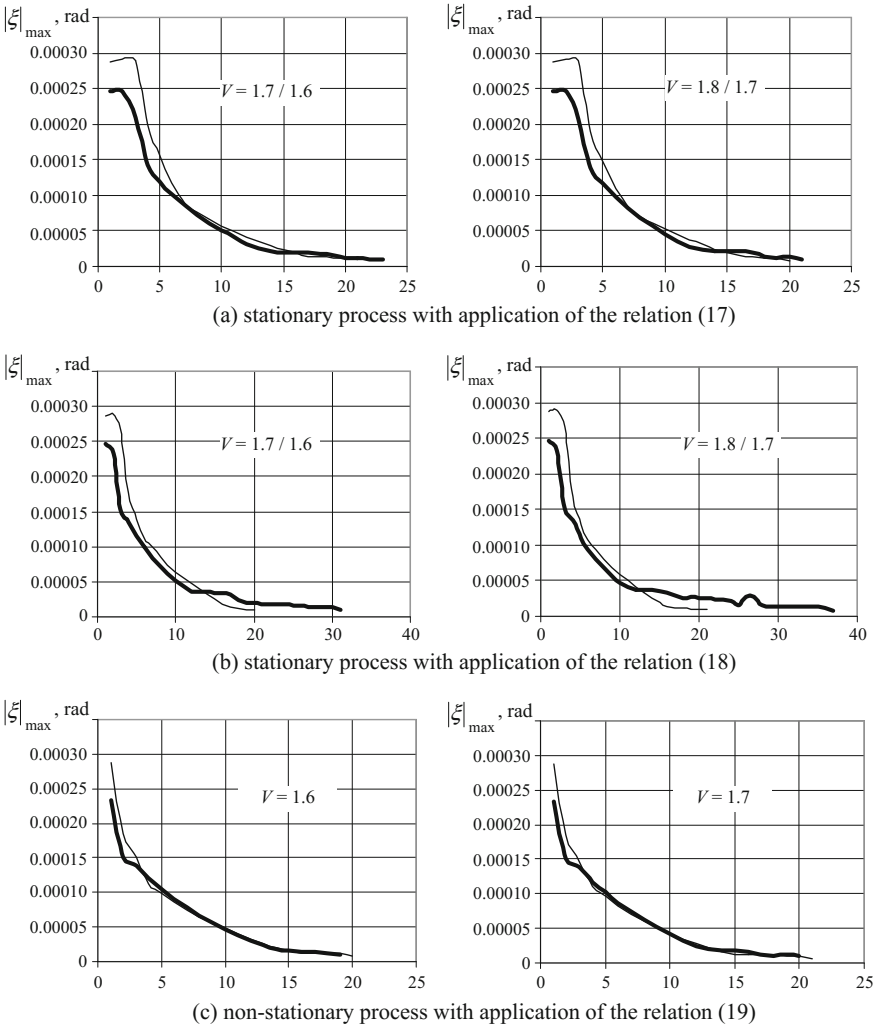

Fig. 5 Convergence of the algorithm of the parameter τ at regulation by (22)

(configuration of discrepancies will be changed more significantly, correspondingly), the less the expectation that the tendency obtained at this iteration will be further kept. No worse and sometimes better results can be obtained when performing the next but one iteration with small values of factors τ for more precise assessment of the velocity of convergence. Performance of these, at first sight, idle iterations allows for forecasting the behavior of discrepancies and, correspondingly, for succeeding in the velocity of convergence.

3 Assessment of the Influence Function of Teeth and Threads

As was stated above, the considered solution of the problem of searching for load distribution in the gearing is based on discretization of the elastic system, its equilibrium state being described by Eq. (1). An important component of the part of this system of equation which determines its solution and participates in implementation of the iteration algorithm is the influence function $\nu_{km\,k'm'}$. This function reflects the reaction of the position of cells that form a continuous flank of the tooth (thread) on the external action by the value of 1 N in one of them. Traditionally, two components of the influence function are singled out: contact and bending-and-shearing (here and further, the subscript 1 indicates the relation of the parameter to the worm thread, and the subscript 2 is for the gearwheel tooth):

$$v_{1,2} = v^{\kappa}_{1,2}(\tilde{x}, \tilde{y}) + v^{u}_{1,2}(\tilde{x}, \tilde{y}). \tag{23}$$

Plotting of the influence functions has been performed within the coordinate systems shown in Fig. 6; for each of them, the counting of the tooth height is done along one of the coordinate axes, and the counting of the tooth length is done along the other one. The initial surface and its unfolding have a common point C which is the center of unfolding: for the gearwheel tooth, this point is at the intersection of the mean cylinder and the pitch surface of the gear rim; for the worm thread, it is at the pitch cylinder.

3.1 Contact Component of the Influence Function

The classic solution of the problem of assessing the contact displacements at the point $i(x, y)$ due to the arbitrarily $k(x', y')$ applied unit normal force is the Boussinesq relation for the semi-space:

$$v(x, y) = \frac{\alpha}{r}, r = \sqrt{(x - x')^2 + (y - y')^2}, \quad \alpha = \frac{1 - \mu^2}{\pi E}. \tag{24}$$

The main and obvious difficulty of applying this function within the following software implementation for the considered approach is the tendency of its value to infinity when considering the deformations in the vicinity infinitely close to the loading point.

The second feature of its application to the analysis of the loaded contact is that teeth have finite dimensions comparable with the dimensions of contact areas. That is why the influence function should additionally consider the closeness of the apex and face edges where the compliance is higher, and also recesses at their roots, where the compliance is conversely lower [10]. We have taken the solutions

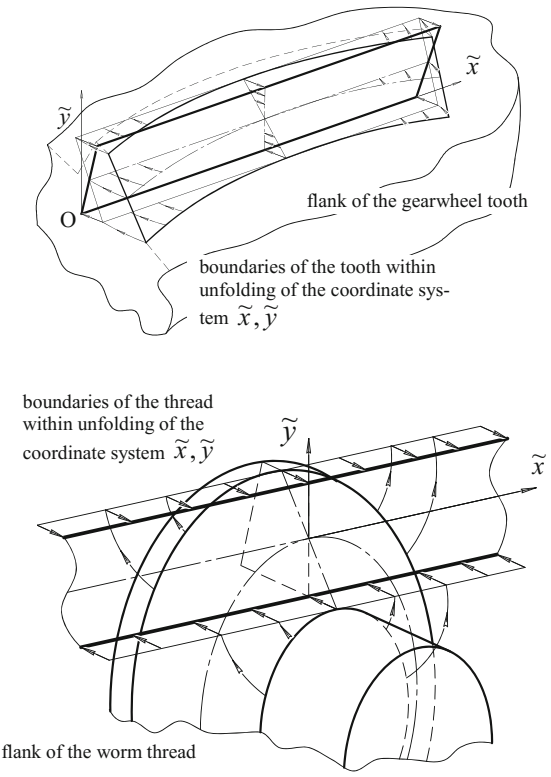

Fig. 6 Coordinate systems for plotting the influence function

obtained in [2, 10] as the basis and augmented them with regard to peculiarities of the geometry of the spiroid gear:

$$v_1^{\kappa}(\tilde{x},\tilde{y}) = \left(\left(1-\mu_1^2\right)/(2rE_1)\right)\cdot(B_1+B_2+B_8), \tag{25}$$

$$v_2^{\kappa}(\tilde{x},\tilde{y}) = \left(\left(1-\mu_2^2\right)/(2rE_2)\right)\cdot\sum_{j=1}^{8}B'_j, \tag{26}$$

$$\begin{cases} for\ r_j^2 \geq r^2 \quad B'_j = 1-\frac{2}{\pi}\arctan\left(\sqrt{r_j^2/r^2-1}\right), \\ for\ r_j^2 < r^2\ B'_j = 1, \end{cases} \quad j=\overline{1,7}$$
$$\begin{cases} for\ r_8^2 \geq r^2 \quad B'_8 = -1+\frac{2}{\pi}\arctan\left(\sqrt{r_8^2/r^2-1}\right), \\ for\ r_8^2 < r^2\ B'_8 = -1, \end{cases} \tag{27}$$

$$\tilde{x}_{\min} = \tilde{y}_p\tan(\Psi), \tag{28}$$

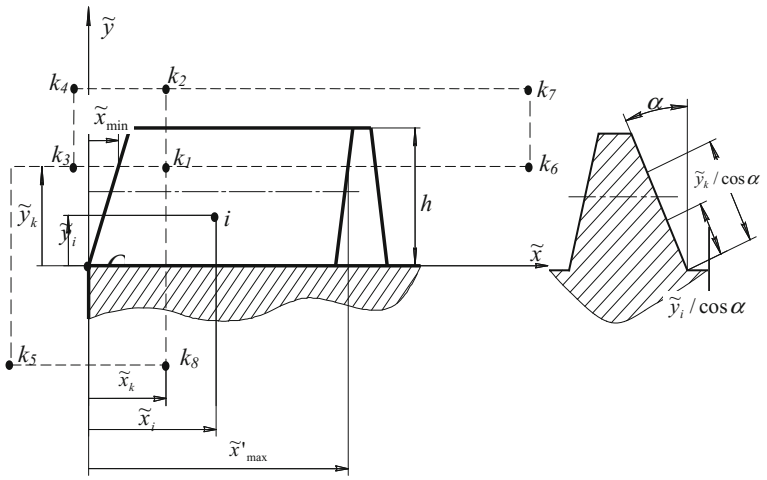

Fig. 7 Definition of contact displacement at the point i for load application at the point k on the gearwheel tooth flank

where r_j is the distance from the point i of the displacement measurement to the point k of load application ($j = 1$) and its jth mirror-like image given in Figs. 7 and 8, accounting for the oblique boundary of the tooth ($\tilde{x}_{\min}$).

Relations (26)–(28) given above allow for assessing the contact displacements with account for the closeness of the tooth and thread apexes, their roots, and two faces of the tooth, one of them having massive basis outside the tooth (Fig. 9). Note here that, similar to the traditional procedure [2, 10, 13], we assume that the convexity (concavity) of the tooth flank does not influence the character of the contact deformations (at least within those tooth areas where these deformations are significant), and that the difference of angles between the tooth flanks on one hand and the faces, apexes and root on the other hand, from the value of 90°, does not significantly influence the values and character of the contact deformations.

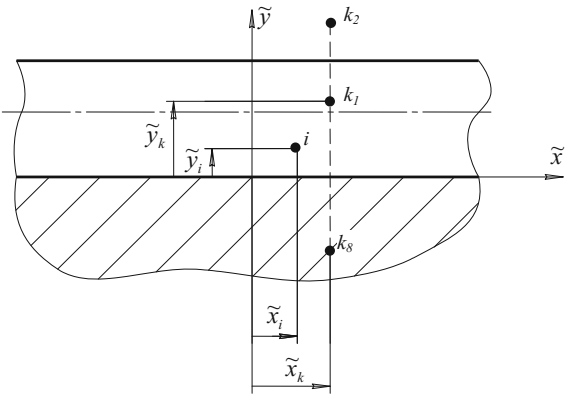

Fig. 8 Definition of contact displacement at the point i for load application at the point k on the flank of the spiroid worm thread

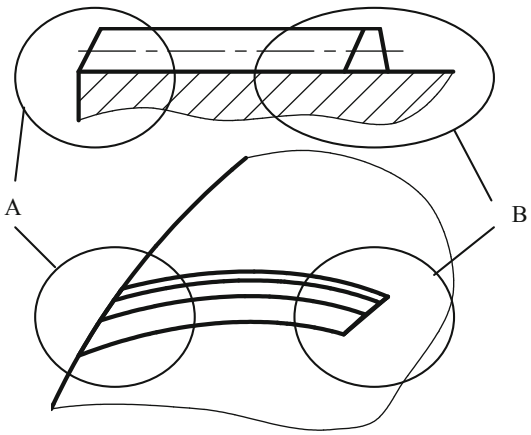

Fig. 9 Areas *A* and *B* of different rigidity of the tooth root

Accounting for the influence of both faces is necessary when the tooth length is less than 9 modules (the value is obtained on the basis of numerical research of tooth compliance); this is the length at which the tooth curvature can be neglected. In other cases, the factors B_1, B_2 and B_6 or B_7 and B_8 should be excluded, depending on which of the faces ends up being closer to the considered point.

3.2 *Influence Function of the Bending and Shearing Compliance*

Prof. E. Airapetov proposed, in [1], the model of the bending displacement of teeth as being

$$w(x, y) = K(x) \cdot K(y), \tag{29}$$

where $K(y)$ is the function characterizing the variation of displacement (in this context) along the height; and $K(x)$ is the function characterizing the variation of displacement along the length (it is constructed on basis of the Fourier composition). After numerous experimental investigations in the field of gear couplings, planetary and double-enveloping worm gears, this method has been developed up to the discretely continuous model of the tooth with the elastic root. We have augmented this model with account for the tooth geometry features for a spiroid gear, and the model ended up taking the following form:

$$v_1^u = \left(h^3 \cos^2 \alpha / \pi D_1\right) k_{1x} k_y k_d, \tag{30}$$

$$v_2^u = \left(h^3 \cos^2 \alpha / \pi D_2\right) k_{2x} k_y k_l k_R, \tag{31}$$

$$\begin{cases} k_y = k_{y2}\left[1 + k_{y1}\tilde{Y}^2\left(\tilde{Y}_k - \tilde{Y}_i/3\right)\right] & for\ 0 \le \tilde{Y} \le \tilde{Y}_k, \\ k_y = k_{y2}\left[1 + k_{y1}\tilde{Y}_k^2\left(\tilde{Y}_i - \tilde{Y}_k/3\right)\right] & for\ \tilde{Y}_k \le \tilde{Y} \le 1 \end{cases}, \tag{32}$$

$$k_{1x} = e^{-\beta\Delta\tilde{X}}\left(\cos\beta\Delta\tilde{X} + \sin\beta\Delta\tilde{X}\right), \tag{33}$$

$$\begin{aligned} k_{2x} = {} & e^{-\beta\Delta\tilde{X}}\left(\cos\beta\Delta\tilde{X} + \sin\beta\Delta\tilde{X}\right) + k_{x1}e^{-\beta k_{x2}\left(\Delta\tilde{X} + \tilde{X}_k\right)}\cos\beta k_{x2}\Delta\tilde{X} \\ & + k_{x3}e^{-\beta k_{x4}\left(\Delta\tilde{X} + 2\tilde{X}_k\right)} \times \left[\cos\beta k_{x4}\left(\Delta\tilde{X} + 2\tilde{X}_k\right) - \sin\beta k_{x4}\left(\Delta\tilde{X} + 2\tilde{X}_k\right)\right], \end{aligned} \tag{34}$$

$$k_l = 1 + k_{l1}(h/l)^{k_{l2}}, \tag{35}$$

$$k_R = 1 - k_{R1}\left(S_{ef2}/R\right)^{k_{R2}}, \tag{36}$$

$$k_d = 1 + k_{d1}\left(h\cos\gamma_1/d_{f1}\right)^{k_{d2}} \tag{37}$$

$$\begin{matrix} \tilde{Y}_i = \tilde{y}_i/h, \Delta\tilde{X} = \left|\tilde{X}_i - \tilde{X}_k\right| = \left|\tilde{x}_i - \tilde{x}_k\right|/h, \\ \tilde{Y}_k = \tilde{y}_k/h, \tilde{X}_k = \tilde{x}_k/h, \end{matrix}. \tag{38}$$

Relative dimensionless coordinates $\tilde{X}$ and $\tilde{Y}$ of the center of the cell i at which the displacement is calculated and cells k of force application are counted from the nearest face for a tooth and from the center of unfolding for a thread. The particular case of the factor k_d is its equality to 1 at an infinitely large diameter of the worm solid and the helix angle of the thread equal to 90°; this corresponds to the problem of an infinitely long plate with an elastic root loaded by a concentrated force.

Numerical simulation has been carried out to specify the type of relation and numerical value of factors which are components of (30)–(38). Simulation was done using the finite element method, and it implied the consequent stamp loading of flanks at their different points, singling the results of contact components out of the obtained results, the components being calculated in accordance with relations (25)–(28), and the consequent approximation of the remaining bending and shearing displacements. An example of these calculation results at loading in the center of the tooth is given in Fig. 10. It was established after the simulation that:

(1) as expected (see Fig. 9), the compliance of the "tooth heel" (the area adjacent to the external diameter of the gearwheel) is higher than the compliance at the center of the unfolding by a factor of 8 when loading along the left flank; and by a factor of 1.7 when loading along the right flank. These values for the "tooth toe" (the area adjacent to the internal diameter of the gearwheel) are 1.4 and 2.7, respectively (Fig. 11);
(2) elastic displacements at thread flanks decrease down to small values at a distance 1/8–1/4 of the thread pitch (smaller values are for cases with big diameters of the worm solid);

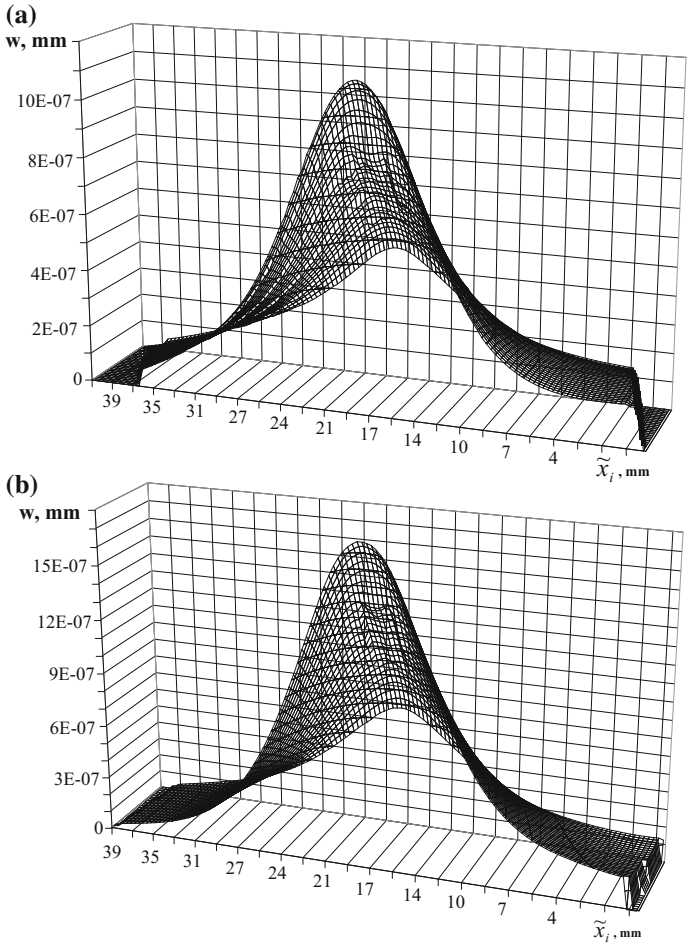

Fig. 10 Bending- and-shearing displacements of a tooth when loading the left (**a**) and right (**b**) flanks at the center C of the tooth

(3) factors which are components of (28)–(36) have the following values (they turned out to be different for the opposite name flanks due to the asymmetry of teeth in a spiroid gear) for the gearwheel tooth:

$$k_{R1} = 10; k_{R2} = 2; S_{ef2} = 0.97 \cdot S_{f2}\left(S_{a2}/S_{f2}\right)^{0.2};$$

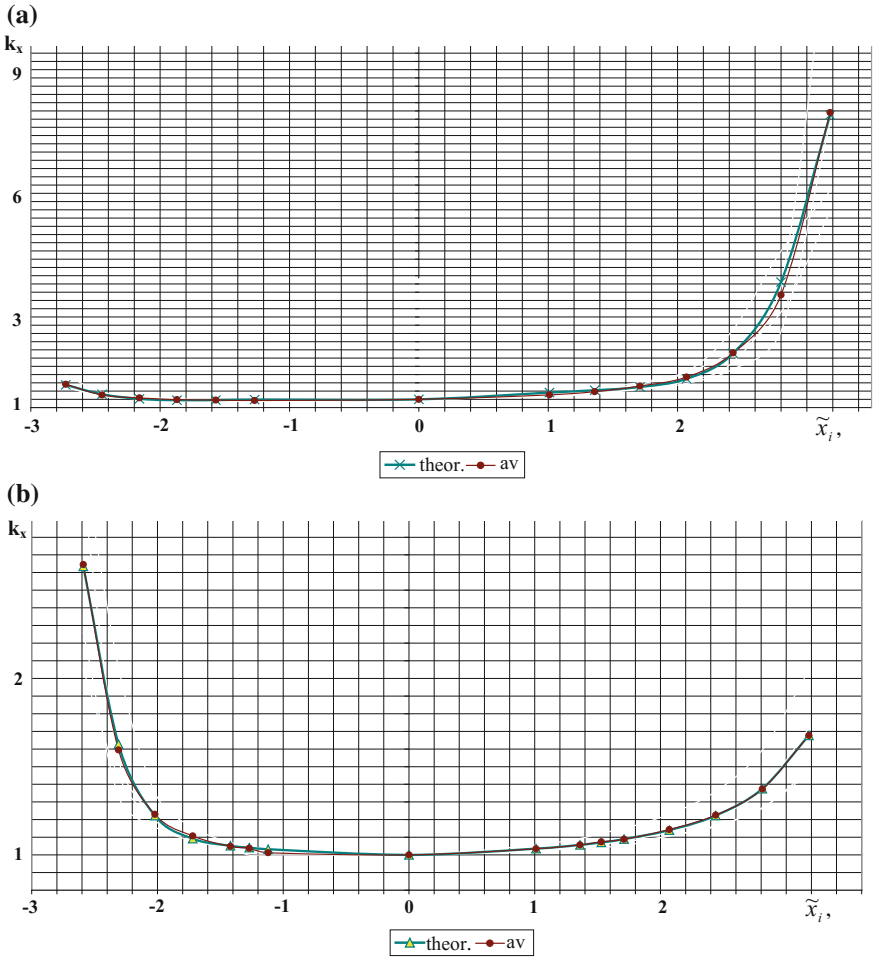

Fig. 11 Variation of the bending compliance along the tooth (loading of the left (**a**) and right (**b**) flanks)

– for the left loaded flank:

$$\beta = 1.18; k_{l1} = 18; k_{l2} = 3.2;$$

$$k_{y1} = 0.063 + 0.0733 \cdot \tilde{Y}_k; k_{y2} = 7.036 + 4 \cdot \tilde{Y}_k;$$

at the toe end:

$$k_{x1} = 4.86;\ k_{x2} = 2.08;\ k_{x3} = 1.4;\ k_{x4} = 1.2;$$

at the cap end:

$$k_{x1} = 0.11;\ k_{x2} = 0.25;\ k_{x3} = 1.5;\ k_{x4} = 1;$$

– for the right loaded flank:

$$\beta = 1.28; k_{l1} = 21; k_{l2} = 3.7;$$

$$k_{y1} = 0.061 + 0.0795 \cdot \tilde{Y}_k; k_{y2} = 7.742 + 1.87 \cdot \tilde{Y}_k;$$

– at the toe end:

$$k_{x1} = 1.25;\ k_{x2} = 0.9;\ k_{x3} = 2.1;\ k_{x4} = 1.9;$$

– at the cap end:

$$k_{x1} = 0.6;\ k_{x2} = 0.08;\ k_{x3} = 2.0;\ k_{x4} = 1.0.;$$

for the worm thread:

– for the left loaded flank:

$$\beta = 1.27; k_{y1} = 0.0632 + 0.1548 \cdot \tilde{Y}_k; k_{y1} = 10.124 - 1.9345 \cdot \tilde{Y}_k;$$

$$k_d = 1 + 3.7\left(h\ \cos(\gamma_1)/d_{f1}\right)^2;$$

– for the right loaded flank:

$$\beta = 1.2; k_{y1} = 0.1206 + 0.1464 \cdot \tilde{Y}_k; k_{y1} = 9.408 + 2.2024 \cdot \tilde{Y}_k;$$

$$k_d = 1 + 2.9\left(h\ \cos(\gamma_1)/d_{f1}\right)^2.$$

Note that application of the finite element analysis is preliminary, a sort of adjusting procedure; its results are valid for a variety of investigated gears, and the main algorithm for assessing the loading state of a multi-pair gear is carried out based on approximating relations.

4 Consideration of Plastic Deformations

First of all, we consider such a level of gear loading and such distribution of contact stresses (established after the first loading cycles) for which contact contortion is not continued (is not progressed). Evidently, a situation of the hyper-loading of a gear is possible when the loading torque and contact stresses are so high that contact contortion at the tooth flanks continues developing after each loading cycle (other fractures are also possible). Though this important case should be detected in calculations, our considered quantitative analysis of the loaded contact does not cover this case.

Putting it all aside, one can single out two statements of the problem of the loaded gear analysis:

- the geometry of the contact flanks is known, and such a load distribution is determined that provides conditions of equilibrium and displacement compatibility; this is practically the analysis of an elastically loaded gear in a pure form;
- load distribution is known; the geometry of the flanks is to be determined, providing conditions of equilibrium and displacement compatibility; it can be, for instance, synthesis of the tooth flanks in accordance with the assigned law of force distribution.

The considered problem of analysis of an elastic and plastic loaded gear is a sort of combination of these two problems: there are areas of elastic contact and areas of elastic-and-plastic contact in such a gear, for which the geometry of the flanks (plastic deformations) should be selected in accordance with the assigned limiting contact stress.

Four types of cell on the loaded teeth are singled out in a discretized model of a loaded gear:

- cells of the first type, in which stresses are so high that contact contortion covers these cells completely; one can consider that the initial micro-roughnesses become completely contorted in this case;
- cells of the second type, in which plastic deformation is specific only for apexes of micro-roughnesses;
- cells of the third type, for which the elastic deformation takes place;
- cells of the fourth type, which do not take part in load transfer.

When loaded elements are rotating, the maximum part of the plastic deformation is displaced along the contact flanks, together with the contact areas, changing them irreversibly (changing the coordinates of points, “drowning” the points into the “tooth solid”). At the consequent loading cycles, the contact surfaces (that are the final object of analysis) will have this very state: changed not only close to the specific considered contact area, but also along the significant part of the tooth flank. That is why the first assessment of contortion cannot be precise: cells that are not contorted, or even loaded at this phase of meshing, will probably be among those contorted at the next phase when the contact area is displaced, with the

contorting load definitely appearing there. This consideration will certainly influence the stress distribution and, consequently, the conditions for the presence of contorted cells and the value of contortion in the analysis. Therefore, in order to specify the set of contorted cells and the values of the simulated contortion for them, another cycle of iterations (external with regard to the algorithm of the load distribution analysis) should be introduced; and it should be carried out after the analysis of load distribution along the whole flank of teeth and threads. Meeting these requirements means repetition of a relatively time-consuming analysis for a rather large (infinitely large at the extreme) number of meshing phases. An alternative can be consideration of a relatively small number of phases with the generation of contortion areas on tooth flanks (sets of points with coordinates being changed at simulation of contortion). After that, approximation of the maximum values of simulated contortions in cells can be carried out. Such an approach is demonstrated in Fig. 12.

Nevertheless, in our opinion, the additional external cycle of iterations is too time-consuming. Calculation of the plastic deformation of contact flanks can be added directly to the algorithm described above for load distribution analysis; in this case, the algorithm is supplemented with the following features (Fig. 13):

- after initial assessment (or beginning with a certain iteration, that is, after obtaining a rather precise distribution of forces) of the contact area, the value of elements approaching and the values of discretely applied forces, the type of each loaded cell is determined; for cells of the first type, the value of contortion is determined (see below);
- the following values are corrected in accordance with the values of discrepancies obtained at each consequent iteration:

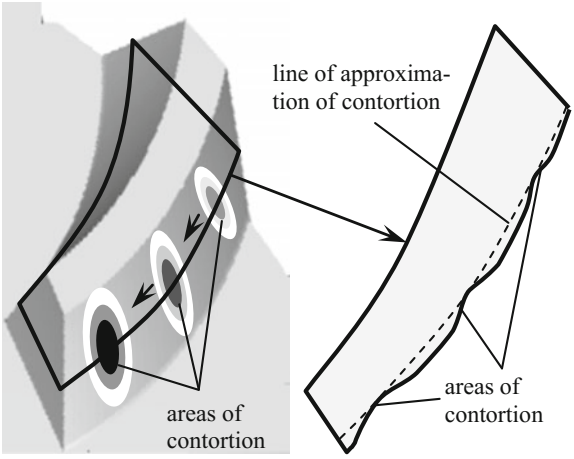

Fig. 12 Approximation of plastic deformation on the tooth flank

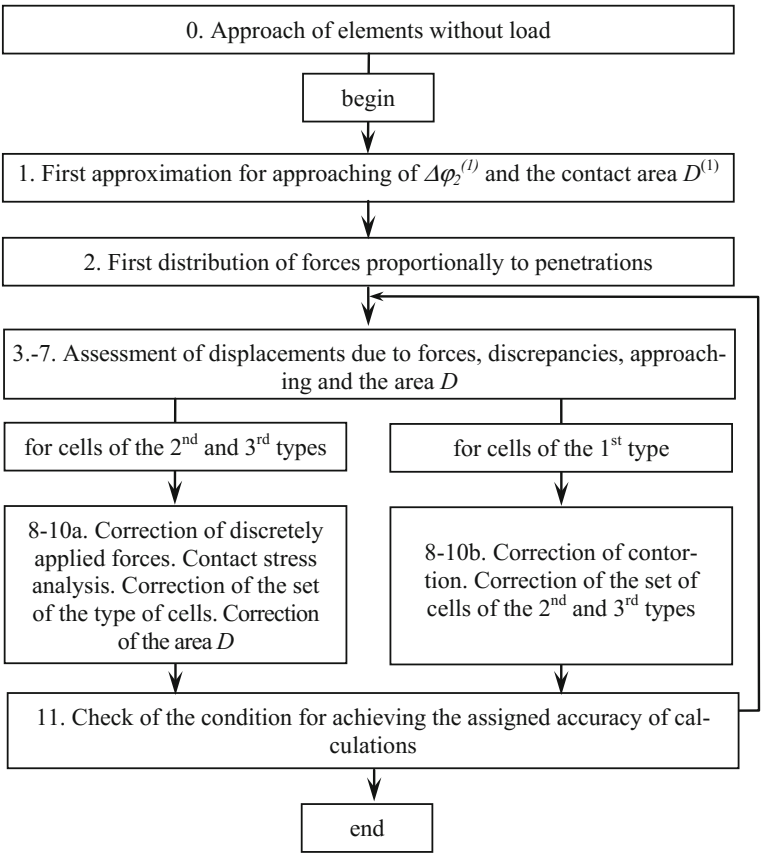

Fig. 13 Scheme of consideration of plastic deformations

for cells of the first type, the value of contortion;
for cells of the second and third types, the values of forces;

– relation of the cell to one or another type can vary:

to contorted ones (type one), on exceeding the allowable limit of the design stress;
to elastically deformed ones (types two and three), on achieving the negative value of contortion.

5 Simulation of Plastic Deformation of the Contact Surface Area (Cells of the 1st Type)

Here, we deal with cells of the 1st type; during calculations, the level of contact stress in them exceeded the assigned limit. The latter is often determined for contact in gears in accordance with the following relation:

$$[\sigma_h] = 2.8\sigma_T, \tag{39}$$

where σ_T is the yield point of the material.

It is reasonable to calculate the values of plastic displacement ${w_{p\,km}}^{n+1}$ and the force ${F_{km}}^{n+1}$ applied at the overloaded kmth cell at step 11, depending on the values obtained for this cell at the current nth iteration: elastic displacement ${w_{h\,km}}^{n}$, acting ${\sigma_{h\,km}}^{n}$ and allowable $[\sigma_h]$ contact stresses:

$$w_{p\,km}^{n+1} = w_{km}^{n}\left(1 - \frac{[\sigma_h]}{\sigma_{h\,km}^{n}}\right), \tag{40}$$

$$F_{p\,km}^{n+1} = F_{km}^{n}\frac{[\sigma_h]}{\sigma_{h\,km}^{n}}. \tag{41}$$

6 Simulation of Deformation of Micro-roughnesses

We accept for the cells of the 1st type that plastic deformation of micro-roughnesses is equal to the height of the profile relative to the mean line (R_P).

In order to calculate deformations of the micro-roughnesses of cells of the 2nd and 3rd types, a numerical model proposed by Izmailov [6] has been taken as the basis; we adapted it to our algorithm with the following features and allowances:

(1) The tooth flank is represented as a certain number of micro-roughnesses in the form of segments of a sphere (see Fig. 14). The actual micro-relief of the surface, which is the alternation of ridges (marks of cuts at tooth machining), is surely different from such a model; however, as is shown in [7], the accepted allowance provides a rather satisfactory level of errors. Dimensions of segments (heights and radii) are random values, which are distributed in accordance with the two-parametrical beta-distribution. Parameters of beta-distribution are chosen based on relations [3, 9] that take into account the results of measurement of real rough surfaces. The dimensions of single recesses in each specific cell are the same, and their number depends on:

- the dimension of the cell itself;
- the radius and height of micro-roughnesses that are average for the tooth.

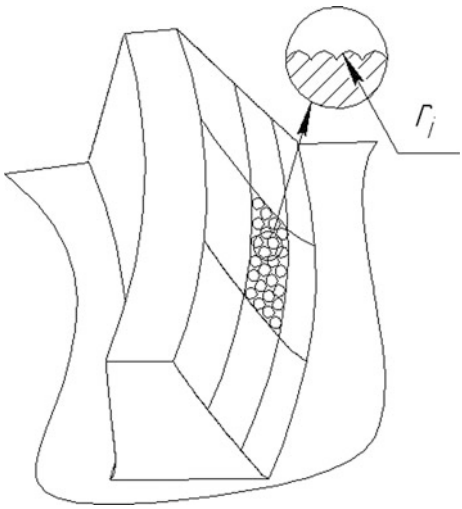

Fig. 14 Single recesses in the cell of the gearwheel tooth flank

The dimension of the cell is chosen so that it could fit at least one single recess.

(2) The force acting on the single recess is equal to

$$F_i = \frac{F_{km}}{n}, \tag{42}$$

where n is the number of single recesses in the given cell.

(3) Relation of cells to the 2nd or 3rd type is carried out based on the dimensionless coefficient α calculated by the formula

$$\alpha = \left(1 + \sqrt{\frac{F_{cr,i}}{F_i}}\right)^{-1}, \tag{43}$$

where $F_{cr,i}$ is the critical force calculated by the formula

$$F_{cr,i} = 14\frac{H^3 r_i^2}{E^{*2}}, \tag{46}$$

where r_i is the radius of rounding of the single recess, E^* is the equivalent Young module, and H is the micro-hardness of the surface. For $\alpha < 0.5$, the contact is considered to be elastic, and the cell is related to the third type; for $\alpha = 0.5$–1, the contact is elastic and plastic, and the cell is related to the second type.

(4) Deformation in cells of the 2nd type is calculated by the formula

$$\delta_{n,i} = \delta_{cr,i}\left(0.5\frac{F_i}{F_{cr,i}} + 0.5\sqrt{\frac{F_i}{F_{cr,i}}}\right), \tag{47}$$

$$\delta_{cr,i} = 5\frac{H^2 r_i}{E^{*2}}. \tag{48}$$

Deformation in cells of the 3rd type is calculated by the formula

$$\delta_{y,i} = \left(\frac{9}{16}\frac{F_i^2}{r_i E^{*2}}\right)^{\frac{1}{3}}. \tag{49}$$

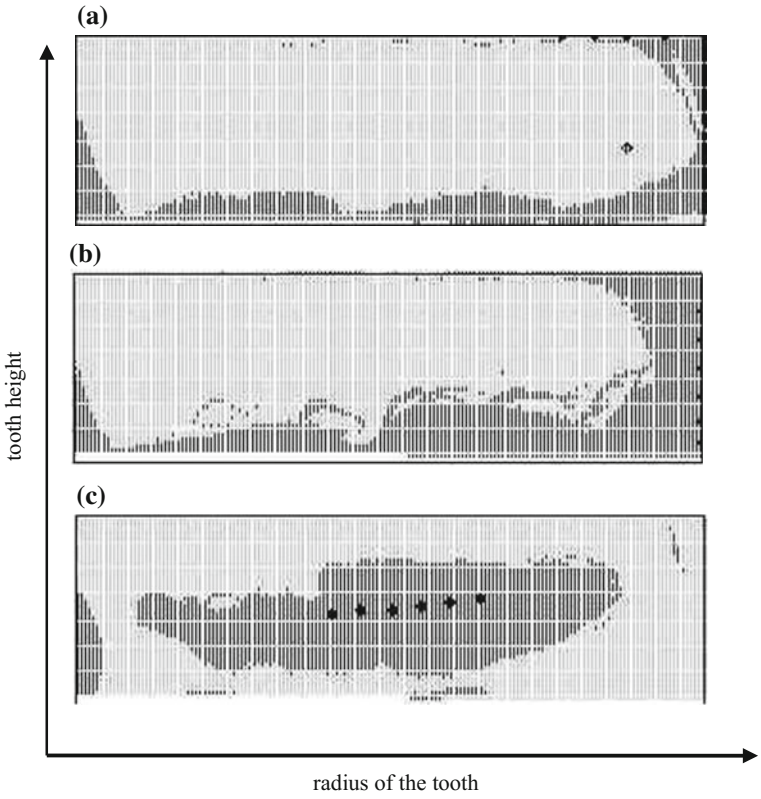

Fig. 15 Projection of the summarized contact pattern onto the axial plane of the gearwheel

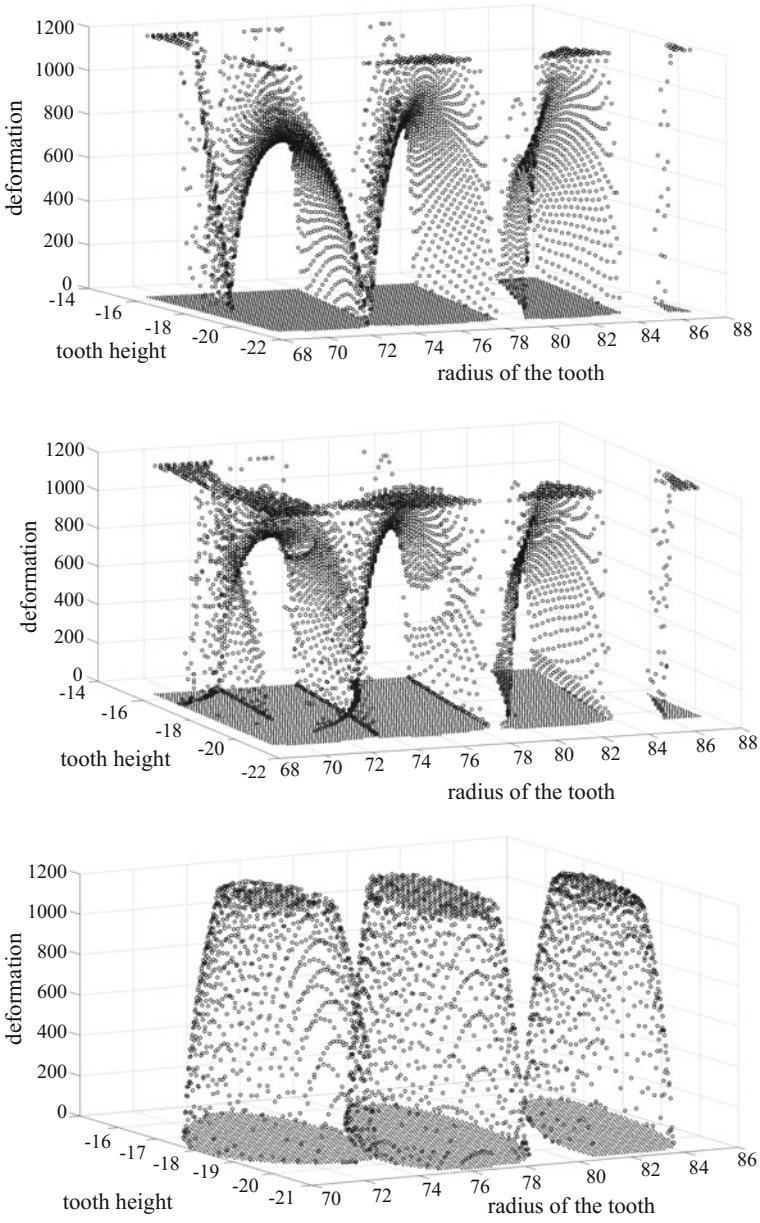

Fig. 16 Distribution of contact stresses along contact areas

7 Examples of Calculations

The example that illustrates the workability of the algorithm is shown in Figs. 15 and 16; several results of calculating the loading of a gear with parameters are given in Table 1 for the loading torque of 4000 Nm and an allowable level of contact stresses at the gearwheel of 1200 MPa. In particular, these Figs. show the summarized contact patterns on the left (concave) tooth flanks in projections on the axial plane of the gearwheel with shadowing of areas subjected to plastic deformation, and the corresponding three-dimensional diagrams of distribution of contact stresses along the contact areas obtained at one meshing phase and conditionally projected onto the flank of one tooth, for the cases:

- of the conjugated contact in the absence of errors (Figs. 15a, and 16a);
- of the conjugated contact accounting for the increased compliance of the gearwheel and worm units (this corresponds approximately to the error of the interaxial angle in a gear 0.1/30) (Figs. 15b, and 16b);
- of the contact which is localized along the tooth height and length (Figs. 15c, and 16c).

In all the cases, the summarized contact pattern is propagated along the entire active tooth flank. The maximum of plastic deformation in a conjugated gear is at the edges of the teeth, a tendency that is strengthened when introducing the errors. Consideration of plastic deformations provides an increase in the area of each individual contact area by 10–12% on average.

8 Conclusions

The algorithms of analysis of load distribution in multi-pair spiroid gearing described in the paper can be applied for both the elastic and elastic-and-plastic statements of the problem. The algorithms are adjusted for high productivity and validity of calculations in accordance with the results of numerical and real experiments. Calculation results are applicable for assessment of the tooth strength of heavy-loaded gears.

References

1. Airapetov, E., Genkin, M., Melnikova, T.: Statics of Double-Enveloping Worm Gears. M., Nauka (1981) (in Russian)
2. Bondarenko, A.: Static loading of double-enveloping worm gearing with account of features of generation, manufacture and assembly errors, compliance of gear elements. PhD Thesis, Kurgan (1987) (in Russian)

3. Demkin, N.: Multi-level models of friction contact. Trenie i iznos, **21**(2), 115–120 (2000) (in Russian)
4. Hohn, B., Steingrover, K., Lutz, M.: Determination and optimization of the contact pattern of worm gears. Proceedings of the International Conference on Gears VDI **1**, 341–352 (2002)
5. Houser, D.: The effect of manufacturing microgeometry variations on the load distribution factor and on gear contact and root stresses. Gear Technol. **6**, 51 (2009)
6. Izmailov, V., Chaplygin, S.: Numerical and analytical simulation of discrete contact of machine parts. Naukovedeniye **6** (2014) http://naukovedenie.ru/PDF/10TVN614.pdf (in Russian)
7. Izmailov, V., Kurova, M.: Application of beta-distribution for analysis of contact of rough solids. Treniye i iznos **IV**(6), 983–990 (1983) (in Russian)
8. Moriwaki, I., Watanabe, K., Nishiwaki, I., Yatani, K., Yoshihara, M., Ueda, A.: Finite element analysis of gear tooth stress with tooth flank film elements. In: Proceedings of the International Conference on Gears VDI, pp. 39–63 (2005)
9. Ogar, P., Tarasov, V., Maksimova, O.: Contacting of a rough surface through the layer of viscous elastic coating. In: Proceedings of the V International Conference "Problems of mechanics of advanced machines", Ulan-Ude (2012) (in Russian)
10. Sheveleva, G.: Analysis of elastic contact displacements on surfaces of parts with limited dimensions. Mashinotroeniye **4**, 92098 (1984) (in Russian)
11. Sheveleva, G.: Numerical method for solution of the contact problem at compression of elastic solids. Mashinovedenye **5**, 90–94 (1981) (in Russian)
12. Sheveleva, G.: Solution of the contact problem by method of consequent loading. Izvestiya vuzov, Mashinostroeniye **9**, pp. 10–15 (9186) (in Russian)
13. Zablonsky, K.: Gears. Load distribution in meshing. K., Tekhnika (1977) (in Russian)

Quality Characteristics of Gearing

D. Babichev and M. Storchak

Abstract Gears are the basis of most of the mechanics that drive machinery, ultimately determining their efficiency and durability. Selection of the parameters of gears is carried out by their quality characteristics. Analysis and synthesis of gears and machine engagements uses three types of quality characteristics: characteristic of gears, characteristic of machine engagements and universal characteristics. Each of these types is divided into local and global quality characteristics. The article suggests a classification of local and global quality characteristics, focused on a common approach to their calculation and display through computer analysis and synthesis of various gears. The developed system of primary characteristics is described, which is a set of simple local quality characteristics. These primary characteristics are invariant to the mechanism scheme and coordinate system used by analysis and synthesis of gears. Using these primary characteristics can calculate any of the considered local and global quality characteristics of the gears or the machine engagements. Analysis of the quality characteristics of synthesized full-strength gears is carried out. To conduct this analysis, a synthesis algorithm is developed. Using this calculation algorithm, the gears with constant tension along the engagement line are synthesized. The sensitivity of the synthesized gears to changes in the axle distance is analyzed. This analysis is carried out for gears with different gear ratios. The complex research is the basis for the development of interactive optimization synthesis of gears with the specified strength properties.

Keywords Computer-aided engineering · Gear · Quality characteristics · Meshing zone · Synthesis

D. Babichev
Institute of Transport, Industrial University of Tyumen, ul. Volodarskogo 38,
Tyumen 625000, Russia
e-mail: babichevdt@rambler.ru

M. Storchak (✉)
Institute for Machine Tools, University of Stuttgart, Holzgartenstrasse 17,
70174 Stuttgart, Germany
e-mail: Michael.storchak@ifw.uni-stuttgart.de

V. Goldfarb et al. (eds.), *Advanced Gear Engineering*,
Mechanisms and Machine Science 51, DOI 10.1007/978-3-319-60399-5_4

1 Introduction

Gears are components in a multitude of machines and facilities, mainly in the aircraft, automotive and tractor industries. The reliability of these machines can be considerably increased if gear drives are used that are optimised with regard to a high load-carrying capacity. The load-carrying capacity of gears is assessed on the basis of two criteria: contact and bending stresses. Hence, it is an important and current challenge to determine tooth profiles with high contact strength and endurance limits.

The determination of tooth profile is executed on the basic of gear analysis and synthesis [1]. Quality characteristics are always considered and calculated through the analysis and synthesis of machine engagements. These characteristics can be divided into three types:

- Quality characteristics of gears. These characteristics are used only in working engagements;
- Quality characteristics of machine engagements. These characteristics are used only in machine engagements;
- Quality characteristics of engagements. These characteristics are used in both working engagements and machine engagements.

Quality characteristics are divided into local characteristics and global characteristics [2]. The local characteristics describe behaviors of surface or conditions of the interaction of two links at a single point of an engagement member, for example, the equivalent radius of curvature at a point of teeth contact. The global characteristics describe properties of a gear, for example, contact ratio.

In the article, a classification of local and global quality characteristics of all types is suggested. This classification point represents the united approach to calculation and presentation by computing analysis and synthesis of different gears. An example of full-strength gear synthesis and the analysis of quality characteristics in accordance with the suggested systematization are carried out.

2 Systematization of Quality Characteristics

The computing and classification of quality characteristics has been the subject of many studies. In [2], it is shown that from all characteristics describing the conditions of contact surfaces at the point, the number of independent parameters is 13. Five of them are geometrical characteristics, three of them are kinematical, four of them are geometrical-kinematical, and one is kinetical. These characteristics are basic. All other characteristics can be calculated through these 13 characteristics.

We suggest systemizing quality characteristics according to three criteria: structure, semantic content and form of presentation. Three kinds of systematization are presented below. Structural systematization of indexes, describing their syntax,

is presented in Fig. 1. The structure of indexes refers to: their type (number, vector, function of one or several variables), degree of their dependence on each other, etc. [3].

Systematization of quality characteristics by the presentation form describing their pragmatics is presented in graphic form in Fig. 2. This is the form in which the information is presented on both computer monitors and on paper. Thus, the graphical forms on paper and on machine carriers are always static. On the monitor, the picture can be both static and dynamic (including as controlled by the user). In the cases when one of the arguments addresses time or transfer, or a curve-lined coordinate, it is possible to show it in a graphic form: current point, special points (for instance, extreme meanings); vector or line (including indication of numerical index value in this position). About the usage of graphic forms: Forms 1, 3, 5. 14, 15, 16 should be used, generally, for unambiguous functions. Form 2 should only be used for unambiguous functions. Forms 11 and 12 are presupposed for visual evaluation of the tooth form obtained: a peaked tooth and a clear cutter interference can be seen there, and the thickness of the tooth in its different reference planes can be analyzed. Forms 13 and 10 must be dynamic on the monitor; forms 11, 16 and 17, contrastingly, should be static, for expedience. All the others are usually static, but, ideally, they will be dynamic, capable of being controlled by the user with an indication of the current numerical values (when transferring such forms to paper, we get a document of higher quality).

Form 8 (the blocking profile) is the most informative of all the forms, but is also the most complex from the mathematical and computer realization points of view. Form 9 (the monogram) is the most diversified by structure, and that is why each monogram of a definite structure requires individual computer realization. Form 17 is frequently used to represent the results of complex calculations. All qualitative indexes, being numerical data, are presented in computers as separate numbers or

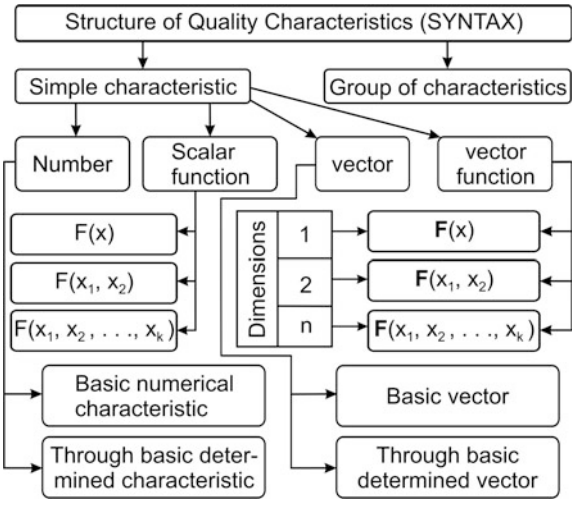

Fig. 1 Structural indexes systematization

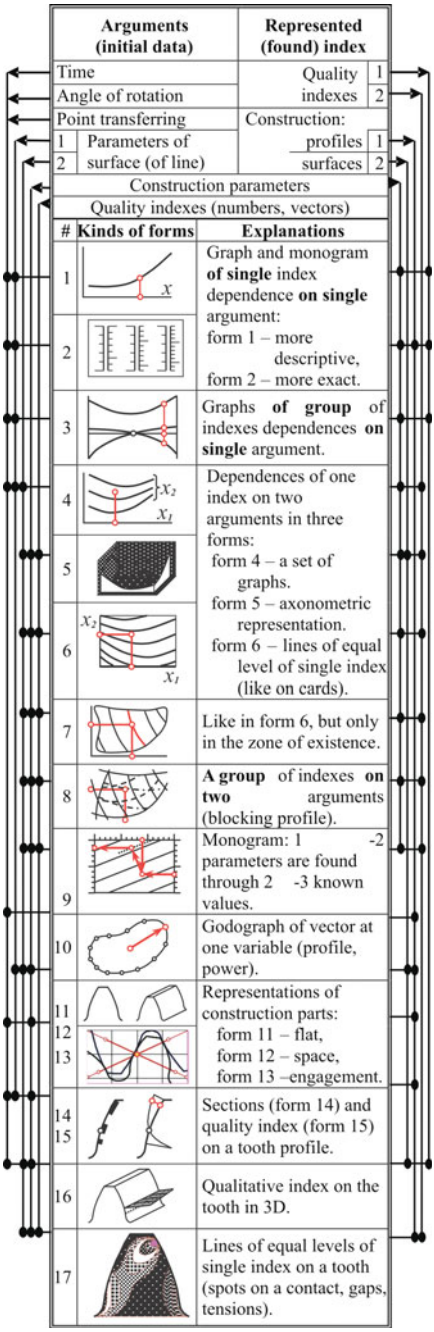

Fig. 2 Systematization of graphic forms

groups of numbers of definite structure. Figure 1 depicts the types of structure of qualitative indexes. In it, the structures of a group of numbers are given, in dependence on: type of qualitative index (vector, structure, etc.), and dimensions of index (1, 2, 3, … n). Thus, Fig. 1 presents the types of data with which a computer system of analysis and synthesis of engagements should operate, in regard to the calculation and representation of their quality characteristics. Figure 2 depicts all the primary kinds of graphic representation of qualitative indexes in 17 forms, pointing out their arguments (time, angle of rotation, etc.) and properties (quality index, construction parameter, etc.). The numbers in Fig. 2 demonstrate dimensions of the index in the representation: 1—line, 2—surface. Thus, Fig. 2 represents the main set of initial graphic forms with which a computer system of analysis and synthesis of engagements should operate.

Thus, structural systematization and systematization of the presentation forms of qualitative indexes (see Figs. 1 and 2) are performed, allowing for the creation of a computer packet representing any qualitative indexes in any admitted form for them without touching upon the question of their calculation. Content (semantic) systematization allows for the development of programs to calculate all main qualitative indexes, without touching upon the question of their representation.

Thus, the systematization carried out is the basis for development of a powerful universal system of geometrical analysis and synthesis of gears, tools and cam mechanisms. This is the system by which a user has abundant possibility of representing the results of analysis and synthesis.

3 Optimisation Synthesis of Full-Strength Gear

Based on the analysis of properties of the meshing zone, the following guiding principles were worked out for synthesising gears:

- The geometric synthesis of gears is solved as a variation problem, namely as the determination of a function (its form and parameters) for describing the tooth profile.
- The segments of the tooth profiles to be synthesised are polyarcs, or sets of arcs of circles and segments of straight lines, allowing for possible breaks in connections of individual segments [1]
- The connecting curves at the root, which have to be synthesised, are arcs of circles or elliptical arches, as well as polyarcs.
- The synthesis has to be carried out separately for the three individual areas of the engagement line: for the area of single tooth contact, the area of double tooth contact, and the area where the teeth enter and leave.
- The three areas are synthesised along the line of engagement according to a given change in contact stresses. Other quality criteria are also used here, such as, e.g., the thickness of the oil film during meshing, cold and warm binding of the teeth, etc.

- In those areas of the engagement line that are far away from the point of engagement, the following conditions have to be used as synthesis criteria: sensitivity of gears to changes in centre distance related to the length of the tooth profile to be synthesised, overlap, the temperature of the oil film, etc.

Mathematically speaking, it is a classic optimisation task to search for the surface form of meshing teeth, which should have a maximum load-carrying capacity. The parameters **x** are established, by which the shape and dimensions of the tooth engagement areas are determined and with which the quality function $F(\mathbf{x})$ goes to an extreme value. At the same time, a number of boundaries in the form of inequalities $P_i(\mathbf{x}) \geq 0$ $\{i = 1, 2, \ldots, n\}$ and equations $Q_j(\mathbf{x}) = 0$ $\{j = 1, 2, \ldots, r\}$ has to be met. It has to be noted that the objective function and the majority of boundaries are nonlinear.

Three different quality functions are used to develop the optimisation synthesis:

- Function $F_H(\mathbf{x})$ determines the contact or rolling fatigue strength of the area of tooth engagement. The contact stresses according to Hertz are used in the initial phase;
- Function $F_F(\mathbf{x})$ determines the bending strength of teeth, here mainly in the root;
- Function $F_\Sigma(\mathbf{x})$ determines both the contact and bending strength of the tooth engagement areas, as well as that of the teeth themselves. This integral function contains the functions $F_H(\mathbf{x})$ and $F_F(\mathbf{x})$ with corresponding weighting coefficients, specified by the user.

Individual quality characteristics are used as limiting factors at the first stage of development of the optimisation synthesis. In addition, the convolutions of individual quality characteristics have to be used as boundaries as well.

The basis when developing an optimisation synthesis is the calculation program for determining tooth profiles. Subsequently, this is developed further and adapted to new requirements. In the program of optimisation synthesis, the quality parameters listed in Fig. 6 have to be calculated and represented in the forms described above. The kinetic quality parameters are analysed with commercial software, of which the calculation results are subsequently used in the optimisation program to be developed. The program creates a library of quality parameters with a supplementary option. It is possible here to take account of the criteria of cold and warm binding, dynamic properties of the friction forces during meshing [1], parameters of the initial engagement phase [4], the parameters of the sensitivity to changes in the centre distance, etc.

Different methods are to be used when developing the synthesis software for calculating cylindrical gears with optimum rolling fatigue strength. These methods are presented in Fig. 3 in the form of a diagram of the underlying calculation algorithm. The scheme contains a total of six calculation blocks. The actual synthesis of the tooth profiles of pinion and gear takes place in block 2. In blocks 3, 4 and 5, the engagement and transition zones of the tooth profiles are combined. Block 6 synthesises the connecting curves of the tooth profiles. All six blocks together guarantee a functioning optimisation synthesis of the tooth profiles.

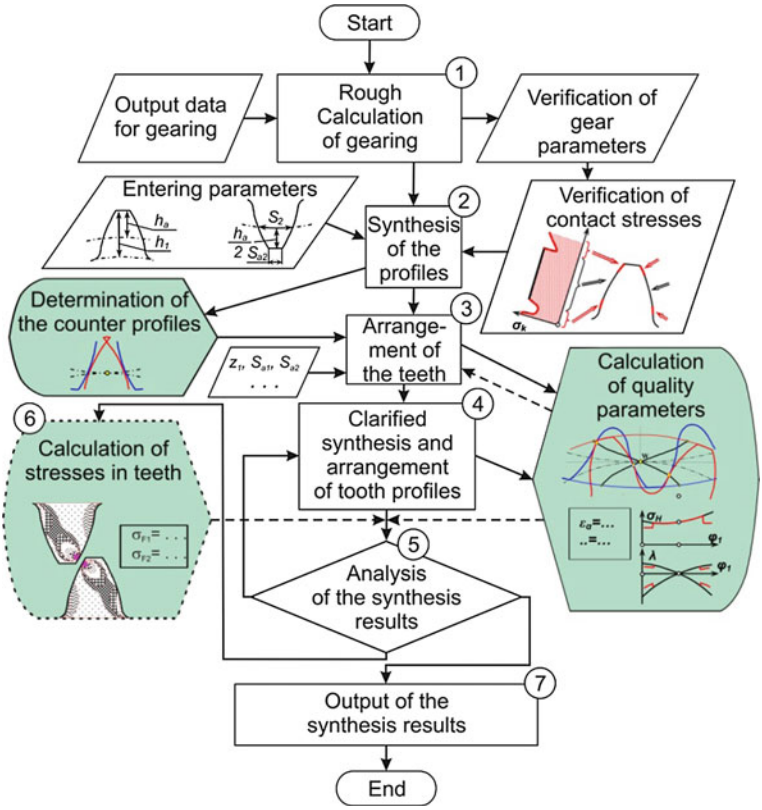

Fig. 3 Flow chart of the algorithm for synthesis of full-strength gears

The method of generalised parameters [5] is used as a basis for creating the synthesis software. The primary result of the synthesis is a polyarc of a circle in the form of some contacting arcs of circles for the synthesised tooth profile [1, 6]. Such polyarcs guarantee that the profile parameters can be definitely calculated. Natural or standardised curved coordinates are used in this process [1].

The connecting curves of the tooth profiles are determined by minimising stresses (mostly bending stresses) in the tooth (see block 6 in Fig. 3). Serving as an initial approximation here is an elliptical arch, which goes through the limiting point of the profile and touches the tooth space.

Based on the performed analyses and the software created for optimisation synthesis, different gears with constant contact stress or uniform rolling fatigue strength along the line of engagement were synthesised. Such gears have minimum weight and dimensions compared with gears with non-uniform rolling fatigue strength, such as, e.g., involute gearings. In addition, there is no danger of interference or undercutting of the tooth in the case of gears with uniform rolling fatigue strength. Figure 4 shows two synthesised gears with uniform rolling fatigue

strength or constant contact stresses of σ_H = 1000 MPa in the middle segment of the engagement line. There are lower contact stresses of σ_H = 700 MPa at the beginning and the end of meshing. Such a reduction in contact stresses at the beginning and the end of the tooth engagement guarantees a smooth or vibration-free operation of synthesised gears. Figure 4 also presents the engagement lines of equivalents for synthesised involute gearings. The engagement lines of different gears only come into contact at the point of engagement at which both gear types have the same contact stress.

Comparing radii of curvature and contact stresses in involute gearings and gears with uniform rolling fatigue strength showed that the latter have considerably larger radii of curvature in the root area than involute gearings. Hence, gears with uniform rolling fatigue strength have a greater load-carrying capacity than involute gearings. This comparison is presented in Fig. 5. Here, Fig. 5a shows, for both gears, how the curvature radii of gear and pinion profiles depend on the rotation angle of the pinion. Figure 5b shows, for both gears, how the contact stresses depend on the rotation angle of the pinion. The contact stresses at the point of engagement are the same for involute gearings and gears with uniform rolling fatigue strength.

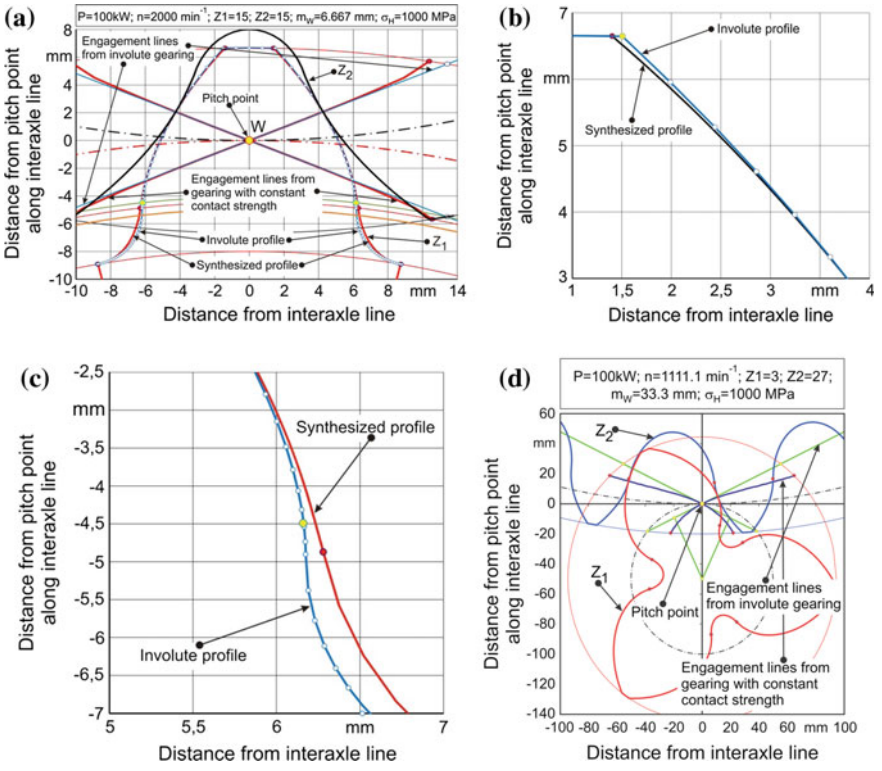

Fig. 4 Gears with uniform rolling fatigue strength and different gear ratios of u = 1 (**a**, **b** and **c**) and u = 9 (**d**)

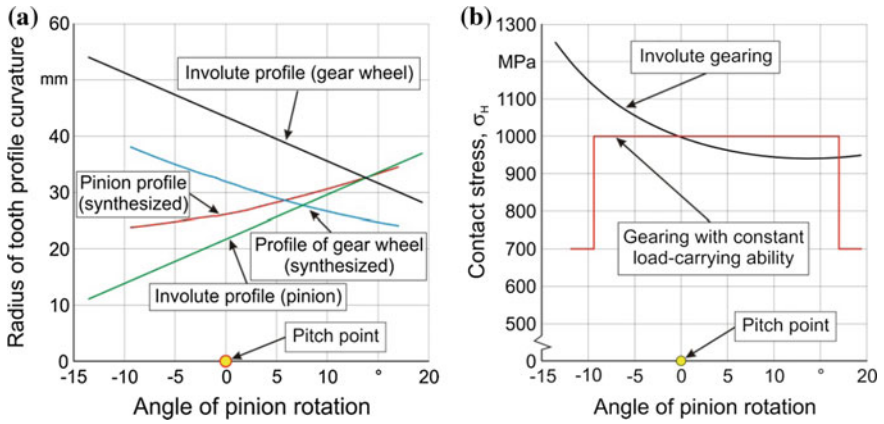

Fig. 5 Contrasting of synthesized and involute gear for curvature radii of tooth profiles (**a**) and contact stress (**b**)

The performed analysis shows that curvature radii in gears with uniform rolling fatigue strength are almost independent of gear ratios. Hence, tooth profiles in such gears are almost independent of the number of teeth as well. When comparing the maximum contact stresses, it can be detected that they are about 25% greater in involute gearings than in gears with uniform rolling fatigue strength at the same torque. In addition, the tooth profiles of these gears are not subject to the undercutting of the tooth.

4 Analysing Quality Properties of Gears in the Meshing Zone

An optimisation synthesis of different gears is founded on quality characteristics. Several publications have analysed the quality characteristics of gears, see, e.g., [4, 7–9], etc. Gear drives are assessed with regard to geometric, kinematic, kinetic, and energetic parameters, as well as others. In addition, these quality characteristics can be divided into two areas: characteristics of the meshing quality, on the basis of which the conditions of tooth contact are assessed, and characteristics of tooth quality, on the basis of which the state of stress deformation and the shape of teeth are assessed. Finally, there are local and global characteristics. Local characteristics describe the properties at one point on the surface of the tooth. Global characteristics describe the properties of the gearing or a gear as a whole. All global characteristics are defined as the sum of the local characteristics on the tooth surface or in the tooth volume.

Figure 6 shows the scheme of the quality parameters that are relevant to cylindrical gears. These quality parameters will be used for the optimisation synthesis. It is important here to analyse the quality parameters, which makes their

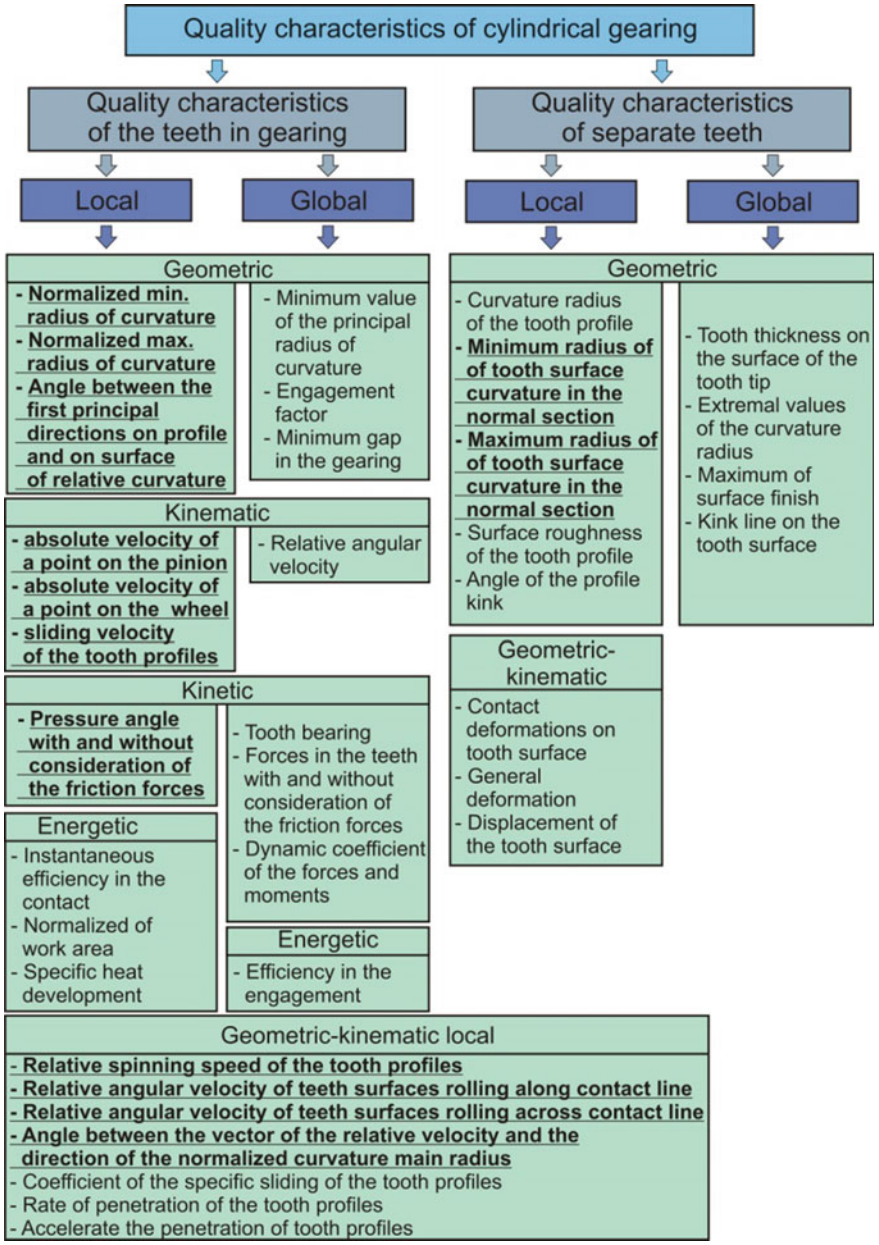

Fig. 6 Scheme of the quality parameters for cylindrical gear drives

illustration helpful. These illustrations will be carried out in different forms: 2-D and 3-D diagrams and nomograms, isolines, locking contours, loci of speed or force, etc.

There are a total of 13 independent quality characteristics with which the quality of tooth contact can be assessed with regard to all curvatures and accelerations, or rather up to the analysis, including second-order derivatives [1]. These independent quality characteristics are divided as follows: five characteristics are geometric, three kinematic, four mixed (geometric-kinematic) and one is kinetic [1]. To calculate the quality characteristics with specially developed software, the following input data were used: centre distance—a_w; width of gear—b_2; gear ratio—u; torque on pinion—T_1; coordinates of the contact point of tooth profiles in the meshing zone; contact stresses according to Hertz—σ_H at this contact point.

To be able to guarantee the optimisation synthesis, the quality characteristics in the meshing zone were analysed with specially created calculation software. The analyses carried out were aimed at deriving regularities to which the curvature shapes of revolving pinion and gear profiles are subject. The zone of meshing was analysed in three different zones:

- analysis of the quality properties at the point of engagement
- analysis of the boundaries for a low zone of meshing
- analysis of the meshing zone close to and far from the point of engagement.

4.1 Rolling Fatigue Strength and Radii of Curvature at the Point of Engagement

A complex of calculation programs was developed for guaranteeing the synthesis of gears with great load-carrying capacity and analysing their quality characteristics. The capacity on the pinion, its rotational speed, transfer ratio, centre distance, width of gear and a particular height of contact strength were used as basic input data. The fundamental input parameters of synthesised profiles include quality characteristics of the synthesised gears in numerical and/or graphic form. An equation system containing the Euler-Savary equation, referring to the correlation of specific radius of curvature and curvature radius of conjugate profiles, and the Hertz equation is used as a mathematical model of the calculation program complex. The system is solved regarding the radii of curvature at any point of either the entire meshing zone or in a small area of the engagement line to be synthesised. Some programs from the developed complex of calculation programs are interactive and guarantee visualisation of the movement of the synthesised gears. Moreover, the results which were obtained with the created complex are shown.

In the calculations, the gear ratio was varied from $u = 1$ to $u = 10$, and the engagement angle at the point of engagement was varied from $\alpha_W = 0°$ to $\alpha_W = 90°$. The results are illustrated in Figs. 7 and 8, showing how both parameters i_{12}, respectively, u and α_W, affect the specific radius of curvature and the contact stresses in the gears. As the engagement angle increases between 0° and 90°, the specific radius of curvature also rises from 0 up to a maximum. This applies to all

gear ratios examined (see Fig. 7a). Figure 7b clarifies the transmission ratio of the specific radius of curvature at the point of engagement to the respective maximum radius of curvature. This ratio applies to all possible engagement angles of this gear.

The contact stresses during meshing change symmetrically for the examined range of engagement angles, reaching a minimum at an engagement angle of 45° (see Fig. 8a). Figure 8b shows the ratio between contact stresses for different transmission ratios and contact stresses for a transmission ratio of 1 (each at the point of engagement). This ratio has the same course for all engagement angles examined.

Figure 9 shows how the engagement angle affects the kinetic characteristics of synthesised gears. Figure 9a presents the ratio of normal and radial forces to the tangential force, depending on the engagement angle. Considering the

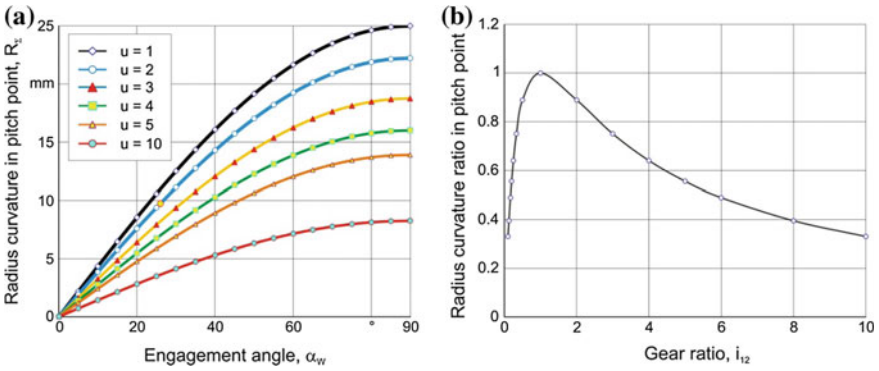

Fig. 7 Effects of engagement angle (**a**) and transmission ratio, respectively, and gear ratio (**b**) on the specific radius of curvature at the point of engagement

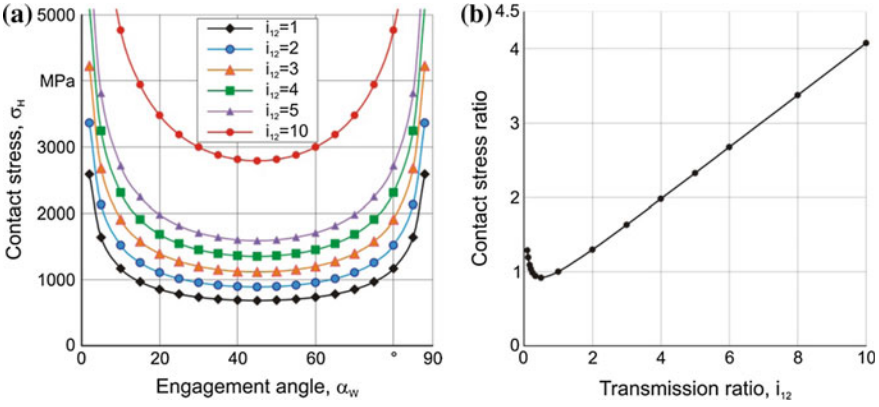

Fig. 8 Effects of engagement angle (**a**) and transmission ratio (**b**) on contact stresses

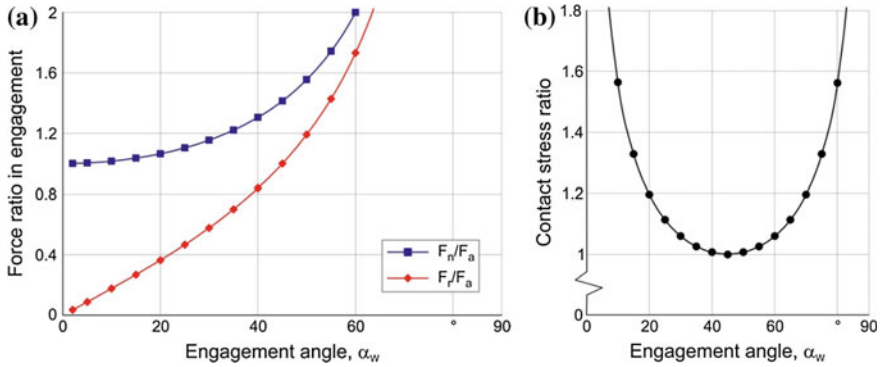

Fig. 9 Varying contact stresses and forces during meshing, depending on the engagement angle

superelevation of the ratio between contact stresses and minimum contact stress (see Fig. 9b) and the superelevation of the components of engagement forces to the tangential force, it can be assumed that an engagement angle of 45° is the optimum.

4.2 Curvature Radii of Profiles in the Meshing Zone with Constant Contact Stresses

In the calculation software, it is possible to model properties of flat gears as a two-dimensional field of arbitrary quality characteristics. As an example, Fig. 10 shows such illustrations of large curvature radii ρ_1 and ρ_2 for gearing with the following parameters: $a_w = 100$ mm, $b_2 = 30$ mm; $i_{12} = 2$; $T_1 = 238.7$ Nm; $\sigma_H = 1000$ MPa.

Analysing fields of curvature for synthesised gears showed that, in general, curvatures far away from the point of engagement change regularly. This applies to the pinion (see Fig. 10a, b) as well as the gear (see Fig. 10c, d). Curvatures behave irregularly in the immediate vicinity of the engagement point. The functions of tooth profile curvatures go to negative infinity for the pinion (see Fig. 10a, b) and positive infinity for the gear (see Fig. 10c, d). Hence, the curvatures of mating profiles change very much if the point of contact is minimally shifted in its vicinity. This may lead to instabilities in the calculation methods if parts of the mating profiles close to the engagement point are established.

When carrying out the calculations, it could be found that a flat zone of meshing is bordered by two straight lines perpendicular to each other. One line is the centre line, and the other is the line perpendicular to the centre line (see Fig. 10).

It follows from analysing Fig. 10 that profile curvature changes regularly far from the point of gear engagement and from the boundaries of the meshing zone. The curvature of mating profiles changes very much if the point of contact deviates minimally from the nearby point of engagement W. This leads to instabilities in the

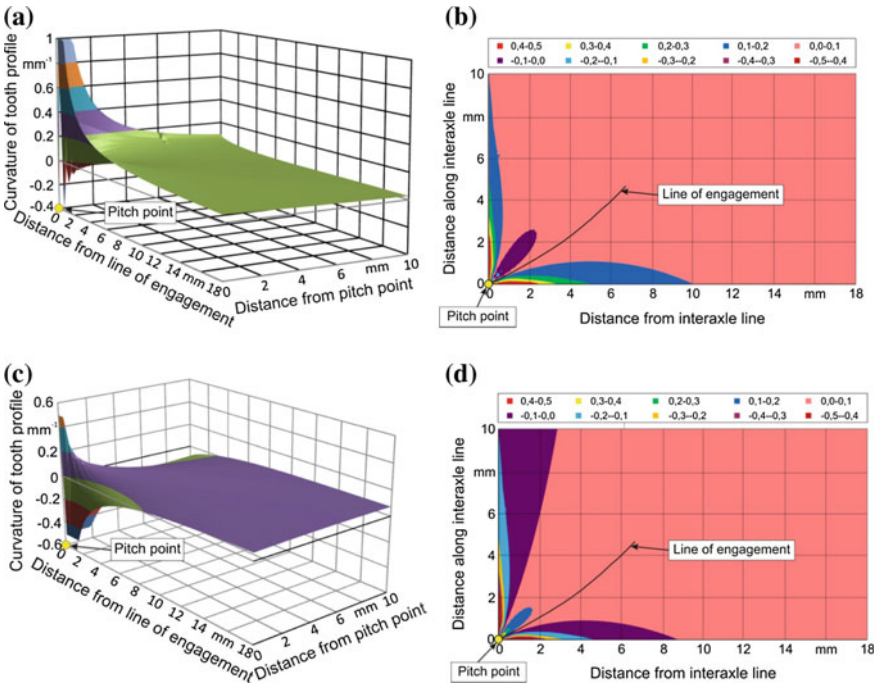

Fig. 10 Curvature fields of tooth profiles for pinions (**a**, **b**) as well as for gears (**c**, **d**)

numerical methods of the synthesis for such points. Hence, the following guiding principle can be concluded: *the line of engagement can cross the boundary lines only at the point of engagement and should not be too close to the boundary lines.*

Owing to the calculations, the duality of the task could be confirmed resulting from the determination of conjugate profiles with given specific curvature at the pitch point. Hence, different pairs with conjugate profiles may transfer the same load or have the same contact stresses during meshing: one pair with large radii of curvature and the other with small radii of curvature for a clearly distinctive convexo-concave contact of the teeth. This duality, however, gets lost at the point of engagement so that the profile pair with the smaller radii of curvature degenerates. Close to the point of engagement, the convexo-concave gear has nearly the same values as the radii of curvature. The values correspond roughly to the distance between the contact point and the engagement point. The functional capability of gears here reacts very sensitively to changes in the centre distance. This leads to the following guiding principle: *profiles with small radii of curvature should not be convexo-concave close to the point of engagement*. Despite the theoretical duality of the task of tooth profile synthesis, there is only one solution for the vicinity of the engagement point—*tooth profiles should have large radii of curvature*.

4.3 Synthesising Conjugate Segments of Tooth Profiles and Their Engagement Lines for the Same Contact Stresses

Based on the examined properties of flat zones of meshing (see Sects. 3.1 and 3.2), an algorithm and a software were created for synthesizing the segments of tooth profiles and their lines of engagement, taking the condition of constant contact stresses into account. Figures 11 and 12 present the possibilities of the software for analysing and synthesising the engagement profiles of gears. The gears here have a maximum contact stress of 1000 MPa regarding the first segment of the engagement line up to the point of engagement and of 600 MPa regarding the second segment of the engagement line after the engagement point.

Figure 11 presents areas of the engagement line and three mating profiles of pinion, gear and rack. Each profile here consists of two segments.

Figure 12 shows the specific curvature of the gear and pinion profile at the point of tooth contact if the angle of rotation of 36° is varied after the point of engagement.

The specific curvature of the tooth profile is the sum of the specific curvatures of tooth profiles for gear and pinion. This specific curvature hardly changes along the line of engagement (see Fig. 12). It also has to be noted that the specific curvature of the pinion's tooth profile takes up negative values in the range of contact stresses of σ_H = 600 MPa. This points to a convexo-concave tooth contact.

A sensitivity to errors in the relative position of gear links is the important index. Figure 13 shows the influence of gear ratio change on the relative distance between axes.

Influence of angle of pinion rotation on the relative distance between axes is presented in Fig. 14. The greatest deviation of relative distance between axes of gear will be by the initial point of teeth contact.

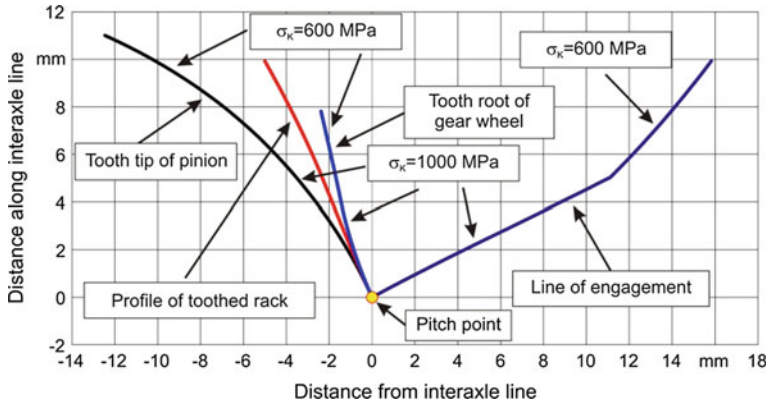

Fig. 11 Example of synthesising the areas of engagement line and profiles

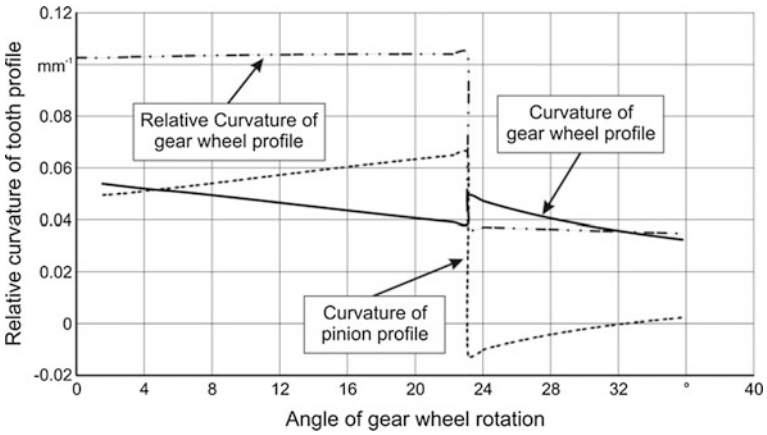

Fig. 12 Varying profile curvature and specific curvature depending on angle of rotation

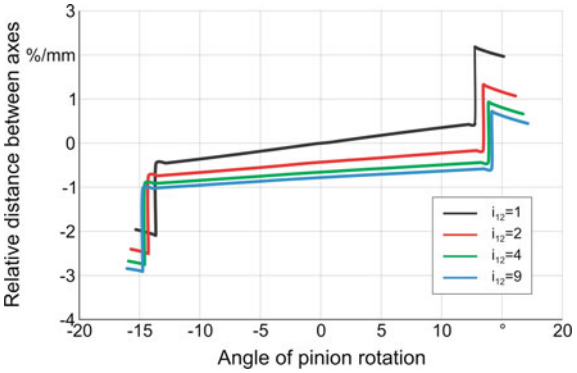

Fig. 13 Influence of gear ratio change on the relative distance between axes

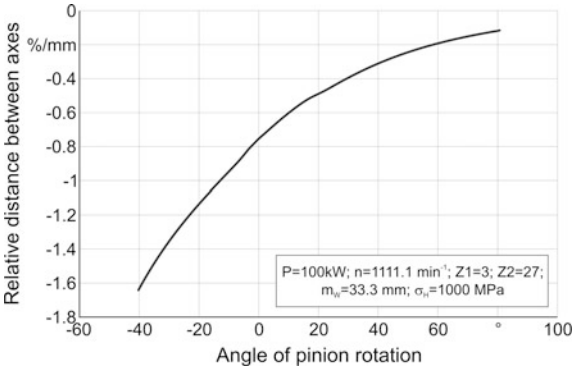

Fig. 14 Influence of angle of pinion rotation on the relative distance between axes

If the start and end sectors of the teeth profile will be modified for the purpose of contact stresses reduced by increasing the radius of profile curvature, the sensitivity of the gear to a change in the distance axes is increased. This increase can be decreased substantially for the benefit of the magnitude and law change selection of contact stress along the teeth modified profiles.

5 Conclusions

The classification of gear quality characteristics was developed. Three systematizations of quality characteristics of engagement operation were carried out: structural, semantic and by the form of presentation. The analysis of local and global quality characteristics of synthesized full-strength gears was realized. For the gear synthesis, a calculation algorithm was developed.

Specifically, a calculation algorithm was developed for the geometric optimisation synthesis of full-strength, cylindrical gear drives. An algorithm and its software realisation were worked out for this concept. Tooth profile forms were generated here which have a constant load-carrying capacity or a uniform rolling fatigue strength along their entire line of engagement. The concept of the synthesis was developed by analysing various methods for increasing the load-carrying capacity of gear drives through optimised gear geometries, and by analysing and selecting quality criteria for evaluating gears, as well as examining the zone of meshing.

The analysis of the curvature radii of the tooth profile in the engagement zone was carried out. Analysing fields of curvature for synthesised gears showed that curvatures far away from the point of engagement change regularly in general. Curvatures behave irregularly in the immediate vicinity of the engagement point. Hence, the curvatures of mating profiles change very much if the point of contact is minimally shifted in its vicinity. This may lead to instabilities in the calculation methods if parts of the mating profiles close to the engagement point are established.

The concept, worked out from a property analysis for the meshing zone of cylindrical gear drives and an analysis of the quality properties of gears to be synthesised, lays the foundations for developing algorithms and a universal calculation program. With this program, it is possible to synthesise the tooth profiles of cylindrical gears according to given quality criteria.

Acknowledgements The presented results were obtained in the project "Development of a concept for the synthesis of cylindrical gears with optimal contact strength," funded by the German Research Foundation (DFG). The authors would like to thank the DFG for their support, which is highly appreciated.

References

1. Babichev, D.T.: Entwicklung der Theorie der Verzahnungen und Formgebung von Oberflächen aufgrund neuer geometrie-kinematischer Auffassungen. Dissertation, Tjumen Staatliche Gas-Öl Universität, Tjumen, 421 S. (2005)
2. Babichev, D., Storchak, M.: Synthesis of cylindrical gears with optimum rolling fatigue strength. Prod. Eng. Res. Dev. **9**(1), 87–97 (2015)
3. Babichev, D.A., Serebrennikov, A.A., Babichev, D.T.: Qualitative indexes of flat engagement operation. Research and Development of mechanical elements and systems. In: Proceedings the 7th International Conference: IRMES, Zlatibor, Serbia, pp. 623–630 (2011)
4. Linke, H.: Stirnradverzahnung: Berechnung, Werkstoffe, Fertigung. Carl Hanser Verlag, München Wien, 840 S. (2012)
5. Vulgakov, E.B.: Theorie der evolventen Verzahnungen. Maschinenbau, Moskau, 320 S. (1995)
6. Shishov, V.P., Nosko, P.L., Fil, P.V.: Theoretische Grundlage der Synthese von Verzahnungen. Lugansk, SNU, 408 S. (2006)
7. Lenskiy, M.F.: Invariant theory of planar pair with point contact. Theor. Eng. **5**, 15–24 (1967)
8. Lenskiy, M.F., Prohorov, V.P.: Generalized characteristics of gears. Theor. Eng. **5**, 67–77 (1971)
9. Litvin, F.L., Fuentes, A.: Gear Geometry and Applied Theory, 2nd ed. Cambridge University Press, 800 p (2004)

Geometric Pitch Configurations—Basic Primitives of the Mathematical Models for the Synthesis of Hyperboloid Gear Drives

V. Abadjiev and E. Abadjieva

Abstract The pitch configurations (circles and surfaces) are the basic primitives, upon which the mathematical models for synthesis of spatial gears with crossed axes of rotation are worked out. These mathematical models are created after the approach to synthesis based on one common point of contact between the operating tooth surfaces of the mating gears, this point being, at the same time, a common point of the pitch configurations. This point is called a pitch contact point. When the pitch circles and surfaces are in a static position, they are treated as geometric characteristics of the designed gears, and determine not only the basic parameters of their structure but also the dimensions of the gears' blanks. If the pitch configurations are put in a rotation according to a given law of motions transformation, then the dimensions and the mutual position of the configurations serve to define the dimensions and the longitudinal and profile geometry of the tooth surfaces contacting at the pitch point. The study deals with the synthesis of geometric pitch configurations for two main cases of three-link hyperboloid gears with externally mating gears: with normal (traditional) orientation of the gears and with inverse (opposite of the traditional) orientation of the gears.

Keywords Mathematical modeling · Synthesis · Hyperboloid gears · Pitch configurations

V. Abadjiev · E. Abadjieva (✉)
Institute of Mechanics-BAS, Sofia, Bulgaria
e-mail: abadjieva@gipc.akita-u.ac.jp

V. Abadjiev
e-mail: abadjiev@imbm.bas.bg

E. Abadjieva
Akita University, Akita, Japan

V. Goldfarb et al. (eds.), *Advanced Gear Engineering*,
Mechanisms and Machine Science 51, DOI 10.1007/978-3-319-60399-5_5

1 Introduction

The mathematical models oriented to the synthesis of spatial gears transforming rotations between crossed axes (hyperboloid gear sets) ensure, in principle, a possibility for their multi-parametrical and multi-criteria optimization. This is explained by the existence of a large number of free parameters which take part in the description of the rotations transformation process. This fact creates possibilities for achieving desired technological and exploitation characteristics of the considered transmissions in their synthesis by looking for suitable combinations of the free parameters. Some of these characteristics are: use of universal and simple equipment for the manufacture of gears; high reliability and durability; low vibration activity and noiselessness; high accuracy of realization of the motions transformation law; high hydrodynamic loading capacity, etc. As a rule, the positive technological and exploitation qualities of the spatial gear mechanisms result from the higher requirements needed to obtain gears' specific kinematical characteristics. Everything mentioned up to now determines, to a great extent, the kinematical character of the chosen approach to the synthesis and the kinematical character of the created models [1–5].

The successful introduction of spatial gearings with new kinematical and strength characteristics in technics depends directly on the creation of adequate mathematical models for synthesis in accordance with the motion transformation processes described by them.

The global structure of each mathematical model for synthesis of a three-link spatial gear mechanism is determined by [6]:

- the purpose the gear-pair is designed for, from a viewpoint of the defined law of motion transformation;
- the geometry and the character of the conjugation of the tooth surfaces (i.e., whether the tooth surfaces contact at a point or along a line);
- the technological reasons for a choice of the instrumental surfaces' geometry and of the kinematics of the technological process by which the active tooth surfaces of the gear set are generated.

The performed and published researches [6–12] determine the authors' opinion about the types of mathematical models that are suitable for the synthesis of hyperboloid gears. Below, we will summarize the basic specific characteristics of one of these models.

The mathematical model for synthesis upon a pitch contact point is based on the assumption that the necessary quality characteristics (that define concrete exploitation and technological requirements to the active tooth surfaces) are guaranteed only at one concrete point P of the active tooth surfaces Σ_1 and Σ_2, and in its close vicinity (see Fig. 1) [9]. This model can be applied for synthesis of spatial gears with both point and linear contact. According to it, the common contact point

P of the conjugate tooth surfaces Σ_1 and Σ_2 is the common point of the circles $H_i^c(i = 1, 2)$ that are called *a pair of pitch circles* $(H_1^c{:}H_2^c)$. The point P is called *a pitch contact point*, the plane T_m, including the tangents to $H_i^c(i = 1, 2)$ at the point P is *a pitch plane*, and $m - m$ is the *pitch normal* to T_m at the point P. The mutual position of these two circles in the fixed space in the case of traditional constructions of hyperboloid gears with externally meshed tooth surfaces is illustrated in Fig. 1. The diameters $d_i(i = 1, 2)$ of $H_i^c(i = 1, 2)$, together with the parameters $a_i, \theta_i, \delta_i(i = 1, 2), \delta$ and a_w, define their mutual position in the fixed space [in the coordinate frames $S_i(O_i, x_i, y_i, z_i), (i = 1, 2)$]. These parameters are related to the definition of the longitudinal and profile orientations of the active tooth surfaces $\Sigma_i(i = 1, 2)$ at the pitch contact point. The pair of rotation surfaces, including the pair of pitch circles whose common normal at P is the straight-line $m - m$, are an analogue of $H_i^c(i = 1, 2)$. These surfaces are called *pitch surfaces.* The pair of circles $(H_1^c{:}H_2^c)$ is directly related with the evaluation of the pitch and of the tooth module of the designed gear set. The parameters $d_i, \delta_i(i = 1, 2)$ define the dimensions of the reference coaxial rotation surfaces, i.e., the blank proportions of the gears depend on them. The above parameters are used when the mounting dimensions of the synthesized gear-set are calculated.

Thus, the mathematical model for synthesis based on a pitch contact point ensures the solution of two basic problems:

- synthesis of the pitch circles/pitch surfaces;
- synthesis of the active tooth surfaces.

The necessary, and preliminarily-defined, geometric characteristics of the synthesized gear set in a close vicinity of the pitch contact point are found by solving these two problems together.

In conclusion, it should be pointed out that the approach to the synthesis of spatial gears described here is based on the following kinematical condition: *The relative velocity vector* $\overline{V}_{12}$ *at the pitch contact point P has to lie both in the pitch plane* T_m *and in the common tangent plane of the tooth surfaces* Σ_1 *and* Σ_2 *contacting at P, this vector being oriented along the common tangent to the longitudinal lines of the active tooth surfaces* $\Sigma_i(i = 1, 2)$.

Therefore, the considered approach to a basic synthesis upon a pitch contact point gives a possibility for the mathematical model and the algorithm (worked out on the model) to have a universal structure for all types of hyperboloid gears. The algorithm can be developed and become an algorithm for an optimizing synthesis. This is achieved through construction of criteria for control of the quality of meshing in the vicinity of the pitch contact point, the criteria taking into account the specifics of the geometry and of the technology of different hyperboloid gears in an adequate way.

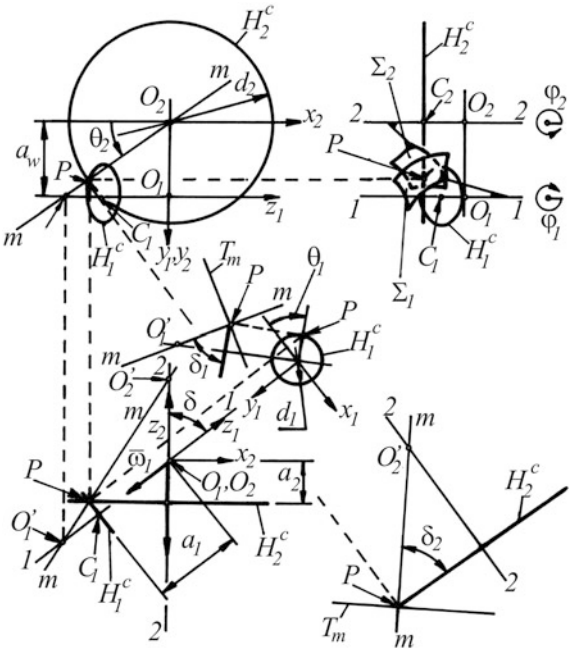

Fig. 1 Geometric and kinematic interpretation of the mathematical model for synthesis based on a pitch contact point: $H_i^c (i = 1, 2)$ are pitch circles; T_m is a pitch plane; $m - m$ is a pitch normal to T_m at the point P; $\Sigma_i (i = 1, 2)$ are tooth surfaces contacting at the point P

2 Pitch Configurations: Essence and Definition

Here, we study the pitch configurations that are basic elements of the mathematical models for synthesis of hyperboloid gears. These elements treat one actual, but still disputable (in terms of content and terminology), part of the meshing theory.

In the theory of spatial gearing, the terms "primary surfaces" and "pitch surfaces" have been used at the same time [13–16]. In most cases, these terms (primary and pitch surfaces) have been used for one and the same surfaces.

Professor F. Litvin gave the following definition of primary surfaces [13]:

"The primary surfaces H_1 and H_2 firmly connected with the movable links of the mechanism are called primary ones if the following conditions are fulfilled: (a) the rotation axis of the primary surface coincides with the rotation axis of the movable link; (b) the surfaces H_1 and H_2 tangent at a given point P of the fixed space, and the velocity of the relative motion of the links 1 and 2 at P lies on the common tangent to the helical lines of the surfaces H_1, H_2 and Q (author's note: Q is a family of coaxial cylinders and the vector (helical) lines of the vector field of the relative motion velocity $\overline{V}^{(12)}$ are situated on them). The second requirement means that they have a common normal at the chosen point, and the velocity vector of the relative motion $\overline{V}^{(12)}$ lies in the common tangent plane of H_1 and H_2. … If $i_{12} =$ constant the primary surfaces could be arbitrary surfaces of revolution only if: (a) the axis of rotation $i - i$ of H_i is an axis of rotation of i-th link; (b) $\overline{V}^{(12)}$ lies in

the common tangent plane of H_1 and H_2. For $i_{12} =$ constant for the primary surfaces could be chosen random surfaces of rotation if: (a) the axis of rotation of $H_i\, i - i$ is the axis of rotation of the i-th link; (b) the common tangent planet to H_1 and H_2 contains $\overline{V}^{(12)}$.

In the theory of gearing, without any restriction to consider small parts of H_1 and H_2 in the vicinity of P, these surfaces are defined as a whole: they have a form of cylinders or cones depending on the vector $\overline{\omega}^{(i)}$ being parallel to the tangent plane or not (author' note: $\overline{\omega}^{(i)}$ is the vector of rotation of the movable link i). Such treatment is possible but not obligatory: H_1 and H_2 could be other surfaces of revolution if they have a common tangent plane at the point P. For the practice, it is convenient as primary surfaces to be chosen cylinders (for worms, cylindrical gears) or cones (for conical and hypoid gears).

In order to avoid any misunderstanding it is necessary to note the following principles:

(a) In the most common case the primary surfaces can not be identified with the axoids; such identification is possible only in the case of gear-pairs with parallel or intersecting axis, and is not permitted for gear sets with crossed axes of rotations; (b) the tooth surfaces Σ_1 and Σ_2 do not coincide with the primary surfaces. Although Σ_1 and Σ_2 tangent at the point P, the normal vectors $\overline{e}^{(\Sigma_i)}$ and $\overline{e}^{(H_i)}$ have different directions. The common tangent plane of Σ_1 and Σ_2 at the point P does not coincide with the common tangent plane of H_1 and H_2 but $\overline{V}^{(12)}$ belongs to each of them; (c) the condition of the simultaneous tangent of H_1, H_2 and Q at the point P is possible but not obligatory…".

Later, Litvin (see [14, 16]) called the primary surfaces "operating pitch surfaces" in accordance with their practical application in the design of spatial gears with crossed axes. They differ from the axoids of the movable links [15]:

"The operating pitch surfaces represents: (i) two cylinders for a worm-gear and helical gears with crossed axes and (ii) two cones for a hypoid gear drives. The chosen surfaces that are called in the technical literature "operating pitch surfaces" must satisfy the following requirements:

(i) The axes of cylinders (cones) have to form the same crossed angle and be at the same shortest distance as for the designed gears.
(ii) The cylinders (cones) must be in tangency at the middle point of contact of the surfaces of the gears to be designed.
(iii) The relative sliding velocity $\overline{V}_{12}$ at point P of tangency of the cylinders (cones) must lie in the plane that is tangent to the cylinders (cones) and $\overline{V}_{12}$ must be directed along the common tangent to the helices of the gears to be designed. The term "helix" is a conventional one. Actually, we have to consider a spatial curve that belongs to the operating cylinders (cones) and represents the line of intersection of the gear tooth surfaces with the operating cylinders (cones). For the case of a helical gear, a cylinder worm, this line of intersection is indeed a helix. For the case of spatial bevel gears and hypoid gears,

the line of intersection is a spatial curve that differs from a helix and might be represented with complicated equations.

(iv) The tangent point P of operating pitch cylinders (cones) will be simultaneously the point of tangency of gear tooth surfaces if the surfaces have a common normal $n-n$ at P and $n-n$ is perpendicular to $\overline{V}_{12}$ …"

In [17], W. Nelson treated the pitch surfaces for one concrete type of spatial gears—the Spiroid®[1] ones. There, he used the terms "primary pitch cone" (the coaxial cone limiting the tips of the Spiroid pinion threads) and "pitch surface" (an envelope of the primary pitch cone in its relative motion with respect to the axis of the second movable link of the Spiroid gear). On the common line of contact of both pitch surfaces, he looked for that pitch contact point which had determined the most suitable spatial curve used as a longitudinal line of the synthesized tooth surfaces of the Spiroid pinion. This is an approach to the choice of such surfaces that does not differ from those already considered.

From the survey conducted, it is established that the pitch configurations have influence when they define such basic characteristics of the gear-pair as: the structure and the geometry of the gear set, the longitudinal and profile orientations of the active tooth surfaces of the gears, pitch value, the tooth module, the strength loading of the gears, the shafts and bearings of the gear mechanism, the efficiency coefficient, etc. All said illustrates the great significance of the development of this scientific field of the theory of gearing from scientific, applied and methodological viewpoints. The authors of the present paper have given up a part of their researches to the mentioned topics in relation to the solution of problems connected with the synthesis and design of spatial gears [6–12]. First of all, our researches have been oriented to the precision of the content of the basic terms*: pitch circles* and *pitch surfaces.* The exact definition of these notions gives us the possibility to precise the applied mathematical models for synthesis of spatial gears on the one hand, and, on the other hand, ensures possibilities for new ideas referring to the creation of hyperboloid gears with new qualities, and new applications in technics, respectively. It is natural that each study in this field will be effective when it leads to creation of an adequate mathematical model, describing the status of the pitch configurations in the process of the spatial transformation of rotations.

Analyzing illustrations in Figs. 1 and 2, and commented upon above, we can conclude that:

- If the law of transformation of rotations $i_{12}=\omega_1/\omega_2=$ constant between fixed crossed axes $1-1$ and $2-2$ (the shortest distance between them being $a_w=$ constant and the angle between them—$\delta=\angle(\overline{\omega}_1,\overline{\omega}_2)=$ constant) is given, and if the position of a point P (treated as a point of contact of conjugate tooth surfaces Σ_1 and Σ_2) in the fixed space is known, then the diameters and the mutual position of the circles $H_i^c(i=1,2)$ are completely and uniquely determined. The circumferential velocity vectors $\overline{V}_i(i=1,2)$ of the common point P,

[1]Spiroid and Helicon are trademarks registered by the Illinois Tool Works, Chicago, Ill.

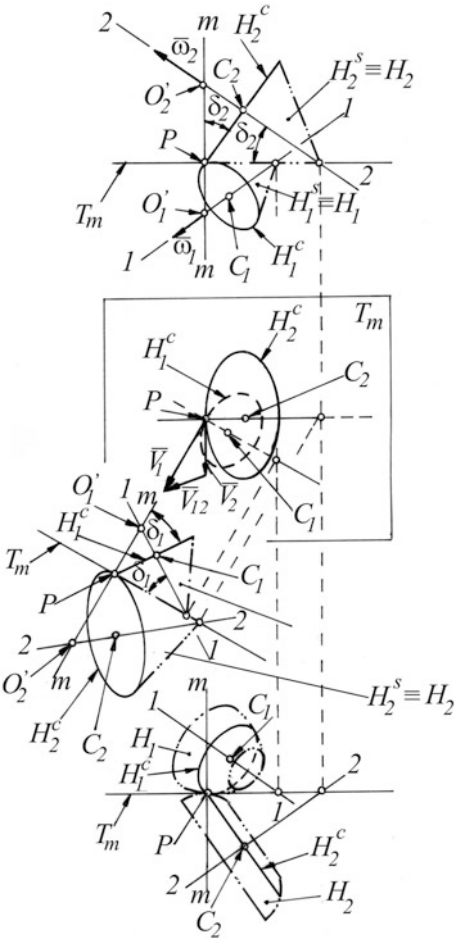

Fig. 2 Pitch configurations: $H_i^c(i = 1, 2)$ are pitch circles; $H_i^s(i = 1, 2)$ are pitch surfaces; $H_i(i = 1, 2)$ are primary surfaces with an arbitrary geometry; P is pitch contact point (pole of meshing); T_m is pitch plane; $m - m$ is pitch normal

and the relative velocity vector $\overline{V}_{12}$ at the same point, (i.e., the plane T_m where the coplanar vectors $\overline{V}_i(i = 1, 2)$ and $\overline{V}_{12}$ lie), as the normal $m - m$ to T_m at the point P are determined in a unique way as well.

- In the case considered in [13], the primary surfaces H_1 and H_2 are not defined in a unique way, since all surfaces of revolution, including the pair of circles $H_i^c(i = 1, 2)$, can be primary surfaces. The primary surfaces, discussed in [13], are simple rotation surfaces (cylinders and cones) tangent at one only point P. In practice, the algorithms for their synthesis define the diameters and the mutual position of the circles $H_i^c(i = 1, 2)$ passing through the common point P.
- It is sufficient to know the mutual position of the crossed axes of rotation $1 - 1$ and $2 - 2$, and the position of the point P (as a common point of the tooth

surfaces Σ_1 and Σ_2) in the fixed space, in order for the circles $H_i^c (i = 1, 2)$ to be completely and uniquely determined (as diameters and mutual position). The plane T_m formed by the tangents to the circles $H_i^c (i = 1, 2)$ at the point P, as the normal $m - m$ to T_m at the point P are uniquely determined as well. The mentioned upper parameters are geometric ones, since the circles $H_i^c (i = 1, 2)$ do not "put in rotation" according to the law $i_{12} = \omega_1/\omega_2$. After the law of rotations transformation begins acting, the geometric parameters defining the diameters and mutual position of $H_i^c (i = 1, 2)$, considered together with the kinematic parameters of the gear set, serve for determination of the longitudinal orientation of the conjugate tooth surfaces $\Sigma_i (i = 1, 2)$, of their pitches and of the gear module.

All said up to now is resulted in this pair of circles to be called *geometric pitch circles* [6–12]. Later, *the geometric pitch circles* will become *pitch circles* only, the plane T_m—*pitch plane*, and the normal $m - m$ to the pitch plane—*pitch normal* (see Fig. 2).

Depending on the position of the pitch circles with respect to the plane T_m, we differentiate:

- *externally contacting pitch circles* when $H_i^c (i = 1, 2)$ are situated in different half-spaces with respect to T_m;
- *internally contacting pitch circles* when $H_i^c (i = 1, 2)$ are situated in one and the same half-space with respect to T_m.

For the externally contacting configurations from Fig. 2, that written above applies to the pitch surfaces, which are alternatives to the pitch circles.

The externally tangent pitch circles have a relation to the synthesis of hyperboloid gears with external meshing (hypoid, Spiroid, helical, wormgears, etc.). As a hypothesis, the synthesis of internally tangent pitch circles can be treated as a stage of the design of new types of spatial gears with internal meshing.

An alternative to the defined pitch configurations are the so-called *kinematical pitch configurations*, consisting of *kinematical pitch surfaces* and *kinematical pitch circles,* whose synthesis is based on the synthesis of *pairs of isokinematical quasi-hyperboloids* [6]. The pitch surfaces, based on the synthesis of the hyperboloids axodes of spatial gears with crossed axes, should participate in the class of kinematic pitch configurations. Analogically to the geometric pitch surfaces, they are called pitch surfaces only [3–5]. The kinematic pitch configurations' synthesis depends on the preliminary given law of transformation of rotations $i_{12} = \omega_1/\omega_2 = \text{constant}$, and the basic geometric parameters $a_w = \text{constant}$ and $\delta = \text{constant}$ (characterizing the structure of the motions transformer) while the geometric pitch configuration synthesis does not take into account the rotations transformation law. Thus, the combination of kinematic and geometric parameters uniquely determines the pair of hyperboloids of revolution (the axodes that contacts along the instantaneous axis of the relative helical motion), the geometric axes of axodes coinciding with the axes of rotation of the hyperboloid gear shafts. In the synthesis of kinematic pitch surfaces, this axis is a locus of the kinematic pitch

points chosen to be poles of meshing of the synthesized hyperboloid gears. If a point from the instantaneous helical axis is chosen as a common point of the tangent tooth surfaces Σ_1 and Σ_2, then the synthesized gear-pair has a minimal sliding velocity in a vicinity of this point (pole of meshing).

In this case, the process of optimization does not include the criterion that controls the magnitude of the sliding velocity between the tangent tooth surfaces. The kinematic pitch surfaces include the chosen conjugate parts from the axodes, as simple surfaces of revolution (cones and cylinders) that are approximations of the rotation hyperboloids at the chosen pole of meshing. If the design of the spatial gears with crossed axes is based on geometric pitch configurations, the chosen pitch contact point is defined by geometric parameters only. These parameters determine the form and dimensions of the geometric pitch surfaces, and of the blanks of the rotating links. Their synthesis does not depend on the sliding velocity at the points of contact of the conjugate tooth surfaces. In this case, the optimization process is being controlled by quality criteria, the sliding velocity here included.

3 Mathematical Model for Synthesis of Pitch Configurations with Normal Orientation of Hyperboloid Gears with External Meshing

Let two crossed axes $1-1$ and $2-2$ (being the axes of rotations of the movable links of a three-link tooth mechanism) be given in the fixed space. Their mutual position is defined by the angle $\delta = \text{constant}$ (the angle between the angular velocity vectors $\overline{\omega}_1$ and $\overline{\omega}_2$ of the moving links $(i = 1, 2)$) and the shortest distance $a_w = \text{constant}$. The concrete study is performed when $\delta \in (0, \pi)$. Each pitch circle H_i^c lies in a plane perpendicular to the axis of rotation $i - i$ of the movable link i and has a radius equal to the distance from the point P to the axis $i - i$. The pitch plane T_m is determined by the tangents at the pitch contact point P to the circles H_1^c and H_2^c. The straight-line $m - m$ is the normal to T_m at P.

The study is performed by means of the notations and the coordinate frames $S_1(O_1, x_1, y_1, z_1)$ and $S_2(O_2, x_2, y_2, z_2)$, introduced in Figs. 3 and 4.

The dimensions and the mutual position of H_1^c and H_2^c are completely determined by the cylindrical coordinates $a_i, r_i, \theta_i (i = 1, 2)$ of the contact point P in the systems $S_i (i = 1, 2)$ and by the angles $\delta_i (i = 1, 2)$ between the planes of $H_i^c (i = 1, 2)$ and the normal $m - m$. The pitch surfaces $H_i^s (i = 1, 2)$—analogs of the pitch circles are illustrated in Figs. 3 and 4.

We represent the radius-vector $\overline{O_1P}$ and the unit vector $\overline{m}$ of the normal $m - m$ by $a_1,\ r_1,\ \theta_1$, and $a_2,\ r_2,\ \theta_2$, and using a_w and δ. Thus, we get the following set of equations:

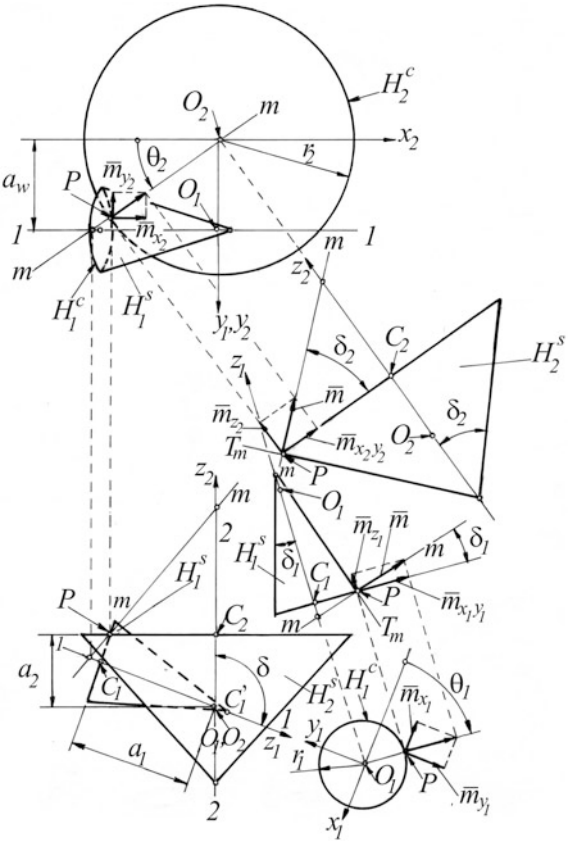

Fig. 3 Externally contacting pitch circles $H_i^c (i = 1, 2)$ and pitch surfaces $H_i^s (i = 1, 2)$, corresponding to hyperboloid gears with external meshing when $z_{2,C_2} > 0$

$$
\begin{aligned}
&r_1 \cos\theta_1 = r_2 \cos\theta_2 \cos\delta \pm a_2 \sin\delta,\\
&r_1 \sin\theta_1 = a_w - r_2 \sin\theta_2,\\
&a_1 = r_2 \cos\theta_2 \sin\delta \mp a_2 \cos\delta,\\
&\cos\delta_1 \sin\theta_1 = \cos\delta_2 \sin\theta_2,\\
&\sin\delta_1 = \sin\delta_2 \cos\delta + \cos\delta_2 \cos\theta_2 \sin\delta,\\
&\cos\delta_1 \cos\theta_1 = \sin\delta_2 \sin\delta - \cos\delta_2 \cos\theta_2 \cos\delta.
\end{aligned}
\tag{1}
$$

Here, the upper signs refer to externally contacting pitch circles $H_i^c (i = 1, 2)$ and pitch surfaces $H_i^s (i = 1, 2)$ when $z_{2,C_2} > 0$ (Fig. 3), and the lower ones—for externally contacting/tangent pitch circles $H_i^c (i = 1, 2)$ and pitch surfaces $H_i^s (i = 1, 2)$ when $z_{2,C_2} < 0$ (Fig. 4). Besides, each of the last three equations in (1) is a consequence of the other two.

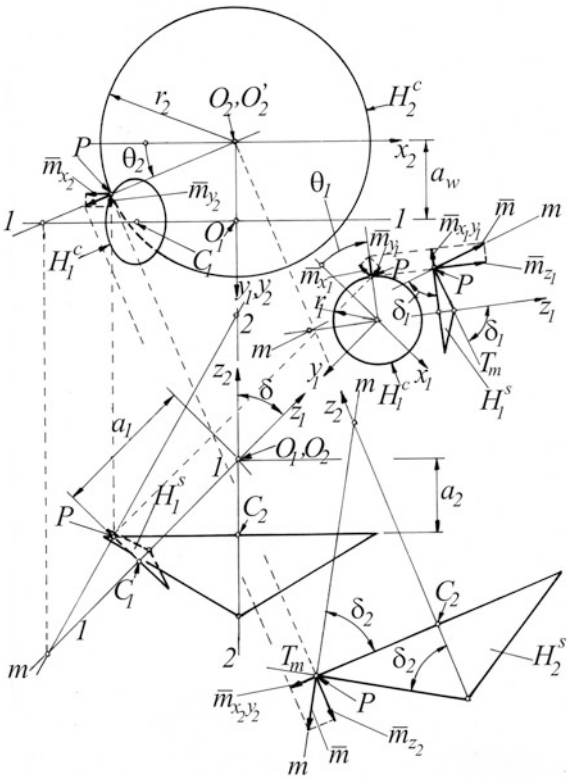

Fig. 4 Externally contacting pitch circles $H_i^c (i = 1,2)$ and pitch surfaces $H_i^s (i = 1,2)$, corresponding to hyperboloid gears with external meshing when $z_{2,C_2} < 0$

Later, the study of the system (1) will be performed taking into account the following geometric conditions: $\theta_1 \in \left[0, \frac{\pi}{2}\right], \theta_2 \in \left(0, \frac{\pi}{2}\right], \delta_1 \in \left[0, \frac{\pi}{2}\right), \delta_2 \in \left[0, \frac{\pi}{2}\right]$, $a_w > 0, r_i > 0 (i = 1,2), a_i \geq 0 (i = 1,2)$.

We will solve and study the set (1) of 5 independent equations with 10 unknowns $\delta, a_w, \delta_1, r_1, a_1, \theta_1, \delta_2, r_2, a_2, \theta_2$. For this purpose, 5 among the unknowns will be considered as free ones. Let them be $\delta, a_w, \delta_1, r_1$ and a_1. We will look for those analytical conditions that the free parameters must fulfill so that the system (1) might have a solution.

It is natural to study the following basic cases: $\delta = \frac{\pi}{2}$ (the axes of rotations $1-1$ and $2-2$ are orthogonal); $\delta \neq \frac{\pi}{2}, z_{2,C_2} < 0; \delta \neq \frac{\pi}{2}, z_{2,C_2} > 0$. The last two cases treat non-orthogonal hyperboloid gears and are illustrated in Figs. 3 and 4, respectively.

3.1 *Synthesis of Orthogonally Tangent Pitch Configurations:* $\delta = \frac{\pi}{2}$

Let us pay attention to the following cases that are essential for the practice:

3.1.1 $\delta_1 = 0$ **and** $a_1 \neq 0$

This case refers to orthogonal hyperboloid gears with external meshing when the coaxial surfaces of the link $i = 1$—reference, root and tip surfaces, are of cylindrical form.

System (1) has the following unique solution:

$$\theta_1 = 0, \tan\theta_2 = \frac{a_w}{a_1}, a_2 = r_1, r_2 = \frac{a_w}{\sin\theta_2}, \delta_2 = \frac{\pi}{2}, \tag{2}$$

in an arbitrary choice of a_w, r_1 and a_1.

The parameters in (2) define the dimensions and the position of the pitch circles corresponding to spatial high reduction gears of type Helicon® [18]. This is the borderline case that separates externally and internally tangent geometric pitch circles (Fig. 5).

3.1.2 $\delta_1 = 0$ **and** $a_1 = 0$

The solution of the set (1) is described with one more parameter δ_2, namely:

$$\theta_2 = \frac{\pi}{2}, \theta_1 = \frac{\pi}{2} - \delta_2, a_2 = r_1 \sin\delta_2, r_2 = a_w - r_1 \cos\delta_2. \tag{3}$$

For the existence of a solution, it is necessary for $\cos\delta_2 \leq \frac{a_w}{r_1}$.

If $a_w > r_1$, the upper condition is always fulfilled.

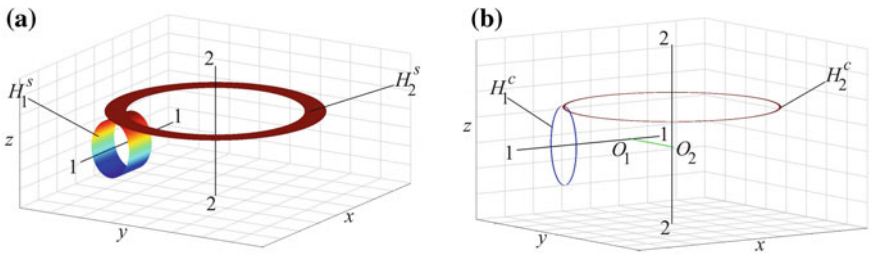

Fig. 5 Pitch configurations for the gears of type Helicon: **a** pitch surfaces $H_i^s (i = 1, 2)$; **b** pitch circles $H_i^c (i = 1, 2)$; $a_w = 100$ mm; $\delta = 90°; \delta_1 = 0°; a_1 = 119.18$ mm; $r_1 = 31$ mm; $\delta_2 = 90°; a_2 = 31$ mm; $r_2 = 155.58$ mm

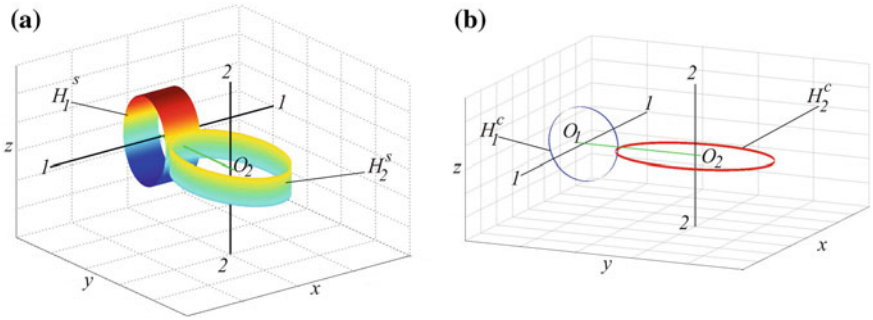

Fig. 6 Pitch configurations for orthogonal worm/helical gears: **a** pitch surfaces $H_i^s (i = 1, 2)$; **b** pitch circles $H_i^c (i = 1, 2)$; $a_w = 100$ mm; $\delta = 90°$; $a_1 = a_2 = 0$ mm; $\delta_1 = \delta_2 = 0°$; $r_1 = 30$ mm; $r_2 = 69$ mm

Pitch configurations corresponding to one particular solution,

$$\delta_2 = 0, \theta_1 = \frac{\pi}{2}, a_2 = 0, r_2 = a_w - r_1, \theta_2 = \frac{\pi}{2}, \tag{4}$$

correspond to orthogonal worm gears or helical gears (Fig. 6).

Solution (4) of (1) is the only one for which the pitch contact point P is situated on the common normal O_1O_2 of the crossed axes $1 - 1$ and $2 - 2$.

Solution (3) of set (1) of the form

$$\delta_2 = \frac{\pi}{2}, \theta_1 = 0, a_2 = r_1, r_2 = a_w, \theta_2 = \frac{\pi}{2} \tag{5}$$

defines the geometric characteristics of toroid gears whose pitch surfaces and circles are illustrated in Fig. 7.

3.1.3 $\delta_1 > 0$

In this case, the condition for the existence of geometric pitch configurations is $a_1 \geq (a_w - r_1) \tan \delta_1$, and the solution to system (1) is:

$$\begin{aligned} \cot \theta_2 &= \frac{r_1 \tan \delta_1 + a_1}{a_w}, \sin\theta_1 = \frac{a_w}{r_1 + a_1 \cot \delta_1}, \\ a_2 &= r_1 \cos \theta_1, \cos\delta_2 = \frac{\sin \delta_1}{\cos \theta_2}, \\ r_2 &= \frac{a_w - r_1 \sin \theta_1}{\sin \theta_2}. \end{aligned} \tag{6}$$

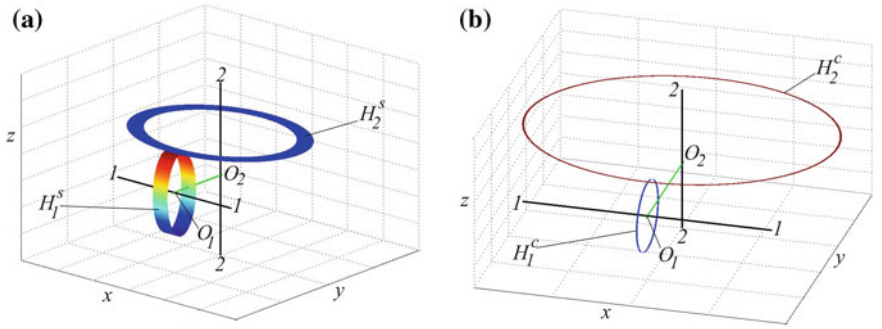

Fig. 7 Pitch configurations for toroid gears: **a** pitch surfaces $H_i^s (i = 1, 2)$; **b** pitch circles $H_i^c (i = 1, 2)$; $a_w = 100$ mm; $\delta = 90°$; $\delta_1 = 0°$; $a_1 = 0$ mm; $r_1 = 31$ mm; $\delta_2 = 90°$; $a_2 = 31$ mm; $r_2 = 100$ mm

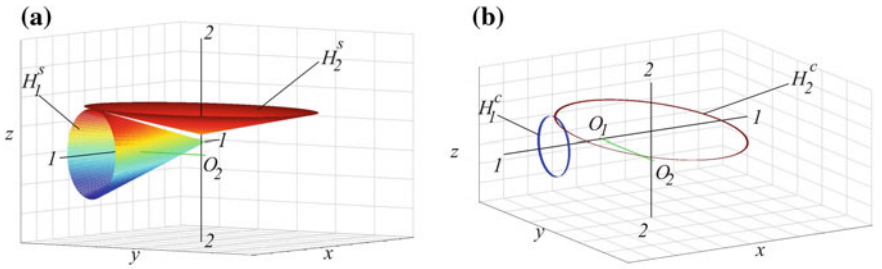

Fig. 8 Pitch configurations for orthogonal hypoid/spiroid gears: **a** pitch surfaces $H_i^s (i = 1, 2)$; **b** pitch circles $H_i^c (i = 1, 2)$; $a_w = 100$ mm; $\delta = 90°$; $\delta_1 = 5°$; $a_1 = 100$ mm; $r_1 = 31$ mm; $\delta_2 = 83°$; $a_2 = 30.89$ mm; $r_2 = 139.57$ mm

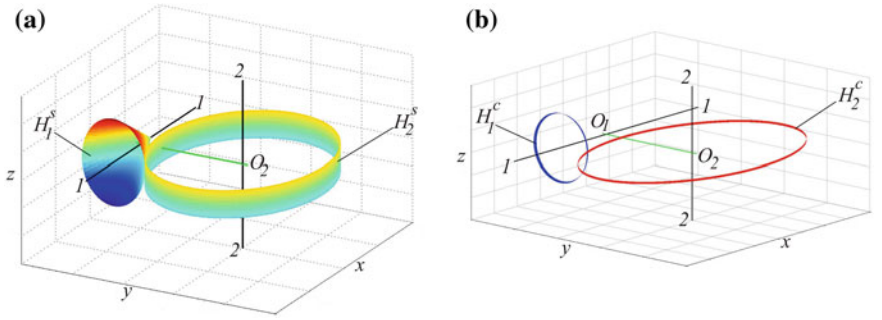

Fig. 9 Pitch configurations of a "common" wormgears: **a** pitch surfaces $H_i^s (i = 1, 2)$; **b** pitch circles $H_i^c (i = 1, 2)$; $a_w = 100$ mm; $\delta = 90°$; $\delta_1 = 30°, a_1 = 39.84$ mm; $r_1 = 31$ mm; $\delta_2 = 0°$; $a_2 = 0$ mm; $r_2 = 79.67$ mm

The parameters of the pitch configurations of orthogonal hypoid gears and gears of type Spiroid [14] are calculated by the relations given in (6). The pitch surfaces and circles are visualized in Fig. 8.

One particular solution of (6) is the case of "common" wormgears, when

$$a_2 = 0, \theta_1 = \frac{\pi}{2}, \tan\delta_1 = \frac{a_1}{a_w - r_1}, \theta_2 = \frac{\pi}{2} - \delta_1, r_2 = \frac{a_w - r_1}{\cos\delta_1}. \tag{7}$$

The pitch surfaces and circles of this type spatial gears are shown in Fig. 9.

3.2 Synthesis of Non-orthogonal Contacting Pitch Configurations When $\delta \neq \frac{\pi}{2}$ and $z_{2,C_2} < 0$

First, it should be pointed out that system (1) has a solution if $\delta \in (0, \pi/2)$, which follows from the condition $a_2 \geq 0$.

The unknown θ_2 is calculated by the formula

$$\cot\theta_2 = \frac{(r_1 \tan\delta_1 + a_1)\sin\delta}{a_w}. \tag{8}$$

To find θ_1, we use the equation

$$\cos(\delta - \delta_1)t^2 - 2\cot\theta_2 \cdot \cos\delta_1 \cdot t - \cos(\delta + \delta_1) = 0, \tag{9}$$

where $t = \tan\dfrac{\theta_1}{2}$.

Let us consider the following cases consecutively:

3.2.1 $\delta + \delta_1 \leq \frac{\pi}{2}$

In this case, it is necessary that $a_1 > 0$ or $\delta_1 > 0$ to be fulfilled.

If, additionally, the condition

$$a_1 \leq a_w \cot\delta - r_1 \tan\delta_1 \tag{10}$$

is satisfied, which presumes $r_1 \leq a_w \cot\delta_1 \cot\delta$, then

$$\tan\frac{\theta_1}{2} = \frac{\cos\delta_1 \cot\theta_2 + \sqrt{D}}{\cos(\delta - \delta_1)}, \tag{11}$$

where $D = \dfrac{\cos^2\delta_1 \sin^2\delta}{a_w^2}\left[(r_1 \tan\delta_1 + a_1)^2 - a_w^2\left(\tan^2\delta_1 - \cot^2\delta\right)\right]$.

If the condition

$$a_1 \geq a_w \cot\delta - r_1 \tan\delta_1 \tag{12}$$

is fulfilled, then

$$\tan\frac{\theta_1}{2} = \frac{\cos\delta_1 \cot\theta_2 - \sqrt{D}}{\cos(\delta - \delta_1)}. \tag{13}$$

If the equality $\delta + \delta_1 = \dfrac{\pi}{2}$ is true, i.e., $\delta = \dfrac{\pi}{2} - \delta_1$, then

$$\theta_1 = 0, \delta_2 = \frac{\pi}{2}, r_2 = \frac{a_w}{\sin\theta_2}, a_2 = a_1\cos\delta - r_1\sin\delta \tag{14}$$

in condition $r_1 \leq a_1 \cot\delta$. Equalities (14) are obtained from (15), and define the pitch configurations of a non-orthogonal spatial face gear-pair (Fig. 10).

3.2.2 $\delta + \delta_1 > \dfrac{\pi}{2}$

In this case, if $a_1 + r_1 \tan\delta_1 \in [a_w\sqrt{\tan^2\delta_1 - \cot^2\delta}, a_w \cot\delta]$, which supposes that $\tan\delta_1 \leq \sqrt{2}\cot\delta$, then θ_1 is calculated by the equality (11).

But if $a_1 + r_1 \tan\delta_1 > \max(a_w \cot\delta, a_w\sqrt{\tan^2\delta_1 - \cot^2\delta})$, then θ_1 is obtained through (13).

For the calculation of the rest of the unknowns in the cases 3.2.1 and 3.2.2, we use

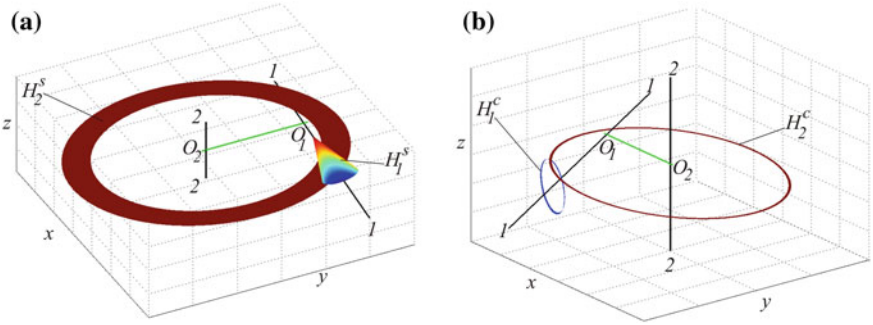

Fig. 10 Pitch configurations: **a** pitch surfaces $H_i^s (i = 1, 2)$; **b** pitch circles $H_i^c (i = 1, 2)$; $a_w = 110$ mm; $\delta = 75°$; $\delta_1 = 15°$; $a_1 = 100$ mm; $r_1 = 20$ mm; $\delta_2 = 90°$; $a_2 = 6.57$ mm; $r_2 = 149.86$ mm

$$a_2 = a_1 \cos\delta - r_1 \sin\delta \cos\theta_1,$$
$$r_2 = \frac{a_w - r_1 \sin\theta_1}{\sin\theta_2}, \cos\delta_2 = \frac{\cos\delta_1 \sin\theta_1}{\sin\theta_2}. \quad (15)$$

3.3 Synthesis of Non-orthogonal Contacting Pitch Configurations When $\delta \neq \frac{\pi}{2}$ and $z_{2,C_2} > 0$

3.3.1 $\delta_1 = 0$

Let consider the following two cases:

If $a_1 = 0$, then the solution to the set of Eq. (1) is in the form

$$\theta_1 = \theta_2 = \frac{\pi}{2}, \delta_2 = 0, a_2 = 0, r_2 = a_w - r_1 \quad (16)$$

when the condition $a_w > r_1$ is satisfied and if $\delta \in \left(0, \frac{\pi}{2}\right) \cup \left(\frac{\pi}{2}, 0\right)$.

Relations (16) describe the pitch surfaces and circles of non-orthogonal worm/helical gears, as shown in Fig. 11. Only in this case of non-orthogonal hyperboloid gears, the common pitch contact point P lies on the common normal O_1O_2 of the crossed axes $1-1$ and $2-2$.

If $a_1 \neq 0$, the solution to (1) is

$$\cot\theta_2 = \frac{a_1}{a_w}\sin\delta, \cot\theta_1 = -\frac{a_1}{a_w}\tan\delta,$$
$$\tan\delta_2 = -\cos\theta_2 \tan\delta, a_2 = r_1 \cos\theta_1 \sin\delta - a_1 \cos\delta, \quad (17)$$
$$r_2 = \frac{a_w - r_1 \sin\theta_1}{\sin\theta_2}.$$

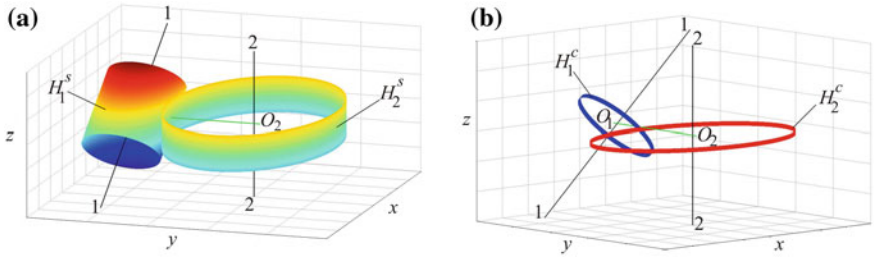

Fig. 11 Pitch configurations for non-orthogonal worm and helical gears: **a** pitch surfaces $H_i^s (i = 1, 2)$; **b** pitch circles $H_i^c (i = 1, 2)$; $a_w = 100$ mm; $\delta = 45°; \delta_1 = \delta_2 = 0°; a_1 = a_2 = 0; r_1 = 31$ mm; $r_2 = 69$ mm

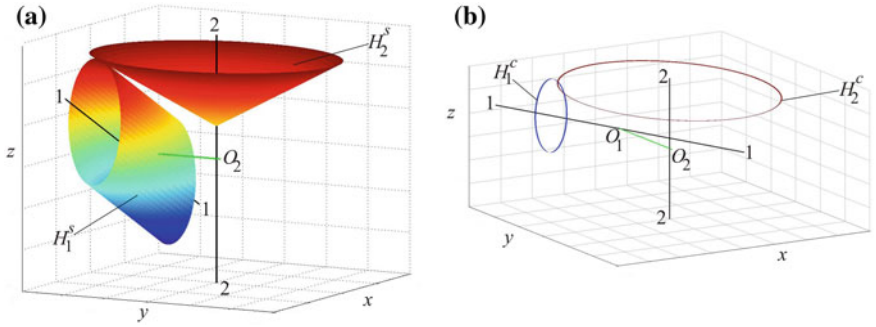

Fig. 12 Pitch configurations for non-orthogonal hyperboloid gears with cylindrical pinion and conical gear: **a** pitch surfaces $H_i^s (i = 1, 2)$; **b** pitch circles $H_i^c (i = 1, 2)$; $a_w = 100$ mm; $\delta = 100°$; $a_1 = 110$ mm; $\delta_1 = 0°$; $r_1 = 31$ mm; $a_2 = 49.25$ mm; $\delta_2 = 76°30'$, $r_2 = 140.20$ mm

The intervals for the unknowns involve the conditions $\delta > \dfrac{\pi}{2}, a_1^2 > (r_1^2 - a_w^2)\cot^2\delta$ (the second condition is true if $r_1 < a_w$).

In Fig. 12, you can see the pitch configurations of non-orthogonal hyperboloid gears with a cylindrical pinion and a conical gear.

3.3.2 $\delta_1 > 0$

Now, we will pay attention to the following cases:

- Let $\delta_1 = \delta - \dfrac{\pi}{2}$, which a priori involves $\delta > \dfrac{\pi}{2}$.

Then, the solution to the set of Eq. (1) is given by

$$\begin{aligned} \cot\theta_2 &= \frac{r_1 \sin\delta_1 + a_1 \cos\delta_1}{a_w}, \tan\frac{\theta_1}{2} = \frac{\sin\delta_1}{\cot\theta_2}, \\ \cos\delta_2 &= \frac{\cos\delta_1 \sin\theta_1}{\sin\theta_2}, a_2 = r_1 \cos\theta_1 \sin\delta + a_1 \sin\delta_1, \\ r_2 &= \frac{a_w - r_1 \sin\theta_1}{\sin\theta_2}. \end{aligned} \tag{18}$$

Algorithm (18) describes the geometric pitch configurations of non-orthogonal hypoid/Spiroid gearing. One concrete design is illustrated in Fig. 13.

The inequalities defined in the paper beginning

$$\theta_1 \in \left[0, \frac{\pi}{2}\right], \delta_1 \in \left[0, \frac{\pi}{2}\right), \delta_2 \in \left[0, \frac{\pi}{2}\right], a_w > 0, r_i > 0 \quad (i = 1, 2), \; a_i \geq 0 \; (i = 1, 2)$$

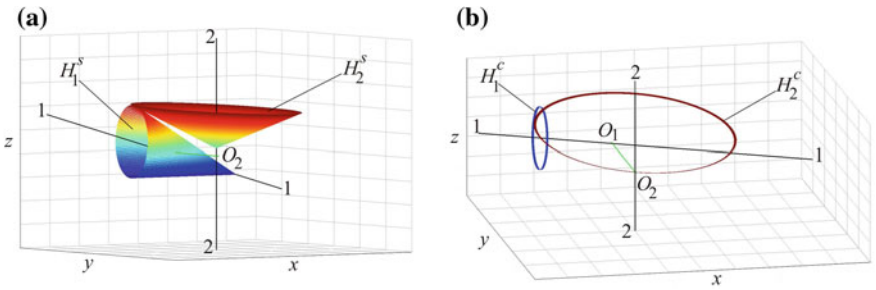

Fig. 13 Pitch configurations for non-orthogonal hyperboloid gears with conical pinion and gear when $\delta - \delta_1 = \frac{\pi}{2}$: **a** pitch surfaces $H_i^s (i = 1, 2)$; **b** pitch circles $H_i^c (i = 1, 2)$; $a_w = 100$ mm; $\delta = 95°$; $a_1 = 110$ mm; $\delta_1 = 5°$; $r_1 = 31$ mm; $a_2 = 40.10$ mm; $\delta_2 = 76°38'$, $r_2 = 143.17$ mm

impose the following restrictions on the free parameters:

If $a_w > r_1$, it is also necessary that $a_1 \geq (a_w - r_1)\tan\delta_1$.

If $a_w < r_1$ it is necessary that $a_1^2 \geq (r_1^2 - a_w^2)\tan^2\delta_1$.

- Let $\delta_1 + \delta = \dfrac{\pi}{2}$, i.e., $\delta = \dfrac{\pi}{2} - \delta_1$.

From the last relation, it immediately follows that $\delta \in \left(0, \dfrac{\pi}{2}\right)$. Then,

$$\cot\theta_2 = \frac{r_1 \sin\delta_1 + a_1 \cos\delta_1}{a_w}. \tag{19}$$

In this case, the set of Eq. (1) has the following two solutions:

$$\theta_1 = 0, \delta_2 = \frac{\pi}{2}, r_2 = \frac{a_w}{\sin\theta_2}, a_2 = r_1 \cos\delta_1 - a_1 \sin\delta_1 \tag{20}$$

which is possible if $a_1 \leq r_1 \cot\delta_1$;

$$\tan\frac{\theta_1}{2} = \frac{\cot\theta_2}{\sin\delta_1}, \delta_2 = \frac{\cos\delta_1 \sin\theta_1}{\sin\theta_2}, r_2 = \frac{a_w - r_1 \sin\theta_1}{\sin\theta_2}, \tag{21}$$

$$a_2 = r_1 \cos\theta_1 \sin\delta - a_1 \cos\delta$$

if the condition $a_1 \leq (a_w - r_1)\tan\delta_1$ is true.

The cases below differ only in regard to the conditions imposed upon the parameters $\delta, a_w, \delta_1, r_1$ and a_1 and the formula for the calculation of θ_1.

The remaining unknowns have been calculated by:

$$\begin{aligned} \cot\theta_2 &= \frac{(a_1 + r_1\tan\delta_1)\sin\delta}{a_w}, \\ \cos\delta_2 &= \frac{\cos\delta_1\sin\theta_1}{\sin\theta_2}, r_2 = \frac{a_w - r_1\sin\theta_1}{\sin\theta_2}, \\ a_2 &= r_1\cos\theta_1\sin\delta - a_1\cos\delta. \end{aligned} \tag{22}$$

Let us describe the cases mentioned:

- If $\delta < \frac{\pi}{2}, \delta_1 + \delta < \frac{\pi}{2}, a_w > r_1$, and $a_1 \le (a_w - r_1)\tan\delta_1$, then θ_1 is calculated by (11).
- If $\delta > \frac{\pi}{2}$, $\delta_1 > \delta - \frac{\pi}{2}$ and $a_1 \ge \max(0, (a_w - r_1)\tan\delta_1)$, then θ_1 is received using (13).
- If $\delta > \frac{\pi}{2}$, $\delta_1 > \delta - \frac{\pi}{2}$ and $a_1 \ge \max(0, (a_w - r_1)\tan\delta_1)$, then θ_1 is calculated by equality (13).
- If $\delta < \frac{\pi}{2}, \delta_1 + \delta > \frac{\pi}{2}, a_w > r_1, a_1 \le (a_w - r_1)\tan\delta_1$, and $(r_1\tan\delta_1 + a_1)^2 > a_w^2(\tan^2\delta_1 - \cot^2\delta)$, then θ_1 is determined by means of (11).

Another variant of the pitch surfaces and circles of non-orthogonal hyperboloid gears of type hypoid or Spiroid is shown in Fig. 14.

- If $\delta > \frac{\pi}{2}, \delta_1 > \delta - \frac{\pi}{2}, a_w > r_1, a_1 \le (a_w - r_1)\tan\delta_1$, and $(r_1\tan\delta_1 + a_1)^2 > a_w^2(\tan^2\delta_1 - \cot^2\delta)$, then θ_1 can be calculated by both (11) and (13).

The pitch configurations illustrated above (Figs. 5, 6, 7, 8, 9, 10, 11, 12, 13 and 14) are obtained from the developed computer program. The coordinate system $S(x, y, z)$, which is shown in all figures, is a basic one. According to it, the location of the coordinate systems S_1 and S_2 (in Figs. 3 and 4) of the corresponding pitch configurations H_i^s and $H_i^c (i = 1, 2)$ is fixed. In the program created, visualization of the coordinate systems S_1 and S_2 is not intended.

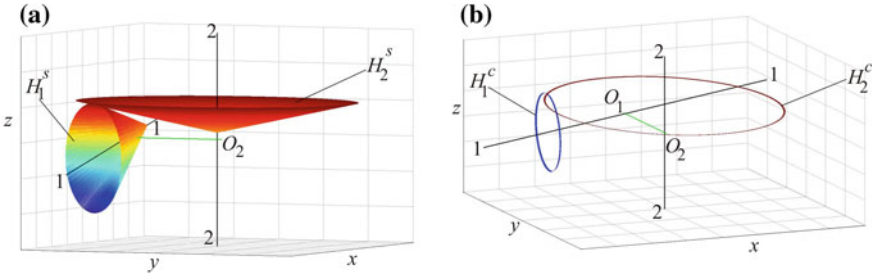

Fig. 14 Pitch configurations for non-orthogonal hyperboloid gears with conical pinion and gear when $\delta_1 + \delta > \frac{\pi}{2}$: **a** pitch surfaces $H_i^s (i = 1, 2)$; **b** pitch circles $H_i^c (i = 1, 2)$; $a_w = 100$ mm; $\delta = 85°$; $a_1 = 110$ mm; $\delta_1 = 10°$; $r_1 = 31$ mm; $a_2 = 21.20$ mm; $\delta_2 = 83°21'$, $r_2 = 148.77$ mm

4 Mathematical Model for Synthesis of Pitch Configurations of Hyperboloid Gears with External Meshing and Inverse Orientation of the Pitch Configurations

The study is performed by the notations and the coordinate frames $S_1(O_1, x_1, y_1, z_1)$ and $S_2(O_2, x_2, y_2, z_2)$ introduced in Fig. 15 [10]. The dimensions and mutual position of H_1^c and H_2^c are completely determined by the cylindrical coordinates $a_i, r_i, \theta_i (i = 1, 2)$ of the contact point P in the systems $S_i (i = 1, 2)$, and by the angle $\delta_i (i = 1, 2)$ between the plane of $H_i^c (i = 1, 2)$ and the normal $m - m$. The analogs of the pitch circles $H_i^c (i = 1, 2)$, which are the pitch surfaces (cones) $H_i^s (i = 1, 2)$

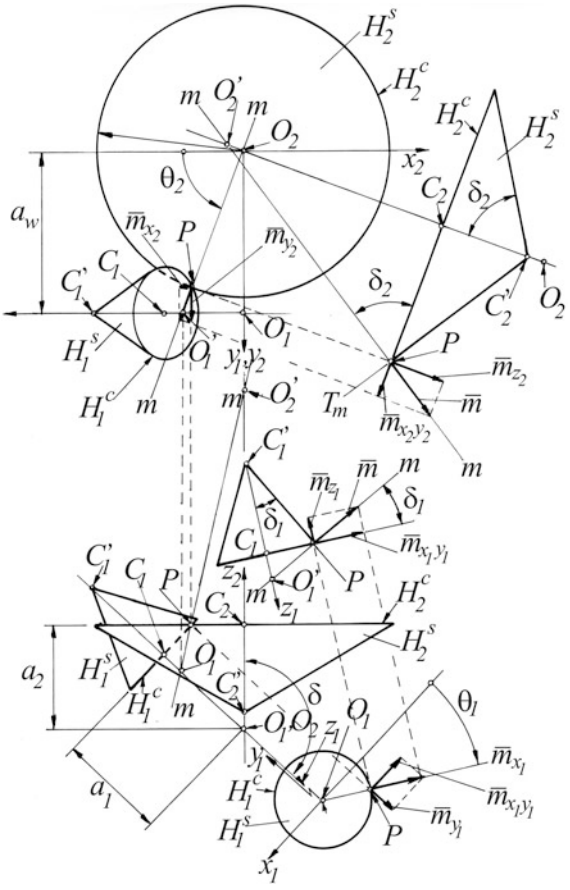

Fig. 15 Externally contacting pitch circles $H_i^c (i = 1, 2)$ and pitch surfaces $H_i^s (i = 1, 2)$ with inverse orientation corresponding to hyperboloid gears with external meshing

are illustrated in Fig. 2. The points of intersection $C_i'(i=1,2)$ of the axes of rotation $i-i(i=1,2)$ and the plane T_m are tips of the pitch cones $H_i^s(i=1,2)$.

Figure 15 is oriented to the synthesis of pitch configurations whose position in the fixed space ensures the design of one special group of non-orthogonal hyperboloid gears. There, the geometric pitch configurations, when they are with *inverse orientation* in the fixed space, can be seen. This type of pitch configurations is characteristic for special constructive types of non-orthogonal spatial gears, which allows for the optimal bearing of both gears from a strength point of view. The geometric characteristics: $\delta > \frac{\pi}{2}; z_{2,C_2} > 0; \angle\left(\overline{C_1C_1'}, \overline{O_1z_1}\right) = 180^\circ; \angle\left(\overline{C_2C_2'}, \overline{O_2z_2}\right) = 180^\circ$ are valid for this class of gears.

Representing the radius-vector $\overline{O_1P}$ and the unit vector $\overline{m}$ of the normal $m-m$ by a_1, r_1, θ_1 and a_2, r_2, θ_2, and using a_w and δ, we get to the following set of equations:

$$\begin{aligned}
&r_1\cos\theta_1 = r_2\cos\theta_2\cos\delta + a_2\sin\delta,\\
&r_1\sin\theta_1 = a_w - r_2\sin\theta_2,\\
&a_1 = r_2\cos\theta_2\sin\delta - a_2\cos\delta,\\
&\cos\delta_1\sin\theta_1 = \cos\delta_2\sin\theta_2,\\
&\sin\delta_1 = -(\sin\delta_2\cos\delta + \cos\delta_2\cos\theta_2\sin\delta),\\
&\cos\delta_1\cos\theta_1 = \sin\delta_2\sin\delta - \cos\delta_2\cos\theta_2\cos\delta.
\end{aligned} \tag{23}$$

We will examine (23), taking into account the following geometric conditions:

$$\theta_1 \in \left[0,\frac{\pi}{2}\right], \theta_2 \in \left(0,\frac{\pi}{2}\right], \delta_1 \in \left[0,\frac{\pi}{2}\right), \delta_2 \in \left[0,\frac{\pi}{2}\right], a_w > 0, r_i > 0, a_i \geq 0 \ (i=1,2).$$

Each of the last three equations in (23) is the consequence of the other two, i.e., (23) is a set of 5 independent equations with 10 unknowns: $\delta, a_w, \delta_1, r_1, a_1, \theta_1, \delta_2, r_2, a_2, \theta_2$. Therefore, each solution to (23) is a function of 5 of them (we will consider them as free ones). We suppose that the independent (free) parameters are $\delta_1, a_w, \delta_1, r_1$ and a_1. We will look for the analytical relations that have to be fulfilled so that the set (23) can have a solution.

4.1 *Synthesis of Non-orthogonally Contacting Pitch Configurations with Inverse Orientation*

After examining the set of Eq. (23), written in accordance with the symbols given in Fig. 15, the following three groups of solutions are established:

4.1.1 $\delta = \frac{\pi}{2} + \delta_1$

Then, the solution to (23) is of the form

$$\begin{gathered} \theta_1 = 0, \delta_2 > \frac{\pi}{2}, r_2 = \frac{a_w}{\sin\theta_2}, a_2 = r_1 \sin\delta - a_1 \cos\delta, \\ \cot\theta_2 = \frac{(a_1 - r_1 \tan\delta_1)\sin\delta}{a_w} = \frac{a_1 \cos\delta_1 - r_1 \sin\delta_1}{a_w}. \end{gathered} \tag{24}$$

The condition for the existence of solution (24) is $a_1 \geq r_1 \tan\delta_1$. This solution is illustrated in Fig. 16a.

4.1.2 $\delta > \frac{\pi}{2} + \delta_1$

In this case, the solution to (23) can be calculated by the formulae

$$\begin{aligned} \cot\theta_2 &= \frac{(a_1 - r_1 \tan\delta_1)\sin\delta}{a_w}, \\ \tan\frac{\theta_1}{2} &= \frac{\cos\delta_1 \cot\theta_2 - \sqrt{D}}{\cos(\delta + \delta_1)}, \\ a_2 &= r_1 \cos\theta_1 \sin\delta - a_1 \cos\delta, \\ \cos\delta_2 &= \frac{\cos\delta_1 \sin\theta_1}{\sin\theta_2}, r_2 = \frac{a_w - r_1 \sin\theta_1}{\sin\theta_2}, \end{aligned} \tag{25}$$

where $D = \frac{\cos^2\delta_1 \sin^2\delta}{a_w^2}\left[(a_1 - r_1\tan\delta_1)^2 + a_w^2\left(\cot^2\delta - \tan\delta_1\right)\right]$.

The condition for the existence of solution (25) is $a_1 \geq r_1 \tan\delta_1$. This solution is illustrated in Fig. 16b.

4.1.3 $\delta > \frac{\pi}{2}, \delta_1 = 0$

Now, the solution to the set of Eq. (23) for the case of pitch configurations with inverse orientation is

$$\begin{aligned} \cot\theta_2 &= \frac{a_1 \sin\delta}{a_w}, \tan\delta_2 = -\cos\theta_2 \tan\delta, \\ \tan\frac{\theta_1}{2} &= \frac{\cot\theta_2 - \sqrt{D}}{\cos\delta}, a_2 = r_1 \cos\theta_1 \sin\delta - a_1 \cos\delta, \\ r_2 &= \frac{a_w - r_1 \sin\theta_1}{\sin\theta_2}, \end{aligned} \tag{26}$$

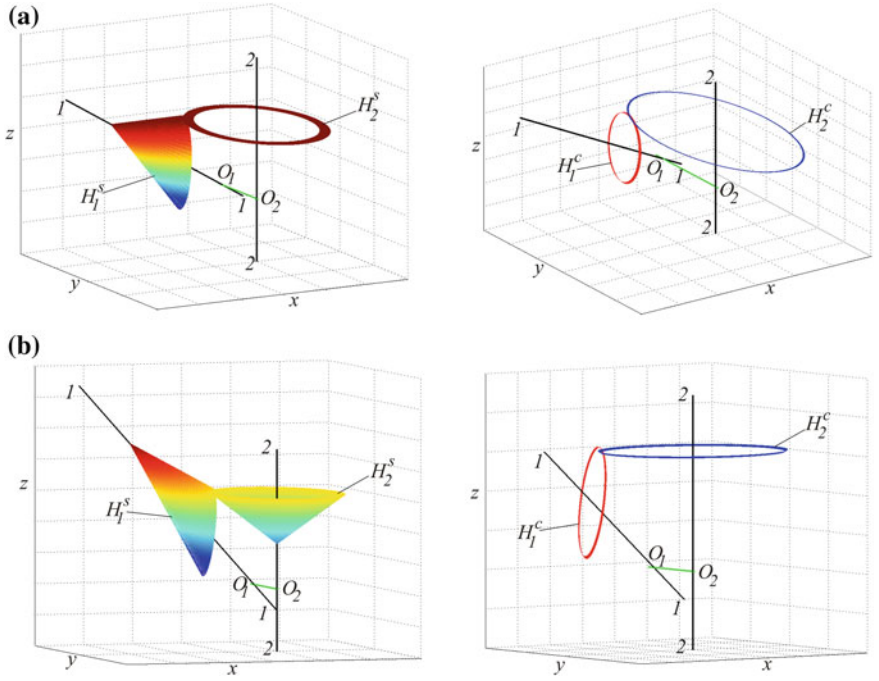

Fig. 16 Pitch configurations with inverse orientation when H_1^s is a rotation cone: **a** H_2^s is a disc, $a_w = 100\,\text{mm}, \delta = 100^\circ, a_1 = 100\,\text{mm}, \delta_1 = 10^\circ, r_1 = 30\,\text{mm}, \delta_2 = 90^\circ, r_2 = 136.75\,\text{mm}, \ a_2 = 46.91\,\text{mm}$; **b** H_2^s is a rotation cone, $a_w = 100\,\text{mm}, \delta = 110^\circ, a_1 = 100\,\text{mm}, \delta_1 = 10^\circ, r_1 = 30\,\text{mm}, \delta_2 = 75^\circ 25', \ r_2 = 126.20\,\text{mm}, a_2 = 61.87\,\text{mm}$

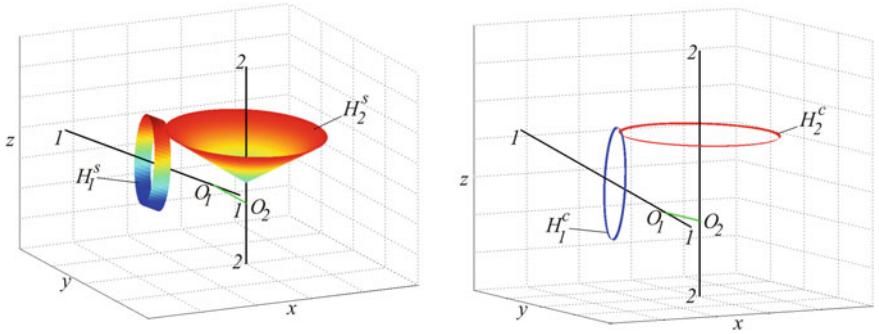

Fig. 17 Pitch configurations with inverse orientation when H_1^s is a rotation cylinder and H_2^s is a rotation cone, $a_w = 100\,\text{mm}, \delta = 100^\circ, a_1 = 100\,\text{mm}, \delta_1 = 10^\circ, r_1 = 30\,\text{mm}, \ \delta_2 = 75^\circ 54', \ r_2 = 129.55\,\text{mm}, a_2 = 45.92\,\text{mm}$

where $D = \cot^2 \theta_2 + \cos^2 \delta$.

The pitch configurations, shown in Fig. 17, are visualized using algorithm (26).

5 Conclusions

Considering one contact point P, which belongs to the conjugate tooth surfaces Σ_1 and Σ_2 as a common point of the geometric pitch circles H_1^c and H_2^c, makes it possible to understand the approaches applied to the construction of mathematical models for synthesis of hyperboloid gears with both externally and internally meshing. In this context, it is essential to remind that the geometric pitch circles are used to define the longitudinal orientation of the tooth surfaces $\Sigma_i (i = 1, 2)$ contacting at P. It has to be pointed once more that these circles can be elements from the coaxial reference, root and tip surfaces. The surfaces, including the geometric pitch circles, are called geometric pitch configurations or simply pitch configurations. The pairs of geometric pitch circles and the pairs of geometric pitch surfaces form the set of geometric pitch configurations. The reference surfaces of the gears are often used as pitch surfaces in the practice of the synthesis of hyperboloid gears. It is possible that one of the pitch surfaces coincides with the tip surfaces of one of the gears. Then, the other pitch surface is an envelope of the first one, and includes the second geometric pitch circle.

In conclusion, one and the same pair of pitch configurations can stay in the base of the synthesis of different spatial gears with crossed axes of rotations, from the viewpoints of both the form of the corresponding geometric pitch surfaces and the realized law of rotations transformation.

The defined and synthesized geometric pitch configurations are basic primitives of the worked out mathematical models oriented to the synthesis and design of spatial gears with crossed axes of rotation.

The presented mathematical model for synthesis of inverse oriented geometric pitch configurations of non-orthogonal hyperboloid gears continues the part of this study that treats normally oriented pitch surfaces and circles related to the same class of mechanisms. The presented algorithms and conditions for their existence are a basic element from the process of design of non-orthogonal gear transmissions with crossed axes. The non-orthogonal character of the structure of these gears, together with the special orientation of their pitch configurations, creates conditions for synthesis of spatial gear mechanisms with innovated qualities.

References

1. Phillips, J.: Freedom in Machinery, Vol. 2 Screw Theory Exemplified. Cambridge University Press, Cambridge (1990)
2. Phillips, J.: General Spatial Involute Gearing. Springer, Berlin (2003)

3. Figliolini, G., Angeles, J.: The synthesis of the pitch surfaces of internal and external skew-gears and their rack. ASME J. Mech. Des. **128**(4), 794–802 (2006)
4. Figliolini, G., Stachel, H., Angeles, J.: A new look at the Ball-Disteli diagram and it relevance to spatial gearing. Mech. Mach. Theor. **42**(10), 1362–1375 (2007)
5. Dooner, D.: Kinematic Geometry of Gearing. Wiley, USA (2012)
6. Abadjiev, V.: Gearing theory and technical applications of hyperboloid mechanisms. Sc. D. thesis, Institute of Mechanics—BAS, Sofia (2007) (in Bulgarian)
7. Abadjiev, V.: On the helical tooth flanks synthesis of skew-axes gear pairs. Mech. Mach. Theor. **36**, 1135–1146 (2001)
8. Abadjiev, V.: Mathematical modelling for synthesis of spatial gears. Proc. Inst. Mech. Eng. Part E J. Process Mech. Eng. **216**, 31–46 (2002)
9. Abadjiev, V., Abadjieva, E., Petrova, D.: Pitch configurations: definitions, analytical and computer synthesis. In: Proceedings of ASME 2011 International Power Transmissions and Gearing Conference, IDETC/CIE 2011, Washington DC, USA (2011) (published on CD)
10. Abadjiev, V., Abadjieva, E., Petrova, D.: Non-orthogonal hyperboloid gears. Synthesis and visualization of pitch configurations with inverse orientation. Compt. Rend. Acad. Bulg. Sci. **64**(8), 1171–1178 (2011)
11. Abadjiev, V., Abadjieva, E., Petrova, D.: Non-orthogonal hyperboloid gears. Synthesis and visualization of pitch configurations with normal orientation, Compt. Rend. Acad. Bulg. Sci. **64**(9), 1311–1319 (2011)
12. Abadjiev, V., Abadjieva, E., Petrova, D.: Synthesis of hyperboloid gear set based on the pitch point approach. Mech. Mach. Theor. **55**, 51–66 (2012)
13. Litvin, F.: Theory of Gearing. In: Nauka (ed.) Moscow (1968) (in Russian)
14. Litvin, F.: Theory of Gearing, NASA Reference Publication 1212, AVSCOM Technical Report 88-C-035, US Government Printing Office, Washington (1989)
15. Litvin, F.: Gearing Geometry and Applied Theory. PTR Prentice Hall, A Paramount Communication Company, Englewood Eliffs, New Jersey 07632 (1994)
16. Litvin, F., Fuentes, A.: Gearing Geometry and Applied Theory. 2nd edn. Cambridge University Press, Cambridge (2004)
17. Nelson, W.: Spiroid Gearing. Part 1—Basic Design Practices, Machine Design. pp. 136–144 (1961)
18. Dudley, D.: Gear Handbook. The Design, Manufacturing, and Application of the Gears. Mcgraw-Hill Book Company Inc., New-York (1962)

Load Distribution in Meshing of Planetary Gearwheels and Its Influence on the Technical and Economic Performance of the Mechanism

F. Plekhanov, V. Goldfarb and E. Vychuzhanina

Abstract The paper presents a method for determination of the laws of load distribution in meshing of gearwheels for a multi-satellite planetary gear. The influence of layout features of the mechanism, its parameters and manufacture errors on compliance of elements, factors of non-uniform load distribution and technical and economic performance is established.

Keywords Planetary gears · Compliance · Load distribution

1 Introduction

Multi-satellite planetary gears are commonly used in mechanical engineering due to their capacity for a number of types of distinctive technical and economic performance: high load carrying capacity at small overall dimensions and mass, low friction power losses, satisfactory vibroacoustic characteristics [1–3]. These gears are most effectively applied in aerospace engineering, transport and hoisting machines, robotics, mechatronic systems, etc.; essentially, any field in which the above-mentioned features prevail in the choice of the type of mechanical drive.

In order to eliminate excessive links and equalize the load in meshing of planetary gearwheels, satellites are usually arranged on spherical bearings, with the sun pinion being placed on the gear clutch. However, such a layout allows for the complete elimination of excessive links only in the case of a three-satellite version. In practice, planetary gears with a greater number of satellites are applied. Inevitable manufacture errors cause non-uniform load distribution in power flows, even in the presence of "floating" and self-aligning elements. In order to provide the workability of a drive in a case of its limited radial dimension, it is necessary to mount each satellite on two bearings, or to produce a multi-row gear [4] which causes non-uniform load distribution along tooth length or rows of satellites. Strain

F. Plekhanov (✉) · V. Goldfarb · E. Vychuzhanina
Kalashnikov Izhevsk State University, Izhevsk, Russia
e-mail: fplehanov@list.ru

V. Goldfarb et al. (eds.), *Advanced Gear Engineering*,
Mechanisms and Machine Science 51, DOI 10.1007/978-3-319-60399-5_6

of individual elements of the mechanism partially compensates for errors in its manufacture which can be used in load equalizing in meshing of gears, increasing the load carrying capacity of the drive and reducing its overall dimensions and mass. In this connection, it is important to establish the influence of manufacture error of a gear, its layout features and the compliance of elements in the technical and economic performance of the drive.

2 Distribution of Load and Bending Stresses by the Length of Gearwheel Teeth

In the presence of excessive links obstructing the self-alignment of satellites, manufacture errors of a planetary gear and deformation of its sun pinion cause the non-uniform distribution of load and bending stresses at the tooth root along its length (Fig. 1). In this case, factors of initial (not accounting for tooth running-in ability) non-uniform distribution of load and bending stresses differ from each other.

Laws of variation of the unit load $W(x)$ and the bending moment $M(x)$ caused by action of the load and its corresponding normal stresses at the root of a straight tooth of the gearwheel can be established according to equations of displacement compatibility written with consideration of tooth torsion relative to the longitudinal axis and its distortion due to deformation of gear elements (the equations are written for the direction of initial mismatch unfavorable in regard to load distribution and when teeth come into contact in their middle part) (Fig. 2):

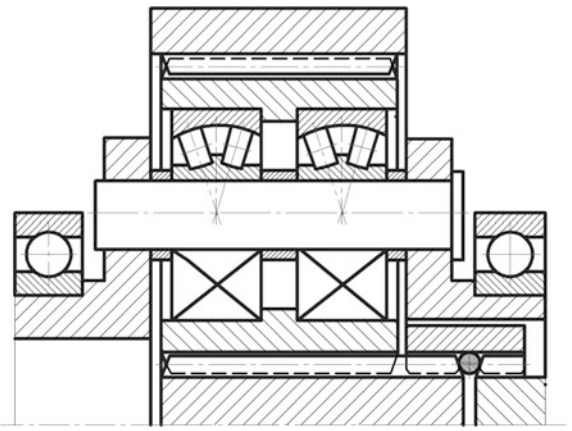

Fig. 1 Planetary gear with non-self-aligning satellites

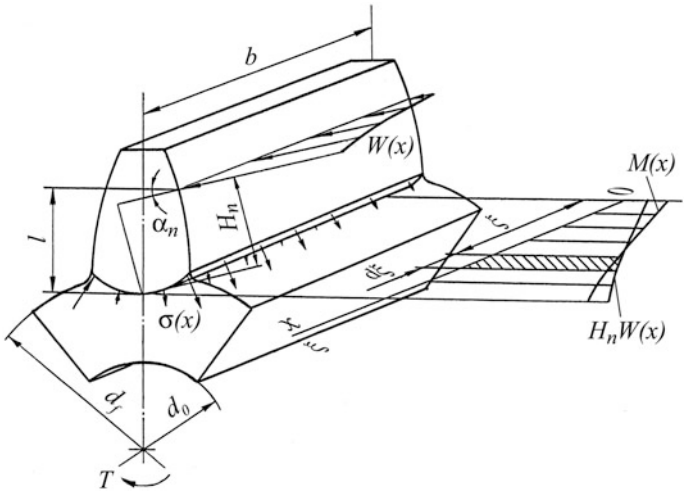

Fig. 2 Element of the sun pinion and diagrams of loads acting on it

$$0.5x[\gamma - (\gamma_0 + \gamma_H)\cos\alpha_W] + 0.5\varphi(x)r_b - \frac{W(x) - W(0)}{C_W} = \frac{H_n}{I_K G}\int_0^x [M(x) - H_n W(\xi)](x - \xi)d\xi, \tag{1}$$

$$0.5x[\gamma - (\gamma_0 + \gamma_H)\cos\alpha_W] + 0.5\varphi(x)r_b - \frac{W(x) - W(0)}{C_W} = \frac{M(x) - M(0)}{H_n C_M} \tag{2}$$

where $\varphi(x)$ is the angle of sun pinion torsion at an arbitrary cross-section with respect to the face end,

$$\varphi(x) = \frac{r_b n_W}{I_P G}\int_0^x W(\xi)(x - \xi)d\xi,$$

γ is the angle of the initial mismatch of teeth in the plane of meshing, γ_0 is the angle of misalignment caused by deformation of the axis and satellite supports, γ_H is the angle of misalignment of the satellite axis caused by deformation of the carrier,α_W is the pressure angle, r_b is the base radius of the sun pinion, H_n is the arm of a force acting on the tooth with respect to the centre of its bending, G is the shear modulus, I_K is the moment of inertia of the lateral section of the tooth (determined according to the approximated relation written for a rectangular section with the width equal to tooth thickness in its middle part and the height equal to its height: $I_K = 0.19HS^3$, where $H = 2.25m$, $S = 0.5\pi m$, m is the module of meshing), n_W is the number of power flows, I_P is the polar moment of inertia of the cross-section for the sun

pinion, C_M is the specific rigidity of the tooth when it is deformed under the action of the bending moment (determined with regard to compliance of a part of the rim adjoining the teeth), and C_W is the specific rigidity of the pinion tooth under its contact deformation, shear and compression deformation,

$$\frac{1}{C_W} = \frac{1}{C_t} - \frac{1}{C_M},$$

where $\frac{1}{C_t}$ is the total specific compliance of the tooth with regard to one half of the contact compliance of the meshing.

Components of rigidity and its reverse value (compliance) are determined through methods of construction mechanics, elasticity theory and experimentalism [1, 5, 6].

In order to obtain analytical relations, let us solve the stated task in parts, having first considered the laws of distribution of the load and bending stresses for rigid elements of the gear, only taking into account the initial mismatch of teeth and their compliance. In this case, expressions (1) and (2) can be represented as a Volterra integral equation

$$W(x) = \lambda^2 \int_0^x W(\xi)(x-\xi)d\xi + F(x), \tag{3}$$

where

$$F(x) = W(0) + 0.5\gamma x C_W + 0.5(\lambda x)^2 \left[0.5\gamma C_t \left(\frac{b}{2} - \frac{x}{3}\right) - W\right],$$
$$\lambda^2 = \frac{H_n^2(C_W + C_M)}{GI_K}.$$

Let us write Eq. (3) in operator form:

$$L[W(x)] = \omega(p) = \frac{p^2 f(p)}{p^2 - \lambda^2}. \tag{4}$$

Turning to the original equation, and transforming the obtained expression with regard to statics, we obtain

$$W(x) = W + \frac{\gamma b C_\Sigma}{2}\left[\frac{2x}{b} - 1 + \frac{2C_W}{\lambda b C_M}\left(sh\lambda x + \frac{1 - ch\lambda b}{sh\lambda b} ch\lambda x\right)\right], \tag{5}$$

$$\frac{M(x)}{H_n} = W + \frac{\gamma b C_\Sigma}{2}\left[\frac{2x}{b} - 1 - \frac{2}{\lambda b}\left(sh\lambda x + \frac{1 - ch\lambda b}{sh\lambda b} ch\lambda x\right)\right]. \tag{6}$$

Here, W is the average unit load in the meshing; b is the tooth length equal to the working width of the rim b_W; and C_Σ is the specific rigidity of the meshing in the absence of a mismatch ($C_\Sigma = 0.5C_t = 0.075E$ [1], E being the Young modulus).

When the load is applied to the tooth at the middle part of its height, the following approximated values of components of Eqs. (5) and (6) will be obtained: $C_W/C_M = 0.5,\ \lambda = 1/m$. Then, the maximum values of the unit load and the moment and corresponding initial factors of non-uniformity are equal to

$$K_W = \frac{W(b)}{W} = 1 + \frac{\gamma b}{2W} C_H(b) = 1 + \frac{\gamma b}{2W} C_\Sigma \left[1 + \frac{m\left(e^{b/m} - 1\right)}{b\left(e^{b/m} + 1\right)}\right], \tag{7}$$

$$K_m = \frac{W(b)}{WH_n} = 1 + \frac{\gamma b}{2W} C_F(b) = 1 + \frac{\gamma b}{2W} C_\Sigma \left[1 - \frac{2m\left(e^{b/m} - 1\right)}{b\left(e^{b/m} + 1\right)}\right]. \tag{8}$$

Figure 3 shows the diagrams of dependences of $W(X) = W(x/b)/W$ and $M(X) = M(x/b)/H_n W$ on the parameter $X = x/b$ for a relative angle of the initial mismatch $\Gamma = E\gamma b/W = 20$ and tooth length $b = 18m$. Figure 4 shows the same dependences for $b = 5m$. Figure 5 presents the dependences of K_W and K_m on Γ.

The most unfavorable case with regard to load distribution along the length of the gearwheel teeth is the case when angles of initial mismatch γ of the teeth at external and internal meshing have opposite signs, and the carrier is fixed. Then, equations for determining the unit loads and bending moment can be presented as follows:

$$W(x) = W(0) + f(x)C_H(b), \tag{9}$$

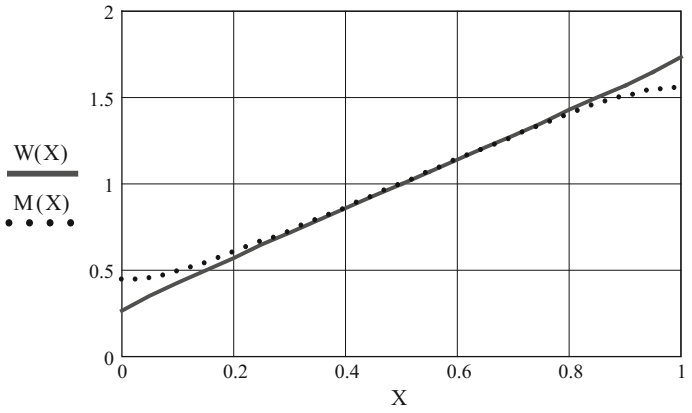

Fig. 3 Distribution of relative load and bending stresses along the gearwheel tooth length for fixed elements of the gear, $\Gamma = 20$, $b = 18m$

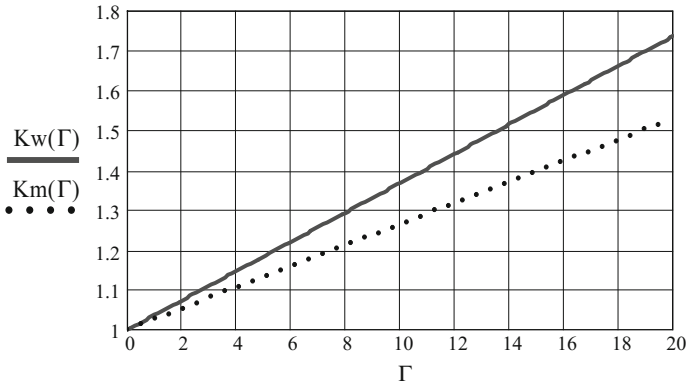

Fig. 4 Distribution of the relative load and stresses along the length of the gearwheel tooth for fixed elements of the gear

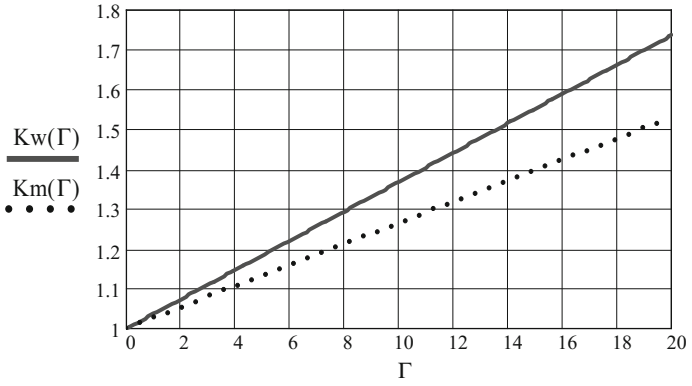

Fig. 5 Factors of non-uniform distribution of load and bending stresses of the tooth versus the relative angle of initial mismatch for fixed elements of the gear and $b = 18m$

$$\frac{M(x)}{H_n} = \frac{M(0)}{H_n} + f(x)C_F(b), \tag{10}$$

where the function of mismatch of the teeth with consideration of torsion of the sun pinion when the torque is transmitted from its face end is

$$f(x) = \gamma x + \frac{r_b^2 n_w}{I_p G} \int_n^x W(\xi)(x - \xi)d\xi. \tag{11}$$

Let us determine the unit load *W(x)* at external meshing of the gear by substituting Eq. (11) for Eq. (9) and differentiating the obtained expression twice:

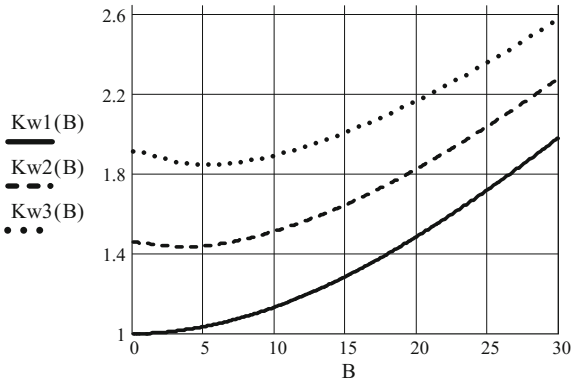

Fig. 6 Factor of non-uniform load distribution along the tooth length for a sun pinion versus *G* and *B*. *Subscripts 1* for Γ = 0; *2* for Γ = 10; *3* for Γ = 20

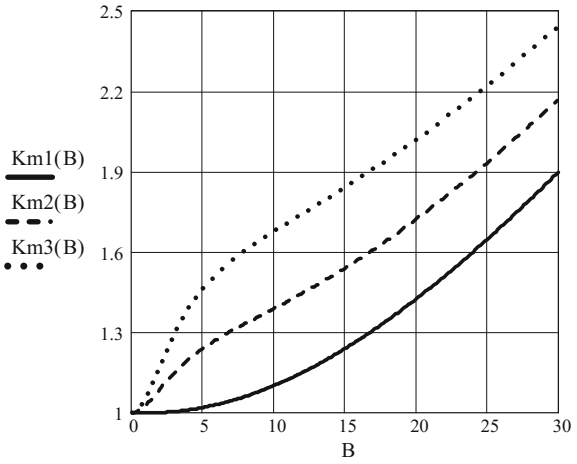

Fig. 7 Factor of non-uniform stress distribution along the tooth length for a sun pinion versus Γ and *B*. *Subscripts 1* for Γ = 0; *2* for Γ = 10; *3* for Γ = 20

$$W''(x) - \frac{r_b^2 n_W C_H(b)}{I_p G} = W''(x) - \mu^2 W(x) = 0. \tag{12}$$

Taking into account the equations $\int_0^b W(x)dx = Wb$ and $W'(0) = \gamma C_H(b)$, the solution to this equation will be as follows:

$$W(x) = \frac{\gamma}{\mu} C_H(b) sh\mu x + \left[W\mu b - \frac{\gamma C_H(b)}{\mu}(ch\mu b - 1) \right] \frac{ch\mu x}{sh\mu b}. \tag{13}$$

Then, applying Eqs. (9), (10) and the equations of statics, we determine

$$\frac{M(x)}{H_n} = W + \frac{C_F(b)}{C_H(b)}[W(x) - W]. \tag{14}$$

Figures 6 and 7 represent diagrams of dependences of non-uniformity factors K_W, K_m on G and $B = b/m$ for a fixed layout of the carrier and the number of teeth of the sun pinion $z = 18$, $n_W = 3$, $d_0 = 0$. Diagrams are plotted according to expressions (13) and (14) and allow for evaluating the pointed strength performances of a multi-satellite planetary gear.

3 Influence of the Compliance of Planetary Gear Elements on Load Distribution Among Satellites

One of the simplest and most efficient layouts of a multi-satellite planetary gear is the gear comprising axes as cantilevers in the carrier jaw, the axes containing spherical bearings and two central gearwheels (Fig. 8). Compliance of cantilever axes and bearings of satellites provides load equalization in meshing of gearwheels, and at corresponding parameters, it can lead to close to uniform load distribution, even in the absence of mechanisms of self-alignment for elements of a planetary gear.

In this connection, it is important to determine the compliance of the axis and the parts in contact with it and to establish the level of its influence on the value of the factor of non-uniform load distribution in meshing of gearwheels.

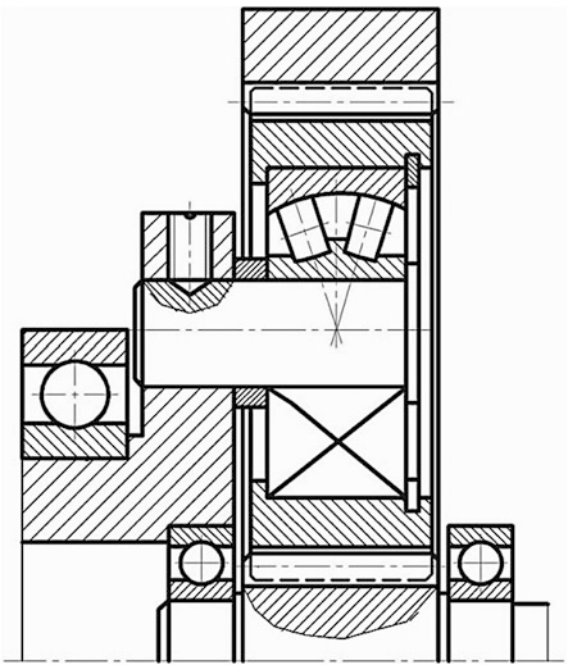

Fig. 8 Planetary gear with cantilever axes of self-aligning satellites

Accounting for distortion of the satellite axis under the action of the force applied to it and increased compliance of the inner ring of the bearing at its face ends, the load on the axis from the bearing side can be presented by the equation (Fig. 9):

$$q(x) = q_m \sin\left(\frac{\pi x}{l}\right) = \frac{\pi P}{2l} \sin\left(\frac{\pi x}{l}\right), \tag{15}$$

where q_m is the maximum value of the unit load.

Then, deflection of a steel axis in the middle part of the area of contact with the bearing ring caused by action of the bending moment and lateral force and determined by known Mohr's formulas will be

$$y_0 = \frac{Pl^3}{IE}\left(\frac{5}{96} - \frac{0.5\pi - 1}{2\pi^3}\right) + \frac{1.11Pl}{SG}\left(0.25 + \frac{0.5}{\pi}\right), \tag{16}$$

where d is the diameter of the satellite axis, I is the axial moment of inertia of its cross-section, S is the area of the lateral cross-section of the axis, and E and G are elasticity moduli of the 1st and 2nd types, respectively.

Let us represent the equation of the deformed axis in the area of its contact with the carrier jaw as follows (see Fig. 9):

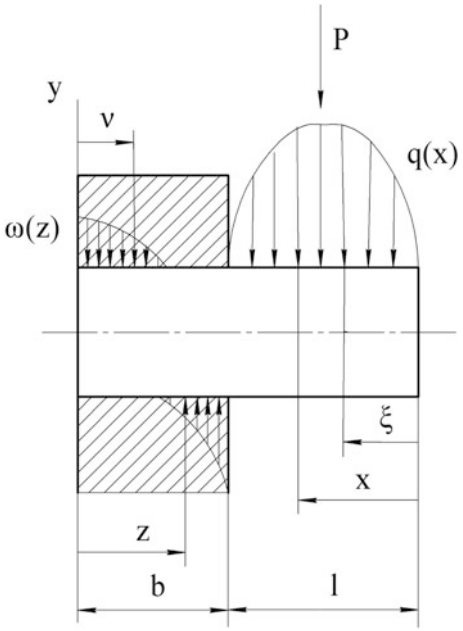

Fig. 9 Loading scheme for cantilever axis of the satellite and the carrier jaw

$$\frac{1}{C_H}\frac{d^2\omega(z)}{dz^2} = \frac{d^2y(z)}{dz^2} = \frac{M(z)}{IE} + 1.11\frac{\omega(z)}{SG}. \tag{17}$$

Here, C_H is the specific contact rigidity of the joint determined experimentally ($C_H \cong E/1.2$ [4]), $M(z) = -\int_0^z \omega(v)(z-v)dv$.

After double differentiation of the equality (17), we obtain

$$\frac{d^4\omega(z)}{dz^4} - \frac{1.11C_H}{SG}\frac{d^2\omega(z)}{dz^2} + \frac{C_H}{IE}\omega(z) = 0, \tag{18}$$

hence,

$$\begin{aligned}\omega(z) = {} & C_1 sh(\alpha z/b)\sin(\beta z/b) + C_2 ch(\alpha z/b)\sin(\beta z/b) \\ & + C_3 sh(\alpha z/b)\cos(\beta z/b) + C_4 ch(\alpha z/b)\cos(\beta z/b),\end{aligned} \tag{19}$$

$$\alpha = b\sqrt{4\frac{C_H}{IE}}\cos\left[0.5\ \arccos\left(\frac{\sqrt{IEC_H}}{1.8FG}\right)\right]$$

$$\beta = b\sqrt{4\frac{C_H}{IE}}\sin\left[0.5\ \arccos\left(\frac{\sqrt{IEC_H}}{1.8FG}\right)\right]$$

In order to determine constants of integration $C_1 \div C_4$, we apply the following boundary conditions and equations of statics:

$$\int_0^b \omega(z)dz = -P;\ \int_0^b \omega(z)(b-z)dz = 0.5Pl;$$

$$\text{for } z = 0\ \frac{d^2\omega(z)}{dz^2} = \frac{1.11C_H}{SG}\omega(z);$$

$$\text{for } z = b\ \frac{d^2\omega(z)}{dz^2} = \frac{-0.5C_H Pl}{IE} + \frac{1.11C_H}{SG}\omega(z).$$

Displacement of the axis in the area of the bearing mounting caused by compliance of the "axis—carrier jaw" contact is

$$\begin{aligned}y_h = {} & \frac{1.2}{E}\left[\omega(z) + \frac{l}{2}\frac{d\omega(z)}{dz}\right]_{Z=b} = \frac{1.2}{E}\{sh\alpha\ \sin\beta[C_1 + 0.5\frac{l}{b}(C_2\alpha \\ & - C_3\beta)] + ch\alpha\ \cos\beta[C_4 + 0.5\frac{l}{b}(C_2\beta + C_3\alpha)] + sh\alpha\ \cos\beta[C_3 \\ & + 0.5\frac{l}{b}(C_1\beta + C_4\alpha)] + ch\alpha\ \sin\beta[C_2 + 0.5\frac{l}{b}(C_1\alpha - C_4\beta)]\}\end{aligned} \tag{20}$$

Correctness of analytical determination of the axis compliance accounting for the deformability of the carrier jaw is proved by SolidWorks finite-element analysis of the mode of deformation of the "satellite axis—carrier jaw" contact. Figure 10 shows the mode of deformation of the carrier jaw for $P = 10000\,N$, $d = 20$ mm, $b = 10$ mm.

In order to determine the factor of non-uniformity of load distribution for satellites, we apply equations of displacement compatibility accounting for the deformation of axes and parts in contact with them (carrier jaw, rolling bearings) along with gear manufacture and assembly errors:

$$\left.\begin{aligned} F_1 = \frac{P_1}{2\cos\alpha_W} = b_W C_\Sigma[\varepsilon - \delta_1 - (y_1 + y_{B1})\cos\alpha_W], \\ \cdots, \\ F_i = \frac{P_i}{2\cos\alpha_W} = b_W C_\Sigma[\varepsilon - \delta_i - (y_i + y_{Bi})\cos\alpha_W], \\ \cdots, \\ F_N = \frac{P_N}{2\cos\alpha_W} = b_W C_\Sigma[\varepsilon - \delta_N - (y_N + y_{BN})\cos\alpha_W], \\ \sum_{i+1}^{N} F_i = b_W \sum_{i=1}^{N} W_i = NWb_W, \end{aligned}\right\} \quad (21)$$

where F_i is the normal force in meshing of the ith satellite with central gearwheels; P_i is the load acting on the ith axis from the side of the bearing ring; W_i is the unit load in meshing of the ith satellite with the stationary gearwheel and pinion; W is the average unit load in meshing of satellites with sun pinions; N is the number of satellites; α_W is the pressure angle (this system of equations corresponds to the equality of angles for internal and external meshing); C_Σ is the specific rigidity of a single-pair meshing ($C_\Sigma = 0.075E$); δ_i is the initial mismatch of teeth (clearance) in meshing of the ith satellite with gearwheels caused by errors of tangential

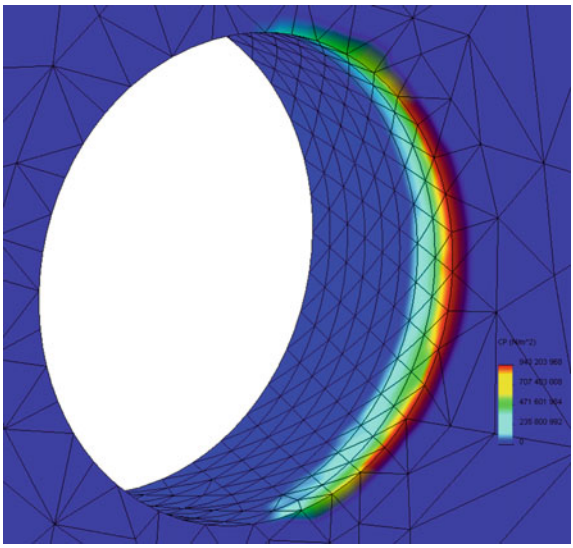

Fig. 10 Computer-aided model of the carrier jaw

arrangement of the axes and pitch of teeth (the clearance in the internal meshing is equal to the clearance in the external one); b_W is the working face width of the satellite; y_i is the displacement of the ith axis at the area of bearing mounting caused by the axis bending, deformation of the carrier jaw and contact deformation of the "axis—bearing ring" contact ($y_i = y_{0i} + y_{hi} + 0.5\pi q_i / C_H$, where q_i is the average unit load acting on the axis of the ith satellite); $\varepsilon = const$; and y_{Bi} is the displacement of the ith satellite caused by the compliance of the rolling bearing (accounting for variation of the bearing compliance within a wide range depending on the load; let us assign its approximate value as $y_{Bi} \cong \frac{5q_i}{E}$).

The initial mismatch of teeth in meshing of gearwheels with the most loaded satellite is absent ($\delta_1 = 0$). Then, knowing the values δ_i, corresponding to the degree of accuracy of gear manufacture, we use Eq. (21) and determine the values F_i, ε and the factor on non-uniform load distribution for power flows $K = F_{\max}/F = W_{\max}/W$.

Figure 11 represents the diagram of dependence of the factor of non-uniform load distribution for satellites of the gear with excessive links (see Fig. 8) on $\Delta = \delta E/W = b_W \delta E/F$ and $\overline{b} = b/l$ for $N = 3$, $\alpha_W = 20^0$, $l = d$, $b_W = l$, $\delta_2 = \delta_3 = \delta$ (the most unfavorable case with regard to load distribution).

According to the analysis performed and the diagrams plotted thereafter, the compliance of cantilever axes leads to considerable reduction of non-uniform load distribution for satellites. But for a small ratio of the carrier jaw thickness to the axis diameter and cantilever length, it is possible to go beyond allowable values (see Fig. 10) of stresses in the area of the "axis—carrier jaw" contact. It is also feasible to reduce the negative influence of manufacture errors for planetary gears on load distribution in meshing of gearwheels by applying satellites with complaint rims;

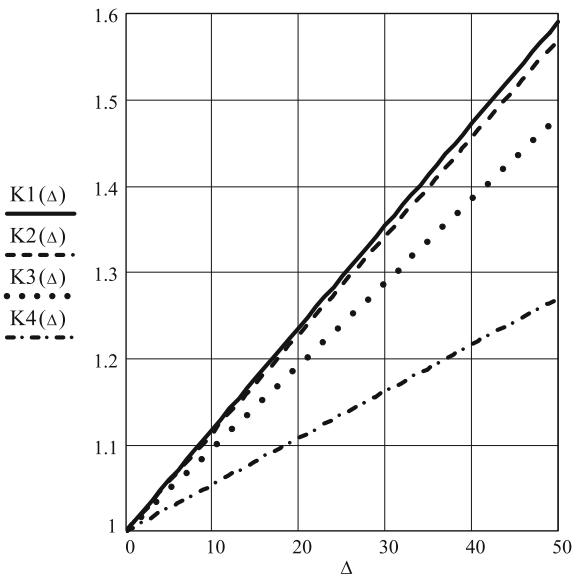

Fig. 11 Factor of non-uniform load distribution for three satellites versus the value of relative initial mismatch of teeth. *Subscripts 1* for $\overline{b} = 2$; *2* for $\overline{b} = 1.5$; *3* for $\overline{b} = 1$; *4* for $\overline{b} = 0.6$

however, the bending strength of this rim can become the limiting factor for the load-carrying capacity of the gear and negatively influence its lifetime.

As for load distribution in meshing of gearwheels and the load-carrying capacity of a mechanical drive, the planetary gear with the "floating" sun pinion, the fixed rigid carrier and single-rim self-aligning satellites mounted on spherical bearings (Fig. 12) is the most efficient. The compliance of this double-support axis of the satellite is determined according to the design scheme shown in Fig. 13, where b is the width of the carrier jaw, l is the half width of the bearing ring for the satellite, and L is the half length of the span between the jaws of the carrier.

The unit load in the area of contact of the satellite axis and carrier jaw $\omega(z)$ is determined through Euler's method according to the expression (19), and in the area of bearing mounting on the axis, according to the formula

$$q(x) = C_5 sh(\alpha x)\sin(\beta x) + C_6 ch(\alpha x)\cos(\beta x). \tag{22}$$

Constants of integration $C_1 \div C_6$, which are components of Eqs. (19) and (22), are determined according to statics equations and boundary conditions:

(1) $\int_0^l q(x)dx = 0.5P = F\cos\alpha_W$;

(2) $\int_0^b \omega(z)dz = 0.5P$;

(3) for $z = b$ $M(z) = 0$, and according to the equation of the deflected axis

$$\omega^{//}(b) = 1.11\frac{C_H\omega(b)}{SG};$$

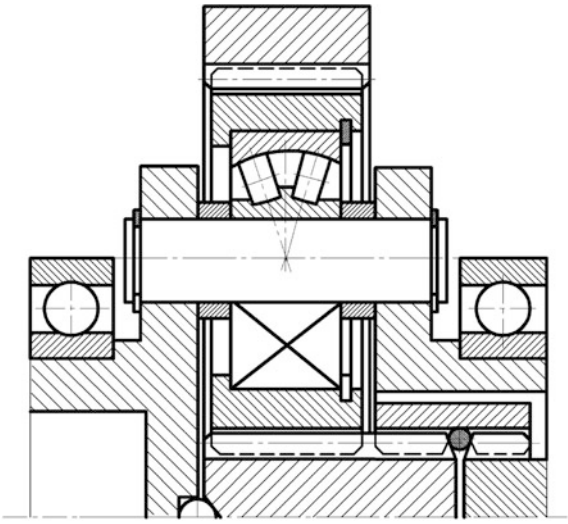

Fig. 12 Planetary gear with self-aligning satellites and a "floating" sun pinion

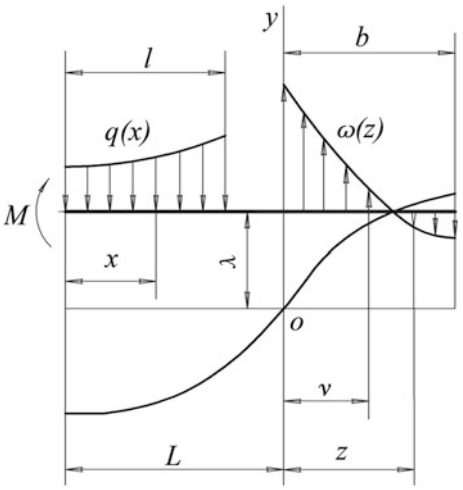

Fig. 13 Design scheme with double-support axis of the satellite

(4) for $z = 0$ $M(z) = M(0) = \int_0^b \omega(z) z dz = IE\left[1.11\frac{\omega(0)}{SG} - \frac{\omega^{//}(0)}{C_H}\right]$;

(5) bending moments at segments for $z = 0$ and $x = l$ are inter-connected by the equation

$$M(l) = IE\left[\frac{q^{//}(l)}{C_H} - 1.11\frac{q(l)}{SG}\right] = 0.5P(L-l) + M(0);$$

(6) inter-relation between angular deformations of segments of the axis is as follows:

$$-\frac{q^{/}(l)}{C_H} = \frac{\omega^{/}(0)}{C_H} + \frac{M(0)}{IE}(L-l) + 1.11\frac{0.5P}{SG} + \frac{0.5P(L-l)^2}{2IE}.$$

Tangential displacement of the satellite caused by deformation of its axis and the contacting jaws of the carrier and bearing ring is

$$y = \frac{\omega(0)}{C_H} + \frac{q(l)}{C_H} + \frac{q^{/}(l)}{C_H}(L-l) + \frac{M(0)}{2IE}(L-l)^2 + \frac{0.5P}{3IE}(L-l)^3. \qquad (23)$$

The factor of non-uniform load distribution for satellites is determined by solving the system of Eq. (19), according to the displacement of the ith satellite y_i and above-assigned values of apposition of bearing rings y_{Bi} obtained from (23).

Results of this analysis are represented as diagrams of dependences $K = F_{\max}/F = W_{\max}/W$ on the relative error $\Theta = b_W \delta E/F$ and the ratio of the half length of the slot between the carrier jaws to the diameter of the satellite axis L/d

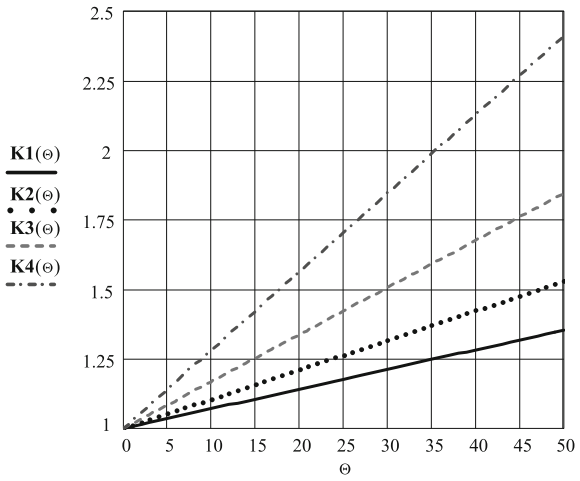

Fig. 14 Factor of non-uniform load distribution for power flows versus the relative error for $N = 5$. *Subscripts 1* for $L/d = 1$; *2* for $L/d = 0.7$; *3* for fixed axes and carrier; *4* for fixed axes, carrier and bearings

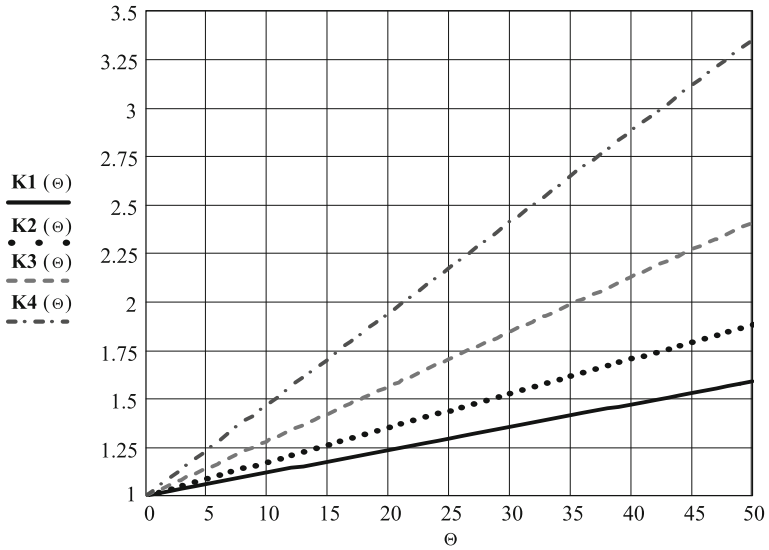

Fig. 15 Factor of non-uniform load distribution for power flows versus relative error for $N = 6$. *Subscripts 1* for $L/d = 1$; *2* for $L/d = 0.7$; *3* for fixed axes and the carrier; *4* for fixed axes, the carrier and bearings

for $0.5 \leq b/d \leq 0.7$; $l/d = 0.5$; $b_w/L = 1.8$ and different numbers of satellites N (Figs. 14, 15 and 16).

The diagrams correspond to the ratio between deviations of satellite axes from a theoretically accurate position that is unfavorable for a gear with a "floating" sun pinion: for $N = 5$ $\delta_1 = \delta_2 = \delta$, $\delta_3 = \delta_4 = \delta_5 = 0$; for $N = 6$ $\delta_1 = \delta_2 = \delta_3 = \delta_4 = \delta$, $\delta_5 = \delta_6 = 0$; $N = 7$ $\delta_1 = \delta_2 = \delta_3 = \delta_4 = \delta$, $\delta_5 = \delta_6 =$

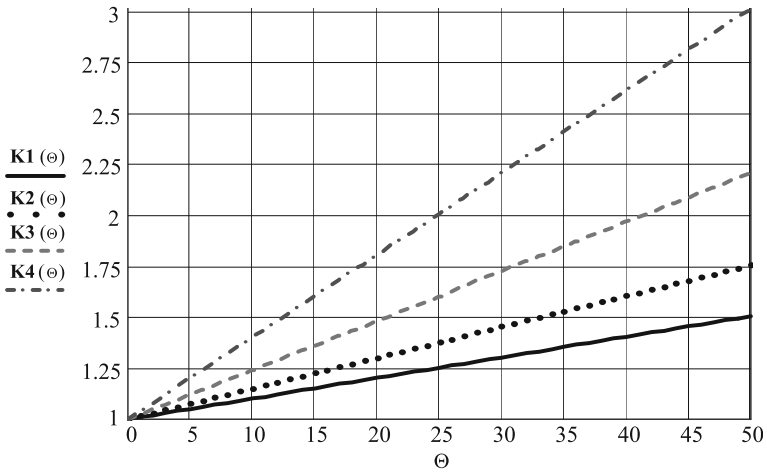

Fig. 16 Factor of non-uniform load distribution for power flows versus relative error for $N = 7$. *Subscripts 1* for $L/d = 1$; *2* for $L/d = 0.7$; *3* for fixed axes and the carrier; *4* for fixed axes, the carrier and bearings

$\delta_7 = 0$ (for an odd number of satellites, the clearances in three of them are eliminated by self-alignment of the sun pinion even at a low load).

An investigation conducted according to the above given method shows that, in case of a "floating" sun pinion and unfavorable deviation of satellite axes from a theoretically precise position, the load carrying capacity of a five-satellite layout does not differ, practically speaking, from this parameter of a gear with six satellites, since the increase in the load carrying capacity due to an increase in the number of power flows is compensated for by the possible increase in the factor of non-uniform load distribution in meshing of gears. The load carrying capacity of a seven-satellite gear in the presence of its manufacturing errors exceeds the pointed technical and economic parameters for five- and six-satellite layouts by approximately 20–30%, which should be considered when analyzing planetary gears.

4 Load Distribution Among Satellite Rows

In the case of a gear with a limited radial dimension, it is reasonable to make each satellite with two or more self-aligning gearwheels that are not rigidly connected to each other and that are fixed on cantilever axes (Fig. 17). In this layout, there is a non-uniformity of load distribution for rows of satellites caused by both gear manufacturing errors and torsion of the sun pinion under the action of a torque applied to it.

The factor of non-uniform load distribution for rims of a double-row satellite is determined by solution of a system of equations:

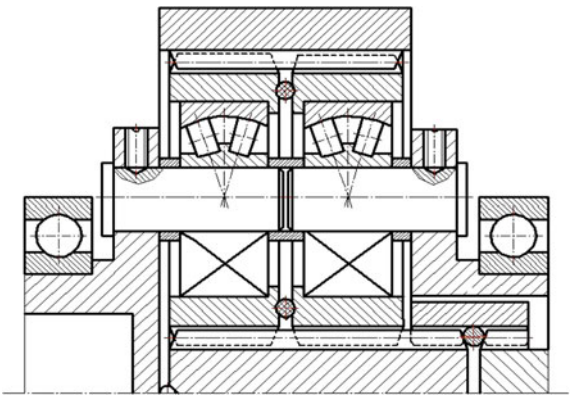

Fig. 17 Planetary gear with double-row satellites and a "floating" sun pinion

$$\left.\begin{array}{c} \frac{q_1 l}{2\cos\alpha_W} = b_W C_\Sigma[\varepsilon - (y_1 + y_{B1})\cos\alpha_W], \\ \frac{q_2 l}{2\cos\alpha_W} = b_W C_\Sigma\left[\varepsilon - \delta - y_\varphi - (y_2 + y_{B2})\cos\alpha_W\right], \\ q_1 + q_2 = 2q = 4W\cos\alpha_W. \end{array}\right\} \tag{24}$$

Here, $\varepsilon = const$; b_W is the face width of one rim of a satellite; δ are clearances between the teeth of the second rim of the satellite and central gearwheels (clearances in both meshes are identical) at tight contact of the teeth in meshing of the first satellite with central gearwheels; q_1 and q_2 are unit loads acting on the axes of the satellite rims from the perspective of the side of the bearings; q is the average unit load; l is the length of the cantilever part of the axis (see Fig. 9); y_{B1} and y_{B2} are displacements of the satellite rims caused by compliance of the rolling bearings; y_1 and y_2 are displacements of the satellite rims caused by deflection of the axes and contact deformation in areas of their contact with carrier jaws and bearing rings (y_{Bi} and y_i are determined in a manner similar to that of a gear with single-row satellites, as shown in Figs. 8 and 9); and y_φ is the half difference of tooth displacements for a sun pinion in its lateral cross-sections by symmetry planes for satellite rims due to torsion:

$$y_\varphi = 0.5\varphi r_b = \frac{0.5 r_b b_W^2}{I_p G}(0.875t_2 + 0.125t_1) \tag{25}$$

where the unit moment of pinion torsion at sections of its contact with the i^{th} rim of the satellite is $t_i = \frac{0.5Nq_i r_b}{\cos\alpha_W}$, r_b is the pinion base radius, I_p is the polar moment of inertia of the pinion cross-section, φ is the difference between angles of torsion for cross-sections, and N is the number of rims of satellites in one row.

Equations are written for the case when the most loaded rim (the first one) of a satellite is located from the side of torque input to the sun pinion (an unfavorable case), and the load is distributed uniformly along the width of separate self-aligning rims of the satellite.

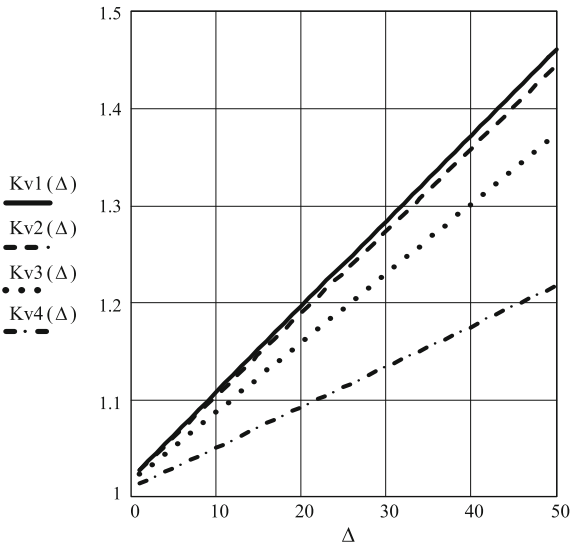

Fig. 18 Factor of non-uniform load distribution among rims of a double-rim satellite versus Δ for $\overline{b}_a = 1$. *Subscripts 1* for $\overline{b} = 2$; *2* for $\overline{b} = 1.5$; *3* for $\overline{b} = 1$; *4* for $\overline{b} = 0.6$

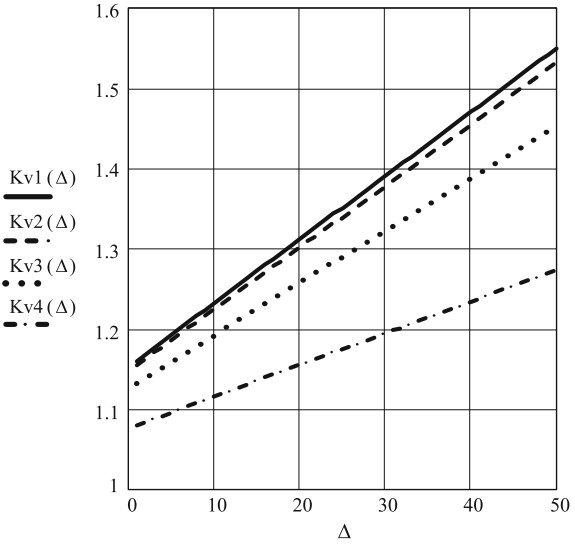

Fig. 19 Factor of non-uniform load distribution among rims of a double-rim satellite versus Δ for $\overline{b}_a = 3$. *Subscripts 1* for $\overline{b} = 2$; *2* for $\overline{b} = 1.5$; *3* for $\overline{b} = 1$; *4* for $\overline{b} = 0.6$

Figures 18 and 19 show diagrams of the factor of non-uniform load distribution among rims of a double-row satellite $K_V = q_1/q$ depending on $\Delta = \delta E/W$ at a number of satellites in a row $N = 3$, $\alpha_W = 20^0$, $\overline{l} = l/d = 1$, $\overline{b}_W = b_W/l = 1$ and different values of relative thickness of the carrier jaw $\overline{b} = b/d$ and the relative width of a sun pinion $\overline{b}_a = 2b_W/d_a$ (d_a is the diameter of the pitch circumference of the sun pinion).

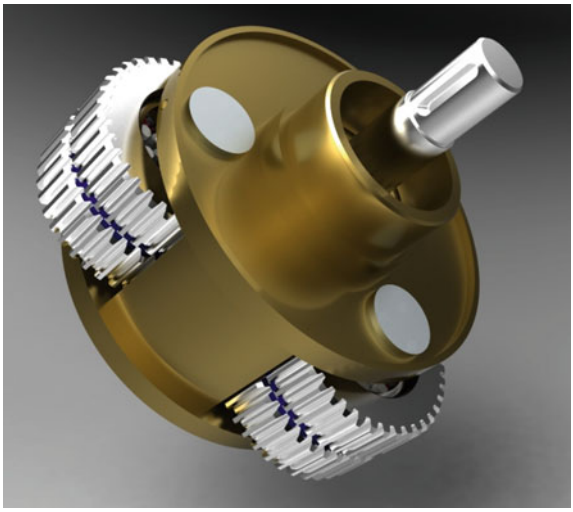

Fig. 20 Assembly unit of satellites for a planetary gear with double-row satellites

Figure 20 shows the assembly unit of satellites for a planetary gear with a limited radial radius. Each satellite is constructed of two self-aligning gearwheels mounted on cantilever axes.

5 Technical and Economic Parameters of Multi-Satellite Planetary Gears

The important technical and economic parameters of a gear are its efficiency and the relation of its mass to the moment at the output shaft. As numerous research works have shown [1], including experimental ones (Fig. 21), the first of the pointed parameters is rather high (about 95%), and the second one is determined by analyzing the contact strength for external gears that limits the load carrying capacity of the drive, and accounting for the gear ratio i, it can be found according to the following approximated relation:

$$M = \frac{0.5\pi\rho KE\left[1 + N(0.5i-1)^2 + 4k_b(i-1) + k_h(i-1)^2\right]}{(\sigma_{HP}/0.418)^2 N(0.5i-1)\sin\alpha_W \cos\alpha_W}\text{kg/Nm}, \qquad (26)$$

where ρ is the density of the gearwheel material; K is the factor considering the non-uniform load distribution among satellites; σ_{HP} is the allowable contact stress of the teeth; k_b is the factor that considers the thickness of the rim of the fixed gearwheel and the gear casing; and k_h is the factor that considers the thickness of the carrier jaws and gear caps.

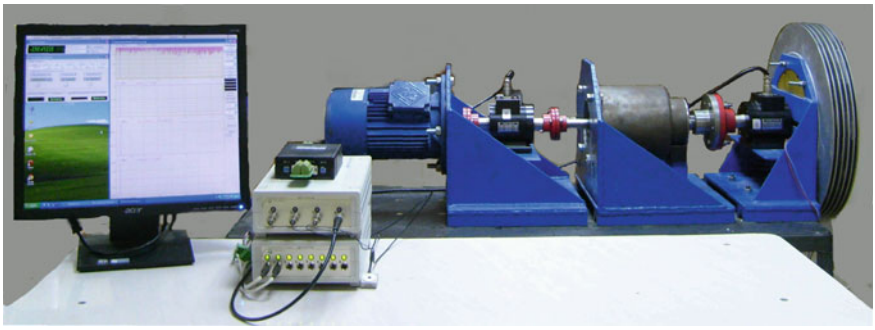

Fig. 21 Experimental apparatus for testing coaxial gears

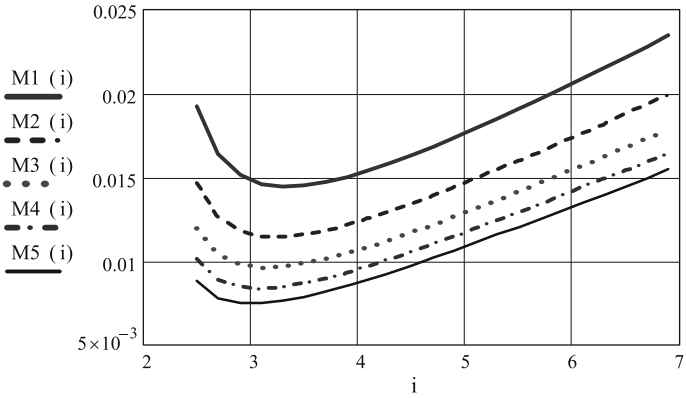

Fig. 22 Relative mass of a gear versus gear ratio and the number of satellites in the absence of manufacturing errors. *Subscripts 1* for $N = 3$; *2* for $N = 4$; *3* for $N = 5$; *4* for $N = 6$; *5* for $N = 7$

Figure 22 shows a diagram of the parameter M depending on the gear ratio and the number of gear satellites at uniform load distribution in meshing of gearwheels, $k_b = 0.2$; $k_h = 0.6$; the material of gear parts is steel, $\sigma_{HP} = 600$ MPa. As we see, the minimum value of the specific mass is $i \cong 3.5$. When the number of satellites is increased, under other equal conditions, the mass-dimensional parameters are improved. The most common configurations in practice are three-satellite layouts or layouts with an odd number of satellites, since the load is distributed less uniformly in the case of an even number of satellites.

The diagram in Fig. 23 is made for a gear with self-aligning satellites and a "floating" sun pinion at $L/d = 0.7$ (see Figs. 12 and 13); values of the non-uniformity factor K for number of satellites $N = 5$ and $N = 7$ correspond to the value of a relative error $\Delta = 30$, for $N = 3$ the value $K = 1$.

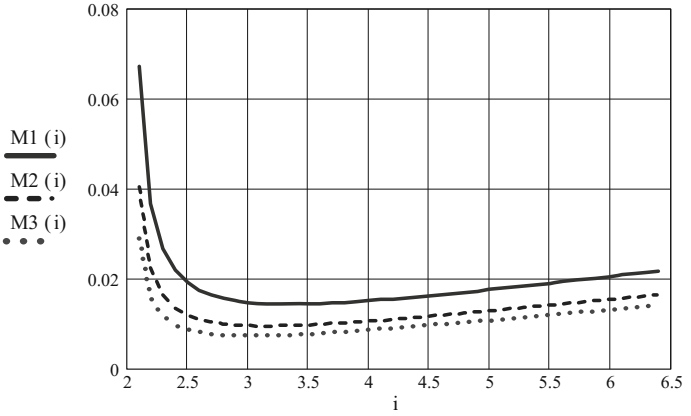

Fig. 23 Relative mass of a gear versus gear ratio and the number of satellites for a gear with a "floating" sun pinion. *Subscripts 1* for $N = 3$; *2* for $N = 5$; *3* for $N = 7$

The relations shown allow for selecting rational values of parameters of a planetary gear providing close to uniform load distribution in meshing of gearwheels and, therefore, a high load carrying capacity of a mechanism at good mass-dimensional parameters and high efficiency.

References

1. Kudryavtsev, V.N., Kirdyashev, Yu.N., Ginsburgm, E.G. In: Mashinostroyeniye, L. (ed.) Planetary Gears. Reference book (1977) (in Russian)
2. Plekhanov, F.I., Goldfarb, V.I.: Rational Designs of Planetary Transmissions, Geometry of Gearing and Strength Parameters (Series: Theory and Practice of Gearing and Transmissions, Mechanisms and Machine Science), pp. 285–300. Springer (2016)
3. Sondkar, P., Kahraman, A.: A Dynamic Model of a Double-Helical Planetary Gear Set. Mech. Mach. Theory **70**, 157–174 (2013)
4. Patent 2581222, RF, MPK F16H 1/32. Multi-row planetary gear / F.I. Plekhanov, A.D. Plekhanov—Publ. 27.10.2015, N30
5. Airapetov, E.L., Genkin, M.D. In: Nauka, M. (ed.) Deformability of Planetary Mechanisms (1973) (in Russian)
6. Plekhanov, F.I.: Investigation of mode of deformation of "satellite axis—carrier jaw" contact for a planetary gear. Izvestiya Vuzov, Mashinostroyeniye **2**, 36–41 (2015). (in Russian)

Actual Issues of Design and Production of Advanced Worm Gears

S. Lagutin, A. Sandler and E. Gudov

Abstract The advanced synthesis of a worm gear in real production should involve not only its geometrical and strength analysis according to the assigned performance characteristics. It must also provide compensation of inevitable manufacture errors, power and temperature deformations by localization of the bearing contact at the assigned area of the tooth flank. This paper considers the methods of solving this problem for both high-loaded worm gears and gearboxes of metallurgical equipment and precision gears of metal-cutting machine-tools.

Keywords Worm gears · Hob · Localization of bearing contact · Longitudinal and profile modification

1 Introduction

For all types of worm gear, including double-enveloping and spiroid ones, the gear ratio exceeds the ratio of the pitch diameters of the worm and gearwheel by a multiple factor. It allows for replacing a multi-stage gearbox with one compact-sized gear. That is why these gears are commonly applied in advanced mechanisms, in particular, in gearboxes for general engineering, screw-down mechanisms, roller conveyor drives for rolling mills, in kinematic chains of various machine-tools including those for gear-machining, etc.

S. Lagutin (✉) · E. Gudov
"Electrostal Plant of Heavy Machines" OJSC,
Moscow Region, Electrostal, Russia
e-mail: lagutin@eztm.ru

E. Gudov
e-mail: gudove@inbox.ru

A. Sandler
"SELECTION" OJSC, Moscow, Russia
e-mail: sandli@aha.ru

V. Goldfarb et al. (eds.), *Advanced Gear Engineering*,
Mechanisms and Machine Science 51, DOI 10.1007/978-3-319-60399-5_7

However, compact sizes provided by a mismatch of pitch surfaces of the worm and gearwheels with the gear axoids intrinsically causes a high sliding speed at contact and, therefore, significant friction losses, accelerated wear, necessity of applying antifriction materials, and low load-carrying capacity and efficiency, as compared to other types of gear. These drawbacks are especially vital at the initial stage of gearbox operation when inevitable manufacture and assembly errors, as well as power and temperature deformations, are shifting the bearing contact to one of the tooth edges during operation, thus increasing the contact stresses and deteriorating the formation of the lubrication layer.

These circumstances should be considered at the stage of design and compensated for in production. That is why the gearing should be designed as that approximated through the deliberate introduction of the parabolic function of errors of rotation angle for the driven element during meshing of one tooth pair. In practice, such a function is implemented by introducing longitudinal and profile modification of one or both conjugated surfaces, that is, their deliberate deviations from theoretically mutually enveloping ones.

The theoretical fundamentals of the local synthesis of general type worm gears are stated in [1–4]. Issues of computer-aided simulation of the localized contact of cylindrical worm gears are considered in [8, 14]. Different manufacturing methods of providing the localized contact, accounting for the functional purpose of the gear, are described in [5, 10–12, 15]. Long-term experience in the design and production of heavy-loaded worm gears at the Electrostal plant of heavy engineering (Moscow region) and of precision worm gears at Russian machine-tool building plants is summarized in the monograph [13].

The present paper proposes the English version of the most urgent chapters of this monograph.

2 The Functional Purpose of Worm Gears and an Integrated Approach to Their Design

Worm gears are divided into two types, according to their functional purpose: index worm gears and power wormgears.

Index worm gears are used in the kinematic chains of various machine tools. In gear-machining equipment that operates by the generating method, as well as in advanced machining centers with rotary tables, they are intended to transmit continuous rotation. These gears are manufactured for precision, as a rule, within degrees of accuracy of the 3rd–5th, according to the Russian Standard GOST 3675-81. Parameters of the kinematic accuracy for such gears have to be calculated according to the required accuracy rating of the machine-tool, or the allowable error of angular rotation of the working table. The smoothness and norms of contact are consequently assigned for the worm, the wheel and the gear as a whole. The same accuracy is required for gears of single rotation that are used in division

mechanisms of machine-tools for profile gear grinding, the sharpening of the front surfaces of hobs, etc. The rotary tables for coordinate boring and milling machine-tools are made with index worm gears of 6th–7th degrees of accuracy. In all cases, a unified set of validation that determines the quality of worm gears is the area of bearing contact with its regulation of the tooth height and width.

Power worm gears are intended for transmitting the torque and power of the drive to actuators. They are manufactured, as a rule, with the accuracy provided by the available manufacturing equipment, and the quality of their production is also controlled according to norms of contact. The main parameters of design are the overall dimensions of the space assigned for the gearbox, load-carrying capacity (torque at the output shaft), and efficiency. It should be considered in design that under other equal conditions, the gears of the 6th–7th degrees of accuracy surpass the gears of the 10th degree by 1.5 times, according to their load-carrying capacity. Smoothness of operation, reducing the wear and increasing the lifetime of gear operation, is of great importance for power gears. In most loaded drives, it is reasonable to apply globoid (double-enveloping) gears.

The essence of designer and technological synthesis of the worm gear under real production conditions is as follows:

1. To assign the tasks to the designer and technologist within development of both working drawings of the gear and the set of technological documentation: the order of manufacturing processes, working drawings of hobs, tool layouts for machining of the gear, and sharpening and relieving for producing the generating worm of the hob.
2. According to the functional purpose of the gear, it is necessary to determine the tolerances for center distances in the assembled gear and machine-tool gearing, and hob parameters (pitch diameter, profile and lead angles of the generating worm).
3. For each step of generating the surfaces of threads for operating and generating worms, it is necessary to determine such layouts for grinding wheel dressing and mounting of its axis ultimately to provide the contact localization for active flanks within the assigned meshing zone.

3 Accuracy Standards and Contact Localization in Worm Gears

It is historically common for production of worm gears to make identical operating and machine-tool settings, that is, to make the shape and position of surfaces of the generating worm coincide with those of the operating one. And the strict conjugation of the operational gearing can be provided theoretically. This property is applied for production of precision gears.

However, inevitable manufacture and assembly errors during the initial period of gear operation cause a shift of the bearing contact to one of the tooth edges, thus abruptly increasing the contact stresses and deteriorating the conditions of formation of the lubrication layer. In this connection, the effective means of increasing the quality of gears is localization of the initial contact at the assigned area of the gearwheel tooth flank, thus eliminating the necessity for long-time running-in.

The technique of manufacture of worm gears with localized contact is based on modification of the parameters of the generating worm, which not only implies the difference in dimensions and parameters of the hob with respect to the operating worm, but adjusts the machine-tool settings for cutting the worm gearwheel.

Strictly speaking, the functionality of localization should not be determined according to the tooth profile or length, but with respect to the nominal line of the instantaneous contact. Localization along this line does not change the instantenous gear ratio, and it prevents the outrun of the bearing contact to tooth edges, completely or partially compensating for the negative influence of errors of the assembly, power and heat deformations of the casing.

Localization in the direction normal to the line of instantenous contact causes discontinuity of the instantenous gear ratio during the meshing of one tooth pair, but it smoothens the edge impacts within tooth re-conjugation, thus allowing for compensation of the pitch errors of gear-cutting and tooth deformation under load.

In gears with a different character of contact line, the profile and longitudinal modifications cause unequivalent effects. In double-enveloping worm gears, the contact lines make up the angle close to 90° with the vector of the worm's tangential velocity. That is why the profile modification mainly reduces the sensitivity to assembly errors and the longitudinal one smoothens the discontinuity of the gear ratio. Similar effects are present in gears with cylindrical worms of ZT type.

In worm gears with ruled **(the term "ruled worm" was introduced long ago and it is widely used in scientific literature—a comment, not to be included into the text)**, in particular, Archimedes worms, the contact lines are stretched along the tooth and the longitudinal modification of the tooth flank compensates for the errors of relative position of worm and gearwheel axes. The influence of pitch and profile errors is reduced through modification of the tooth flanks in the direction perpendicular to the contact lines, that is, through profile localization.

3.1 Basics of Profile Localization Analysis

The profile localization of contact in gears with cylindrical **ruled** (or close to them) worms is provided by deliberate deviation of the upper and lower parts of the tooth profile "into" the tooth solid, that is, by creation of the reduced concavity for the profile of a hob-generating surface with respect to the worm thread profile.

The pointed profiles do not coincide organically, since they are generated in different production operations: for the operating worm, it is the grinding of the thread flank; for the generating worm, it is the sharpening of the front surface and relieving of the flanks of the hob.

The task of designers is to choose the most efficient basic thread profile for the operating and generating worms and to regulate the value of the reduced concavity of the pointed profiles, as applied to a specific degree of gear accuracy. The technologist has to develop the methods for implementation of the desired localization.

Smoothness of operation for a worm gear depends on a combination of errors of the axial pitch of the worm threads f_{Pxr} and of the tangential pitch of the wheel teeth f_{Ptr}.

Negative values of f_{Pxr} and positive values of f_{Ptr} reduce the actual tooth pitch, that is, the distance along the line of action between the points of contact of the driving pair of teeth and the subsequent pair. Entry into the mesh will be accompanied here by a "rigid" impact of the thread addendum and tooth dedendum. The reverse combination of pitch errors causes a "soft" impact at re-conjugation, that is, the contact of the upper edge of the worm thread with the tooth dedendum outside the conventional line of action. This phenomenon is less risky, but it should be eliminated.

Taking into account the axial angle α of the thread profile, the total influence of errors f_{Pxr} and f_{Ptr} on deviation of the base pitch is determined by the square-law summation of their allowable values with high probability

$$f_P = \left(f_{Pt}^2 + f_{Px}^2\right)^{0.5} \cos\alpha. \tag{1}$$

The expression (1) determines the maximally sufficient value (the arrow) f_{max} of the reduced concavity f of axial profiles of the generating and operating worms. At the same time, since the value f affects the cyclic error of the tooth mesh frequency f_{zz0r} in a gear, under the most unfavorable combinations of errors ($f_{Ptr} + f_{Pxr}$), it should be related to the tolerance f_{zz0} for the cyclic error according to the inequality

$$(|f_{Ptr}| + |f_{Pxr}|)\cos\alpha - f \le f_{zz0}. \tag{2}$$

Hence, by identifying the pitch errors with the tolerances, let us determine the minimum required value of f_{min} when producing gears with the localized contact:

$$f_{min} = (|f_{Pt}| + |f_{Px}|)\cos\alpha - f_{zz0}. \tag{3}$$

In worm gears with localized contact, the parameter of operation smoothness f_{hsr} (the distance between the active flank of the worm thread and the coaxial generating surface of the hob applied to finish the machining of gearwheel teeth) becomes irrelevant, since it is replaced by the value f of the profile localization.

The authors found the relation between values of f_{max} and f_{min} determined by expressions (1) and (3) with tolerances f_{Pt}, f_{Px}, f_{zz0}, f_{hs} for different degrees of

accuracy, according to the Russian standard GOST 3675-81. It is stated that the required value of the reduced concavity f should correspond to the range

$$f_{\text{hs}} \leq f \leq 2.0 f_{\text{hs}}. \tag{4}$$

The reduced concavity of the hob-generating surface with respect to the worm thread profile is formed due to the concavity of the front surface of teeth obtained during sharpening (Fig. 1) and the concavity of the profile of the relieved tooth flanks of the hob with respect to the profile of the ground worm thread (Fig. 2).

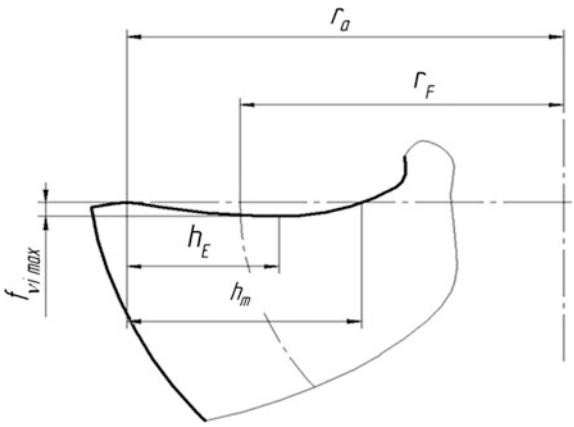

Fig. 1 Profile of the generating helical front surface of the hob teeth

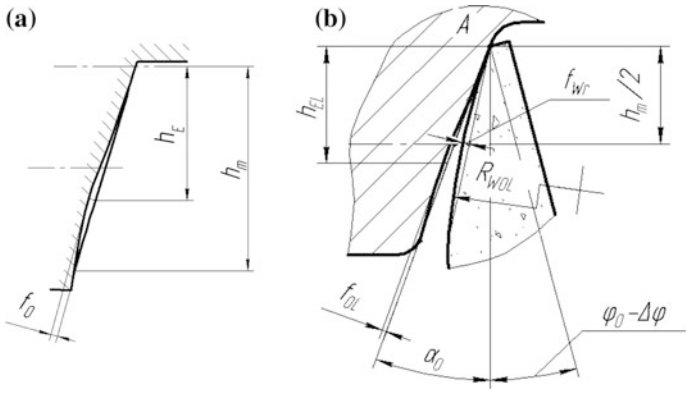

Fig. 2 Profiles of relieved surfaces of the hob teeth in the case of localized contact

Figure 1 presents the front surface profile of the hob with the following parameters:

m is the axial (or normal) module of the hob;
r_F is the radius of the pitch cylinder of the generating worm;
r_a is the radius of the outer cylinder of the active profile of the hob tooth;
$h_m = 2$ m is the height of the active profile of the hob tooth;
$f_{vi\ max}$ is the maximum deviation of the generatrix from the radial straight line;
$h_E = 2h_m/3$ is the distance from the boundary of the active segment of the profile to the point of maximum concavity of the generating line of the front surface.

Figure 2a shows the profile of the relieved surface for which the helix angle λ_r is greater than the helix angle λ for the thread of the generating surface (the right flank of the tooth of the right-hand hob). In this case, the distance from the internal cylinder of the active flank of the thread to the maximum value of the concavity is $h_E = 2h_m/3$. In Fig. 2b, the helix angle λ_r of the shank is less than the angle λ (the left flank of the tooth of the right-hand hob), in this case, $h_{EL} \approx 0.5774h_m$.

The concavity of the profile of flanks for the hob teeth is provided by adjusting the set-up parameters for the radial-axial relief [11]. In this case, different adjusting methods are used for two flanks of the tooth, which is why coordinates of maximums for the concavity of profiles of the front and relieved surfaces do not coincide and are separated by distance: ≈0.67 m for one flank of the tooth and ≈0.49 m for the other flank.

The influence of both components on the value of the reduced concavity of the profile of the generating surface for the hob should be considered when producing worm gears with the 3rd–5th degrees of accuracy.

The influence of the deviation f_{vi} of the generating line for the front surface of teeth on the axial profile of the generating surface will be related here with the radial relief angle $\lambda_b = |\lambda_r - \lambda|$ by the expression

$$f(f_{vi}) = f_{vi} \tan \lambda_b \tag{5}$$

For the flank of the hob teeth where the angle $\lambda_r > \lambda$, the optimal value is $\lambda_b \approx 5°$, and for the opposite flank, it is $\lambda_b \approx 7°$.

For worm gears of the 6th and lower quality degrees of accuracy, the required value of the profile localization is provided only as a result of relieving the hob teeth, since the increase in the allowable value of the concavity of the profile of the generating surface leads to an essential decrease in the influence of the concavity of the generating surface for the front flank of the tooth.

Analysis and implementation of manufacturing parameters of certain processes (grinding of worm threads, sharpening and relieving of the hob teeth, including the techniques for analysis of set-up parameters for worm-grinding, sharpening and relieving machines) are stated in detail in [13].

3.2 Alternative of Profile Modification

The profile localization of the contact in a worm gear requires the science-intense analysis of machine-tool settings and grinding wheel profiling at grinding operations for helical and relieved surfaces of the worm and the hob. In this relation, the authors have developed and tested an alternative method for providing the smoothness of worm gear operation based on a combination of tolerances for manufacture of the worm and the hob.

Parameters of smoothness include the parameter of identity f_{hs}, pitch errors f_{px} of the worm threads and f_{pt} of the gearwheel teeth, and allowable deviations of the profile f_{f1} of the worm thread and f_{f2} of the gearwheel tooth. The mutual relation of these parameters should be considered when designing both worms and hobs. In particular, it is necessary to consider the influence of the difference in angles of the worm and hob profiles on the combination of base pitches.

In [9], it was shown that in order to provide smoothness of gear operation, the base pitch of the driving element should be greater than that of the driven one. As applied to worm gears, this means that the base pitch of the worm p_b should be greater than the base pitch of the gearwheel, that is, the gearwheel should be cut by the hob with the pitch $p_{b0} < p_b$.

Sources of the error f_{pbr} of the base pitch of the worm are the error f_{pxr} of its axial pitch p_x and deviation of the angle $\Delta\alpha_1$ of the thread profile.

$$f_{pbr} = f_{pxr}\cos\alpha_1 - \pi m \sin\alpha_1 \Delta\alpha_1. \tag{6}$$

With a worm as the driving element of the gear, the increase in the base pitch is inadmissible, that is, the condition $f_{pbr} \geq 0$ should be fulfilled. It follows from (6) that the following condition should be fulfilled for this purpose:

$$\Delta\alpha_1 \leq f_{pxr}/(\pi m \tan\alpha_1). \tag{7}$$

That is, in order to compensate for the negative value of the error of the base pitch f_{pxr} of the worm, it is necessary to assign the tolerance $\delta\alpha_1$ for the pressure angle of its thread only as a negative deviation and to determine it through the expression

$$\delta\alpha_1 \leq -f_{px}/(\pi m \tan\alpha_1). \tag{8}$$

The sign of equality in expression (8) determines the upper value of the tolerance $\delta\alpha_1^{max} = -f_{px}/(\pi m \tan\alpha_1)$ for the pressure angle of the worm thread.

The lower value of the tolerance $\delta\alpha_1^{min}$ is determined by the tolerance range for the worm thread profile f_{f1} provided by standards. Hence:

$$\delta\alpha_1^{\min} = -f_{px}/(\pi m \tan\alpha_1) - f_{f1}\cos\alpha_1/2m. \quad (9)$$

Positive values of errors f_{ptr} of the tangential pitch of the gearwheel and f_{pxr0} of the axial pitch of the hob increase the base pitch of the gearwheel. It is also increased while decreasing the pressure angle of the generating worm during re-sharpening of the hob. The influence of these factors should be compensated for by decreasing the base pitch of the hob through assigning positive deviations (both the upper and the lower) for the angle α_0 of the profile of relieved flanks of teeth.

When designing a hob, the upper value of this tolerance $\delta\alpha_0^{\max}$ should be calculated according to the formula

$$\delta\alpha_0^{\max} = \left(f_{px} + f_{pt}\right)/(\pi m \tan\alpha_1) + f_{f2}\cos\alpha_1/(3m), \quad (10)$$

where f_{px} is the positive part of the tolerance for the pitch error of the generating worm taken to be equal to the pitch tolerance of the worm, and f_{pt} is the positive part of the tolerance for the tangential pitch of the gearwheel.

Formula (10) implies that the 1/3 part of the tolerance f_{f2} for the gearwheel tooth profile should be related to the error appearing due to faceting.

The first component of expression (10) determines the minimum value of the angle α_0 necessary to provide the smoothness of meshing. It corresponds to the deviation of the pressure angle for a completely re-sharpened hob.

$$\delta\alpha_{0c}^{\min} = \left(f_{px} + f_{pt}\right)/(\pi m \tan\alpha_1). \quad (11)$$

The second component of expression (10) determines the sum of the tolerances for manufacture and for variation of the angle α_0 during re-sharpening.

It is reasonable to distribute the value $f_{f2}\cos\alpha_1/3m$ between the pointed tolerances for manufacture and re-sharpening in equal portions. Then, ***when manufacturing a new hob***, the upper limit of the tolerance for the angle α_0 should be:

$$\delta\alpha_0^{\max} = \left(f_{px} + f_{pt}\right)/(\pi m \tan\alpha_1) + f_{f2}\cos\alpha_1/6m. \quad (12)$$

The allowable number for re-sharpening is calculated through the remaining value of the tolerance $\delta\alpha_{0i} = f_{f2}\cos\alpha_1/6m$. Thus, when designing the worms and hobs, the necessary clearance Z_z in the meshing during the instance of teeth re-conjugation is stated to provide the smoothness of gear operation—causing the base pitch for the driving element to exceed the base pitch of the driven one:

$$Z_z = \left(2f_{px} + f_{pt}\right)\cos\alpha_1. \quad (13)$$

If the pressure angle of the generating surface is assigned for the applied hob tolerances for deviations of the pressure angle of the worm thread, it should be analyzed according to (8) and (9), and after that, the profile of the helical surface of the worm thread should be corrected.

Therefore, in addition to the requirements stated in the Russian standard GOST 3675-81, it is necessary to regulate the following parameters of the worm and the hob:

- Upper and lower allowable deviations of the pressure angle of the operating worm, which should be negative deviations with respect to the nominal value;
- Upper and lower allowable deviations of the pressure angle of lateral flanks of teeth during manufacturing and re-sharpening of the hob, with both deviations being positive with respect to the nominal value.

3.3 Analysis of Parameters and Technique of Longitudinal Localization

The theoretical lines of instantenous contact in a completely conjugated worm gear with a cylindrical, in particular, Archimedes worm are stretched along the gear-wheel tooth and over its whole width. In real gears, the total bearing contact should be concentrated in the middle part of the tooth, so that the assembly errors will not shift the contact to the boundaries (edges) of the gear rim. Modification of the gearwheel tooth flank along the tooth length (called longitudinal localization) is aimed at compensation for these errors.

The most common methods for longitudinal localization of the contact for worm gears of the 6th–12th degrees of accuracy is the application of hobs having an increased diameter [5, 12–15]. And it is important to assign such a diameter of the hob and manufacturing tolerances that allow for compensating the manufacturing errors of gearbox parts and for obtaining the gear with a specific degree of accuracy and the required quality parameters.

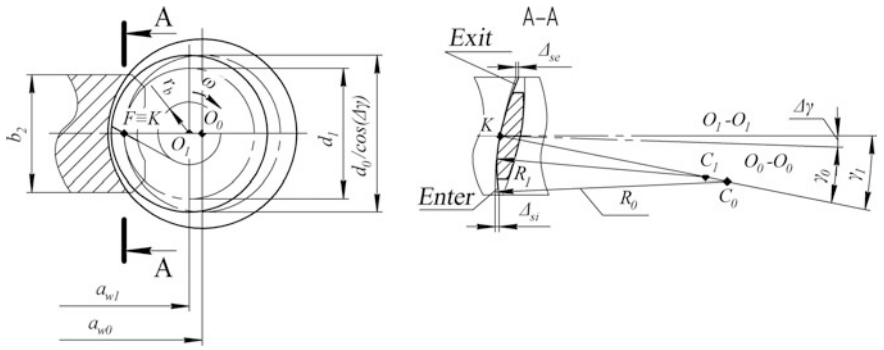

Fig. 3 The combined scheme of the operating and machine-tool meshing for the *centre* of the bearing contact arranged on the *middle* plane of the gear

3.3.1 Machine-Tool Meshing for Application of Hobs with the Increased Diameters

Figure 3 shows the combined scheme of meshing of the orthogonal worm gear and the machining of gearwheel teeth by a hob with an increased diameter. The diameter d_0 of the pitch cylinder of the hob is greater than the diameter d_1 of the pitch cylinder of the worm, however, these cylinders make contact with each other at the pitch point F. Let us consider the version of the arrangement of the nominal centre of the bearing contact (the point K) on the middle plane of the gear.

The left side of this figure shows the section of the gear by a plane perpendicular to the worm axis and passing through the gearwheel axis. The section A–A is drawn tangentially to the pitch cylinder of the worm (and the hob) through the straight line parallel to the gearwheel axis at the distance equal to the radius $r_2 = 0.5m_x z_2$ of the pitch cylinder of the gearwheel.

This straight line is the axis of meshing that possesses a number of properties [4]:

(1) In the case of linear, as well as localized, contact, all contact normal lines of the gear intersect this axis;
(2) In a completely conjugated gear, this axis definitely lies on the surface of the meshing, which is a set of lines of instantenous contact;
(3) In a gear with longitudinally localized contact, the points of instantenous contact of active flanks generate the line of meshing in a fixed space, the line intersecting the pointed axis by necessity.

Due to these properties, when synthesizing a gear with longitudinal localization, it is necessary to choose the centre K of the bearing contact exactly on this axis: either on the middle plane of the gear by aligning it with the point F, or by shifting it with respect to F towards the worm leaving the meshing.

To synthesize such a gear, it is necessary and sufficient to rotate the axis of the hob so that its generating surface could contact the active flank of the worm exactly at this point, that is, normal lines to two surfaces should coincide at the point K.

The normal line to any helical surface is skewed with its axis at a distance equal to the radius r_b of the base cylinder of the equivalent involute worm:

$$r_b = 0.5m_{x1}z_1/(\tan^2\alpha_{x1} + \tan^2\gamma_1)^{0.5} \tag{14}$$

That is why the straight line passing through the point K tangential to the circle with the radius r_b represents a projection of the common normal line at the design point. Simultaneously, this tangent line shows the direction of displacement of the centre of the bearing contact along the tooth flank at worm rotation.

In the picture on the right side of Fig. 3, the axis of the worm O_1–O_1 is arranged horizontally, and the axis of the hob O_0–O_0 is rotated with respect to it at an angle $\Delta\gamma$. The shaded area is the section of the worm thread by the plane A–A tangential to the pitch cylinder of the worm. This section is in contact with the section of the thread of the hob-generating surface by the same plane at the design point K.

The straight line KC_0 represents the common normal line to longitudinal profiles of threads. This line makes up the angle γ_1 (equal to the pitch lead angle of the worm) with the worm axis O_1–O_1 and the angle γ_0 (equal to the pitch lead angle of the hob-generating surface) with the projection of the hob axis. Points C_1 and C_0 represent the centers of curvature of the considered sections of the worm and the hob, and the distances $C_1K = R_1$ and $C_0K = R_0$ are the radii of curvature of the pointed sections. Values R_1, R_0 are determined by the expressions

$$R_1 = 0.5d_1/(\tan\alpha_{x1}\cos^3\gamma_1), R_0 = 0.5d_0/(\tan\alpha_{x0}\cos^3\gamma_0) \tag{15}$$

where α_{x1}, α_{x0} are axial pressure angles of the worm thread and the generating surface of the hob, respectively.

In order to arrange the design point K on the pitch cylinder of the worm at the middle plane of the gear, the hob axis should be rotated towards increasing the tooth helix angle at an angle $\Delta\gamma$ equal to

$$\Delta\gamma = \gamma_1 - \gamma_0. \tag{16}$$

When the worm is rotating in the direction shown by the arrow ω, the active part is that side of the profile which passes through the point K; and the "*Enter*" and "*Exit*" points of the worm out of the meshing are shown on the right side of Fig. 3.

The arrow of the convexity (curvature) δ_1 of the surface of the worm thread along the gearwheel tooth in the considered section is determined to be

$$\delta_1 = b_2^2/(8R_1\cos^2\gamma_1)\,. \tag{17}$$

As for the generating surface of the hob having an increased diameter due to the increase of the curvature radius of the thread by the value $\Delta R = R_0 - R_1$, the arrow of the convexity in the same section will be decreased by the value

$$\Delta\delta = -b_2^2\Delta R/(8R_1^2\cos^2\gamma_1), \tag{18}$$

where the minus sign shows that deviations of $\Delta\delta$ and ΔR have opposite signs.

3.3.2 Compensation for the Influence of Errors of Assembly and Machine-Tool Meshing

Standards for the accuracy of the worm gears with non-adjustable arrangement of axes, including the Russian standard GOST 3675-81, assign the allowable values for the following errors: deviations of the center distance f_{ar} in the gear (worm – worm gearwheel) and f_{acr} at machining (hob - gearwheel); deviations of the cross angle $f_{\sum r}$ in the gear and $f_{\sum cr}$ at machining; shifts of the middle plane of the gearwheel f_{xr} in the gear and f_{xcr} at machining.

The technique for calculating the increase in the pitch diameter of the hob with respect to the operating worm necessary to compensate each of the pointed pairs of errors is given below; and limitations imposed on this parameter by the assigned value of the bearing contact along the gearwheel width are considered.

The error of the gear center distance depends on the accuracy of producing the bores for the worm and gearwheel shaft supports in the casing of the gearbox. The error of the machine-tool center distance is determined by the accuracy of the gear-milling machine-tool, by the manufacture accuracy of the master worm with the thickness of its thread, considering the assigned backlash in the gear, and by tolerances for the center distance adjusted according to the master worm.

That is why, at equal pitch diameters d_1 of the operating worm and d_0 of the generating worm, the actual values of center distances in the gear a_{w1} and in machine-tool meshing a_{w0} differ from each other. Let us determine the influence of this difference on the formation of contact along the helical surface of the thread.

As is known, one of the properties for the helical surface is the increase of its curvature and helix angle with decrease of the current radius. Therefore, the decrease in a_{w0} with respect to a_{w1} is the most risky at formation of the bearing contact. In this case, the generating worm forms a more concave tooth surface than the surface enveloped by the thread of the operating worm with the axis shifted from the gearwheel axis at a greater distance. The initial contact of active flanks is valid for that face end of the gearwheel where the worm thread enters the meshing.

To make the curvature of the helical surface of the generating worm less than the curvature of the thread of the operating worm under the most unfavorable combination of errors, it is necessary to increase the pitch diameter d_0 of the hob and to provide the nominal of the center distance a_{w0} equal to

$$a_{w0} = a_{w1} + 0.5(d_0 - d_1). \tag{19}$$

For a gear of the assigned degree of accuracy, the maximum value of the error of the center distance does not exceed the sum of absolute magnitudes of allowable values of components:

$$f_a + f_{ac} = 1.75 f_a. \tag{20}$$

Having assigned the value $(a_{w0} - a_{w1}) = 1.75 f_a$, we obtain the required increment Δd_{0a} of the diameter d_0 of the hob with respect to the diameter d_1 of the worm:

$$\Delta d_{0a} = (d_0 - d_1) = 3.5 f_a. \tag{21}$$

The error $f_{\sum r}$ of the cross angle of the gear occurs when manufacturing the gearbox casing due to deviation from the perpendicularity of the axes of the bores for the worm and gearwheel supports (or the assigned value of the angle between them). According to the Russian standard GOST 3675-81, the symmetrical tolerance for this deviation is assigned by the linear value $f_{\sum}$ at the width b_2 of the gearwheel rim. The error $f_{\sum cr}$ of the cross angle at machining occurs at the

gear-milling machine-tool, first, due to mounting errors of the hob axis, and second, due to non-perpendicularity of the axis of the mounting bore of the gearwheel and its mounting face end. The standard assigns the symmetrical (±) tolerance for deviation of the cross angle at machining $f_{\sum c} = 0.75 f_{\sum}$ for these two components.

The gearbox casing, the gearwheel and the hob are produced by machine-tools with differently-directed errors. It is impossible to control the mutual compensation of these errors. Values of $f_{\sum}$ stated by the Russian standard do not provide the contact concentration at the middle of the gearwheel tooth. For the 6th–12th degrees of accuracy, the absolute values $f_{\sum}$ vary from 9 to 160 μm, essentially exceeding the thickness (≤ 5 μm) of the paint layer fixing the location and length of the bearing contact at the inspection and measuring machine.

That is why, practically speaking, the only means of compensation of the total error of the cross angle for stable localization of the contact is the longitudinal modification of the gearwheel teeth through application of hobs having the increased diameter of the generating surface. In order to prevent the shift of the bearing contact to the face edges of the teeth, the arrow of concavity for the surface of the generating worm along the tooth length should be decreased by the value Δδ.

By equating Δδ to the absolute value of the tolerance $\left|f_{\sum}\right|$, and accounting for (18), let us determine the value of the necessary increase in the diameter d_0 of the hob with respect to the diameter d_1 of the worm:

$$\Delta d_{0\sum} = (d_0 - d_1) = 4 f_{\sum} d_1^2 / (b_2^2 \tan \alpha_{x1} \cos \gamma_1). \tag{22}$$

The value $f_{\sum}$ in formula (22) surpasses the influence of angular errors of mounting the gearwheel and the hob axis over gear-cutting operations.

The shift f_{xr} of the middle plane of the worm gearwheel in the gear is limited by the symmetrical tolerance $\pm f_x$ and it is formed by design dimension chains of the worm gearbox. The shift f_{xcr} of the middle plane of the gearwheel at machining is limited by the tolerance $\pm f_{xc} = 0.75 f_x$ and it is determined by a manufacturing dimension chain for the setting of the gear-milling machine-tool. Methods for the valid control of these parameters at manufacturing have not yet been developed.

In this connection, values of tolerances $\pm f_x$ and corresponding values of $\pm f_{xc}$ given in the Russian standard GOST 3675-81 are applied as allowable errors of the master link in calculation of the pointed dimension chains.

The shift of the middle plane is controlled according to the dimension of the total bearing contact given in the same standard.

In the practice of single or low-batch production, the quality of this parameter is achieved through application of compensators in the layout of the gearwheel shaft assembly. Compensators are bushings or rings, their length being machined by measurements. One of compensators “helps” the gearwheel approach the position at which the required bearing contact along the tooth length is formed. The second compensator closes the axial play of the trust bearing of the gearwheel shaft.

For series production of large gears having the 6th–12th degrees of accuracy, for compensation of errors f_{xr} and f_{xcr}, it is also reasonable to implement the increase in the diameter of the hob with respect to the worm diameter on the value Δd_{0x}:

$$\Delta d_{0x} = 2f_x d_1/(K_b b_2), \tag{23}$$

where K_b is the design factor of the relative length of the bearing contact.

Since tolerances for errors f_{xr} and f_{xcr} are symmetrical, the value f_x in (23) should be taken to be equal to the absolute value of the tolerance $|f_x|$. Values of the factor K_b, according to the Russian standard GOST 3675-81 for different degrees of accuracy, are given in Table 1. When calculating the value Δd_{0x}, the greatest value of K_b shown in the table should be used.

When applying the hob with the increased diameter, it is necessary to provide the equality of base pitches (or basic modules $m_{b1} = m_{b0}$) of threads of the operating and generating worms by correction of the worm thread parameters. For Archimedes gears, the equality of axial modules $m_{x1} = m_{x0}$ should be provided at the same time. In this case, the values of axial pressure angles and pitch lead angles of threads are related by the equation

$$\tan^2\alpha_{x1} + \tan^2\gamma_1 = \tan^2\alpha_{x0} + \tan^2\gamma_0. \tag{24}$$

Methods for correction of the worm (or hob) axial profile providing this equality are stated in greater detail in Sect. 4.

When choosing the hob diameter, it is necessary to consider the value of the backlash Z_b between active surfaces at the boundary of the bearing contact. This backlash should not exceed the thickness of the paint layer fixing the bearing contact at the control and measuring machine. By assigning the boundary of the bearing contact at the distance $(K_b b_2/2)$ from the middle plane of the gearwheel, let us determine the value Z_b at the worm pitch cylinder, accounting for the hob parameters:

$$Z_b = 0.25(K_b b_2)^2[(\sin\alpha_{x1}\cos^3\gamma_1)/d_1 - (\sin\alpha_{x0}\cos^3\gamma_0)/d_0]. \tag{25}$$

Having assigned the ultimate value of the clearance $Z_b \leq 5$ mcm, let us determine, from (25), the maximum allowable increase Δd_{0m} in the pitch diameter of the hob d_0 with respect to the worm diameter d_1:

$$\Delta d_{0m} = d_0 - d_1 = 4Z_b d_1^2/(K_b^2 b_2^2 \sin\alpha_{x1}\cos^3\gamma_1), \tag{26}$$

where the least value of the factor K_b (shown in Table 1) should be taken.

Table 1 Design factors K_b of the length of the bearing contact

Degree of accuracy	6, 7	8, 9	10	11, 12
Factor K_b	0.54–0.6	0.43–0.5	0.34–0.4	0.2–0.3

Analysis of the design values of the necessary increase Δd_{0a}, $\Delta d_{0\sum}$, Δd_{0x} in the pitch diameter d_0 of the hob depending on the required degree of accuracy (6th–12th) of gear production [12] showed the following:

1. The increase Δd_0 in the pitch diameter of the hob relative to the operating worm should be considered according to the condition of obtaining the minimum necessary dimension of the length of the bearing contact for the maximum backlash at its boundary (no more than 0.005 mm).
2. For gears of the 9th–10th degrees of accuracy, the allowable values of $[f_a]$ and $[f_{ac}]$ should be stiffened, as compared to the Russian standard GOST 3675-81, proportionally to the allowable value of the increase Δd_{0m} in the hob diameter:

$$[f_a] = \Delta d_{0m}/3.5. \tag{27}$$

3. For gears of the 9th–12th degrees of accuracy assembled without compensators, the tolerances f_x for the shift of the middle plane should be stiffened in manufacturing dimension chains according to the condition

$$[f_x] = \Delta d_{0m} K_b b_2/(2d_1). \tag{28}$$

3.3.3 Features of Contact Localization in Precision Gears

Precision worm gears are mainly applied in kinematic chains of gear-machining machine-tools. The accuracy of such gears should be two degrees higher than the accuracy of the machined parts and it should correspond to the 3rd–5th degrees of accuracy. The edge contact is inadmissible, so both longitudinal and profile localizations are necessary.

The finishing machining of the precision gear is implemented by master machine-tools that do not allow for varying the angle of the hob axis setting. That is why the pitch diameter of the finishing hob should be equal to the pitch diameter of the operating worm. Under such conditions, the contact localization along the tooth length is made by an additional machining of some segments of tooth flanks about 10–15% of the face width from both of its sides. This eliminates the possibility of edge contact near the gearwheel face ends.

Moreover, in order to provide longitudinal localization, the nominal of the machine-tool center distance at gear machining is taken to be equal to $a_{w0} = a_w + f_{ac}$, and when manufacturing the gear casing, only the negative tolerance f_a is assigned for the center distance a_w of bores for the worm and gearwheel supports.

The profile localization of the bearing contact is provided in a similar fashion, as was described in Sect. 3.1.

4 The Principle of Priority of Gear-Cutting Tools in the Individual Production of Power Gears

The need to manufacture single samples of worm gears, including those for spare parts for the existing equipment, initiated the requirement for designers to widen the range of machined products without widening the range of available tools.

When there is no hob with parameters identical to the parameters of the design drawing, in order to obtain the conjugated gear, it is necessary to follow the principle of priority of the gear-cutting tool. This principle implies the selection of a hob that has a close (greater in priority) diameter and the correction of parameters of the operating worm. The correction of the worm module and/or the pressure angle should provide the equality of base pitches at the design point. The calculation of the hob-setting parameters should provide the longitudinal localization.

Experience shows that proper selection of the hob from the available range and obtainment of the localized contact in a gear is a task that is solvable in practice. First of all, such a hob should be selected from the list of available ones that has the base pitch p_{b0} maximally close to the base pitch p_{b1} of the worm. Here, one can consider both hobs with the Archimedes generating surface intended for Archimedes wormgears and hobs according to the Russian standard GOST 9324-80 "Finishing single-thread hobs for cylindrical gears with the involute profile".

4.1 Selection of Hob Parameters

The initial information needed for the analysis is the assigned parameters of the gear. As for the gears with the Archimedes worms most common in practice, these parameters are: the axial module m_{x1}, the number of threads z_1, the pitch diameter of the worm d_1 and the pressure angle α_{x1} at the axial section of the worm.

The base pitch of the Archimedes worm is determined by the expression

$$p_{b1} = \pi m_{x1} \cos \gamma_1 \cos \alpha_{n1}, \tag{29}$$

where $\alpha_{n1} = \text{atan}\,(\tan \alpha_{x1} \cos \gamma_1)$ is the pressure angle of the worm at the normal section, and $\gamma_1 = \text{atan}\,(m_{x1} z_1/d_1)$ is the pitch lead angle of the thread.

The main parameters of the hob are: the number of threads z_0 and the pitch diameter d_0; the module m_{x0} and the pressure angle α_{x0} at the axial section for Archimedes hobs; the module m_{n0} and the pressure angle α_{n0} at the normal section for involute hobs, the pitch helix angle γ_0:

$$\gamma_0 = \text{atan}(m_{x0} z_0/d_0) = \text{asin}(m_{n0} z_0/d_0). \tag{30}$$

For both types of hobs, the parameters of the axial and normal sections are mutually related by the known expressions

$$m_{n0} = m_{x0}\cos\gamma_0, \quad \tan\alpha_{n0} = \tan\alpha_{x0}\cos\gamma_0. \tag{31}$$

For the Archimedes hob, the base pitch is determined as

$$p_{b0} = \pi m_{x0}\cos\gamma_0\cos\alpha_{n0}. \tag{32}$$

The base pitch of the hob for cutting involute cylindrical gearwheels is not related to the hob diameter and the pitch lead angle of the thread:

$$p_{b0} = \pi m_{n0}\cos\alpha_{n0}. \tag{33}$$

In any case, in order to provide the conjugacy of elements of the obtained gear, the following condition should be strictly fulfilled:

$$p_{b0} = p_{b1}. \tag{34}$$

4.2 *Worm Correction in the Application of Archimedes Hobs*

The requirement of equality for the base pitches of the Archimedes worm and the Archimedes hob means that the following condition should be strictly fulfilled:

$$m_{x0}\cos\gamma_0\cos\alpha_{n0} = m_{x1}\cos\gamma_1\cos\alpha_{n1}. \tag{35}$$

We consider the parameters of the hob $m_{x0,}$ γ_0 and α_{x0} as being the assigned ones, and the parameters of the worm m_{x1} and α_{x1} can be varied within certain limits, keeping its pitch diameter and the helix angle γ_1 of the thread. The axial profile m_{x1} of the worm can be kept equal to the initial one, or it should be varied discretely based on setting possibilities of the worm grinding machine-tool. That is why the angle of the worm profile should be considered to be the main, continuously varied parameter. This angle α_{n1} is determined from (35) at the normal section

$$\cos\alpha_{n1} = m_{x0}\cos\alpha_{n0}\cos\gamma_0/(m_{x1}\cos\gamma_1). \tag{36}$$

Then, the axial pressure angle α_{x1} is determined by the formula

$$\tan\alpha_{x1} = \tan\alpha_{n1}/\cos\gamma_1. \tag{37}$$

Strictly speaking, condition (37) determines the conjugacy of the active flanks of the worm thread and the gearwheel teeth only within the differential vicinity of the design point of contact. In order to provide the conjugacy of these surfaces along

the entire height of the thread, the worm should be made quasi-Archimedes and its axial profile should be outlined along the convex curve described by the expression

$$x(r) = \int_{r_{p1}} \tan \alpha_x(r) \partial r, \tag{38}$$

where r is the current radius at the active thread profile, which varies within the range from r_{p1} to r_{a1};

$r_{p1} = a_w - 0.5d_{a2} \cos(\alpha_{a2} - \alpha_{x1})$ is the radius of the lower boundary point of the active profile; and $r_{a1} = d_{a1}/2$ is the outer radius of the worm.

The current value of the axial pressure angle α_x is determined from (37) for the current value r and the corresponding lead angles of the worm threads $\gamma_1(r) = \text{atan}\,(m_{x1}z_1/2r)$ and the hob $\gamma_0(r) = \text{atan}[m_{x0}z_0/(2r - d_1 + d_0)]$.

The axial profile of the modified worm is shown in Fig. 4. Its curvature at the current point M is determined by the expression

$$K(r) = \frac{\partial}{\partial r}[\alpha_x(r)] \cos \alpha_x(r). \tag{39}$$

The required axial profile can be approximated by the arc of a circle, parabola or ellipse, depending on the type of contour follower applied at the worm grinding machine-tool. Its arrow of the convexity f_n is determined by the following expression with sufficient accuracy for practical purposes:

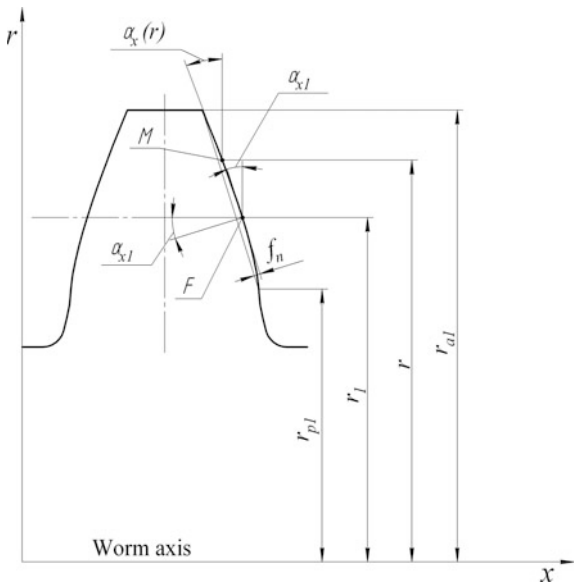

Fig. 4 The axial profile of the thread of the modified worm

$$f_n \geq m_x^2 K(r_1)/\left(2\cos^2\alpha_{x1}\right), \tag{40}$$

where $K(r_1)$ is the curvature calculated according to (39) for the radius $r = r_1$.

The sign > in this expression means that the bearing contact in the gear will be localized along the height of the tooth, thus allowing for smoothening of the negative influence of errors of the pitch and profile on the smoothness of gear operation.

Note that the required convexity of the axial profile is, as a rule, less than that of the organic error of grinding by the conical grinding wheel.

In the case when the axial modules of the worm m_{x1} and the hob m_{x0} are equal to each other, the expression (36) is simplified to

$$\cos\alpha_{n1} = \cos\alpha_{n0}\cos\gamma_0/\cos\gamma_1, \tag{41}$$

and the angle α_{x1} is directly related to the angles α_{x0}, γ_1 and γ_0 by the formula

$$\tan\alpha_{x1} = \sqrt{\tan^2\alpha_{x0} - \tan^2\gamma_1 + \tan^2\gamma_0}, \tag{42}$$

and, revealing the value of the derivative $d[\alpha_x(r)]/dr$ at the design point, formula (40) can be reduced to the following:

$$f_n \geq m_x\cos^2\alpha_{x1}(\tan^3\gamma_1 - \tan^3\gamma_0)/(z_1\sin\alpha_{x1}). \tag{43}$$

If the hob pitch diameter d_0 exceeds the diameter of the worm d_1 by 1–2 modules, then for a single-thread gear, the axial pressure angle calculated by formula (42) turns out to be less than the standard one $\alpha_{x1} = 20°$ by 0.5°–2°. In this case, the necessary arrow f_n of the profile convexity is within the tolerance f_f according to the 8th degree of accuracy and is provided by application of a conical grinding wheel without its special dressing.

Application of hobs having increased diameters automatically provides the longitudinal localization of contact along the face width and reduces the gear sensitivity to manufacture and assembly errors.

In a case of production necessity, the hobs with diameter d_0 less than the worm diameter d_1 can be used for cutting the gearwheel teeth. All the formulas indicated above for correction of the worm profile remain valid here. However, in order to avoid edge contact, the gearwheel teeth should be machined in three transitions. This version of the machining technique is described in detail in [13].

4.3 Application of Involute Gear-Cutting Hobs

If the tool shop of the enterprise does not have Archimedes hobs with parameters rather close to the worm, then hobs specified by the standard GOST 9324-80 and

intended for machining the involute spur and helical gearwheels can be used for cutting the worm gearwheel teeth. The calculation technique in this case is similar to that stated above, differing from it in only two circumstances.

First, since for these hobs, the normal module m_{n0} is standardized instead of the axis module m_{x0}, the condition for equality of base pitches is reduced to

$$m_{n0} \cos \alpha_{n0} = m_{x1} \cos \gamma_1 \cos \alpha_{n1}. \tag{44}$$

Hence, the required angle of the worm profile is determined according to formula (37) and does not depend on the lead angle γ_0 of the hob thread, which affects only the setting parameters of the hob axis at gear-cutting.

Second, strictly speaking, in this case, the operating worm of the gear can be the involute one, having the radius of the base cylinder

$$r_{b1} = 0.5 z_1 m_{x1} / (\tan^2 \alpha_{x1} + \tan^2 \gamma_1)^{1/2}. \tag{45}$$

For single-thread gears, such a version is even more convenient in production, since it is provided by the worm grinding with the conical wheel at parallel axes of the wheel and worm with the theoretical accuracy.

The axial profile of the involute worm is determined from the function of the current radius r by integral (39) or directly by the equation

$$x(r) = 0.5 m_x z_1 [\tan \theta(r) - \theta(r)], \tag{46}$$

where $\theta(r) = \text{acos}(r_{b1}/r)$ is the current pressure angle of the face involute.

Having differentiated Eq. (46), the variable pressure angle of the axial section of the thread will be determined by the following expression:

$$\alpha_x(r) = \text{atan}[\tan \gamma_1(r) \tan \theta(r)]. \tag{47}$$

The curvature of the axial profile can be determined by substitution of $\alpha_x(r)$ into expression (39). At the design point located on the pitch cylinder of the worm, this expression is reduced, after transformations, to

$$K(r_1) = \tan^2 \gamma_1 \cos^3 \alpha_{x1} / (r_1 \tan \alpha_{x1}). \tag{48}$$

The required arrow of the convexity of the axial profile of the thread f_n is determined by expression (41), with sufficient accuracy for practical analysis.

For single-thread gears, the normal module of the hob m_{n0} can be chosen to be equal to the axial module of the worm m_{x1}. The deviation of the worm axial profile from the straight line is rather insignificant, and condition (44) is fulfilled through correction of the thread profile according to the expression

$$\cos \alpha_{n1} = \cos \alpha_{n0} / \cos \gamma_1. \tag{49}$$

Example 1 Gear parameters are $z_1 = 1$, $z_2 = 42$, $a_w = 120$, $m_{x1} = 4$, $d_1 = 72$, $\gamma_1 = 3°\,11'$. Parameters of the hob are $\alpha_{n0} = 20°$, $m_{n0} = 4$, $z_0 = 1$, $d_0 = 78{,}6$, $\gamma_0 = 2°55'$.

The corrected axial angle of the worm profile is $\alpha_{x1} = 19°47'$, and the required arrow of convexity is $f_n = 0.002$ mm, that is, it is negligibly low. According to expression (16), the angle $\Delta\gamma$ of the turn of the hob axis is $\Delta\gamma = 0°16'$.

For the manufacturing of multi-thread worm gears, the hob module m_{n0} has to be selected to be less than the worm axial module m_{x1}. In this case, the profile curvature described by Eq. (48) can be sufficiently significant and it has to be realized by means of a dressing device of the worm grinding machine-tool.

Example 2 The worm has the parameters $m_{x1} = 10$, $z_1 = 4$, $d_1 = 80$, $\gamma_1 = 26°34'$, and the base module $m_{b1} = 8.505$. The most suitable involute hob has $m_{n0} = 9$, $z_0 = 1$, $d_0 = 114.5$, $\gamma_0 = 4°30'$ and $m_{b0} = 8.457$. Being corrected according to (44), the worm pressure angle becomes $\alpha_{x1} = 19°47'$. The maximum deviation of the profile (46) from a straight line comes to $f_n = 0.68$. To provide a practically sufficient accuracy, such a profile may be replaced by a circular arc with the radius R = 76.0.

The angular correction of the worm according to Eq. (44) is also applied when manufacturing the gears with the Archimedes worm and the involute cylindrical gearwheel that must perform a helical motion along its axis [6]. These gears are applied, for example, in adjustment mechanisms of mill rollers of screw rolling. They minimize the number of links and the amount of clearances in the kinematic chain mechanism, thereby improving the accuracy of rolled products.

4.4 Design of Duplex Worm Gears

The reversible worm gears (both power and index ones) need to meet the requirement of the backlash-free meshing, and this backlash-free character should be maintained in regard to the wearing-out of the gearwheel teeth. In these gears, the worm has a different axial pitch along the left flank of the thread p_L than the pitch along the right flank, and correspondingly, the axial modules m_{xL} and m_{xR} are also different. This provides the thread thickness variable along the worm axis. As the gearwheel teeth are worn out, the worm is periodically shifted in the axial direction and a thicker segment of the thread is introduced into meshing, thus eliminating the backlash. Such types of gear are called Duplex.

In Fig. 5, such a gear is shown at the middle section and at the section by the plane *A–A* tangent to the pitch cylinder of the worm.

The difference between the right and left pitches $\Delta p_x = p_L - p_R$ is usually taken within the range (0.1–0.2) of the average module. In previously known layouts of such gears, the axial pressure angle at both flanks of the thread was equal to the standard $\alpha_{x1} = 20°$. Cutting of the gearwheel teeth was implemented either with a

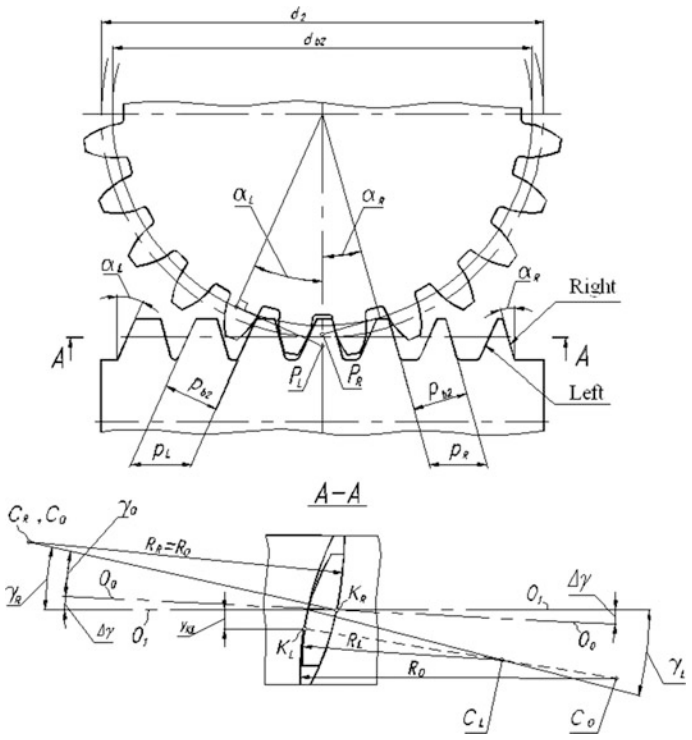

Fig. 5 Duplex worm gears

special hob with a generating surface identical to the active flank of the worm threads, or by two cuts of a single-cutter flying blade with different tangential feeds for each flank of the tooth. Neither method is particularly manufacturable. Moreover, tooth profiles are produced asymmetrically, and the profile corresponding to the greater module is undercut.

In order to eliminate these drawbacks, it is proposed that gearwheel teeth be cut with an Archimedes hob that has an increased diameter as compared to the worm diameter; and one which has a standard value of the module m_{x0}, axial pressure angle α_{x0} and their corresponding meshing module m_{b0}. Equality of base pitches for each of the flanks of the thread is provided by correction of axial pressure angles of the worm according to the condition

$$m_{bL} = m_{bR} = m_{b0}. \tag{50}$$

Let us consider the consequence of calculating the parameters of the worm and hob-setting through a specific example with the following initial data:

For the gear : $a_w = 165, z_1 = 2, z_2 = 24, d_1 = 90, m_{x\,cp} = 10.0; m_{xL} = 10.4; m_{xR} = 9.86.$
For the hob : $m_{x0M} = 10.0; d_0 = 120.0; z_0 = 2, \alpha_{x0} = 20^\circ, m_{b0} = 9.2838, \gamma_0 = 9^\circ 28'.$

According to this initial information, we consequently determine:
Axial pitches for the left and right profiles of the worm:

$$p_{xL} = \pi m_{xL} = 32.672\,\text{mm}, p_{xR} = \pi\, m_{xR} = 30.976\,\text{mm}.$$

The difference between axial pitches of the left and right profiles:

$$\Delta p_x = p_{xL} - p_{xR} = 1.696\ \text{mm}.$$

Pitch helix angles of the worm thread:

$$\gamma_L = \text{atan}\ (m_{xL} z_1/d_1) = 13^\circ 00' 48'', \text{similarly}\ \gamma_R = 12^\circ 21' 32''.$$

Normal angles of the worm thread profile:

$$\alpha_{nL} = \text{acos}[m_{b0}/(m_{xL} \cos\ \gamma_L)] = 23^\circ 37' 24'', \text{similarly}\ \alpha_{nR} = 15^\circ 26' 36''.$$

Axial angles of the worm thread profile:

$$\alpha_{xL} = \text{atan}(\tan \alpha_{nL}/\cos \gamma_L) = 24^\circ 10' 32'',\ \text{similarly}\ \alpha_{xR} = 15^\circ 47' 30''.$$

If the obtained values for α_{xL} or α_{xR} go out of range (15°–25°), initial values for m_{xL} and m_{xR} should be corrected, keeping, if possible, the assigned difference of Δp_x, and the calculation is repeated.

After this, we determine the radii of curvature of the section of the thread by the plane tangent to its pitch cylinder:

$$R_R = 0.5 d_1/(\tan \alpha_{xR} \cos^3 \gamma_R) = 170.7, R_L = 0.5 d_1/(\tan \alpha_{xL} \cos^3 \gamma_L) = 108.4.$$

And the greater of them (the first one in our case) is compared to the radius of curvature of the similar section of the hob thread:

$$R_0 = 0.5 d_0/(\tan \alpha_{x0} \cos^3 \gamma_0) = 171.8.$$

The condition $R_0 > R_R$ means that the longitudinal localization of the bearing contact is provided in the gear. If this condition is not fulfilled, it is necessary to choose the hob of greater diameter and repeat the calculation. At the other flank of the thread, the value of R_L will obviously be less than R_0.

The machine-tool center distance at gear-cutting is:

$$a_0 = a_w + 0.5(d_0 - d_1) = 180\text{mm}.$$

The hob axis should be turned towards the increase of the tooth inclination by the angle $\Delta\gamma = \gamma_R - \gamma_0 = 2°53'47''$. Then, the design contact point on the right flank of the tooth will be located on the middle plane of the gear and the bearing contact will be spread practically over the whole width of the gearwheel. On the left flank of the tooth, the bearing contact is localized in the longitudinal direction and its center is shifted by the value Y_{KL} towards the worm entering the meshing:

$$Y_{KL} = -R_0 R_L[\sin(\Delta\gamma + \gamma_0) - \sin\gamma_L]/(R_0 - R_L) = 3.24 \text{ mm}.$$

The proposed method of machining eliminates the necessity of manufacturing the special tool for gear-machining of gears with the variable thickness of the worm thread, and it increases the manufacturing efficiency of the gear-cutting process.

Experience showed the viability of the method for synthesis of worm gears with the localized contact based on the priority of the gear-cutting tool.

5 Modification of Double-Enveloping Worm Gears

Globoid, or double-enveloping, worm gears have a higher load capacity than the single-enveloping gears with a cylindrical worm. This advantage is especially appreciable for center distances exceeding 200 mm [7, 13]. That is why double-enveloping gears are commonly applied in power drives, in particular, rolling mills, in spite of manufacturing difficulties.

Experience in the production of double-enveloping worm gears showed that a number of specific manufacturing features should be stated in the technical documentation within their design. These are, in particular, parameters of the machine-tool meshing and setting of cutters when machining the modified worm.

As is known, in the classical double-enveloping Cone worm gear, the active flank of the worm threads is generated through rotation of the straightline generatrix tangent to the profile circle of the gearwheel. In such a gear, the initial bearing contact is a narrow strip located across the gearwheel tooth near its middle plane. During the running-in, the wear of surfaces takes place both for the gearwheel tooth and the worm thread. The run-in area is formed on the tooth flank, and gradually spreads over a considerable part of its surface.

Wear of the worm thread is also non-uniform. The maximum wear takes place at the input segment of the thread. The wear becomes minimal at the middle part of the thread and increases again when approaching the thread output. Such a running-in continues over 150–200 h, after which the geometry of the active flanks of threads and teeth is stabilized and the velocity of wear multiply decreases [7].

Change of the thread geometry during wearing-out is called *natural* modification. It is achieved by a long-term and expensive running-in process. If the

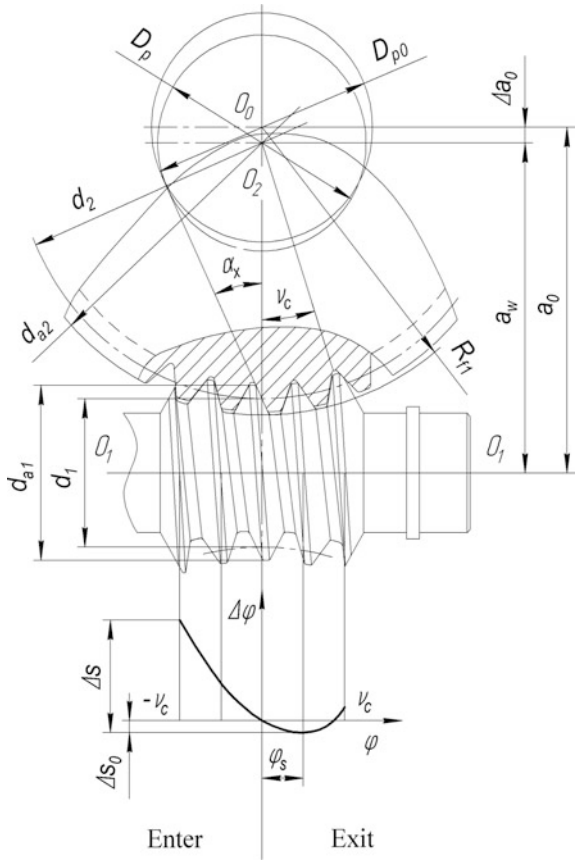

Fig. 6 Double-enveloping worm gear modified by the *AU* method

deviation close to its natural modification is provided at cutting of the worm thread, the time of running-in is multiply reduced and the gear can operate under maximum load from the very beginning.

Various methods for machine-tool modification of the double-enveloping worm thread during its cutting are known. The most common of them is the method in which the modification law that is closest to the assigned one is provided by a simultaneous deviation of the center distance and the gear ratio from nominal values to greater ones. Since both flanks of the thread in this case are modified at one machine-tool setting, it is called the "*AU* double-flank correction-free method."

Figure 6 shows the schemes of the machine-tool meshing for cutting the double-enveloping worm by the *AU* method and the curve line of the modification law, with its maximum value at the input ΔS and extreme value ΔS_0 at the point $\varphi = \varphi_s$.

When calculating modification by the *AU* method, the following parameters are determined: the tooth number of the generating gearwheel z_{20}, the increase in the

machine-tool center distance at worm cutting $\Delta a_0 = a_0 - a_w$, the pitch diameter of the generating gearwheel d_0, and the diameter of its profile circle D_{p0}.

The modification law (in radians) is described depending on the angle of rotation φ of the rectilinear generatrix for the thread by the following expression:

$$\Delta(\varphi) = \text{asin}[\sin\alpha_x + (2\Delta a_0/d_2)\cdot(\sin\alpha_x - \sin(\alpha_x + \varphi - K_u\varphi))] + K_u\varphi - \alpha_x \quad (51)$$

Here, $K_u = (z_{20} - z_2)/z_{20}$ is the factor of variation of the machine-tool gear ratio.

The advanced technique for the development of modified double-enveloping worm gears is considered in detail in [7, 13]. It comprises analysis of parameters for worm modification, elements of designing two- or four-teeth flying cutters for generating gearwheel teeth, and methods for evaluation of the load-carrying capacity and efficiency of these gears.

6 Conclusions

Any real worm gears have to be designed as approximated ones in order to compensate for inevitable manufacturing errors, as well as strength and heat deformations.

For single-enveloping worm gears, especially those with an Archimedean worm, the profile localization of the bearing contact allows for reducing the drive sensitivity to pitch errors of its elements. For profile localization, the designer should define and specify the equivalent concavity of profiles of the active and generating worms. An alternative method is also proposed to ensure the smooth operation of the gears through the appointment of mutually-related tolerances for pressure angles and pitches of the worm and the hob manufacturing of worm wheel teeth.

The assembly errors are compensated for and the edge contact is eliminated in such gears by the longitudinal localization of the bearing contact at the middle of the tooth width. The simplest, though not the only, method of longitudinal localization is to use worm hobs with increased diameter. It is shown that, in this case, worm profile correction is needed, along with proposed methods for its calculation.

In double-enveloping worm gears, the impact of the longitudinal and profile localization of the contact on the drive sensitivity to assembly and pitch errors is directly opposite. The method for machine-tool modification of the double-enveloping worm thread is considered.

In the individual production of power worm gears, it is proposed that production be guided by the principle of the priority of a tooth-cutting tool. In particular, this principle is used in the design of Duplex gears.

When longitudinal and/or profile contact localization is applied, it is necessary to specify the size and location of the bearing contact in the design documentation, taking into account the functional purpose of worm gears and the requirements for the accuracy and load-carrying capacity of the gear drive.

The problem of the synthesis of real worm gears with localized contact is as inexhaustible as the problem of the synthesis of spiral bevel and hypoid gears.

Acknowledgements The authors express their appreciation to the editor Natalya Barmina, Ph.D., for her invaluable help in the preparation of the English version of this paper.

References

1. Goldfarb, V.I.: Fundamentals of the theory of computer-aided geometrical analysis and synthesis of general type worm gears. Thesis for DSc in Engineering, Izhevsk, 415 p. (1985) (in Russian)
2. Lagutin, S.A.: Local synthesis of general type worm gearing and its applications. In: Proc. of the 4th World Congress on Gearing and Power Transmissions, vol. 1, pp. 501–506. Paris (1999)
3. Lagutin, S.A.: Synthesis of spatial gearings by aid of meshing space. In: Proceedings of International Conference "Power Transmissions-03", vol. 1, pp. 343–346. Varna, Bulgaria (2003)
4. Lagutin, S.A.: Analogs of axes of meshing in general type worm gearing. In: Theory and Practice of Gearing and Transmissions: In Honor of Professor Faydor L. Litvin, IX, pp. 145–158. Springer International Publishing AG Switzerland. ISBN: 978-3-3 19-19739-5 (2016)
5. Lagutin, S.A., Verhovski, A.V., Dolotov, S.V.: Technological design of worm gears with a localized contact. In: Proceedings of 2nd International Conference "Power Transmissions 2006", pp. 177–182. Novi Sad, Serbia (2006)
6. Lagutin, S.A., Gudov, E.A.: Special types of worm gears for rolling mills. In: Proceedings of the International Conference on Gears, pp. 1337–1347. Munich, Germany, VDI-Berichte 2108.2 (2010)
7. Lagutin, S., Gudov, E., Fedotov, B.: Manufacturing and load rating of modified globoid gears. Balkan J. Mech. Transm. (BJMT) **1**(2), 45–53 (2011)
8. Litvin, F.L., Fuentes, A.: Gear Geometry and Applied Theory, 2nd edn, 800p. Cambridge University Press (2004)
9. Ostrovski, G.N., Gushchin, V.G.: Spur gears with opposite deviations of base pitches. Izv. VUZov. Mashinostroenie **3**, 54–57 (1980) (in Russian)
10. Sandler, A.I.: Technological prerequisites for tooth-to-tooth accuracy of worm gears. In: Proceedings of International Conference "Power Transmissions-03", vol. 2, pp. 130–131. Varna, Bulgaria (2003)
11. Sandler, A.I., Lagutin, S.A.: Technique of profile localization of bearing contact in worm gears. In: Proceedings of the International Conference on Gears, pp. 1233–1244. Munich, Germany. VDI-Berichte 2108.2 (2010)
12. Sandler, A.I., Lagutin, S.A., Gudov, E.A.: Longitudinal contact localization in worm gears. Russ. Eng. Res. **34**, 480–486 (2014)
13. Sandler, A.I., Lagutin, S.A., Gudov, E.A.: Theory and practice of manufacturing of general type worm gears. Infra-Engineering, 346 p. Moscow-Vologda (2016) (in Russian)
14. Su, D., Yang, F.: Advancement in design, modelling and simulation of worm gearing with less sensitivity to Errors. In: Proceedings of the 10th World Congress on the TMM, vol. 6, pp. 2287–2292. Oulu, Finland (1999)
15. Vintila, H., Miloiu, G., Visa, F., Tiseanu, C.: Numerical research regarding contact localization at cylindrical worm gears. In: Proceedings of the 9th World Congress on the TMM, vol. 1, pp. 442–446. Milano (1995)

Multi Axis CnC Manufacturing of Straight and Spiral Bevel Gears

C. Gosselin

Abstract Multi Axis CnC gear manufacturing offers gear-makers the sort of versatility in tooth shape and tooling that no dedicated gear-cutting machine can offer, but that versatility usually comes at the expense of production volume. However, any gear-cutting machine, whether dedicated or CnC, is affected by build and wear errors that are transmitted to the workpiece. The same applies to the tools. Manufacturing errors on the tooth flank topography resulting from machining and tooling can be quite significant, and must therefore be controlled by Closed Loop. Commercially-available Computer Aided Manufacturing programs rely on a point cloud, such as IGES or STEP files, to describe the tooth flank topography. Despite being a very general approach, this method requires an external Tooth Flank Generator to create the point cloud, and therefore Closed Loop cannot be applied effectively. This document presents an integrated approach to Tooth Flank Generation, Closed Loop, and multi-axis CnC manufacturing of straight-bevel and spiral-bevel gears, in which a Unified Model is applied to different gear types. The Unified Model is used to calculate tooth flank topography, generate CMM target coordinates and use CMM output to minimize manufacturing errors. The machine settings describing tool and workpiece positions and movements in a gear-cutting machine, either before or after Closed Loop, are used to define equivalent positions and movements in a multi-axis CnC machine. Actual examples of gears cut and corrected on 5 Axis CnC machines show that the presented method is general, fast, and accurate.

Keywords Gears · Spiral-bevel · Straight-bevel · Coniflex · Simulation · Closed loop · CnC manufacturing

C. Gosselin (✉)
Involute Simulation Softwares Inc., Quebec, Canada
e-mail: HyGEARS@HyGEARS.com

V. Goldfarb et al. (eds.), *Advanced Gear Engineering*,
Mechanisms and Machine Science 51, DOI 10.1007/978-3-319-60399-5_8

1 Introduction

Multi axis CnC gear manufacturing is fast becoming mainstream in the gear industry, as it offers gear-makers the versatility in tooth shape and tooling that no dedicated gear cutting machine can offer. The cost for this versatility is decreased output volume when compared to dedicated gear-cutting machines. However, in some instances, such as very large spiral-bevel gears, multi axis CnC machines may be the only option, since gear machine makers such as Gleason and Klingelnberg do not offer machines capable of cutting spiral-bevel gears beyond ~ 2 m in diameter. And for modules up to 3.5 mm, most 5 Axis CnC machines can easily cut spiral-bevel gears using Face Mill cutters, or Coniflex™ straight-bevel gears using dish-type cutters.

Any gear-cutting machine, whether dedicated or multi-axis CnC, is inherently affected by build and wear errors that are transmitted to the workpiece. The same applies to tools. Such manufacturing errors can be quite significant in the way they affect the kinematics of a gear set, and must therefore be controlled. The Closed Loop (i.e., Corrective Machine Settings), used to control such manufacturing errors, has been in use since the early 1980s [5] in dedicated spiral-bevel gear-cutting machines, and is therefore well known. It has been expanded to spur, helical, Beveloid, straight-bevel and Coniflex gears.

Commercially available Computer Aided Manufacturing programs mostly rely on a point cloud, such as IGES or STEP files, to describe tooth flank geometry. The selected tool is then guided by the user along the tooth flank to generate the part program driving the CnC machine. Despite being a very general approach, this method can be slow, is error prone, and requires an external Tooth Flank Generator to create the point cloud, such that Closed Loop cannot be applied effectively.

This document presents an integrated approach to Tooth Flank Generation, Closed Loop, and multi-axis CnC manufacturing of straight-bevel and spiral-bevel gears, in which a Unified Model for the simulation of gear manufacturing is applied to different gear types. The Unified Model is used to calculate tooth flank topography and generate target files that are fed into a CMM whose output is then used to determine new machine settings, minimizing the differences between the manufactured part and the design simulation. The Unified Model and the machine settings describing tool and workpiece positions and movements in a gear-cutting machine, either before or after Closed Loop, are used to define equivalent positions and movements in a multi-axis CnC machine.

2 The Tooth Flank Generator

A Tooth Flank Generator can be described as a group of software functions defining the shape of a tool and its movements relative to a workpiece and solving the resulting equations within the boundaries of a given blank. Since the vast majority

of gears are generated, the generating process should be the basis of any Tooth Flank Generator.

The generating process [1] is based on the concept of a cutter blade representing one tooth of a theoretical generating gear meshing with the workpiece. The fundamental equation of meshing can be written as

$$\bar{N} \cdot \bar{V}_r = 0 \tag{1}$$

Equation (1) states that, at any point, the relative speed vector of the contacting tool and workpiece surfaces must be in a plane perpendicular to their common normal.

When applied using the reference frames of Fig. 1, Eq. (1) yields an unbounded generated surface in the workpiece reference frame. The generated surface is a function of the machine settings and three variables, respectively, cutter position α_c (angular or linear), work piece roll angle α_3, and position S of a point along the edge of the cutter blade:

$$S = f(\alpha_c, \alpha_3) \tag{2}$$

The solution of Eq. (2) is a series of contact points between the cutter blade and the workpiece describing a line along the path of the cutter blade. The envelope of a series of such lines yields a generated tooth, as shown in Fig. 3. Equation (2) is solved numerically in real time.

The Tooth Flank Generator, which uses the Unified Model of Eq. (3), includes work and tool adjustments and movements found in gear-cutting machines. In CnC controlled machines, machine settings can be continuously altered during generation, thus allowing for significant improvements in the kinematics of gear sets.

Figure 1 below represents the most general case in the simulation of cutting processes, and is therefore the basis for the Unified Model of the Tooth Flank Generator. The implicit equation of the general tooth surface is

$$\vec{X} = \vec{D}[\alpha_c]_1[\tau]_3[J]_1[R][L_{1m}]_1[\Gamma]_2[P][\alpha_3]_3[R_c]_3 \tag{3}$$

$$\vec{D} = \begin{bmatrix} S\cos(\phi) \\ 0 \\ (R \pm S\sin(\phi)) \end{bmatrix}. \tag{4}$$

Vector $\vec{D}$ in Eq. (4) is the position of a point along a Face Mill cutter blade. In Eq. (3), vector $\vec{D}$ is rotated by cutter phase angle α_c, tilt angle τ and swivel angle J, translated to the origin of the machine by vector R, rotated by cradle angle L_{1m} and root angle Γ, translated to the origin of the workpiece by vector P, rotated by roll angle α_3 and finally rotated by R_c, the Face-Hobbing-cutter-to-work-piece timing relationship (when applicable). Figure 2 shows the general definition of a Face Mill cutter blade (Fig. 3).

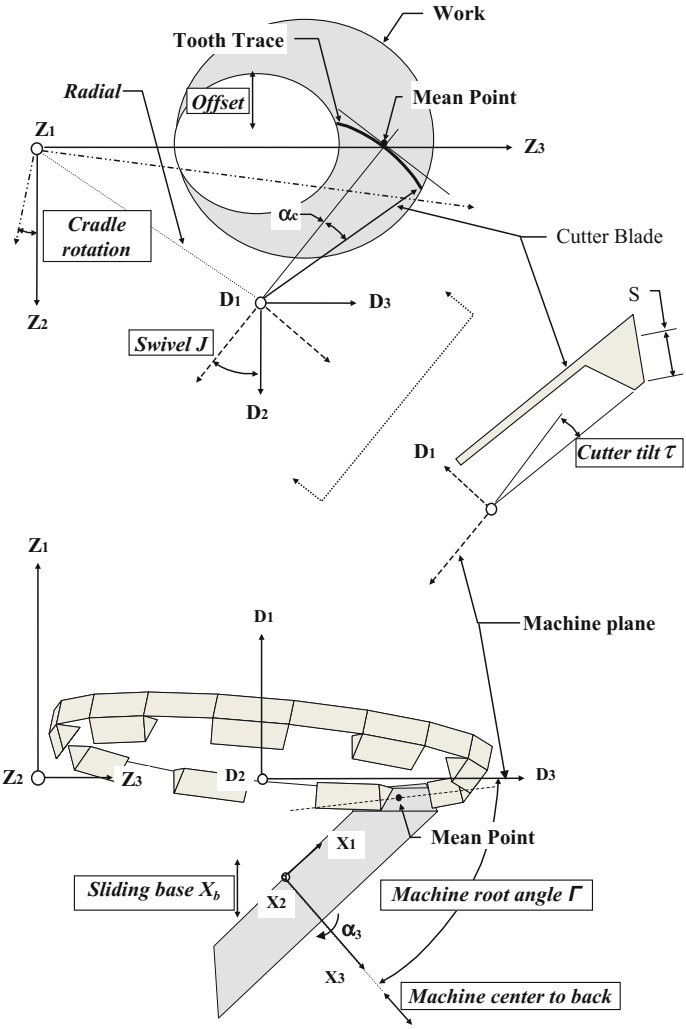

Fig. 1 Reference frames for face milling simulation

Similarly, Eq. (5) defines vector $\vec{N}$, the normal vector to the cutter blade at point S, and Eq. (6) gives the transformations required between the reference frames of the cutter blade and the work piece, from which translations R and P have been omitted.

$$\vec{N} = \begin{bmatrix} \sin(\phi) \\ 0 \\ \mp\cos(\phi) \end{bmatrix}. \tag{5}$$

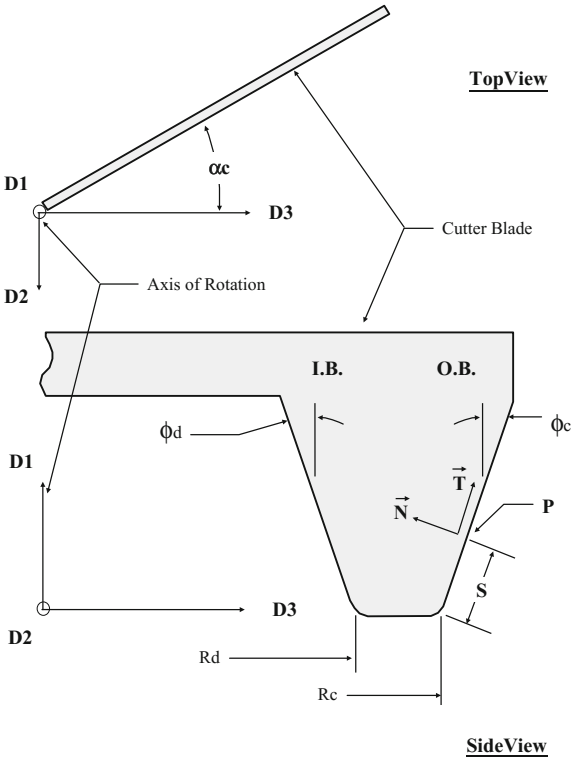

Fig. 2 Face mill cutter reference frame

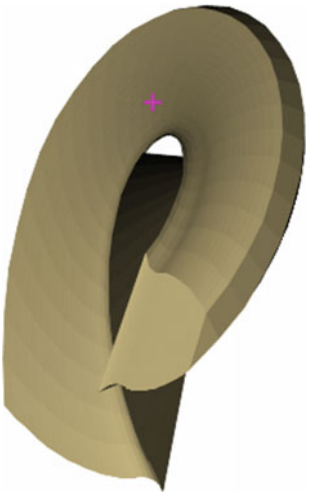

Fig. 3 Generated tooth

$$\vec{N}_x = \vec{N}[\alpha_c]_1[\tau]_3[J]_1[L_{1m}]_1[\Gamma]_2[\alpha_3]_3[R_c]_3. \quad (6)$$

In Eqs. (3) and (6), rotations and translations can be expanded into Taylor series to allow for higher order manufacturing flexibility on CnC controlled machines.

For straight-bevel gears cut by a 2-tool generator, the terms involving cutter tilt τ, cutter swivel J and Face Hobbing rotation R_c are dropped from Eqs. (3) and (6), and cutter phase angle α_c becomes a translation of the tool. For Coniflex™ gears, the terms involving cutter swivel J and Face Hobbing rotation R_c are dropped from Eqs. (3) and (6).

3 Calibration of the Tooth Flank Generator

Fundamentally, the Tooth Flank Generator is aimed at digitally reproducing the same tooth surfaces as would be cut on an actual machine. It is therefore important to establish the exactness of the simulation such that one can assume that the tool movements in a CnC machine will replicate the desired tooth surface independently of the tool used.

In order to calibrate the Tooth Flank Generator, its output must be compared to something reliable and universally accepted in the industry. For this purpose, two sources stand out for spiral-bevel gears: The Gleason Works and Klingelnberg GmbH, the world leaders in spiral-bevel gear manufacturing technology.

3.1 Comparison with Gleason's CAGE

The output of the Tooth Flank Generator described in the previous section is compared to the CMM Nominal obtained from Gleason's CAGE software.

Using the Basic machine settings for an 8 × 39 Face Milled spiral-bevel pinion, Fig. 4 below shows the differences between the CAGE simulation (red lines for the OB, blue lines for the IB) and the simulation based on the presented Tooth Flank Generator (black lines). Except for two points at the heel at the bottom of the OB and IB flanks of the tooth (upper and lower right corners), the Tooth Flank Generator output is identical to that of CAGE within 0.0002 mm.

3.2 Comparison with Klingelnberg's KiMOS

The output of the Tooth Flank Generator described in the previous section is compared to the CMM Nominal obtained from Klingelnberg's KIMoS software.

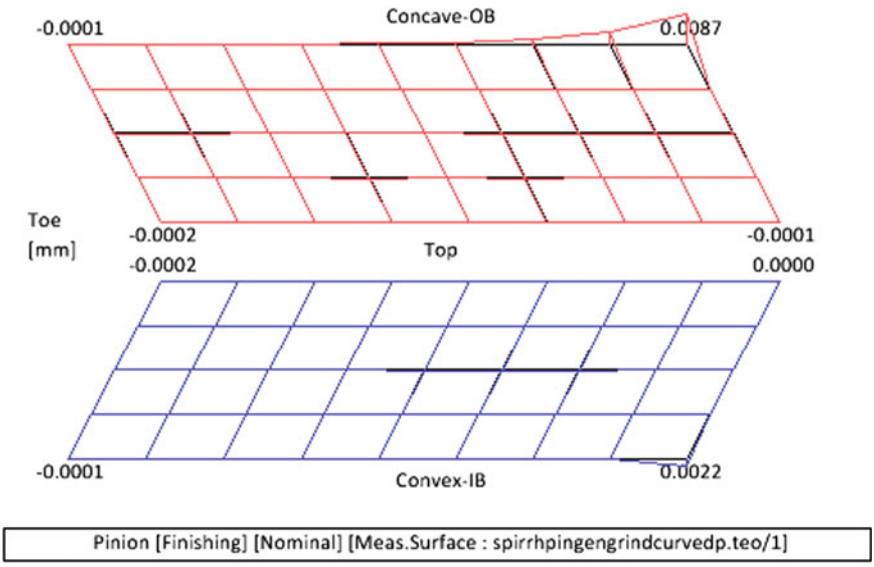

Fig. 4 Comparison with CAGE—8 × 37 face milled spiral-bevel pinion

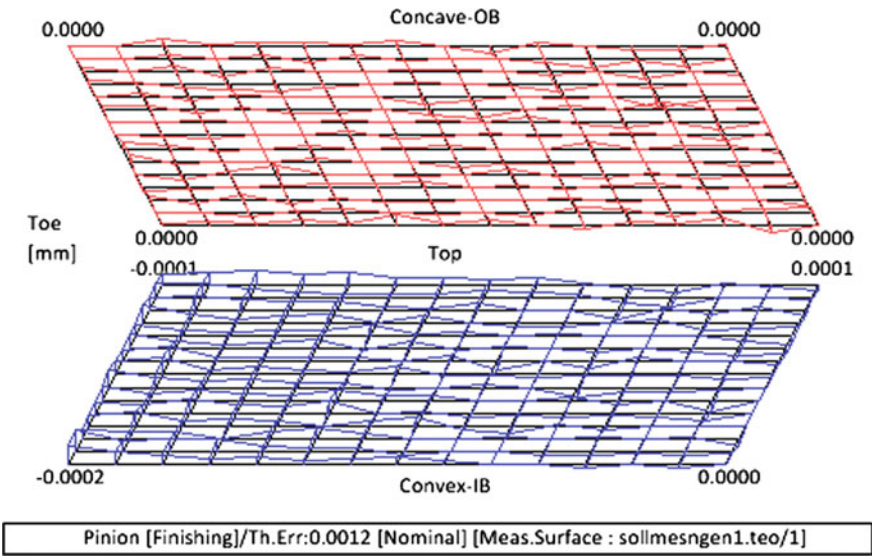

Fig. 5 Comparison with KIMoS—8 × 37 face milled spiral-bevel pinion

Using the same Basic machine settings as for the above 8 × 39 Face Milled spiral-bevel pinion, Fig. 5 below shows the differences between the KIMoS simulation (red lines for the OB, blue lines for the IB) and the simulation based on the

presented Tooth Flank Generator (black lines). The deviations noted with Gleason's CAGE near the fillet at the heel have disappeared, and the Tooth Flank Generator output is identical to KIMoS' output within 0.0002 mm.

4 Closed Loop

The Closed Loop, an essential part of any gear manufacturing software, calculates changes in machine settings to remove surface errors caused by machine and tool, and matches the manufactured tooth surface to the designed tooth surface [2–4].

The following surface errors are generally considered adequate to describe the quality of a tooth flank and are used in the Closed Loop. Average surface errors are calculated as follows:

- Pressure angle error:

$$\Phi = \frac{\sum_{col=1}^{j} \frac{\left[\sum_{row=1}^{i} \frac{\varepsilon_{i,j}-\varepsilon_{1,j}}{y_{i,j}-y_{1,j}}\right]}{i}}{j}; \tag{7}$$

- Spiral angle error:

$$\Psi = \frac{\sum_{row=1}^{i} \frac{\left[\sum_{col=1}^{j} \frac{\varepsilon_{i,j}-\varepsilon_{i,1}}{x_{i,j}-x_{i,1}}\right]}{j}}{i}; \tag{8}$$

- Lengthwise crowning error:

$$\Xi = \frac{\sum_{row=1}^{i} \frac{(2\varepsilon_{i,mid}-(\varepsilon_{i,1}+\varepsilon_{i,j}))}{2}}{i}; \tag{9}$$

- Bias error:

$$\zeta = \Phi_1 - \Phi_j; \tag{10}$$

- Profile curvature error:

$$\xi = \frac{\sum_{col=1}^{j} \frac{(2\varepsilon_{mid,j}-(\varepsilon_{1,j}+\varepsilon_{i,j}))}{2}}{j}; \tag{11}$$

where

- i is the index of row data along the face width,
- j is the index of column data depthwise,

- *mid* is the index of the mid-column or mid-row data,
- $\varepsilon_{i,j}$ is the error value at point ij of the measurement grid,
- $x_{i,j}$ is the distance between points along the face width,
- $y_{i,j}$ is the distance between measurement points depthwise.

Surface Matching, the algorithm used in Closed Loop, is based on the response of the error surface, i.e., the difference between the simulated and measured tooth surfaces (Fig. 6) to changes in selected machine settings. Sensitivity factors are obtained by changing machine settings, recalculating the error surface and solving Eqs. (7)–(11).

In the Surface Matching algorithm, a combination of machine settings is sought such that the theoretical surface matches the measured surface. To achieve this, the following objective functions are to be satisfied:

$$\Phi(m_i) - T_1 \leq L_1, \tag{12}$$

$$\Psi(m_i) - T_2 \leq L_2, \tag{13}$$

$$\Xi(m_i) - T_3 \leq L_3, \tag{14}$$

$$\zeta(m_i) - T_4 \leq L_4, \tag{15}$$

$$\xi(m_i) - T_5 \leq L_5, \tag{16}$$

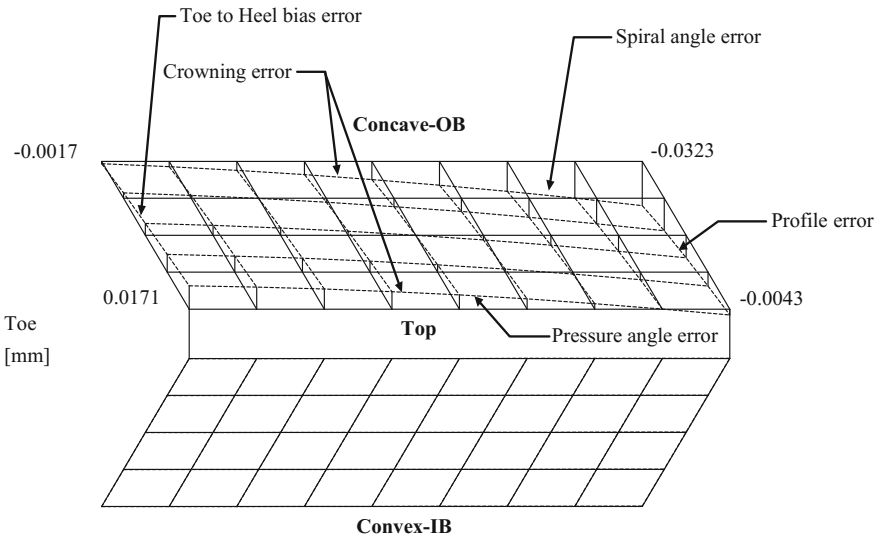

Fig. 6 Error surface

where

- m_i are the considered machine settings,
- Φ and Ψ are the averaged pressure and spiral angle errors,
- Ξ and ζ are the lengthwise crowning and bias error values,
- ξ is the profile curvature error,
- T_i are target surface deviations,
- L_i are the tolerances within which the objective functions can be considered satisfied.

A Newton-Raphson-based solution is used to solve the above functions. The solution yields new settings for a dedicated machine, which are converted to a 5 Axis CnC machine.

5 Tools Used in CnC Gear Manufacturing

Thanks to the flexibility in movement and tool orientation offered by multi-axis CnC machines, virtually any tool type can be used to cut gears. The most frequently found tools are:

- Face Mill cutter,
- Coniflex™ dish type cutter,
- Conical Side Milling Tool, or CoSIMT for short,
- End Mill,
- Ball Mill.

Other tools are also used in applications such as Skiving for internal gears and splines, but are not used for straight or spiral-bevel gears, and therefore will not be considered here.

5.1 Face Mill Cutter

Face Mill cutters used to cut spiral-bevel gears in multi-axis CnC machines are no different from those used in dedicated spiral-bevel gear-cutting machines, with the exception of the chucking head, for which a special adapter may be required.

Cutters up to $\sim$7.5″ diameter can be used on an average multi-axis CnC machine. Beyond 7.5″ diameter, power and stiffness requirements may not be satisfied, which limits the gear module that can be cut on a normal multi-axis CnC machine with a Face Mill cutter.

Face Mill cutters come in three basic embodiments:

(i) with solid blades (Fig. 7) for which no adjustment is possible; this is usually found on small diameter cutters;

Fig. 7 Solid face mill cutter (*Photo courtesy* Harbin Tool Works)

Fig. 8 Face mill cutter with detachable blades (*Photo courtesy* Weiku.com)

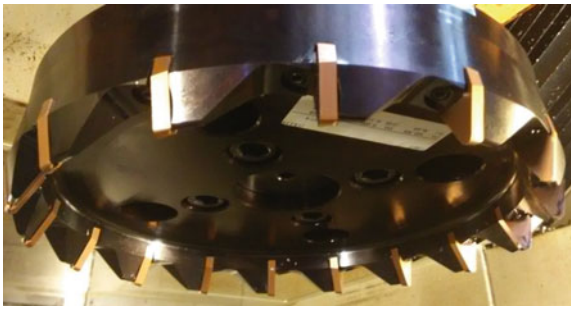

Fig. 9 Face mill cutter with replaceable inserts (*Photo courtesy* Sandvik Coromant)

(ii) with detachable blades (Fig. 8) for grinding and radial adjustment; usually found in medium to large size cutters;
(iii) with replaceable inserts (Fig. 9) for which no adjustment is possible; this is an economical solution for roughing prior to heat treatment and finish

grinding, since the inserts are rather inexpensive when compared to roughing with a cutter with detachable blades, or to solid grinding for which grinding wheels are expensive, need to be dressed and wear out rapidly.

In cases (i) and (ii) above, blades need to be sharpened at given intervals. Case (iii) requires the inserts to be changed when needed.

The basic geometry of a Face Mill cutter is described in Fig. 10 below, in which the cutting edge of the blade can be straight or circular. The Average Diameter is given at the center of the Point Width and denotes a cutter used in completing cycles, such as Spread Blade™, Duplex Helical™ and Formate™.

Figure 11 below shows a variant of the basic Face Mill cutter, but with TopRem™, in which a section of the blade has a different angle in order to create a protuberance at the bottom of the tooth. A protuberance is often to be desired for the purpose of preventing tool contact with the fillet at the finishing operation after heat treatment, and also applies just as much to grinding as to lapping.

Cutting cycles such as Fixed Setting™ and Modified Roll™ usually require one roughing cutter, such as the Basic Face Mill cutter in Fig. 10, and two finishing cutters (Fig. 12), one for the Convex flank (I.B.) and one for the Concave flank (O.B.), for which the machine settings are usually different.

5.2 *Coniflex™ Dish Type Cutter*

Coniflex™ cutters (Fig. 13) are used to cut straight-bevel gears with lengthwise crowning. These are available either in solid form (Fig. 13) or with replaceable blades that can be ground. While cutting cycles are short, Coniflex cutters quickly

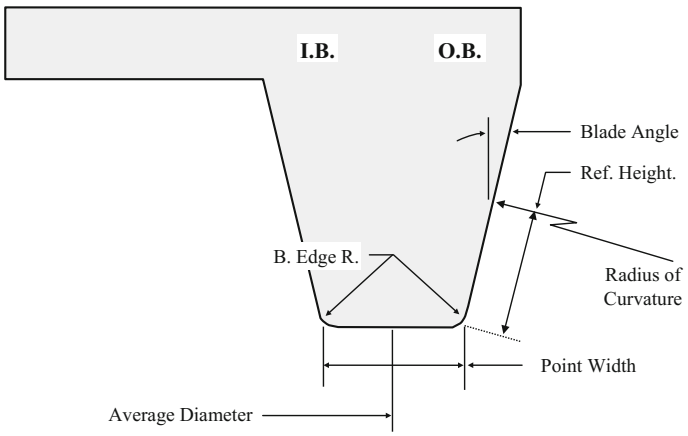

Fig. 10 Basic face mill cutter

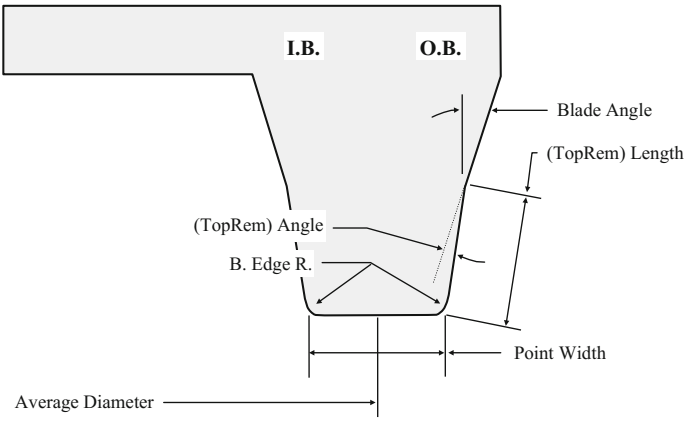

Fig. 11 Face mill cutter with TopRem™

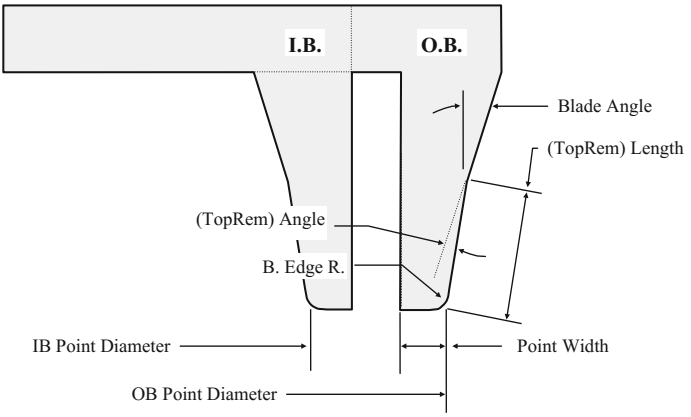

Fig. 12 Fixed setting cutter with TopRem™

grow in diameter with the module. Available in sizes of 4.25″, 9″ and 15″, only the smaller variant of 4.25″ diameter is really practical on multi-axis CnC machines because of power requirements and weight considerations when the diameter reaches 9″ and above.

The original, mechanical Coniflex™ machines from the Gleason Works use two interlocking cutters (Fig. 14), such that both the left and right tooth flanks are cut simultaneously. In multi-axis CnC cutting, only one cutter can be used at any given time, and therefore the left and right tooth flanks are cut in two separate cycles. While this cutting cycle may appear to be somewhat slower than that of the conventional mechanical machine, cutter tilt can be modified freely in CnC machines and thus offers more flexibility in the design of Coniflex gear sets.

Fig. 13 Coniflex™ cutters (*Photo courtesy* The Gleason Works)

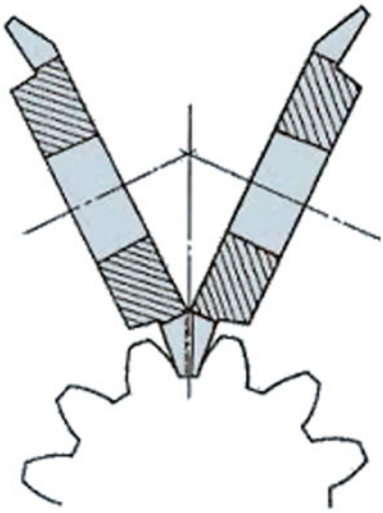

Fig. 14 Coniflex™ cutters (*Photo courtesy* Arrow Gear)

5.3 Conical Side Milling Tool (CoSIMT)

A Conical Side Milling Tool, or CoSIMT, is a milling tool of variable shape. It can be found either with solid blades (Fig. 15) or with replaceable inserts. CoSIMT tools typically have high feed rates, and are thus well-suited to gear milling. The initial tool cost of the CoSIMT body is easily offset by the superior output.

CoSIMT tools can be used to cut any tooth shape with a convex profile curvature. This therefore excludes Face Gears for which the profile curvature is concave.

Fig. 15 CoroMill 327 CoSIMT (*Photo courtesy* Sandvik Coromant)

CoSIMT are offered in various shapes and sizes. Figure 16 shows the general definition of a CoSIMT, for which the *Outside Angle* can be positive, null or negative, which results in the tools shown in Fig. 17. The *Inside* cutting edge is on the same side as the arbor.

- When the *Outside Angle* is positive, both the Outside and Inside cutting edges are on a Convex cone, which results in a single contact point between the tool and the work piece in the lengthwise direction; thus, it is good if the lengthwise curvature is concave, such as the OB side of spiral-bevel gears.
- When the *Outside Angle* is null, the Outside cutting edge is a plane, and therefore offers advantageous cutting conditions for straight-bevel, spur and helical gears with no lengthwise crowning.
- When the *Outside Angle* is negative, a Concave cone results, and the tool can now be used to cut gear teeth with a convex lengthwise curvature, such as Coniflex and the IB side of spiral-bevel gears.

Theoretically, the cutting edges could also be curved, as shown in the upper right corner of Fig. 16. Although not yet offered on the market, curved blades would allow for a cost-effective generation of Face Gear teeth in which the profile curvature is concave, whereas the current option is to use Ball Mill tools that are much slower.

5.4 End Mill Tools

End Mill tools present a shape similar to that of a drill bit (Fig. 18), except that they are designed to cut with their side flukes. Depending on the End Mill diameter, the

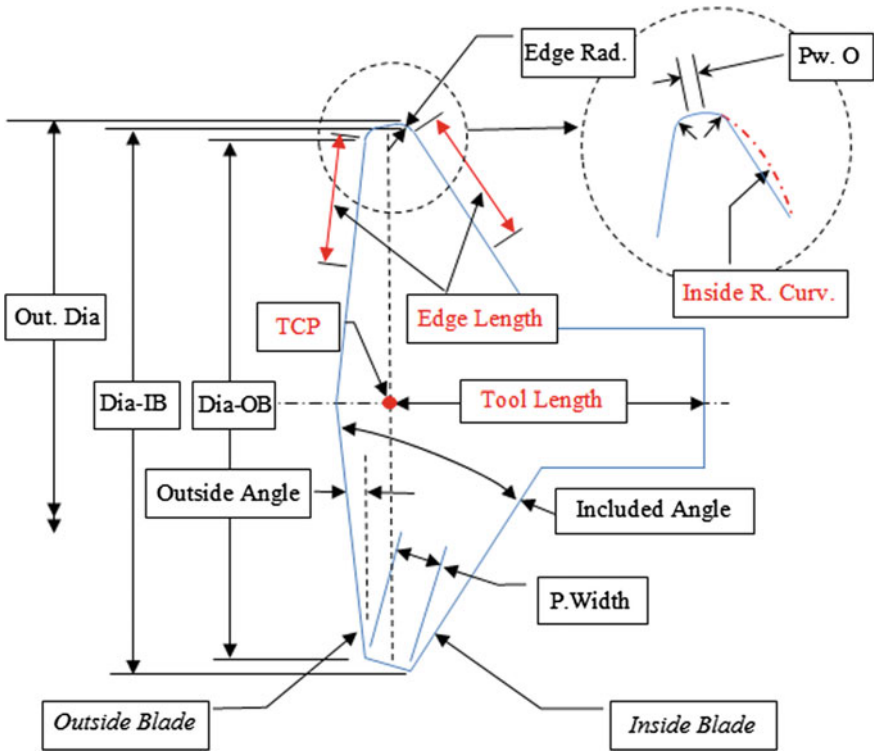

Fig. 16 CoSIMT general definition (*Photo courtesy* Involute Simulation Softwares)

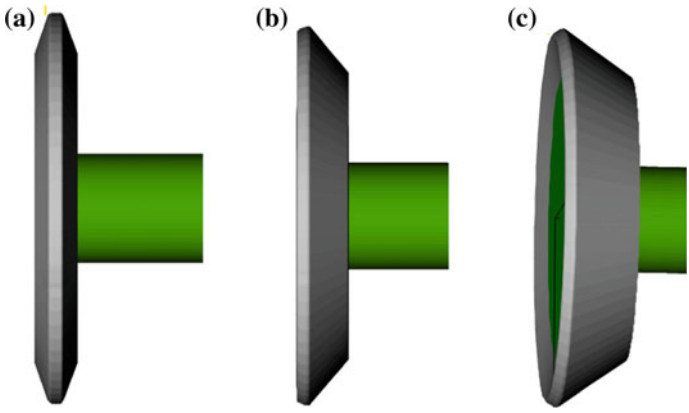

Fig. 17 **a** Positive *outside angle*, **b** null *outside angle* and **c** negative *outside angle*

Fig. 18 End mill tools

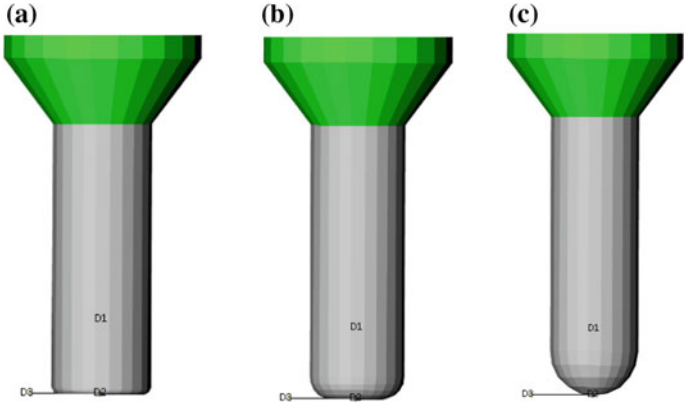

Fig. 19 **a** Square end mill, **b** bull nose end mill and **c** ball nose end mill

depth of cut, whether the removed material is a slot or a profile, and the type and hardness of the material, feed rates in steel vary from less than 100 mm/min for the smaller diameters to more than 1500 mm/min for the larger diameters.

Two significant advantages of End Mill tools are their wide range of dimensions and comparatively low cost. Major disadvantages include their high wear and slow feed rates for small diameter tools, which is often the case when cutting gears of small to medium size modules for which slot width is limited to less than 6 mm.

End Mill tools can be broadly classified as follows (Fig. 19):

- *Square*: no edge radius; normally a small break-edge; used to open a tooth flank gap (roughing operation) or to finish cutting the tooth flank;
- *Bull Nose*: edge radius less than ½ the End Mill diameter; used to open the gap in the fillet (roughing operation), or to finish cut the fillet;
- *Ball Nose*: edge radius equal to ½ the End Mill diameter; used to open the gap in the fillet (roughing operation), or to finish cut the fillet.

5.5 Ball Mill Tools

Ball Mill tools present a shape with a sphere at the cutting end (Fig. 20), usually followed by a contraction, a tapered section and a stem of constant diameter. Only the sphere end is meant to cut.

Functionally speaking, Ball Mill and Ball Nose tools are interchangeable when cutting a tooth fillet, since only the spherical end of the End Mill tool is used. The Ball Mill tool (Fig. 21) has the advantage of a slight contraction between the cutting

Fig. 20 Ball mill tool

Fig. 21 Ball mill tool

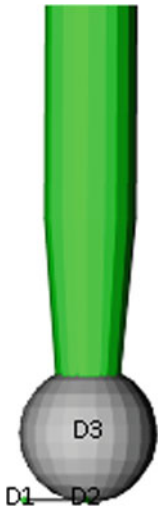

sphere and the tapered section leading to the stem, which allows for introducing a protuberance, i.e., negative stock, into the fillet without damaging the tooth profile, whereas the straight section of a Ball Nose tool immediately above the spherical end may remove some material on the profile if negative stock is important.

The contraction above the cutting sphere of a Ball Mill tool also introduces a weakness because of the reduced section, and thus feed rate and cutting depth may have to be reduced.

Similarly to End Mill tools, Ball Mill tools are available in a wide range of dimensions at comparatively low cost. Major disadvantages include their high wear and slow feed rates for small diameter tools, which is often the case when cutting gears of small to medium size modules for which slot width is limited to less than 6 mm. Ball Mill tools also tend to cut in the same area of the sphere when finishing a tooth flank, thus accelerating wear.

6 Conversion from Dedicated to CnC Machine

Figure 22 below shows a Face Mill cutter in a dedicated machine. In the approach proposed here, the Face Mill cutter is replaced by another tool (such as a Conical Side Milling Tool, i.e., CoSIMT), which is forced to follow the path of one cutter blade of the Face Mill cutter (Fig. 23). This approach is extended to Coniflex,

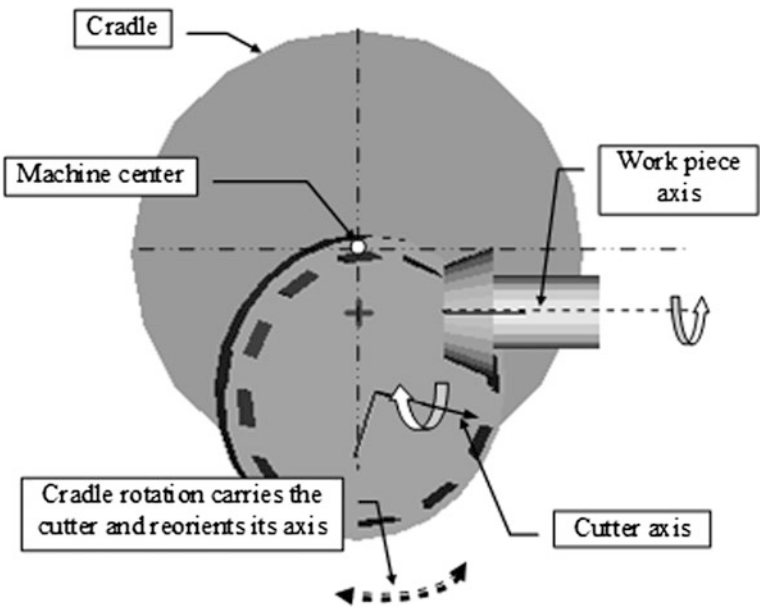

Fig. 22 Ref. cutter and work piece relative position

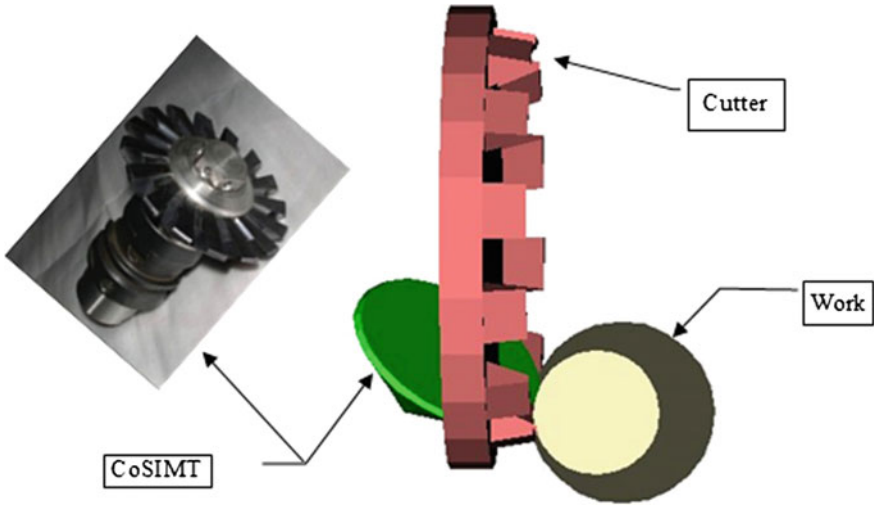

Fig. 23 Ref. cutter and CoSIMT

End Mill and Ball Mill tools, and readily lends itself to the use of Closed Loop described above.

The conversion from a conventional gear-cutting machine to a multi-axis CnC machine is based on two conditions:

(i) Maintaining the location of the tool in relation to the origin of the reference frame attached to the workpiece, and
(ii) Maintaining the relative orientation and phase angle between the axis of the tool and that of the workpiece (Fig. 22).

Referring to Eq. (3), the position of the center point of a Face Mill cutter, in the workpiece reference frame, is given as

$$\vec{X}_c = \begin{bmatrix} 0 \\ 0 \\ 0 \end{bmatrix} [R][L_{1m}]_1[\Gamma]_2[P][\alpha_3]_3. \tag{17}$$

Referring to Eq. (6), the orientation of the axis of a Face Mill cutter, in the workpiece reference frame, is given as

$$\vec{N}_c = \begin{bmatrix} 1 \\ 0 \\ 0 \end{bmatrix} [\tau]_3[J]_1[L_{1m}]_1[\Gamma]_2[\alpha_3]_3. \tag{18}$$

The axis of rotation of the workpiece being

$$\vec{X}_3 = \begin{bmatrix} 0 \\ 0 \\ 1 \end{bmatrix}, \tag{19}$$

Angle Λ between the axis of the cutter and that of the workpiece is therefore

$$\Lambda = \vec{X}_3 \cdot \vec{N}_c. \tag{20}$$

Multi-axis CnC lathes and milling machines can come in different architectures, as explained in the following section. All 5 axis architectures can accommodate any angle Λ between the axis of the tool and the workpiece.

Tools include dish-type cutters for Coniflex™ straight-bevel gears, Face Mill cutters compatible with the CnC machine size, and Conical Side Milling Tool cutters (or CoSIMT), such as Sandvik's InvoMill, End Mill and Ball Mill tools. Basically, End Mill, Ball Mill and CoSIMT tools can cut any tooth shape, including Face Hobbed gears. Each tool type requires a specific definition for Eqs. (17) and (18) in order to calculate angle Λ in Eq. (20).

7 CnC Machine Architectures

5 Axis CnC machines found in the market comprise three main architectures, as described below. Machines are offered with a variety of controllers, which allow the CnC machine manufacturer to define the names and signs of all the axes (i.e., rename the axes as desired). The coordinates in part programs fed to the controller can be given as:

(i) *Machine coordinates*, i.e., in a fixed reference frame attached to the machine body; angles A, B and C are used to tilt the turntable, pivot the machine head, and rotate the workpiece;

(ii) *Workpiece coordinates*, i.e., in a reference frame rotating with the workpiece with a zero along the axis of rotation, such as the pitch apex of bevel gears; angles A, B and C are used to tilt the turntable, pivot the machine head, and rotate the workpiece;

(iii) *Workpiece coordinates and tool unit vector*, i.e., as in (ii) above for the linear axes; however, a unit vector gives the orientation of the tool axis which the controller converts into angles A, B and C to tilt the turntable, pivot the machine head, and rotate the workpiece.

7.1 Tilting Turntable

The turntable (Fig. 24) on which the workpiece is installed can both rotate by angle C about its axis of symmetry and tilt by angle A about axis X. The machine head/turntable can be translated along axes X, Y and Z.

This machine type is well-adapted to small workpieces with short shafts. When the parts become large, weight considerations become predominant and tilting precision suffers. Turntable tilt angle A is usually limited around ±100°.

7.2 Pivoting Tool Head

The turntable (Fig. 25) on which the work piece is installed is fixed in orientation and rotates by angle C about axis Z; the tool head pivots by angle B about axis Y. The machine head/turntable can be translated along axes X, Y and Z. Tool pivot angle B is usually limited around ±100°.

This machine type is well adapted to cutting pinions on long shafts when embodied as a lathe. In lathes, the OD of the part is limited by the travel of the head in the radial direction. Also, machine head pivot is only allowed in one direction when a short shaft work piece is mounted directly on the turntable to prevent collisions. The axis of the turntable can also be vertical, and in this case, is well-suited to cutting large bevel gears on short shafts.

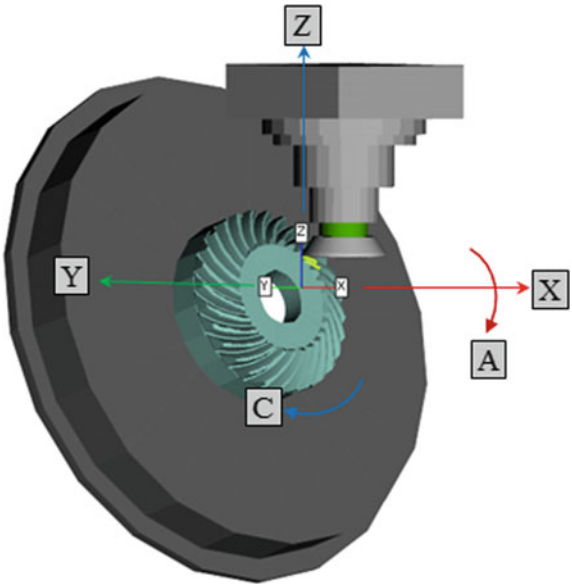

Fig. 24 Tilting turntable 5 axis CnC machine

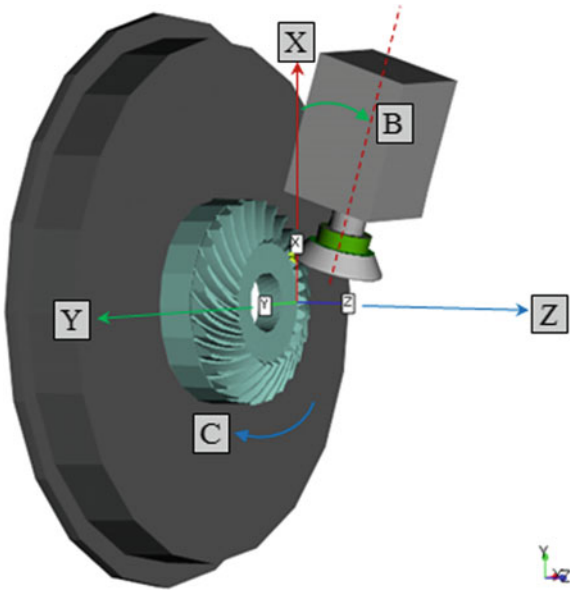

Fig. 25 Pivoting tool head 5 axis CnC machine

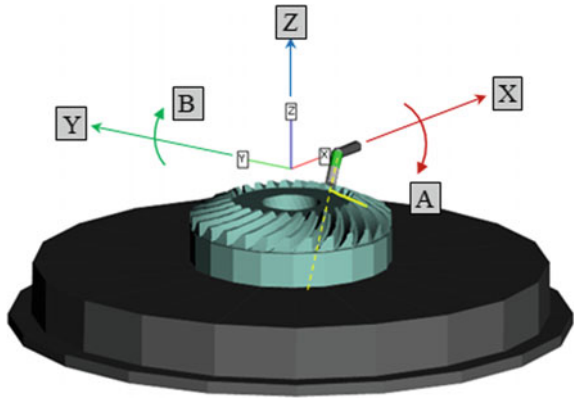

Fig. 26 Tilting and swiveling tool head 5 axis CnC machine

7.3 Tilting and Swiveling Tool Head

The turntable (Fig. 26) on which the workpiece is installed is fixed; the tool head tilts by angle B about axis Y and swivels by angle A about axis X. The machine head can be translated along axes X, Y and Z. Turntable rotation is used solely for indexing.

This machine type is well-adapted to cutting bevel gears of large diameter. Indexing precision is affected by the weight of the workpiece. The overhung machine head can be an issue with heavy tools.

8 Cutting Cycles with Multi Axis CnC Machines

Given the different tool types and shapes described above, different cutting cycles are to be expected in order to offer flexibility and allow for cycle optimization. Several cutting cycle possibilities are presented below for each tool type.

8.1 Face Milling Cutter

Spiral-bevel gears can be either generated (with or without helical motion and modified roll) or non-generated, i.e., Formate™ cut.

Basically, the cutting cycle of a generated spiral-bevel workpiece involves (Fig. 27):

- Plunging the tool to a given depth, at Toe or Heel,
- Generating the part, either in an up-roll or down-roll direction,
- Retracting the tool above the blank and returning the tool to its plunging position,
- Indexing the workpiece to cut the next tooth gap.

Single-roll or double-roll can also be desired; single-roll (Fig. 27) implies that, after plunging the tool, the part is generated either in an up-roll or down-roll direction, at the end of which the tool is retracted (dotted line) and returned to its starting location, and the cycle recommences for the next tooth gap.

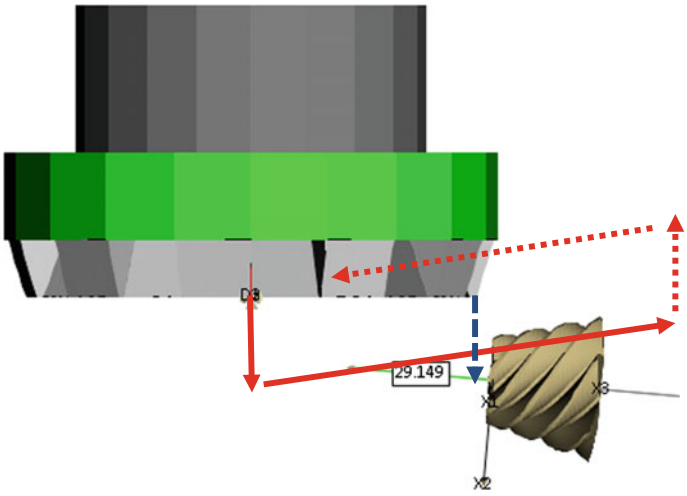

Fig. 27 Single-roll *external* plunge

In double-roll (Fig. 28), the tool is plunged to a *set in* position, i.e., before full depth, and the part is generated in one direction, either up-roll or down-roll; at the end of the rolling motion, the tool is plunged *full depth* and returns to the starting end of the tooth gap while generating. The tool is then retracted (dotted line) and the cycle recommences for the next tooth gap.

Several factors can affect tooth flank quality and cycle time:

- Height to which the tool is retracted above the blank;
- Whether the tool is plunged full speed *outside* the blank (outside Toe in Fig. 27) and rolling then begins, or the tool is plunged at a lower feed rate at the very beginning of the rolling motion (at Toe in Fig. 29) i.e., in the tooth itself;
- How many tooth gaps are skipped when indexing, such as to spread tool wear, heat generation and indexing errors around the part.

For non-generated gears, basically a simple plunge cut is needed. The cycle can also be used to *rough* generated parts, but without generation.

8.2 *Coniflex™ Cutter*

Coniflex bevel gears can be cut using dish-type cutters such as those shown in Figs. 13 and 14. Coniflex bevel gears are always generated.

On a multi-axis CnC machine, the cutting cycle involves (Fig. 30):

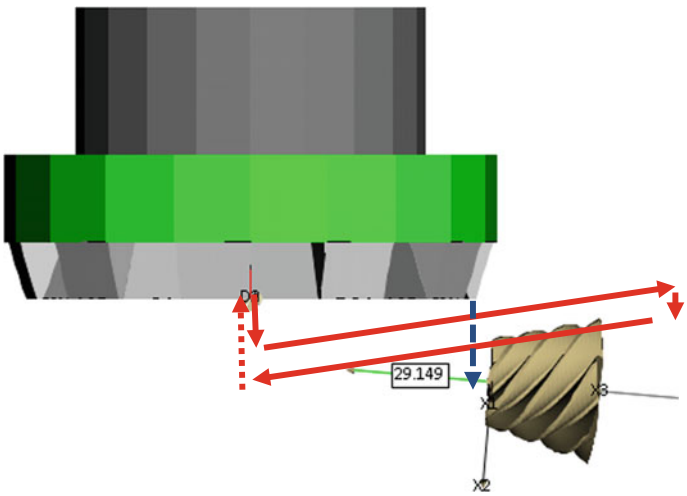

Fig. 28 Double-roll *external* plunge

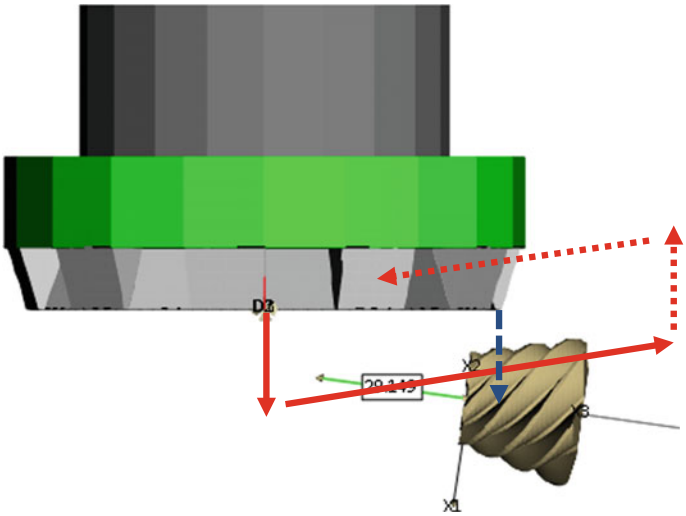

Fig. 29 Single-roll *internal* plunge

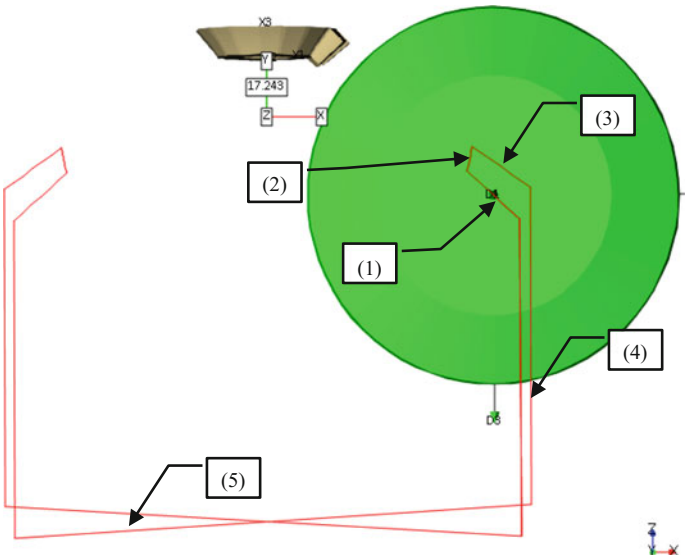

Fig. 30 Coniflex cycle on a 5 axis CnC machine

- Plunging the tool from a position above the blank (1),
- Rolling one tooth flank (2),
- Retracting the tool (3),

- Indexing the part and recommencing the cycle until all the tooth flanks on one side of the teeth have been generated;
- and subsequently withdrawing the tool (4) beyond the apex of the part and moving it to the opposite side of the workpiece (5) where the other tooth flanks are generated in the same manner.

8.3 CoSIMT, End Mill and Ball Mill Tools

These tools share similarities that allow us to treat them as a group. Specifics will be noted in the text when required.

Generally speaking, cutting cycles involve either moving the tool *along the face width*, or in the *depthwise* direction. It is also advantageous to consider the tooth flank and the fillet separately in order to use the most appropriate tool for each.

- *Along the face width*: each time the tool reaches the end of the tooth, it is stepped down progressively from the tooth tip to the fillet (Fig. 31); when the bottom is reached, the tool is retracted and returned to the starting position to cut another tooth flank; this can be inversed, starting at the tooth bottom and finishing at the tooth tip.
- *Depthwise direction*: the tool follows the tooth flank from tip to fillet (Fig. 32); the cycle can then advance the tool along the face width and backtrack from the fillet to the tip along the tooth profile; or else, the tool is retracted, advanced along the face width, and the cycle starts again from the tooth tip to the fillet.

Cutting depthwise is especially well-adapted to CoSIMT tools that have a flat face, as depicted in Fig. 32, where, in this case, the Inside Blade angle is null.

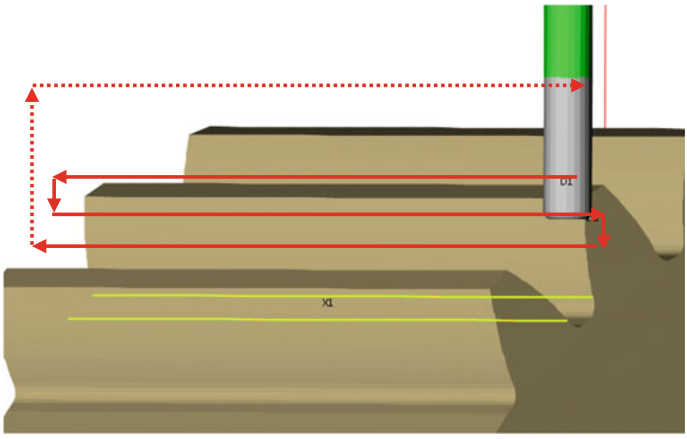

Fig. 31 Cutting *along the face width*

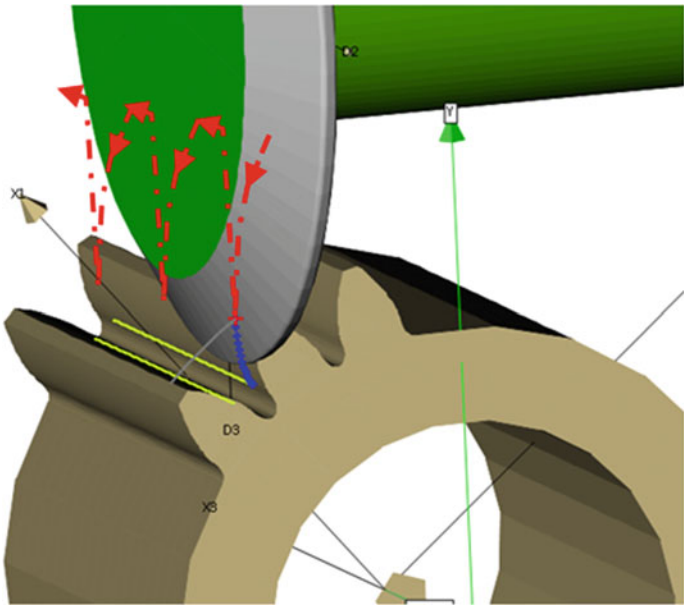

Fig. 32 Cutting *depth wise*

However, scalloping will occur along the face width near the bottom of the teeth, as shown in Fig. 33, and one or more tool passes along the face width may be required to ensure a smooth finish near the fillet.

- *In the fillet*: given that the tool must be spherical to cut the fillet, a cutting cycle *along the face width* gives the best results. This usually implies Ball Nose or Ball Mill tools whose radius is less than that of the fillet, thus possessing a slow feed rate. A faster approach is to use a CoSIMT tool (Fig. 34) with a feed rate several times that of a Ball Nose or Ball Mill tool.

Let us now consider the End Mill tool shown in Fig. 35, in several cutting positions along the profile of a spur gear tooth (this will make things easier to visualize): it is clear that scallops will be left on the profile because of the limited number of tool positions. Knowing the equation of the tooth surface, provided by the Tooth Flank Generator, allows for calculating the height of the scallop and optimizing the cycle for surface quality versus consumed time.

When a Ball Mill is used, as in Fig. 36, scallop height will be much larger if the depthwise step is the same as for an End Mill, which implies a greater number of—and more closely spaced—depthwise tool passes to achieve the desired tooth surface quality. Cycle time can be as much as 10 times more than for an End Mill to achieve the same surface quality.

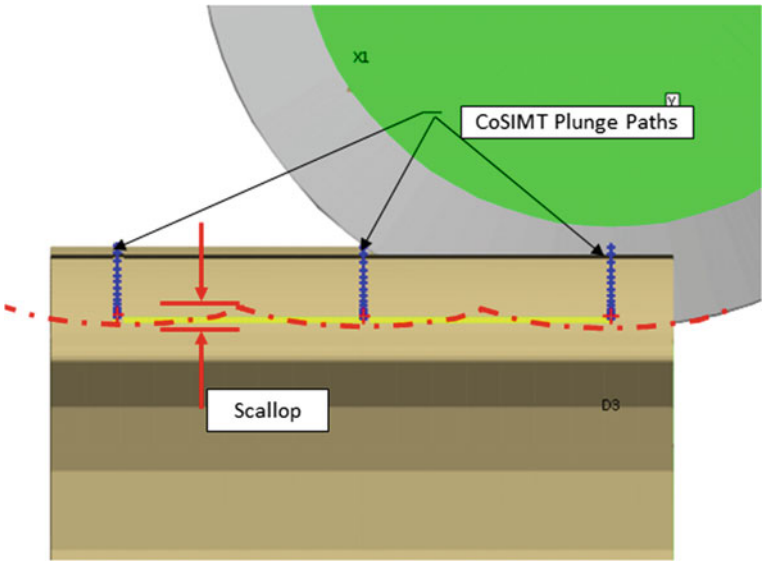

Fig. 33 Scalloping when cutting depth wise

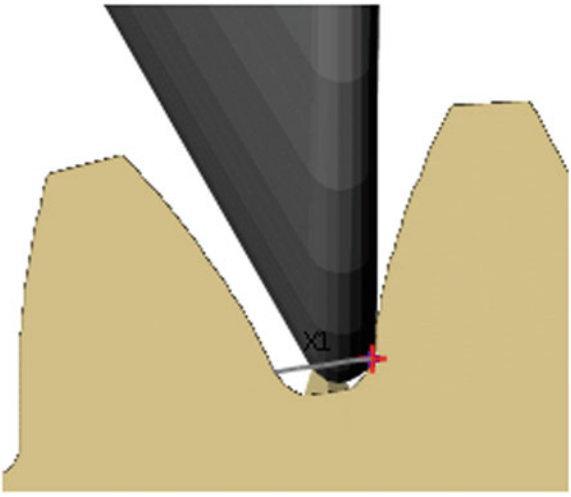

Fig. 34 Fillet finishing with a CoSIMT tool

To cut the tooth flank, it is therefore desirable to use a tool with a straight cutting edge or, if available, a concave cutting edge, rather than a tool with a convex cutting edge such as a Ball Mill. CoSIMT and End Mill tools fall into this category.

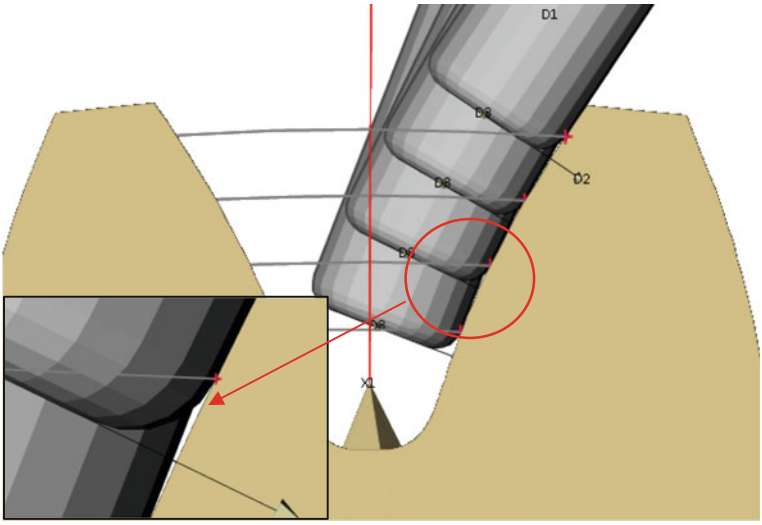

Fig. 35 End mill tool and tooth profile scalloping

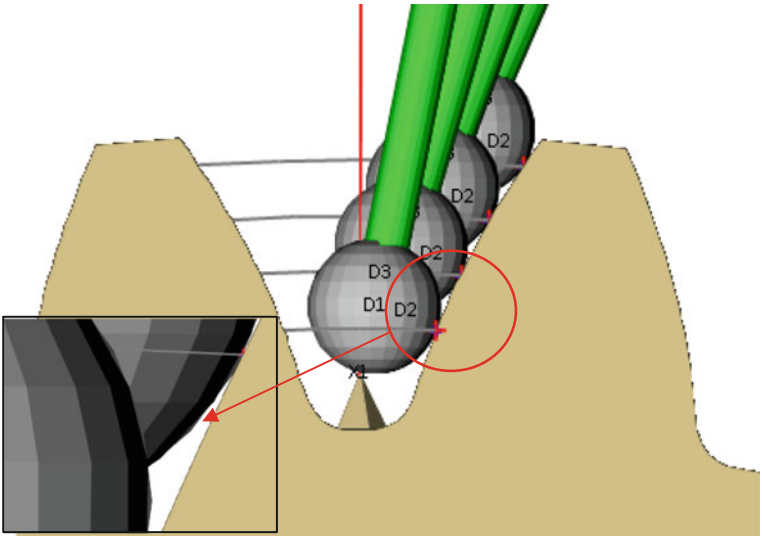

Fig. 36 Ball mill tool and tooth profile scalloping

9 Applications

The following examples demonstrate the effectiveness of the methods presented above using different gear geometries, tools, and 5 Axis CnC machines. Closed Loop, while possible with commercial CAM software based on clouds of points,

such as STEP files, describing the tooth surfaces, is much slower and does not offer the same effectiveness as that based on a Tooth Flank Generator (as presented above).

9.1 Application 1: 32 Tooth, 1.25 mm Module, Coniflex Pinion; Dish-Type Cutter

This pinion was cut on a tilting turntable type 5 Axis CnC machine. The first cut yielded the results shown in Fig. 37. Helix (fb) and pressure (fa) angle errors are visible on both tooth flanks (Table 1).

Figure 38 shows the same part after the 1st Closed Loop iteration, where pressure and helix angle errors have all but disappeared (Table 2).

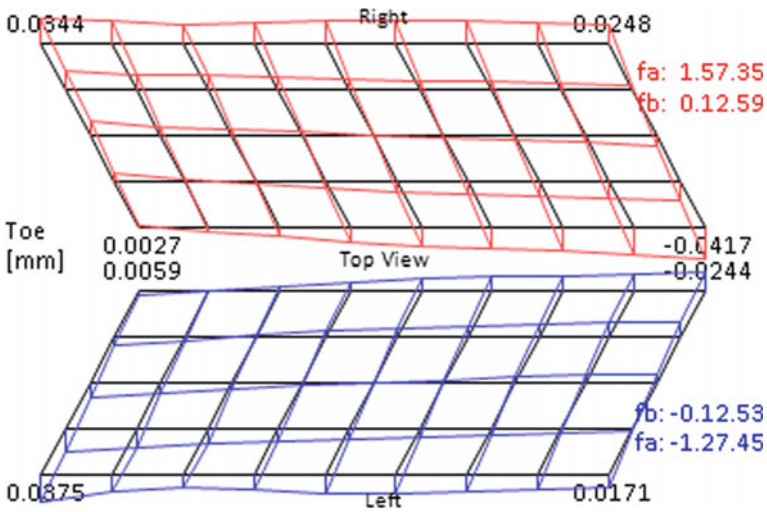

Fig. 37 Error surface after 1st cut

Table 1 Averaged surface errors after 1st cut

Average error	Right flank	Left flank
Tooth thickness	0.0087	
Pressure angle	1.57.35	−1.27.45
Helix angle	0.12.59	−0.12.53
Lengthwise crowning	−0.0029	−0.0050
Profile curvature	−0.0024	−0.0032

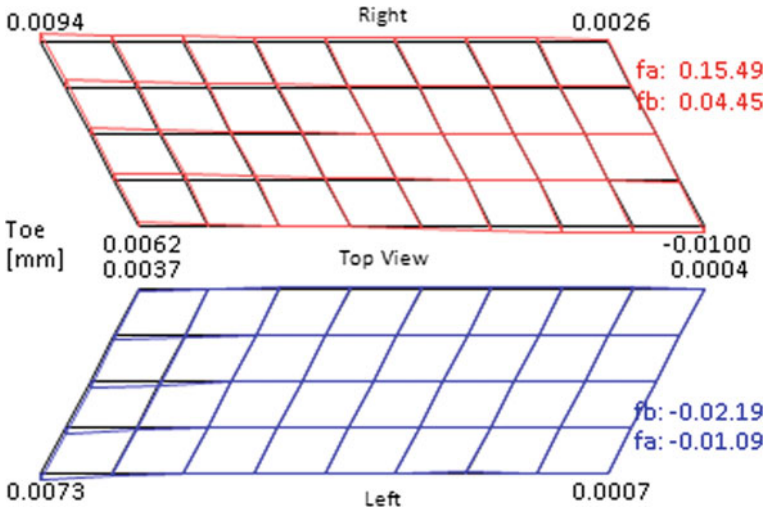

Fig. 38 Error surface after correction

Table 2 Averaged surface errors after correction

Average error	Right flank	Left flank
Tooth thickness	0.0087	
Pressure angle	0.15.49	−0.01.09
Helix angle	0.04.45	−0.02.19
Lengthwise crowning	−0.0024	−0.0049
Profile curvature	0.0017	0.0019

9.2 Application 2: 26 Tooth, 1.5 mm Module, Duplex Helical Spiral-Bevel Pinion

This pinion was cut on a tilting turntable type 5 Axis CnC machine using a 2″ Face Mill cutter. The 1st cut yielded the results shown in Fig. 39. Pressure (fa), spiral (fb) angle and bias errors are visible.

Figure 40 shows the error surface after the 1st Closed Loop iteration. Clearly, pressure, spiral and bias errors have been corrected.

9.3 Application 3: 28 Tooth, 12.68 mm Module, Duplex Helical Spiral-Bevel Gear

This gear was cut on a tilting turntable type 5 Axis CnC machine using a 160 mm diameter Conical Side Milling Tool (CoSIMT). The 1st cut yielded the results shown in Fig. 41. Slight pressure angle errors (fa) are visible; the spiral angle error

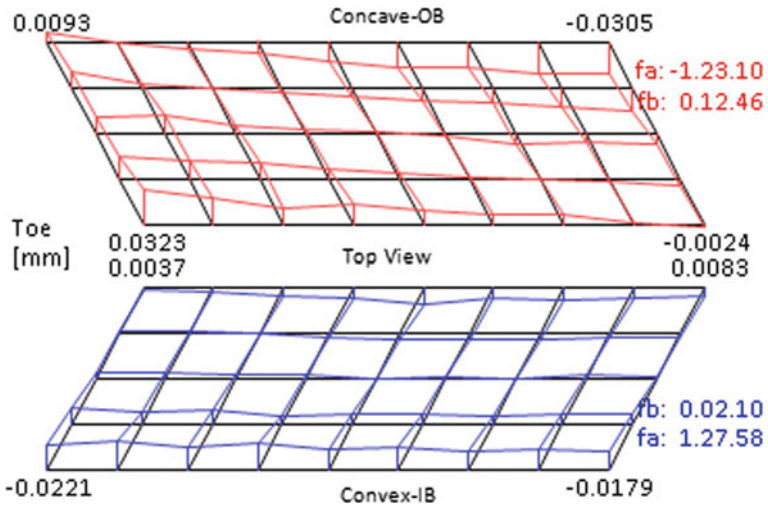

Fig. 39 Error surface after 1st cut

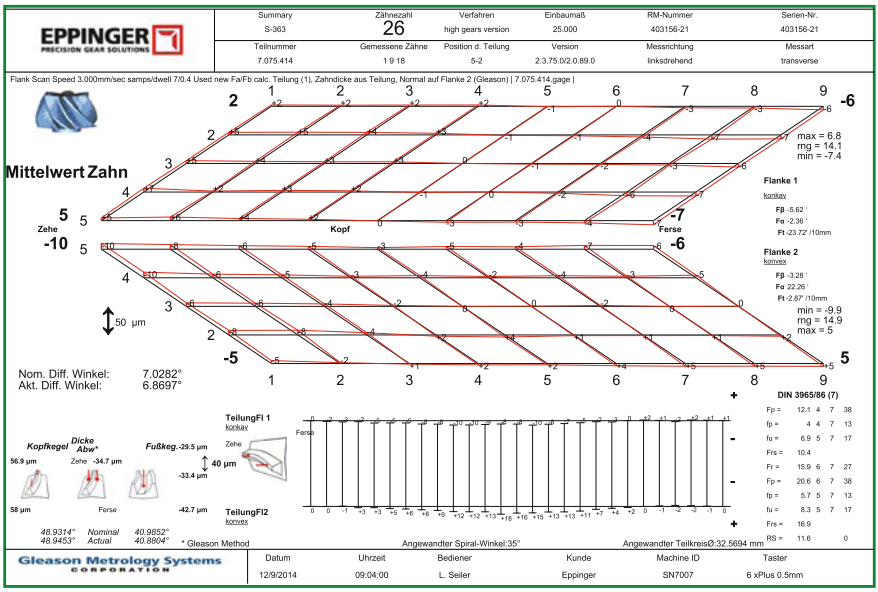

Fig. 40 Error surface after correction

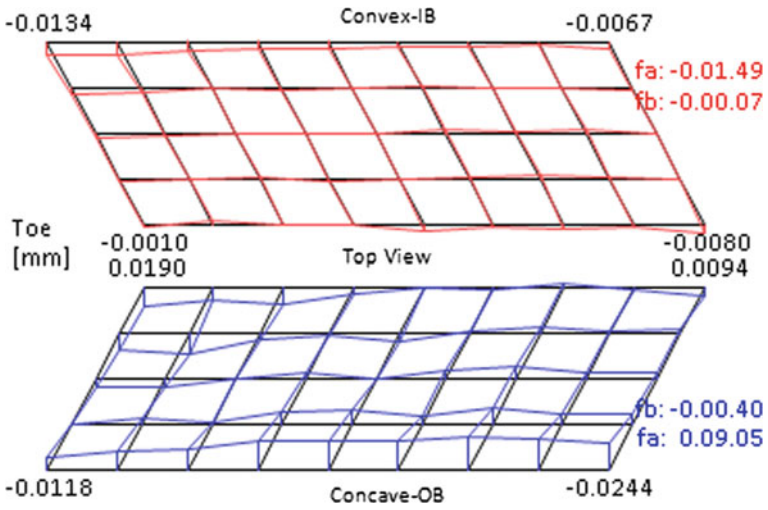

Fig. 41 Error surface after 1st cut

Table 3 Averaged surface errors after 1st cut

Average error	Convex flank	Concave flank
Tooth thickness	0.1031	
Pressure angle	−0.01.49	0.09.05
Helix angle	−0.00.07	−0.00.40
Lengthwise crowning	0.0025	−0.0077
Profile curvature	0.0051	0.0070
Warp factor	−0.01.36	0.0354

(fb) is close to zero; some lengthwise crowning is present on the Concave flank, some bias is visible on both tooth flanks, and thickness error is significant at +0.1031 mm (see Table 3).

The results shown in Fig. 42 are obtained after the 1st correction. Table 4 lists the residual errors. The initial pressure angle and bias (warp) errors have disappeared.

However, since both tooth flanks are cut simultaneously in the Duplex Helical process, correcting bias can introduce some lengthwise crowning, as is visible in Table 4.

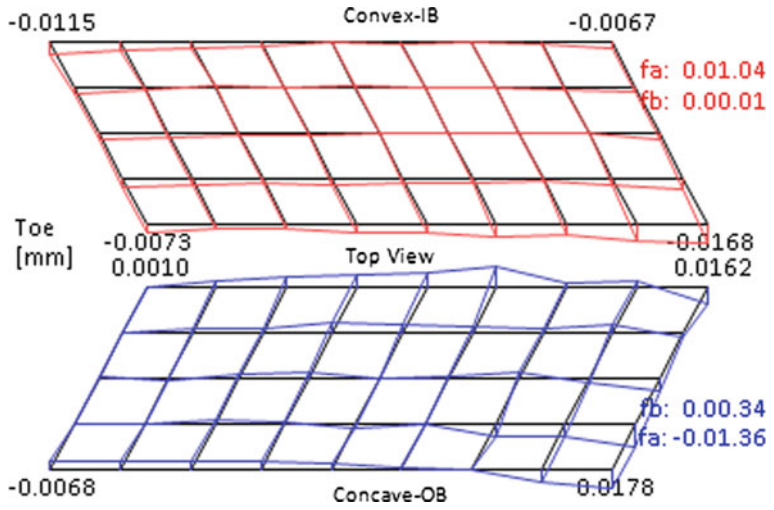

Fig. 42 Error surface after correction

Table 4 Averaged surface errors after correction

Average error	Convex flank	Concave flank
Tooth thickness	−0.0454	
Pressure angle	0.01.04	−0.01.36
Helix angle	0.00.01	0.00.34
Lengthwise crowning	0.0055	−0.0124
Profile curvature	0.0046	0.0038
Warp factor	0.00.15	0.00.13

9.4 Application 4: 39 Tooth, 1.15 mm Module, Duplex Helical Generated Spiral-Bevel Gear Electrode

The copper electrode (Fig. 43) was cut on a tilting turntable type 5 Axis CnC machine using a 1.0 mm diameter End Mill tool for the flanks and a 0.8 mm diameter Ball Mill tool for the fillets. The 1st cut yielded the results shown in Fig. 44, in which virtually no error can be seen. Closed Loop is therefore not required here.

When cutting copper, a comparatively soft material, tools do not wear at the same rate as when cutting steel. Given that the machine used was new and of a very high quality, and that the tools were within the advertised dimensions, the excellent results shown in Fig. 44 are not surprising.

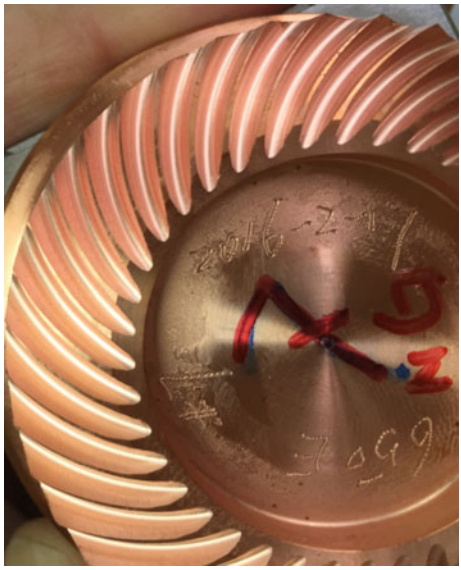

Fig. 43 Generated spiral-bevel gear electrode

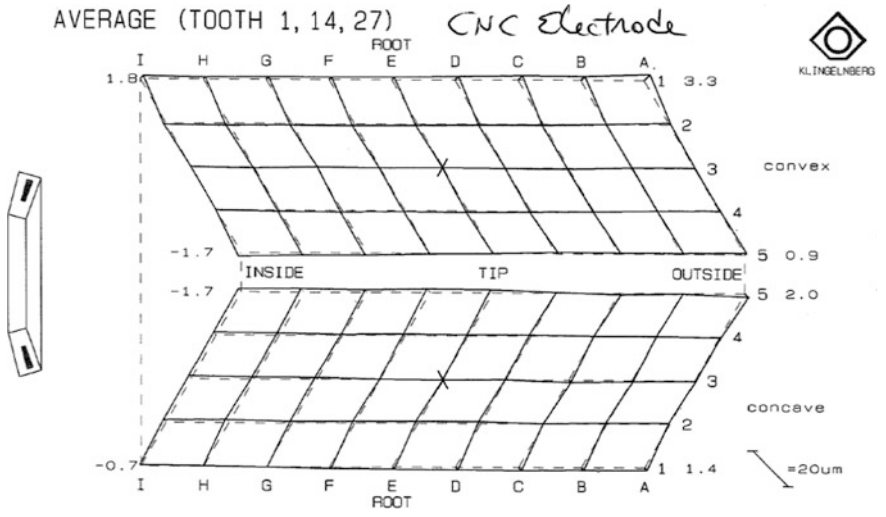

Fig. 44 Error surface at 1st cut

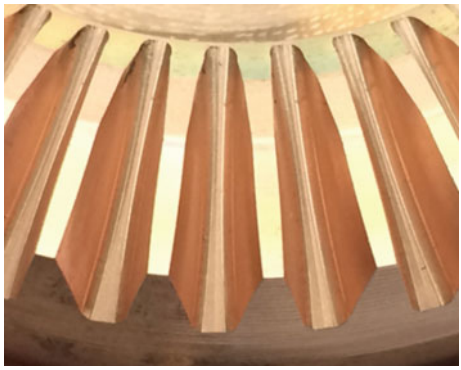

Fig. 45 Straight-bevel gear copper electrode

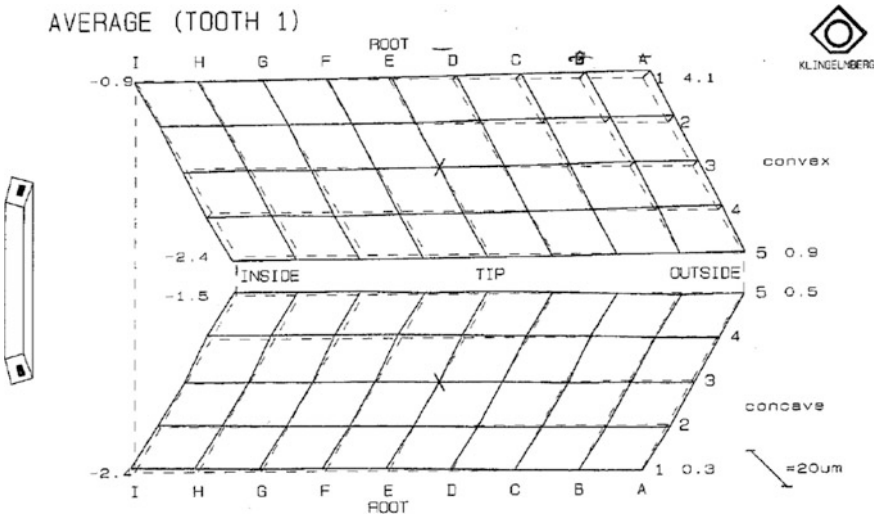

Fig. 46 Error surface at 1st cut

9.5 Application 5: 38 Tooth, 1.348 mm Module, Straight-Bevel Gear Electrode

The copper electrode (Fig. 45) was cut on a tilting turntable type 5 Axis CnC machine using a 1.0 mm diameter End Mill tool for the flanks and a 0.8 mm diameter Ball Mill tool for the fillets. The 1st cut yielded the results shown in Fig. 46, in which virtually no error can be seen. Again, Closed Loop is not required.

10 Conclusions

The methods presented in the previous sections describe a system for simulating gear manufacturing processes, controlling manufacturing through Closed Loop (i.e., Corrective Machine Settings), and using the manufacturing capabilities of multi-axis CnC machines.

In practice, the presented Tooth Flank Generator and Closed Loop have been in industrial use for more than two decades, and have proven effective and reliable. Multi-axis CnC manufacturing has been in industrial use for several years and has allowed for the production of now countless gear sets.

Multi-axis CnC gear manufacturing allows for cutting quality gears on machines that can also be put to other uses. Tooling is flexible, and any tooth flank topography can be addressed through the presented methodology. The combination of the presented Tooth Flank Generator, coupled to Closed Loop, ensures manufacturers of a quality production.

Acknowledgements Fixed Setting, Modified Roll, Duplex Helical, Spread Blade, Formate, Coniflex, TopRem are all Trade Marks of The Gleason Works, Rochester, NY, USA.

References

1. Gosselin, C., Thomas, J.: A unified approach to the simulation of gear manufacturing and operation. International Conference on Gears. T.U.M., Munich, 7–9 Oct 2013
2. Gosselin, C., Thomas, J.: Integrated closed loop in 5 Axis CnC gear manufacturing. International Conference on Gear Production 2015. T.U.M., Munich, 5–6 Oct 2015
3. Gosselin, C., Shiono, Y., Kagimoto, H., Aoyama, N.: Corrective machine settings of spiral bevel and hypoid gears with profile deviations. World Congress on Gearing, Paris, 16–18 Mar 1999
4. Gosselin, C., Nonaka, T., Shiono, Y., Kubo, A., Tatsuno, T.: Identification of the machine settings of real hypoid gear tooth surfaces. ASME J. Mech. Des. **120** (1998)
5. Krenzer, T.J.: Computer aided corrective machine settings for manufacturing bevel and hypoid gear sets. AGMA Paper 84-FTM-4, Oct 1984

Increase in Contact Strength of Heavy-Loaded Rolling Bearings for Gear Drives and Transmissions

E. Tesker

Abstract Special rolling bearings are applied in layouts of various types of machine. The serviceability of these bearings greatly affects the main performance characteristics of power gears and gear drives. A special class of gear contains parts which are subjected to different advanced hardening treatment. The reason for the failure for such bearings is progressive contact fractures. Trouble spots for these fractures originate in sub-surface layers of the structurally non-homogeneous material obtained as a result of hardening treatment. In this relation, the study of kinetics and ways of generation of sub-surface (depth) contract failures is vital for the purpose of developing a method for analysis and an increase in the load-carrying capacity of the part under cyclic and dynamic loads. Trends of surface layer generation for heavy-loaded bearing parts of planetary turnover mechanisms (PTM) for mobile machines have been studied. The features of contact loading are revealed for parts of power gears with a surface hardened layer obtained through the use of various hardening treatments. Methods for depth contact stress analysis are proposed, design relations are obtained which allow for determining, in each specific case, the position of a risky zone where the trouble spots of fatigue depth fractures can appear. A method for analysis is proposed which permits determining the values of the hardened layer parameters necessary to provide high resistibility to contact fractures. Examples of the analysis of depth contact strength are given for the bearing parts of PTM for the mobile machine.

Keywords Rolling bearings · Hardened surface layers · Loading · Load-carrying capacity · Depth contact fracture · Way of fracture · Cyclic and dynamic loads · Contact fractures

E. Tesker (✉)
Volgograd State Technical University, Volgograd, Russia
e-mail: agromash-vlg@rambler.ru

V. Goldfarb et al. (eds.), *Advanced Gear Engineering*,
Mechanisms and Machine Science 51, DOI 10.1007/978-3-319-60399-5_9

1 Introduction

One of the key problems of advanced mechanical engineering is the increase in reliability and technical level of heavy-loaded gears and transmissions in which the shaft supports are the rolling bearings.

The practice of operation shows that the main reason for the insufficient serviceability of gears is the progressive contact fracture of operating surfaces.

A special class comprises single-purpose bearings for gearboxes with parts that have been subjected to advanced hardening treatment. The reason for the failure of such bearings is progressive contact fractures. Trouble spots for these fractures originate in the very hardened layer or in the material core.

Analysis of conditions for generation of depth fractures and the development of methods for analysis of surface hardened parts are the vital problem, since the existing methods for design and analysis of the load-carrying capacity of surface hardened bearings do not fully consider the features of contact loading for parts with a structurally non-homogeneous surface hardened layers and kinetics and reasons for the generation of fatigue fractures.

2 Stressed State of Surface-Hardened Parts Under Contact Loads

The layout of the planetary turnover mechanisms (PTM) for the mobile machine has been chosen as the object of study (Fig. 1).

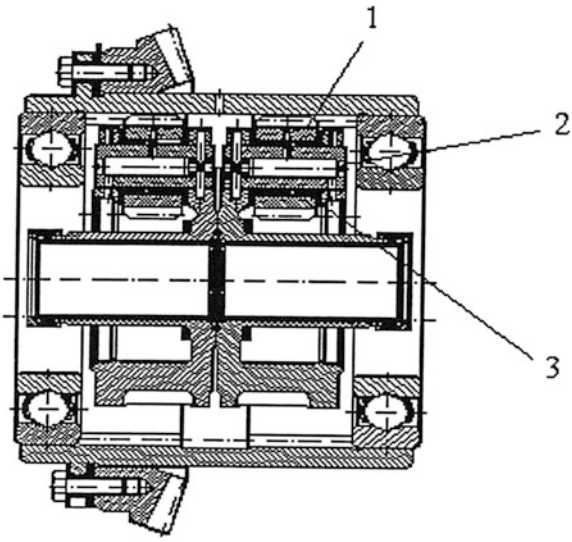

Fig. 1 Typical layout of PTM. *1* satellite, *2* satellite axis, *3* needle of the bearing

Analysis of the loaded state for parts of the bearing with cylindrical surfaces shows that, similar to the contact of two cylinders, the most loaded zone is not only the zone of the layer surface ($\sigma_{z\ max} = p_0$), but also the deeper layers of the material located at a depth of z = 0.786b from the surface of contact (Fig. 2).

Expressions for components of stresses σ_x, σ_y, σ_z, τ_{zy}, τ_{zx}, τ_{yx} at the boundaries of the contact area (y ≈ 0.8b) are determined in accordance with formulas of the elasticity theory [1, 2]:

$$\begin{aligned}
\sigma_x &= -p_0 2\mu \frac{z}{b}\left(\sqrt{\frac{b^2+u}{u}} - 1\right);\\
\sigma_y &= -p_0 \frac{z}{b}\left(\sqrt{\frac{b^2+u}{u}}\left(2 - \frac{b^2 z^2}{u^2 b^2 z^2}\right) - 2\right);\\
\sigma_z &= -p_0 \frac{bz^3}{u + b^2 z^2}\sqrt{\frac{b^2+u}{u}};\\
\tau_{yz} &= -p_0 \frac{byz^2}{u^2 + b^2 z^2}\sqrt{\frac{u}{b^2+u}};\\
\tau_{zx} &= \tau_{xz} = 0; \tau_{xy} = \tau_{yx} = 0,
\end{aligned} \tag{1}$$

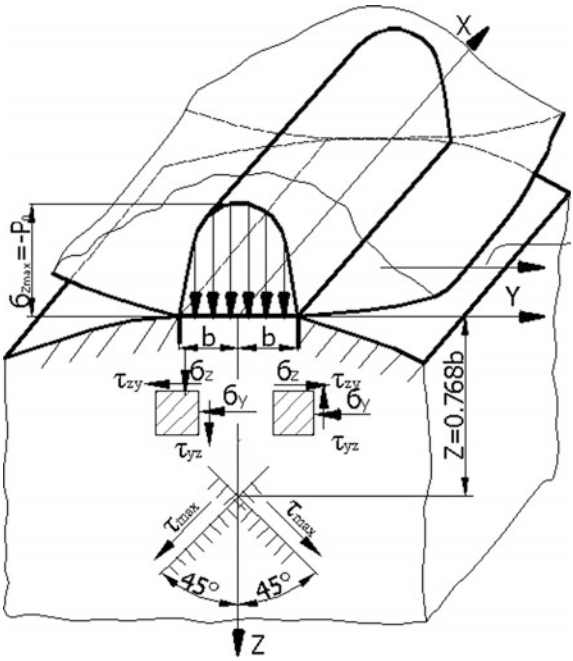

Fig. 2 Scheme of stresses at the contact of two cylinders

where b is the half width of the contact band; y is the coordinate of the point along the width of the contact area; z is the coordinate of the point along the depth; μ is the Poisson factor; and u is the maximum root of the equation

$$\frac{y^2}{b^2+u}+\frac{z^2}{u}=1. \tag{2}$$

In order to study the conditions for the contact interaction of heavy-loaded rolling supports of a PTM, and to create methods for analysis of the depth contact strength on its basis, a generalized mathematical model has been developed. This model is based on the fact that the load-carrying capacity of parts with a surface hardened layer is determined not only by distribution of equivalent tangential stresses with the distance from the surface to the considered point with the coordinate $z = z_i$, but also by the laws of variation of the contact endurance limits with regards to the thickness of the structurally non-homogeneous layer.

On this premise, one can state that the depth contact fractures will first appear at a certain distance from the contact surface $z_i = z_{min}$, in such zones where the value of the function of the safety factor h(z) is a minimum, that is,

$$h(z)=\tau_k(z_{min})/\tau_{eq}(z_{min})\le n_{min}. \tag{3}$$

Here, τ_k is the contact endurance limit for the hardened layer, and τ_{eq} are the equivalent tangential stresses determined in accordance with formulas of the elasticity theory.

The condition (3) is represented as a diagram demonstrating the law of variation of stresses and properties of the material along the depth of the surface layer of contacting parts (Fig. 3).

In order to obtain the relations $\tau_k(z)$, the laws of variation of micro-hardness along the thickness of the surface layer material have been studied. These surface layers have been obtained through the use of various surface hardening treatments

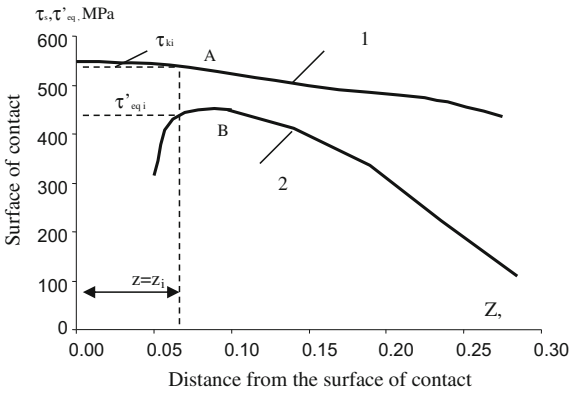

Fig. 3 Laws of variation of stresses and properties of the material along the length of the surface layer. *1* Distribution of contact endurance limits along the thickness of the layer (τ_k); *2* diagrams of equivalent stresses τ_{eq}; $z = z_i$—current coordinate and its corresponding values of equivalent stresses $\tau_{eq\ i}$

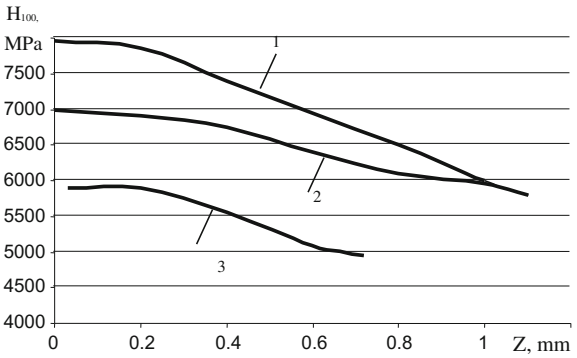

Fig. 4 Variation of micro-hardness along the thickness of case-hardened layers with different versions of hardening treatment. *1–3 Curved lines* obtained through the formula (4). *Points* correspond to experimental values of the micro-hardness for local volumes

(case-hardening, nitro-carburizing, laser hardening, nitriding). The obtained curved lines of hardness distribution are shown in Fig. 4.

Relations (4–5), which were obtained after the processing of experimental data, describe the laws of hardness variation depending on the layer of thickness δ, and the hardness on the surface Hs and in the core Hc of the material of the bearing parts.

For case-hardened parts of bearings,

$$H = \frac{H_n}{\left(\frac{H_n}{H_c} - 1\right)\left(\frac{z}{\delta_c}\right)^2 + 1}. \tag{4}$$

For parts of bearings treated by laser,

$$H = \frac{H_n}{\left(\frac{H_n}{H_c} - 1\right)\left(\frac{z}{\delta_c}\right)^4 + 1}. \tag{5}$$

The root-mean-square relative error of design and experimental values does not exceed 6%; and the maximum deviations of the measured values from those of the design are within the ranges of $\pm|\delta|$.

When applying the developed model of the contact interaction of the surface-hardened parts of bearings, methods have been developed for analysis of the depth contact strength of bearings for transmissions under static and cyclic contact loads. In each specific case, the model and design relations allow for determining, through calculations, the coordinate $z = z_{min}$, that is, the location of this risky zone where plastic deformations (under overloads) or trouble shots of fatigue cracks can appear.

3 Methodology for Analysis of the Depth Contact Strength of Surface Hardened Parts

The design model of the depth contact strength under cyclic loads is based on relations which characterize the variation of properties of the bearing material with the distance from the surface towards the material core, and also on equations determining the cyclic contact stresses which cause fatigue fractures in the surface layer.

At the interaction of two cylinders with parallel axes (Fig. 2), the tangential stresses $\tau_{zy}(\tau_{yz})$ hold the highest risk with regard to the appearance of sub-surface fractures. It is evident that these stresses act on areas which are parallel and perpendicular to axes z and y and separated from the plane of symmetry by the distance $y = \pm 0.85b$ (here, b is the half-width of the contact area). The maximum span of stress $\tau_{zy}(\tau_{yz})$ variation is at the boundaries of the contact area ($y = \pm b$) at a depth of 0.5b. At this depth, the tangential stresses are $\tau_{zy} = \pm 0.25 p_0$; and, therefore, the amplitude of these stresses is $\tau_{zy} = 0.5\ p_0$ (where p_0 is the maximum normal contact stress acting along the axis of symmetry of the contact band). Equivalent tangential stresses τ_{eq}, which are determined by the equation given immediately below, are taken to be the strength criterion under the action of cyclic contact loads:

$$\tau_{eq} = \tau_{zy} + k\sigma_y. \tag{6}$$

The chosen strength criterion almost completely corresponds to advanced representations of the terms for the appearance of fatigue fractures. The fatigue strength at any point of the area of the part making contact (located at a certain distance z from the contact surface) will be determined in accordance with the relation of diagrams of cyclic stresses τ_{eq} and the surface endurance limit to be defined by the formula (7) (Fig. 5).

$$\tau_k(z) = cH(z). \tag{7}$$

Therefore, in accordance with the proposed model, for the case of cyclic contact loading of rolling bearings for transmissions and drives, the fatigue fractures first appear in the zone $z = z_{min}$ with the lowest safety factor of cyclic strength n_{min}. The coordinate $z = z_{min}$ that determines the position of this zone can be found by the equation

$$\frac{d}{dz} n(z) = \frac{d}{dz}\left(\frac{\tau_k(z)}{\tau'_e(z)}\right) = 0. \tag{8}$$

Then, we have equations that describe the terms of the contact strength of bearings under cyclic loads for case-hardened parts:

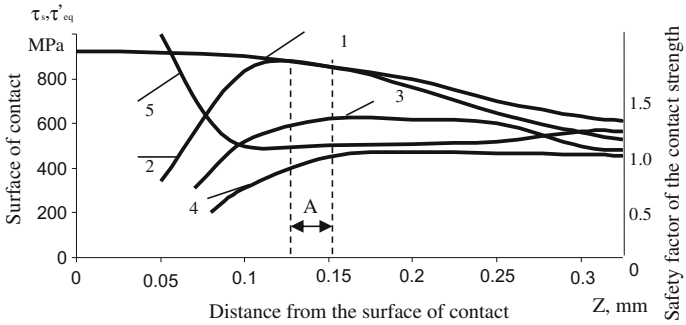

Fig. 5 Distribution of stresses under static loads and values of the safety factor of the contact strength n in different zones of the contacting surface: A the area ($n_{min} \approx 1$) where contact fractures can appear at operation of bearings; *1* diagram of allowable stresses τ_s which are limited by the material yield point at different zones of the hardened layer; *2–4* diagrams of equivalent stresses τ_{eq} for different diameters of rolling solids (needles) (4, 6, 16 mm, respectively); *5* diagram characterizing the laws of variation of the safety factor of the contact strength n(z)

$$\frac{d}{dz}\left(\frac{cH}{\left[\left(\frac{H_n}{H_c}-1\right)\left(\frac{z}{\delta_c}\right)^2+1\right](\tau_{xy}+k\sigma_y)}\right)=0. \tag{9}$$

In the case of laser hardening,

$$\frac{d}{dz}\left(\frac{cH}{\left[\left(\frac{H_n}{H_c}-1\right)\left(\frac{z}{\delta_c}\right)^4+1\right](\tau_{zy}+k\sigma_y)}\right)=0. \tag{10}$$

As an example, Fig. 6 shows the possible arrangement of curve lines $\tau_z(z)$ and $\tau_{eq}(z)$ calculated for the contact of real surfaces.

When analyzing the loading of the contact zone of bearing parts, it is necessary to consider cases of twist and mismatch that lead to a considerable increase in stresses determined by the elasticity theory (see Figs. 7, and 8).

At great values of angles of twist for rolling bodies and small values of convergence of contacting surfaces, the contact of parts takes place only at the portion of the contact line L (Fig. 8).

Figure 8 shows that even a small increase in the angle of twist leads to a considerable increase in loads on the bearing. That is why when determining the limiting allowable load acting on the bearing, the factor k_γ has been introduced. It accounts for the increase in contact pressure caused by the radial twist of rolling bodies. In order to determine the numerical values of this factor, the concept of the total factor of overload $k_\sum$ has been introduced. It represents the product of factors

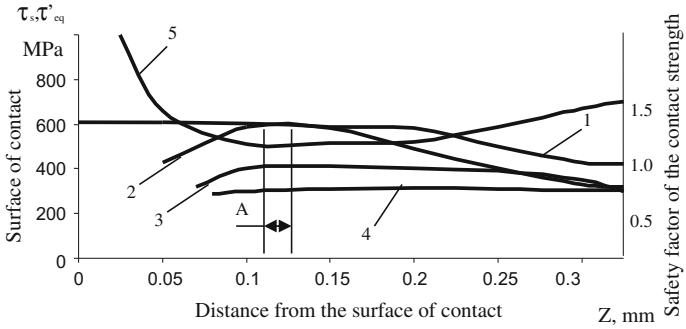

Fig. 6 Values of the safety factor of the contact strength (function n(z)) at different zones of the hardened surface layer (curve 5): *A* the area ($n_{min} \leq 1$) where primary contact fractures can appear; *1* the diagram of allowable stresses $\tau_{k(z)}$; *2–4* diagrams of equivalent tangential stresses $\tau_{eq}(z)$ for different diameters of needles (4, 8, 16 mm, respectively)

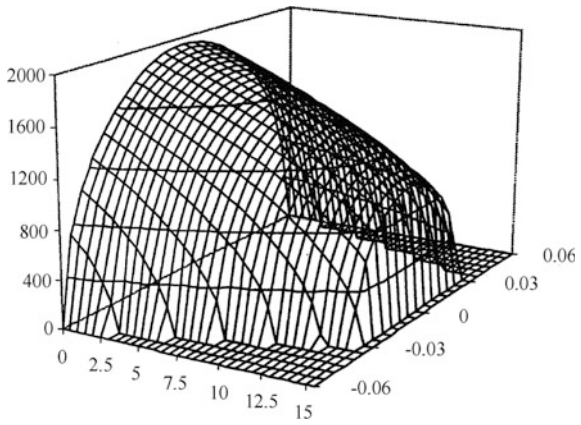

Fig. 7 Distribution of normal contact stresses along the contact area for the angle of twist $\gamma = 0.00005$ rad

considering the dynamic loads in meshing of pinions for a PTM and the factors of non-uniform load distribution between satellites and non-uniform load distribution between rolling bodies in the bearing.

The influence of the angle of twist on the factor of overload is shown in Fig. 9.

An experimental study of the contact strength of bearing parts for a PTM of the mobile machine has been carried out during tests at the stand with the closed power circuit. In order to choose the testing modes, corresponding to real loading conditions, contact strength analysis of bearing parts for a PTM has been preliminarily performed by means of the methods developed for analysis of the depth contact strength. The values of parameters and factors involved in design formulas have been determined accounting for the features of design and operation of a PTM. The calculation results for specific conditions of contact loading are shown in Figs. 10 and 11.

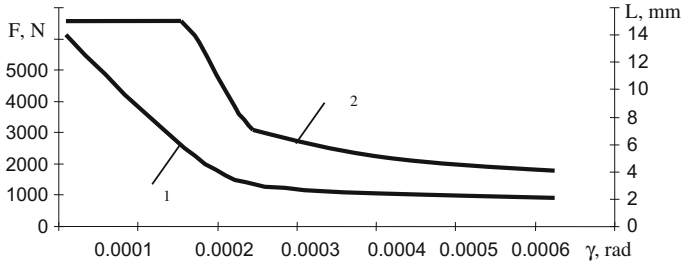

Fig. 8 Diagrams of variation for the ultimate force of the contact load (F) and the length of the contact line (L), depending on the angle of twist γ: *1* the ultimate force F; *2* the length of the contact line L

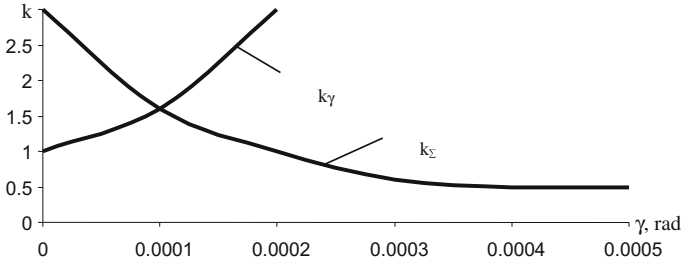

Fig. 9 Influence of the angle of mismatch γ on the value of the overload factor

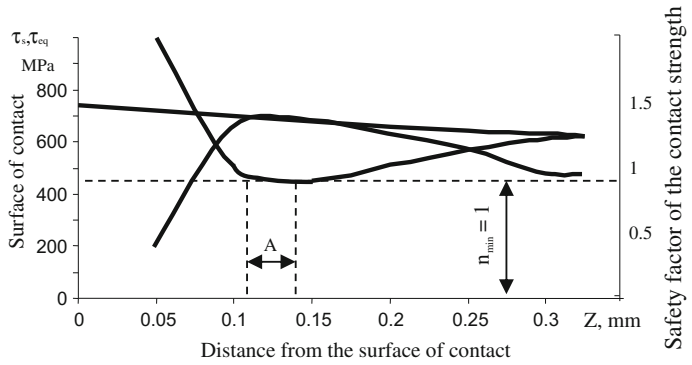

Fig. 10 Diagrams of stress distribution and properties of the material at the surface layer of bearing parts for a PTM under static loads (overloads) and the corresponding values of safety factors of the contact strength n in different zones of the contacting surface of case-hardened parts: *1* allowable stresses in accordance with the contact strength; *2* equivalent tangential stresses; *3* distribution of the safety factor of the contact strength along the thickness of the hardened layer

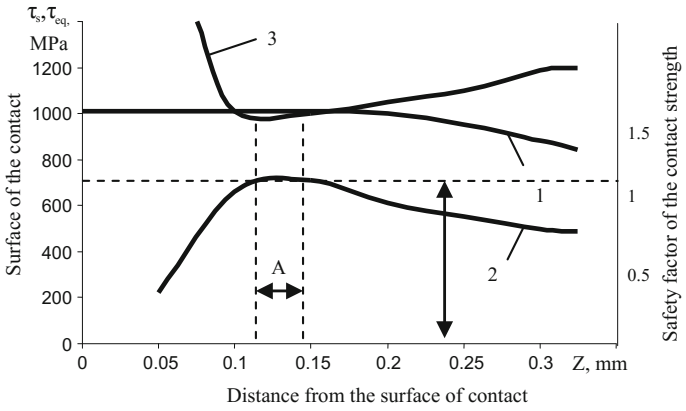

Fig. 11 Diagrams of stress distribution at the surface layer of bearing parts for a PTM under static loads (overloads) and the corresponding values of safety factors of the contact strength n in different zones of the contacting surface hardened by laser. A is the area where primary contact fractures can appear

Contacting parts with surface hardened layers have been subjected to analysis. The parts have the following characteristics of physical and mechanical properties: $E_o = E_u = 2.1 \times 10^5$ (МРПа); Poisson's factors $\mu_0 = \mu_u = 0.3$; hardness of the satellite axis core $H_c = 3500$ (MPa); surface hardness at case-hardening $H_n = 6200–7000$ (MPa); surface hardness at laser treatment $H_n = 8000–8500$ (MPa); the depth of the hardened layer at case-hardening $\delta_c = 0.7$ mm; the depth of the hardened layer at laser treatment $\delta_c = 0.5$ mm; radii of the curvature of contacting parts $R_0 = 14.6$; $R_u = 2$ mm. The design value of the thrust in the contact is $F_{eq} = F_u = 10.5$ kN.

Strength analysis under cyclic loads has been performed for two cases of surface hardening: case-hardening and laser treatment. The design value of the thrust in the contact is $F_{eq} = F_u = 6.7$ кN.

The calculation results are shown in Figs. 12 and 13.

The diagrams show that the minimum values of the safety factor for the analyzed PTM are: for case-hardened parts of the bearing, $n_{min} \approx 1.1$, for parts hardened by laser, $n_{min} > 1.3$. This is stipulated by higher values allowable for parts hardened by laser ($\tau_s \approx 1000$ MPa, $\tau_k \approx 670$ MPa), which in turn are stipulated by a higher degree of hardness on the metal surface after laser hardening ($H_n = 8000–8500$ MPa). Moreover, the specific feature of laser hardening is the resulting high hardness being found practically throughout the entire depth of the hardened layer. Thus, for example, in the zone of action of maximum equivalent stresses at a depth of $z = 0.08–0.15$ mm, the laser-hardened layer possesses the high degree of hardness close to that of the surface. At the same time, at case-hardening and nitro-carburizing, the material of a part has a hardness at the zone of action of maximum equivalent stresses that is considerably lower that the surface hardness.

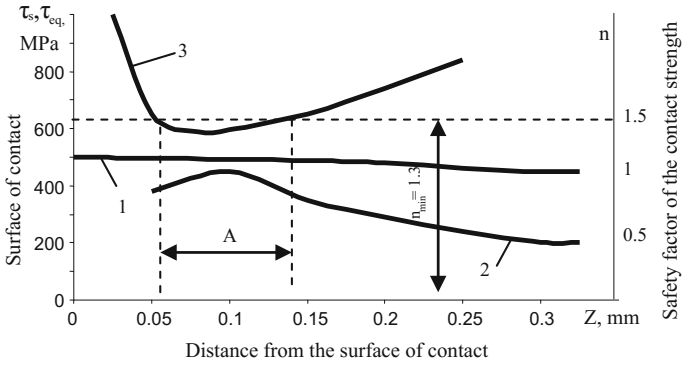

Fig. 12 Diagrams of stress distribution at the surface layer of bearing parts for a PTM under cyclic loads (overloads) and the corresponding values of safety factors of the contact strength *n* in different zones of the contacting surface that is case-hardened. *A* is the area where primary contact fractures can appear

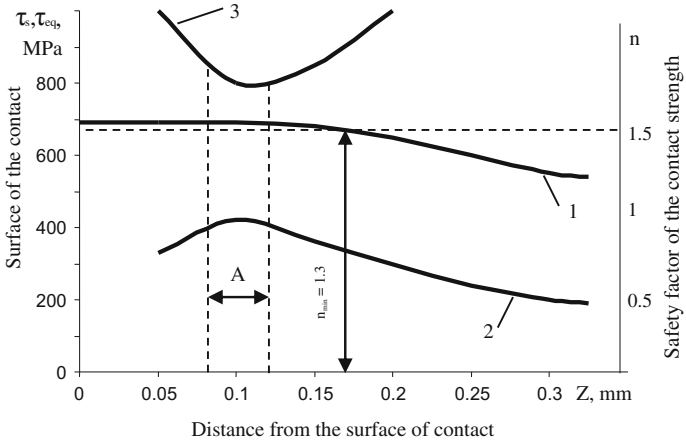

Fig. 13 Diagrams of stress distribution at the surface layer of bearing parts for a PTM under cyclic loads (overloads) and the corresponding values of safety factors of the contact strength *n* in different zones of the contacting surface hardened by laser. *A* is the area where primary contact fractures can appear

Experiments have shown that fatigue fractures in operating surfaces do not appear if the values of the safety factor in the risky zone are $n_{min} > 1.3$. Tests of case-hardened parts showed that if the condition $n_{min} > [n_{min}]$ is not fulfilled, the fractures appear at depths close to those of the design. Thus, at a depth of 0.07–0.14 mm, fatigue cracks have been detected that led to lamination of significant areas of the surface and failure of parts. Similar fractures have been detected when investigating the failed bearing parts for a PTM after long-term operation (more

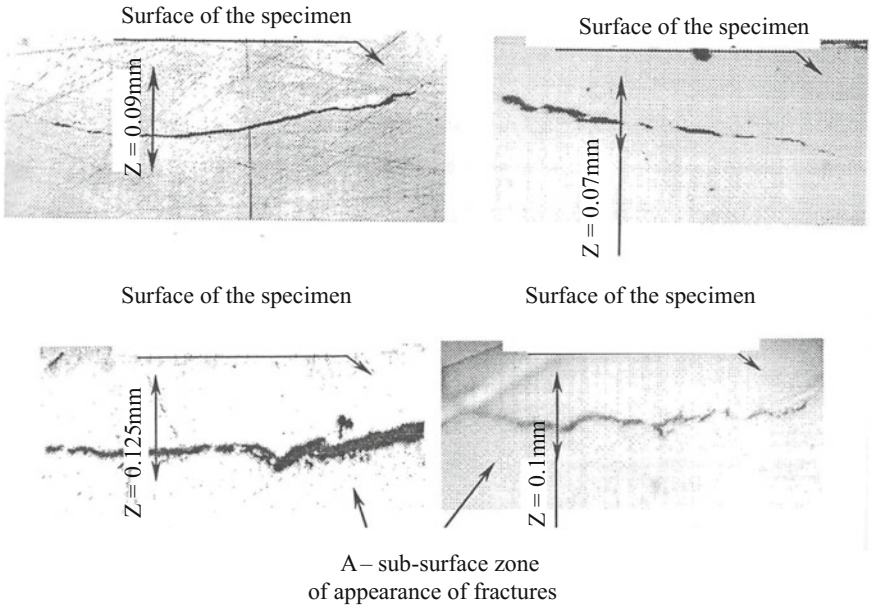

Fig. 14 Character of fractures and arrangement of fatigue cracks in the surface layer after stand tests

than 6000 motor hours). The character of fractures and cracks at the lateral micro-section is shown in Fig. 15. It is determined that the calculated depth of location of the risky zone (zone A, see Figs. 13 and 14) practically coincides with the zone of generation of sub-surface cracks revealed during the experimental study.

On the basis of the studies performed on the depth contact strength and load-carrying capacity of bearings for a PTM, a new method has been proposed for analysis of the depth contact strength of bearings. Its flow-chart is shown in Fig. 16.

The theoretical and experimental studies performed allowed for development of recommendations as to the choice of optimal properties of surface—hardened bearings that operate under the action of high contact loads.

It is recommended that the effective hardness H^{ef}, the effective thickness of the layer δ^{ef} and the relation δ^{ef}/δ_c (that is, the relation of the effective thickness of the layer to the total thickness of the hardened layer) be indicated in technical documentation as features of the properties of the surface layer, along with the surface hardness.

The effective thickness of the hardened layer, accounting for the provision of the required safety factor of the depth cyclic contact strength $n_{min} \geq 1.1$, is determined by the expression

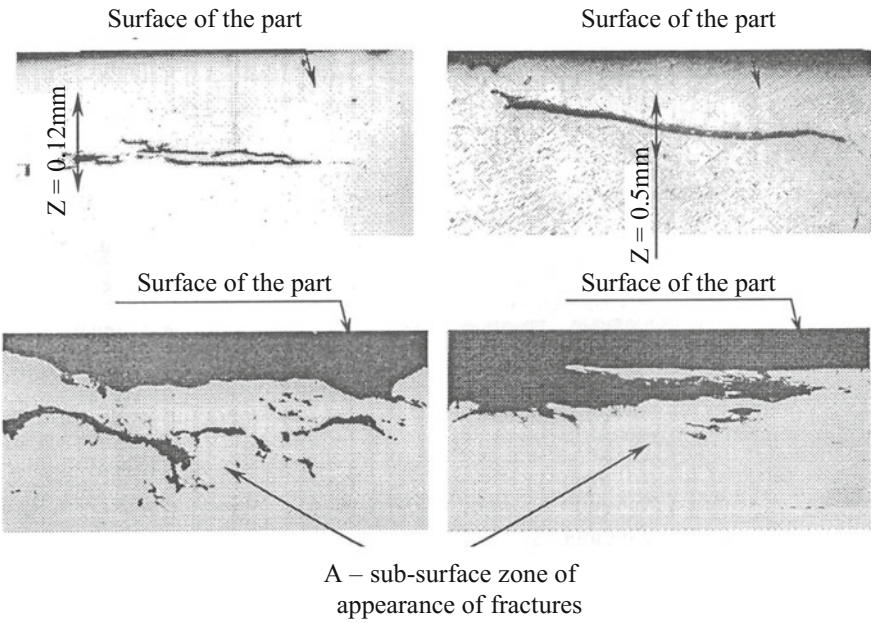

Fig. 15 Character of fractures and arrangement of fatigue cracks on parts that failed after long-term operation

$$\delta_y^{\text{ef}} = 1.386 \times 10^{-5} \sigma_n [n] \cdot p_{\text{red}}. \tag{11}$$

If the maximum stresses act under the hardened layer, the effective thickness of the hardened layer must be equal to the total thickness of the layer, that is, $\delta^{\text{ef}} = \delta_c$.

In order to prevent depth fractures at the boundary of the layer and the core (when the condition of the depth strength is fulfilled in the zone of maximum equivalent stresses at the thickness $z_{\max} = \delta^{\text{ef}}$), it is necessary to provide the definite relation between the total δ_c and the effective δ^{ef} thicknesses of the hardened layer.

This relation is as follows:

$$\frac{\delta_c}{\delta_y^{\text{ef}}} = \sqrt{\frac{[n]\sigma_n - 4.1H_c}{0.85H_c}}. \tag{12}$$

The necessary hardness of the hardened layer at the thickness δ^{ef} can be determined by the equation that describes the hardness distribution H(z) along the thickness of the case-hardened layer,

$$H^{\text{ef}} = \frac{H_n}{\left(\frac{H_n}{H_c} - 1\right) \cdot \left(\frac{\delta_y^{\text{ef}}}{\delta_c}\right) + 1}. \tag{13}$$

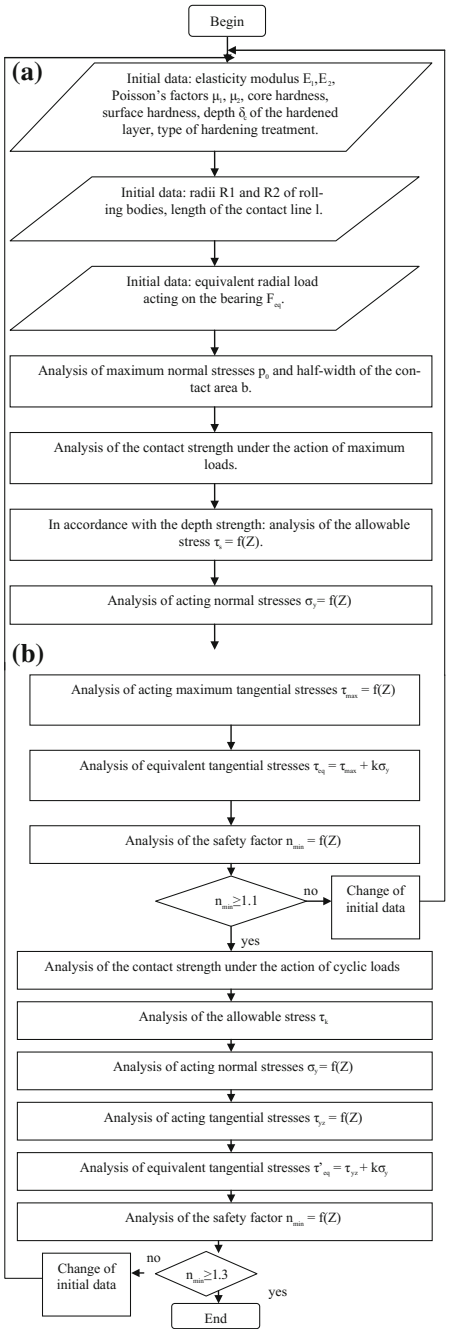

Fig. 16 Flow-chart of the analysis of the depth contact strength under the action of maximum loads (**a**) and cyclic loads (**b**)

In case of laser treatment,

$$H^{\mathrm{ef}} = \frac{H_n}{\left(\frac{H_{nlas}}{H_{cn}} - 1\right) \cdot \left(\frac{\delta_\gamma^{\mathrm{ef}}}{\delta_c}\right) + 1}. \tag{14}$$

The necessary value of H^{ef} should meet the requirement $H^{ef} \geq 0.22\sigma_{\mathrm{H}}[n]$.

Therefore, the increase in the load-carrying capacity of surface-hardened rolling supports can be provided by the choice of the required characteristics of hardened layers. Application of the developed methods for analysis of contacting parts allows for calculating these characteristics in accordance with the condition of the depth contact strength.

On the basis of the investigation results and analysis, it is recommended that the following values of characteristics of hardened layers for heavy-loaded bearings for the planetary mechanism of the mobile machine be assigned:

$$H \geq 7500\,\mathrm{MPa};\ \delta^{ef} \geq 0.5;\ [n]_{min} \geq 1.5. \tag{15}$$

4 Conclusions

1. The analysis has been performed for the loading state of bearings for the planetary mechanism of the transmission; the factors that influence the serviceability of bearings and the criteria that determine the limiting state of operating surfaces have been revealed.
2. The mathematical model has been developed that describes the conditions of the contact loading of surface hardened bearings for power gears.
3. New methods have been developed for analysis of the contact strength of surface hardened bearings under static and cyclic loading. They are distinguished, since the design relations have been obtained accounting for the laws of stress variation from the surface to the core of the main metal. The analysis allows for determining not only the limiting contact stresses that do not cause fractures, but also the optimal characteristics of the surface layers of bearing parts (H^{ef}, δ^{ef}, H_n, H_c).
4. It is established that the angular twist of rolling bodies of the bearing for a PTM has an influence on the distribution of contact loads; and it is proposed that we take this fact into account by the factor k_γ. The technique for its determination has also been presented.
5. It is established that in order to provide the required safety factors of the depth strength, eliminate contact fractures and increase the durability of bearings for the planetary mechanism, the thickness of the hardened layer with the highest hardness ($H_V > 8000$ MPa) should be no less than 0.5 mm.

6. When testing bearings hardened by laser, the effect of self-organizing for friction surfaces has been revealed. It implies that the wave-like micro-relief "oil pockets" are generated on the surface during operation. This causes an increase in the oil absorption of the contact, an improvement in lubrication conditions (especially for transient modes), a decrease in the rate of wear and, correspondingly, an increase in durability. Therefore, the increase in the wear of bearing parts hardened by laser is achieved as a result of the total effect of optimization of properties of the hardened layer and improvement of the lubrication condition for transient modes. Laser treatment of operating surfaces is recommended as an effective method for increasing the load-carrying capacity of rolling bearings for power gears.

References

1. Pinegin, S.V.: Contact Strength and Resistance to Rolling. Mashinostroyeniye, Moscow (1969) (in Russian)
2. Saverin, M.M.: Contact Strength of the Material. Mashgiz, Moscow (1946) (in Russian)

Features of the Relationship Between Vibration, Lubrication and Noise of Gears

V.L. Basinyuk, V.E. Starzhinsky, A.I. Mardasevich, S.V. Shil'ko and E.M. Petrokovets

Abstract The realization of a method of a complex estimation of the manufacture and assembly quality of gear-based mechanical drives for parameters of vibration, noise, and lubricating film thickness using the amplitude spectra analysis is described.

Keywords Mechanical drive · Gears · Quality criteria · Vibration · Noise

1 Introduction

Up to now, gears have been one of the most common elements of mobile transmission technology and process equipment. Moreover, they are constantly being improved in almost all industrialized countries. This is due to, on the one hand, the technological and methodological software computation that has been developed, design, manufacture, production quality control and monitoring of the technical state of gears during operation, and on the other hand, to the relatively low cost of manufacturing a sufficiently large resource. The use of modern materials and hardening technologies, as a rule, allows us to provide the required parameters of reliability and technical and economic indexes of gears.

The existing approaches to assessing the quality of mechanical drives include the monitoring and verification of compliance with the technical requirements of the results of design, manufacturing and assembly of the basic components. The complex criteria of the drive quality are:

V.L. Basinyuk · A.I. Mardasevich
Joint Institute of Mechanical Engineering NASB, Minsk, Belarus
e-mail: vladbas@mail.ru

V.E. Starzhinsky (✉) · S.V. Shil'ko · E.M. Petrokovets
Metal-Polymer Research Institute NASB, Gomel, Belarus
e-mail: star_mpri@mail.ru

V. Goldfarb et al. (eds.), *Advanced Gear Engineering*,
Mechanisms and Machine Science 51, DOI 10.1007/978-3-319-60399-5_10

– the vibration generated with the drive, characterized not only by the correctness of the design, precision of the manufacturing and assembly of the transmission, but also, to a certain extent, its real dynamic loading [1, 2];
– the noise emitted from the drive, the parameters of which characterize the above indicators, as well as the correctness of the choice of material, the housing arrangement, and the parameters of the related structural elements and compliance requirements of environmental safety.

In some cases, the noise parameters characterize the conditions of the frictional interaction in terms of gear meshing [3], including the thickness of the lubricating film, which has a direct impact on the gear's lifetime [4–6] and the noise that it generates. It is worth noting the following [3]:

– the vibration and noise are interconnected, but the influence of tooth friction on them is different;
– the vibration parameters are most sensitive to longitudinal oscillations, including resonant ones, taking into account the transmission of vibrations of the shaft, bearing units and housing in the primary transducer (usually the piezoelectric);
– the parameters of sound pressure are most sensitive to the longitudinal and torsional oscillations, including the resonant ones, which are seen in very limited numbers in the vibration, but have a significant impact on the frictional conditions of the teeth in some cases, taking into account the effect of the internal environment on the gearbox, the housing walls, bearing units and external air, or another medium;
– the assessment of the conditions of the gears' interaction on the lubricating film thickness [4, 7–9] does not fully reflect the lubrication effect on the gearing resource, since the ratios of the lubrication thickness to the geometric mean roughness in surfaces in contact [10] and surface topography [11–13] are important;
– the analysis of vibrations and noise usually does not so assess the important parameters for the evaluation of resources in compliance with the required structure and properties of raw materials, as well as the hardening treatment. However, the deviations of these parameters can be characterized by the elevated change gradients of vibration and noise in operation, relative to the predictable ones, to some extent, caused by higher wear, compared with a predictable one and/or contact chipping friction surfaces of the teeth in operation [3].

The goal of the paper is to establish the features and the relationship of parameters of the amplitude spectra of the vibration, noise and lubricating film thickness, as well as the effect of the functioning modes of the gear on the thickness of the lubricating film in the process of engagement.

2 Research Method

A testing unit with an open power circuit was used for the experimental studies. Its design ensures the smallest possible number of elements of the kinematic chain and components, vibrations of which could distort the amplitude spectra of the

parameters studied. The test had a spur gear transmission ratio equal to the unit, i.e., $z_1 = z_2 = 40$, and the module $m = 3$ mm, which allowed us to reduce the variations in the dynamic loading of the individual pairs of teeth due to the random nature of the combination of the pinion and gear base pitch errors at each subsequent complete revolution. Gears were mounted on shafts by cylindrical surfaces with a torque transmission by keyed joint. The shafts were installed in the housing with sufficient hard-row tapered roller bearings.

The casing of the test gear was carried out using a window covered with a thin plate made of PMMA. It provided a low level of noise absorption and distortion, resulting in the propagation of sound from the gear to the measuring microphone.

The research into the amplitude spectra was performed at angular velocities of rotation $\omega = 50$, 100, 150 and 200 rad/s and a torque $T = 0$, 100 and 200 Nm. The following signals of primary transducers with reference to real time scale were recorded:

- the voltage of the piezoelectric sensor U_H (mV) by which the vibration accelerations of the gear bearing support were recorded;
- the voltage of the microphone U_L (mV) by which the sound waves were recorded. They characterize the noise generated by the gear and stand elements;
- the voltage U_h (mV) (for the stabilized current $I = 1.5$ A), starting from which, using the calibration curves obtained previously, the lubricating film thickness was recorded in the gear meshing.

Since these voltages and their corresponding physical quantities are connected by linear relations, the frequency content of their spectra is identical and can be used to analyze the results.

The typical character of the relative change in the thickness of the lubricating film on the engagement phase (ratio of the current value of the lubricating film thickness h to the lubricating film thickness in the pitch point h_0) is shown in Fig. 1 at various speeds and loading modes of the tested gear, and the amplitude spectra of the thickness fluctuations of the lubricating film, vibrations and noise—in Fig. 2 [3].

3 Analysis of the Results

The thickness of the lubricating film, except for the idle run mode, raises the power function of 0.6–0.8 by increasing the circumferential speed and the associated rolling speed. This fact correlates well with the results of studies [8, 11–13]. At the same time, the certain laws of change h were established as being slightly different from the results in these studies. For example, the dynamic interaction of the teeth at engage and disengage is significantly affected as a destabilizing lubricating film of the edge or median impacts when entering or leaving the teeth out of engagement on the real thickness h in the gearing. Variations h reach the maximum values

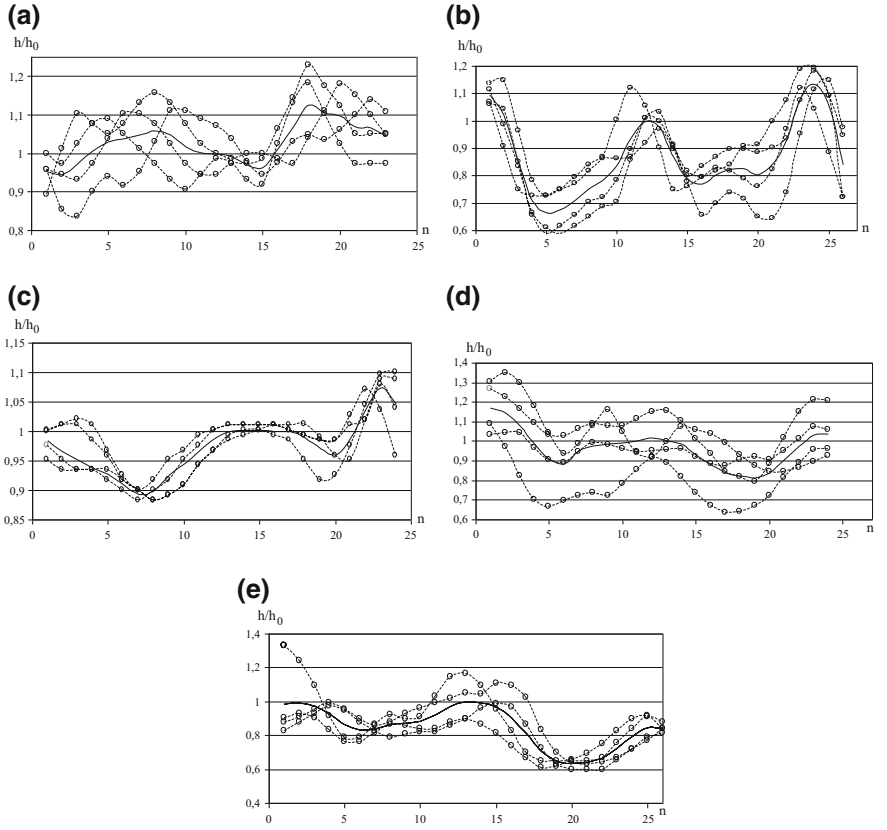

Fig. 1 The typical character of the relative change in the thickness of the lubricating film on the engagement phase at different speeds and load conditions of functioning of the test gear pair: **a** V_0 = 3 m/s, idling; **b** V_0 = 3 m/s, T = 100 Nm (σ_{H1} = 800 MPa); **c** V_0 = 3 m/s, T = 200 Nm, (σ_{H1} = 1150 MPa); **d** V_0 = 6 m/s, T = 100 Nm (σ_{H1} = 800 MPa); **e** V_0 = 9 m/s, T = 100 Nm (σ_{H1} = 800 MPa)

(Fig. 1a–d) in areas of tooth changeover. While, as noted in [8], the lubricant comprised between the teeth is not squeezed out instantaneously when entering, the new pair of teeth engages or disengages the upstream rotational pair of teeth.

This not only provided an acceptable mode of lubrication of the contact surfaces, but also contributed to the damping of the edge and middle impacts to some extent. In general, changes in the lubricating film thickness in these regions and along the line of engagement can be characterized by the following features.

At lightly loaded slow-speed transmission mode for large value h, its variation along the line of engagement was of a pronounced stochastic character. The minimum values h were recorded in tooth changeover and pitch point after a change in the opposite direction of the sliding speed of working surfaces of the teeth. The maximum value h corresponds to the engagement portion of the line between these

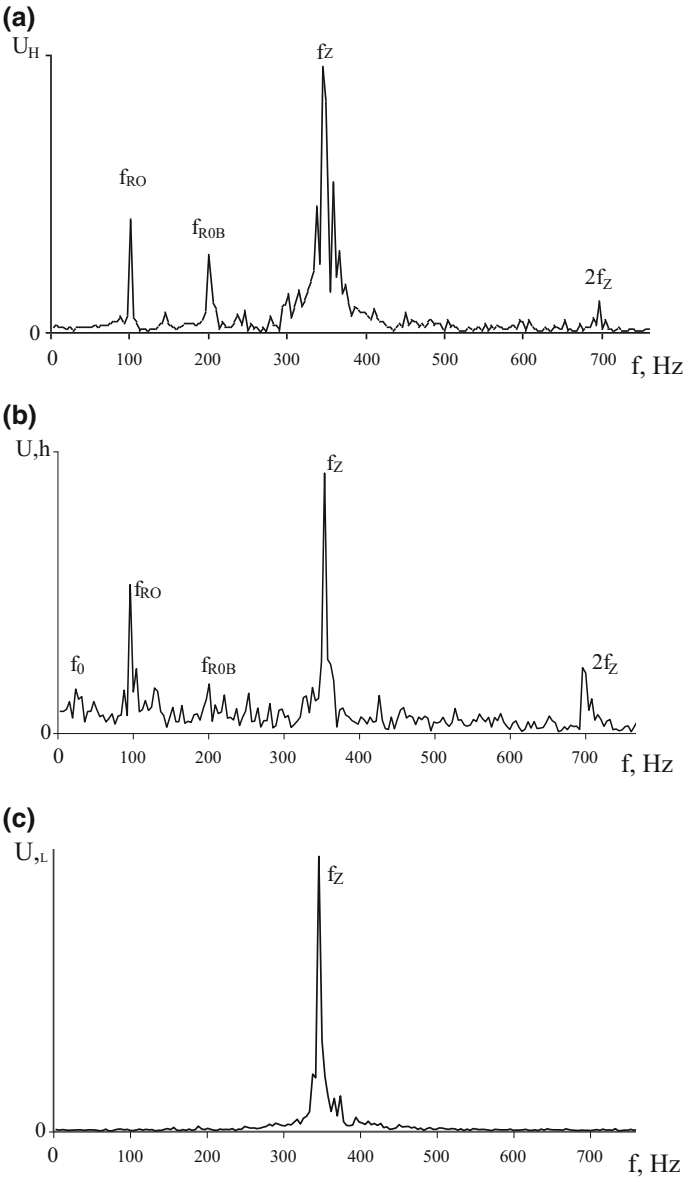

Fig. 2 Typical types of amplitude spectra of the noise oscillation (**a**), the lubricating film thickness (**b**) and the vibrations (**c**). f_0 is the negotiable rate, f_{R0} is the natural frequency of torsional vibrations, f_{R0B} is the natural frequency of the stand elements associated with gears, f_Z is the tooth mesh frequency

two points, which is characterized by a relatively stable interaction of the teeth. Minimum average values h were different from the lubricating film thickness at the pitch point by only 5–10%.

Change in the thickness of the lubricating film was close to the deterministic calculated value with respect to the loaded and heavy-loaded conditions in double tooth meshing [3]. The greatest value h was achieved at the pitch point, as well as at the entry and exit zones of tooth meshing. The "extrusion" time of the excess lubricant from the meshing zone was t = (0.06–0.08) t_T = (0.1–0.12) t_p.

The value h is greater than the value of the lubricating film thickness h_0 at the pitch point by 1.1–1.2 times at tooth changeover. Zones of minimum lubricating film thickness with these modes are arranged between the pitch and the entrance and exit points of engagement of the teeth, where the average values h were smaller than those of the lubricating film thickness at the pitch of 30–40%.

It should be noted that the change in the thickness of the lubricating film differed somewhat from that calculated by increasing the circumferential speed and the associated rolling velocity. This fact was also observed in [8]. The value h was first increased and then stabilized at a certain level and even slightly decreased, while it began to rise again at $V_0 \geq 12$ m/s with increasing circumferential speed at contact stresses σ_{H1} = 800 MPa and σ_{H2} = 1150 MPa. This effect can be explained by the influence on the lubrication thickness h of dynamic and static loads, as well as the high-speed and thermal modes of interaction between the contacting surfaces. Theoretical analysis of the influence of these factors on the value h in [5, 6] showed the possibility of such a change in the thickness of the lubricating film at a level similar to that when changing gear operation modes.

The value h along the lines of engagement was varied stochastically with minor deviations from the mean at high circumferential speeds ($V_0 > 10$ m/s). Standard deviations σ_h and coefficients of variation v of the lubricating film thickness were non-linearly dependent on the circumferential speed and the contact pressures. In all cases, an increase in the speed V_0 contributed to the increase of these indicators. At idling, the value σ_h increased from 0.2–0.28 to 0.35–0.44 μm, v from 7–10 to 18–22%, and the value v increased in power function at a nearly linear increase σ_h. The deviation σ_h increased from 0.22–0.3 to 0.4–0.5 μm, but up to V_0 = 6 m/s, the value v decreased from 20–23 to 16–21%, and then increased to 22–34% (T = 100 Nm) in the gears loaded by torque (T = 100 Nm). Trends of change σ_h and v were close to the above.

Standard deviation σ_h and coefficient of variation v were monotonically increased, respectively, from 0.09–0.16 to 0.32–0.36 μm and from 9–0.16 to 17–0.20% in heavy-loaded transmissions (T = 200 Nm), stabilizing at the top level. This is associated with a stationary mode of contact interaction and consistency in the thickness of the lubricating film. The increase in amplitude values of forced oscillation and natural vibrations of gears [3] is significantly affected by the values σ_h and v. This is due to the increase in dynamic loading level at the edge or median base impacts.

The nature of the change in the thickness of the lubricating film on the engagement phases is significantly changed by varying the circumferential speed

and gear loading. Variations in the thickness are reduced with increasing circumferential speed and loading, but the process of their change comes closer to that of the stochastic one.

Thus, the methodological approaches, built on the use of deterministic algorithms for determination of h, are limited. They do not take into account the variations of combinations of base pitch errors in transmission ratios, being unequal to the unit, the variations within manufacturing deviations in the confines of tolerances on total profile error, the stochastic nature of the conditions of the dynamic interaction between the teeth and the amplitudes of the oscillations generated, or the influence of the topography of the interacting surfaces. This makes it difficult to use the dependences obtained on the basis of these approaches for the detailed calculation of the thickness of the lubricating film in the absence of comprehensive experimental data on specific groups of transmission, modes of operation and characteristics of lubricants.

The existing analytical dependences and calculation methods of the thickness of the lubricating film can be used to determine the approximate values of the lubricating film thickness h at the pitch point, as well as the evaluation of the viscosity of lubricants, speed, load and thermal modes of gearing on the thickness of the lubricating films and durability of the tooth-working surfaces. in many cases in the absence of such data. It is advisable in some cases to introduce the coefficient k_g, taking into account the effect of the dynamic nature of the tooth interaction, the natural and forced oscillations of the system and changes in the conditions of tooth interaction by moving the contact zone along the line of engagement [2].

Analysis of the amplitude spectra of noise, vibrations and oscillations of the lubricating film thickness showed the following.

The forced vibrations with a tooth frequency f_Z, caused by errors in the manufacture of the gear according to the smoothness norms and related fluctuations in stiffness along the engagement phase, were not only decisive under almost all speed and load conditions of the test gear pair, but also have the most significant effect on the spectra of noise, vibrations and changes in the lubricating film thickness. The only exception was the idle run, in which the greater amplitude was the second harmonic.

In the spectrum of noise, the most significant amplitude corresponds to tooth frequency f_Z at a relatively low angular speed of rotation and heavy loaded operation mode with a thin lubricating film. This confirms a correlation between the noise and frictional interaction of gears, to some extent.

In other cases, the forced longitudinal oscillations, as well as the mechanical torsional vibrations with the natural frequency of torsional vibrations which arise mainly due to a kinematic error in gear manufacturing, strongly influence the composition of the noise amplitude spectrum.

The tooth mesh frequency f_Z was basically the second largest and only under certain conditions—the first or third after frequency of oscillations having the frequency value f_{R0} of natural torsional vibrations [3] in the amplitude spectrum of the oscillation of the lubricating film. This fact indicates a significant influence of the dynamic processes in the teeth contact on the torsional vibrations and confirms

the appropriateness of the account of this factor when choosing a lubricant and evaluating its impact on gear lifetime. Furthermore, the most similar compositions were the amplitude spectra of the noise and vibrations of the lubricating film, indicating the correlation between the noise and friction conditions in the gearing.

The forced vibrations with a tooth mesh frequency are due to an error primarily in the gear manufacturing for smoothness standards and the engagement rigidity periodically changing with a frequency f_Z. They have the most significant impact on all drive parameters, including the frictional characteristics, as well as the noise and vibrations generated in the meshing process. The degree of this effect was not only dependent on the accuracy of the gears, but also the mode of their operation and the inertial and stiffness parameters of the mechanical system in radial and circumferential directions, as well as the associated natural torsional vibrations.

4 Conclusions

Mechanical vibrations and noise generated by gears, as well as the value of and change in the thickness of the lubricating film, have a significant impact on the resource. This is advisable to take into account when we develop the systems for monitoring the manufacture and assembly quality, as well as the residual lifetime to operation. The most effective one includes a comprehensive assessment of the quality of manufacturing and mechanical drive monitoring systems based on analysis of the parameters of noise, vibrations and lubricating film thickness. Tribotechnical parameters of the gear may be determined through comparative analysis of the vibration and noise parameters [3], in some cases, in connection with the use of non-standardized equipment for registration of the thickness of the lubricating film.

Acknowledgements The authors would like to acknowledge the Belarusian Republican Foundation for Fundamental Research (project T16R-202) for their support.

References

1. Basinyuk, Ya.V., Ishin, N.N., Basinyuk, V.L., Mardasevich, A.I.: Vibration monitoring of internal dynamic loading, accuracy parameters and wear of individual pairs of teeth by gearing. Mech. Eng. Autom. Comput. **4**(10), 48–53 (2001) (Vestnik of Brest State Technical University) (in Russian)
2. Starzhinsky, V.E., Shalobaev, E.V., Shil'ko, S.V., et al.: Elements of Drive Devices. Calculation, Design, Technology. Belaruskaya Navuka, Minsk (2012) (in Russian)
3. Basinyuk, V.L.: Dynamics, Lubrication and Noise of Gears. MPRI NASB, Belarus (2006) (in Russian)
4. Petrusevich, A.I.: The Main Conclusions of the Contact and Hydrodynamic Lubrication Theory. Publishing House AS USSR, DTS, vol. 2, pp. 209–233 (1951) (in Russian)

5. Van, K.L., Chzhen, Kh.S.: Numerical determination of dynamic stress, lubricating film thickness and surface temperature for spur gears. Part I. Research. In: Proceedings of American Society of Mechanical Engineers (Series: Design and Engineering Technology). Mir, vol. 1, pp. 81–92 (1981) (in Russian)
6. Van, K.L., Chzhen, Kh.S.: Numerical determination of dynamic stress, lubricating film thickness and surface temperature for spur gears. Part II. Results. In: Proceedings of American Society of Mechanical Engineers (Series: Design and Engineering Technology). Mir, vol. 1, pp. 92–99 (1981) (in Russian)
7. Kodnir, D.S., Ratner, I.D.: Contact and hydrodynamic calculation of gears. Reliab. Qual. Gears. **18-67-73**, 2–12 (1967) (in Russian)
8. Raiko, M.V.: Lubrication of Gears. Tekhnika (1970) (in Russian)
9. Skurka, I.S.: Elastohydrodynamic lubrication of rolling bearings. In: Proceedings of American Society of Mechanical Engineers (Series: Problems of Friction and Lubrication). Mir, vol. 2, pp. 110–121 (1970) (in Russian)
10. Kragelsky, I.V., Alisin, V. (eds.) Friction, Wear and Lubrication: Handbook. Mashinostroenie, Russia (1979) (in Russian)
11. Chzhu, D., Chzhen, Kh.S.: Influence of surface roughness on egd lubrication of point contacts. In: Proceedings of American Society of Mechanical Engineers (Series: Problems of Friction and Lubrication). Mir, vol. 4, pp. 36–43 (1988) (in Russian)
12. Tonder, K.: Effect of one-dimensional roughness of the inclined orientation of the microscopic irregularities in the hydrodynamic lubrication. part 2: moving rough surface. In: Proceedings of American Society of Mechanical Engineers (Series: Problems of Friction and Lubrication). Mir, vol. 3, pp. 103–107 (1988) (in Russian)
13. Tonder, K.: The Consequences of a number of common theories of roughness in the case of lubrication of surfaces with parallel ridges. In: Proceedings of American Society of Mechanical Engineers (Series: Problems of Friction and Lubrication). Mir, vol. 2, pp. 16–20 (1986) (in Russian)

Development of Geometric Descriptors for Gears and Gear Tools

D. Babichev

Abstract Important parameters of *a gear tool* are values of deflection of the machined surface at its different points, appearing due to errors of tool set-up, its re-sharpening and so on. An important parameter of *a gear* is its sensitivity to variation in the mutual arrangement of links appearing at gear assembly and due to deformations by loads and temperature influence. It is almost impossible for a production engineer, designer, product assembler or repairman to find this information; it can be obtained through complicated computer-aided analysis, individually tailored to each specific tool and gear. The place for keeping this information may be geometric descriptors of tools and gears proposed in this paper. The geometric descriptor will allow the manufacturers to solve multiple complex tasks quickly and reliably: (a) to obtain the proper location of the bearing contact in a gear; (b) to estimate the behavior of the bearing contact and the value of cyclic variations of the gear ratio when a gear is operated; (c) to assign deviations in tool-setting parameters in order to compensate for organic errors in the re-sharpening of tool front surfaces; (d) to determine the re-sharpening parameters in order to decrease organic errors in re-sharpening or obtain the required modification of tooth surfaces and other tasks. Theoretical basics for creating geometric descriptors are kinematic methods of the classical theory of gearing, developed later in the theory of real gearing. Choosing the most valuable references for development of geometric descriptors, we have to list works [11–20, 22–24]. The previous theoretical works written by the author are essentially useful for computer-aided design of generating processes, which precedes the development of geometric descriptors [2–4, 6, 7]. In these works, investigations of generating processes are carried out through applying: (i) the concepts of fans, wedges and bunches of normal lines [2–4, 7] (one can determine surfaces generated by jogs on generating solids, including those of secondary cutting); (ii) multi-parametric enveloping [2] (surfaces of shear are determined within tool supply and withdrawal); (iii) interrelated systems of curvilinear coordinates: integral, natural, unified, regulated [3] (one can even describe the geometry of all cutting edges for any edge-type tool as a

D. Babichev (✉)
Industrial University of Tyumen, Tyumen, Russia
e-mail: babichevdt@rambler.ru

V. Goldfarb et al. (eds.), *Advanced Gear Engineering*,
Mechanisms and Machine Science 51, DOI 10.1007/978-3-319-60399-5_11

continuous, smooth surface differentiable at all points with two unified regulated curvilinear coordinates on it [7]). The paper also presents: (a) analysis of features for gear machining cutting by edge-type tools and requirements for the geometry of operating flanks of teeth; (b) specification of types of geometric descriptor (paper, computer-aided and combined) and of tasks solved by their means; (c) statement of theoretical basics of development of geometric descriptors; (d) approximate contents of works on development of a system of geometrical descriptors for tools and gears; (e) theoretical investigations and specification of developed computer-aided programs aimed at development of geometrical descriptors; (f) results of computer-aided simulation through these programs for generation of helical surfaces by solids of revolution, i.e., fundamentals of geometric descriptors for disk-type cutters and disks for profile grinding; (g) structure of paper geometric descriptors and basic components of one sheet of such a descriptor. The present paper does not provide examples of geometric descriptors for specific tools and gears.

Keywords Theory of generation · Machine-tool meshing · Gear · Geometry of meshing · Geometric descriptor

1 Introduction

Many industrial and household products have descriptors with their technical parameters and consumer properties.

Important parameters of gear tools are, in particular, values of deflection of the machined surface at its different points, appearing due to tool re-sharpening, errors in tool set-up or other reasons. This information is necessary for a production engineer to be able to: (a) estimate the influence of tool set-up errors on deflections of the machined surface; (b) determine the deliberate deviations of tool setting parameters to compensate for organic errors in re-sharpening; (c) determine parameters of sharpening for front surfaces of tools in order to obtain the required modification of tooth surfaces, for example, within localization of tooth contact in a gear; and to solve other similar tasks.

An important parameter of a gear is its sensitivity to variation in mutual arrangement of gear links appearing at gear assembly and due to deformations during its operation because of both loads and temperature influence. Proper presentation of these parameters could, in particular, essentially simplify derivation of an optimal bearing contact in a gear at its assembly, repair and maintenance.

It is almost impossible for a production engineer, a designer, a product assembler or a repairman to find this information; it can be obtained through complicated computer-aided analysis, individually tailored to each specific tool and gear. That is why they need a source of such information that is convenient in use and allows for solving the mentioned tasks. It is proposed that a system be developed of geometric descriptors for tools and gears to be used as the required source.

Apparently, the task of development of *geometric* descriptors has not been brought up either in Russia or abroad. The "Description of hobs at their production and operation" described in [16] solves other tasks and pursues other aims: following the re-sharpening number and amount of metal cut at front surfaces during hob operation, determination of the hob's lifetime, etc. There is a reason to believe that the *geometric component* added to such a *description* would be very useful.

There have only been two publications by the author *on geometric descriptors*: [5, 21] in 2011 and 2012, respectively. They were published in Russian and they considered geometric descriptors of gear cutting tools. The publications remained unmarked. In recent years, this idea was discussed in private conversations with gear experts. Their typical opinion is that industry needs such descriptors very much, but their development would require labor of great intensity, both in theoretical investigations and especially in the programming implementation of a system of computer-aided generation and application of descriptors. This work can be carried out only by a development team with sufficient financing. But it is already reasonable and timely to state the necessity of such a task and to work towards solving its theoretical aspects. Tolerances for the manufacture of tooth elements of advanced gears often do not exceed several micrometers, and in their production, the urgent problem arises in regard to both the geometric features of the tool and the details of the appearance of organic errors in generation by enveloping methods. Geometric descriptors would facilitate the transition to a higher level of production of gears and tools.

Geometric descriptors are also of great interest for enterprises with worn-out batches of gear cutting machine-tools which have lost the accuracy required for production. In order to use them to produce gears of proper quality, the gears need to be designed with an essentially greater level of contact localization than is required for more precise gears. The greater value of contact localization can be also obtained through special sharpening of the edge-type gear cutting tool. The geometric descriptor, in particular, will allow a production engineer to determine the shape of the tool front surface at its sharpening.

Geometric descriptors of tools can also stimulate practical implementation of new tools and gear machining techniques. For instance: (a) cutting the gearwheels for worm gears by unified hobs [11, 23] (a single-thread hob can be used here to machine gearwheels meshed with a multi-thread worm and to obtain, in this case, the localized contact); (b) a new production method for gear machining of spiroid gearwheels by cutting heads at continuous generation [22]. Geometric descriptors would be helpful in this case for estimation of suitability of available tools for cutting specific worm (spiroid) gearwheels; revealing the quality parameters of obtained gears (first of all, the assessment of the degree of contact localization and multi-pair character of meshing).

This work is the first English publication on geometric descriptors. The text is presented in as close to layman's terms as possible to make the information comprehensible for those who are unfamiliar with all the geometrical details of gears and gear machining tools. That is why the paper states the requirements for tooth flanks of advanced gears and features of edge-type tools at the very beginning.

Then, it considers the concept of a geometric descriptor, the tasks to be solved with its help and the principle of its development. The paper also gives an example of investigations to be made prior to development of a geometric descriptor, especially investigation of the generation of helicoids (helical surfaces with constant pitch) by a disk-type tool, specifically by solids of revolution—disk grinding wheels.

2 Basics of Development of Geometric Descriptors

2.1 Requirements for the Geometry of Tooth Flanks

Representation of gear geometry underwent fundamental changes in the 20th century. At the beginning of the century, it was thought that, theoretically, conjugated surfaces should participate in meshing, these conjugated surfaces giving the uniform rotation of the driven gearwheel when contacting each other at uniform rotation of the driving wheel. It was supposed in this context that manufacture and assembly errors of gear elements were absent and that no deformations occurred due to both load and temperature. By the middle of the century, the profile and longitudinal modification of teeth had become common for responsible gears (first of all, spur and helical, bevel and hypoid). That is, the tooth flank for one of the gearwheels was deliberately deviated from that of the theoretically conjugated one. The tooth thickness at the outside surface was decreased at profile modification, thus reducing the impact power of the teeth at the instant of their re-conjugation. The tooth thickness at tooth flanks was decreased at longitudinal modification, thus eliminating the appearance of edge contact of the teeth at misalignment of the axes due to gear manufacturing and assembly errors, and deformations under load.

In the 1980s, a new approach towards optimal tooth modification appeared. Contact, bending and other deformations were taken into account for all gear elements: teeth, gearwheels, bearings, shafts, joints and casings. Modification of teeth was assigned after complicated computer-aided analysis of the mode of deformation for gear elements, accounting for re-conjugation and the multi-pair character of meshing.

The largest contribution to the development theory of localized contact in bevel and hypoid gears was made by F.L. Litvin, along with his followers (Leningrad). M.G. Segal (Saratov) developed and implemented the method for designing and cutting bevel gears, assigning values for deviations at eight boundary points of tooth flanks. Methods for gear synthesis with computer-aided simulation of mode of deformation of gear elements were successfully developed by: G.I. Sheveleva (Moscow) for bevel gears; M.L. Erikhov and his followers (Kurgan) for spur, helical and bevel gears; V.I. Goldfarb (Izhevsk) and his followers for worm-type gears; “Salyut” Inc. (Moscow) for spur gears, and other scientific schools.

At the present time, the following gears are considered to be the best: (a) those with point contact at the nominal point (at the middle of a tooth); and (b) those with small deviations in the solid of a part of the gearwheel flanks at the boundaries.

2.2 Features of Complex Edge-type Tools

The teeth of all edge-type tools are identical (Fig. 1). They have front and back surfaces, forming the cutting edges (main elements of the tool—Fig. 2) at the points of intersection. Very high demands are made on the shape of the cutting edges, namely, they generate the flanks of teeth on gearwheels. One problem for complex

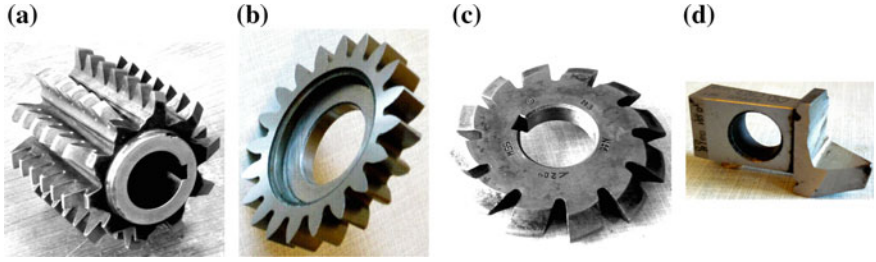

Fig. 1 Edge-type tools for cutting gearwheels: **a** involute hob; **b** shaping cutter; **c** disk-type hob; **d** cutter of a cutting head for spiral bevel gear machining

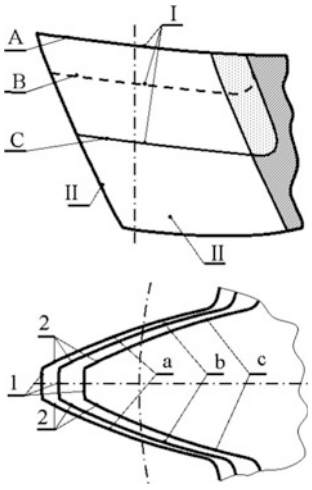

Fig. 2 Tooth and cutting edges of edge-type tools: *I* front surface. *II* back flanks. *1*, *2* top and side cutting edges: *A*, *a* for a new tool, *B*, *b* for a tool re-sharpened by 40%, *C*, *c* for a tool depleted by re-sharpening

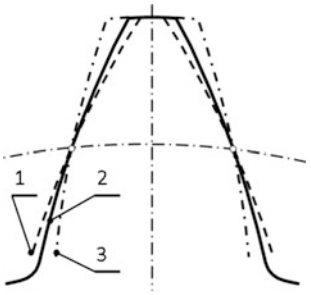

Fig. 3 Organic errors of edge-type tools: *1* new, *2* re-sharpened by 40%, *3* depleted by re-sharpening

edge-type tools is that, after their re-sharpening, the cutting edge leaves out a certain nominal surface, and it becomes all the more vital the farther the front surface strays from its nominal position. When the cutting edge leaves the nominal surface, the surface of the product will deviate from that required. This deviation results in an organic error of generation.

It is common to design an edge-type tool so that the organic error will be absent at the re-sharpening of the tool by 40% of its allowable value. As a rule, a tool that is new and re-sharpened to its maximum will cause organic errors with opposite signs (see Fig. 3). Maximum organic errors appear at the machining of wheels for worm gears: single- and double-enveloping [16, 17] and spiroid [23]. This is related to the significant sensitivity of the shape of tooth flanks for such gearwheels to variation in the hob diameter due to its re-sharpening.

There are many works on the generation of helical surfaces (which are very common in tools and gearwheels) and on investigations into the geometry for shaping cutters, involute hobs and other gear-cutting tools. In particular, they cover the following issues: (a) influence of re-sharpening on the shape of the product surface; (b) influence of errors of mutual arrangement of the tool and blank on the shape of the machined surface; (c) influence of mutual arrangement of gearwheels in a gear drive on the character of tooth contact.

There are to ways to correct organic errors in gear machining by edge-type tools: (a) changing the shape of the front re-sharpened surface; (b) changing the parameters of the tool setting with respect to the blank. One of the tasks to be solved by means of geometric descriptors of tools is to give a production engineer the possibility of reducing the organic errors of tooth flank generation to a minimum.

2.3 Geometric Descriptor of a Tool and Tasks Established with Its Application

A geometric descriptor is a document containing several pages/appendices with nomograms that allows for:

(a) determination of deviations at assigned points of the machined surface which appear due to the re-sharpening of the tool and errors in its setting and motion at gear machining—*the direct task*;
(b) determination of the parameters of the tool setting, motion and refurbishment so as to obtain the assigned deviations of the shape of the machined surface from the nominal enveloping surface—*the reverse task*.

Let us explain the above through several examples of tasks and manners of their establishment through application of geometric descriptors.

Example 1 The geometric descriptor of the grinding wheel for machining a helical surface with constant pitch of: worms, gearwheels (including the spur variety) and other parts. The main element of the geometric descriptor is the nomogram connecting the deviation of the product profile from the nominal one at any point depending on the assigned:

(a) diameter of the grinding wheel (at its invariable profile);
(b) errors of the grinding wheel position with respect to the product (for all parameters of its setting);
(c) errors of the grinding wheel profile—displacement of the whole profile and deviations at any assigned point.

The following points can be assigned here at the profile of a product or grinding wheel: (a) the point at the outside cylinder; (b) the lowest active point; (c) the point at the reference (nominal) cylinder; (d) any other point.

Nomograms in the descriptor allow for establishment of both the *direct* and *reverse* tasks. They are necessary for a designer to be able to assign the rules of the contact in a gear, and for a production engineer to be able to correct the parameters of gear machining and obtain the required bearing contact.

Example 2 *The geometric descriptor of the disk-type hob for machining a helical surface with constant pitch.* According to the contents of the descriptor, the established tasks and the methodology of application, it is close to the descriptor of the grinding wheel. The difference is that, instead of variation of the wheel diameter at the invariable axial profile, the tool re-sharpening for its front surface is accounted. The shape of the back flank inherent to the tool and the shape of the front surface to be re-sharpened are considered here. Such a supplement to the descriptor is very significant and rather complex in its computer-aided implementation.

Example 3 *The geometric descriptor of the involute hob—the main edge-type gear machining tool.* According to its functional possibilities, this descriptor is similar to the descriptor of the disk-type hob, but much more complicated. First, the content of the descriptor and a part of the established tasks are different for tools which machine worm and spur or helical gearwheels. Second, the involute hob is intended for cutting gearwheels with different numbers of teeth and factors of addendum modification. And it is desirable to have one descriptor per hob, rather than a series of descriptors for one hob per each of the products.

Who creates nomograms for geometric descriptors and how. A descriptor itself, with appendices—nomograms and instructions for application, are generated by means of special software.

Let us consider in more detail the manufacturing tasks which are established by means of geometric descriptors of tools.

Task 1 (direct). It is necessary to determine the influence of the tool position on the shape of the machined surfaces of a gearwheel:

- to determine the value of deviations from the assigned position at specified points of the surface generated by the tool on the tooth of a gearwheel. The task is established for the design position and motion of the tool and blank.
- to determine the variation of these deviations for the assigned errors of position and motion of the tool with respect to the blank. Establishment of this task will allow for estimating the applicability of this tool (for cutting a specific gearwheel) with the front surface present upon it.

Task 2 (reverse). It is necessary to determine for a specific tool:

- the position and parameters of tool motion with respect to the blank, so that the deviation of the generated surface from the design at the assigned points of the tooth will be a minimum.
- the allowable limits of errors for tool setting, so that the deviation of the generated surface from the design will be within the tolerance range.

Establishment of this task will allow for determining such optimal position and motion of this tool in machining a specific gearwheel that will provide minimum organic error of generation and provide the opportunity to specify technically-based tolerances for position and motion of the tool within gear machining.

Task 3 (reverse). It is necessary to determine the shape of the front surface of the tool and the profile of the grinding disk for re-sharpening of this surface, providing the modification of the machined surface of the tooth that minimally deviates from the required design surface. Establishment of this task diminishes the urgency of the problem of variation of organic errors of generation due to the re-sharpening of gear cutting tools.

Task 4 (reverse). Correction is necessary for position, motion or parameters of front surfaces of the tool based on measurements (by an involute profile measuring device or control-measuring machines) of gearwheels previously cut by this tool. Establishment of this task allows for at least partial compensation for the influence of a large group of random factors (not involved in geometric descriptors) affecting the generating process: deformations and dynamic processes in the system “machine—equipment—tool—part”, errors of kinematic chains, and others.

2.4 Types of Geometric Descriptor

The three following types of descriptor are proposed:

Type 1. Paper descriptor, with diagrams and nomograms as its basis, created by a computer program for a specific tool according to one of two techniques:

(1) Based on its measurement at the control-measuring machine. This technique is preferable, but expensive equipment is required in this case.
(2) Based on computer-aided simulation of generating processes according to which the tool is made at the tool-making plant and, perhaps, accounting is made for measurement of several tools within one dimension type at the control-measuring machine (to obtain the statistics for a group of tools and to check the validity of accounted parameters of generation within tool manufacture). This technique is less reliable than the first one and it is appropriate only for mass production (with use of the control-measuring machine).

Drawbacks of the first type of descriptor are as follows: it is hard to provide the establishment of all tasks considered in Sect. 2.3 (especially for hobs); and it is time-consuming to solve optimization tasks here.

Type 2. Computerized descriptor, with a package of software programs as its basis, intended for establishment of all the tasks described in the previous section. Such a descriptor consists of the program package and documentation of its application.

Type 3. Combined descriptor, including:

1. Extractions from the paper descriptor—nomograms for establishing the simple tasks, with instructions and examples of their application.
2. Package of software programs for establishing complex optimization tasks, with documentation of its application.

We suppose that the main type of geometrical descriptor should be the third type —the combined type.

2.5 Tools and Gears for the Priority Certification

The most common gears in machines are the spur and the helical. That is why the system of geometric descriptors should first of all be developed for tools that machine spur and helical gearwheels: worm and disk-type hobs, shaping cutters (see Fig. 1), grinding wheels, and others. It is reasonable to choose the following sequence of the development process:

The first descriptor is for wheels for profile grinding. They are used to machine, in particular, precise involute gearwheels of high-speed and heavy-loaded gear

drives, and that is why it is necessary to consider even the very smallest organic errors of generation. And since it is also the easiest geometry tool, its descriptor will be simpler than the others, including the software part. It will allow for gaining experience in the development and implementation of geometric descriptors and the creation of a computer-aided system of certification.

The second descriptor is for disk-type module and shape cutters. They will help in mastering the technique of establishing the tasks that are common to all edge-type tools: geometry of cutting edges, variation after re-sharpening, and others.

The third descriptor is for hobs—the basic tool for cutting gearwheels. As was mentioned above, they are the geometric descriptors with the most complicated development process. And several types are necessary: for machining both the gearwheels of worm-type gears and spur and helical gearwheels, involute and non-involute ones.

The fourth descriptor is for shaping cutters and generating cutters.

The consequent descriptors for other tools: module and shape end-milling cutters, milling cutters for spline grooves, honing tools, etc.

2.6 Contents of Works on Development of a System of Geometric Descriptors for Tools and Gears

Let us describe the list and sequence of steps necessary to be taken when developing such a system:

1. Systematization of types and a structure of geometric descriptors and tasks established by their means.
2. Development of the list, structure and type of diagrams and nomograms necessary to be included in geometric descriptors of tools. These graphic images are individualized for each specific tool. Their list and structure are different for various types of tool.
3. Development of mathematical models and algorithms:
    - To analyze the geometry of front and back surfaces of edge-type tools (including random and deliberate deviations in position, motion and shape of grinding wheels for relieving and sharpening).
    - To analyze the geometry of tooth surfaces generated by cutting edges which are lines of intersection of complex front and back surfaces (including intended or undeliberate deviations in position and motion of the tool with respect to the blank).
    - To process data of measurement of gearwheels and tools at control-measuring machines (for individual and batches of gearwheels or tools).
    - To develop software programs for creation of nomograms and texts of descriptors.
    - To develop software programs which are the components of the descriptor.

4. Development of software packages for solving the tasks described above.
5. Investigation of geometry of tools and gears with the help of developed software in order to determine the properties and main relations specific to these types of tool and gear.
6. Sample certification of tools and gears (based on the two previous points).
7. Refinement of a system of certification and production of gearwheels with the assigned modification of tooth flanks obtained through a special sharpening of available tools and preliminary deviations in position and motion of the tool with respect to the blank.
8. Refinement of a system of certification of gears in order to control the position and dimensions of the contact pattern when producing and repairing gears.

2.7 *Theoretical Studies and Computer-Aided Design Allowing for Creation of Geometric Descriptors*

The theoretical foundation of the development of geometric descriptors is the classic theory of gearing that had been created by the beginning of 1970s, and its further development as the theory of real gearing. The most valuable publications by scientists of this period that can be helpful in the development of geometric descriptors are:

Shishkov [20]—the concept of "penetration velocity"; Litvin [14, 15]—kinematic and matrix methods for analysis of meshing; Zalgaller [24]—analysis of the classical theory of envelopes; Sheveleva [19]—the concept of "wrapping" and techniques of contact stress analysis; Segal [18]—the effective method of contact localization; Korostelev [12]—kinematic parameters of load-carrying capacity of spatial gearing; Lagutin and Sandler [13, 16, 17]—the concept of "meshing space" and generation for the cases of grinding the tools surfaces and production of worm gears; Goldfarb, Trubachev et al. [11, 22, 23]—numerous investigations of worm-type gears and new types of tools for cutting of gearwheels and worms.

The main results of theoretical investigations by the author related to this theme have been stated in PhD and DSc theses [3, 6] and published in works [1, 2, 4, 5, 7–10, 21]. These studies are focused on development of kinematic methods of the theory of gearing and theoretical basics of *computer-aided simulation* of generating the surfaces of gears and tools. In [6], the methodology of the numerical analysis of gearing is developed, which does not require analytic investigation of geometry and kinematics of specific gears and machine meshing. In [8], the computer-aided implementation of this methodology is described. One of the elements of this ideology is application of generalized systems of coordinates and motions to which any active and machine meshing are reduced. In [3, 4], fundamentals of an alternative theory of generation are developed and stated based on new geometric and kinematic images and concepts: a fan, a wedge and a bunch of normal lines in jogs of profiles and surfaces [2]; acceleration of implementation [1].

An integral component of the alternative theory of generation is the application of consequent and multiple-parameter envelopes [2] and discrete and continuous curvilinear coordinates, including natural [3] and regulated with controllable placement of points along profiles [3, 21]. A distinctive feature of the developed theory of generation is that not only is the separate most important segment of a tooth considered, but so is the whole profile or surface of the tooth (or root or even the whole gear rim) [3, 7]. The profound technique for the description of any edge-type tool (shaping and various milling cutters) is developed, enabling the finding of both the generated surface and the dynamic angles of cutting. The initial tool surface will have continuous smooth curvilinear coordinates in this case [7].

Software programs developed on the basis of theoretical investigations and used when creating the geometric descriptors. Let us consider the most acclaimed programs developed by Taisin and Babichev within the project [21]:

1. *Subprogram* ***Profil*** **is** intended to work with plane lines and profiles. It allows for composing complex profiles (including those containing jogs) out of segments of typical lines in an interactive mode. Visualization of the created profile is made during this composition (see Fig. 4).

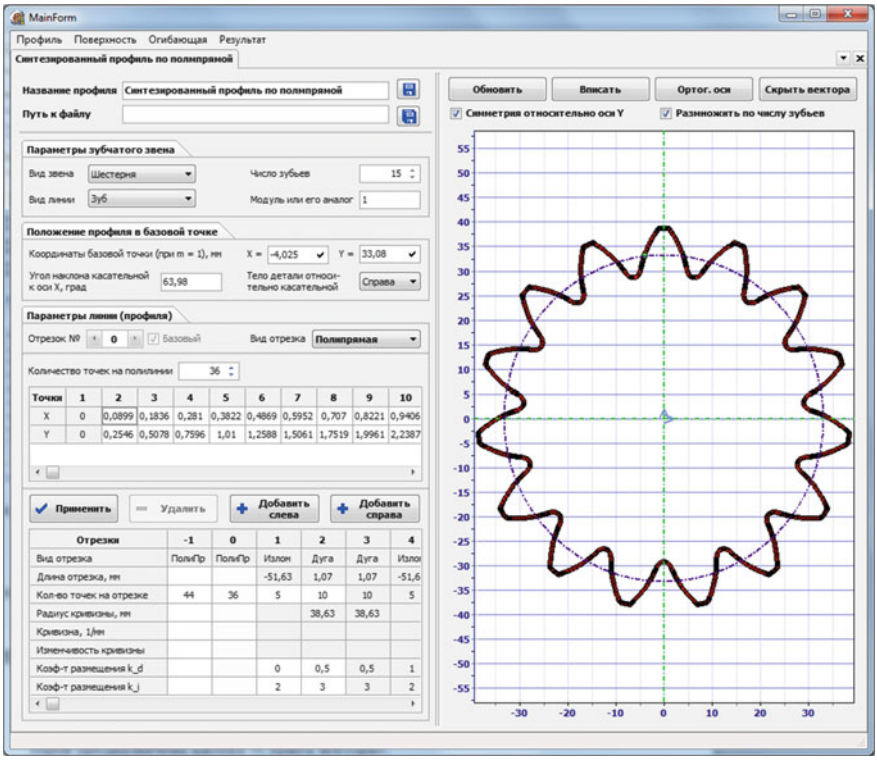

Fig. 4 The main window of the subprogram *Profil*

The profile can consist of a number of various segments (straight line, arc, involute, jog, poly-straight line, poly-arc). The subprogram ***Profil*** contains procedures and functions for determining:

- Cartesian coordinates of the point assigned by a curvilinear coordinate unique to the whole profile;
- Projections of the unit normal vector and unit vector of the tangent to the line at this point, including *the jogs of the profile* (!) where fans of normal and tangent lines are located;
- Curvature and radius of curvature at the given point.

The most attractive feature of the program is that it allows a user to control the location of points on profiles (their number and non-uniformity of location for each typical segment, including jogs).

2. *Subprogram* ***EasySurf*** assigns the areas of surfaces generated by motion of plane and space segments of lines. In the general case, the motion of the generating segment can be helical with constant or variable pitch (its special cases are linear and rotary types of motion). The generating segment of the line itself does not change its dimensions and shapes in motion.
3. *The main program* ***GrindTool*** determines the profile of the grinding wheel used to form the final designed spur or helical gearwheel, cylindrical worm, helical groove of the drill or other helical surfaces with a constant pitch. Such a surface is called a helicoid in mathematics. It is often encountered in machine parts and tools. The surface of the grinding wheel determined here can also be the initial tool surface (ITS) of form milling cutters and end-mill gear cutters for machining the pointed parts. Cutting edges of milling cutters should be located on this ITS.
4. *The main program* ***GrindZub*** analyzes the geometry within gear grinding. The main established task is to determine the surface generated by a grinding wheel. The question arises here—what is the purpose of determining the surface for which the profile of the grinding wheel has already been designed? It is evident that this exact known surface of the part (the synthesized gearwheel) will be obtained according to the designed tool (grinding wheel). This statement is valid only in the case when the grinding wheel is mounted (and will be transmitting) with respect to the part in a strictly determined way. Due to errors of mounting and motion and due to wheel dressing, deviations in the surface generated by grinding from the required designed surface occur. And though these deviations are small, they should be considered when manufacturing precise gears.

In order to develop a geometric descriptor for a specific tool or a gear according to the steps and programs described above, it is necessary to perform a thorough preliminary investigation of the appropriate type of machine-tool or operating gearing. An example of part of such an investigation prior to development of descriptors for tools with the initial tool surface as a surface of rotation is presented below in Sect. 3.

Prior to proceeding to that section, let us explain several features of the generation of surfaces by bodies of rotation for purposes of comprehension. Figure 5a shows the convolute worm. It is generated at the thread-turning lathe by a cutter with rectilinear cutting edges: two lateral and one vertex. These three edges belong to one plane (on the front surface, see Fig. 2) and generate two jogs (two singular points on the continuous profile of the cutter) in areas where they meet. The front surface (a plane) passes through the straight line intersecting the worm axis at the right angle. There is the "model" of the cutter (three rectilinear segments with two jogs between them) at the root of the worm profile in the normal cross-section. The surface of space is generated by a helical motion of the cutter profile with respect to the worm solid (see line ***I*** in Fig. 5a).

If the same convolute worm is generated not by the cutter but by the tool with the initial tool surface as the body of rotation (for instance, to grind all the space surfaces of such a worm), then it turns out that:

(1) contact of the grinding wheel surface with flanks of the worm space will be along spatial curves (see line ***II*** (ABC) in Fig. 5a);
(2) the surface of the grinding wheel will not be conical (as a consequence of the previous statement);
(3) jogs as screw lines on the worm surface can be obtained by the grinding wheel only for a specially selected cross angle during grinding (at other values of the cross angle, the transient surface will appear on the worm (see line 6–6 generated by the point of the jog 6 in Fig. 5b).

An important (and upsetting) circumstance is that the shape of the contact line ***II*** in Fig. 5a and the profile of the grinding wheel depend on the diameter of the grinding wheel and cross angle during grinding.

Another upsetting feature of the generation process is demonstrated in Fig. 5b. It shows that the continuous profile (or the surface) generates, as a rule, a continuous

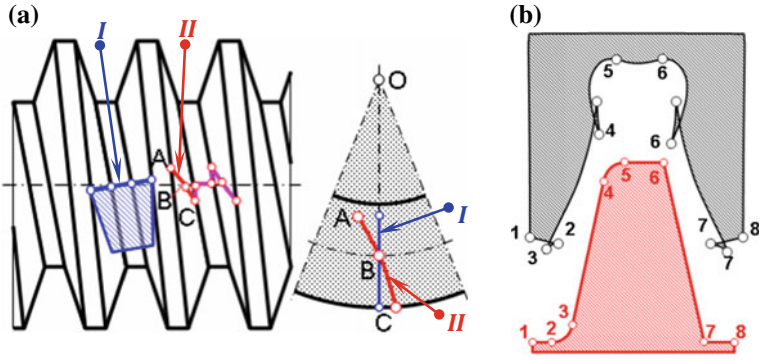

Fig. 5 Problems of the generating process: **a** *I* generation by a cutter: plane line of contact of the tool and a part; *II* generation by a grinding wheel: complex spatial lines of contact of the initial tool surface and the part; **b** undercut and looping of the conjugated profile

conjugated profile (or surface) of the part root (see this in more detail in [4]). But this continuous conjugated profile can be self-intersecting, that is, looping. It is the reason begind undercut (sloping "fish tails"; see lines 4–5 and 6–6 in Fig. 5b) and the impossibility of gear machining for a section of the assigned profile (abrupt "fish tails"; see lines 2–3 and 7–7 in Fig. 5b).

All upsetting features of generation processes should be revealed and rated quantitatively during investigation prior to the development of descriptors and should be considered during said development.

3 Investigations Preceding Development of Geometric Descriptors of Tools (by Example of the Descriptor of a Tool for Profile Gear Grinding)

3.1 Choice of a Gear Pair for Profile Gear Grinding

The object of profile grinding became a pinion of one of uniform-strength gears synthesized by us [9]. Uniform strength means the planar gearing (including spur gears) where Hertz contact stresses along the line of action are constant, that is, σ_H = const. Synthesis of such gears is reduced to establishment of a variation task [9]: it is necessary to determine a function $f(x,y)$ (line of action) and conjugated profiles $\mathbf{r}_1 = \mathbf{r}_1(u_1)$ and $\mathbf{r}_2 = \mathbf{r}_2(u_2)$ for which the chosen quality parameter (the contact stress σ_H) is equal to the assigned value at all points of the given line of action.

Figure 6 shows one such synthesized gear. Its parameters are: power at the pinion shaft P_1 = 100 kW; pinion speed n_1 = 1500 rpm; gear ratio u = 2; center distance a_w = 150 mm; face width b_2 = 36 mm; pinion tooth number z_1 = 15;

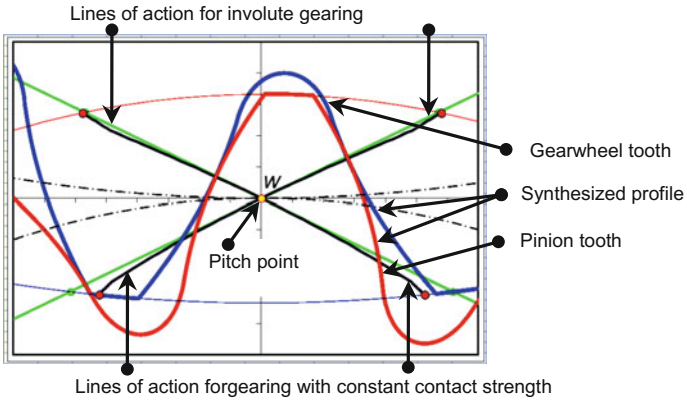

Fig. 6 Uniform-strength gear (contact stresses σ_H = const)

pressure angle at the pitch point $\alpha_w = 25.562°$; contact stresses on the main part of the line of action $\sigma_H = 1000$ MPa, and at the beginning and at the end of the line of action $\sigma_H = 700$ MPa (assuming that one tooth pair is in the contact); addendum factors for gearwheels: $h^*_{a1} = 1$ and $h^*_{a2} = 1$; module at pitch circles $m_w = 6.667$ mm; tooth thicknesses at addendum circles: $S_{a1} = S_{a2} = 3.106$ mm; contact ratio $\varepsilon = 1.327$.

For comparison, Fig. 6 also shows lines of action for an involute gear with the same pressure angle at the pitch point W $\alpha_w = 25.562°$ and the same contact stresses $\sigma_H = 1000$ MPa. According to Fig. 6, the lines of action for a synthesized gear slightly differ from the straight lines that are the lines of action in the involute analog. That is why pressure angles are close to their corresponding values for an involute gear. The tooth shape is also close to the involute one—according to analysis, deviation of profiles from involutes for a synthesized gear is less than 0.1 mm at addendums and up to 0.3 mm at dedendums as compared to the involute analog.

Figure 7 shows diagrams of quality parameters of the synthesized uniform-strength gear as compared to parameters of the involute analog. The most important quality parameter is Hertz contact stress σ_H. The values of σ_H are the same at the pitch points of both gears. Beyond the pitch point, the value σ_{Hmax} for the involute analog is greater than for the uniform-strength gear in all meshing phases.

At the beginning of tooth contact, the value σ_{Hmax} is 2.1 times greater; at the zone of a single-pair meshing, it will be greater by 10%; at the instant of the tooth coming out of the meshing, the value σ_H is greater by 30% (see Fig. 7e). The reason lays in the character of variation of profile curvature radii R along the line of action (Fig. 7 a–c): at the pinion root, the value of R is from 23 to 27 mm; at the gearwheel tooth root, there is even a small concave segment.

The value of the factor υ_{1max} of the specific sliding at the pinion tooth root in the uniform strength gear is 2.3–3.0 times less than in the involute analog (υ characterizes the intensity of an abrasive tooth wear).

The pinion of the equal strength gear shown in Fig. 6 is also the object of profile grinding, because it is better to carry out refinement of techniques, algorithms and programs for the development of geometric descriptors as applied to complex profiles consisting of diverse curves and determined by means of program software.

Results of the pinion synthesis shown in Fig. 6 are taken as the initial data for the subprogram **Profil**. After processing, they are transmitted to the main programs ***GrindTool*** and ***GrindZub***. They are the arrays: of coordinates of points of the synthesized profile; of projections of the tangent and normal lines and radii of curvature to the profile at all determined points.

3.2 Investigation of the Machine-Tool Gearing with the Initial Tool Surface as the Surface of Rotation

This section describes the results of investigating the generation process for the pinion dedendum with parameters determined in the Sect. 3.1. At the investigation,

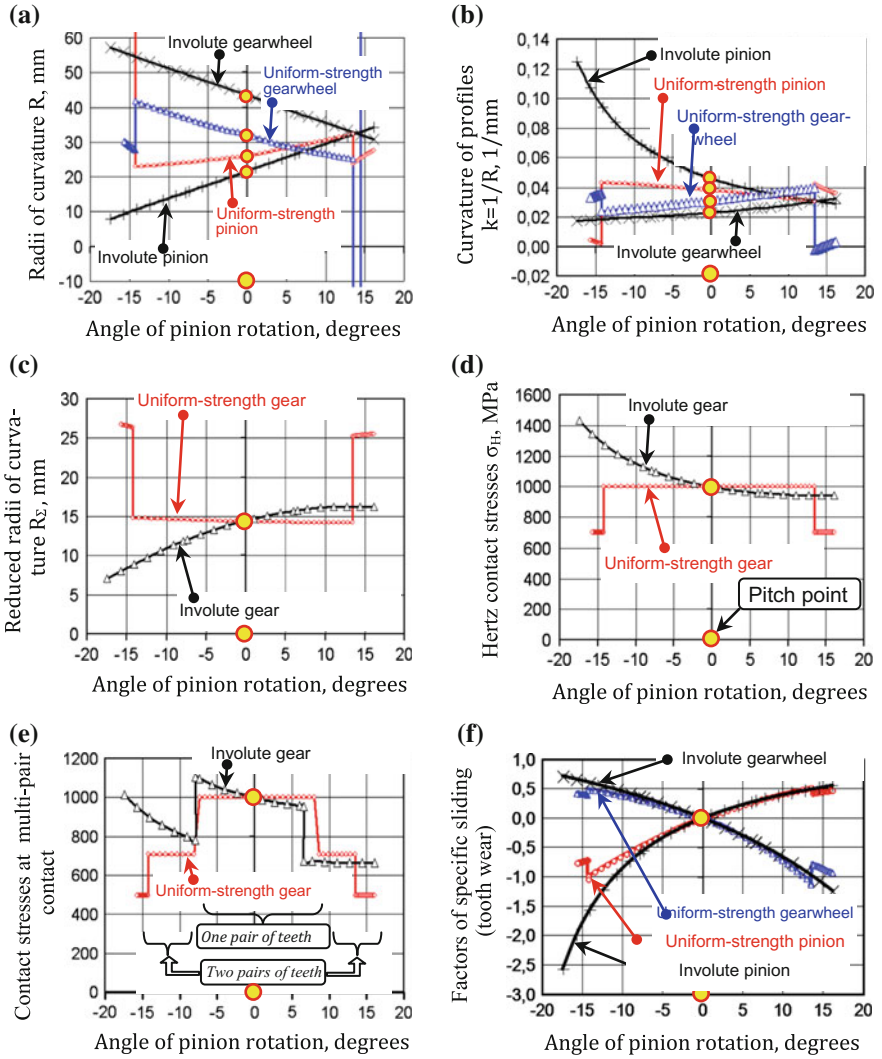

Fig. 7 Comparison of quality parameters along the whole meshing line for involute and uniform-strength gears: **a** curvature radii of tooth profiles for a pinion and gearwheel at contact points; **b** curvatures of tooth profiles; **c** reduced radii of curvature at points of tooth contact; **d** Hertz contact stresses for a single-pair tooth contact; **e** Hertz contact stresses for a single- and double-pair tooth contact; **f** specific sliding of teeth

a helix angle on pitch diameter was equal $\beta_w = 20°$ and cross angle in machine meshing $\gamma = 110°$. This investigation was carried out with the ***GrindTool*** and ***GrindZub*** programs. Figures 8, 9, 10, 11 and 12 present a selection of diagrams—results of operation of the program ***GrindTool***. Figure 8 shows the difference between normal sections of dedendums of the helicoid for the same face

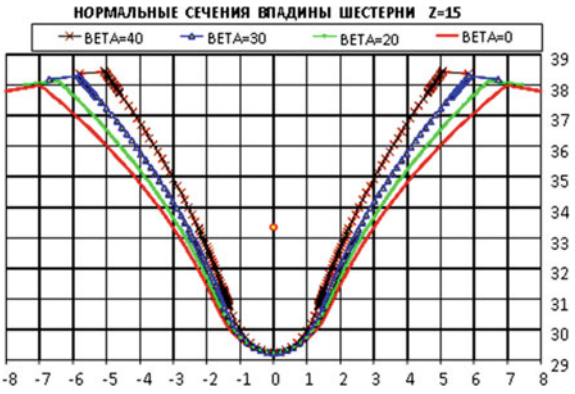

Fig. 8 Normal cross-sections of the helicoid at different helix angles of the tooth line β_w

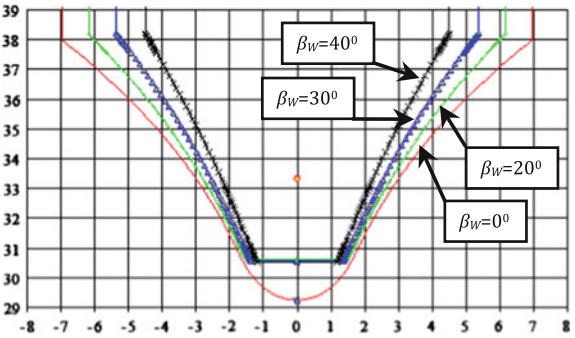

Fig. 9 Profiles of grinding wheels at different helix angles of the tooth line β_w

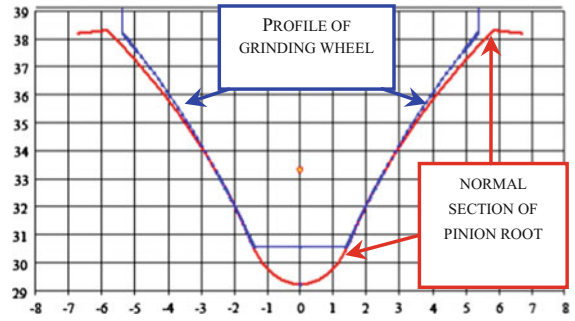

Fig. 10 Profile of normal section of the pinion with $\beta_w = 30°$

cross-section at different tooth helix angles. Figure 9 shows the difference in profiles of grinding wheels intended to machine flanks of helicoids with the same face section but with different helix angles. Note that the profile of the grinding wheel is identical to the root profile only for the angle $\beta_w = 0$. Figure 10 shows the

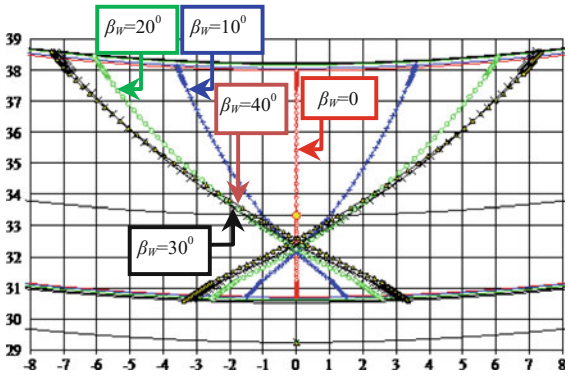

Fig. 11 Location of contact lines on the grinding wheel at different β_w

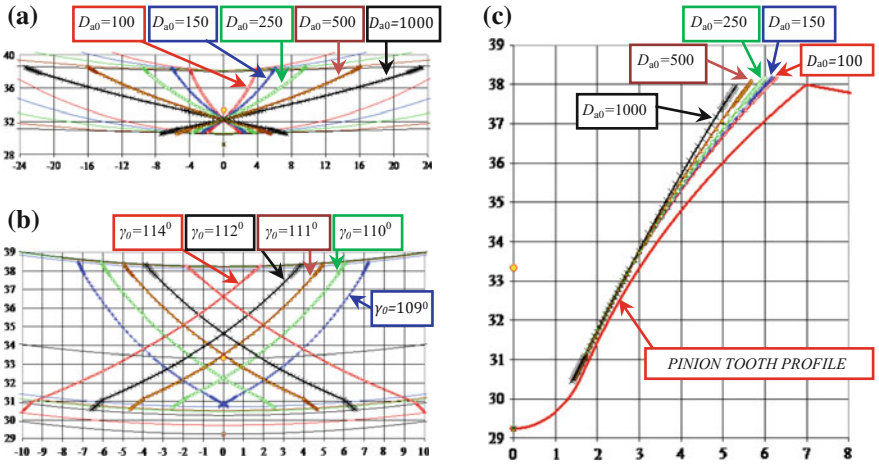

Fig. 12 Influence of the grinding wheel outer diameter D_{a0} and the cross angle γ_0 in gear machining on location of contact lines and wheel profile: **a** influence of D_{a0} on contact lines; **b** influence of γ_0 on contact lines; **c** influence of D_{a0} on the profile of the grinding wheel

difference between the *profile of the grinding wheel and profile of the normal cross-section* β_w = 30°. The greater the value β_w, the greater this difference is. Figure 11 shows that for the same face cross-sections of helicoids, the lines of contact of surfaces of grinding wheels with surfaces of helicoids are different at various inclination angles of the tooth line. Note that only for the angle β_w = 0 (spur gear) is the line of contact of tool surface and the machined part the plane line—the axial cross-section of the grinding wheel surface (see the red line for β_w = 0). In all other

cases, the lines of contact (they are also called the characteristic lines) are spatial curves. And the greater the helix angle β_w, the farther this line goes from the center distance.

Figure 12a shows the influence of the grinding wheel outer diameter D_{a0} on the line of contact (characteristic). It turned out that this influence is very significant. Thus, for a small diameter D_{a0} = 100 mm, approximately 8 mm of the tooth line are in machining: 6 mm from the right and 6 mm from the left side of the tooth. And for a large diameter D_{a0} = 1000 mm, approximately 46 mm of the tooth line are in machining: 30 mm for each side of the tooth. Therefore, the greater the diameter of the wheel, the larger the minimum tool overrun required when machining a helical gearwheel: for D_{a0} = 100 mm, it is equal to ΔS_Z = 6 mm, for D_{a0} = 1000 mm, it is ΔS_Z = 30 mm. This means that movement of the tool along the axis of the machined gearwheel should be greater than ($b + 2 \cdot \Delta S_Z$), where b is the face width.

If D_{a0} is changed, the tool (in this case, the grinding wheel) profile should also be changed: Fig. 12c shows the dependence of the grinding wheel profile on its diameter D_{a0}. At the right, the large-scale face profile of the machined helical pinion is shown by the red solid line. At the left, there are five profiles of grinding wheels for five different outer diameters D_{a0}. It is clear that segments of a tool machining the dedendum differ insignificantly. However, segments machining the addendum are significantly different: when D_{a0} is changed two times, variation of the profile reaches 0.2–0.3 mm at the segment machining the points at the addendum. That is, organic errors in profiling (not considering the diameter of the grinding wheel) can become 100 times greater than the required accuracy of tooth profile manufacturing.

Note that all diagrams in Figs. 8, 9, 10, 11, and 12a, c are plotted for machining at the cross angle γ equal to $\gamma = (90° + \beta_w)$. That is, it was accepted that the tool is planned according to its design position with respect to the blank for which the tool inclination angle $(90° - \gamma)$ is equal to the helix angle of the tooth (β_w) *on the pitch diameter* (d_w). But according to the theory of tool design, it is known that the other angle of tool inclination, with respect to the blank, can be used; let us designate it γ_0. Figure 12b shows the influence of this cross angle γ_0 on the location of the contact lines during grinding of pinion teeth.

The general conclusion from Figs. 8, 9, 10, 11 and 12: for the considered profile of a gear dedendum, there is a rather wide range of variation in parameters for the tool (D_{a0}), the gearwheel (β_w) and their mutual arrangement (γ_0). When machining typical cylindrical gears and worms by profile grinding, there are no difficulties associated with undercut, looping or self-intersecting of the required tool profile. That is why there is a rather wide range of variation in tool parameters and tool position for achieving the improvement of quality parameters of gear machining and their optimization.

Examples of operation of the program ***GrindZub*** are not given here, since they differ slightly from the examples given in Figs. 8, 9, 10, 11 and 12.

3.3 *What a Paper Descriptor Should Represent and How It Should Be Developed on the Basis of Performed Study for Specific Types of Machine-Tool and Active Meshing*

We suppose that a paper geometrical descriptor for a specific meshing (machine-tool or active) will include several sheets. The structure of all sheets is similar (Fig. 13): there are two groups of scales along the edges (input and output for the established tasks) and a group of nomograms (the basis of geometrical descriptors) is located in the middle. There are also two types of scale on each nomogram: input and output. Scales of variable parameters and quality parameters can be multilevel, for example: dimensions are pointed in millimeters and inches (linear-dependent scales); or backlashes in a gear can be measured in normal and circular directions (scales with non-linear dependence). Scales of consequently applied nomograms indicate the same parameter (in Fig. 13, this relation is symbolized by dashed lines). It is desirable to make colored lines of relations and fills and to relate these colors logically with tasks to be established and types of variable parameter and quality parameter.

Each of the sheets of any descriptor is intended to establish several similar tasks (both direct and reverse) by means of available nomograms. When establishing the direct task, the input data are assigned at left scales (Fig. 13) and the result is obtained at right scales. When establishing the reverse task, the method is opposite: the input data is on the right scales and the results are on the lef. In order to simplify the work with descriptors, "trajectories of motion" are plotted on nomograms between the right and left scales for each task to be established. A part of sheets for certain tools can be similar. For example, one-two sheets of the geometrical descriptor of a disk-type cutter can be identical to one-two sheets of the descriptor of a grinding wheel for profile grinding. They are, in particular, the sheets with nomograms relating the deviations in the generated surface with parameters of

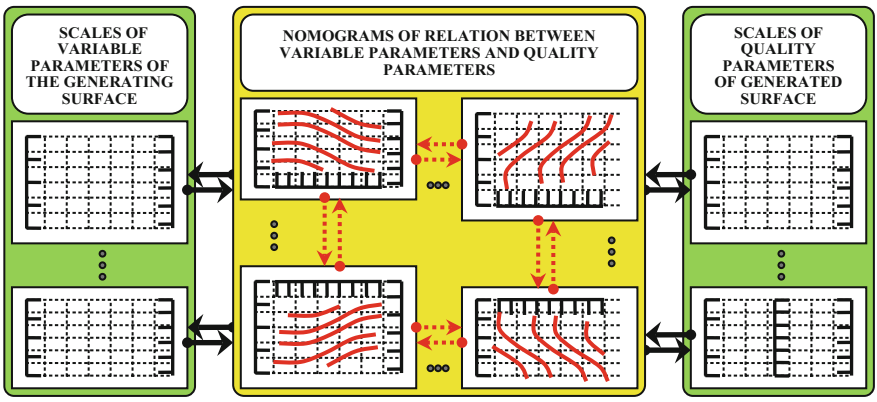

Fig. 13 Basic components of one sheet of the paper geometrical descriptor

mutual arrangement of axes of the tool and machined gearwheel. It is valid, for example, for establishing the task of determining the tool displacement after its re-sharpening (dressing), providing the required backlash in the gear.

The foundations of the development of nomograms (i.e., the main components of geometrical descriptors) are various arrays of results of thorough investigation of a specific gearing. It is reasonable to carry out the development of nomograms by means of software programs created for this purpose. It is similar to the method of development of *dynamic* blocking contours [10].

4 Conclusions

1. In order to manufacture a quality gear, one should take into account both the geometrical features of tools and the details of appearance of organic errors of surface formation by generation methods. This is impossible to do without computer-aided analysis. One easy-to-use representation of this analysis can be geometric descriptors of gears and gear-machining tools.
2. The paper described the idea of development of these descriptors, procedure and contents of the project to create them. The geometrical descriptor, in particular, will assist a designer in assigning tolerances for a gear, including rules of tooth contact, and a production engineer in determining parameters of tool shape and position providing the required accuracy of the product and obtaining the assigned bearing contact.
3. Three types of geometrical descriptors have been proposed: paper, computerized and combined; tasks established by their means have been considered. Combined descriptors are recommended as basic ones for complex edge-type tools.
4. The structure of paper geometrical descriptors and methodology of their creation are developed:

    - the basis of a geometrical descriptor is a nomogram, which demonstrates the relations and numerical dependencies between input and output parameters of the task to be established;
    - such a descriptor consists of several pages with nomograms for establishing one or two simple tasks;
    - complex tasks are established by specially developed computer-aided programs for combined descriptors;
    - paper geometrical descriptors for specific tools are generated by a special program software—the main (and the most expensive) element of the proposed system of certification;
    - the theoretical basic for creating a special program software is a number of kinematic methods of the theory of gearing focused on computer-aided methods of analysis of generation processes.

5. The paper presented: the performed theoretical studies and developed computer-aided programs intended for creation of geometrical descriptors; and the results of computer-aided simulation carried out by means of these programs for generation of helical surfaces by solids of revolution, the simulation being the basis for the creation of geometric descriptors of disk-type cutters and wheels for profile grinding.
6. Information presented in this paper is the result of the first (initial) stage of works on this project. The next planned step will involve the following tasks:
   - to finalize the list, structure and types of diagrams, schemes and nomograms to be included for geometric descriptors;
   - to finalize the software for the generation of diagrams and nomograms for the descriptors of wheels for profile gear grinding;
   - to create some sheets of the first version of the descriptor of grinding wheels.

References

1. Babichev, D.T.: Acceleration of cutting-in is an important factor of the process of surfaces formation by means of bending. In: Proceedings of the 7th International Conference "Research and Development of Mechanical Elements and Systems", IRMES 2011, 8.6, s. 611–618, Zlatibor, Serbia (2011)
2. Babichev, D.T.: Development of kinematic method of theory of gearing to determine areas of tooth flanks produced by jogs of generating solids. In: Theory and Practice of Gearing and Transmissions: In Honor of Professor Faydor L. Litvin. Mechanisms and Machine Science, vol. 34, pp. 159–188. Springer (2016)
3. Babichev, D.T.: Development of the theory of gearing and generation of surfaces basing on new geometric and kinematic representations. Doctor of Science in Technology Thesis, Tyumen SOGU, Tyumen (2005) (in Russian)
4. Babichev, D.T.: Fundamentals of the alternative theory of generation based on new geometric concepts. In: Proceedings of the International Conference "Technics of Drives 03", I–58, pp. 270–275, Sofia, Bulgaria (2003) (in Russian)
5. Babichev, D.T.: Geometric descriptor of the tool is the means of estimating the error of gear-machining and modification of surfaces at tooth contact localization. In: Proceedings of the National Technical University "KhPI". "Issues of mechanical drive", vol. 28, pp. 3–13, NTU "KhPI", Kharkov (2011) (in Russian)
6. Babichev, D.T.: Issues of investigation of geometry and kinematics of spatial gearing. Ph.D. in Engineering Thesis, Sverdlovsk, UPI (1971) (in Russian)
7. Babichev, D.T.: Reference tool surface of edge-type tools. In: Proceedings of IFToMM International Conference "Theory and Practice of Gearing". pp. 412–421, Izhevsk (1998) (in Russian)
8. Babichev, D.T., Plotnikov, V.S.: To the development of software complex for computer-aided numerical investigation of gearing. Mechanics of Machines, Issue 45, pp. 36–43, Moscow, Nauka (1974) (in Russian)
9. Babichev, D.T., Storchak, M.G.: Synthesis of cylindrical gears with optimum rolling fatigue strength. In: Production Engineering. Research and Development, vol. 9, N1, pp. 87–97. Springer (2015)
10. Goldfarb, V.I., Tkachev, A.A.: Design of involute spur and helical gears. ISTU Public House, New approach, Izhevsk (2004) (in Russian)

11. Goldfarb, V.I., Trubachev, E.S., Lunin, S.V.: System of hobs unification for gear-wheel cutting of worm-type gears. In: Proceedings of the ASME International Conference IDENC'07, Las-Vegas, USA (2007)
12. Korostelev, L.V.: Kinematic parameters of load-carrying capacity of spatial gearing. J. Izv. Vuzov. Mashinostroeniye **N10**, 5–15 (1964) (in Russian)
13. Lagutin, S.A.: The meshing space and its elements. J. Sov. Mach. Sci. **4**, 69–75 (1987)
14. Litvin, F.L.: Theory of Gearing, 2nd edn. Nauka, Moscow (1968) (in Russian)
15. Litvin, F.L., Fuentes, A.: Gear geometry and applied theory, 2nd edn. Cambridge University Press, 800 p. (2004)
16. Sandler, A.I., Lagutin, S.A., Gudov, E.A.: Theory and practice of manufacturing of general type worm gears. "Infra-Engineering", 346 p., Moscow-Vologda (2016) (in Russian)
17. Sandler, A.I., Lagutin, S.A.: Grinding of helical and relieved surfaces. M. Mashinostroeniye (1991) (in Russian)
18. Segal, M.G.: Types of localized contact of bevel and hypoid gears. J. Sov. Mach. Sci. **N1**, 56–63 (1970). (in Russian)
19. Sheveleva, G.I.: Theory of generation and contact of moving solids. In: Mosstankin, M. (ed.) (1999) (in Russian)
20. Shishkov, V.A.: Surface cutting by generation method. In: Mashgiz, M. (ed.) (1951) (in Russian)
21. System of rating and certification of gear-machining tools. Report of the project headed by Babichev D.T., Tyumen State Oil and Gas University, Tyumen (2012) (in Russian)
22. Trubachev, E.S.: Several issues of tooth generating process by two-parametric families of generating lines. In: Theory and Practice of Gearing and Transmissions: In Honor of Professor Faydor L. Litvin. Mechanisms and Machine Science, vol. 34, pp. 97–116. Springer (2016)
23. Trubachev, E.S., Savelyeva, T.V.: Statement of the task of developing the dimension type of single-thread spiroid hobs. In: Theory and Practice of Gearing. Proceedings of the Scientific Technical Conference with International Participation, Izhevsk, pp. 202–207 (2004) (in Russian)
24. Zalgaller, V.A.: Theory of Envelopes. Nauka, Moscow (1975). (in Russian)

S-gears: From Metal to Polymer Solution

G. Hlebanja and J. Hlebanja

Abstract The paper addresses the gradual development of S-gears from a heavy industry start up to the present state with polymer gears. The curved and half symmetric path of contact implies a concave-convex contact in a vicinity of the meshing start (and end), higher reduced radii of curvature and improved lubrication conditions. Specimens of both gear geometries, which were made of tempered and nitrided alloyed steel, were tested on an FZG testing machine, and results confirmed the theoretical foundations of S-gears. Lastly, the rack profile is defined by a parabolic-type function, which in turn defines the path of contact and finally gears with arbitrary number of teeth. This concept is considered for polymer gears as well. A special testing machine was built to enable testing of small plastic involute (E-) and S-gears. Initial results combining gear pairs made of polyacetal and nylon confirm the theory of S-gears. Improved performance of S-gears, compared to E-gears, is based on the fact that S-gears exhibit a lower amount of sliding.

Keywords S-gears · Curved path of contact · Polymer gears · Sliding

1 Introduction

Involute gears, which transmit power through convex–convex contact, are prevailingly used in contemporary machines. This is due to their gradual development over centuries and improvements in both manufacturing technologies and materials. However, the intrinsic property of the involute gear is its curvature radius function in the dedendum part when approaching the base circle. Values, in general, are small and limited to zero approaching the base circle, therefore implying high

G. Hlebanja (✉)
Faculty of Technologies and Systems, Higher Education Centre, Novo Mesto, Slovenia
e-mail: gorazd.hlebanja@guest.arnes.si

J. Hlebanja
Faculty of Mechanical Engineering, University of Ljubljana, Ljubljana, Slovenia
e-mail: joze.hlebanja@siol.net

V. Goldfarb et al. (eds.), *Advanced Gear Engineering*,
Mechanisms and Machine Science 51, DOI 10.1007/978-3-319-60399-5_12

contact loads in this area. Additionally, for gears with a low number of teeth, the dedendum flank is comparatively very short, thus invoking excessive sliding and friction losses and the possibility of premature damage in this area. Yet another problem is undercutting of the dedendum area. This is why there exists a permanent need for improved gears, with such features as a convex-concave contact, a stronger root, improved curvature radii, better lubrication conditions, etc.

2 Early Development

This paper deals with the gradual development of an S-gear shape, which is an answer to the above-stated requirements. So, the aim was to define tooth flanks of adequate characteristics. This was achieved by the curved path of contact, which implies a concave–convex fit of the meshing gear teeth flanks. The path of contact is a sequence of contact points of the meshing gear pair, which transmits rotation, where each contact point complies with the law of gearing. The path of contact should also warrant sufficiently high contact ratio. The contact load in the kinematic pole C depends on the initial pressure angle α_C. The starting pressure angle α_A is limited due to the contact ratio and contact load. The condition for manufacturing gears of the same module with an arbitrary number of teeth by the same tool profile is the half-symmetrical path of contact.

Gears are designed with regard to their root strength and flank durability. The path of contact shape and the root fillet influence the root thickness, whereas the flank shape essentially influences its durability. The basic factors influencing flank durability are the reduced radius of curvature and amount of sliding. Higher radii imply lower Hertzian pressure. The sliding circumstances are essentially improved in the case of convex-concave contact. The research showed that areas of the path of contact with a higher curvature imply lower sliding and higher reduced radii of curvature. Due to necessity of the stronger oil film in the meshing start zone, the path of contact curvature in that area should be higher and the path of contact takes on a distinctive S-form.

This tooth flank form was used in grooved roller gears for rolling mills. It was successfully installed in the Sisak rolling mill, with variations in other facilities. Gears were helical, $\beta = 28°$, and transmitted 1500 kW at 80 up to 160 rpm. Material was alloy steel 30CrMoV9. The tooth profile is illustrated in Fig. 1. Initially, the involute gearing was installed, suffering severe scuffing in the gear teeth dedendum and addendum areas. S-formed gearing was an essential improvement, operating for several decades, as was also reported in Niemann and Winter [17].

Further research was oriented towards spur gears with the module of about 5 mm, for which the path of contact should be defined in such a way as to ensure smaller flank pressure, better lubrication and less sliding, and which would be linear or almost linear in the vicinity of the kinematic pole C. Figure 2 illustrates such a path of contact and its proportions, with the basic characteristic of gradual increase

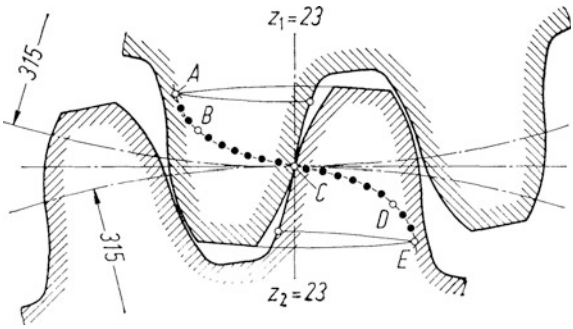

Fig. 1 Industrial implementation for rolling mills [11]

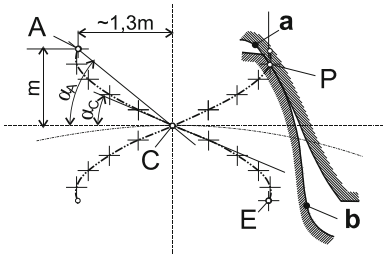

Fig. 2 S-gears defined by the path of contact with a gradual curvature increase

of curvature towards the meshing start and end area and corresponding pinion (a) and gear (b) flanks [13].

Typical characteristics, like reduced flank curvatures, amount of sliding, Hertzian stress curve, contact velocities, oil film thickness and flank temperatures, based on the flash temperature concept, were analyzed for E- and S-gears. It was discovered that all parameters, developed over the path of contact, show relevant improvement in S-gears compared to E-gears [13, 14, 18].

Some experiments on the FZG-machine were carried out. Therefore, E- and S- gears were compared regarding damages that might appear during operation: (a) fracture due to overloading; (b) damage of tooth flanks due to pitting; (c) cold and hot scuffing; and (d) wear of tooth flanks. The gears were made of alloyed steel 42CrMo4, which was heat treated to 28–30 HRC prior to toothing. Experimental lots comprised hardened and tempered gears and hardened, tempered and plasma nitrided gears. The technical data of the gears are collected in Table 1.

The basic indicator with regard to endurance against tooth fracture is the tooth root stress, which depends on the tooth root thickness and fillet radius. The S-gear teeth were stronger by approximately 20% [18] in this particular case.

Experimental results with regard to pitting indicated that the load capacity for hardened and tempered S-gears was slightly increased, whereas for hardened, tempered and plasma nitrided S-gears, the load capacity was higher than that for E-gears [13].

Hardened, tempered and plasma nitrided S- and E-gears have been tested with regard to scuffing on a standardized FZG machine according to the load levels

Table 1 Technical characteristics of the tested gears

Feature	Designation	S-gears		E-gears	
		Pinion	Gear	Pinion	Gear
Module	m [mm]	4.575		4.5	
Number of teeth	z	16	24	16	24
Profile shift	x [mm]	–	–	+0.233	+0.12
Pitch circle diameter	d_w [mm]	73.2	109.8	73.2	109.8
Pressure angle (in kinematic pole)	α_w [mm]	20 or 22		22.438	
Face width	b [mm]	20		20	
Centre distance	a [mm]	91.5		91.5	
Rotational frequency	n [min^{-1}]	2100	1400	2100	1400
Circumferential speed	v_t [m/s]	8.048		8.048	
Gear quality according to DIN 3962					
Pitch deviation	f_p	7–8		7	
Total pitch deviation	F_p	7–8		7	

prescribed by DIN 51354 [3]. Gears were dipped in ISO VG100 oil without additives, with the oil's temperature kept at 90 °C. The time span for the load levels was 15 min. E-gears exhibited scuffing damage on the addendum part of the flanks at the load level 11, whereas in S-gears, no such damage appeared, even at level 12. The oil temperature in the casing during experiments increased due to friction losses of the operating gears. Temperature measurements clearly indicated that the oil was less heated in the case of S-gears due to lower losses. The temperature difference was approximately 10% [13]. With regard to wear, it was discovered that loss of weight in S-gears was approximately half of that in E-gears [13].

The above research was focused on spur gears and later continued with other gear types (helical gears, crossed helical gears, ZS worm drives, internal S-gears for planetary gear trains) in order to explore their usability [15]. Yet another proposal involved cylindrical worm-gearings with a progressively curved shape of teeth flanks, the so-called parabolic worm gear drives [9] and so-called UPT (uniform power transmission) gears [6].

3 S-Gears

The logical idea was then to define the rack profile formally (Eq. 1). Such a rack could be regarded as a cutting tool which can produce gears with an arbitrary number of teeth along a single, curved path of contact:

$$y_P = a_p(1 - (1 - x_P)^n) \tag{1}$$

where y_P defines the upper part of the half symmetric rack profile, with a unit being the module. x_P, y_P are Cartesian coordinates of the rack profile, with the kinematic pole C being the origin. The rack-shaping parameters are the exponent n and the height or form factor a_p. These parameters can be optimized in order to achieve the desired properties of the gear teeth, e.g., thicker root, the size of the convex-concave area, initial pressure angle, curvature of the path of contact, etc., which are, however, always derived from the rack [7, 12]. The third influencing factor, the inclination angle α_{p0} or the succeeding initial pressure angle α_{w0}, can be calculated from the first derivative of y_P in C and is used to form the rack profile (and consequently the gear tooth profile) instead of n or a_p. The way in which the rack profile defines the path of contact and a pinion and a gear flank derive from the path of contact is shown in Fig. 3.

Figure 4 illustrates half-symmetric S-rack profiles with various initial pressure angles α_w and form factors a_p, namely $\alpha_w = 12°$, 18° and 22°. The contact ratios ε of the corresponding paths of contact are $\varepsilon = 1.51$, 1.24, and 1.05. Pinions having 20 teeth each are also presented in Fig. 3. One can observe that the active length of

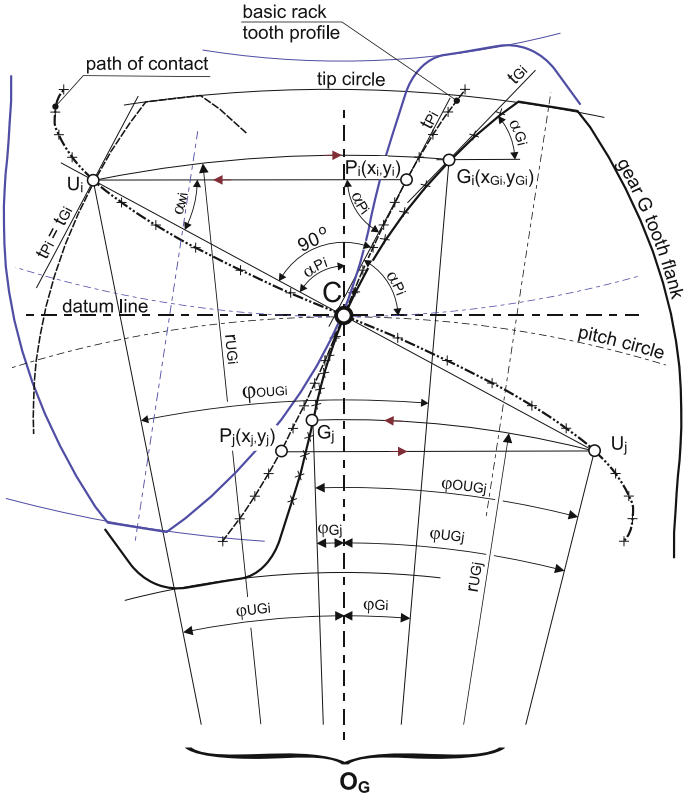

Fig. 3 Development of the S-gear tooth flank from the basic rack profile [12]

the dedendum becomes shorter for lower pressure angles while the contact ratio increases at the same time. The pressure angle is of particular importance, since it influences the flank load, the load capacity, the curvature radii, and the contact ratio.

The lowering of the form factor a_p increases the curvature of the rack profile. Lower values of n induce a thinner root, which becomes thicker for higher values. On the other hand, higher values also induce a sharper tooth tip [16].

3.1 Some Features

Important features of the S-gears include:

- radii of curvature and flank pressure,
- velocity circumstances and oil film thickness and
- rolling and sliding ratio.

An intrinsic feature of S-gears is that their tooth flanks become concave in the dedendum flank. The concave area is short for gears with a low number of teeth and extends to the vicinity of the kinematic pole for a high number of teeth. Regardless of the number of teeth, this assures convex-concave contact in the meshing start and end areas. Therefore, the contact circumstances in this critical area are improved. One can agree that concave-convex contact and the curved path of contact imply higher reduced radii of curvature, which then imply lower Hertzian pressure [12].

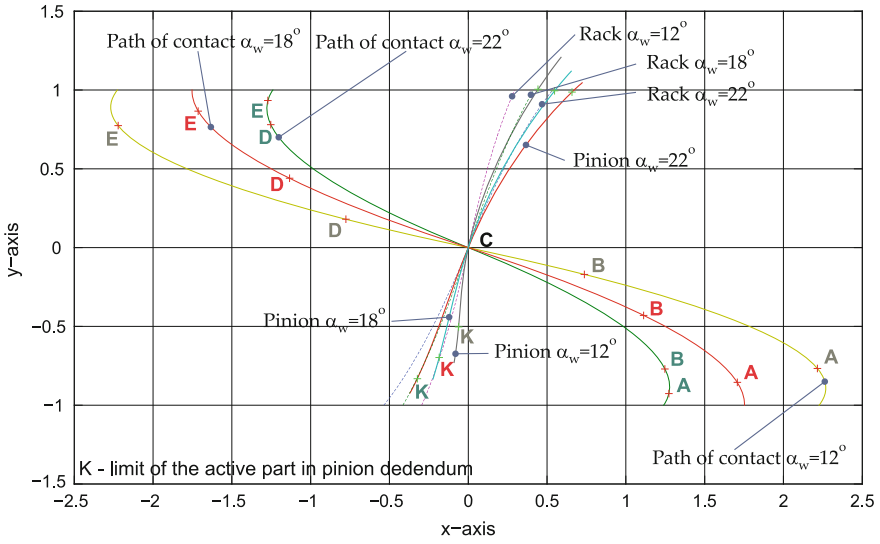

Fig. 4 Rack profiles, paths of contact and pinions for various pressure angles ($\alpha_w = 12°$, $\alpha_w = 18°$, $\alpha_w = 22°$)

Velocity circumstances in the gear tooth contact, appearing along the path of contact, decisively influence oil film thickness and depend on the tooth flank geometry. Absolute velocities, relative velocities of the teeth flanks, and the contact point movement velocity in the direction tangential to the path of contact can be distinguished with regard to the direction tangential to the teeth flanks at the contact point.

Figure 5 illustrates a situation in the vicinity of the meshing start area. The absolute velocities of the gear tooth flank and the pinion are represented by the vectors $\boldsymbol{v_S}$ and $\boldsymbol{v_P}$, respectively. The relative velocities $\boldsymbol{v_{rS}}$ and $\boldsymbol{v_{rP}}$ act tangentially to the corresponding teeth flanks, whereas $\boldsymbol{v_{At}}$ is the velocity of the contact point in the direction of a tangent to the path of contact. Thus, expressions for $\boldsymbol{v_S}$ and $\boldsymbol{v_P}$ are

$$\vec{v}_S = \vec{\omega}_S \times \vec{r}_S \text{ and } \vec{v}_P = \vec{\omega}_P \times \vec{r}_P \tag{2}$$

The velocity components in the direction of teeth flank surfaces influence oil film formation; the corresponding velocities of the pinion $\boldsymbol{v_{rS}}$ and the gear $\boldsymbol{v_{rP}}$ are

$$\vec{v}_{rS} = \vec{v}_S - \vec{v}_{At} \text{ and } \vec{v}_{rP} = \vec{v}_P - \vec{v}_{At} \tag{3}$$

The sliding velocity $\boldsymbol{v_g}$ is defined as the difference of the absolute velocities of teeth flanks at the contact point or as the difference of the relative velocities:

$$\vec{v}_g = \vec{v}_S - \vec{v}_P = \vec{v}_{rS} - \vec{v}_{rP} \tag{4}$$

The prevailing factors conserving the oil film thickness are the dynamic viscosity (oil property) and the sum of relative velocities, which are higher in the vicinities of the meshing start and meshing end points, due to the curved path of contact. Material properties (elasticity), geometry and load have a lower influence on the oil

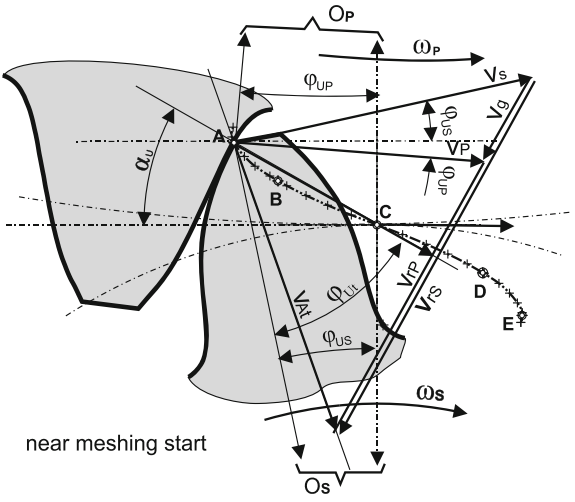

Fig. 5 Velocity circumstances for S-gears in the meshing start area [7]

film. Therefore, it should be noted that the curved path of contact induces a system velocity (tangential to the path of contact) and relative velocities tangential to the current contact. Since the latter are high, they positively influence the oil film thickness [7].

Figure 6 illustrates the contact density of the driving dedendum s_1 with simultaneous contact points designated by $G'_{1/i}$, and those of the driven addendum s_2 designated by $G_{2/i}$. One can observe that the dedendum part is shorter, which depends on the number of teeth—the smaller the number of teeth, the shorter the length of the dedendum. The initial pressure angle in C influences the size of the dedendum as well—higher pressure angles impose longer dedendum lengths (Fig. 4). Accordingly, the addendum part is longer, which indicates that the driving dedendum contact point density is higher than in the driven gear addendum.

The density difference therefore indicates the amount of sliding of the partner with the longer intermediary path that has the lesser density. So, if we designate the path on the dedendum partner with s_{1i} and the path on the addendum flank with s_{2i}, we can formally write

$$\Delta s_i = s_{2i} - s_{1i} \tag{5}$$

The smaller of the two, s_{1i} or s_{2i}, gives us the value for pure rolling and the difference Δs_i gives us the value of sliding. The situation is reversed for the upper side, above C.

The most important features of S-gears compared to E-gears with regard to usage with plastic materials are:

- lower sliding due to relatively large contact lengths of gear pair dedendums and consequently lower friction and contact temperature,
- convex-concave contact zones in the vicinity of the meshing start and meshing end and higher reduced radii of curvature.

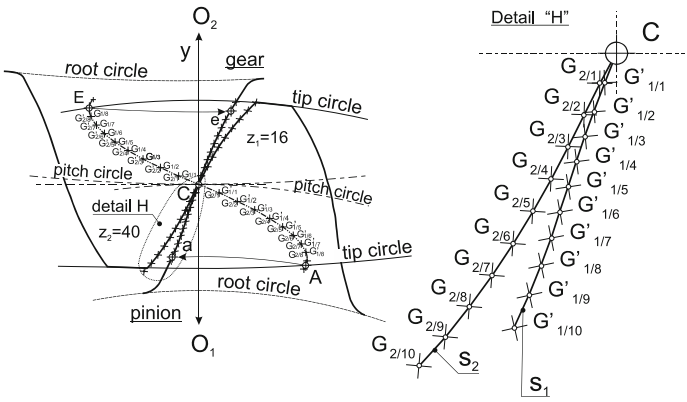

Fig. 6 Contact density

4 S-gears Made of Polymers

Gears made of polymers are in daily use in high-tech appliances, in part due to their qualities of low maintenance, wear resistance, low noise, vibration dampening, immunity from corrosion, low inertia, light weight, and low manufacturing cost in mass production. Their deficiencies, such as lower load, accuracy of molded gears, dimensional problems due to thermal expansion, sensitivity to temperatures, etc., do not represent obstacles in the use of plastic gears. Extensive research has delivered new and improved materials, with better thermal and load characteristics. On the other hand, superb lifetime behavior of gear trains for high-tech devices made of polymers is expected.

4.1 Experimental Gear Shape and Materials

As already stated, S-gears have some outstanding characteristics, so there is interest in their use in a polymeric version. However, such gears should be experimentally proven. The most straightforward way is to test their durability and compare E- and S-gears. The first test gears were molded, and basic parameters were $m = 1.0$ mm, $z_1 = z_2 = 20$, and $b = 6.0$ mm. The selected material combination was:

- polyoxymethylene (acetal) (POM-C) and
- polyamide (nylon) (PA6, PA66).

This material combination is quite common for plastic gears, due to its good dynamic friction coefficient and price criterion. Both materials can be used in precision engineering, the automotive industry, electrical engineering, etc. And both materials are distinguished by their slide and wear properties, strength, toughness, etc. POM-C is also characterized by good machinability, whereas PA66 is challenging in this context. Both materials have a long-term service temperature of around 100 °C. Detailed technical characteristics can be found in the corresponding data sheets [4, 5].

It was discovered that the center distance, 20 mm, of S-gears was deviating by about +0.1 up to 0.2 mm, which means up to 20% of the module size. It has already been agreed that S-gears can mate even with disrupted axis distance [8], but the efficiency of such action has not yet been defined precisely. And the same molding tool was used for both materials. As a result, the Wöhler curves did not show a sufficient and accurate distinction between the two gear types. This implies that the design of molds should be carried out with consideration of the actual shrinkage of particular materials, which is not an easy task. Another consideration is that the quality of molded gears is rather low and we need to consider how it influences the precise flank geometry, particularly in the case of S-gears.

Considering past experience, it was decided that new gears should be cut and better quality and shape conformity for both, S- and E-gears should be assured.

Fig. 7 Involute (*above*) and S-gears (*below*) made of PA66 (*left*) and POM-C (*right*)

So, the decision was made to use the same size gears, that is, $m = 1.0$ mm, $z_1 = z_2 = 20$, $b = 6.0$ mm. For the initial pressure angle of the S-gears, $\alpha_{w0} = 18°$ was chosen. Figure 7 shows the cut gears, one made of POM-C (the driving gear) and one of PA66 (the driven gear).

4.2 Gear Measurements

Shrinkage is inherent in the injection molding process. Despite databases and shrinkage models for various materials and process parameters, it is difficult to propose the correct values for a particular product and situation, e.g., injection molded gears.

This is why a coordinate measuring machine (CMM) for gears should be used to measure the gears produced and compare them to the theoretical shape. Deviations make necessary corrections of the mold possible, achieving far greater accuracy in the final product.

LH54 Gear (Wenzel GearTec) with 4th axis rotary table, designed for measuring all types of gears (gear, shaft, worms, etc.) according to different standards for gear teeth quality, was used during our work. This machine with Metrosoft CM software is also used for measurement of basic geometric elements and free form surfaces (based on the CAD model). With a scanning 3D probe, a large number of measured points can be achieved. The machine has an active damping system and a good thermal stability through the use of dark granite for a base and axes air bearings to

meet special requirements of high precision measurements. The machine is improved to cover additional gear tooth flank shapes, e.g., S-gears.

Since the quality of molded gears is rather low and it influences the precise flank geometry, particularly in the case of S-gears, milled gears of the same materials were produced. Table 2 collects quality grades for molded and milled E-gears, which clearly show the difference for app. 2 grades in favor of milled gears. S-gears exhibited similar values; however, they cannot be compared directly due to different forming parameters. Milling is also of interest for production of gears in which the expense of the molding tool cannot be justified.

4.3 Testing Machine

Temperature behavior of mating, loaded gears is yet another important phenomenon to be observed, since temperature increase directly influences gear durability. There is a contact temperature model at disposal for the involute gears. VDI 2736, Blatt 2 [19] has brought a new proposal for a temperature model for E-gears. Definitively, this equation cannot deal with S-gears. So, experimental work is necessary in this context as well.

A testing machine was designed and built in LECAD, University of Ljubljana, for experiments with small polymeric gears [10]. The layout of the machine is simple and robust and consists of a framework on which two asynchronous electro-motors are mounted. On the motor rear side, there are two fans to remove redundant heat. Two small gears are mounted in such a way to adapt center

Table 2 Quality grades of molded and milled E-gears according to DIN 3961/62 [1, 2]

Inspected parameter		Milled		Molded	
		Left	Right	Left	Right
Total profile deviation	F_α	12	10	12	11
Profile form deviation	$f_{f\alpha}$	5	7	10	10
Angular profile deviation	$f_{H\alpha}$	12	11	12	12
Total lead deviation	F_β	6	7	9	10
Lead form deviation	$f_{f\beta}$	6	5	8	8
Angular lead deviation	$f_{H\beta}$	6	8	10	11
Pitch deviation	f_p	8	8	10	11
Composite pitch deviation	F_p	8	9	10	10
Runout deviation	F_r	10		10	

distance. Power transmission from the motors to the shafts is by belts. Each motor speed is governed by a frequency inverter. So, load is implemented by a speed difference. It is important to have the possibility of measuring contact temperature by a fast thermal camera, so the machine was designed in such a way to enable a frontal view (Fig. 8).

Comparative lifetime experiments with S- and E-gears made of PA66 and POM-C produced by milling started earlier this year. First results are collected in self-describing Wöhler curves (Fig. 9) [20]. Temperature measurements are in accordance with lifetime experiments. Experiments with higher torque, e.g., 1.6 Nm, were rather short, so full temperature recording was made available and revealed that gears collapsed above 90 °C.

Tests were designed to deliver Wöhler curves for each material and geometry combination. So, they were conducted for various loads, ranging from 1.0 Nm up to 1.6 Nm, incrementing by 0.1 Nm. The rotational frequencies ranged from 1392 rpm at 1.0 Nm and slightly decreasing down to 1273 rpm at 1.6 Nm. The temperatures at the contact spot were observed for the first 20 min in all

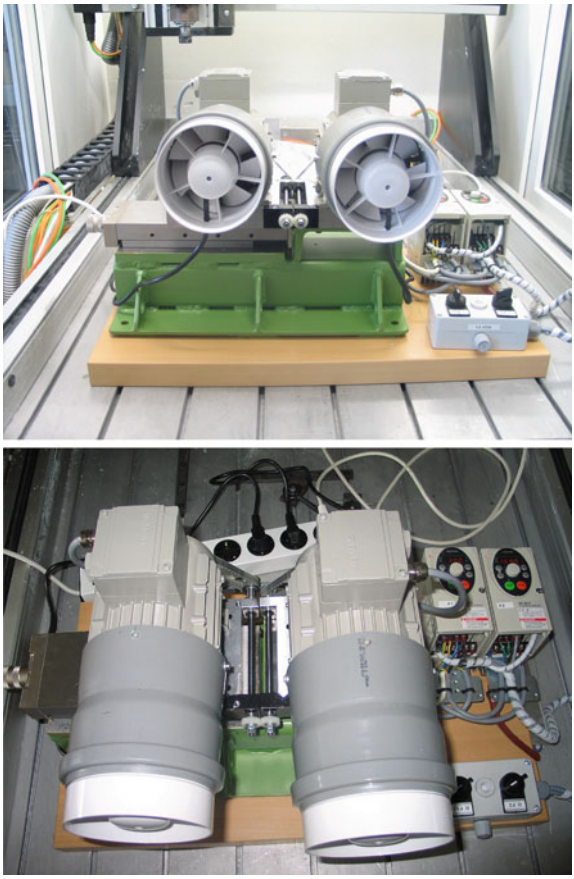

Fig. 8 Testing machine for small gears

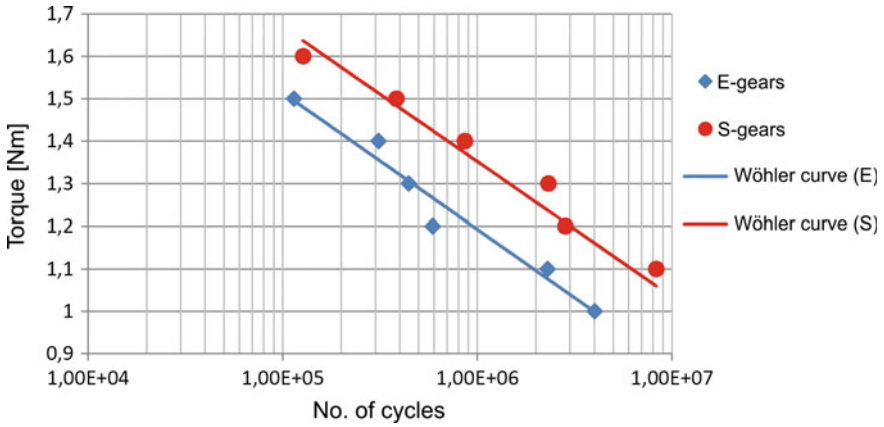

Fig. 9 Wöhler curves for milled E- and S-gears [20]

measurements. General observations are that the temperature increased from 20 °C to a working level that was in correlation with a load level. The temperatures of E-gears were higher than those of S-gears for about 15 K in all cases. Figure 10 shows the temperature development for the E- and S-gear experiment at the load level 1.5 Nm at 1298 min^{-1} from the experiment start to the gear damage, which appeared at app. 90 °C.

These encouraging results led to the production of several testing machines, already described. The plan is to generate a statistically relevant number of experiments. However, gears should be manufactured, actually milled, which takes some time. The Koepfer gear-hobbing machine with professional cutting tools, which have been produced for both gear geometries, is used for testing gear production.

5 Conclusions

The S-gear tooth flank profile was first successfully implemented in a heavy duty industry about 50 years ago. The curved path of contact implied a convex-concave contact (near meshing start and end), lower reduced radii of curvature and thicker oil film. That is why some experiments with gears with the module m = 4.5 mm (4.575 mm for S-gears) have been conducted on the FZG machine. Specimens were made of a hardened, tempered (and nitrided) alloyed steel. Results with regard to pitting, scuffing, wear, and oil temperature (inducing losses) favored S-gears.

Finally, the S-rack profile was defined by a parabolic-type function. The rack then defines the path of contact, and subsequently the gears. The defining parameters should be carefully chosen in order to assure design requirements. In this way, one could design gears with increased root thickness, gears with a low initial pressure angle, etc.

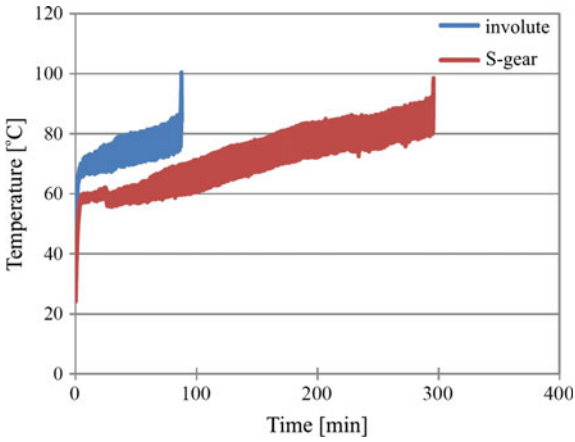

Fig. 10 Temperature development from the start to the collapse (T = 1,5 Nm, n = 1298 min^{-1}) [20]

The S-gear tooth flank profile features a concave shape in the lower part of the dedendum so that the mating gears exhibit the convex-concave contact in the vicinity of the contact start and contact end. The S-gear tooth flank shape also assures higher comparative reduced curvature radii. Therefore, the contact load is lower. The relative velocities in the contact surface are higher due to the curved path of contact, which implies better lubrication, a factor of particular importance with metallic gears. Due to their S-shape, the velocity characteristics of mating gears are improved, especially in both external areas with high relative velocities and comparatively low sliding velocity. This concept was also used in the development and testing of polymeric S-gears.

The most important features of polymeric S-gears are lower sliding due to relatively larger contact lengths of dedendum-addendum of a gear pair (and consequently lower friction and contact temperature), convex-concave contact zones in the vicinity of meshing start and meshing end, and higher reduced radii of curvature, particularly in the meshing start and end zones.

It has also been proven that the S-gears mate even with changes in the axis distance. So, they are not sensitive in the context of cycloidal gears. However, the true impact of the variation in axis distance in the context of efficiency still has to be assessed. Recent experimental work with milled gears has shown that the lead form deviation had a greater impact on S-gear performance.

Experimental work with regard to S-gears made of POM, PA66 and other polymeric and composite materials, milled or molded, has just begun. First results of the lifetime experiments proved the theoretical considerations, indicating that, in fact, S-gears develop lower temperatures than E-gears due to their lower sliding, corresponding lower friction, and lesser developed heat. However, a sufficient number of tests should be conducted to confirm the initial results. Several testing machines are at our disposal now. And after initial problems with cutting technology and improved choice of gear materials, we can expect more relevant results in the near future.

Acknowledgements The authors wish to express their gratitude to Podkrižnik d.o.o., Nazarje, Slovenia, for their exceptional support of the experimental work, and LECAD; University of Ljubljana, Slovenia, for conducting the experiments.

References

1. DIN 3961: Toleranzen für Stirnradverzahnungen; Grundlagen, Beuth Verlag (1978)
2. DIN 3962-1: Toleranzen für Stirnradverzahnungen; Toleranzen für Abweichungen einzelner Bestimmungsgrößen, Beuth Verlag (1978)
3. DIN 51354: Prüfung von Schmierstoffen; FZG-Zahnrad-Verspannungs-Prüfmaschine; Allge-meine Arbeitsgrundlagen, Beuth Verlag (1990)
4. Ensinger: TECAFORM AH Natural—Stock Shapes, Technical Data Sheet, Ensinger (2014)
5. Ensinger: TECAMID 66 natural—Stock Shapes, Technical Data Sheet, Ensinger (2014)
6. Hlebanja, G., Hlebanja, J.: Uniform power transmission gears. J. Mech. Eng. **55**(7/8), 472–483 (2009)
7. Hlebanja, G.: Specially shaped spur gears: a step towards use in miniature mechatronic applications. Balkan J. Mech. Transm. **1**(2), 25–31 (2011)
8. Hlebanja, G., Hlebanja, J.: Influence of axis distance variation on rotation transmission in S-gears: example on heavy duty gears. In: International Conference on Gears, Oct 2013, Garching: Europe invites the world (VDI-Berichte, ISSN 0083-5560, 2199). pp. 669–679. VDI-Verlag, Düsseldorf (2013)
9. Hlebanja, G., Hlebanja, J., Čarman, M.: Cylindrical wormgearings with progressively curved shape of teeth flanks. J. Mech. Eng. **55**(1), 5–14 (2009)
10. Hlebanja, G., Kulovec, S., Hlebanja, J., Duhovnik, J.: S-gears made of polymers. Ventil. **20**(5), 358–367 (2014). ISSN 1318-7279
11. Hlebanja, J.: Konkav-konvexe Verzahnung Ermitlung der Zahnflanken und einige Grenzfälle. Antriebstechnik Jg. **15**(6), 324–329 (1976)
12. Hlebanja, J., Hlebanja, G.: Spur gears with a curved path of contact for small gearing dimensions. International Conference on Gears, Garching near Munich, Germany, Oct 2010: Europe invites the world, (VDI-Berichte 2108). pp. 1281–1294. VDI-Verlag, Düsseldorf (2010)
13. Hlebanja, J., Okorn, I.: Charakteristische Eigenschaften von Zahnrädern mit stetig gekrümmter Eingriffslinie. Antriebstechnik Jg. **38**(12), 55–58 (1999)
14. Hlebanja, J., Okorn, I.: Investigation of tooth surface-durability of non-involute spur gears. In: International Conference on Gears: Tagung Dresden, 22–24 Apr 1996, VDI Berichte, Düsseldorf, pp. 443–450 (1996). ISSN 0083-5560, 1230
15. Hlebanja, J., Hlebanja, G.: Anwendbarkeit der S-Verzahnung im Getriebebau: Nichtevolventische Verzahnungen weiterentwickelt. Antriebstechnik Jg. **44**(2), 34–38 (2005)
16. Kulovec, S., Duhovnik, J.: Variation of S-gear shape and the influence of the main parameters. In: International Conference on Gears, Oct. 2013, Garching near Munich, Germany: Europe invites the world, (VDIBerichte 2199). pp. 1535–1541. VDI-Verlag, Düsseldorf (2013)
17. Niemann, G., Winter, H.: Maschinenelemente, Band II, 2. Erw, Auflage, Springer (1989)
18. Okorn, I.: Research of tooth flank durability of gears with progressively curved path of contact—Ph.D. Thesis (in Slovene). University of Ljubljana (2000)
19. VDI 2736, Blatt 2: Thermoplastische Zahnräder, Stirnradgetriebe, Tragfähigkeitsberechnung, VDI Richtlinien, VDI, Düsseldorf (2013)
20. Zorko, D., Duhovnik, J.: Testing of polymeric involute and S-gears. Intermediate report (in Slovene). LECAD, Faculty of Mechanical Engineering, University Ljubljana (2016)

Aspects of Teaching "Advanced Gears" for Future Mechanical Engineers Within "Bachelor of Sciences" Programs at Technical Universities

V. Goldfarb, E. Krylov, O. Perminova, N. Barmina and L. Vasiliev

Abstract Innovative development of important mechanical engineering industries necessitates very high demands on graduates of engineering universities who plan to devote their professional activity to gears, specifically: their qualification by the time of graduation, their knowledge, abilities and skills in regard to innovation, and their communication abilities. The present paper analyzes the recent trends and fundamental aspects of higher education in Russia with regard to the successful training of gear experts at a technical university within the Bachelor program. Issues related to the teaching of various courses involving gears within the curricula of mechanical engineers and obtainment of a BS are also considered in the paper. Attention is paid to foreign language (English) competences for future gear experts. Agreement on the valid syllabi for mechanical engineers and requirements specified for graduates by the present manufacturing industry is studied through the example of one of the most sought-after majors in the field of mechanical engineering.

Keywords Gears · Innovation development of production · Teaching gears in technical universities

1 Introduction

As is known, gears find wide application in all engineering spheres, in many cases defining the important technical and economic parameters of corresponding machines and devices. Though gears represent a traditional type of mechanism (cases of the application of gears in the 2nd century BC are known), nevertheless, they have been continuously upgraded [2, 11]. Development of gears and methods

V. Goldfarb · E. Krylov · O. Perminova · N. Barmina (✉)
Izhevsk State Technical University, Izhevsk, Russia
e-mail: barmina-nat@mail.ru

L. Vasiliev
Saint Petersburg University, St. Petersburg, Russia
e-mail: l.vasilyev@gsom.pu.ru

V. Goldfarb et al. (eds.), *Advanced Gear Engineering*,
Mechanisms and Machine Science 51, DOI 10.1007/978-3-319-60399-5_13

for their design, simulation and production in the 20th century and further into the 21st century was strongly affected by the introduction of computers.

In accordance with various estimations, the world market for production and consumption of gears increases annually by 4–6%. This explains the interest in gears of scientists, designers, manufacturers and consumers of these products, and also of economists who study the trends in different spheres of production for the purpose of economic forecasts on their development and reasonable planning.

The four most significant markets for gears include the car industry, general-purpose mechanical engineering (including machine-tool engineering, lifting and handling engineering, etc.), the aerospace industry and ship-building.

The largest gear manufacturers in the world are the USA, Japan, Germany, Italy, France and others.

Along with the car industry (representing about 80% of all gear consumption), one of the most significant markets for gears is valve engineering as a part of general-purpose mechanical engineering. In the last 20 years, successful developments have been made in Russia in the field of investigation, production and operation of new drives for pipeline valves that are highly competent with traditional world analogs.

Prospects for further wide application of gears are related to the increase in their load-carrying capacity with simultaneous reductions in mass and overall dimension and cost parameters.

Therefore, innovative development of important mechanical engineering industries necessitates very high demands on graduates of engineering universities who plan to devote their professional activity to gears, specifically: their qualification by the time of graduation, their knowledge, abilities and skills in the field of innovation, and also their communication abilities.

Nowadays, gear experts are required to continuously upgrade the drive equipment, and develop new mechanisms on the basis of already existing gears while accounting for the rapid appearance of new methods for design, analysis, production and testing of gears.

At the present time, there is an obvious contradiction between the necessity to increase the efficiency of an innovative manufacturing system, insufficient rates of reformation of the educational system and low-performing levels of professional competences of engineering experts, a clear indication of the urgent need for development of innovative mechanisms for formation of professional competences as applied to the requirements for training an expert engineer.

Recent trends and fundamental aspects of development of higher education in Russia with regard to the successful training of gear experts at a technical university within the bachelor program are further studied in this paper. Issues related to the teaching of various courses involving gears within the training of mechanical engineers and obtainment of a BS are also considered. Agreement on the valid syllabi for mechanical engineers and requirements specified for graduates by the present manufacturing industry is studied through the example of one of the most popular majors in the field of mechanical engineering—“Design and manufacturing

preparation of mechanical engineering production" (DMPMEP) at the Federal State Budget Education Institution of Higher Education "Kalashnikov Izhevsk State Technical University" (Kalashnikov ISTU).

2 Recent Trends and Fundamental Aspects of Higher Education in Russia with Regard to Training Gear Experts at a Technical University Within the Bachelor Program

Changes in the educational system related to the formation of scientific and educational complexes, the extension of paid educational services, and the integration of education and industry are forcing us to reconsider approaches to higher professional education. Let us further consider some statistical data related to higher educational institutions and the number of enrolled students. At present, there are 950 institutions of higher education (IHE) in the territory of the Russian Federation, more than 60% of which have obtained state status. Table 1 shows that the number of IHE has not grown recently.

The recent trends require the development of an educational infrastructure to react flexibly to the changes in the present production specifications. Particular requirements are specified for students of the "Design and manufacturing preparation of mechanical engineering production" major, since this is the exact scope that is subject to extremely rapid innovations in the field of gears. Peculiarities in the efficient progressive development of mechanical engineering production require the creation of a systematic interaction between employers and students in order to result in the accumulation and application of new knowledge and improvement of the process of formation of professional competences.

Orientation of education to the individual professional developments within the system of training and retraining of gear experts for our regional industry illuminates the problem of creating the conditions for activation of self-knowledge, self-development of students and experts, and alteration of their attitude towards their own achievements in the field of professional activity.

The traditional system of professional training of students of the "Design and manufacturing preparation of mechanical engineering production" major is

Table 1 Dynamics of the number of IHE and their students

Indicators	2005	2010	2015
Number of IHE	1071	980	950
Number of state IHE among them	662	578	548
Number of students (in thousands)	6884	5647	5209
Student enrollment (in thousands)	1743	1399	1192
Numbers of graduates (in thousands)	1012	1468	1226

characterized by excessive differentiation, insufficient mobility and variability, doubling of the contents at different stages of education and orientation towards studying specific (sometimes out of date) techniques. Modernization of the professional training of gear experts actualizes the innovative educational process's ability to excel with regard to integration of the subjects and harmonization of their interests. Trends towards training reformation directed at integrating subjects of educational, manufacturing and innovation processes imply the following activities:

- Correction of educational programs (development of the range of additional programs of different education levels and profiles, introduction of elements of multi-profiles and variative training).
- Development of strategic partnership (improvement of practical education, formation of social control, enlargement of the number of strategic partners, provision of homogeneity in manufacturing support).
- Control of education quality (introduction of innovative educational techniques, adoption of international standards of training and development of a system of quality control, quality auditing, organization of new majors in training mechanical engineers, special training of the teaching staff).
- Development of individual trajectories of training mechanical engineers (development of techniques for personal enhancement, formation of models of expert competences and professional and psychological features of the personality, optimization of training terms, mobility and differentiation of training).

Development of the successive professional training of mechanical engineers for the "Design and manufacturing preparation of mechanical engineering production" major implies structural reorganization of the whole educational process, beginning from secondary school and continuing on into professional educational institutions with organizations of scientific research and production engineering activities. The result of implementing the system of enhanced professional training will be an alignment of the training quality with the requirements of the innovative industrial production complex.

As applied to the Udmurt Republic of the Russian Federation, the program of development for training engineering personnel in the field of gears is first related to implementation of the program of development of mechanical engineering and the metal machining industries. Dynamics of characteristics for activity of the industrial enterprises of the Udmurt Republic are determined by the growth of the industrial production index due to the growth in production volumes of such enterprises as "Votkinsky zavod" OJSC, "Izhevsky motozavod Aksion holding" OJSC, "Elecond" OJSC, "IEMZ "Kupol" OJSC, and "Reduktor" OJSC. The rate of growth of the shipped products within the mechanical engineering industry for the last year was 109.5%, and the cost of the shipped products of their own production exceeded 350 billion rubles. The Udmurt industrial enterprises have developed programs of professional improvement for themselves. In 2016, "Sarapulsky radiozavod" OJSC organized various types of education for its 2600+ employees and "ChMZ" OJSC involved about 3600 of its employees. It cost about 8 million

rubles to train the personnel of "ChMZ" OJSC. Another enterprise, "Concern Kalashnikov" OJSC, paid great attention to education, and now has its own educational production center, while for the higher professional education, it created strong links with Kalashnikov ISTU [12].

Meeting the requirements for innovative development of the industrial sector of the Udmurt Republic in regard to the professional training of gear experts accounting for enhanced education demands the creation of a principally new educational process for training mechanical engineers. The special terms of this education are: provision of integration of education, science and production, innovative character of content in the training and educational process, competence of the teaching staff and readiness of the students. The personality of a student and his/her potential are the determining factors in the enhanced training, since his/her interest in constant self-improvement in regard to professional activity makes it possible to create the process of efficient generation and the development of competences.

Analysis of availability of gear experts for enterprises has shown that the main problem is in disagreement on the specifications required by employers in regard to the level of professional training of experts and the ability of the educational system to meet these specifications. The specific character of mechanical engineering and its innovative development necessitates agreement as to the contents and techniques of education designed to fit the demands of production and the character of innovations, and consideration of the globalization processes and world achievements. Therefore, generation of professional competences for future gear experts requires introduction of new, activity-oriented educational techniques to be implemented within the integration of education, science and production.

In spite of the variety of investigations dedicated to the problem of the professional training of mechanical engineers, little attention is paid to the development of conceptual fundamentals of the educational process when training gear experts, due to the specifics. There are no investigations revealing the interaction of factors in the professional growth of the expert, reflecting both professional needs and preferences and trends in the development of mechanical engineering. In this regard, determination of the aspects of forming professional competences for mechanical engineers with regard to the enhanced training is very urgent.

The innovative educational complex of the DMPMEP department implies the process of development of student competences with regard to their individual features. It allows for flexible reactions to individual changes in the professional competences of the student, and gives him/her a right to choose his/her own professional educational trajectory, thus providing for a continuously enhanced training of engineers for the gear industry. In order to obtain the qualitative professional competences, it is necessary to provide certain conditions of formation of a future gear expert, one of them being the individual trajectory of accumulation of professional competences.

Analysis of publications has shown that there are several approaches to the aspect of formation of an individual educational trajectory. The most developed approach is the pedagogical one, which interprets individual educational trajectories

as a definite sequence of elements within the educational activity. The basis for studying the individual trajectory of the student is the model of directions of achieving the educational standard, when the choice of how to implement the standard depends on the individual features of each student.

The innovative approach to training gear experts implies the development of content in accordance with the professional functions of the employee, problems to be solved and the competence necessary to solve them; for this purpose, the structurization of description components into educational programs is carried out with regard to inter-disciplinary links. Differentiation of educational levels within the multi-level system is based on the development of the various levels of competence achieved by the student. Techniques for the development of competences implement the conditions for establishing the competence experience: consideration of cognitive problems within a professional situation; variability of educational routes allowing creative abilities and individuality to be revealed; increase in the role of individual styles, approaches, and personal systems of the cognitive and practical professional activity of students when passing from one education level to the next.

The infrastructure component of studying the educational trajectory is widely represented in works on models of continuous education, since the idea of continuous education is not a mechanical motion from pre-school to the post-graduate education; it represents a harmonic process of cyclic renewal of the personality at each stage. One can consider here the experience of technopolises, business-incubators and technoparks as the most successful types of integration of science and production within a system of continuous education and training experts for innovative production. Taking into account that, based solely on the optimal combination of three components (educational, scientific and production) within the educational process, one can train a many-sided expert, the development of a principally new, distributed educational scientific production environment for steering experts in the prioritized directions of science and engineering based on innovative techniques of education and deep integration of the scientific, educational and production processes is possible only within innovative educational university complexes [1].

Therefore, when creating the trajectory for training the expert within innovation economics, it is necessary to assess the individual level of development of professional competences of the future mechanical engineer and to choose the proper educational vector. In general, the process of training a gear expert can be presented as stages in a life cycle, in accordance with the model of cycles for intellectual activity characterizing the accumulation of intellectual capital based on obtainment of information and fresh knowledge and the subsequent comprehension of techniques, links and principles.

In the most general case, the life cycle of training a mechanical engineer can be represented as the consequent increment of professional competence through stages of origin, formation, growth, stabilization and recession over the entirety of their time employed within the industry. The stage of origin is characterized by professional self-determination and choice of direction of activity or education. During

this period, a person can change across several types of activity or educational institutions in order to choose a more suitable course that allows for self-determination in the range of future works. After determination of the area of professional activity, the subsequent stage of formation involves mastery of profession and acquisition of basic necessary professional competences. An expert achieves a certain level of professional competences, which is determined with regard to the developed indices based on individual assessment of the employee. With regard to the individual abilities of the expert, different versions of passing through stages to achieve a certain level are possible. The following stage is characterized by the growth of qualification, accumulation of experience, and both acquisition of new and consolidation of previously acquired knowledge and skills. A certain limit for improving the skills at a definite level is reached, thus leading to uniform stable work characterized by the stabilization stage. In the case of an absence of positive assessment results for improving the professional level, the regression period occurs, characterized by a freeing of the expert [16].

The process of the consequent passing of different stages of the life cycle implies an assessment of the employees to reveal the potential for development of their professional competences. At the stage of formation of the mechanical engineer at each level, the performed assessment allows for determining the level of starting potential; and in a case of possibility for its increment, it is reasonable to continue the formation process on the next level up. Otherwise, an engineer is passing to the next stage purely by consequence. Similar processes are considered at stages of growth and stabilization and, in the case of the potentials being revealed, passage to the stage of formation of an employee of the next higher level takes place. If the assessment does not give a positive result, the consequent transition to the next stage of the life cycle takes place. At the stage of origin, we deal with the professional self-determination of the future mechanical engineer and the primary study of the specific character of gears. At this stage, the enterprise needs to unmask the presence of the professional affection of pretenders and to choose possible candidates for training. During the formation process, the choice of the most suitable candidates takes place on the basis of assessment. Adaptation and accumulation of experience at the stage of growth gradually lead to stable work; the performed assessment will allow for revealing the potential possibilities of making decisions about promotions and the circulation of employees. The proposed approach of considering the employee within the stages of the life cycle implies determination of possible professional levels and the development of requirements for each level with respect to the stages of the lifecycle within the model of professional competences.

For each stage of accumulation and formation of professional competences of the mechanical engineer, it is necessary to make up a list of courses of fundamental, humanitarian, practical and profile (special) cycles. At different stages, the education should involve both basic chapters of these courses and specially developed "advanced" chapters of the educational process. In certain cases, special educational modules consisting of several inter-related courses are developed. The practical

cycle should be related to the real design of gears, and it should encourage the development of business, designing and manufacturing activity. When investigating the issue of the formation of professional competences within the study of basic skills at the university, the activity that will further turn into production creativity, possibility and a desire to develop innovative production must be determined.

3 Studying "Advanced Gears" Within MMS and Machine Design Courses for Future Mechanical Engineers

Let us consider the content of courses that include the study of gear through the example of one of the most sought-after majors at Kalashnikov ISTU related to the training of mechanical engineers. This major within the Bachelor program is called "Design and manufacturing preparation of mechanical engineering production" (DMPMEP). The professional activity of the graduates of this major is often related to the design and manufacture of various gears and gear mechanisms.

The typical structure of the **Theory of machines and mechanisms (TMM)** course, as a rule, includes two parts related to the design of gear mechanisms: the geometric synthesis of toothed gearing, and analysis and synthesis of gear trains. Gear train force analysis is included in the investigation of dynamics of a whole mechanism made by Assur groups. Some University course syllabi contain the issues related to Wildhaber-Novikov tooth profile design, bevel gears, worm gears, gears with cycloidal profiles, and strain wave gearing [4, 8, 14].

The introductory part of the corresponding section provides basic definitions and a classification of the simple gears according to various criteria, such as: type of gear ratio, location of the gear axes in space, shape of a tooth profile, shape of a tooth line, shape of a generating gear tooth surface, and others.

Within the study of the *geometric synthesis of toothed gearing*, the fundamental law of gear-tooth action is derived from the basis of the higher kinematic pair theory. The law has its two statements, one for analysis and one for the synthesis of a gearing. The courses mostly focus on the involute gearing, when each mating profile is generated as the involute of a circle. The mathematical equation of the involute, as well as the properties of the involute curve and the involute gearing, is investigated in detail.

During the practical lessons, students learn to identify the basic dimensions of the teeth and the qualitative parameters of gearing in the course of solving problems associated with tooth thickness along the arc of a circle of arbitrary radius, the lengths of the arc of contact and the path of contact, the contact ratio, and the relative sliding ratio.

The geometry of the teeth and all gear parameters are defined by the gear manufacturing process. The TMM course considers two principle machining manufacturing processes, including gear forming (form milling, broaching) and

gear generation (milling with a hob, gear shaping with a pinion-shaped cutter, gear shaping with a rack-shaped cutter). By virtue of clarity, the gear shaping with a rack-shaped cutter is the most popular in the study of manufacturing processes. In this case, generation commences by aligning the rack's reference line with the pitch circle of the gear blank about to be cut. A cutting rack may be displaced transverse to its reference line from the pitch diameter of the gear in order to avoid teeth undercutting in the course of generation.

During the practical lessons and labs, students explore a way to eliminate the possible undercutting of a tooth due to the profile shift of a cutting tool. After doing this, students are expected to be able to calculate the parameters of engagement of modified (corrected) gears, such as the operating pressure angle α_w and center-to-center distance a_w with zero backlash, tooth thickness along the arc of the pitch circle, the diameter of dedendum circle d_f, the diameter of addendum circle d_a, and others. During calculations carried out for the purpose of learning, it is necessary to verify the correctness of selecting the profile shift coefficient x so as not to let the tooth crest thickness become too thin. Students are given an idea of how to calculate coefficients suitable for a range of operating criteria, including the use of graphical methods.

The profile shift coefficient x, as one of the most important geometrical parameters, must be controlled when cutting teeth. For the indirect (and quite accurate) measurement of the shift coefficient, the instrumentally controlled dimensions can be used, which depend on x and, at the same time, allow for direct measurement through the use of standard or special tools, such as the vernier caliper, the gear-tooth caliper, or special templates. Wherein, depending on the method used, it is controlled, those dimensions are: the tooth height to the chord $\bar{h}_{ay}$, tooth thickness along the chord $\bar{S}_y$ (both used to determine the actual values of s, or x); constant chord $\bar{S}_c$, span measurement W.

Thus, in the process of studying the theory and applying the relevant knowledge in practice, students acquire skills related to the design of involute gears cut by a standard tool rack. When making the project, the students also learn to make drawings of the involute gearing.

The aim of the *kinematic analysis of toothed gearing* is to determine the angular velocities of gears and gear ratios. The first topic of the corresponding section is to examine the kinematics of simple and compound gear trains with gears rotating about fixed axes. In a multi-stage gear train, the number of stages is equal to the number of meshings, its overall gear ratio being defined as the product of the ratios of series-connected stages.

Gear ratio i is defined both algebraically and graphically. In the latter case, a method of calculation is based on the construction of the velocity triangles. This method is also used for kinematic analysis of epicyclic mechanisms, for which angular velocity diagrams are built to scale.

To determine the gear ratios of planetary and differential gear trains, Russian courses mostly employ a method of motion inversion (an analog of tabular method) and formula method (R. Willis's method).

Students apply the Willis formula in two alternative forms. The general formula view is useful for describing the kinematics of almost any planetary gear:

$$i_{ab}^{H} = \frac{\omega_a - \omega_H}{\omega_b - \omega_H}$$

In the particular case in which, for example $\omega_b = 0$, the Willis formula takes the form: $i_{aH}^{b} = 1 - i_{ab}^{H}$. The first formula is more versatile and is suitable for any planetary or differential gear trains, while the second is used only for the stages that include fixed-axis gears.

The study material focuses on the kinematic analysis of closed-loop gear trains in which members of the differential gear train form a rigid kinematic constraint in the form of a circuit, closing the differential stage. Some courses pay attention to the complex combined mechanisms, in particular, bi-planetary gearboxes.

A *gear mechanism design* comprises the choice of its kinematic scheme and selection of its parameters. The main condition for the design of a gear mechanism is to provide a predetermined gear ratio. A typical TMM tutorial focuses on the problem of selecting the number of teeth.

When selecting the number of teeth in the planetary and differential mechanisms, one must take into account the conditions of alignment, assembly condition, and some others. To avoid getting too large or too small a number of teeth, the design conditions are shaped as proportions. Formulae expressing design conditions form a closed non-homogeneous linear system of algebraic equations that can be solved for the numbers of teeth according to Cramer's Rule or by other means.

Analysis of the results of all kinds of TMM-relevant learning activity of students allows for identifying the most common difficulties and errors. These include, in particular, errors in counting the number of moving bodies within a complex gear train; determining the number of two-degrees-of-freedom kinematic pairs; identifying idle degrees of freedom; determining the number of one-degree-of-freedom kinematic pairs; kinematic analysis of the gear train and finding the angular velocity of the gears and the linear velocity vectors of teeth points; sign detection for gear ratios; determining the gear ratio of the differential stages of gear trains (for example, using the Willis method); determining the sizes of the tooth; analyzing the geometry of the involute gearing; determining qualitative parameters of gearing, and others [9]. A properly planned educational process helps to reduce the number and frequency of these errors.

The successful acquisition of competences by students, related to the analysis and design of gear trains in the course of TMM, becomes possible provided that the syllabus contains practical lessons, labs and a course project, the latter being one of

the most important types of learning activity, giving students the possibility of applying the knowledge acquired in a practice problem.

The syllabus of a **Machine Design** course also provides implementation by the students of a course project to design a drive unit with a gearbox as its most important component. At the initial step of calculation, the kinematics and force parameters of a drive unit are determined. Then, the material for the gears is selected, including determination of the hardness and heat treatments and of the allowable contact and bending stresses. Thereafter, the design calculation of the gear train geometric parameters is performed; the results are tested according to the determining calculation. This allows for calculating the loading of the gear shafts and making a drawing of the gearbox. Furthermore, the design scheme is established for the gear shafts and a determining calculation for bearings is carried out. Typically, in the course of the project, the largest amount of computational and other operations falls on the gear train design.

In general, the scope of knowledge related to gears obtained within the professionally-oriented courses is wide enough, which is why its versatile analysis is beyond the area of the present paper and deserves its own thorough individual study.

Gears in this or that form are studied within several other courses, for instance, Material Science, Strength of Materials, Advanced Techniques in Mechanical Engineering, etc. When finishing the Bachelor program, the mechanical engineering graduate should possess a clear understanding of the place and role of gear mechanisms within advanced manufacturing and mastery of definite skills for designing and analyzing various gear-based mechanisms.

Let us consider another aspect which is no less important within the training of an in-demand mechanical engineer given the present state of international and manufacturing activity—knowledge of a foreign language (English) [6, 7].

In 2001–2002, ten leading world engineering universities took part in a research (SPINE—Successful Practices in International Engineering Education) [5]. Partner universities in this research were, in particular, the Massachusetts Institute of Technology (USA), Queen Technical University (Sweden), Imperial College (Great Britain), and the Federal Polytechnic School in Lausanne (Switzerland). The purpose of the SPINE project was a comparative analysis of courses of engineering education in different countries, assessment of their quality, and revelation of the concepts, methodologies and means of education proving their efficiency in accordance with the chosen criteria. The review was proposed to 543 professors, 1517 engineers and managers, and 66 rectors, deans, and other supervisory personnel. Means of quality and quantity analysis were applied to study: the structure of universities, the educational process, international collaboration, collaboration with industry, the competences of an engineer, and the authority of universities. An engineer should possess the following common professional competences:

- presentation skills,
- leadership abilities,
- skills of project management,
- capability for teamwork,

- capability for acquiring common (general culture) education,
- language competence (not English),
- language competence (English),
- communicative competence,
- social competence,
- competence in the field of finance,
- marketing competence,
- legal competence.

Emphasis was on a high rank of communicative and language competences—experts of all categories gave the rating 5.4 out of a possible 6 for these competences. Assessment of the real situation gave 4.0–4.5 for communicative competence and 4.4–4.7 for language (English) competence out of a possible 6. It was concluded in the project that communicative and language (English) competences, along with the capability for teamwork, presentation skills and the development of leadership characteristics, are related to the most important general professional competences [5].

In accordance with the review of 100 engineers employed in Australian industry, more than 70% of their working time was spent dealing with documents [15]. The real object is preceded by its ideal image represented by explanatory notes, schemes, drawings, and mathematical calculations. Globalization of markets requires that all the developed documentation (including drawings) be made understandable and easily translated into any language.

The portions of course syllabi that relate to gears are among the most difficult to learn and require significant classroom time. A significant reduction in contact hours during the transition from the Russian higher school to a two-level model will, in our opinion, have an effect on the categorization of the students' team into two unequal groups. The first one is represented by the conditionally average and weak students who, without going deeply into the essential questions, will acquire receptive skills only.

The more talented and, most importantly, motivated students will form a second, smaller group. To acquire the relevant competences, they will have to make additional efforts in the process of learning, self-study, attending electives, performing research projects, participating in competitions at various levels, and participating in professional societies. The objective of the Technical University is to provide conditions for implementing the potential of this category of students. Its positive examples are considered to be of student participation in international competitions in MMS (with the obligatory inclusion of the tasks related to the gearing) [9, 10] and in the activities of the IFToMM [3].

The most active students comprising the second group are more likely to dedicate their professional activity to scientific research and project engineering directly related to gears at advanced manufacturing mechanical engineering enterprises.

4 Analysis of Agreement on Valid Syllabi for Mechanical Engineering Students and Requirements Specified for Graduates by the Manufacturing Industry

One of the most sought-after majors for mechanical engineering graduates is the above-mentioned "Design and manufacturing preparation of mechanical engineering production." Bachelors for this major are successfully trained at Kalashnikov ISTU.

Analysis of types of professional activity allowed for identifying five variable blocks of professional training with the necessary professional competences for the workplace: project design, manufacturing, operation and maintenance, scientific research, and management and control; it also facilitated grouping them into two main blocks of training: project design and innovation manufacturing [13].

Such identification provides an opportunity to define the courses within a syllabus in accordance with the professional competences necessary for the workplace; their set is chosen by the university, together with an employer with regard to the advanced object-oriented training of Bachelors.

The syllabus for training the experts in the above-mentioned major implies various types of education (lectures, practical and laboratory works, term papers and term projects, etc.) for more than 30 courses within all five blocks.

One of the methods for evaluation of an agreement on syllabi and requirements specified for graduate-engineers by manufacturing enterprises is the survey of graduates who now successfully work for modern mechanical engineering enterprises. The review involved graduates who obtained the B.S. degree in the considered major in 2004–2015 and whose professional activity is in one way or another related to investigation, development, production, testing and operation of gears and gear-based mechanisms.

70% of respondents found their job related to their major as far back as in their time studying at the university. All the rest found their job immediately after graduation from the university. None of the respondents answered that they had had difficulties in finding a job or that it took any significant amount of time to find a good job.

Respondents related their professional activity to one or several of five blocks:

A project design—53%
B manufacturing—46%
C operation and maintenance—7%
D scientific research—30%
E management and control—15%

46% of respondents emphasized that the knowledge obtained during their study in the Bachelor program was enough to commence professional activity successfully. 54% said that it was not enough, and that that was why they had decided to start their MS programs in the same major immediately after graduation from the Bachelor program.

In general, the level of training offered by the experts in the "Mechanical engineer" major at the DMPMEP Department of Kalashnikov ISTU satisfied 85% of the respondent graduates.

One of the questions posed to the graduates was: What theoretical knowledge and practical skills did you lack at the beginning of your professional activity? Almost all of them answered that theoretical knowledge was enough, but they lacked a significant number of certain practical skills in the development of manufacturing processes, in work with engineering and design documentation, in work with metal working equipment, and in practice writing down the programs for CNC machine-tools.

Knowledge in the field of gears obtained when studying for the Bachelor program was enough to commence professional activity for 77% of the respondents. 11% answered that the insufficient volume of knowledge was completely replenished during their further study in the Master's Degree program; and another 12% noted that their professional activity was not so closely related to gears, so it was hard for them to answer this question for sure.

After that, the graduates were offered the opportunity to assess the quality of teaching for practically all professionally-oriented courses from the point of view of their validity and applicability within their professional activity on a scale from one to ten (0 was for unsatisfactory, 10 was for maximum useful courses). Results of this assessment are given in Table 2.

Among all of the above-enumerated courses, the most important ones from the point of view of becoming an engineer and an expert in the field of gears proved to be (in descending order of priority):

1 Machine parts (Fundamentals of machine design)
2 Theory of mechanisms and machines
3 Mechanical engineering technology
4 Accuracy rating. Metrology, standardization and certification
5 Strength of materials
6 Material science
7 Methods for computer-aided design.

In general, the results of the review showed a good agreement on the syllabus for training mechanical engineers at the "Design and manufacturing preparation of mechanical engineering production" Department. However, the results given in Table 2 indicate the necessity for continuous monitoring of the validity of these aspects of those courses, and the necessity of paying greater attention to acquiring practical skills for future professional activity.

Table 2 Results of assessment for the quality of the obtained knowledge from the point of view of their validity and applicability within real manufacturing conditions

Name of the course	Average value
Methods for computer-aided design	9.57
Metrology, standardization and certification	9.43
Accuracy rating	8.86
Mechanical engineering technology	8.64
Machine parts (Fundamentals of machine design)	8.57
Advanced techniques of machining and assembly	8.46
Manufacturing tooling	8.46
Computer science	8.43
CAD of manufacturing processes	8.42
Systems of computer-aided engineering analysis	8.31
Fundamentals of mechanical engineering	8.29
Design of blanks in mechanical engineering	8.29
Material science	8.21
Introduction to professional field of work	8.17
Computer-aided methods for solving engineering problems	8.09
Computer-aided practice of mechanical engineering	8.00
Techniques for manufacturing processes	8.00
Theory of mechanisms and machines	7.86
Quality management	7.73
Programming languages	7.64
Strength of materials	7.57
Algorithm development and applied programming	7.38
Automation of manufacturing processes	7.36
Fundamentals of logic control	7.33
Mathematical modeling of processes in mechanical engineering	7.14
Theory of computer-aided control	7.00
Microprocessor systems in control of manufacturing objects	6.90
System analysis and decision-making	6.25
Electronics and microprocessor engineering	6.22
Control of objects and systems	6.13
Control of discrete systems	6.00

5 Conclusions

Nowadays, gear experts should continuously improve the machinery, and develop new mechanisms on the basis of already-existing gears, accounting for the rapid appearance of new methods of design, analysis, production and testing of gears and gear mechanisms. Within the advanced innovative development of gear production, strict requirements are specified for graduate engineers who plan to devote their professional activity to gears; these requirements imply the development of high

skills and abilities, innovative knowledge, and communicative capabilities by the time of their graduation.

Obvious contradictions between the necessity to increase the efficiency of activity of an innovative manufacturing system, insufficient rates of reformation of the educational system and a low-performing level of professional competences of engineering experts allow for stating the urgency for the development of innovative mechanisms for forming professional competences as applied to requirements for training an expert engineer.

Analysis of the contents of different courses related to gears within the training of mechanical engineers in the Bachelor program shows a good fundamental theoretical preparation of future gear engineers.

Results of the review carried out for graduates of one of the most sought-after majors, "Design and manufacturing preparation of mechanical engineering production" at Kalashnikov ISTU, indicate good agreement on the valid syllabi for mechanical engineers and requirements specified for graduates by the present manufacturing industry. Nevertheless, results of the review revealed the necessity for continuous monitoring of the validity of aspects of those courses, and the necessity of paying greater attention to acquiring practical skills for future professional activity.

References

1. Astafyev, N.: Innovation Development of University Complexes, UGTU-UPI, Ekaterinburg (2008) (in Russian)
2. Babichev, D., Lagutin, S., Barmina N.: Russian school in the theory and geometry of gearing. Part 1. Its origins and golden period of 1935–1975. Front. Mech. Eng. FME-15028-MA. **11**(1), 44–59 (2016).
DOI 10.1007/s11465-015-0360-z
3. Barmina, N., Karelina, M, Krylov, E.: MMS study in Russian universities: the recent past and the desired future. In: Proceedings of IFToMM Permanent Workshop on History of Mechanism and Machine Science (2015)
4. BMSTU lectures on theory of machines and mechanisms. http://tmm-umk.bmstu.ru/index_2.htm
5. Bodmer, C., et al: Successful practices in international engineering education. SPINE Final Report. www.ingch.ch/pdfs/spinereport.pdf
6. Chmelikova, G.: Doctoral students and necessary academic skills. In: R&E Source. Special issue 4, 2015, online. ISSN 2313-1640, pp. 28–31. http://journal.ph-noe.ac.at/index.php/resource/article/view/241/280
7. Chmelikova, G.: Preparing the postgraduate students for academic environment by specific training and by utilizing technologies. In: Proceedings of IEEE 13th International Conference on Emerging eLearning Technologies and Applications (ICETA 2015), CD-ROM, pp. 119–124. IEEE, 2015, Starý Smokovec, The High Tatras, Slovakia. 1. vyd. Piscataway, 26–27 Nov 2015. ISBN 978-1-4673-8533-6
8. Frolov, K., Popov, S., Musatov, A., Lukichov, D.: Theory of Mechanisms and Machines. Vyschaya shkola, Moscow (1987) (in Russian)

9. Goldfarb, V., Krylov, E., Elensky, A.: Analysis of the participant solutions of the first student international Olympiad on mechanism and machine science. Mech. Mach. Theory **70**, 293–297 (2013)
10. Goldfarb, V., Krylov, E., Elensky, A.: The first student international olympiad on mechanism and machine science—the challenge in MMS education. J. Mech. Eng. Autom **3**(3), 152–158 (2013)
11. Goldfarb, V.: Theory and practice of gearing in machines and mechanisms science. In: Technology developments: the Role of mechanisms and machine science and IFToMM, pp. 133–139. Springer, Berlin (2011)
12. http://mintorg.udmurt.ru/industry/index.php
13. http://www.istu.ru/oo/standarts/standart_151900.62.pdf
14. Kuniver, A.: Geometry synthesis of spatial gears. ISTU, Izhevsk (2003) (in Russian)
15. McGregor, H.: Engineers at work: developing communication skills for professional practice. In: Proceedings of the Society for Technical Communication Conference, Orlando (2000)
16. Prajova, V., Perminova, O., Faizullin, R.: Principles of organizations' interaction while forming mechatronics specialists' professional competences in a regional industry cluster. Procedia. Eng **96**, 370–373 (2014)

Kinematics of Bevel Biplanetary Gear

J. Drewniak, T. Kądziołka and S. Zawiślak

Abstract In the present paper, we present a method of kinematical analysis of a complex gear, i.e., a bevel biplanetary gear. As an introduction, the structure, operating rules and some remarks on application are given. Afterwards, the relationships allowing for determination of the speed gear ratio are derived. The considerations are performed for two variants of the considered gear—by means of the Willis formulas. The utilized relationships are verified by means of the drawing-analytical method, in which equations of the equilibrium of forces acting on particular pairs of wheels are used, considering a sequence of two-pair subsystems from an input to an output.

Keywords Bevel biplanetary gear · Transmission gear ratio · Willis equation · Equilibrium equations

1 Introduction

Biplanetary gears belong to a subsection of mechanisms which are not too frequently analyzed or applied. Nevertheless, some of them are considered in the monograph [1], and biplanetary mechanisms were utilized in devices patented [2, 3] in the USA. The authors also considered cylindrical biplanetary gears [2, 4].

J. Drewniak (✉)
Dept. of Found. of Machine Building, Faculty of Mechanical Engineering and Computer Science, University of Bielsko-Biala, Bielsko-Biała, Poland
e-mail: jdrewniak@ath.bielsko.pl

T. Kądziołka
Vocational High School, Nowy Sącz, Poland
e-mail: tkadziolka@pwsz-ns.edu.pl

S. Zawiślak
Dept. of Informatics and Automation, Faculty of Mechanical Engineering and Computer Science, University of Bielsko-Biala, Bielsko-Biała, Poland
e-mail: szawislak@ath.bielsko.pl

V. Goldfarb et al. (eds.), *Advanced Gear Engineering*,
Mechanisms and Machine Science 51, DOI 10.1007/978-3-319-60399-5_14

Moreover, some other types and/or layouts of these gears were considered, e.g., so-called open or compound (complex, coupled) gears [2, 4, 5] (Fig. 1).

However, bevel biplanetary gears belong to an advanced class of mechanism which could be good objects for analysis, e.g., for PhD students and young researchers within the field of MMT Science.

In Fig. 2a, b, two versions of bevel biplanetary gear are presented. Among other factors, these gears consist of two planetary mechanisms:

- an external (main) mechanism built of the following parts: sun wheel 1, planet gears 2 and 6, and fixed wheel 7, as well as external arm h,
- an internal mechanism which consists of wheels 3 and 5 and planet gear 4, as well as internal arm H.

In the first variant (Fig. 2a) of biplanetary gear, the satellite 2 of the external mechanism is united with the wheel 3 of the internal mechanism, and additionally, the internal arm H is united with the satellite 6 of the external mechanism. However, in the second variant (Fig. 2b), the satellite 2 is united with the internal arm H and the internal wheel 3 is united with the satellite 6 of the external mechanism.

The characteristic feature of these gears is that the internal planet gear 4 performs a complex movement around three axes: its own, the vertical (perpendicular to the main axis) and the main axis of the gear.

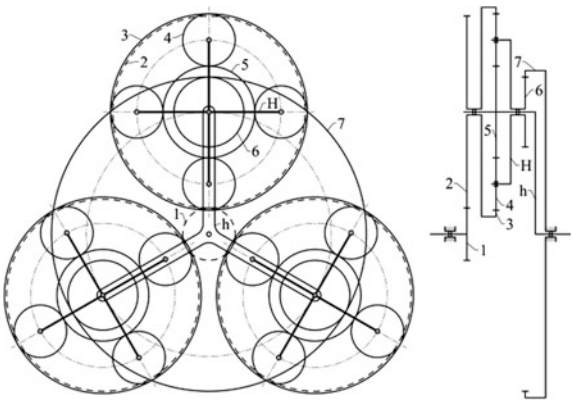

Fig. 1 Front view and general scheme of cylindrical biplanetary gears

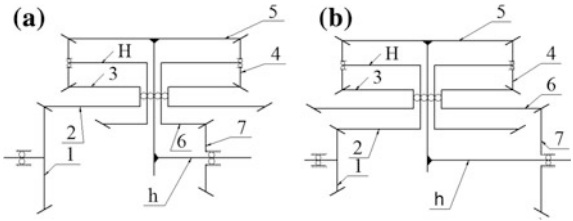

Fig. 2 Kinematical schemes of biplanetary gears: **a** variant according to [2], **b** own variant

In general, cylindrical and bevel biplanetary gears are used as driving links of work elements of mining and agricultural machines. The gears considered below are not widely applied or even applied at all in real, industrial systems. The essential drawback of these mechanisms is the lack of possibility of reaching adequate high transmission values unless their dimensions (and simultaneously their mass) are essentially enlarged. But, in consequence, high centrifugal forces are generated in the internal mechanism, which is an additional inconvenience. However, due to the complicated structure and complex movements of geared wheels and their arms, the considered bevel biplanetary gears could be recognized as interesting mechanisms themselves, additionally creating a challenging task for performance of versatile analyses, i.e., geometrical, kinematical and those focusing on strengths—especially for advanced students' classes (e.g., postgraduate studies) within the range of such subjects as theory of mechanism and machine and design of such complicated mechanisms.

2 Gear Train Value for the First Variant of the Gear

2.1 Considerations Based on the Willis Approach

According to the definition of the gear train transmission value (speed ratio) $i^7_{1,h}$ of the gear sun wheel 1 to the external arm h, in case the wheel 7 is held fix, will be initially calculated.

For the assumed notation, we can write the following formula:

$$i^7_{1,h} = \left(\frac{n_1}{n_h}\right)_{n_7=0}, \tag{1}$$

where $n_1 = n_N = n_{in}$ is a velocity of sun wheel 1, i.e., the input velocity of the gear, whereas $n_h = n_{out}$ is a velocity of arm h, i.e., the output velocity of the gear (Fig. 2a). Aiming for determination of this speed ratio, i.e., $i^7_{1,h}$, the base ratio of the internal gear should have previously been calculated, while in the case when the whole epicyclic gear has a rotational velocity equal to $-n_h$, one should consider the kinematics of the system in relation to the arm h. Then, the relative rotational velocities of the particular geared wheels of the gear are equal to, respectively, $n^h_j = n_j - n_h$ for $j = 1, 2, \ldots, 7$, whereas we have the following equalities: $n^h_5 = n_5 - n_h = -n_h$ (because $n_5 = 0$), $n^h_7 = n_7 - n_h = -n_h$ (because $n_7 = 0$), and $n^h_3 = n_3 - n_h = n_2 - n_h = n^h_2$ (because $n_3 = n_2$).

Similarly, the relative rotational velocity of internal arm H in relation to arm h is equal to $n^h_H = n_H - n_h$.

The base ratio of the internal gear, consisting of gears 3, 4 and 5 and arm H, for the given relative velocities n^h_3, n^h_4, n^h_5 and n^h_H, can be calculated based on the Willis formula:

$$i_{3,5}^{H} = \frac{n_3^h - n_H^h}{n_5^h - n_H^h}, \tag{2}$$

as well as based on the formula of the ratio for wheels 3, 4 and 5, in relation to arm H. The second formula mentioned can be expressed utilizing the teeth numbers (similarly as to a gear having fixed axes):

$$\begin{aligned} i_{3,5}^{H} &= \left(\frac{n_3^h - n_H^h}{n_4^h - n_H^h}\right) \cdot \left(\frac{n_4^h - n_H^h}{n_5^h - n_H^h}\right) = \left(\frac{n_3^h - n_H^h}{n_5^h - n_H^h}\right) \\ &= \left(-\frac{z_4}{z_3}\right) \cdot \left(+\frac{z_5}{z_4}\right) = \left(-\frac{z_5}{z_3}\right) = -1; \end{aligned} \tag{3}$$

Furthermore, the following formula can be written:

$$i_{3,5}^{H} = -1 = \frac{n_3^h - n_H^h}{-n_H^h}, \tag{4}$$

because $n_5^h = n_5 - n_h = 0$ and $z_3 = z_5$.

Additional remarks have to be entered, i.e., some special rules for local ratios were assumed—namely the minus sign is assigned to the ratio of numbers of teeth out of meshing (e.g., $(-z_4/z_3)$) and the plus sign is assigned to the ratio of teeth in meshing (e.g., $(+z_5/z_4)$).

Aiming for determination of the investigated transmission of the biplanetary gear, it is necessary to calculate the unknown relative velocities n_3^h and n_H^h in the above-written formula (4). These notions should be determined as a function of the variables n_h and/or n_1, based on two conditions for the transmission $i_{H,7}^h$ (transmission from to arm H to wheel 7) and the transmission $i_{3,1}^h$ (transmission from wheel 3 onto wheel 1 in relation to arm h):

$$i_{H,7}^h = \frac{n_H^h}{n_7^h} = \frac{n_6^h}{n_7^h} = \frac{z_7}{z_6}, \tag{5}$$

and therefore

$$n_H^h = n_7^h \cdot \left(\frac{z_7}{z_6}\right) = -n_h \cdot \frac{z_7}{z_6}, \tag{6}$$

because: $n_7^h = n_7 - n_h = -n_h$.

Similarly,

$$i_{3,1}^h = \frac{n_3^h}{n_1^h} = \frac{n_2^h}{n_1^h} = -\frac{z_1}{z_2}, \tag{7}$$

consequently

$$n_3^h = n_2^h = n_1^h \cdot \left(-\frac{z_1}{z_2}\right) = (n_1 - n_h) \cdot \left(-\frac{z_1}{z_2}\right), \tag{8}$$

because $n_3 = n_2$, and consequently we also have: $n_3^h = n_2^h$.

Therefore, the ratio of teeth numbers z_5/z_3, i.e., formula (4) describing the kinematical transmission $i_{3,5}^H = -1$, finally has the form (9). After some additional transformations, we can write the relationship (10):

$$-1 = \frac{(n_1 - n_h) \cdot \left(-\frac{z_1}{z_2}\right) + n_h \cdot \frac{z_7}{z_6}}{n_h \cdot \frac{z_7}{z_6}}, \tag{9}$$

$$\frac{n_1}{n_h} = \left(1 + 2 \cdot \frac{z_2}{z_1} \cdot \frac{z_7}{z_6}\right). \tag{10}$$

Therefore, the formula (1) for kinematical transmission of the biplanetary gear can be written in the following form:

$$i_{1,h}^7 = \left(\frac{n_1}{n_h}\right)_{n_7=0} = 1 + 2 \cdot \frac{z_2}{z_1} \cdot \frac{z_7}{z_6}. \tag{11}$$

The exemplary value can be calculated for the following assumed number of teeth for the consecutive wheels of the considered biplanetary gear: $z_1 = 50$, $z_2 = 200$, $z_3 = 60$, $z_4 = 40$, $z_5 = 60$, $z_6 = 28$, $z_7 = 28$; therefore, the value of kinematical transmission is equal to

$$i_{1,h}^7 = 1 + 2 \cdot \frac{z_2}{z_1} \cdot \frac{z_7}{z_6} = 1 + 2 \cdot \frac{200}{50} \cdot \frac{28}{28} = 9.0. \tag{12}$$

Further consideration will be performed to compare the achieved results with another approach.

2.2 *Utilization of Equilibrium Equations for Consecutive Subsystems of Geared Wheels*

The equilibrium equations for geared wheels and arms are derived based on the adequate geometrical charts presented in Figs. 3, 4, 5, 6, 7 and 8. The schemes were made for the considered biplanetary gear, but the manner of consideration is a general one. According to Fig. 3, the input torque T_1 is equal to

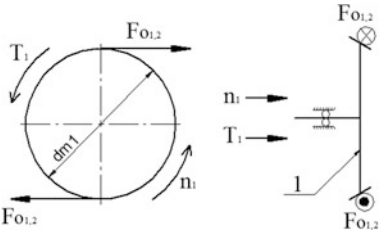

Fig. 3 Tangential forces acting upon sun wheel 1 (in the case when $s_2 = 2$)

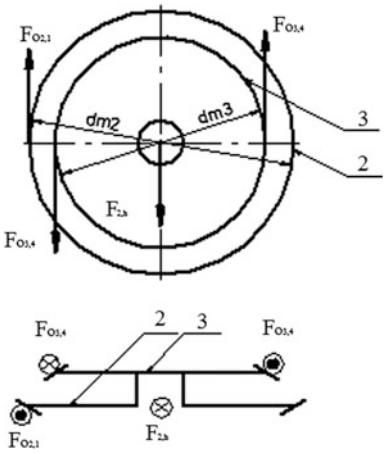

Fig. 4 Tangential forces acting upon gears 2 and 3

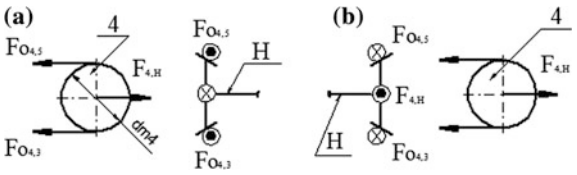

Fig. 5 Tangential forces acting upon satellite 4 (**a** and **b**)

$$T_1 = s_2 \cdot F_{o1,2} \cdot r_{m1}, \tag{13}$$

where s_2 is the number of satellites 2 (minimum $s_2 = 2$), r_{m1} is the mean pitch radius of wheel 1, and $r_{m1} = m_{mn1,2} \cdot z_1$, $m_{mn1,2}$ is the mean normal module of wheel 1 and 2 (according to the standard ISO 10300).

Based on the above formula, one can calculate the tangential force $F_{o1,2}$ exerted by gear 2 against gear 1 (radial force $F_{r1,2}$ is omitted, because only $F_{o1,2}$ is transmitted force):

$$F_{o1,2} = \frac{T_1}{s_2 \cdot r_{m1}}. \tag{14}$$

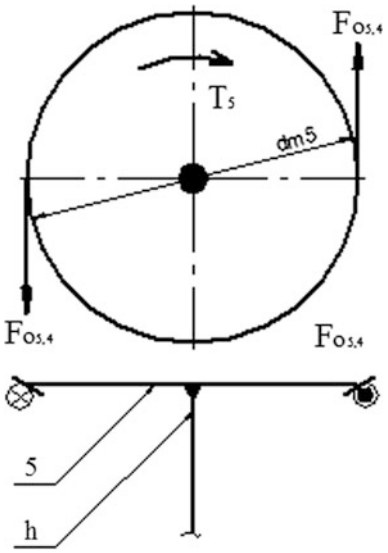

Fig. 6 Tangential forces acting on wheel 5 connected with arm h

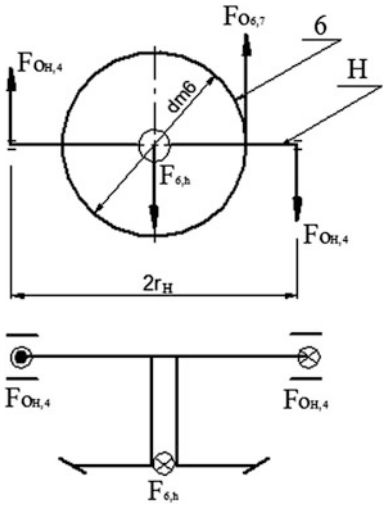

Fig. 7 Tangential forces acting upon gear 6 and arm H

Based on Newton's third law, the equality of tangential forces can be written as (considering the adequate form of notation)

$$F_{o2,1} = F_{o1,2} = \frac{T_1}{s_2 \cdot r_{m1}}. \tag{15}$$

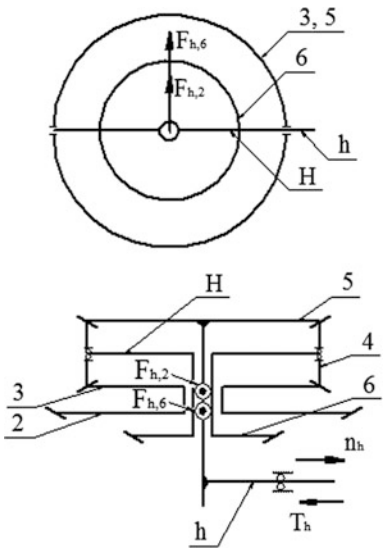

Fig. 8 Tangential forces acting upon arm h

The condition of equilibrium for wheels 2 and 3 can be written as follows (Fig. 4):

$$s_2 \cdot F_{o2,1} \cdot r_{m2} = s_4 \cdot F_{o3,4} \cdot r_{m3}, \tag{16}$$

where s_4 is the number of satellites 4 (minimum $s_4 = 4$), and $r_{m2} = m_{mn1,2} \cdot z_2$ as well as $r_{m3} = m_{mn3,4,5} \cdot z_3$ and $m_{mn3,4,5}$ is the mean normal module of gears 3, 4 and 5.

Based on Eq. (16), it is possible to determine the tangential force $F_{o3,4}$ exerted by satellite 4 against gear 3:

$$F_{o3,4} = \frac{s_2 \cdot F_{o2,1} \cdot r_{m2}}{s_4 \cdot r_{m3}} = \frac{T_1 \cdot r_{m2}}{s_4 \cdot r_{m1} \cdot r_{m3}}. \tag{17}$$

Therefore, the tangential forces $F_{o4,3}$ of gear 3 on gear 4 (Fig. 5a, b) are equal to (using Newton's third law)

$$F_{o4,3} = F_{o3,4} = \frac{s_2 \cdot F_{o2,1} \cdot r_{m2}}{s_4 \cdot r_{m3}} = \frac{T_1 \cdot r_{m2}}{s_4 \cdot r_{m1} \cdot r_{m3}}, \tag{18}$$

because $\vec{F}_{o4,3} = -\vec{F}_{o3,4}$ and $F_{o4,3} = F_{o3,4}$.

Based on the equilibrium conditions for satellite 4 (Eqs. (19) and (20)), it is also possible to determine the force $F_{4,H}$ of internal arm H on satellite 4 (relation (21)) (see Fig. 5a, b):

$$F_{o4,3} + F_{o4,5} - F_{4,H} = 0, \tag{19}$$

$$F_{o4,3} \cdot r_{m4} - F_{o4,5} \cdot r_{m4} = 0, \tag{20}$$

$$F_{4,H} = 2 \cdot F_{o4,3} = \frac{2 \cdot T_1 \cdot r_{m2}}{s_4 \cdot r_{m1} \cdot r_{m3}}, \tag{21}$$

because $F_{o4,3} = F_{o4,5}$, as well as the equilibrant force $F_{oH,4}$:

$$F_{oH,4} = F_{4,H} = \frac{2 \cdot T_1 \cdot r_{m2}}{s_4 \cdot r_{m1} \cdot r_{m3}}. \tag{22}$$

Based on the relationship (18), it is possible to determine the tangential force $F_{o5,4}$, of gear 4 on gear 5 (Fig. 6):

$$F_{o5,4} = F_{o4,5} = \frac{T_1 \cdot r_{m2}}{s_4 \cdot r_{m1} \cdot r_{m3}}. \tag{23}$$

According to the schemes presented in Fig. 7, we can write the equation of equilibrium of arm H and gear 6 as follows:

$$s_4 \cdot F_{oH,4} \cdot r_H = s_6 \cdot F_{o6,7} \cdot r_{m6}, \tag{24}$$

where r_H is the radius of arm H, r_{m6} is the mean pitch radius of wheel 6, $r_H = r_{m6}$ and s_6 denotes the number of geared wheels 6 (minimum $s_6 = 2$).

Based on Eq. (24), it is possible to determine the tangential force $F_{o6,7}$ of gear 7 on gear 6:

$$F_{o6,7} = \frac{s_4 \cdot F_{oH,4} \cdot r_{m3}}{s_6 \cdot r_{m6}} = \frac{2 \cdot T_1 \cdot r_{m2}}{s_6 \cdot r_{m1} \cdot r_{m6}}. \tag{25}$$

Having the relationships for determination of the forces $F_{h,2}$ and $F_{h,6}$ of gear 2 and 6, respectively, on external arm h, which can be written as $F_{h,2} = F_{o2,1}$ and $F_{h,6} = F_{o6,7}$, it is possible (see Fig. 8) to determine the formula for calculation of the output moment T_h.

The assumption is made that the efficiency of the gear is equal to one (i.e., $\eta_{1,h}^7 = 1$), and therefore, we have

$$T_h = s_2 \cdot F_{h,2} \cdot r_{m1} + s_6 \cdot F_{h,6} \cdot r_{m7}. \tag{26}$$

Then, the output moment T_h (as a function of the input moment T_1) can be easily calculated:

$$T_h = T_1 + \frac{2 \cdot T_1 \cdot r_{m2} \cdot r_{m7}}{r_{m1} \cdot r_{m6}} = T_1 \cdot \left(1 + \frac{2 \cdot r_{m2} \cdot r_{m7}}{r_{m1} \cdot r_{m6}}\right). \tag{27}$$

And finally, we can derive the formula for the gear train value of the bevel biplanetary gear:

$$\left|i_{1,h}^{7}\right| = \frac{T_h}{T_1 \cdot \eta_{1,h}^{7}} = 1 + \frac{2 \cdot r_{m2} \cdot r_{m7}}{r_{m1} \cdot r_{m6}} = 1 + \frac{2 \cdot z_2 \cdot z_7}{z_1 \cdot z_6}. \tag{28}$$

According to Fig. 8, the direction of rotation of arm h (opposite to the direction of action of the passive moment T_h) is compatible with the direction of rotations of sun wheel 1 (compatible with the direction of action of the active rotational moment T_1 (Fig. 3)). Therefore, the value of the kinematical transmission is positive $i_{1,h}^{7} > 0$, similar to that in the formula (11). A similar approach has been utilized for the derivation of the formulas for calculation of the transmission of the 2nd variant of the biplanetary gear.

3 Gear Train Value for the Second Variant of the Gear

3.1 Utilization of the Willis Formula

The structure (functional scheme) of the second variant of biplanetary gear (Fig. 2b) differs slightly from the structure of the previous gear. Therefore, the manner of derivation of the formula for calculation of speed ratio gear train value $i_{1,h}^{7}$ will be similar. Even the initial formula for speed ratio $i_{1,h}^{7}$ of the analyzed gear is the same as it was previously (1).

The basic ratio of the internal planetary gear (consisting of the following parts: geared wheels 3, 4 and 5 and arm H, for the given relative velocities n_3^h, n_4^h, n_5^h and n_H^h) can be derived based on the Willis formula:

$$i_{3,5}^{H,h} = \frac{n_3^h - n_H^h}{n_5^h - n_H^h}. \tag{29}$$

Moreover, it can be calculated based on the relationship for ratio of wheels 3, 4 and 5, in relation to arm H, as a function of teeth numbers (as for a gear of fixed axes):

$$i_{3,5}^{H,h} = \left(\frac{n_3^h - n_H^h}{n_4^h - n_H^h}\right) \cdot \left(\frac{n_4^h - n_H^h}{n_5^h - n_H^h}\right) = \left(\frac{n_3^h - n_H^h}{n_5^h - n_H^h}\right) = \left(-\frac{z_4}{z_3}\right) \cdot \left(+\frac{z_5}{z_4}\right) = -1, \tag{30}$$

namely,

$$i_{3,5}^{H,h} = -1 = \frac{n_3^h - n_H^h}{-n_H^h}, \tag{31}$$

because $n_5^h = n_5 - n_h = 0$ and $z_3 = z_5$.

Aiming for determination of the desired speed ratio of the biplanetary gear, we have to determine the unknown relative velocities n_3^h and n_H^h (utilized in the above formula (31)) as the functions of notions: n_h and/or n_1, based on two conditions for some special (local) ratios. These ratios are as follows: ratio $i_{H,7}^h$ (i.e., the ratio of arm H to gear 7) and ratio $i_{3,1}^h$ (i.e., the ratio of gear 3 to gear 1, in relation to arm h):

$$i_{1,H}^h = \frac{n_1^h}{n_H^h} = \frac{n_1^h}{n_2^h} = -\frac{z_2}{z_1}, \tag{32}$$

and consequently

$$n_H^h = n_1^h \cdot \left(-\frac{z_1}{z_2}\right) = -(n_1 - n_h) \cdot \frac{z_1}{z_2}, \tag{33}$$

because $n_1^h = n_1 - n_h$ and $n_2 = n_H$, namely $n_2^h = n_H^h = n_H - n_h$.

Similarly, we have the following formula:

$$i_{3,7}^h = \frac{n_3^h}{n_7^h} = \frac{n_6^h}{n_7^h} = \frac{z_7}{z_6}, \tag{34}$$

and therefore

$$n_3^h = n_6^h = n_7^h \cdot \left(\frac{z_7}{z_6}\right) = -n_h \cdot \left(\frac{z_7}{z_6}\right), \tag{35}$$

because $n_3 = n_6$. Consequently, we also have that $n_3^h = n_6^h$ and $n_7^h = n_7 - n_h = -n_h$.

Finally, the ratio of teeth numbers z_5/z_3, considered in formula (31), after some consecutive transformations, has the same form as given in (37):

$$-1 = \frac{-n_h \cdot \frac{z_7}{z_6} + (n_1 - n_h) \cdot \frac{z_1}{z_2}}{(n_1 - n_h) \cdot \frac{z_1}{z_2}}, \tag{36}$$

$$\frac{n_1}{n_h} = \left(1 + \frac{z_2 \cdot z_7}{2 \cdot z_1 \cdot z_6}\right). \tag{37}$$

Based on the afore-mentioned considerations, in conclusion, we can state that the formula for determination of the ratio (1) for the biplanetary gear can be expressed as follows:

$$i_{1,h}^{7} = \left(\frac{n_1}{n_h}\right)_{n_7=0} = 1 + \frac{z_2 \cdot z_7}{2 \cdot z_1 \cdot z_6}. \tag{38}$$

For the second version of the biplanetary gear, the following teeth numbers were assumed: $z_1 = 20$, $z_2 = 200$, $z_3 = 60$, $z_4 = 40$, $z_5 = 60$, $z_6 = 40$, $z_7 = 80$, thus the kinematical transmission has the following value:

$$i_{1,h}^{7} = 1 + \frac{z_2 \cdot z_7}{2 \cdot z_1 \cdot z_6} = 1 + \frac{200 \cdot 80}{2 \cdot 20 \cdot 40} = 11.0. \tag{39}$$

3.2 *Calculations Based on Utilization of the Equilibrium Equations for Consecutive Geared Wheels*

The equilibrium equations of geared wheels and arms are derived utilizing figures comparable to those discussed in Sect. 2.2. Similarly, as the in case of the first variant of the gear, for the given moment T_1, one can determine the forces $F_{o1,2}$ and $F_{o2,1}$ (see formulas (13)–(15)):

$$F_{o1,2} = F_{o2,1} = \frac{T_1}{s_2 \cdot r_{m1}}. \tag{40}$$

It should be highlighted that the manner of description of the discussed forces and geometrical gears' parameters are the same as for the afore-analyzed gear (in Sect. 2.2).

The equilibrium rotational condition for wheel 2 and arm H (as a subsystem) can be expressed by the following relationship:

$$s_2 \cdot F_{o2,1} \cdot r_{m2} = s_4 \cdot F_{oH,4} \cdot r_H. \tag{41}$$

Therefore, the tangential force $F_{oH,4}$ acting on arm H, in the point of position of bearings for satellite 4, is equal to

$$F_{oH,4} = \frac{s_2 \cdot F_{o2,1} \cdot r_{m2}}{s_4 \cdot r_{m3}} = \frac{T_1 \cdot r_{m2}}{s_4 \cdot r_{m1} \cdot r_{m3}}. \tag{42}$$

Based on the condition of equilibrium for satellite 4 (Eqs. (43) and (44)), we can determine the tangential forces $F_{o4,3}$ and $F_{o4,5}$ exerted, respectively, by gears 3 and 5 against satellite 4 (relation (45)):

$$F_{o4,3} + F_{o4,5} - F_{4,H} = 0, \tag{43}$$

$$F_{o4,3} \cdot r_{m4} - F_{o4,5} \cdot r_{m4} = 0, \tag{44}$$

$$F_{o4,3} = F_{o4,5} = 0,5 \cdot F_{oH,4} = \frac{T_1 \cdot r_{m2}}{2 \cdot s_4 \cdot r_{m1} \cdot r_{m3}}. \tag{45}$$

Based on Newton's third law, we can determine the tangential forces acting on the teeth of wheel 5 and wheel 3:

$$F_{o5,4} = F_{o3,4} = F_{o4,3} = \frac{T_1 \cdot r_{m2}}{2 \cdot s_4 \cdot r_{m1} \cdot r_{m3}}, \tag{46}$$

because: $\vec{F}_{o5,4} = -\vec{F}_{o4,5}$ and $\vec{F}_{o4,3} = -\vec{F}_{o3,4}$. Consequently, we also have that: $F_{o5,4} = F_{o4,5}$ and $F_{o4,3} = F_{o3,4}$.

Having calculated the tangential force $F_{o3,4}$, it is possible to determine the tangential force $F_{o6,7}$ (48) based on the equilibrium equation for wheels 3 and 6 (47):

$$s_4 \cdot F_{o3,4} \cdot r_{m3} = s_6 \cdot F_{o6,7} \cdot r_{m6}, \tag{47}$$

$$F_{o6,7} = \frac{s_4 \cdot F_{o3,4} \cdot r_{m3}}{s_6 \cdot r_{m6}} = \frac{T_1 \cdot r_{m2}}{2 \cdot s_6 \cdot r_{m1} \cdot r_{m6}}. \tag{48}$$

Based on the second equilibrium equation for wheel 2 and arm H (i.e., considering projection of forces on the rotational axis of wheel 2 (Eq. (49)) and the same equilibrium condition for wheels 3 and 6 (Eq. (50)), we can write the following equations:

$$F_{o2,1} - F_{oH,4} + F_{oH,4} - F_{2,h} = 0, \tag{49}$$

$$F_{o3,4} - F_{o3,4} + F_{o6,7} - F_{6,h} = 0. \tag{50}$$

We can determine the forces of influence of arm h on wheel 2, $F_{2,h} = F_{o2,1}$, and on wheel 6, $F_{6,h} = F_{6,h}$. Moreover, considering vector equations, it can be written that $\vec{F}_{2,h} = -\vec{F}_{o2,1}$ and $\vec{F}_{6,h} = -\vec{F}_{6,h}$.

Based on Newton's third law, it is possible to determine the relationships of mutual effect of wheels 2 and 6 on arm h:

$$F_{h,2} = F_{2,h} \quad \text{and} \quad F_{h,6} = F_{6,h}, \tag{51}$$

where the vector equalities are as follows: $\vec{F}_{h,2} = -\vec{F}_{2,h} = \vec{F}_{o2,h}$ and $\vec{F}_{h,6} = -\vec{F}_{6,h} = \vec{F}_{o6,h}$.

Based on the rotational equilibrium of the arm (52), we can finally determine the output rotational moment (torque) T_h via the formula (53):

$$s_2 \cdot F_{h,2} \cdot r_{m1} + s_6 \cdot F_{h,6} \cdot r_{m7} - T_h = 0, \tag{52}$$

$$T_h = T_1 + \frac{T_1 \cdot r_{m2} \cdot r_{m7}}{2 \cdot r_{m1}} = T_1 \cdot \left(1 + \frac{r_{m2} \cdot r_{m7}}{2 \cdot r_{m1} \cdot r_{m6}}\right). \tag{53}$$

The expression for the torque T_h can be utilized for derivation of the formula for calculation of the kinematical transmission $i_{1,h}^7$ for the second variant of the biplanetary gear:

$$\left|i_{1,h}^7\right| = \frac{T_h}{T_1} = 1 + \frac{r_{m2} \cdot r_{m7}}{2 \cdot r_{m1} \cdot r_{m6}} = 1 + \frac{z_2 \cdot z_7}{2 \cdot z_1 \cdot z_6}. \tag{54}$$

Similarly, as in case of the first variant of the considered gear (Fig. 2a), the direction of rotation of arm h is compatible with the direction of rotation of sun wheel 1, and therefore the speed value has a positive value $i_{1,h}^7 > 0$, as previously.

4 Final Remarks and Conclusions

The majority of biplanetary gears have relatively low transmissions in relation to their complex kinematical structure. Nevertheless, due to the complicated motion of the satellites of the internal planetary mechanism, those gears have some range of application in the operational working links of coal mine machinery, as well as some medical equipment. The complex motions of satellites are interesting to study and precisely known. The universal method of analysis consists in utilization of the Willis approach and formulas [2, 4]. Another effective method is the so-called Kutzbach scheme of velocities, however, the range of application is restricted to biplanetary cylindrical gears [4]. Therefore, in the present paper, we propose a general method based on utilization of equilibrium conditions for the elements passing the drive throughout a gear, i.e., geared wheels and arms—aiming at determination of the most important characteristic of a particular gear, i.e., kinematical transmission (the ratio).

References

1. McCarty Jr, W.L.: Therapeutic method for effecting translatory continuous passive motion of the temporomandibular joint. U.S. Patent No. 5,467,785, 21 Nov 1995
2. Cyplakov, J.C.: Bi-Planetary Mechanisms. Mas'inostroenie. Moskwa (1966, in Russian)
3. McCarty Jr, W.L.: Therapeutic method and apparatus for effecting translatory continuous passive motion of the temporomandibular joint. U.S. Patent No. 5,374,237, 20 Dec 1994

4. Drewniak, J., Deptuła, A., Kądziołka, T., Zawiślak, S.: Kinematics of biplanetary epicyclic gear. International Conference Computational Kinematics, Poitiers 2017 (accepted for publishing)
5. Kolovsky, M.Z., Evgrafov, A.N., Semenov, Y.A., Slousch, A.V.: Kinematic and parametric analysis of mechanisms. In Advanced Theory of Mechanisms and Machines, pp. 79–120. Springer, Berlin (2000)

Tool Profiling for the Grinding of Helical Surfaces

V. Medvedev and A. Volkov

Abstract The methods of synthesis and analysis of the tool shape for grinding different types of helical surfaces are presented in the paper. The formation (synthesis) of the flank of the tool for grinding the general-type external thread is described in detail. The problem of the mathematical simulation (analysis) of screw processing using the tool of the given profile to test the possibility of manufacturing at the required accuracy is also solved. Features of synthesis and analysis techniques for grinding internal threads, as well as Archimedean and involute worms, are considered briefly. Examples of the proposed technique application for grinding the buttress external thread and involute worm are presented.

Keywords Grinding · Helical surface · Cylindrical single-thread · Archimedean worm · Involute worm · Abrasive wheel

1 Introduction

Parts with helical surfaces are used to transmit movements and forces in machines and mechanisms. Investigation into the processing of these items has been described in a large number of scientific papers [1, 3–6]. Grinding by a profile abrasive wheel is one of the main methods of obtaining an accurate helical surface.

For modern machine-tools, it is possible to obtain an arbitrary profile of the grinding wheel. As a rule, the tilt of the tool spindle is used for grinding helical surfaces. However, the use of the tilt angle for grinding internal threads on long workpieces is limited. The fundamental possibility of grinding certain types of thread without tilting the tool spindle by an appropriate selection of the profile of

V. Medvedev (✉) · A. Volkov
MSTU «STANKIN», Moscow, Russia
e-mail: vladimir.ivanovich.medvedev@gmail.com

A. Volkov
e-mail: volkov411@gmail.com

V. Goldfarb et al. (eds.), *Advanced Gear Engineering*,
Mechanisms and Machine Science 51, DOI 10.1007/978-3-319-60399-5_15

the grinding wheel is shown in [10]. However, this method is not applicable to all types of thread.

The purpose of this paper is to describe the method for determining the tool axial section that is necessary for grinding a helical surface at an arbitrary tilt angle of the grinding wheel axis with a given accuracy.

The grinding of external and internal single-start threads, and Archimedean and involute worms, is considered in the paper. The case of grinding external threads is discussed in detail. The profiling of tools for grinding the other helical surfaces is briefly described, with emphasis on the fundamental differences.

2 Grinding of an External Thread. Problem Statement

We consider the process of grinding an external thread with an abrasive wheel (Fig. 1). Tool 1 represents a rotation body. The tilt angle β of the tool spindle is the angle between the tool axis 2 and the axis 4 of blank 3. The distance between the axes is a_w.

As a rule, the tilt angle β is equal to the angle β_0 of the lifting thread helix (or to the helix angle β_0) on the average diameter d_2

$$\beta_0 = \arctan\frac{s}{\pi d_2}, \tag{1}$$

where s is the thread pitch. However, these angles may be different.

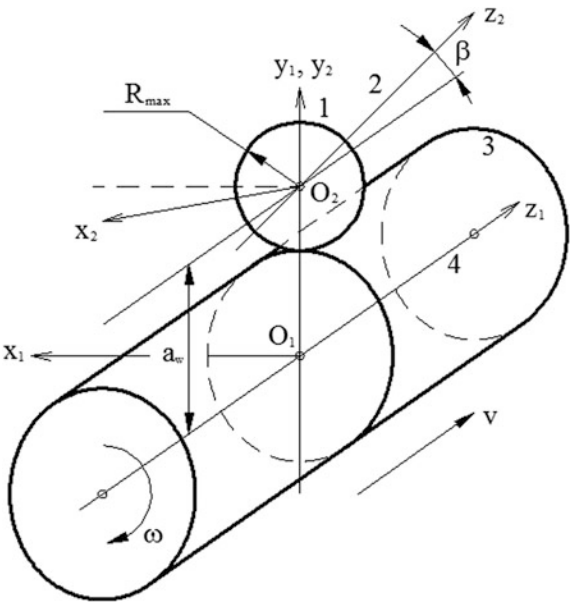

Fig. 1 Schematic representation of grinding the external single-thread

During processing, the blank performs a helical motion (Fig. 1). It consists of rotational movement about an axis at an angular velocity ω and translational movement along the axis of a linear velocity $v = p\omega$. Here, p is a helical parameter equal to

$$p = \pm\frac{s}{2\pi}. \tag{2}$$

The plus sign in Eq. (2) corresponds to the right-hand thread, and the minus sign is for the left-hand one.

Processing is carried out using the duplex method. Side clearances due to the thread on the bolt are not provided.

The problem is to build a tool surface for grinding the thread with the required accuracy.

The solution of the problem consists of several stages.

1. Description of the required profile in the axial section of space between the turns of the external helical thread.
2. Formation of the lateral surface of space between the turns of the external helical thread.
3. Determination of the axial section of the grinding wheel surface (synthesis).
4. Definition of the thread surface by simulating processing by a given grinding wheel (analysis).
5. Calculation of the error of thread processing.

3 Description of Mathematical Models for the Machining of the External Thread

3.1 Description of the Required Profile in the Axial Section of Space Between the Turns of the External Helical Thread

Different types of thread are characterized by the shape of the axial section of the thread. Here, we represent the most general description of the profile of any given thread. The contour of the axial-section (Fig. 2) is defined in the moving *Oxrz* system, which is rigidly connected to the blank. The *z*-axis is directed along the axis of the bolt. Coordinate axis *r* is perpendicular to the *z*-axis, and it passes through the apex A of the basic triangle ABC (Fig. 2). The sides AB and AC, respectively, are inclined at an angle α_1 and α_2. The base BC of the ABC triangle is equal to the thread pitch *s*. When viewed in a positive direction along the *z*-axis, the blank rotation is clockwise (Fig. 1).

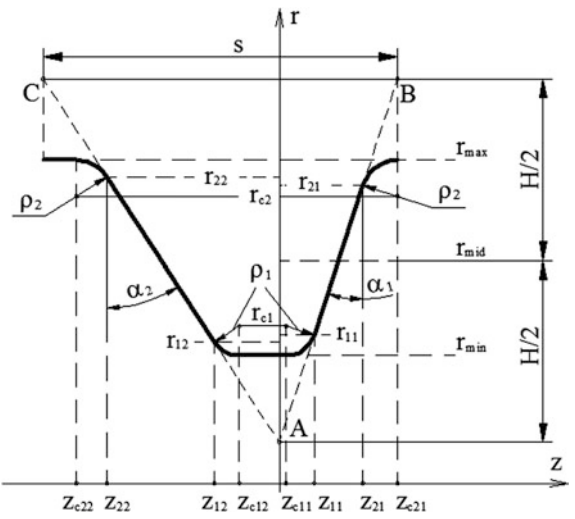

Fig. 2 Periodic part of the axial section of an arbitrary external thread

In the most general case, an axial section consists of several conjugated curves: two arcs of a circle of radius ρ_2 at the top, two inclined line segments with profile angles α_1 and α_2, two arcs of a circle of radius ρ_1 at the root of the thread, and the straight segment that represents the bottom of space between turns of the external helical thread. It should be noted that the thread profile may comprise only a portion of the above pairs of curves.

The radial section of the male thread (Fig. 2) is determined by the function

$$z_i(r) = \begin{cases} z_{1i} \pm (r - r_{1i}) \tan \alpha_i, & r_{1i} \le r \le r_{2i}; \\ z_{c1i} \pm \sqrt{\rho_1^2 - (r - r_{c1})^2}, & r < r_{1i}; \\ z_{c2i} \mp \sqrt{\rho_2^2 - (r - r_{c2})^2}), & r > r_{2i}. \end{cases} \tag{3}$$

We assume that on the left side of the thread (to the right in Fig. 2), the value of the z coordinate is greater than that on the right (left in Fig. 2). For the left side of the thread in Eq. (3), the upper sign and $i = 1$ are chosen. For the right side, the lower sign and $i = 2$ are chosen. The range

$$r_{min} \le r \le r_{max} \tag{4}$$

is the domain of the function $z_i(r)$.

3.2 Formation of the Lateral Surface of Space Between the Turns of the External Helical Thread

Let us consider a fixed right orthogonal Cartesian coordinate system $O_1x_1y_1z_1$ (Fig. 1). The axis z_1 coincides with the axis of the screw. The axis y_1 is directed along the line of the shortest distance between the axis z_1 of the blank and the tool axis of rotation in a direction from the first to the second axis. The mobile system $Oxrz$ (Fig. 3) performs a helical motion relative to the system $O_1x_1y_1z_1$. The position of the system $Oxrz$ is determined by the angle ζ of rotation. The angle is measured from the axis y_1. In the initial position (when $\zeta = 0$), the system $Oxrz$ coincides with the system $O_1x_1y_1z_1$.

The lateral surface of space between the turns of the external helical thread in the system $O_1x_1y_1z_1$ is a set of points with coordinates that are given by the relation

$$\mathbf{r}^*(r,\zeta) = \begin{bmatrix} x^* \\ y^* \\ z^* \end{bmatrix} = \begin{bmatrix} -r\sin\zeta \\ r\cos\zeta \\ z_i(r) + p\zeta \end{bmatrix}, \tag{5}$$

where the function $z_i(r)$ is defined by the relation Eq. (3).

3.3 Determination of the Axial Section of the Grinding Wheel Surface (Synthesis)

Let us consider a fixed right Cartesian orthogonal reference system $O_2x_2y_2z_2$, associated with the tool (Figs. 1 and 3). The origin of this system O_2 is displaced relative to the point O_1 in the positive direction of the axis y_1 by the distance

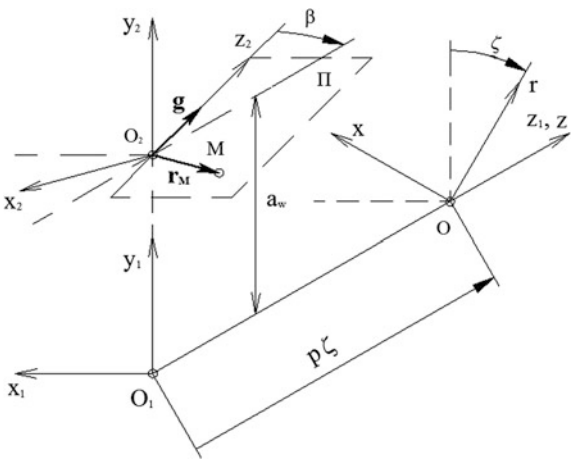

Fig. 3 Coordinate systems

$$a_w = r_{min} + R_{max},$$

where R_{max} is the radius of the grinding wheel. The axis z_2 coincides with the axis of rotation of the tool and is formed by rotating the axis z_1 at an angle β around the axis y_1. The axis y_2 coincides with the axis y_1.

A grinding wheel is a body of revolution with the axis z_2. We define an axial section of the grinding wheel.

The grinding wheel is tangent to the surface in Eq. (5) of the external helical thread along some curve L. During processing of the blank, the curve L is immovable in space. It represents the generatrix of the desired tool surface. The curve is defined by the relations [12]:

$$x = x^*(r, \zeta(r)); \quad y = y^*(r, \zeta(r)); \quad z = z^*(r, \zeta(r)). \tag{6}$$

The function $\zeta(r)$ is found from the following considerations. Two smooth surfaces at the point M of tangency have a common normal $\mathbf{n}$. Let us consider the plane Π (Fig. 3), which contains the tool axis and the point of tangency M. The normal $\mathbf{n}$ is located in the plane Π and intersects the tool axis z_2. Thus, a normal $\mathbf{N}$ to a plane Π is perpendicular to the vector $\mathbf{n}$, i.e.,

$$(\mathbf{n}, \mathbf{N}) = \mathrm{n_x N_x} + n_y N_y + n_z N_z = f(r, \zeta) = 0. \tag{7}$$

We define vectors in Eq. (7).

We define the vector $\mathbf{N}$ in the system $O_1 x_1 y_1 z_1$ as the vector product of two vectors located in the plane Π (Fig. 3). The first factor is the direction vector of the tool axis

$$\mathbf{g} = \begin{bmatrix} \sin\beta \\ 0 \\ \cos\beta \end{bmatrix}.$$

The second factor is the vector drawn from the point O_2 (0, a_w, 0) of the disk axis to the point M (x_1, y_1, z_1) of the external helical surface.

Then, the vector $\mathbf{N}$ can be represented as

$$\mathbf{N} = \mathbf{g} \times \mathbf{r}_M = \begin{bmatrix} N_x \\ N_y \\ N_z \end{bmatrix} = \begin{bmatrix} -\cos\beta(r\cos\zeta - a_w) \\ -\sin\beta(z_i(r) + p\zeta) - r\sin\zeta\cos\beta \\ \sin\ \beta(r\cos\zeta - a_w) \end{bmatrix}.$$

The normal $\mathbf{n}$ to the external helical surface is defined by

$$\mathbf{n} = \frac{\partial \mathbf{r}^*}{\partial \zeta} \times \frac{\partial \mathbf{r}^*}{\partial r},$$

where

$$\frac{\partial \mathbf{r}^*}{\partial \zeta} = \begin{bmatrix} -r\cos\zeta \\ -r\sin\zeta \\ p \end{bmatrix}; \quad \frac{\partial \mathbf{r}^*}{\partial r} = \begin{bmatrix} -\sin\zeta \\ \cos\zeta \\ \partial z_i/\partial r \end{bmatrix}.$$

By solving Eq. (7), one can obtain the angle $\zeta(r)$ for the given r. Then, using Eqs. (3), (5) and (6), we determine the coordinates of the point M of the curve L in the system $O_1x_1y_1z_1$.

The coordinates x_2, y_2, z_2 of the same point of the external helical surface in the system $O_2x_2y_2z_2$ are obtained using the relations

$$x_2 = x_1\cos\beta - z_1\sin\beta; \quad y_2 = y_1 - a_w; \quad z_2 = x_1\sin\beta + z_1\cos\beta. \tag{8}$$

The shape of the axial section of the wheel are defined as a function

$$z_2 = z_2(R(\zeta)), \quad R(\zeta) = \sqrt{x_2^2 + y_2^2}, \tag{9}$$

where $R(\zeta)$ is the distance from the axis of the grinding wheel to a point on the tool flank.

The flank of the grinding wheel can be obtained by rotating the axial section in Eq. (9) about the z_2 axis. We note that the grinding wheel has two flanks intended to process the left and right sides of the external helical surface.

The function of Eq. (9) is defined as a table

$$z_{2i} = z_2(R(\zeta(r_i))); \quad (i = 1, 2, \ldots, N),$$

where

$$r_i = r_{max} - (r_{max} - r_{min})/(N-1). \tag{10}$$

The solution of Eq. (7) is carried out for values of the parameter r that decreases from an initial value r_{max} to a final value r_{min} with a certain constant step.

The solution to Eq. (7) must satisfy the condition

$$R(\zeta(r_i)) \le R_{max} \tag{11}$$

at values of r_i belonging to the interval in Eq. (4). In order to avoid the self-intersection of points of the function $R(r)$, another requirement is imposed for the monotonous increase in R with a decrease in r

$$R(r_i) < R(r_{i+1}). \tag{12}$$

The tilt angle β in Eq. (7) is, in general, a freely pre-determinable parameter, but the flank of the grinding wheel cannot be obtained for any value of the angle β. This may be due to the following factors.

As an example, Eq. (7) has no solutions for some values of r_i in the interval in Eq. (4). The obtained tool contour has self-intersection points (the inequality in Eq. (12) is not true) and cannot be practically realized. A meaningless solution is possible in which a part of the obtained contour is located out of the circle $R = R_{max}$.

The search of the proper tilt angle β and construction of the generatrix L of the tool surface starts from the value obtained using Eq. (1).

Equation (7) is solved with respect to the parameter ζ at the decreasing values r_i that are defined by the relation in Eq. (10). If the root is not found at some $r_{i,}$ we decrease the value of β, and repeat construction of the generatrix L. If the root ζ at the current r_i exists, by means of Eqs. (8) and (9), the values of z_{2i} and $R(\zeta(r_i))$ are determined. If the inequality in Eq. (11) does not hold, the process of formation of the surface, and the process of searching for the tilt angle are completed. If the inequality in Eq. (12) is not accomplished for values of $r_{i,}$ corresponding to rounding of the thread base, then the curve L is complemented by the arc tangent to the already-constructed part of the curve and to the circle $R = R_{max}$ and the process is completed here. If the inequality in Eq. (12) is not true at a value r_i, which is greater than that mentioned above, after diminishing the β parameter, an attempt to construct the curve L is performed again from the very beginning.

In a case of the absence of top rounding by using the above algorithm, only the part of the surface of the tool is defined. This is the part which carries out a final processing of the surface of the blank (the very last layer of material is removed). However, the entire tool surface that is located in the space between threads must be of a proper shape. That is why we add a straight line segment to the curve, and a tangent to its end that corresponds to the minimum value of R. The segment ends at the point $R = a_w - r_{max}$.

3.4 *Definition of the Thread Surface by Simulating the Processing Using a Given Grinding Wheel (Analysis)*

To determine the surface of the external helical thread, we will use the same reference frames as that for formation of the tool surface.

Assume that the form of the flank of the grinding wheel in the system $O_2x_2y_2z_2$ is defined by means of functions $z_{2s}(R)$. The subscript s defines the flank of the circle ($s = 1$ corresponds to the right side, and $s = 2$ is for the left one). It is required that we determine the shape of the axial section of the screw by the plane $x = 0$ in the coordinate system $Oxrz$ as a function $z_s^{\circ}(r)$.

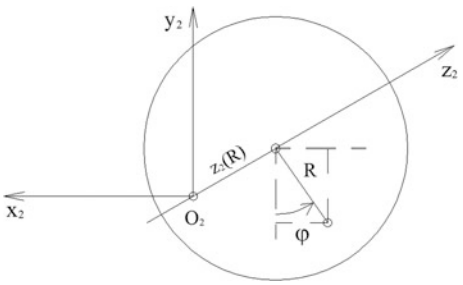

Fig. 4 Parameters of the flank of the grinding wheel

We write down the coordinates of an arbitrary point of the flank of the wheel in the $O_2x_2y_2z_2$ system as a function of the parameters φ and R (Fig. 4)

$$x_2 = -R\sin\varphi; \quad y_2 = -R\cos\varphi; \quad z_2 = z_2(R), \tag{13}$$

where R is the distance from the point to the circle axis; the angle φ is measured from the negative direction of the axis y_2 counterclockwise when viewed along the z_2 axis in the positive direction.

Transition to the fixed system $O_1x_1y_1z_1$ is described by relations

$$x_1 = x_2\cos\beta + z_2\sin\beta; \quad y_1 = y_2 + a_w; \quad z_1 = -x_2\sin\beta + z_2\cos\beta. \tag{14}$$

The coordinates of the tool surface point in the mobile system $Oxrz$ can be written as

$$x = x_1\cos\zeta + y_1\sin\zeta; \quad r = y_1\cos\zeta - x_1\sin\zeta; \quad z = z_1 - p\zeta. \tag{15}$$

Here, ζ is the parameter that defines the motion of the blank relative to the grinding wheel.

The relations in Eq. (15) are the parametric equations of a family of surfaces with the parameters R, φ, ζ. The envelope of this family is a helical surface. However, the theory of enveloping is inappropriate for describing the thread surface. This is due to the fact that the surface in Eq. (13) of the wheel is determined in a tabular form for a finite number of points by means of Eq. (11). Moreover, the envelope does not always coincide with the really machined surface. We will therefore use a more appropriate model [7–9] to find the thread surface that takes into account the process of material removal. We call this model a wrapping model.

The flank with the number s (s = 1, 2) of the grinding wheel is given in a tabular form in the system $O_2x_2y_2z_2$ by its values in grid nodes. The nodes are located in the interval

$$R_{min} \le R_{si} \le R_{max}. \tag{16}$$

The axial cross-section of the screw by the plane x = 0 is defined in the system of coordinates $Oxrz$ at points that are at an equal distance from each other

$$r_j^* = r_{min} + (j-1)(r_{max} - r_{min})/J, \quad (j = 1, 2, \ldots, J+1). \tag{17}$$

We define the relative positions of blank and tool on the set ζ_k (k = 1, 2, …, K) by values of the angle ζ that are located on the interval

$$-\zeta_{max} \le \zeta \le \zeta_{max}.$$

Here, ζ_{max} is the maximum angle of rotation of the blank, at which a point on the tool surface can be in the plane x = 0. The angle ζ_{max} can be determined by the cosine theorem of the triangle O_1O_2C (Fig. 5). The upper circle is the radial section of the tool; the lower circle is the radial section of the blank. It is proposed that the tilt angle β is small and that the elliptic section of the tool may be considered to be a circle.

Let A_k be the area of the tool section by the plane x = 0 in the position ζ_k . We call B_k the part of the area A_k that satisfies the condition in Eq. (16). The axial section of spacing between turns of the external helical thread (the space where the material is removed) is constructed as a union of all the areas B_k. If the boundaries of B_k are determined to be polygonal lines with vertices (r_j^*, z_{sjk}^*), then the searched-for coordinates z_{1j}° of the nodes on the left side of the thread are approximately equal to the maximum of quantities z_{1jk}^*.

$$z_{1j}^\circ = \max_k z_{1jk}^*.$$

Coordinates z_{2j}° of the nodes on the right side of the thread are approximately defined as follows:

$$\min_k z_{2jk}^*.$$

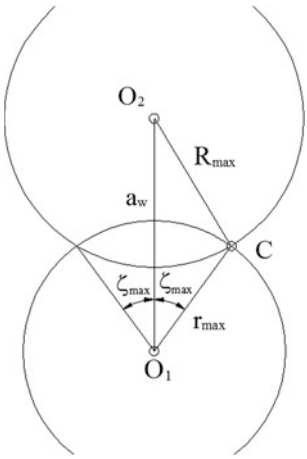

Fig. 5 The scheme for determining the maximum angle of rotation of the blank at the processing of the axial section O_1C by the grinding wheel

Computing coordinates z^*_{1jk} of the nodes is carried out as follows. Assume that the functions $z_{2s}(R)$ describing the flanks of the tool in the $O_2x_2y_2z_2$ system are defined at some points R_{si} by the values $z_{2si} = z_{2s}(R_{si})$. Let us consider a point of the grinding wheel surface with coordinates (R_{si}, z_{2si}). We denote (r_{sik}, z_{sik}) as the coordinates of the same point in the system $Oxrz$ obtained using Eqs. (13), (14) and (15) at an angle ζ_k of rotation. The angle φ necessary for transformation of the coordinates in Eq. (13) is determined by means of the equation $x = 0$. We substitute the expressions in Eqs. (13) and (14), as well as the values ζ_k and R_{si}, into the first of the equalities in Eq. (15). The obtained equation $C_1\cos\varphi_{sk} + C_2\cos\varphi_{sk} = C_3$ is easily solved analytically with respect to φ_{sk}, because the coefficients C_1, C_2, C_3 do not depend on unknown φ_{sk}. Then, using linear interpolation, we define the coordinates z^*_{sjk} of the nodes $r = r^*_j$. If

$$r_{sik} \le r^*_j \le r_{s,i+1k},$$

then

$$z^*_{sjk} = z_{sik} + (r^*_j - r_{sik})(z_{si+1k} - z_{sik})/(r_{si+1k} - r_{sik}).$$

3.5 Calculation of the Error of Thread Processing

Deviation of the obtained contour of an external helical thread from the desired contour is computed separately for the right ($s = 1$) and left ($s = 2$) sides of the thread. The deviation is defined as the difference of the two values. The first value is obtained by means of the wrapping model as a result of a simulation of thread processing. The second value is calculated using Eq. (3) for a given contour. Both values are determined at the points r^*_j specified by Eq. (17). There are two options: the point belongs to the straight part of the contour or the point belongs to the arc of a circle.

In the first case, the deviation Δ_{sj} of the point number j is computed along the axis z

$$\Delta_{sj} = \left| z^\circ_{sj} - z_s\left(r^*_j\right) \right|.$$

In the second case, the normal deviation is computed.

If the point j belongs to the arc of a circle ($r^*_j < r_{1s}$), then

$$\Delta_{sj} = \left| \sqrt{(r^*_j - r_{c1})^2 + (z^\circ_{sj} - z_{c1s})^2} - \rho_1 \right|.$$

If the point with the number j is on the rounding of the top of the thread ($r_j^* > r_{2s}$), then

$$\Delta_{sj} = \left| \sqrt{(r_j^* - r_{c2})^2 + (z_{sj}^\circ - z_{c2s})^2} - \rho_2 \right|.$$

The error of processing is considered to be the maximum deviation for all points.

4 Examples of Calculation of the External Thread

The technique for synthesizing and analyzing the male thread grinding process is implemented in the form of software modules.

Example 1 Let us consider the example of grinding of the exterior buttress thread with the parameters given in Table 1.

In this case, the tool surface is obtained at the initial value β_0 of the angle β that is obtained using the relation in Eq. (1). The inequalities in Eqs. (11) and (12) are valid for all points of the contour. The axial cross-section of the tool for grinding the buttress thread of Example 1 is shown in Fig. 6.

The external helical thread surface can be conventionally divided into two parts (Fig. 7). The first part is the working surface, intended for contact with the surface of the nut thread; the second part is the transient surface, which is located within the radial clearance.

The axial section of each flank of the tool consists of the part close to the straight line, which is for processing the working surface of the thread, and the area close to the arc of a circle intended for profiling the transient surface. The small circles on each flank of the tool divide the contour into parts that form the straight and arched parts of the thread contour.

Table 1 The values of input data for calculation of the exterior buttress thread

Parameter	Designation	Value
Outer screw diameter, mm	$d_{max} = 2r_{max}$	22.0
Basic effective diameter, mm	$d_2 = 2r_{mid}$	20.5
Core screw diameter, mm	$d_{min} = 2r_{min}$	18.529
Axial pitch, mm	s	2.0
Profile angle (left side of thread)	α_1	3°
Profile angle (right side of thread)	α_2	30°
Radius of thread root rounding, mm	ρ_1	0.249
Radius of thread tip rounding, mm	ρ_2	0.0
Diameter of grinding wheel, mm	$D_{max} = 2R_{max}$	400.0

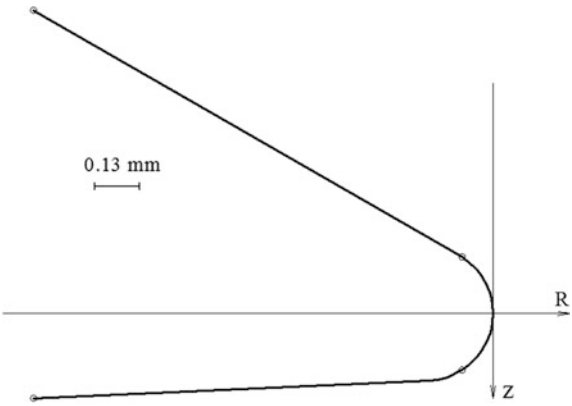

Fig. 6 Axial tool section for processing the outer buttress thread with a pitch s = 2 mm (Example 1)

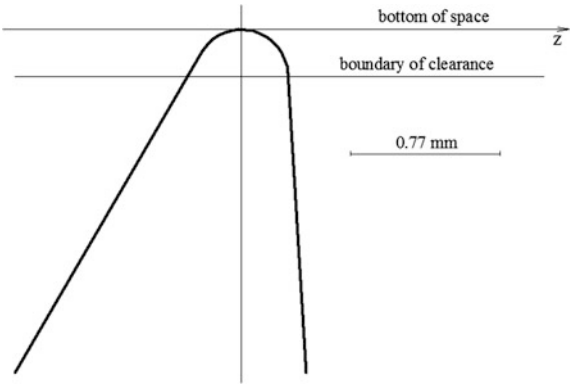

Fig. 7 Space of the buttress thread for Example 1

The results of the analysis show that the entire surface of the cavity can theoretically be made with an accuracy of 0.0001 mm.

Example 2 Let us consider a thread of the same type and diameter with a larger pitch s = 8 mm. We will not take into account the conditions in Eq. (11) and Eq. (12) at synthesis. In this case, the maximum value of the tilt β, which ensures the existence of roots in Eq. (7) at any point of the interval in Eq. (4), is equal to $0.8\beta_0$. The obtained form of the grinding wheel (Fig. 8) for processing of the side of the thread with the angle of the profile of 3º is unrealizable. This is due to the fact that the curve has two features. Firstly, the curve corresponding to the surface of the grinding wheel, for machining the surface of the thread profile angle of 3º (lower curve in Fig. 8), is outside the outer boundary of the instrument, i.e., the circumference $R = R_{max}$. This indicates that absolutely precise machining of the straight portion of the thread contour is impossible. Secondly, the axial section of the surface of the grinding wheel has a loop. To get a shape for the grinding wheel that may be realized, reconstruction of the profile of the grinding wheel (Fig. 9) is necessary.

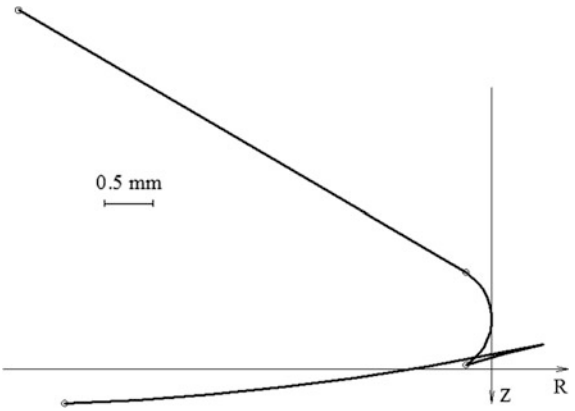

Fig. 8 Axial section of the tool for grinding the buttress external thread with the pitch s = 8 mm before reconstruction (Example 2)

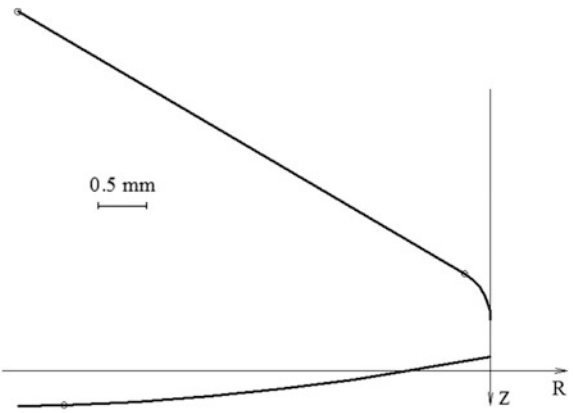

Fig. 9 Axial section of the tool for grinding the buttress external thread with the pitch s = 8 mm after reconstruction (Example 2)

Machining of the working part of the screw is accomplished by the surface of the wheel represented in Fig. 8 as two almost straight lines. Machining of the transient surface is accomplished by the surface of the wheel represented in Fig. 8 by a strongly curved line. Numerical experiments have shown that absolutely accurate processing of both parts of the surface (working part and transient surface) by one and the same tool is impossible. The tool surface for precise machining of the working surface on the top of the external helical thread may be constructed in the case of a relatively small tilt angle. Construction of the surface for processing the external helical thread in the vicinity of the root is possible at a larger tilt only. Moreover, the consecutive processing by means of two tools with different tilt angles is also impossible, because the subsequent processing corrupts the desired surface obtained after the previous processing.

The algorithm presented in item 3.3 is based on the idea that the precise machining of the working part of the surface is more important than the precise machining of the transient surface. By imposing the condition in Eq. (11), we will

remove the loop, together with the surface for machining of the transient surface of the screw. An edge is formed on the wheel. This generates a transient surface distinct from the one required. The maximum error of transient surface machining is 0.15 mm. A part of the tool surface that produces machining of the working external helical surface is also removed. That is why the maximum error of 0.022 mm of processing of the working surface occurs on the boundary of the radial clearance.

The defining domain of the surface of the grinding wheel intended for surface machining of the thread with a profile angle of 3º (the lower curve in Fig. 8) does not reach the boundary of the portion of the grinding wheel that must be located inside the cylindrical blank. The curve is extended to the left up to $R = a_w - r_{max}$ (compare Figs. 8 and 9).

Example 3 Let us consider machining of the buttress thread of the same diameter with the pitch $s = 5$ mm. In the case in which the inequalities in Eqs. (11) and (12) are not used in the process of tool synthesis, the obtained tool contour has a loop, but in distinction from the previous example, the entire contour is located inside the circle $R = R_{max}$. Also unlike the previous example, in this case, the tool for the precise machining of the working surface of the external helical thread may be formed. In the case in which the inequality in Eq. (12) is not true in the vicinity of the external helical thread root, we finish the process of forming the exact tool surface. The remaining part of the tool surface is assumed to be toroidal. This assumption provides the maximum processing error of the transient surface of 0.12 mm (Fig. 10).

Numerical experiments have shown that manufacturing of metric, round and Whitworth screws within the range defined by the Russian Standard GOST may be carried out without tilting the tool spindle. The entire side surface of the thread of the above-mentioned types can be processed with a high accuracy.

The working surface of the acme thread with a large pitch cannot always be manufactured with high precision (1 μm) without the use of the tool spindle

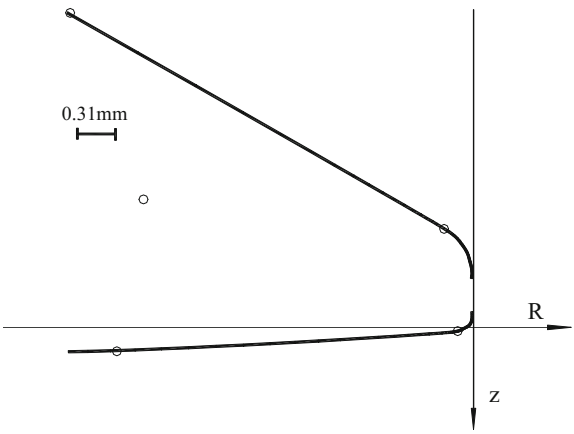

Fig. 10 Axial section of the tool for grinding the buttress external thread with the pitch s = 8 mm after reconstruction (Example 3)

inclination. Precision of machining of the fillet surface is usually very low. Application of the spindle tilt allows for making a theoretically precise work surface. The error in processing the transient surface is several hundredths of a millimeter.

For example, in the case of the acme thread of diameter of 24 mm with a pitch of $s = 8$ mm, the fillet surface may be obtained with an accuracy higher than 0.01 mm. The maximum deviation of the obtained profile from the theoretical thread profile occurs within the radial clearance. The working part of the flank, which is intended for contact with a nut surface, can theoretically be manufactured precisely.

Grinding a buttress thread is not possible without a tool spindle tilt. If the helical surface has a small pitch, when using the tilt, the tool working surface and rounds of the external helical surface can be manufactured with a theoretical error of less than 0.001 mm. Accuracy decreases with an increase of the thread pitch. The theoretical error of manufacturing of the working surface can reach hundredths of a millimeter. An error in processing of the transient surface can reach 0.1 mm or more.

5 Processing of the Internal Thread

The technology of grinding an internal thread is a little different from that for the male thread. The scheme of internal thread grinding, using a grinding wheel, is shown in Fig. 11. The same reference systems are used below, along with the same notations as in Sects. 2 and 3.

The task is to build a tool for grinding a surface of the female thread with the required accuracy at a minimum tilt of the tool axis.

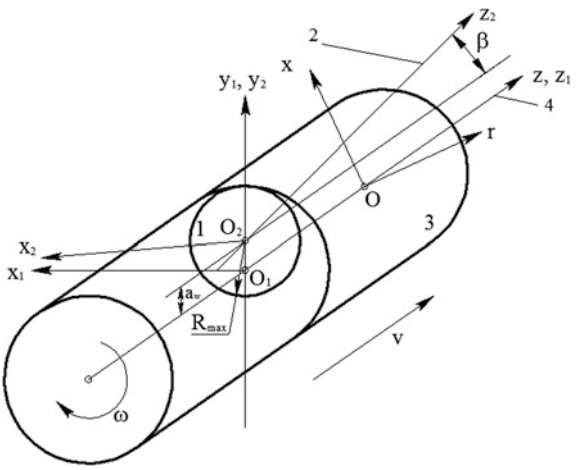

Fig. 11 Scheme of grinding the internal single-thread

The technique for determining the surface of the tool for grinding an internal thread is similar to the technique described above for machining of the external thread.

There is a difference in the description of the internal thread. This is shown in Fig. 11 and is defined by the function

$$z_i(r) = \begin{cases} z_{1i} \mp (r - r_{1i}) \tan \alpha_i, & r_{2i} \le r \le r_{1i}; \\ z_{c1i} \pm \sqrt{\rho_1^2 - (r - r_{c1})^2}, & r > r_{1i}; \\ z_{c2i} \mp \sqrt{\rho_2^2 - (r - r_{c2})^2}), & r < r_{2i}. \end{cases} \quad (18)$$

The signs and lower indexes are the same as those of the function in Eq. (3). The domain of the function in Eq. (18) is the interval in Eq. (4).

Calculation of the thread parameters, which are shown in Fig. 12 and are contained in Eq. (18), is presented in [10, 11, 13] for the most common types of thread.

The minimum angle tilt of the tool axis is defined as follows. The calculation starts with the angle $\beta = 0$. Often, however, machining at a small tilt angle β of the tool axis is not possible. This is due to the absence of the required profile or impossibility for practical implementation of the resulting profile. In these cases, the value of β is increased and further attempts are repeatedly made to build the tool contour.

With the aid of software modules developed for synthesis and analysis, the following dependences have been established. The minimum angle β, at which machining is possible, increases with the rise of the tool diameter D and the lead angle β_0, as well as with the decrease in the angle α of the thread profile. The most difficult for manufacturing are the acme and buttress threads with a large helix angle and a small angle of the thread profile located in deep orifices.

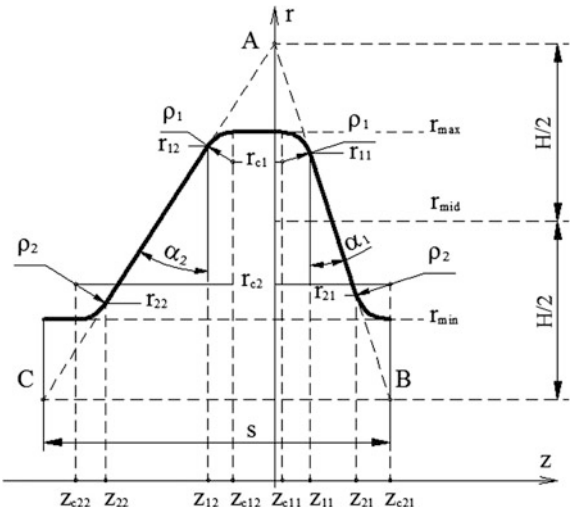

Fig. 12 The axial section of an arbitrary internal thread

6 Processing of Archimedean and Involute Worms

The axial section of the Archimedean worm can be described by the relation in Eq. (2). Therefore, algorithms for constructing the axial section of the grinding wheel and the axial section of the Archimedean worm are similar to those discussed above. The difference lies only in the parameters characterizing the size and shape of the screw that are used as input data.

The axial section of the involute worm, symmetric with respect to the r-axis, is somewhat different from the one described above with the aid of Eq. (2). It consists of two circular arcs and the axial section of an involute helicoid, and is defined by the following relation (Fig. 13) [2]:

$$z_i(r) = \begin{cases} \pm z_s \pm p(\tan\theta - \theta), & \theta = \arccos(r_b/r), \quad r_1 \le r \le r_2; \\ z_{c1} \pm \sqrt{\rho_1^2 - (r - r_{c1})^2}, & r < r_1; \\ z_{c2} \mp \sqrt{\rho_2^2 - (r - r_{c2})^2}, & r < r_2. \end{cases}$$

As was previously the case, the upper sign corresponds to the left side of the thread, and the lower sign corresponds to the right side. Here, r_b is the radius of the base circle; p is the screw parameter; and θ is the parameter defining the point of axial section of the involute helicoid.

Let us define the coordinate values r_1 and r_2 of the points of conjugation of the circular arcs and an axial section of the involute helicoid. For this purpose, we compose a system of equations to obtain the parameters φ_2 and θ_2 that define the upper point of conjugation.

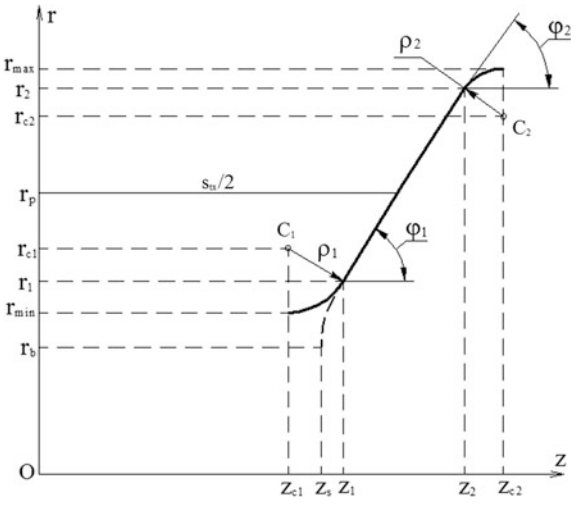

Fig. 13 The axial section of the left side of the involute worm thread

$$\frac{r_b}{\cos\theta} - [r_{\max} - \rho_2(1 - \cos\varphi)] = 0, \tag{19}$$

$$\tan\varphi = \frac{dr}{dz} = \pm\frac{r_b}{p\sin\theta}.$$

The second equation determines the tangent of the angle φ of inclination of the tangent to the axial cross-section of the involute helicoid within an interval r_1 $r \leq r_2$. To calculate φ_1 and θ_1 for the lower conjugation point of the parameters instead of Eq. (19), the following equation is used:

$$\frac{r_b}{\cos\theta} - [r_{\min} + \rho_1(1 - \cos\varphi)] = 0.$$

Coordinates (r_1, z_1) and (r_2, z_2) of the conjugation points are calculated using the relations

$$r = \frac{r_b}{\cos\theta}, \quad z = \pm z_s \pm p(\tan\theta - \theta).$$

The quantity z_s in Eq. (18) is a half-width of spacing on the base cylinder of the radius r_b. It is related to the axial pitch width of the space s_{tx} as follows:

$$z_s = s_{tx}/2 - p(\tan\theta_0 - \theta_0),$$

where $\theta_0 = \arccos(r_b/r_p)$ corresponds to the point of intersection of the helicoid with the pitch cylinder.

Coordinates z_{c1}, r_{c1} and z_{c2}, r_{c2} of the centers of the arcs are associated with the values of z_1, r_1, z_2, r_2 by relation

$$z_{c1} = z_1 - \rho_1\sin\varphi_1; \quad r_{c1} = r_{min} + \rho_1;$$
$$z_{c2} = z_2 + \rho_2\sin\varphi_2; \quad r_{c2} = r_{max} - \rho_2.$$

Solution of the problem of synthesis for the flank of the grinding wheel and analysis of the grinding process is done in the same way as for external threads.

7 Example of the Synthesis of the Profile of the Grinding Wheel for Machining an Involute Worm

Example 4 In Fig. 14, the radial section of the tool and the axial section of the involute worm are shown. Parameters are given in Table 2. Calculation of the worm geometry was carried out on the basis of Russian Standards GOST 19036-94 and GOST 19650-97. It is assumed that there is no backlash. Deviations from the

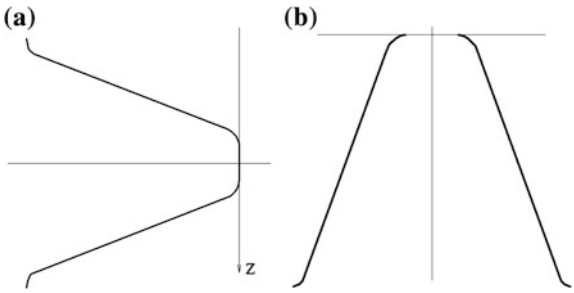

Fig. 14 Axial sections: of the tool (**a**), of the worm ZI (**b**) for Example 4

Table 2 Input data for calculation of the worm

Parameter	Designation	Value
Type of worm	ZA or ZI	ZI
Pitch, mm	m	5.0
Coefficient of pitch diameter, mm	q	8.0
Number of worm threads	z_1	1
Helical parameter, mm	p	2.5
Pitch profile angle in axial (for ZA) or normal (for ZI) section	α_n	20° 0′ 0″
Lead angle on pitch (for ZA) or base (for ZI) cylinder	γ_b	21° 10′ 56″
Outside tread diameter, mm	$d_a = 2r_{max}$	50
Bottom diameter, mm	$d_f = 2r_{min}$	28
Radius of pitch cylinder, mm	r_b	6.4516
Radius of fillet curve, mm	ρ_{f1}	1.0
Radius of top rounding, mm	ρ_2	0.25
Diameter of grinding wheel, mm	D_{max}	400.0
Chordal thread thickness, mm	s_{a1}	7793

required working surface are negligible. They are caused, apparently, by the interpolation errors at simulation of grinding. The maximum deviation of the fillet surface and the rounding of the thread top are 0.01 and 0.005 mm, respectively.

8 Conclusion

The technique described in the paper allows for making an informed choice about grinder setting and tool parameters for the machining of various types of helical surface.

The software modules implementing the presented methods are used in the grinding machine MSH520 model by Machine-Tool Plant JSC “MSZ-Salut”.

References

1. Kosarev, V., Grechishnikov, V., Dymov, M.: Defining the profile of the original surface of the tool in the processing of internal threads tool with planetary motion. STIN **3**, 28–32 (2011). (in Russian)
2. Litvin, F.: Theory of Gearing. Fizmatgiz, Moscow (1960). (in Russian)
3. Litvin, F., De Donno, M., Lian, Q., Lagutin, S.: Alternative approach for determination of singularity of envelope to a family of parametric surfaces. Comput. Methods Appl. Mech. Eng. **167**, 153–165 (1998)
4. Ljukshin, V.: Theory Screw Surfaces in the Design of Cutting Tools. Moscow, Mechanical Engineering (1968) (in Russian)
5. Sandler, A., Lagutin, S., Gudov, E.: Longitudinal contact localization in worm gears. Russ. Eng. Res. **34**, 480–486 (2014)
6. Sandler, A., Lagutin, S., Gudov, E.: Theory and Practice of Production of the General Type Worm Gears. Educational and Practical Guide. Moscow-Vologda, Infra-Engineering (2016) (in Russian)
7. Sheveleva, G.: Theory of Generation and Contact of Meshing of Moving Bodies. Moscow, Stankin (1999). (in Russian)
8. Volkov, A.: Methods for identifying undercutting in bevel and hypoid gears with circular teeth. Prob. Mech. Eng. Reliab. Mach. **4**, 66–74 (2000). (in Russian)
9. Volkov, A., Medvedev, V.: Designing and Technological Calculations of Bevel Gears with Circular Teeth. Tutorial. Moscow, Publishing house of the MSTU "STANKIN" (2007) (in Russian)
10. Volkov, A., Gazizov, A., Dzyuba, V., Medvedev, V.: Grinding of the inner thread without tilt of the tool spindle. J. Mach. Manuf. Reliab. **43**(5), 422–428 (2014)
11. Volkov, A., Gazizov, A., Medvedev, V.: Grinding of long holes with the screw surface. Vestnik nauchno-tehnicheskogo razvitija **1**, 16–24 (2015). (in Russian)
12. Volkov, A., Gazizov, A., Medvedev, V.: Substantiation of possibility external thread grinding on CNC Machines without Tilting the Tool Spindle, vol. 1, pp. 8–13. Vestnik MSTU "STANKIN" (2016) (in Russian)
13. Volkov, A., Gazizov, A., Grechishnikov, V., Medvedev, V.: Grinding of Single-pass Internal Thread by Abrasive Wheel on CNC Machines, vol. 3, pp. 49–53. Vestnik MSTU "STANKIN" (2016) (in Russian)

Practice of Design and Production of Worm Gears with Localized Contact

E. Trubachev, T. Savelyeva and T. Pushkareva

Abstract The paper considers the mathematical model, the main idea and examples of the practical application of a new approach to the design and production of worm gears with localized contact. Features of design for special and series worm gears under various limitations are distinguished; recommendations on the choice of parameters are given.

Keywords Worm gear · Hob · Fly-cutter · Gear design · Contact localization

1 Introduction

One of the most important results of applying our developed method for localized contact synthesis in worm-type gears [9] turned out to be an abrupt decrease in the range of expensive hobs used in diversified production of worm and spiroid gears [1, 6]. This presented an opportunity for a rather simple and effective solution to practical problems for production of both series and non-series (special) worm gears. A great number of such solutions appeared over the course of the last decade at the Institute of Mechanics of Kalashnikov Izhevsk State Technical University and from within the innovative production enterprise "Mechanik" Ltd. This deserves, in our opinion, an overview of the accumulated experience, since similar works are also vital for other enterprises that produce worm gears [3, 5].

E. Trubachev (✉) · T. Savelyeva · T. Pushkareva
Institute of Mechanics, Kalashnikov Izhevsk State Technical University, Izhevsk, Russia
e-mail: truba@istu.ru

V. Goldfarb et al. (eds.), *Advanced Gear Engineering*,
Mechanisms and Machine Science 51, DOI 10.1007/978-3-319-60399-5_16

2 Idea and Algorithm of the Design Method

The method for analysis of machine-tool meshing parameters for generation of worm-type gearwheel teeth by means of a helicoid generating surface has been proposed in [9]. Later, it became the foundation for development of the algorithm [8] for spiroid and worm gear design on the basis of applying the assigned gear cutting tool (in the important particular case, the standard one). The scheme shown in Fig. 1 essentially corresponds to this algorithm; however, we further assume that it can also be applied to the case in which tool parameters are not assigned or are not completely determined.

The main idea of the method implies that the geometric parameters of the generating worm and its arrangement with respect to the gearwheel blank are selected in accordance with the conditions of:

– meshing of three surfaces [4], that is, the conjugated surfaces of the worm and the gearwheel and the desired generating surface at arbitrarily assigned design points:

$$\begin{aligned} &\mathbf{n} \times \mathbf{v}_{12} = \mathbf{n} \times (\mathbf{v}_1 - \mathbf{v}_2) = 0, \\ &\quad \Rightarrow \mathbf{n} \times (\mathbf{v}_0 - \mathbf{v}_1) = \mathbf{n} \times \mathbf{v}_{01} = 0, \\ &\mathbf{n} \times \mathbf{v}_{02} = \mathbf{n} \times (\mathbf{v}_0 - \mathbf{v}_2) = 0, \end{aligned} \tag{1}$$

where $\mathbf{n}$ is the common normal to three pointed surfaces, $\mathbf{v}_{0(1,\ 2)}$ are velocities of their motion in meshing, and $\mathbf{v}_{12}$, $\mathbf{v}_{02}$ and $\mathbf{v}_{01}$ are relative velocities of surfaces.

Here and further on, indices $_0$, $_1$ and $_2$ are related to the generating worm, the operating worm and the gearwheel, respectively; and indices $_R$ and $_L$ relate to parameters of the right and left flanks of teeth and threads and their meshing.

– constancy of the pitch and profile of surfaces of the operating and generating worms-helicoids, for which the following relations (invariant with respect to the choice of the coordinate system) are valid [10]:

$$\tan\ \gamma = -\frac{\mathbf{n} \cdot \mathbf{e}_t}{\mathbf{n} \cdot \mathbf{k}}, \tag{2}$$

$$\tan\ \alpha_x = -\frac{\mathbf{n} \cdot \mathbf{e}_r}{\mathbf{n} \cdot \mathbf{k}}, \tag{3}$$

where α_x is the axial angle of the helicoid profile, γ is the lead angle for its pitch line, and $\mathbf{e}_t$, $\mathbf{e}_r$ and $\mathbf{k}$ are the unit vectors of the tangential, radial and axial directions with respect to the axis of the helicoid.

The system composed of Eqs. (1)–(3) has a rather simple analytic solution [9] in which the preliminary assigned parameters are the machine-tool cross angle Σ_0,

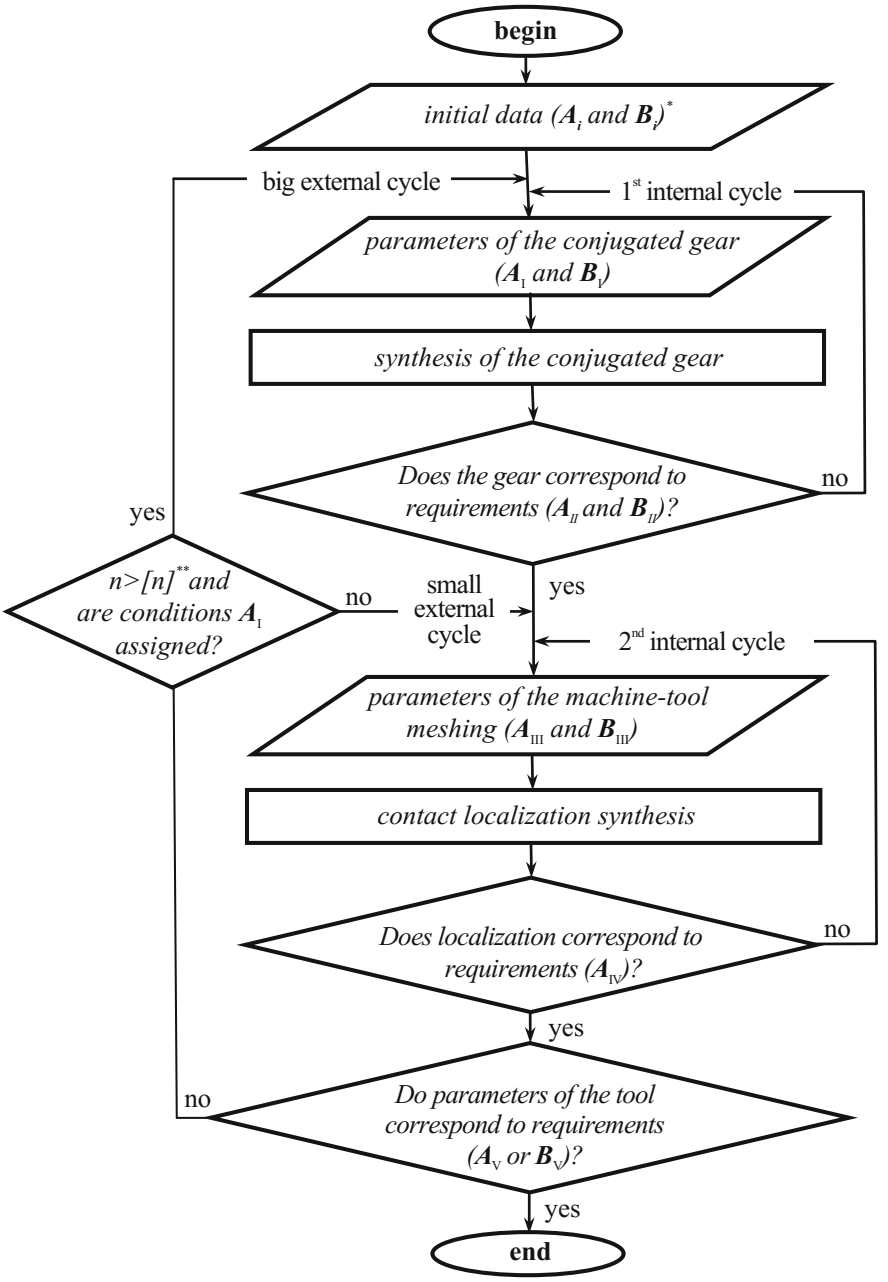

Fig. 1 Algorithm of the worm gear design when applying the assigned gear-cutting tool. *$\boldsymbol{A_i}$ are limitations-inequalities, $\boldsymbol{B_i}$ are limitations-equalities, **n is the number of iterations for a small external cycle

the number of threads z_0 and the axial module m_{x0} of the generating worm, and the parameters obtained in accordance with conditions (1)–(3) are the center distance in the machine-tool meshing a_{w0}, pressure angles $\alpha^1_{x0R,L}$ and the pitch diameter d_0 of the generating worm.

Figure 1 presents the limitations for optimization: they are the groups of parameters $\boldsymbol{A_i}$ and $\boldsymbol{B_i}$, which are related to the following ith steps of the design:

1. Input (assignment) of parameters of the conjugated gear.
2. Evaluation of conformity for the conjugated gear to the assigned requirements.
3. Input of initial (assigned) parameters for the machine-tool meshing.
4. Evaluation of conformity to the assigned requirements for localized contact.
5. Evaluation of conformity to the available (required) one for the generating worm.

3 Limitations and Components of the Target Function

Let us consider the essence and several examples of limitations $\boldsymbol{A_i}$ and $\boldsymbol{B_i}$ assigned at statement of the design problem and considered at different steps. In the first step, limitations $\boldsymbol{A}_{\mathrm{I}}$ and $\boldsymbol{B}_{\mathrm{I}}$ affect the following parameters:

– the gear ratio u_{12} (allowable limits of its variation or the strictly assigned value);
– the outer diameter of the worm d_{a1} and the maximum diameter of the gearwheel d_{ae2}, the center distance a_w and the cross angle Σ (limitations of the casing space, overall dimensions of blanks, possibility of assembly of the worm unit, and worm rigidity);
– the axial module m_{x1} of the worm (can be limited by rational values of the addendum modification factor of the worm $x = f(m_{x1})$ and the standard row of modules).

In the case when it is necessary to cut only the gearwheel that is conjugate with the existing worm, the limitations imposed on all worm parameters are related to the type $\boldsymbol{B}_{\mathrm{I}}$, that is, they have to be equal to those assigned.

In the second step, we need the correspondence of the analyzed conjugated gear to the assigned requirements (limitations $\boldsymbol{A}_{\mathrm{II}}$): level of the efficiency and load-carrying capacity (torques $[T_2]$ allowable in accordance with various criteria, fitting the limitation of the absence of undercutting and pointing at machining of gearwheel teeth and undercutting at the grinding of worm threads. The version of maximization of η and $[T_2]$ is also possible, that is, they are included in the target function of optimization. Iterations at the 1st internal cycle (Fig. 1) are subjected to meeting these requirements.

In the third step, limitations $\boldsymbol{A}_{\mathrm{III}}$ and $\boldsymbol{B}_{\mathrm{III}}$ set the allowable values of the machine-tool center distance a_{w0}, the machine-tool cross angle Σ_0 and the number of threads z_0 of the generating worm.

In the forth step, local and non-local specifications are the basis for evaluation of the geometry of the modified surface of the gearwheel teeth and correctness of the design parameters of the machine-tool setting. The following limitations $\boldsymbol{A}_{\mathrm{IV}}$ are considered here:

- allowable maximum values of the longitudinal and profile modification of teeth (corresponding to the allowable concentrations of the load and the tooth-to-tooth error at transfer of meshing which appear due to contact localization);
- allowable minimum values of the longitudinal and profile modification of teeth (corresponding to the allowable sensitivity of the meshing to the action of manufacture and assembly errors);
- completeness of surface profiling at generation (this is practically always related to the ratio of diameters and lengths of the operating and generating worms and the heights of their thread profiles);
- desirable distribution of the modification field along the tooth (contact localization on a definite area of the tooth);
- absence of pointing or undercutting of the tooth of the worm gearwheel or undercutting of the thread of the generating worm;
- absence of pointing of the tool that produces the generating worm.

Parameters of contact localization can also be components of the target function of optimization. In order to fulfill the conditions $\boldsymbol{A}_{\mathrm{IV}}$ or at optimization, iterations at the 2nd internal cycle (Fig. 1) are made.

The fifth step determines the application of the existing gear-cutting tool or, regarding the algorithm, the evaluation of the correspondence of the generating worm parameters to those chosen from a certain set of discretely assigned values, that is, limitations $\boldsymbol{A}_{\mathrm{V}}$ or $\boldsymbol{B}_{\mathrm{V}}$. These parameters are: the number of threads z_0, the axial module m_{x0}, the length of the cutting part b_0, the pitch diameter d_0, pressure angles $\alpha_{x0R,L}$, curvature radii $\rho_{x0R,L}$ and factors of the height h_0^* and thickness s_0^* of thread profile.

The set and type of limitation ($\boldsymbol{A}_{\mathrm{V}}$ or $\boldsymbol{B}_{\mathrm{V}}$) depends significantly on the choice of method for implementation of the generating worm, that is, the application of a fly-cutter or a hob for gear-cutting. In the first case, limits on the possible correction of parameters are determined by the tool rigidity; and they are limited, for example, by a wish to apply the existing mandrel with diameter $d_{mandrel}$ for the fly-cutter. When the existing hob is applied, parameters are assigned unambiguously, and their required values are obtained at the iterative mode of the design process. As is seen in Fig. 1, the corresponding external cycles can imply a return to steps I (big external cycle) or III (small external cycle) of assigning the parameters of the operating or machine-tool meshing. As a rule, during the design process, the version of the return to step III is first implemented. Then, as the possibilities of achieving the required or optimal solution have been exhausted, we return to step I, accordingly.

Let us further consider the examples of implementation of the analysis for practical cases, differing by the purpose of gears, the degree of responsibility and,

therefore, the assignment of the target function of optimization and the set of limitations $\boldsymbol{A_i}$ and $\boldsymbol{B_i}$.

4 Simple Case: Gear Parameters Are Strictly Assigned

The simplest design situation is that for the case in which it is necessary to meet the limitations $\boldsymbol{B}_\mathrm{I}$ of the first step focusing on producing a special and relatively simple tool—a fly-cutter. This situation appears when there is no available hob with somewhat similar parameters and gear parameters cannot be changed significantly. The typical case is the production of responsible repair pairs for complex manufacturing equipment (there is even a simpler case in which the repair problem is solved by substituting the whole gearbox, but it will not be considered here). Note that a delusion can appear here: if the situation is simple, one should always tend to reduce the design process to it. However, it is simple only from the point of view of design; and in production, it can lead to difficulties that are sometimes irresistible. These difficulties are related to the relatively low accuracy and productivity of the method for gear-cutting by means of the fly-cutter.

In this case, the design process is generally traditional. First, a conjugate meshing is designed in accordance with the assigned, and usually strict, limitations. Sometimes, the design is reduced to the checking process when the gear to be designed, in fact, repeats the prototype being replaced (often after interpretation of the specimen without a drawing). Furthermore, the machine-tool meshing with optimization of localized contact follows. Perhaps the main feature here is the accounting for conditions for application of the already available range of mandrels for fly-cutters.

Let us consider a number of gear designs for this typical case. Table 1 presents the main parameters of gears cut by fly-cutters reproducing single-thread worms at gear generation.

In all cases, parameters of the conjugated gear have been restricted by limitations of type $\boldsymbol{B}_\mathrm{I}$ (their equality to the assigned ones). While maintaining the initial parameters at the first stage of design and, therefore, meeting the limitations,

Table 1 Examples of gears for the case of a strictly assigned operating meshing

№	a_w, mm	u_{12}	m_{x1}/m_{x0}, mm	Σ_0	d_1/d_0, mm	$d_{mandrel}$, mm
1.	33	24:2	1.5/1.498	87.00	30/33.47	25.0
2.	64	30:2	3.15/3.105	85.00	33.7/35.40	22.8
3.	70	30:1	3.5/3.495	89.88	35/35.76	22.8
4.	164	45:1	6.0/6.0	89.85	58/60.14	44.0
5.	180	62:2	5.0/4.895	85.80	50/52.12	28.0
6.	180	40:1	6.3/6.3	89.90	100.8/110.29	95.0

the $\boldsymbol{B}_{\text{II}}$ type of limitations (keeping the operation performances) eliminates additional iterations at the big external and the 1st internal cycles (Fig. 1).

In this case, localized contact should be optimized. The profile localization is provided by the corresponding selection of the profile curvature radii for the worm ρ_{x1} (Fig. 2b, d) or the tool ρ_{x0} (Fig. 2a, c, e, f). When applying the fly-cutter, it is possible to implement profile modification by any of these versions by choosing the most reasonable one from the manufacturing and structural points of view with regard to this gear. When applying the hob, the only version is, as a rule, the selection of the curvature for the worm profile at keeping the initial profile of the tool. The value of the profile curvature is taken with account of limitations $\boldsymbol{A}_{\text{II}}$ and $\boldsymbol{A}_{\text{IV}}$.

Longitudinal localization is provided by variation of the cross angle at machining Σ_0 and/or the axial module of the generating worm m_{x0}. Since these variables affect the design parameter d_0, one should account for limitations-inequalities $\boldsymbol{A}_{\text{V}}$ for its choice related to the available mandrel (or the desirable one, for instance, in accordance with layout considerations) for the cutter by applying the small external cycle of iterations. Thus, for samples, shown in Table 1, one of the design conditions is the application of available mandrels, including, for example, one and the same mandrel for gears № 2 and № 3.

Note that the equal degree of modification can be obtained at various combinations of m_{x0} и Σ_0 (correspondingly, for significantly different d_0). Let us give some recommendations for the choice of these parameters.

Intervals of acceptable combinations of parameters m_{x0} and Σ_0 are narrow, and the relation between parameters of the machine-tool setting and parameters of the modification fields is not obvious in the general case. Therefore, the first approximation at the iteration mode often determines the convergence to the optimal solution and, consequently, the time needed to find it. In the simplest case, the machine-tool meshing which is identical to the operating one is chosen at the first approximation. Usually, it makes sense when the numbers of threads of the operating and generating worms are equal to each other, and the difference between the diameter of worm roots and the diameter of the available mandrel is relatively small. The required longitudinal modification can be provided here by variation of one of the pair of the above-mentioned parameters, which is convenient for the setting of the gear-hobbing machine (the module taken from the range of standard values or the orthogonal machine-tool meshing). The example can be gears № 4 and № 6 in Table 1: when designing their machine-tool settings, the required localization and limitations of the mandrel diameter are provided by variation of the cross angle Σ_0 only.

Limits of the reasonable variation of the value Σ_0 mainly depend on the difference between the numbers of threads of the operating and generating worms $\Delta z = z_1 - z_0$. For $\Delta z = 0$, such a range is within the limits from 87.5° up to 91°; and for $\Delta z = 1$, it is from 84° up to 87.5°. As a rule, a higher level of tooth modification corresponds to the smaller values of the machine-tool cross angle and the module of the generating worm.

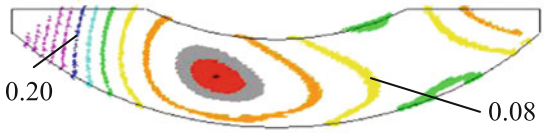

(a) worm ZK; ρ_{x0}= –190 mm; $\Delta z = 1$;

(b) ρ_{x1}=150 mm; ρ_{x0}=∞; $\Delta z = 1$;

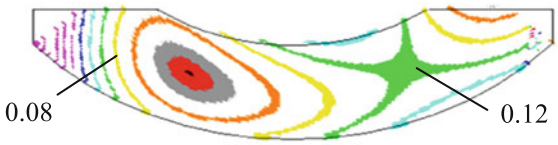

(c) worm ZK; ρ_{x0}= –250 mm; $\Delta z = 1$;

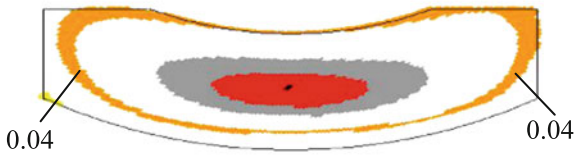

(d) ρ_{x1}=150 mm; ρ_{x0}=∞; $\Delta z = 0$;

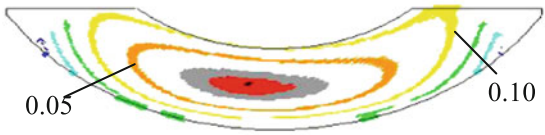

(e) worm ZK; ρ_{x0}= –200 mm; $\Delta z = 0$;

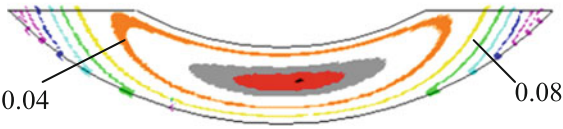

(f) worm ZK; ρ_{x0}= –200 mm; $\Delta z = 0$;

Fig. 2 Modification fields for gears: **a** № 2; **b** № 1; **c** № 5; **d** № 3; **e** № 4; **f** № 6; « 0.04 » are modification levels, mm

Distribution of modifications along the gearwheel tooth length is often unacceptably asymmetrical relative to the design point. Asymmetry essentially depends on the difference between the numbers of threads for the operating and generating worms (for instance, versions a, b, c in Fig. 2 for $\Delta z = 1$ and versions d, e, f in Fig. 2 for $\Delta z = 0$). An extremely large modification at the tooth face end from the worm thread entering the mesh can be corrected by shifting the design point to this face end: at first approximation, it is 3–5% of the total length of the tooth.

As for the considered simple case, iterations are concentrated at the second internal and small external cycles (Fig. 1), without addressing the first one and organizing the big external cycle of iterations, which is essentially simplifying the search for the solution.

5 More Complex Case: Application of the Existing Hob

In case of applying the hob from the range of existing ones, it is necessary to provide the conformity for its design parameters to the assigned ones. This is achieved through introduction of iterations at the big external cycle (Fig. 1) with variation of parameters of the first step, thus leading to additional iterations at the 1st internal cycle, since it is required that we provide the values of operation parameters within the range allowable in accordance with limitations $\boldsymbol{A}_{\mathrm{II}}$.

Let us consider certain features of the design procedure for such a case by example of the gears having the main parameters given in Table 2. Note that gearwheels for all gears have been cut with single-thread hobs. Moreover, hobs specified by the Russian standard GOST 9324–80 and intended for machining involute spur and helical gearwheels have been used for cutting gears № 8, № 9 and № 10.

In the fifth step of the design procedure, after searching for the first approximation with regard to the above-mentioned recommendation and optimizing at the 2nd internal cycle (Fig. 1), the parameters of the generating worm can take values different from those assigned in accordance with limitations $\boldsymbol{B}_{\mathrm{V}}$. Differences between the obtained design and the required parameters of the tool involve the values of discrepancies which should be accounted for at the following cycle of

Table 2 Examples of gears designed in accordance with the assigned hobs

№	a_w, mm	$u^{*}_{12\ initial} \rightarrow u_{12\ accepted}$	$m_{x1\ initial}/m_{x0} \rightarrow m_{x1\ accepted}$, mm	$d_{1\ initial}/d_0 \rightarrow d_{1\ accepted}$, mm	$[\alpha_{x0L/R}] \rightarrow \alpha_{x1L/R}$, °	Σ_0, °
7.	52.5	28:1 → 31:1	2.5/2.5 → 2.46	35/35 → 28	20.18 → 17.5	89.3
8.	60.0	24:2 → 24:2	2.5/2.5 → 2.5	60/74 → 60	20.44 → 20.0	87.2
9.	96.4	22:1 → 44:2	6.3/3.0026 → 2.963	50.4/72.5 → 58	20.00 → 17.0	86.8
10.	103.5	33:1 → 33:1	4/4 → 4.005	75/79.1 → 75	20.01 → 19.8	89.8

*The subscript $_{initial}$ designates the initial values of parameters (parameters of a reference gear), the subscript $_{accepted}$ designates the parameters accepted after the design procedure

iterations (big external cycle—Fig. 1). For this purpose, the corresponding corrections are introduced to the values of the homonymic parameters of the operating worm [8] assigned at step I with account for limitations $\boldsymbol{A}_{\mathrm{I}}$:

$$\Delta m_{x0j} = m_{x0j} - [m_{x0}],\ m_{x1j+1} = m_{x1j} + \Delta m_{x0j}, \tag{4}$$

$$\Delta \alpha_{x0R,Lj} = \alpha_{x0R,Lj} - \left[\alpha_{x0R,L}\right],\quad \alpha_{x1R,Lj+1} = \alpha_{x1R,Lj} + \Delta \alpha_{x0R,Lj}; \tag{5}$$

$$\Delta s^*_{0j} = s^*_{0j} - \left[s^*_{0j}\right],\quad s^*_{1j+1} = s^*_{1j} + \Delta s^*_{0j}. \tag{6}$$

Here, j is the number of iteration of the big external cycle, $\Delta m_{x0}, \Delta \alpha_{x0R,Lj}, \Delta s^*_{0j}$ are the values of discrepancies, respectively, for the module, pressure angle and thread thickness factor for the generating worm; and the values in square brackets are assigned in accordance with limitations $\boldsymbol{B}_{\mathrm{V}}$. When varying the parameters of the first step, provision of the required strength, rigidity and durability (providing limitations $\boldsymbol{A_2}$) is also evaluated, thus increasing the number of iterations as compared to simple cases.

Similar to simple cases, for a more complex case of applying the existing hob, it is possible to obtain the required tooth modification by correction of only one of two parameters, that is, the module of the operating worm m_{x1} while maintaining the orthogonality of the operating and machine-tool meshing or only machine-tool cross angle Σ_0 (gear № 8 in Table 2) while maintaining the same modules of the worm and hob (for example, the standard ones).

Dr. Eng. S. A. Lagutin [4] was the first to pay attention to the possibility of applying the same modules for the operating and generating worms at localized contact synthesis in the worm gear. He found a simple relation between the parameters of the worm and hob for this important and convenient case. However, in the general case of gear design, it is necessary to search for the combination of Σ_0, m_{x1}, d_1 and the position of the design point presenting an optimal picture of tooth modification. It is evident from the information given in Table 2 and Fig. 3 that the above-mentioned recommendations on the choice of the design point position, machine-tool cross angle Σ_0 and relations between modules of the operating and generating worms are also generally valid for more complex cases.

Providing the level of tooth modification within the interval $(0.02–0.05)m_{x1}$ can require a correction of parameters d_1, m_{x1}, α_{x1}, and s^* and, in certain cases, of the gear ratio u_{12}. Such a correction inevitably leads to a certain change in the operation parameters of the gears, as compared to the initial ones available prior to optimization synthesis. Both positive and negative effects are possible here, and this circumstance should be given due attention. However, in most cases, the correction is acceptable. Thus, in the worst cases for gears shown in Table 2, the decrease in efficiency did not exceed 1 to 2%, and that of torques, the result of contact failures of teeth, was under 10%, which turned to be acceptable; application of the existing tooth cutting tool gave an essential economy.

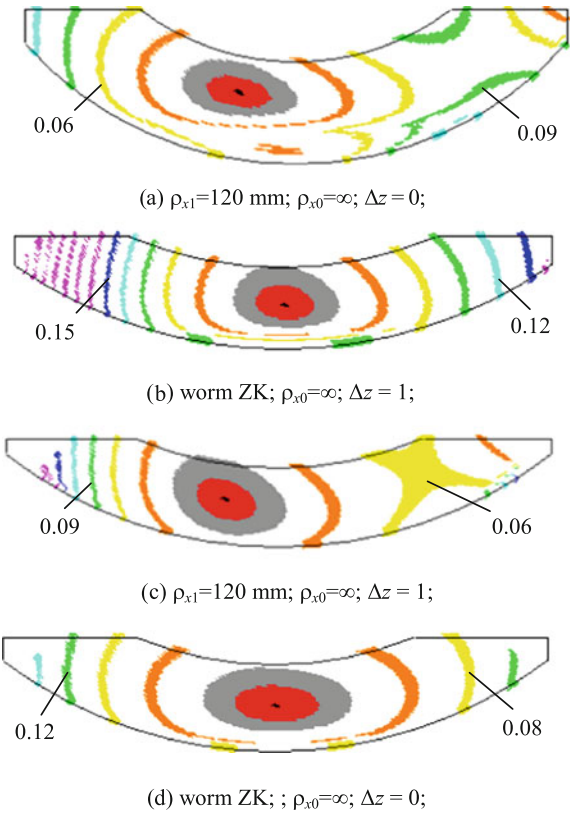

Fig. 3 Modification fields for gears: **a** № 7; **b** № 8; **c** № 9; **d** № 10

6 Features of Design for Highly Responsible Gears

A number of highly responsible gears which were designed and introduced into series production required a very thorough and versatile analysis. Let us consider two specific cases.

A heavy-loaded low-speed gear. We paid great attention in our works on this theme (for instance, [2]) to a special selection of parameters of the non-orthogonal worm gear, when the worm gearing becomes similar to the spiroid one in accordance with its properties: contact ratio (Fig. 4), arrangement and path velocity of contact lines, sensitivity to the action of errors. Consequently, it becomes more suitable for application in low-speed (rotational frequency of the output shaft does not exceed 200 rpm) and heavy-loaded (contact stresses are 1000–2000 MPa) drives for pipeline valves.

We have designed a range of such non-orthogonal worm gears for the gearbox of the torque of 64,000 Nm (Σ = 75°, a_w = 260 mm) [7]. In all gears, the contact has

been localized in both length and height; and gearwheels have been cut by standard involute gear hobs. The main parameters of gears and machine-tool settings and the main operation performances of gears are presented in Table 3. The obtained theoretical and operational modification fields and bearing contacts are shown in Figs. 5 and 6. Note that the efficiency of such gears turned to be a little less (by 2.5% on average) compared to their orthogonal analogs. But in this case, bending loads on teeth decreased abruptly, gear sensitivity to the action of errors was reduced and the possibility arose of applying heat-hardened steel for gearwheels; in total, it led to an abrupt increase in the gear strength.

The important feature of the design and production of these gears has been the choice of the level of the longitudinal and profile modification. As opposed to orthogonal worm gears, and similar to spiroid ones, the longitudinal modification of teeth had an impact mainly on the contact ratio actually implemented (and additionally, on the tooth-to-tooth accuracy, however, this feature is not crucial for the considered gears); and profile modification had an impact on load distribution along contact lines (areas). The actual bearing contacts obtained under load reveal the correctness of the accepted degree of contact localization (Fig. 6).

Note that in order to localize the contact in non-orthogonal gears, it is reasonable to follow recommendations on the change of the machine-tool cross angle, as compared to the cross angle of the gear, which has been described above for the orthogonal version.

A loaded gear with the increased requirements for tooth-to-tooth accuracy and the backlash. It was required that we master series production of worm pairs with the centre distance of 100 mm in which the motion smoothness and the bearing contact were rated by the 6th degree of accuracy in accordance with the Russian

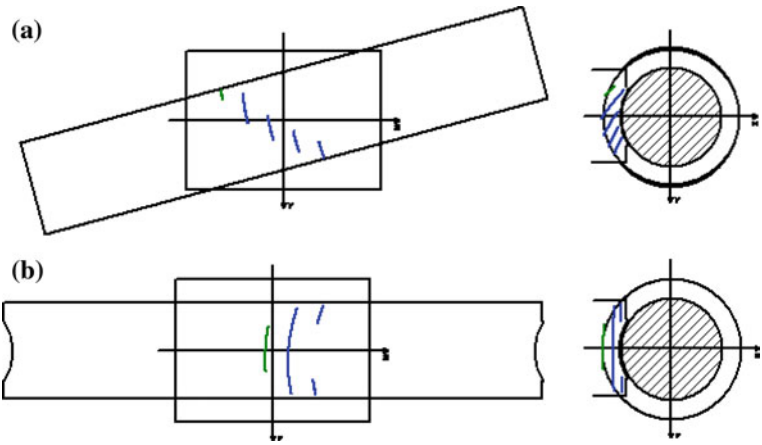

Fig. 4 Modification fields: **a** gear № 13; **b** orthogonal analog

Table 3 Non-orthogonal low-speed heavy-loaded gears

№	u_{12}	m_{x1}/m_{x0}, *mm*	d_1/d_0, *mm*	Σ_0,°	η,%	$\tilde{\sigma}_F$[b], *MPa*	
						thread	tooth
11.	81:2	4.967/5.008	102.2/87.9	70.7	45.9/(46.7)[a]	114/(285)	261/(492)
12.	68:2	6.070/6.011	106.0/97.6	72.3	49.4/(50.7)	96/(231)	111/(210)
13.	57:1	7.207/7.017	103.7/101.1	77.4	37.1/(37.9)	153/(474)	150/(399)

[a]Values in brackets correspond to orthogonal analogs
[b]Conditional values of bending stresses applied for comparative analysis

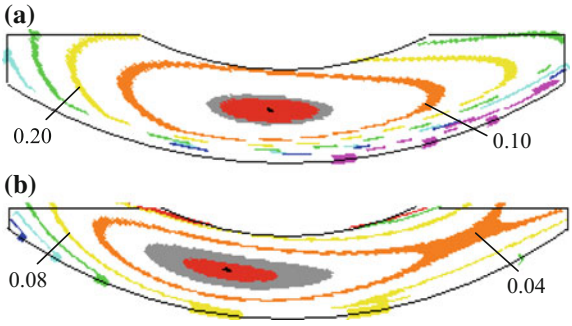

Fig. 5 Modification fields for gears **a** № 12; **b** № 11

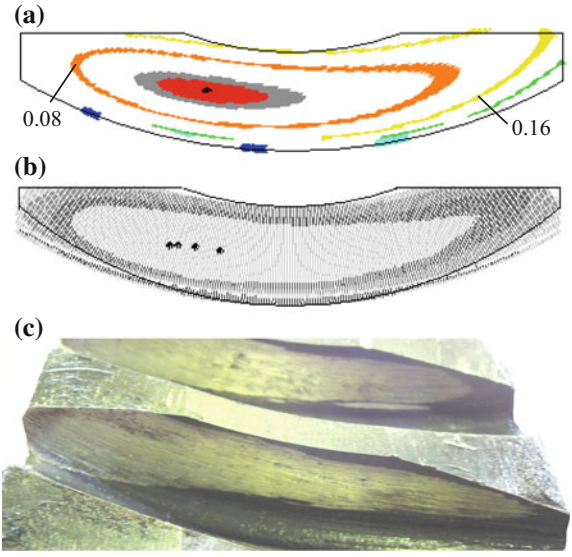

Fig. 6 Gear № 13:
a modification field;
b designed bearing contact;
c actual bearing contact under load

Table 4 Versions of a highly responsible gear

№	u_{12}	m_{x1}, *mm*	d_1, *mm*	η,%	σ_H, %	σ_F, %	
						thread	Tooth
14.	48:1	3.250	44.0	68.9	100.0	100.0	
15.	50:1	3.172	45.2	65.4	96.4	109.3	106.8
16.		3.189		65.5	96.5	109.1	112.9
17.		3.201		65.6	96.1	103.5	103.9
18.	51:1	3.182	41.0	66.6	97.4	110.8	100.0
19.	50:1	3.175	44.0	66.1	96.7	127.0	111.0

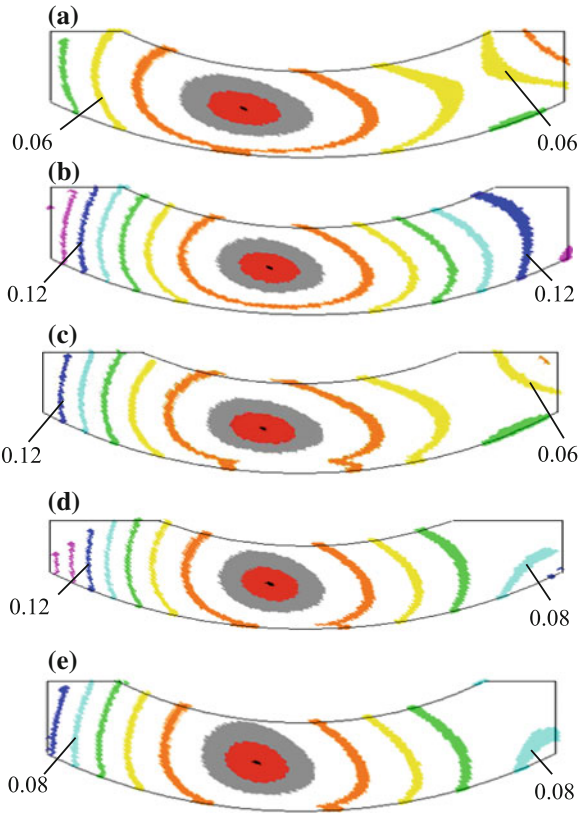

Fig. 7 Modification fields for gears: **a** № 15—0.06 mm*; **b** № 17—0.12 mm; **c** № 18; **d** № 19; **e** № 16—0.08 mm; *for gear №s 15, 16 and 17, localization within a definite range of values is provided

State Standard GOST 3675-81 (this corresponds to the standard DIN 3974-2); and the backlash had to be within the 0.03–0.06 mm range. Of course, the problem of producing a gear of the 6th degree of accuracy was mainly the problem of ensuring the appropriate level of manufacturing (equipment, tool, mounting and measuring means). However, within this range of manufacturing problems, no less important a task is the design of a gear that corresponds to the following requirements:

(a) High load-carrying capacity, both for the contact and bending strength;
(b) Application of the available precision tool, that is, involute gear hobs of a high degree of accuracy;
(c) Relatively low sensitivity of the bearing contact and backlash to the errors of the axial position of the gearwheel (assembly without adjustment).

Table 4 presents the main parameters of the versions of the gears considered. The first of the enumerated versions (gear № 14) was called the basic one: it was given by the customer as the result of designing a drive comprising a worm gear. Note here that the number of considered gears was indeed considerably greater; Table 4 presents only the "final gears" which possess better loading characteristics (contact σ_H and bending σ_F stresses on teeth), as compared to the basic version.

Three versions (gear №s 15-17) have been chosen from gears presented in Table 4 for practical implementation as those closest in accordance with the set of comparisons with the reference gear. The different degree of longitudinal localization of the contact (Fig. 7a, b, e) is provided in these gears, this degree having been chosen after practical development – directly for experimental specimens.

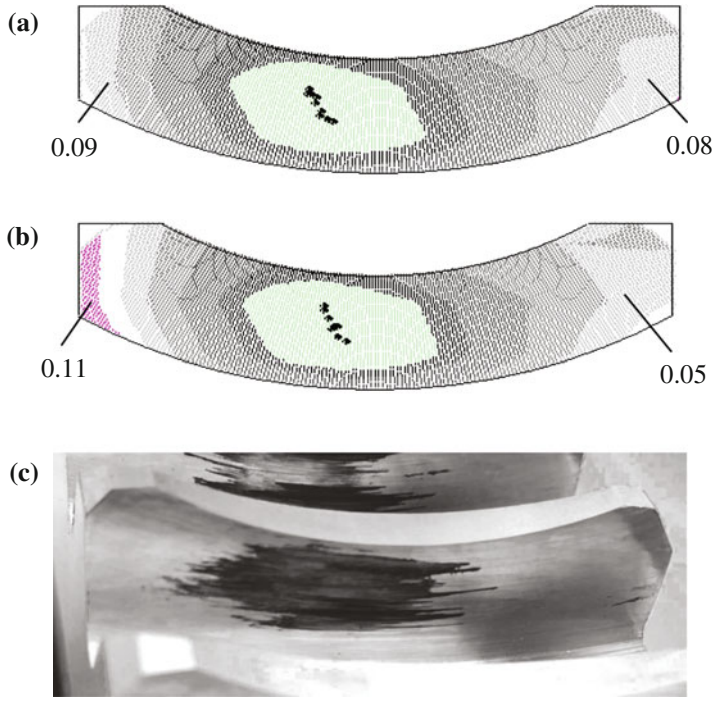

Fig. 8 Gear № 16: **a** design bearing contact at the nominal axial arrangement of the gearwheel ($f_x = 0$); **b** design bearing contacts at the axial shift of the gearwheel $f_x = 200$ μm; **c** actual bearing contact after running-in

Our developed technique here allowed us to take into account another additional limitation (which should be referred to the set $\boldsymbol{B}_{\text{III}}$): the coincidence of machine-tool settings for cutting the gearwheels for the pointed versions ($\Sigma_0 = 88.8°$, $a_{w0} = 107.7$ mm). In essence, we have obtained a new, previously unknown result: one and the same gearwheel (a number of interchangeable gearwheels) can be used to mesh with somehow differing worms and to obtain the various degrees of contact localization and acceptable load characteristics. It allowed for an abrupt reduction in the time and other costs for development of the design solution.

During the working out of design decisions, gear № 16 was chosen (Fig. 7e). Its initial bearing contact turned out to have acceptable dimensions and, as expected, a low sensitivity to the action of errors (Fig. 8).

7 Conclusions

Examples of application of our developed method and software for analysis of worm gears with localized contact which have been considered in this paper illustrate possibilities for the quick and efficient solution of a number of practical problems. In our opinion, these possibilities have not been completely uncovered. For example, we deliberately did not include all existing examples of worm gears which have been produced in practice in the number of gears considered. This was done to emphasize the basic trends of the choice of parameters and assessments of gears. However, it does not mean that the method for analysis and the results presented are not applicable for those cases which would require solutions outside common tendencies. For those cases, the pointed trends also assist significantly in the search for a non-standard solution. No doubt, such solutions are also of great interest, especially for more complex cases of multi-thread gears.

The paper, for practical reasons, did not address the issue of generation and a specific type of target function. This issue is urgent from the point of view of complete formalization of the considered optimization problem and it deserves special consideration. Note here that for an experienced design engineer, the absence of this function is explicitly not the irresistible obstacle. Often, it is enough to make a subjective ranking and practical checkup of different assessments, which have been pointed out above.

In our opinion, further development should involve supplementation of the method of analysis with more specified ranges of recommended parameters, empiric relations plotted in accordance with these or those criteria and, perhaps, unification of parameters of gears and tools.

References

1. Goldfarb, V.I., Trubachev, E.S., Lunin, S.V.: System of hobs unification for gearwheel cutting of worm-type gears. In: Proceedings of the 10th ASME International Power Transmission and Gearing Conference, DETC2007-34916, Las-Vegas, USA (2007)
2. Goldfarb, V.I., Trubachev, E.S., Puzanov, V.Y.: New possibilities of non-orthogonal worm gears. In: Proceedings of the 3rd International Conference "Power Transmissions 09", Greece, Chalcidice, pp. 139–145 (2009)
3. Lagutin, S.A., Verhovski, A.V., Dolotov, S.V.: Technological design of worm gears with a localized contact. In: Proceedings of 2nd International Conference "Power Transmissions 2006", Novi Sad, Serbia, pp. 177–182 (2006)
4. Lagutin, S.A.: Local synthesis of general type worm gearing and its applications. In: Proceedings of the 4th World Congress on Gearing and Power Transmissions, Paris. vol. 1, pp. 501–506 (1999)
5. Sandler, A.I., Lagutin, S., A., Gudov, E.A.: Theory and practice of manufacturing of general type worm gears. Infra-Engineering, Moscow-Vologda, 346 p (2016) (in Russian)
6. Trubachev, E.S., Glazyrin, A.V., Savelyeva, T.V.: New solution of the problem for hobs unification at design and production of cylindrical worm gears. In: Proceedings of the Scientific Conference on Gears. Izhevsk, pp. 298–301 (2008) (in Russian)
7. Trubachev, E.S., Puzanov, V.Y.: Contact localization in worm gears at arbitrary cross angles. In the World of Scientific Discoveries, 1.1, Krasnoyarsk, pp. 53–69 (2012) (in Russian)
8. Trubachev, E.S., Savelyeva, T.V.: Optimization problem at computer-aided design of spiroid gears on the basis of single-thread unified hobs. Informational Mathematics Jnl, 1(5), Moscow, Publishing house of physical and mathematical literature, pp. 121–130 (2005) (in Russian)
9. Trubachev, E.S.: Method for synthesis of parameters for the machine-tool meshing with a Helicoid generating surface. In: Advanced Information Techniques. Problems of Investigation, Design and Production of Gears, Izhevsk, pp. 163–169 (2001) (in Russian)
10. Trubachev, E.S.: Vector field of normal lines and its application in investigation of the geometry of Spiroid gearing with the Helicoid worm. In: Problems of Design of Mechanical Engineering and Informatization Units, Izhevsk, pp. 3–14 (1999) (in Russian)

Optimization of Requirements for Accuracy of Base Surfaces for Spur and Helical Gearwheels at Their Tooth Cutting

M. Kane

Abstract The paper describes the character of the joint influence of errors for base surfaces for blanks of spur and helical gearwheels (mounting bore and rim face end) on the position of the blank at tooth cutting. Possible versions of gearwheel blank mounting at tooth cutting are considered. It is shown that implementation of this or that version at tooth cutting is of a random character. The following issues are substantiated: the important role of the influence of the blank mounting error for providing accuracy parameters of teeth at their cutting; the necessity of applying statistical methods for the experimental study of the mutual relations between errors of blank bases and accuracy parameters of teeth at their cutting. A technique for such investigation is proposed and investigation results are presented for a wide range of conditions of gear machining. Techniques for preliminary choice and optimization of requirements for accuracy of base surfaces of spur and helical gearwheel blanks before their tooth cutting are described. These requirements provide the necessary accuracy of teeth at the assigned conditions of gear machining.

Keywords Parameters of tooth accuracy for spur and helical gearwheels · Parameters of accuracy of base surfaces for spur and helical gearwheels · Optimization of requirements for accuracy of base surfaces for spur and helical gearwheels · Statistical analysis of influence of errors of base surfaces for blanks on the accuracy of gearwheel teeth at their cutting

1 Introduction

Base surfaces of the blank for a spur or helical gearwheel are surfaces of the blank mounting on a machine-tool and orientation relative to the coordinate system at tooth cutting. For spur and helical gearwheels, they are usually the mounting bore

M. Kane (✉)
Belorussian National Technical University, Minsk, Republic of Belarus
e-mail: kane_08@mail.ru

V. Goldfarb et al. (eds.), *Advanced Gear Engineering*,
Mechanisms and Machine Science 51, DOI 10.1007/978-3-319-60399-5_17

and the rim face end. Sometimes the blank outer diameter is used for its centering. Besides the evident relation between errors of gearwheel teeth at cutting and errors of their base surfaces, the character and degree of these relations have been poorly studied. The most detailed study of the influence of the blank base errors (diameter clearance ΔD in "blank—machine tool mandrel" contact and runout of the reference face end of the blank E_T,) on various parameters of tooth accuracy at tooth milling is presented in works by B. A. Taits, M. A. Esterzon, S. M. Shreibman [1, 5, 6]. Whereas B. A. Taits considered individual influence of separate accuracy parameters of blank bases on different accuracy parameters of teeth (he paid the most attention to the influence of E_T on the error of tooth direction $F_{\beta r}$), M. A. Esterzon and S. M. Shreibman noted that ΔD and E_T jointly influence the position of a blank on the machine-tool and parameters of tooth accuracy at their milling. However, in order to choose the requirements for the accuracy of bases, they proposed empiric formulas connecting the allowable values ΔD and E_T with separate parameters of tooth accuracies (variation of measuring center distance (MCD) per one revolution of the gearwheel F''_{ir} and $F_{\beta r}$). Authors of the performed investigations pointed to the significant role of errors of blank base surfaces in forming the accuracy parameters of teeth at their cutting. According to their estimation, the percentage of errors of base surfaces for gearwheel blanks before tooth cutting reaches 80% in the error $F_{\beta r}$ after tooth cutting, 64% in the error F''_{ir}, and 28% in the accumulated pitch error along the gear rim F_{pr}. There were no studies on the influence of radial runout of the blank E_r on tooth accuracy after tooth cutting in the investigations performed, though the presence of E_r can increase variation of cutting forces and error of teeth at their tooth cutting. Taking the above into account, the following task has been determined: to study the joint influence of errors of base surfaces (bases) of blanks for spur and helical gearwheels and machining conditions on the type of blank mounting at tooth cutting and on generation of different parameters of tooth accuracy after this operation. Another aim of the work is to develop recommendations on the preliminary choice of requirements for accuracy of blank bases and technique for the optimization of these requirements accounting for machining conditions.

2 Analysis of Influence of Errors of Blank Bases and Machining Conditions on the Type of Blank Mounting at Tooth Cutting

Nowadays, as a rule, gear cutting of spur or helical flange-type gearwheels for cars, tractors and machine-tools is performed on machine-tools with a vertical axis at their gearwheels, which are mounted on the plane and fixed mandrel. Clamping of the workpiece is performed at the face end of a rim or hub opposite the supporting one, with application of pneumatic, hydraulic or screw devices. Machining errors

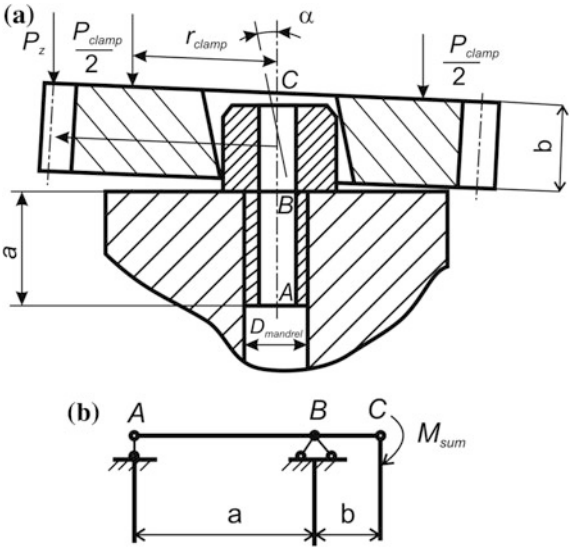

Fig. 1 Scheme of the mounting of a spur or helical gearwheel at tooth milling: **a** scheme for action of force; **b** design scheme

for base surfaces of a blank (hole or face end) can cause its skew at mounting (Fig. 1a).

Clamp forces trying to press the blank to the base surfaces of the device create the torque M_{clamp} acting on the central mandrel at definite conditions:

$$M_{\text{clamp}} = (P_{\text{clamp}} r_{\text{clamp}})/2, \tag{1}$$

where P_{clamp} is the clamping force and r_{clamp} is the distance between the point of force application P_{clamp} and the axis of the mandrel rotation.

Torque from the cutting force applied at the pitch radius r of the gearwheel usually acts in the same direction

$$M_{cut} = P_z r. \tag{2}$$

The total torque trying to press the blank to the support and even deform the mandrel will be equal to

$$M_{\text{total}} = M_{\text{clamp}} + M_{\text{cut}}. \tag{3}$$

When analyzing deformations, the mandrel can be considered either as a cantilever fixed bar or as a double-support cantilever bar. Considering that $a \approx (2 \div 3)\, D_{\text{mandrel}}$, let us assign the design scheme as the scheme of a double-support cantilever bar with arrangement of supports at points A and B (Fig. 1b).

When the part is mounted on a gear hobbing machine-tool, the versions of its position shown in Fig. 2 become possible. Conditions of the part mounting and features of the fit for each of these versions are given in Table 1.

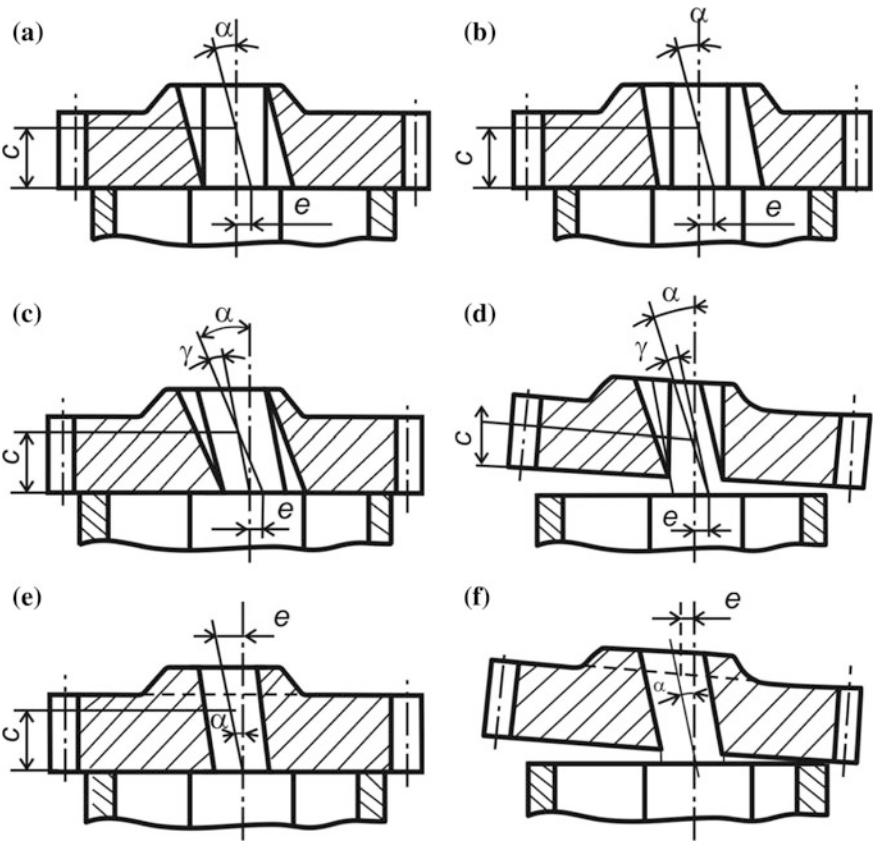

Fig. 2 Possible versions of mutual arrangement of a part and mounting elements of the appliance at tooth milling

Analysis shows that the most specific dimensions and errors for the considered gearwheels are: d_a = 100–200 mm, D_{hole} = 30–80 mm, $B \approx L_{\text{hole}}$ = 20–80 mm, $E_{\text{т}}$ = 50–120 μm. In order to bend the mandrel up to a position of complete contact between the blank face end and the mandrel for $\Delta D_{\text{o}} = 0$, the torque M_{total} = 0.5–6000 Nm is necessary, and for ΔD_{o} = 0.04–0.09 mm, it is M_{total} = 0–5900 Nm. Since modern gear hobbing machine tools have P_{clamp} = 20–60 kN and P_z = 2–10 kN (at machining gearwheels of the pointed dimensions and made of medium-carbon and low-carbon steels like 45, 40X, 18XГT, 25XГT, 20XH3A), for the given dimensions of gearwheels M_{clamp} = 500–3000 Nm, M_{cut} = 100–1000 Nm, M_{total} = 600–4000 Nm. The steel's chemical composition and properties are in accordance with the Russian standards GOST 1050-74 and GOST 4543-71. Therefore, gearwheels with pointed dimensions and errors of bases under the action of M_{clamp} and M_{total} can take any of the positions shown in Fig. 2 at tooth cutting.

Table 1 Versions and conditions of mounting the blank in the mandrel

Versions of mounting the blank	Conditions of mounting the blank	Note
Figure 2a, b	$D_{\text{mandrel max}} \leq D_{\text{hole min}} - \frac{bE_T}{d_a}$	A part freely fits the base surface of the appliance not deforming the mandrel. The clearance ΔD_o in "mandrel–gearwheel" contact is taken up completely (version *a*) or partially (version *b*)
Figure 2c	$D_{\text{hole min}} > D_{\text{mandrel max}}$ $\frac{y_{\text{bend}}}{b} \geq \frac{E_T}{d_a} - \frac{\Delta D_o}{b}$	The value of the clearance ΔD_o is not enough to compensate for the runout E_T and the mandrel is bent under the action of the clamping and cutting forces. A part either makes contact with the base surfaces of the appliance (version *c*) or touches them at one point or along some arc of a circumference (version *d*)
Figure 2d	$D_{\text{hole min}} > D_{\text{mandrel max}}$ $\frac{y_{\text{bend}}}{b} < \frac{E_T}{d_a} - \frac{\Delta D_o}{b}$	
Figure 2e	$D_{\text{hole max}} \leq D_{\text{mandrel min}}$ $\frac{y_{\text{bend}}}{b} \geq \frac{E_T}{d_a}$	A blank is mounted on the mandrel metal-to-metal. In this case, under the actions of M_{total}, the mandrel is bent, after which the blank either fits tightly on the base surfaces of the appliance (version *e*) or touches it at the point or along the arc of a circumference (version *f*)
Figure 2f	$D_{\text{hole max}} \leq D_{\text{mandrel min}}$ $\frac{y_{\text{bend}}}{b} < \frac{E_T}{d_a}$	

Note. Accepted designations: $D_{\text{mandrel max}}$ is the maximum dimension of the mounting diameter of the mandrel; $D_{\text{hole min}}$ is the minimum dimension of the hole in a blank; b is the height of the mounting surface of the mandrel taken to be equal to the width of the gearwheel hub B; y_{bend} is the deformation of the upper face end of the mandrel (point C, Fig. 1a) under the action of the bending torque M_{total}: $y_{\text{bend}} = M_{\text{total}}(2ab + 3b^2)/6EJ$, where J is the axial moment of inertia of the cross-section B of the mandrel (Fig. 1b) and E is the elasticity modulus for the mandrel material. Designations of other components of equations are either given above, or are evident from Fig. 1

Analysis of the versions of blank-mounting for a gearwheel at tooth milling presented in Fig. 2 shows that:

1. Errors of base surfaces of gearwheel blanks at their mounting can either partially compensate or worsen each other's action in regard to the accuracy of tooth machining. In versions *a* and *b*, the presence of E_T decreases the value of eccentricity e caused by the clearance ΔD_o. In versions *d* and *f*, the angle between the part and the axis of rotation caused by E_T is decreased due to the small value of ΔD_o and the high rigidity of the mandrel. In versions *e* and *f*, even in the absence of ΔD_o, there is an eccentricity e varying along the tooth length due to the mandrel skew caused by E_T.
2. Mounting of a part according to each of the versions and the position of the part at mounting according to versions *b, d* and *f* is, as a rule, of a random character, since it is related to a great number of independent factors, many of which are also random. These factors are: geometrical dimensions of the gearwheel and their relations (diameters of the gear rim and mounting bore, face width and

length of the bore), values of errors of base surfaces for the blank, dimensions and rigidity of the mounting mandrel, values of cutting and clamping forces, orientation of the part with respect to mounting elements of the appliance, and some others.

3. Depending on the version of the part mounting, the parameters of the mutual arrangement of the part and mandrel also differ: the skew angle α between the geometrical axis of the part and axis of its rotation, the distance C between the intersection point of these axes and the base face end of the part at similar values of errors of base surfaces $E_{\text{т}}$ and ΔD_{o}. Values α and C, in turn, mainly predetermine the degree of influence of base surface errors on the accuracy of tooth machining and, in particular, on the value of eccentricity e between the geometrical axis and the axis of rotation of the machined part.

Due to a mismatch of the axis of rotation of the blank with its geometrical axis caused mainly by errors in the hole generation, the gear rim of the cut gearwheel is arranged eccentrically relative to the geometrical axis of the gearwheel. That is why, when operating and measuring the gearwheel, its kinematic errors and errors of the backlash are revealed when measuring the radial runout of the gear rim F_{rr}, variations of MCD per one revolutions of the gearwheel F''_{ir} and limiting deviations of MCD + $E_{a''S1}$, − $E_{a''i}$, the kinematic error of the gearwheel F'_{ir}, and the total composite error of the gearwheel pitch F_{pr}.

Since parameters of kinematic accuracy are related, to some extent, to parameters of tooth-to-tooth accuracy, one can also expect the presence of indirect mutual relations between the accuracy parameters of base surfaces and the parameters of tooth-to-tooth accuracy, namely, variation of MCD at one tooth f''_{ir}, local kinematic error f'_{ir}, deviation of meshing pitch f_{pbr}, and error of the tooth profile f_{fr}. The same effect can be expected for the relation between the accuracy parameters of base surfaces and variation of the base tangent length F_{vwr} which is the component of the kinematic error of the gearwheel.

Runout of the base face end results in a skewing of the geometrical axis of the blank and axis of its rotation, which in turn results in lead errors $F_{\beta r}$ that are sinusoidal on the gearwheel circumference.

The radial runout of the outer diameter of the blank E_r causes deviation of the cutting depth and, therefore, cutting force and elastic pressing out of elements of a technological system at tooth cutting per one revolution of the gearwheel. Under definite conditions, this can become the source of kinematic errors of the gearwheel. And the value E_r can indirectly end up being related to the parameters of smoothness of gear operation.

Since (as was stated above) the influence of the base surfaces of the blank on the accuracy of gearwheel tooth cutting is interrelated, one can expect the dependence of practically all the pointed parameters of the gear rim accuracy on each of the accuracy parameters of the base surfaces ($E_{\text{т}}$, ΔD_{o}, E_r).

3 Investigation of the Influence of Errors of Bases for Blanks of Spur and Helical Gearwheels on Parameters of Tooth Accuracy at Tooth Cutting

3.1 Technique for Experimental Investigation

Let us note the following main features of the process of developing the errors of bases of blanks for spur and helical gearwheels in errors of the gear rim at tooth cutting:

1. The process is of a random character, since it depends on a great number of factors which are, in turn, random.
2. Each accuracy parameter of the gear rim is simultaneously influenced by several assorted errors of the base surfaces.
3. The accuracy parameters of base surfaces for blanks of spur and helical gearwheels for the considered methods of their machining are not interrelated by random values, their distribution being capable of being described by the normal law.

Moreover, it should be considered that the technological system (TS) of metal-cutting machine tools as a whole, and tooth cutting in particular, is a "poorly organized" complicated system in which physical processes determined by the influence of various factors are not subject to individual description.

For an objective estimation of the degree of relation and type of single- and multi-factor inter-relation of accuracy parameters of teeth with errors of the base surfaces of spur and helical gearwheels for the different dimensions, types and conditions of their tooth machining, the following technique was proposed.

In order to gather experimental data, machining of a series of blanks was performed at one gear hobbing or gear shaping machine-tool, then at gear shaving machine-tools in a definite sequence. Machining at each machine-tool was carried out by one tool. Prior to machining, the equipment and facilities were checked for correspondence to technical specifications imposed on them within the assigned machining conditions. To obtain statistically valid results that accounted for machining conditions and the lifetime of the gear cutting tool, the number of series was taken to be $n = 50$ pieces. In some cases, when there was a possibility of gear hobbing one part at a time, the number n reached 100 pieces. Prior to gear machining, runouts of the base face end $E_{\text{т}}$ and outer rim E_r on the expandable (ball-type) mandrel were measured, and in the case of its absence, the control mandrel with a small taper angle (1:5000–1:10000) was applied. Values of $E_{\text{т}}$ and E_r were taken to be equal to the arithmetical mean of 3–5 measurements of the corresponding parameter at different mountings of the part in the mandrel. Measurement of the diameter D_{o} of the mounting hole was performed in two or three cross-sections along the part height and in each of these cross-sections in two mutually perpendicular planes. The value D_{o} was taken to be equal to the average of 4–6 measured values.

In order to arrange experimental data and check the pre-conditions of applying the correlation-regressive analysis (CRA), processing of measurement results was begun with preliminary analysis of the experimental material.

Pre-conditions of the successful application of CRA in terms of a passive experiment are [2]:

1. The results of the observation of parameters are normally distributed random values.
2. Independent variables (arguments) are not mutually correlated.
3. The dependent variable generates a stationary random process.
4. Dispersions obtained at various observations (repeated, sequential, etc.) of parameters are equal to each other or homogeneous, that is, the process is ergodic.
5. Experimental data are based on results of a number of independent tests (observations) forming the random sampling of the given general entity.
6. The error of measurement of each parameter is less than the range (limit) of measurement of said parameter.

We checked the fulfillment of pre-conditions 1, 3 and 4. It was shown that in order to describe distribution of accuracy parameters for spur and helical gearwheels at the considered operations of their machining, the law of normal distribution can be applied, and the considered processes of machining are stationary and ergodic in compliance with definite limitations (requirements of standards and technical documentation).

At the first stage of processing the results of gearwheel measurements, enormously different data were excluded, mainly by means of the Irwin criterion. A statistical check of the randomness and independence of the observation results was made by means of the criterion of sequential differences for each set of observations.

To estimate the degree of the mutual relation of the accuracy parameters of teeth (y_1, …, y_i, …, y_n) and the accuracy parameters of bases (x_1 … x_j … x_κ), we analyzed the factors of pair correlation $r_{y_i x_j}$, correlation ratios $\eta_{y_i x_j}$ and factors of multiple correlation $R'_{y_i, x_j \ldots x_k}$(in a standardized scale).

The relevance of the difference between $r_{y_i x_j}$ and $\eta_{y_i x_j}$ was estimated by means of the Romanovsky criterion ξ.

The performed analysis allowed for stating the insignificance of the difference between the pointed characteristics for all measured accuracy parameters of the gear rim. That is why we will only give the analysis of calculation results for $r_{y_i x_j}$ from this point on. Significance of the correlation factors was checked by means of the Student t-test.

For preliminary choice of the type of relation between the considered accuracy parameters of the base and the accuracy parameters of the gear rim, empirical regression lines (examples are shown in Fig. 3) were plotted according to the experimental data obtained for different types and conditions of gear machining.

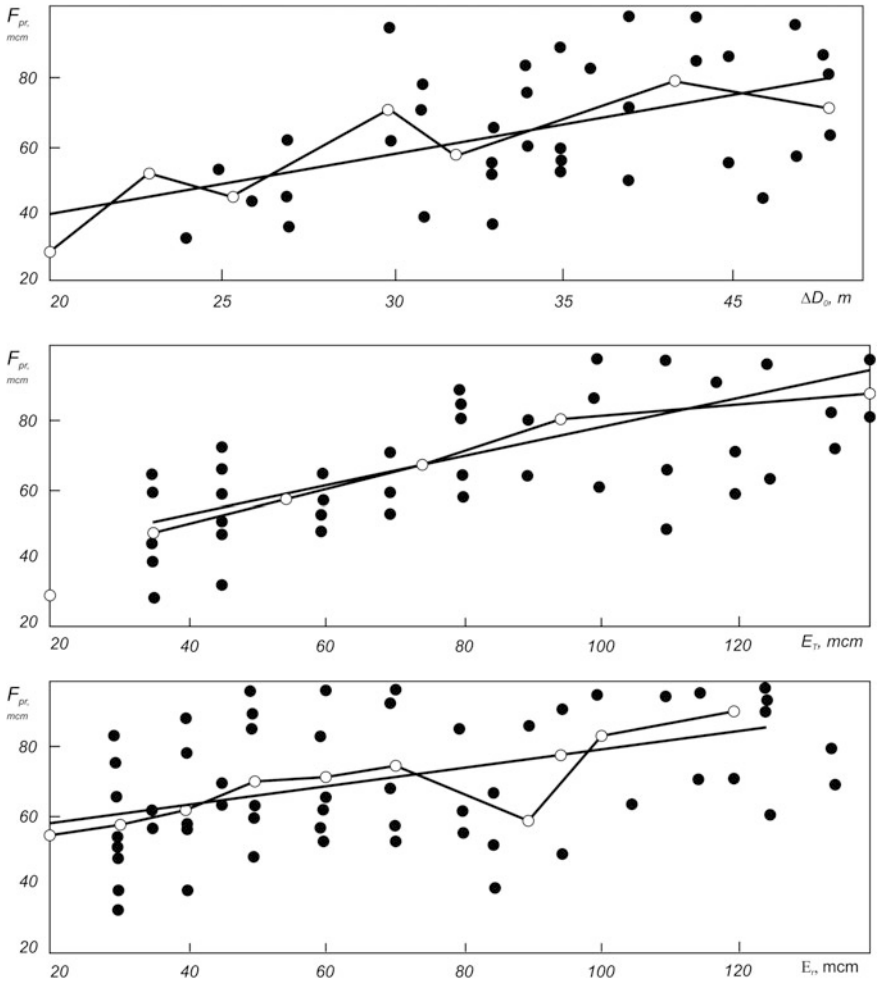

Fig. 3 Examples of empirical regression lines for the accumulated error of the pitch F_{pr} as a function of the error of base surfaces of blanks (ΔD_o, E_T, E_r) at gear hobbing under laboratory conditions

Analysis of regression lines and relations given in works by B. A. Taits, V. I. Golikov, M. A. Esterzon, S. M. Shreibman et al. allowed for proposing that, apart from the linear relation, there can be relations described by an exponential function between investigated parameters:

$$y = a_0 + a_1 E_T + a_2 D_0; \tag{4}$$

$$y = a_0 + a_1 E_T + a_2 \Delta D_0 + a_3 E_r; \tag{5}$$

$$y = a_0 E_T^{a_1} \Delta D_0^{a_2}; \tag{6}$$

$$y = a_0 E_{\mathrm{T}}^{a_1} \Delta D_0^{a_2} E_r^{a_3} \tag{7}$$

where y is one of the measured parameters of the gear rim accuracy and a_0, a_1, a_2, a_3 are constant factors of the equation depending on the properties of a technological system and the type of interrelation.

In order to determine the type of interrelation which describes the dependence of this parameter of gear rim accuracy on the accuracy parameters of bases in the best way, each of the investigation parameters of the gear rim accuracy, 5–10 dimension types of gearwheel and all the studied types and conditions of gear machining became a version for computer-aided analysis of the factors of the Eqs. (4)–(7) and a number of parameters necessary to estimate the adequacy of each of the dependencies, namely:

1. factors of multiple correlation $R_{y_i x_j \ldots x_k}$,
2. Student t-test for significance of $R_{y_i x_j \ldots x_k}$;
3. Fisher's ratio test for model adequacy. If $F < F_{\text{table}}$ (for the considered conditions $F_{\text{table}} = 1.55$), then the hypothesis of adequacy is accepted;
4. the mean relative error of the relation equation $\varepsilon_{\text{mean}}$ in % or the approximation factor in relative units.

3.2 Results of the Experimental Investigation

To get experimental data, 60 batches of gearwheels were machined and measured under conditions of manufacturing, and 20 batches of gearwheels, under those of the laboratory. The machining of gearwheels under manufacturing conditions was implemented at the Minsk Gear Works, the Minsk Tractor Works, the Volgograd Tractor Works, and the Minsk Automobile Plant; and under laboratory conditions, it was carried out at the Vitebsk Machine Tool Plant. The main characteristics of the investigated gearwheels and the conditions of their gear machining are given in Table 2.

Blanks at gear hobbing and gear shaving in all the cases were mounted on a mandrel and face end of the appliance. Gearwheels with spline holes were centered mainly with regard to the outer diameter of the splines, and in certain experiments, to the inner diameter. One or two blanks were mounted on the machine-tool at gear hobbing. When two blanks are hobbed simultaneously, the influence of the bases on the accuracy of gear machining was investigated only for the lower part in the set.

Under manufacturing, the value E_{T} in blanks was within the range 0.02–0.3 mm, E_r within 0.03–0.4 mm, and the hole was made according to the 6th–8th accuracy degrees of quality according to the Russian Standard GOST 25346-82. Under

Table 2 Basic parameters of investigated gearwheels and conditions of gear machining. The steel's chemical composition and properties correspond to Russian State Standards GOST 1050-74 and GOST 4543-71

Conditions of gear machining	m, mm	z	α°	d_{a1}, mm	b_1, mm	L_{hole}, mm	L_{hole} / $D_{mandrel}$	D_o, mm	Type of hole	Material of gearwheel
Manufacturing	3.5–5.0	23–41	20	80–210	20–30	35–120	0.20–1.02	40–70	Spline, smooth	Steel 18ХГТ, steel 25ХГТ, steel 30ХГТ, steel 25ХГМ, steel 20ХНР
Laboratory	2.0–6.0	25–51		60–303	16–40	25–40	0.15–0.75	25–60	Smooth	Steel 40Х, steel 45

Conditions of gear machining	Degree of accuracy according to Russian Standard GOST 1643–81 after gear hobbing and gear shaping	Machine-tools applied for gear hobbing and gear shaping (Russian designations of machine-tool grade)
Manufacturing	8–11	5З А З ОП, 5А312, 5Б312, 5К32, 5Д32, 5Е32, Module ВС–Б12, 5А122, 5А140П
Laboratory	8–10	5А312, 5Б312, 5К32

Conditions of gear machining	Scheme of gear hobbing	Class of hob accuracy according to Standard GOST 9324–80	Material of the hob cutting part	Cutting modes for gear hobbing		Characteristics of shapers according to Standard GOST 9323–79	
				V_1, mm/min	S_0, mm/rev	Type of shapers	Class of accuracy
Manufacturing	With co-current feed, with contrary feed	B	P18, P6M5, P9M4K8, P9K10	30–55	1.5–2.5	Disk, straight tooth	A, B
Laboratory	–	A, B	P18	25–35		–	–

Conditions of gear machining	Cutting modes for gear shaping		
	Rotary feed S_{rotary}, mm/double pass	Radial feed S_{radial}, mm/double pass	V_1, m/min
Manufacturing	0.25–0.40	0.05–0.08	14–22
Laboratory	–	–	–

laboratory conditions, the value E_T was kept within 0.008–0.150 mm, E_r within 0.01–0.20 mm, and the hole was made according to the 5th–7th accuracy degrees.

Having analyzed $r_{y_i x_j}$ and $R_{y_i x_j \ldots x_k}$, accepted as estimating the degree of relation between the accuracy parameters of the gear rim and those of the bases ($E_{\text{т}}$, ΔD_0, E_r) and validating the obtained values, it was established that the influence of E_r on the major part of the accuracy parameters of gearwheels (besides F_{pr}) is insignificant at gear hobbing and gear shaping, though the values $r_{y_i E_r}$ in all cases were different from zero. That is why the values $r_{y_i E_r}$ are not presented in Table 3, but when investigating the type of relation between the accuracy parameters of the gear rim and the base parameters, the influence of E_r was further analyzed.

As analysis showed, the values $r_{y_i x_j}$ and $R_{y_i x_j \ldots x_k}$ at gear hobbing with co-current and contrary feed do not differ significantly. That is why, in Table 3, these versions of machining conditions are not emphasized.

Analysis of the results given in Table 3 allows for making the following conclusions.

1. Accuracy parameters of bases ($E_{\text{т}}$, ΔD_{o}) at gear hobbing and gear shaping mainly influence the kinematic accuracy and tooth contact parameters. It was established that at gear hobbing and gear shaping, there is a low relation between the diametric clearance ΔD_{o} and the parameters of tooth-to-tooth accuracy f'_{ir}, f''_{ir} and f_{ptr}. Obviously, this relation is established indirectly, through the influence of errors of blank base surfaces on the parameters of kinematic accuracy for gearwheels F'_{ir}, F''_{ir} and F_{pr}. Values of relation between the accuracy parameters of bases and the parameters of tooth-to-tooth accuracy f_{pbr}, f_{fr} proved to be invalid.
2. Values of relation between the accuracy parameters for the gear rim and the accuracy parameters of base surfaces for blanks at gear hobbing and gear shaping vary within one and the same range, which is why we accepted the identity of these values.

Table 3 Main investigation results for the degree of relation between accuracy parameters of teeth and base surfaces for spur and helical gearwheels

Parameters of the relation	Parameters of the gear rim accuracy									
	F''_{ir}	F_{rr}	F_{pr}	F'_{ir}	$F_{\beta r}$	f''_{ir}	f_{pt}	f'_{ir}	$+E_{a''S}$	$-E_{a''i}$
	Gear hobbing, gear shaping									
$r_{yiE_{\text{T}}}$	*0.385* 0.392	*0.33* 0.322	*0.37* 0.371	*0.344* –	*0.541* 0.423	*0.236* 0.28	*0.244* 0.295	*0.202* –	*0.209* 0.284	*0.304* 0.249
$r_{y\Delta D_{\text{o}}}$	*0.422* 0.588	*0.381* 0.556	*0.462* 0.491	*0.418* –	*0.322* 0.312	*0.299* 0.32	*0.268* 0.318	*0.302* –	*0.315* 0.316	*0.294* 0.281
$R_{yE_T \Delta D_{\text{o}}}$	*0.454* 0.591	*0.436* 0.57	*0.633* 0.645	*0.584* –	*0.637* 0.611	*0.314* 0.344	*0.297* 0.341	*0.328* –	*0.324* 0.32	*0.302* 0.296

Note Values of accuracy parameters given in the numerator are obtained under manufacturing conditions, and those in the denominator, under laboratory conditions

3. The degree of relation between the accuracy parameters of bases and the accuracy parameters of the gear rim can vary within a wide range, even for the given type and condition of gear machining. This is demonstrated by a scattering in values $r_{y_i x_j}$ and $R_{y_i, x_j \ldots x_k}$. In general, this range is wider for manufacturing conditions than for laboratory ones. This can be explained by the wider range of variation of different factors influencing the relation between the parameters investigated under manufacturing conditions than those investigated under laboratory ones. The range of variation of $r_{y_i x_j}$ and $R_{y_i, x_j \ldots x_k}$ at gear hobbing and gear shaping is within the limits 150–600%. That is why, for specific conditions of gear machining, the most precise model of relation between the accuracy parameters of base surfaces for blanks and the accuracy parameters of the gear rim can only be obtained experimentally.
4. The obtained results allow for objective and mathematically-proven estimation of not only the degree of single—and multiple-factor relations between the accuracy parameters of bases and the accuracy parameters of the gear rim, but also of the portion of errors of the bases in the total error (dispersion) of this or that accuracy parameter of the gear rim for different types and conditions of gear machining. This can be done by means of the determination factor $(R'_{y_i x_j \ldots x_k})^2$. Thus, at gear hobbing under manufacturing conditions, the portion of errors of bases in the total error F'_{ir} can reach 54% ($R_{F'_{ir} E_r \Delta D_{o\max}} = 0.732$), F_{pr} − 72%, F_{rr} − 57%, F''_{ir} – 26%, $F_{\beta r}$ – 62%, and so on.

This information allows for choosing the ways and methods for increasing the accuracy of different parameters of the gear rim at gear hobbing and gear shaping.

5. An increase in the accuracy and rigidity of equipment improves the degree of influence of the base surfaces of blanks on the accuracy of gear machining. This is proven by the fact that the values $r_{y_i x_j}$ and $R_{y_i, x_j \ldots x_k}$ analyzed under manufacturing conditions are less than those for laboratory conditions of gear machining.

After analyzing the degree of relation between different accuracy parameters of the gear rim and the accuracy parameters of bases for those accuracy parameters of the gear rim for which this relation turned to be significant, this type of relation was chosen to approximate it to a greater extent.

The analysis performed showed that the adequacy of relations between many accuracy parameters of the gear rim and the accuracy parameters of bases is improved if the value E_r is considered in these relations. However, this improvement of adequacy is insignificant. Thus, values of the mean relative error of the equation of relation $\varepsilon_{\text{mean}}$ calculated with and without accounting for E_r differ by no more than 2–3%. Application of the Romanovsky criterion for estimating the significance of the difference between values $R_{y_i x_j \ldots x_k}$ calculated with and without accounting for E_r also allowed for proving the insignificance of the difference between them. That is why the influence of E_r can be neglected, in practice,

when analyzing the dependence between the considered accuracy parameters of the gear rim on the accuracy of base surfaces.

In order to describe the interrelation between the major part of the considered accuracy parameters of the gear rim and the accuracy parameters of base surfaces at gear hobbing and gear shaping, the relation (4) can be applied. Exclusion is for such accuracy parameters as f'_{ir},—$E_{a''i}$ (under laboratory and manufacturing conditions). The degree of relation between these parameters and the accuracy parameters of the bases is so low here that it is impossible to select the equation that describes these relations adequately.

4 Technique for Preliminary Choice and Optimization of Requirements for the Accuracy of Base Surfaces for Spur and Helical Gearwheels at Their Tooth Cutting

4.1 Technique for Optimization of Requirements for the Accuracy of Bases for Blanks of Spur and Helical Gearwheels at Their Tooth Cutting

The term "optimal" is valid here, under these conditions, for the maximum allowable values of accuracy parameters of base surfaces for gearwheels providing the necessary accuracy of teeth at their cutting. The following requirements are usually regulated: for gearwheels of automobile and tractor transmissions, F''_{ir} and $F_{\beta r}$ are specific; for gearwheels of metal cutting equipment, it would be F_{pr} and $F_{\beta r}$. Only the parameters of kinematic accuracy and tooth contact are highlighted here, since they are closely related to the accuracy parameters of base surfaces for gearwheel blanks at their tooth cutting.

The task of assigning the allowable and optimal maximum for these machining condition requirements for the accuracy of base surfaces for blanks $E_{\text{т}}$ and ΔD_{o} can be considered to be the task of maximizing the target function

$$U = E_T + \Delta D_0 \rightarrow \max \tag{8}$$

with fulfillment of limitations, which can be written as follows, taking into account the investigations carried out previously:

(a) for gearwheels of automobile and tractor transmissions,

$$\left.\begin{aligned} F''_i &\geq a_1 + b_1 E_{\text{T}} + c_1 \Delta D_0 \pm \alpha_1 \\ F_\beta &\geq a_2 + b_2 E_{\text{T}} + c_2 \Delta D_0 \pm \alpha_2 \end{aligned}\right\}; \tag{9}$$

(b) for gearwheels of gearboxes and feeds for machine tools,

$$\left.\begin{aligned} F_p &\geq a_1 + b_1 E_\mathrm{T} + c_1 \Delta D_0 \pm \alpha_1 \\ F_\beta &\geq a_2 + b_2 E_\mathrm{T} + c_2 \Delta D_0 \pm \alpha_2 \end{aligned}\right\}. \tag{10}$$

It should also comply with the boundary conditions

$$\left.\begin{aligned} E_\mathrm{T} &\geq 0 \\ \Delta D_\mathrm{o} &\geq 0 \end{aligned}\right\}. \tag{11}$$

This task is related to the class of linear programming problems.

In limitations (9) and (10), F_i'', F_p, F_β are allowable values of the corresponding accuracy parameters of the gear rim according to the standard GOST 1643-81 at the given operation of gear machining; a_1, a_2, b_1, b_2, c_1, c_2 are factors of the regression equations obtained experimentally; and α_1, α_2 are halves of confidential intervals of the predictive error for the output parameter for each of the obtained equations of regression.

The value α can be calculated both by the relations given in [4] and according to the approximated formulae

$$\alpha = t_{\beta,n-k-i}\sigma_y \sqrt{1 - (r^2_{yE_T} + r^2_{y\Delta D_\mathrm{o}})}, \tag{12}$$

where $t_{\beta,n-k-1}$ is the Student inversion distribution for the accepted confidential probability β and the number of degrees of freedom $(n - k - 1)$; k is the number of the variable in equations of regression; n is the number of the parts sample; and σ_y is the mean square deviation of the output parameter y (the parameter y is the accuracy parameter of the gear rim to be considered as being related to the accuracy parameters of bases of blanks at their optimizing).

Values $t_{\beta,n-k-1}$ are given in publications on mathematical statistics.

Since in each of the two equations in systems (9) and (10), the values F_i'', F_p, F_β, a and α are known, they can be transposed to one part of the inequality, and after that, the value A can be obtained by algebraic sum. However, since values $\pm\alpha_1$ and $\pm\alpha_2$ are components of the inequality, the following four systems of inequality will be obtained after different transformations of inequalities taking into account the sign of the value α:

$$\left.\begin{aligned} b_1 E_\mathrm{T} + c_1 \Delta D_\mathrm{o} &\leq A_1 \\ b_2 E_\mathrm{T} + c_2 \Delta D_\mathrm{o} &\leq A_2 \end{aligned}\right\}. \tag{13}$$

Let us consider the two most specific versions of conditions for solving this task.

1. On the phase plane, the systems of Eqs. (11) and (13) describe the closed area of possible values of independent variables (Fig. 4a). Here, the linear form U reaches the maximum values at the apex C of the convex polygon, the coordinates of the apex being determined by solving the system of inequalities (13) as the system of linear equations. Since we have four systems of inequalities, we need to solve four systems of equations and accept the minimum of four determined values of E_T and ΔD_o (Fig. 4c) as the solution.
2. The systems of limitations (11) and (13) determined the unclosed area of possible values of the variable (Fig. 4b). The form of U is maximized at the point C. An unambiguous solution is possible only when imposing the additional limitation on the variable with the ordinate along which the area is unclosed. In our case (Fig. 4b), this limitation is the relation

$$\Delta D_o \leq C. \tag{14}$$

Similar limitations can be chosen according to operational regulations for the optimized parameter (for example, according to the influence of the value δD_o on the dynamic loads in a gear), based on available recommendations, etc.

Solving the inequality (14) jointly with one of inequalities in the system (13) as a system of equations, we determine the value of the second variable (in our example it is E_T (Fig. 4d)). The least value is also chosen from two possible values of the second variable.

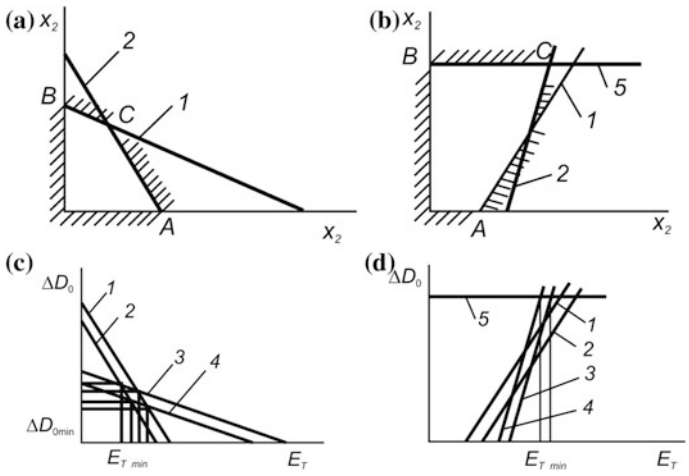

Fig. 4 Schemes for solving the task of optimization of requirements for the accuracy of base surfaces of blanks for gearwheels

Therefore, according to the proposed technique, the definition of optimal requirements for the accuracy of base surfaces for the given operation of gear machining should be carried out through the following steps:

1. Statistical relations between the accuracy parameters of base surfaces $E_{\text{т}}$ and ΔD_{o} and the two main regulated parameters of the gear rim accuracy, characterizing the kinematic accuracy and tooth contact, are determined experimentally.
2. The area of possible values $E_{\text{т}}$ and ΔD_{o} is determined graphically by means of calculated regression equations and chosen restrictions.
3. Solving the systems of corresponding equations, the maximum allowable values of $E_{\text{т}}$ and ΔD_{o} are determined, accounting for the error of the regression equation.

Along with the optimization of requirements for the accuracy of base surfaces of blanks for gearwheels accounting for the properties of a technological system of gear machining equipment and the required accuracy of gear rim machining, the proposed technique also allows for regulating the requirements for the accuracy of base surfaces of the appliance for the investigated gear machining operation.

The allowable value of the runout for the support surface of the device can be the actual runout of this surface $E_{\text{т appl actual}}$ at the time of the experimental study of the influence of bases for blanks on the accuracy of gear machining to further optimize the requirements for the accuracy of base surfaces of blanks. This is because the allowable values of errors of bases for blanks determined by such an experiment provide for the necessary accuracy of gear machining, accounting for the face runout present within the experiment and equal to $E_{\text{т appl actual}}$.

The same is also valid for the radial runout of the base surface of the appliance (mandrel) $E_{r\text{ appl actual}}$ at gear cutting. That is, the value $E_{r\text{ appl actual}}$ available within the experiment is also automatically considered in this method for determining the allowable values of the accuracy of base surfaces of gearwheels, and that is why $E_{r\text{ appl actual}}$ can be taken, under these conditions, as the allowable value for the base surface of the appliance.

The tolerance δD_{appl} for the diameter of the mandrel of the appliance (where the gearwheel is mounted at gear cutting) can be determined according to the condition

$$\bar{\delta} D_{\text{o}} + \bar{\delta} D_{\text{appl}} \leq \Delta \bar{D}_{\text{o}}, \tag{15}$$

where δD_{o} is the tolerance for the diameter of the mounting surface of the gearwheel at gear cutting.

The value ΔD_{o} is determined according to the above-described technique. One value of δD_{o} or δD_{appl} should be assigned.

The value δD_{appl} can be taken into account for recommendations given in the corresponding standards and technical documentation. Considering that distribution of dimensions of gearwheel holes and the mounting surfaces of machine-tool mandrels is subject to the normal law [3], the value δD_{o} can be determined by

solving the dimension chain (15) through the probabilistic method. Assigning $P = 0.27\%$, $t = 3$, and $\lambda = 1/9$, we have

$$\delta D_{\mathrm{o}} = \sqrt{\Delta D_{\mathrm{o}}^2 - \delta D_{\Pi \mathrm{p}}^2}. \tag{16}$$

4.2 Technique for Preliminary Choice of Requirements for the Accuracy of Bases for Blanks of Spur and Helical Gearwheels at Their Tooth Cutting

We computed the optimal values of E_T and ΔD_o according to the technique described in Sect. 4.1 for all investigated batches of gearwheels. Since the accumulated experimental information covered a wide range of dimensions of gearwheels, accuracy of bases for blanks and gear rims, and other conditions of tooth cutting, for the considered conditions, it became possible to establish relations between the maximum allowable values of E_T and ΔD_o at tooth cutting and the geometrical dimensions of gearwheels and the degree of gear rim accuracy necessary to be achieved after gear hobbing and gear shaping. We determined the influence of allowable values of E_T and ΔD_o on such conditions of tooth cutting as face width b of the machined gearwheels (designated further as X_1), outside diameter d_a (X_2), the ratio of the mounting hole length to the diameter of the base face end L_{hole}/D_{base} (X_3), the degree of accuracy after tooth cutting according to the Russian Standard GOST 1643-81 (X_4), and the diameter of the mounting hole of the gearwheels D_o (X_5). If the gearwheel has different degrees of accuracy according to norms of kinematic accuracy and tooth contact, then the least of the two values should be taken as X_4. If the standard DIN or ISO is applied, one must increase the value of the degree of accuracy according to these standards by a unit, which should be provided, and take it as X_4, since the tolerance, according to the Russian Standard GOST 1643-81, is approximately one degree higher than that in accordance with the corresponding standards DIN 3962 or ISO 1328. Six types of regression equations were analyzed and those relations were chosen that were the most adequate for experimental data.

For gearwheels of automobile and tractor transmissions, these relations are as follows:

$$\begin{aligned} E_T = (&82661 + 145514X_{30} - 43358X_4 + 2115 \cdot 10^{-2}X_1^2 + 160 \cdot 10^{-2}X_2^2 \\ &- 118250X_3^2 + 7058X_4^2 - 52 \cdot 10^{-2}X_5^2 - -46 \cdot 10^{-4}X_2^3 + 15063X_3^3 \\ &- 285X_4^3 - 295X_1X_4 - -278X_2X_3 + 412X_3X_5 + 15X_2X_4) \cdot 10^{-6} \text{ mm} \end{aligned} \tag{17}$$

$$\begin{aligned}\Delta D_o = (&1810689 - 118650X_5 + 83765X_3 + 2354X_5^2 \\ &+ 88X_4^3 - 1439 \cdot 10^{-2}X_5^3 - 665X_1X_3 - 12630X_3X_4 \\ &+ 154X_4X_5 + 452 \cdot 10^{-3}X_2^2) \cdot 10^{-6} \text{ mm}\end{aligned} \quad (18)$$

These relations or table recommendations, obtained according to them and given in the State Standard of the Belarus Republic [7] developed by us, can be used for the preliminary choice of allowable errors of base surfaces of blanks for spur and helical gearwheels m = 3.5–5 mm prior to their gear hobbing or gear shaping.

5 Conclusions

Errors of base surfaces for blanks of spur and helical gearwheels wield great influence on tooth accuracy at gear hobbing or gear shaping. Errors of bases for blanks comprise anywhere from 26 to 72% of the errors of separate parameters for teeth at their cutting.

Errors of bases for blanks of spur and helical gearwheels jointly influence the major part of the accuracy parameters for teeth at their cutting. Most of all, they influence the parameters of kinematic accuracy and tooth contact. The degree of this influence depends on a large number of factors: the ratio of the gearwheel dimensions, the rigidity and accuracy of a technological system of the gear cutting equipment, forces of blank cutting and clamping, etc. The considered relations are of a random character, and statistical methods should be used in their study.

A scattering of values for the degree of relation between the errors of bases for blanks and the accuracy parameters of teeth at their cutting under manufacturing conditions is 150–600%. That is why the most accurate model of these relations can be obtained only experimentally while machining the sample batch of gearwheels under the given conditions of tooth cutting.

The method for choosing the requirements for the accuracy parameters of base surfaces for blanks of spur and helical gearwheels prior to tooth cutting (recommended nowadays in most reference books, common in practice and based on the degree of influence of errors of separate base surfaces on separate parameters of teeth after their cutting,) does not correspond to the nature of the highlighted relations. It also does not allow for optimizing the requirements for the accuracy of bases for blanks and using the possibilities of a machine-tool in full to provide the necessary accuracy of teeth. Our proposed method for optimization of the requirements for the accuracy of base surfaces for blanks of spur and helical gearwheels prior to their tooth cutting is free of these drawbacks, in our opinion. The practice of applying this method showed that it allows for increasing the accuracy of teeth after their cutting by 20–40%.

References

1. Esterzon M.A.: Accuracy of gearwheels manufactured with basing along the rim face end// Stanki i instrument. 1965. N 3
2. Kane, M.M.: Fundamentals of investigations in mechanical engineering: Study guide for higher educational institutions. Vysheyshaya shkola, Minsk (1987)
3. Kane, M.M.: Engineering support of the quality of high-loaded gears with involute spur and helical gearwheels: DSc Thesis. BGPA, Minsk (1996)
4. Khal'd A.: Mathematical statistics with technical application. M.: Izd. inostrannoy literatury (1956)
5. Production of gearwheels: Reference book. Editor B.A. Taits. M.: Mashinostroyeniye (1990)
6. Shreibman S.M.: Foundation and achievement of the necessary accuracy of base surfaces of gearwheels (according to the assigned accuracy of gearwheels): Ph.D. Thesis, M: Stankin (1965)
7. State standard of Belarus Republic STB 1251-2000 «Spur and helical gearwheels. Methods for designing the manufacturing processes». Minsk, Gosstandart, 2000—50 p

Optimization of HCR Gearing Geometry from a Scuffing Point of View

M. Rackov, M. Vereš, M. Čavić, M. Penčić, Ž. Kanović, S. Kuzmanović and I. Knežević

Abstract The paper deals with an issue of increasing the resistance of HCR external involute gearing from a scuffing point of view. It reports on a difference between involute gears with low contact ratio (LCR) and those with high contact ratio (HCR). The paper describes scuffing as the most significant damage done to the teeth flanks of HCR involute gears. In the case of warm scuffing, it is the combined action of high pressure between surfaces, high sliding speeds, and excessive contact temperature, resulting from pressure and sliding speed values, which consequently cause oil film rupture between the teeth flanks. Adopting a suitable geometry of the tooth curve profile, certain values of addendum heights for the meshing wheel will be defined according to the criteria of specific slips and corrected head shapes of the teeth of both wheels. The paper deals with the assessment and theoretical analysis of the impact of the HCR tooth profile resistance to scuffing on the basis of integral temperature criterion according to the Winter-Michaelis criterion. The basic relations for assessing the scuffing properties of an HCR involute gearing profile are derived, as well as the optimization of

M. Rackov (✉) · M. Čavić · M. Penčić · Ž. Kanović · S. Kuzmanović · I. Knežević
Faculty of Technical Sciences, University of Novi Sad, Novi Sad, Serbia
e-mail: racmil@uns.ac.rs

M. Čavić
e-mail: scomaja@uns.ac.rs

M. Penčić
e-mail: mpencic@uns.ac.rs

Ž. Kanović
e-mail: kanovic@uns.ac.rs

S. Kuzmanović
e-mail: kuzman@uns.ac.rs

I. Knežević
e-mail: ivanknezevic@uns.ac.rs

M. Vereš
Faculty of Mechanical Engineering, Slovak University of Technology in Bratislava, Bratislava, Slovakia
e-mail: miroslav.veres@stuba.sk

V. Goldfarb et al. (eds.), *Advanced Gear Engineering*,
Mechanisms and Machine Science 51, DOI 10.1007/978-3-319-60399-5_18

geometrical parameters of HCR gearing based on theoretical considerations on the properties of HCR gearing in terms of its resistance to warm scuffing combined with geometrical constraints against interferences. Finally, the results of the obtained optimization are compared with experimental results provided in previous research. A significant benefit in a theoretical area is the generalization of the integral temperature criterion for involute HCR gearing. By optimizing the criterion for the integral temperature of involute HCR gearing, the minimal flash temperature is obtained and the condition for the occurrence of scuffing is minimized.

Keywords HCR involute gearing · Scuffing · Flash temperature criterion · Integral temperature criterion · Optimization

1 Introduction

Nowadays, mechanical transmissions are produced in millions of special series, in the context of the automotive industry (for transferring mechanical energy from the engine to the wheels, starting an engine, moving the window, etc.), or in the area of railway engineering, industries of construction machinery, etc. Special transmissions are also used in agricultural, industrial, construction and mining equipment. Obviously, they are also used as universal mechanical transmissions in all fields of mechanical engineering, in first and foremost for connecting motors, i.e., driving units [1–3]. In this paper, mechanical transmissions for the automotive industry will be researched, i.e., the focus will be on the gears used in this type of transmission.

Mechanical transmissions, being integral parts of a driving system, when operated properly, significantly influence the reliability of the system as a whole. However, they can be found in a state of failure and thus be the cause of unplanned delays in production. Despite the fact that all conditions are provided for undisturbed functioning, failures of one or more elements can occur, causing unplanned delays, and hence leading to improper operation, or the current termination of the working of gear transmission [2].

Because of the role of transferring mechanical energy from the driving engine to the driven machine, the failure of mechanical gear transmission means the immediate termination of the entire system, the termination of its production and a delay in production, which can cause large financial losses for users of mechanical transmissions [2, 4].

Bearing in mind the great use and importance of mechanical transmissions, they need to provide high reliability in order for the delays in production or losses thus incurred to be as small as possible. Proper operation of transmissions greatly affects the quality and reliability of other machines and mechanisms into which they are incorporated. This means that during the construction of each element in a mechanical transmission, care should be taken in relation to their reliability, and at the same time, in relation to the optimal design and the requirement for achieving better technical characteristics of the transmission. To ensure a reliable and long

service life, and in general, the high quality operation of the mechanical units and systems into which they are installed, it is necessary to examine in detail the characteristics of the proper operation of a mechanical transmission, the characteristics of their work at various loads, and the reasons for accidents and breakdown situations [2, 4].

Scientific and technological progress in engineering has led to increasing improvement in the use of resources, a reduction in energy intensity of production and an increase in reliability and efficiency during operation. This trend is also reflected in the field of the development of gears, which, in recent years, has seen the ability to transmit power increased, while, at the same time, the volume and weight of gears has been reduced.

Increasing the transmitted power of a gear relative to the unit of volume is, however, associated with an increase in thermal load transfer. Apart from the usual kinds of tooth damage (fracture in the heel and the formation of pitting), the increased heat load has uncovered another kind of damage, so-called scuffing. Boundary curves representing the main kinds of tooth damage are shown in Fig. 1, depending on the transmitted torque and the peripheral speed for the same lifetime [5–7].

Problems of tooth scuffing mainly occur during such transfers, which cannot be used for lubrication oils with EP additives (EP—extreme pressure). Examples of EP additives include sulphur, chlorine, phosphorus and lead. Scuffing can occur in the gear reducer for gas turbines, in which non-additive-enhanced oil is commonly used. The oil in transmissions of diesel driven ships and in the gearboxes of diesel locomotives does not provide adequate protection against scuffing.

Naturally, scuffing may arise in other cases, even assuming that the gear lubrication oils do have additives. In such cases, scuffing occurs in overloading transfers that operate at the higher peripheral speed of transfers with poorly chosen tooth geometry or that influence an excessive increase in oil temperature operation (e.g., high ambient temperature, etc.) [5].

In any case, progressive scuffing means serious damage to the shape of the tooth profile, which subsequently means removing the teeth from the service. Increased

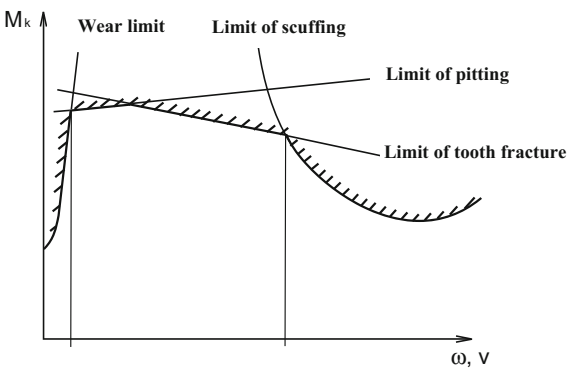

Fig. 1 Typical load carrying capacity limits of case carburized gears [7]

noise transmission over the standard border may refer, in some cases, to the reason for exclusion from the transfer operation.

The problem related to the involute gear with an extended duration of the contact period, known in the literature as HCR (High Contact Ratio), is discussed in this paper. Due to the larger path of action and the higher peripheral speed, scuffing can occur more frequently in HCR gear teeth. The objective of this paper is to analyze and discuss the possibilities for reducing the occurring of scuffing as tooth damage on external HCR gears.

In recent years, while introducing higher demands on the capacity of teeth, and while developing new materials with high resistance to pitting or high flexural strength, it has become obvious that the limit factor at the design of spur gears may, in many cases, just be scuffing [5–7].

The majority of standard methods and procedures only apply for LCR (low contact ratio) gears [5, 8, 9]. This type of damage of HCR gears has not, to date, been sufficiently researched. It has been identified that the process of scuffing can occur in HCR gears while gear processing, resulting in a direct impact on their working life.

2 Effect of Higher Contact Ratio on the Noise Level of Gearing

There is a new option involving minimizing the size of gearing, and thus the size of gearwheels as well. Reducing the dimensions of the gear leads to a greater heat load caused by the reduction of the material volume for the transfer of heat energy formed in the teeth meshing. Increased thermal stress in mechanical transmission can cause scuffing of tooth flanks. Besides the heat stress, the tendency towards scuffing damage is also dependent on the gear load, the peripheral speed, the gearing geometry, the quality of the tooth flanks and the properties of the lubricating oil. When crossing the limit criteria, the damage of tooth flanks by scuffing can lead to damaging of the gear, which is possible even after a very short time of operation [5, 7].

In the era of modern technological development, there is continuing research into new forms of tooth which could potentially meet the most demanding requirements. The intent of this article is primarily to reduce the noise of mechanical transmissions, improve them (automotive transmissions to begin with), reduce their size and increase their efficiency, all while increasing the transmitted power. In involute gear drives, the majority of geometric parameters affects the properties of this type of gearing and cannot be changed to a great extent. Therefore, it is necessary to focus on those factors which affect the properties of teeth and which still have not been sufficiently examined in detail, even though they have a significant impact on the desired characteristics of the transfer.

One such parameter is the coefficient of contact ratio of involute gears (ε_α) [5, 10]. Today, nearly all automotive transmission gears have involute gears, for which the coefficient of the contact ratio is equal to or greater than 2. Such a type of gear in the literature is generally marked as HCR (High Contact Ratio) teeth. The correct geometry for the proposed HCR gearing is complicated by the fact that there is much more to the internal primary and secondary teeth, as well as to interference, than in standard involute profiles. In terms of strength characteristics, the proposed HCR gearing is also problematic, mainly due to the lack of extensive experimental test results of such transfers. Likewise, the problem is that the current standards for strength calculation of involute gearing are contemplated with higher ε_α. Those factors hinder the optimization of geometrical parameters of HCR gearing as a virtually arbitrarily defined objective function. The aim of the article is therefore to contribute to a greater knowledge of the properties of HCR gearing, especially in terms of its resistance to scuffing and further development of the strength calculation of gearings with HCR teeth.

Contact ratio can be defined as the number of pairs of teeth in contact during the course of action. The physical significance of the contact ratio lies in the fact that it is a measure of the average number of teeth in contact during the period in which a tooth comes in and out of contact with the mating gear [3, 5, 6].

The correct working of the gear will be assured if the value of the path of contact is higher than that of the base pitch [3, 6, 11]. The ratio between the length of contact g_α, and the pitch on the base cylinder p_b is provided by the following formula:

$$\varepsilon_\alpha = \frac{\text{length of contact}}{\text{base pitch}} = \frac{g_\alpha}{p_b} = \frac{\sqrt{r_{a1}^2 - r_{b1}^2} + \sqrt{r_{a2}^2 - r_{b2}^2} - a_w \sin \alpha_{wt}}{p_t \cos \alpha_{wt}}. \quad (1)$$

Referring to Fig. 2, the progression of tooth contact has been represented for LCR gears. At the point A, the contact commences. Each of the pairs carries a load of $F/2$. At the internal point B, the whole load is on the second pair as the first pair leaves the mesh at the point E; therefore, there is a single tooth contact. This single pair bears the load until the point D is reached. Double-pair engagement begins from here onwards, until the former pair departs from the mesh. The minimum acceptable contact ratio for smooth operation is 1.2. Gears should not generally be designed having contact ratios less than about 1.2, since inaccuracies in mounting might reduce the contact ratio even more, increasing the possibility of impact between the teeth, as well as an increase in the noise level. To ensure smooth and continuous operation, the contact ratio must be as high as possible, which the limiting factors permit. A minimum contact ratio of 1.4 is preferred, and the larger one is better. Contact ratios for conventional gearing are generally in the range from 1.4 to 1.6; hence, the number of tooth engagements is either one or two [12, 13].

When HCR gearing is used, it is not necessary to achieve a greater gear load capacity; nevertheless, there is a greater risk of interference due to a greater height of the teeth. The advantage of HCR gearing is also higher resistance (load distribution

is shared between more pairs of teeth simultaneously) and lower relative noise level, which can be significantly reduced by using the integer HCR factor ε_α.

HCR profiles are more complicated than standard involute profiles; they have greater predisposition for interference and pointed tip thickness, but also an undercut of the teeth during production (primary production interference) [11, 12].

The coefficient of the contact ratio is the main indicator of HCR gearing, which differs from the commonly used standard profiles.

The geometry of involute HCR gearing is presented in Fig. 3, where the difference in geometry between HCR gearing and the standard involute gearing can be observed. Likewise, there is a difference in length of the line of action g_a (the tooth pitch on the base cylinder p_{bt} is the same as in Fig. 2).

General distribution of the applied force at the characteristic points of LCR and HCR gear tooth flanks is shown in Fig. 4. When comparing both these kinds of gearing, it is obvious that, in the case of LCR gearing, the maximum force is applied when one pair of teeth is in contact (between points BD, Fig. 4a). This can be considered to be 100% of the value of the force F. The greatest applied force in

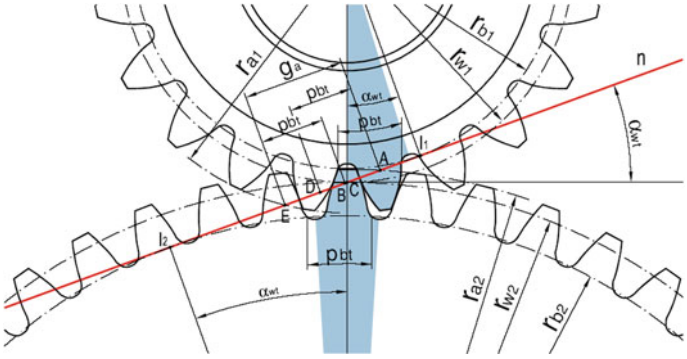

Fig. 2 Geometry of the standard involute gearing [11]

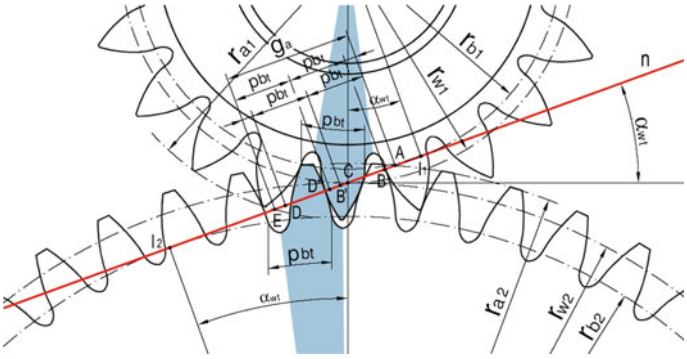

Fig. 3 Geometry of involute HCR gearing [11]

the HCR gearing (between points BB' and DD') can be considered that of about 50%, when two pairs of teeth are in contact. Consequently, the size of the applied force is decreased when three pairs of teeth are in contact. Hence, the value of involute gearing 2/3*F* is decreased to 1/3*F*, and the value 1/3*F* is decreased to 1/6*F*, meaning that the load distribution is more favorable in HCR gearing [11, 12].

Often, gears in the mechanical gearboxes of automobiles are designed with greater gear ratio, integer transverse contact ratio ($\varepsilon_\alpha \geq 2$) and overlap ratio ($\varepsilon_\alpha$ 1). These gears are characterized by their increased strength capacity [14].

While a one or two teeth pair in contact change at the mesh of the standard gear, two teeth pairs are permanently in contact at the mesh of an HCR gear with $\varepsilon_\alpha = 2$. Advantages of an HCR gear with $\varepsilon_\alpha = 2$ are based on the smoother change of stiffness at the mesh and the smooth division of the total carried force between two teeth pairs.

When $\varepsilon_\alpha > 2$, three pairs of teeth occur in contact along the line of action, thereby representing triple tooth contact (Fig. 5). Triple tooth contact generally has a higher load capacity and lower gearing noise. Also, the favorable property of this HCR gearing includes increasing the resistance of fatigue damage.

In high precision and heavily loaded spur gears, the effect of gear errors is negligible, so the periodic variation of tooth stiffness is the principal cause of noise and vibration. High contact ratio spur gears could be used to exclude or reduce the variation of tooth stiffness [13, 14].

Increasing the noise of a gear pair is largely conditioned by the load increase. Increasing the applied force affects the greater elastic deformation of the teeth, including greater internal dynamic forces.

The main cause of internal dynamic forces is engaging different variants of involute tooth shapes, as well as changing the number of teeth pairs in contact. Dynamic forces between the teeth depend on the speed of rotation and the number of teeth of the pinion and gear wheel.

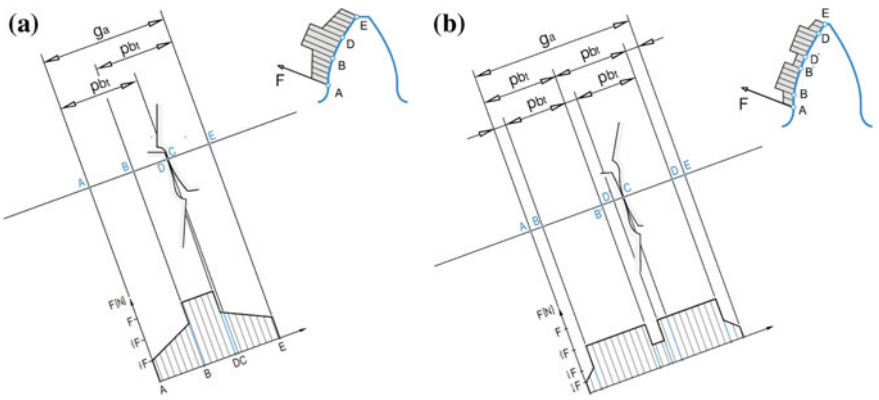

Fig. 4 Distribution of tooth load during **a** low contact ratio (LCR) and **b** high contact ratio (HCR) [11]

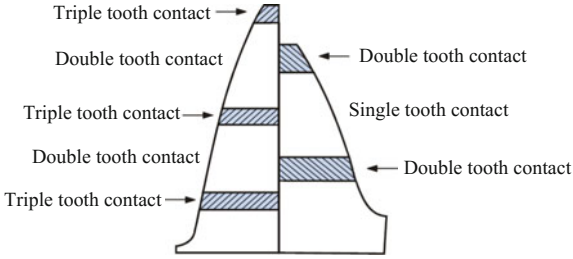

Fig. 5 Comparison of the gearing profiles

By changing some parameters, dynamic forces can be reduced. Introducing and changing the helix angle β, or changing the contact ratio ε_α, can accomplish a quite significant reduction in noise levels of a gear pair.

It is well known that increasing the average number of teeth in contact leads to excluding or reducing the vibration amplitude. First, it was established experimentally that dynamic loads decrease with an increase in the contact ratio in spur gearing [15]. Then, in order to get a further reduction of the vibration, HCR gear profiles can be optimized. Sato et al. [16] found that HCR gears were less sensitive with respect to manufacturing errors. In particular, such kinds of gear allow for larger tolerance in the tip relief length. Moreover, they found that, in the absence of a pressure angle error, the best contact ratio should be about 2; otherwise, it was better to have a contact ratio of about 1.7 or higher than 2.3. Kahraman and Blankenship [17] published an experimental work on HCR gear vibration; they found that the best behavior was obtained with an integer contact ratio, even though other specific non-integer (rational) contact ratios could minimize the amplitude of some specific harmonics of the static transmission error. It is important to note that in Ref. [17], HCR gears were obtained by modifying the outside diameter; the other macro-geometric parameters, e.g., the number of teeth, were left unchanged.

According to the results of different measurements of gear pair, the reduction of noise proved to be greatest using HCR gearing with the value of the contact ratio $\varepsilon_\alpha = 2$. A decrease in noise is caused by $\varepsilon_\alpha = 2$, because there are always two pairs of teeth in contact, meaning that when one pair of teeth comes out of contact, another pair of teeth is coming into contact; hence, the applied force is considerably smaller, since it is divided between two pairs of teeth.

3 Geometric Parameters of the Objective Function Defining the Correct Mating HCR Gearing

According to Eq. (1), it follows that $\varepsilon_\alpha = f(g_\alpha, p_{bt})$. Tooth pitch on the base circle of LCR gearing is equal to the base pitch on HCR gearing, and it is considered to be constant. This means that achieving the greatest value of the contact ratio ε_α has to be obtained by the greatest possible increase in the length of the line of action g_α. The length of the line of action g_α is calculated in following equation [3, 5, 6]:

$$g_\alpha = \sqrt{r_{a1}^2 - r_{b1}^2} + \sqrt{r_{a2}^2 - r_{b2}^2} - a_w \sin \alpha_{wt}, \tag{2}$$

where the tip diameters of the pinion and gear wheel are as follows:

$$r_{a1} = r_1 + (h_a + x_1 \cdot m_n), \tag{3}$$

$$r_{a2} = r_2 + (h_a + x_2 \cdot m_n). \tag{4}$$

From Eqs. (3) to (4), it is clear that the length of the line of action g_α is directly dependent on the addendum height h_{a1}, h_{a2} and factors of addendum modification x_1, x_2. Optimization of the geometric parameters of HCR gearing can be based on the objective function to achieve the maximum value of the contact ratio ε_α for a given centre distance a_w. The main optimization parameter at this level can be the addendum heights of teeth h_{a1}, h_{a2}, and factors of addendum modification x_1 and x_2. For a given distance between the centers of the wheels, x_c can be defined as the relationship between x_1 and x_2 [11, 12].

Addendum heights h_{a1} and h_{a2} can be found from the following equations:

$$h_{a1} = h_{a1}^* \cdot m_n, \tag{5}$$

$$h_{a2} = h_{a2}^* \cdot m_n, \tag{6}$$

where h_{a1}^* and h_{a2}^* are addendum heights for the module equal to one. Furthermore, it follows that

$$x_2 = x_c - x_1. \tag{7}$$

Consequently, this implies that the contact ratio is the objective function of both addendum heights and the addendum modification factor of pinion $\varepsilon_\alpha = f(h_{a1}^*, h_{a2}^*, x_1) = \max$, i.e., optimization parameters h_{a1}^*, h_{a2}^*; x_1 makes a nonlinear optimization of triple constraint, with limitation requirements defined for [11, 12]:

- removal of the meshing interference,
- minimum arc thickness of the tooth tip $s_{a1,2}$,
- distribution x_c to x_1, x_2 has to be performed through balancing specific slips, strength, or a particular condition, respectively compromising their combinations [11, 12].

Therefore, the most favorable solution is obtained by increasing the addendum height. However, there are a lot of geometrical and manufacturing constraints that have to be satisfied, thus limiting the increase of the contact ratio. Description of the geometrical and manufacturing constraints and their solution are thoroughly explained and solved in [11, 12].

Due to the high load capacity of HCR gear, and since thermal power is reduced, there is a great possibility that scuffing may occur, even before pitting. The origin of fatigue damaged tooth flanks (scuffing and pitting) directly depends on the load transfer.

4 Scuffing as the Most Important Damage of HCR Tooth Flanks

Scuffing tends to occur at the head of the large slip rates with the impact of high temperatures. It appears most often in high speed and highly stressed gearings. Scuffing is not a fatigue phenomenon, as it may occur at the beginning of the operation [7, 18]. There are several analytical methods for predicting the risk of scuffing; however, the threshold for determining whether a gear set will scuff remains mostly dependent on empirical results. The method for evaluating the risk of scuffing is a function of oil viscosity and additives; the operating bulk temperature of the gear; sliding velocity; the surface roughness of the gear teeth; gear materials and heat treatments; and surface pressure. The risk of scuffing is defined by comparing the calculated tooth contact temperature with the limiting scuffing temperature; this is accomplished through gear scuffing tests for each gear lubricant [7, 18].

Scuffing is not a fatigue phenomenon, and it may occur instantaneously. Based on the severity of the damage, scuffing can be categorized as mild, moderate, or severe. Scuffing is classified as mild if it occurs only on small areas of the teeth and is confined to the peaks of the surface asperities (Fig. 6a). It is generally non-progressive. Moderate scuffing occurs in patches that cover significant portions of the teeth. If the operating conditions do not change, moderate scuffing may be progressive. Severe scuffing (Fig. 6b) occurs on significant portions of the gear tooth (for example, the entire addendum, the entire dedendum, or both). In some cases, the surface material may be plastically deformed and displaced over the tip of

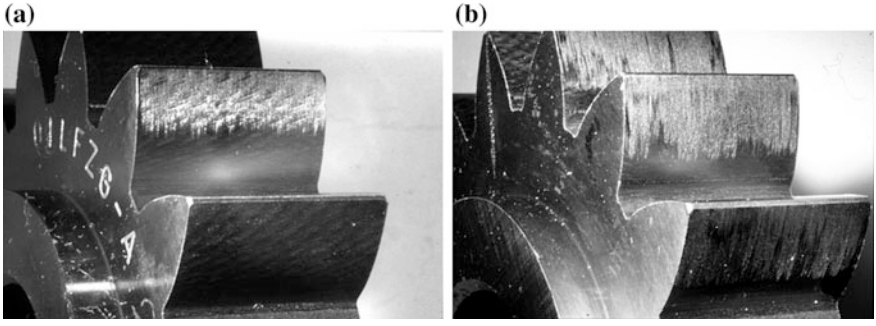

Fig. 6 Light scuffing (**a**), severe scuffing (**b**) [7]

the tooth or into the root of the tooth. Unless corrective measures are taken, severe scuffing is usually progressive [18].

Scuffing is severe adhesion that causes the transfer of metal from one tooth surface to another due to welding and tearing. The damage typically occurs in the addendum, dedendum, or both, away from the operating pitch line, in narrow or broad bands that are oriented in the direction of sliding. Scuffing may occur in localized patches if it is due to load concentrations. The scuffed area appears to have a rough or matted texture [7].

Scuffing is the process that occurs when the surfaces of two contacting bodies are joined by localized welding and then pulled apart. A material transfer occurs between the two contacting surfaces due to high metal-to-metal contact, and hence produces a weld. The high metal-to-metal contact is the result of a local failure of the gear lubricant, which has been caused by frictional heating due to high sliding speed and high surface pressure. This type of scuffing is called warm scuffing.

The scuffing traces appear in the form of streaks or scratches with rough bottoms and sides, often emerging as bands of variable depth and width oriented in the direction of the height of the tooth, affecting isolated zones or their whole width. The scuffing traces are generally more clearly marked at the tooth tip and root of the teeth in the high sliding zones.

In the case of warm scuffing, it is, in fact, the combined action of high pressure between surfaces, high sliding speeds, and excessive contact temperature resulting from pressure and sliding speed values, which causes the rupture of oil film between the tooth flanks. During the start-up or running-in of certain gears, some local scuffing of lesser importance, which is characterized by shallow traces and very fine roughness, may appear at certain points of the teeth in the zone where the contact pressure is at a maximum. In general, after a certain period of operation at reduced load, these localized traces of scuffing diminish by wear. Once this happens, the gear may operate under its nominal load. In this case, a slight increase in the lubricant viscosity will allow for better safety in service. On ground gears, localized scuffing can be observed at the tip and root of the teeth as the result of insufficient tip relief or too great a deviation in the profile. Identical phenomena can also appear near the tooth ends due to insufficient longitudinal correction or too great a helix deviation [7, 18].

When the failure occurs a long time after the start-up of the gearing, it is caused by an accidental faulty lubrication or an overload resulting from the continuous use of the machine in a manner for which it was not designed. However, if the failure occurs a short time after the start-up, one should examine whether the amount of heat generated by the gear is compatible with the choice of the gear geometry and the choice of lubricant. Objective signs of scuffing include a rapid increase of friction coefficient, wear, vibration, and a temperature increase in the total surface of the meshing wheels and lubricating oil, as well as increased noise transfer [19, 20]. Intensity of scuffing can be assessed by the change in the roughness of the tooth profile in relation to its width perpendicular to the direction of the slip. If there are deep scratches from 3 to 7 pm, they can be the cause of scuffing. When the process of scuffing gears begins, it may, depending on the conditions of friction,

stop after some time (surfaces with smooth flanks) or, conversely, the amount and intensity of scuffing characters in service may increase over time. Then, it is the case of limiting, or progressive scuffing [18].

Scuffing damage can be prevented through design changes or operational/break-in changes. Design-related changes include optimizing the gear geometry/accuracy and the use of nitrided steel. Operational and break-in changes include the use of high viscosity lubricants with anti-scuff additives, reduced lubricant temperatures, and the running-in of new gearboxes at reduced loads.

5 Calculating the Tooth Scuffing Resistance According to the Criterion of Integral Temperature

One of the hypotheses about the development of the scuffing phenomenon involves a temperature criterion. It is based on the assumption that there is a limit temperature of the surface of the teeth at which scuffing occurs. These criteria can be divided into those based on local instantaneous surface temperature and those based on the mean temperature of the surface of the teeth.

Theoretically, the best criterion among these criteria is the sophisticated Blok criterion (1937). Blok was one of the earliest researchers to study scuffing and to propose a hypothesis to explain the experimental observations. In his study, he suggested that scuffing would only take place if a critical temperature is reached at the sliding interface [21]. This is based on the assumption that for each combination of oil and gears of the material, there is still a critical temperature at which the oil loses its lubricating properties and will not protect the surfaces of the teeth from intermediate metal contact. It is assumed that the lubrication is effected by alloyed mineral oil. When the local temperature in the contact area between two tooth flanks reaches the critical value, then scuffing occurs. Critical instantaneous temperature, according to this theory, for a particular combination of metal-lubricating oil is constant and does not depend on the operating conditions of the transmission. Corresponding to the temperature disorientation of oil molecules on the metal surface, it is close to the evaporation temperature of the oil, and therefore does not depend on whether the teeth are in contact or in hydrodynamic boundary friction.

Instantaneous local temperature ϑ_C at the current contact of teeth meshing together on a Blok criterion consists of two components: the local instantaneous temperature (flash temperature, Blitztemperatur, ϑ_{Bl}), which both causes friction and increases the second component, the tooth bulk temperature ϑ_0; hence, it can be written as [21]

$$\vartheta_C = \vartheta_0 + \vartheta_{Bl}. \tag{8}$$

For the practical calculation of safety against scuffing of gearing, more favorable temperature criteria are those based on the mean surface temperature. One of the reasons is the fact that, when used, it is not necessary to know the local coefficient

of friction, radii of curvature, etc. These criteria, based on the mean temperature of the surface of the teeth, are the Lechner criterion (1966), the Seitzinger criterion (1971), the Winter-Michaelis criterion (1975) and calculation according to the Schauerhammer criterion (1978).

The Winter-Michaelis criterion of integral temperature (median average contact temperature) is among the most modern criteria for assessing resistance to tooth scuffing. It is based on defining the contact surface temperature of teeth in relation to the Blok theory. The calculation consists of identifying the instantaneous temperature along the mating line under the Blok and adding tooth bulk to a constant temperature. The comparative average temperature of the surface is then determined as the quotient of the integral thus calculated during the unsteady temperature along the mating line and a length image. The calculation of safety against scuffing of the teeth is a relatively simple one, and provides good agreement with measured or detected data in practice, both for pure mineral oils, but also for doped and synthetic oils. For these reasons, the integral temperature criterion appears to be the best comprehensive method published so far for calculating gearing resistance to scuffing. Therefore, in addition to the Blok criterion, it became a part of the standard DIN 3990 [8].

This paper will present the relations of integral temperature criterion for spur involute gears with high contact ratio (HCR). Since the Winter-Michaelis criterion is based on the Blok hypothesis (Eq. 8 [21]), it is first necessary to derive the formula for calculation of the instantaneous local flash temperature ϑ_{Bl}.

The instantaneous local temperature ϑ_C at the momentary contact of teeth meshing, together with the Blok criterion, consists of two components: the local instantaneous flash temperature (Blitztemperatur, ϑ_{Bl}), which causes friction, and the tooth bulk temperature ϑ_0.

5.1 *Local Instantaneous Flash Temperature* ϑ_{Bl} *for the Mated Teeth of HCR Spur Gears*

For calculation of the local instantaneous flash temperature ϑ_{Bl}, it is necessary to determine the place where the rise in temperature is the highest in the transition of the heat source.

According to Blok (flash temperature criterion), it is possible to express the flash temperature (local instantaneous flash temperature) at any point of meshing along the contact path, using the following formula:

$$\vartheta_{Bl} = 0.62\,\mu \left(\frac{F_n}{b}\right)^{0.75} \left(\frac{E_r}{\rho_r}\right)^{0.25} \frac{\left|v_{\rho 1} - v_{\rho 2}\right|}{\sqrt{\lambda_1\,\rho_1\,c_1\,v_{\rho 1}} + \sqrt{\lambda_2\,\rho_2\,c_2\,v_{\rho 2}}}. \tag{9}$$

Usually, in the literature, it is marked that $\lambda\ \rho\ c = B_M$, so it follows that

$$\vartheta_{Bl} = 0.62\,\mu w^{0.75}\left(\frac{E_r}{\rho_r}\right)^{0.25}\frac{\left|v_{\rho 1} - v_{\rho 2}\right|}{\sqrt{B_{M1}\,v_{\rho 1}} + \sqrt{B_{M2}\,v_{\rho 2}}}, \tag{10}$$

where

ϑ_{Bl} is the flash temperature (local instantaneous flash temperature);
μ is the mean coefficient of friction;
w is the normal unit load ($w = F_n/b$),
F_n is the normal force, b is the gear width;
E_r is the reduced modulus of the elasticity of the gear wheel;
ρ_r is the reduced radius of curvature at the point of mesh;
$v_{\rho 1,2}$ is the tangential velocity at the X profile point;
$\lambda_{1,2}$ are the coefficients of thermal conductivity of the wheel materials; and
$\rho_{1,2}$ are the specific densities of the wheel material.

6 General Principles of the Integral Temperature Criterion in HCR Involute Gearing

The integral temperature criterion is based on the middle temperatures of surface calculated on the basis of the Blok theory according to Eq. (10). The comparative medium temperature of surfaces ϑ_i (the integral temperature) consists of two temperatures: the medium value of local instantaneous flash temperature along the action line ϑ_{Blm} and the tooth bulk temperature ϑ_O [21].

Therefore, integral temperature is calculated from the following relationship:

$$\vartheta_i = \vartheta_0 + B\vartheta_{Blm}, \tag{11}$$

where B is a weighting factor which takes into consideration qualitatively different temperatures influencing the actual tooth bulk temperature ϑ_O and temperature ϑ_{Blm}, which is defined only as a comparative temperature, and does not reflect the actual size of the temperature at the contact points [21].

The medium value of the local flash temperature is determined from Eq. (10), which takes into account the medium friction coefficient μ_m taken along the meshing, so that the proportion of the integral local flash temperature ϑ_{Bl} taken along meshing and the length of the engagement line represent the temperature ϑ_{Blm}, i.e.,

$$\vartheta_{Blm} = \frac{\int_0^l \vartheta_{Bl}\,dx}{l}. \tag{12}$$

For determining the integral temperature ϑ_i from Eq. (11), it is necessary to determine the tooth bulk temperature ϑ_0. It can be assumed that the tooth bulk temperature principally consists of two parts. The first is the tooth surface temperature when it is not in contact (approximately equal to the temperature of the oil). The other part depends on the size of the difference between the integral temperature and the oil temperature, as well as from the values of the coefficients of thermal convection in the gear material and thermal transfer from the gear to the oil. If the coefficients of thermal convection and thermal transfer are included in the dimensionless coefficient A, it can be written that

$$\vartheta_0 = \vartheta_{oil} + A(\vartheta_i - \vartheta_{oil}). \tag{13}$$

The coefficients A and B in Eq. (13), resp. (11), are determined experimentally by measuring the temperature at the surface of the teeth. If Eq. (13) is substituted into Eq. (11), then it has the following form:

$$\vartheta_i = \vartheta_{oil} + \frac{B}{1-A}\,\vartheta_{Blm}, \tag{14}$$

or, simplified,

$$\vartheta_i = \vartheta_{oil} + C\vartheta_{Blm}, \tag{15}$$

where

$$C = \frac{B}{1-A}. \tag{16}$$

6.1 Calculating the Integral Temperature for HCR Involute Gearing

The size of the integral temperature is determined from Eq. (15), as

$$\vartheta_i = \vartheta_{oil} + C\frac{\int_0^l \vartheta_{Bl}\,dx}{l}. \tag{17}$$

The integral in Eq. (17) can be expressed in the form

$$\frac{1}{l}\int_0^l \vartheta_{Bl}\,dx = \vartheta_{Bl\,E}\,X_\varepsilon, \tag{18}$$

where $\vartheta_{Bl\ E}$ is the local flash temperature at the reference point of meshing E for the contact between teeth with the contact ratio $\varepsilon_\alpha = 1$, and X_ε is a dimensionless factor taking into account the distribution of the load between mating teeth, the contact ratio of the head of the pinion and gear wheel, and the geometric characteristics of the curve tooth profile [5].

If ϑ_{Bl} and $\vartheta_{Bl\ E}$ are expressed in Eq. (18) using (10), it follows that

$$X_\varepsilon = \frac{\int_0^l \frac{F_{bt}^{0.75}}{\rho_r^{0.25}} \left|\sqrt{v_{t1}} - \sqrt{v_{t2}}\right| dx}{\frac{F_{bt\,E\,\varepsilon_\alpha=1}^{0.75}}{\rho_{r\,E}^{0.25}} \left|\sqrt{v_{t1}} - \sqrt{v_{t2}}\right| l}, \tag{19}$$

and then

$$\vartheta_i = \vartheta_{oil} + C\vartheta_{Bl\mathrm{E}} X_\varepsilon, \tag{20}$$

where

ϑ_i is the integral temperature;
ϑ_{oil} is the oil temperature;
$\vartheta_{Bl\ E}$ is the local flash temperature at the reference point E with the contact ratio $\varepsilon_\alpha = 1$; and
X_ε is the factor of load distribution for HCR involute gearing (Fig. 7).

6.2 Determining the Factor X_ε for HCR Involute Gearing

HCR gearing is different from the standard profiles in different load distributions along the contact line and, obviously, there are also greater tangential velocities at the beginning and end of the meshing. If Eq. (10) is analyzed more deeply, it is

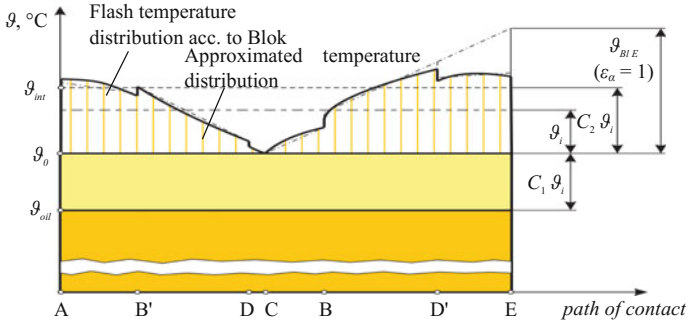

Fig. 7 Temperature distribution along the path of contact for HCR involute gearing

evident that, from the geometric parameter point of view, the main influence on the resistance to scuffing of the teeth can be attributed to the values of the tangential velocities and the value of the reduced radius of curvature.

It is obvious that, for determination of the factor of load distribution (X_ε), it is necessary to identify load distribution, the size of the radii of curvature and the tangential speed at any contact point. Basically, the main difference between the calculation of the integral temperature intensity for standard gearing and that for HCR gearing is determination of the factor of load distribution X_ε. Relations for X_ε are determined as a part of the area under the course curves of the local flash temperatures along the meshing (Fig. 7) and local flash temperatures at the point $E\varepsilon_\alpha = 1$ multiplied by the length of the meshing line (equivalent areas). The considered load distribution along the contact line is shown in Fig. 8 [12].

Equation (19) for involute gear can be simplified if it is considered that

$$\begin{aligned} v_{\rho 1} &= \rho_1\,\omega_1 \\ v_{\rho 2} &= \rho_2\,\omega_2\,. \\ u &= \frac{\omega_1}{\omega_2} \end{aligned} \tag{21}$$

Therefore, if considering the load distribution along the contact line (Fig. 8), and if the endpoint of contact, i.e., the point on the head of the pinion (point E), is considered to be the reference point for the calculation, then

$$X_\varepsilon = \frac{\int_0^l \frac{F_{bt}^{0.75}(x)}{\rho_r^{0.25}(x)} \left|\sqrt{\rho_1(x)\,\omega_1} - \sqrt{\rho_2(x)\,\omega_2}\right| dx}{l\,\frac{F_{bt\,E\,\varepsilon_\alpha=1}^{0.75}}{\rho_{rE}^{0.25}} \left|\sqrt{\rho_{1E}\,\omega_1} - \sqrt{\rho_{2E}\,\omega_2}\right|} \quad \text{or}$$

$$X_\varepsilon = \frac{\int_0^l F_{bt}^{0.75} \left|\sqrt[4]{\frac{\rho_1}{\rho_2}} - \sqrt[4]{\frac{\rho_2}{u^2\rho_1}}\right| dx}{l\,F_{bt\,E\,\varepsilon_\alpha=1}^{0.75} \left|\sqrt[4]{\frac{\rho_{1E}}{\rho_{2E}}} - \sqrt[4]{\frac{\rho_{2E}}{u^2\rho_{1E}}}\right|}. \tag{22}$$

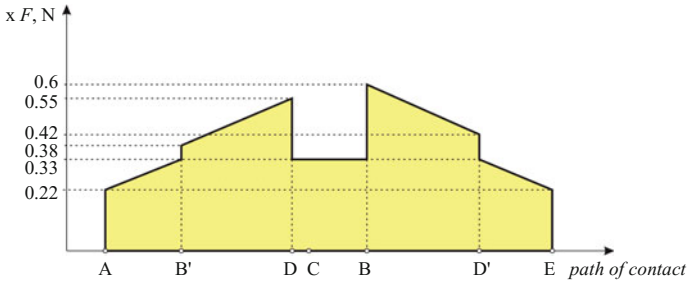

Fig. 8 Load distribution along the contact line for HCR involute gearing

However, Winter and Michaelis, in their criteria, foresaw a simplified waveform of temperatures along the contact line. Theoretical values of these temperatures apply strictly, and only at points C and E, with the change in temperature between these points being linear (Fig. 9) [12, 22]. In fact, this meshing could not occur with different radii of curvature of involute of both wheels, since the tangent at any individual point is linear, and the deviation between the actual and linear course for considering temperature is negligible.

The overall surface (P) under the flash temperature line during the entire contact of path of action can be replaced with the surface of a rectangle. The width of this rectangle is the same value as the contact line, while the height represents the integral temperature ($\vartheta_{Bl\ E}$):

$$\vartheta_{Bl} = P = \overline{AE} \cdot \vartheta_{Bl\,\mathrm{int}} = \vartheta_{Bl\,E} \cdot X_{\varepsilon} \cdot X_G \cdot X_M. \tag{23}$$

According to Fig. 9, it is possible to derive the relationship for the factor of load distribution (X_{ε}) for HCR involute gearing.

First of all, the overall surface is to be divided into six separate parts, and the relations for calculating these areas are as follows:

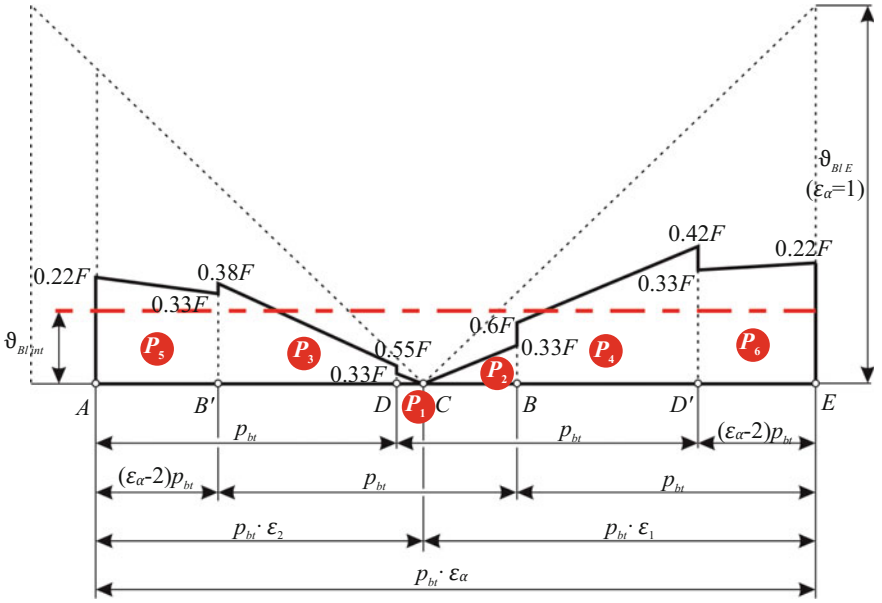

Fig. 9 Linear distribution of temperature along the path of contact for HCR involute gearing

$$
\begin{aligned}
P_1 &= \frac{\overline{CD}}{\overline{CE}}\,\vartheta_{BlE\varepsilon_\alpha=1}\cdot(0.33)^{0.75}\cdot\frac{\overline{CD}}{2},\\
P_2 &= \frac{\overline{CB}}{\overline{CE}}\,\vartheta_{BlE\varepsilon_\alpha=1}\cdot(0.33)^{0.75}\cdot\frac{\overline{CB}}{2},\\
P_3 &= \left(\frac{\overline{CB'}}{\overline{CE}}\,\vartheta_{BlE\varepsilon_\alpha=1}\cdot(0.38)^{0.75}+\frac{\overline{CD}}{\overline{CE}}\,\vartheta_{BlE\varepsilon_\alpha=1}\cdot(0.55)^{0.75}\right)\cdot\frac{\overline{B'D}}{2},\\
P_4 &= \left(\frac{\overline{CD'}}{\overline{CE}}\,\vartheta_{BlE\varepsilon_\alpha=1}\cdot(0.42)^{0.75}+\frac{\overline{CB}}{\overline{CE}}\,\vartheta_{BlE\varepsilon_\alpha=1}\cdot(0.6)^{0.75}\right)\cdot\frac{\overline{BD'}}{2},\\
P_5 &= \left(\frac{\overline{CB'}}{\overline{CE}}\,\vartheta_{BlE\varepsilon_\alpha=1}\cdot(0.33)^{0.75}+\frac{\overline{CA}}{\overline{CE}}\,\vartheta_{BlE\varepsilon_\alpha=1}\cdot(0.22)^{0.75}\right)\cdot\frac{\overline{AB'}}{2},\\
P_6 &= \left(\frac{\overline{CD'}}{\overline{CE}}\,\vartheta_{BlE\varepsilon_\alpha=1}\cdot(0.33)^{0.75}+\vartheta_{BlE\varepsilon_\alpha=1}\cdot(0.22)^{0.75}\right)\cdot\frac{\overline{D'E}}{2}.
\end{aligned}
$$

Secondly, the area under the polygon and line segments showing the tooth bulk temperature ϑ_O are provided by the following expression:

$$
\begin{aligned}
P &= \sum_{i=1}^{6} P_i\\
&= \frac{p_{bt}\vartheta_{BlE\varepsilon_\alpha=1}}{2\,\varepsilon_1}\left[-0.543\varepsilon_1\varepsilon_2+0.204\varepsilon_2^2+0.123\varepsilon_1^2+0.759\varepsilon_2+1.001\varepsilon_1-0.539\right].
\end{aligned}
\tag{24}
$$

Equation (22) for the factor of load distribution can be written in the following form:

$$
X_\varepsilon = \frac{P}{l\cdot\vartheta_{BlE\varepsilon_\alpha=1}}.
$$

Considering that $l = AE = \varepsilon_\alpha\, p_{bt}$, it follows that

$$
X_\varepsilon = \frac{1}{2\,\varepsilon_1\varepsilon_\alpha}\left[-0.543\varepsilon_1\varepsilon_2+0.204\varepsilon_2^2+0.123\varepsilon_1^2+0.759\varepsilon_2+1.001\varepsilon_1-0.539\right].
\tag{25}
$$

For comparison, Winter and Michaelis derived that for LCR gearing the following applies [5, 22]:

$$
X_\varepsilon = \frac{1}{2\,\varepsilon_1\varepsilon_\alpha}\left[0.18(\varepsilon_1^2+0.7\varepsilon_2^2)+0.82\varepsilon_1-0.52\varepsilon_2-0.33\varepsilon_1\varepsilon_2\right].
$$

6.3 Calculating Local Flash Temperature $\vartheta_{Bl\ E}$ for HCR Involute Gearing

To compare the resistance of particular types of gearing against scuffing, it is necessary to identify local flash temperatures ϑ_{BlE} at the reference point. The reference point is defined by the integral temperature for HCR involute gearing as the endpoint of contact line on the head of the pinion, i.e., the point E on the contact line.

The temperature at the reference point E can be expressed using Eq. (9):

$$\vartheta_{BlE} = 0.62\,\mu_m \left(\frac{F_{nE}}{b}\right)^{0.75} \left(\frac{E_r}{\rho_r}\right)_E^{0.25} \frac{\left|v_{\rho 1E} - v_{\rho 2E}\right|}{\sqrt{B_{M1}\,v_{\rho 1E}} + \sqrt{B_{M2}\,v_{\rho 2E}}}. \tag{26}$$

If the normal force F_{nE}, acting at the point E of the straight tooth (spur gear) is expressed, the tangential force F_0 on the rolling circle can be obtained from $F_{nE} = F_0/\cos\alpha_E$. Additionally, if it is considered that the gearing of both gear wheels is made of standard steel (i.e., $B_{M1} = B_{M2} = B_M$), Eq. (26) can be expressed in the following form:

$$\vartheta_{BlE} = 0.62\,\mu_m \left(\frac{w}{\cos\alpha_E}\right)^{0.75} \left(\frac{E_r}{\rho_r}\right)^{0.25} \frac{\left|\sqrt{v_{\rho 1E}} - \sqrt{v_{\rho 2E}}\right|}{\sqrt{B_M}}, \tag{27}$$

where $w = F_0/b$.

The values E_r and B_M depend only on the material of the meshing gear wheels. Then, the coefficient of material X_M can be defined by the expression

$$X_M = \frac{E_r^{0.25}}{B_M^{0.5}}. \tag{28}$$

For standard steel, it follows that

$$\sqrt{B_M} = \sqrt{\lambda\,\rho\,c} = \sqrt{50 \cdot 7800 \cdot 10^{-9} \cdot 482 \cdot 10^3} = 13.7\ \mathrm{Nmm^{-1}\,s^{-0.5}\,K^{-1}}$$

$E_r = 2.26 \cdot 10^{11}\ \mathrm{Nm^{-2}}$.

Then, the coefficient of material is calculated as $X_M = 50\ \mathrm{K\ N^{-0.75}\ s^{0.5}\ m^{-0.5}\ mm}$.

If Eq. (28) is substituted into Eq. (27), and ρ_{rE}, $v_{\rho 1E}$, $v_{\rho 2E}$ are substituted for the relations (21), after modification and arrangement, it follows that

$$\vartheta_{BlE} = \mu_m\, w^{0.75}\, v_0^{0.5}\, a^{-0.25}\, X_M\, X_G, \tag{29}$$

where X_G is a dimensionless coefficient of the gear geometry

$$X_G = 0.62\sqrt{u+1}\,\frac{\sqrt{\sin\alpha_{wt} + \frac{l_E}{r_1}} - \sqrt{\sin\alpha_E - \frac{l_E}{u\,r_1}}}{\sqrt[4]{u\,\sin\alpha_{wt} - \frac{l_E^2}{r_1^2\,\sin\alpha_{wt}} + \frac{l_E}{r_1}(u-1)}\cdot\sqrt[4]{\cos^3\alpha_{wt}}},$$

which can be modified in the following form:

$$X_G = 1.24\sqrt[4]{\frac{\mathrm{tag}\alpha_{wt}}{\cos^2\alpha_{wt}}}\cdot\frac{\sqrt{u+1}}{2}\cdot\frac{\sqrt{\rho_{1E}} - \sqrt{\rho_{2E}}}{\sqrt[4]{\rho_{1E}\rho_{2E}}}. \tag{30}$$

The product of the first two factors in the expression (30) is, for $\alpha_{wt} = 20°$, approximately equal to one. In [8], the factor X_G is presented in a simplified form as

$$X_G = \frac{\sqrt{u+1}}{2}\cdot\frac{\sqrt{\rho_{1E}} - \sqrt{\rho_{2E}}}{\sqrt[4]{\rho_{1E}\rho_{2E}}}. \tag{31}$$

However, for the pressure angle different from 20°, there is a lower accuracy in the calculations (for example, for $\alpha_{wt} = 25°$, there is a deviation of X_G of about 8%).

6.4 Calculating Medium Temperature of the Tooth Surface ϑ_{Blm} for HCR Involute Gearing

The size of the local instantaneous flash temperature ϑ_{BlE} is determined from the general Eq. (29). With respect to this relationship and Eqs. (15) and (20), there is an equation

$$\vartheta_{Blm} = \mu_m\, w^{0.75}\, v_0^{0.5}\, a^{-0.25}\, X_M\, X_G\, X_\varepsilon. \tag{32}$$

If the medium value of the coefficient of friction μ_m along the contact line is considered to be constant, then the general influence on the medium temperature value ϑ_{Blm} will be expressed with the product of the coefficients X_G and X_ε. Therefore, the occurrence of scuffing depends on the factor of load distribution (X_ε) and the factor of gear geometry (X_G).

The product of coefficients $X_G \cdot X_\varepsilon$ is crucial for assessment of the impact on the size of the temperature ϑ_{Blm}, and thus on the resistance to scuffing of HCR involute gearing. It is clear that there is strong dependence of the temperature ϑ_{Blm} on the shape of the tooth [8]. So, it is very important as to what profile is used for teeth meshing (involute, cycloidal, Novikov, etc.), since it determines the temperature in contact and the occurrence of scuffing.

If Blok's intensity of the local flash temperature of standard and HCR gearing is compared with comparable geometric characteristics, it is apparent that these temperatures are higher for HCR gearing. Figure 10 shows the plotting of Blok's local

flash temperatures along the contact path for gearing loaded by M_{k1} = 1000 Nm, and with the peripheral speed v_o = 12 m/s, for LCR gearing with $\varepsilon_\alpha \approx 1.6$. Local flash temperatures for HCR gearing with $\varepsilon_\alpha \approx 2$ are presented in Fig. 11. It is obvious that the values of local flash temperatures are smaller for LCR involute gearing than for HCR involute gearing. Therefore, it should be taken into account that the occurrence of tooth damage on scuffing is more possible for HCR involute gearing [12].

7 Optimization of Geometrical Parameters of HCR Gearing Based on Theoretical Considerations on the Properties of HCR Gearing in Terms of Its Resistance to Warm Scuffing

The main goal of the paper is to extend the validity of the integral temperature criterion (according to Winter and Michaelis) on external HCR involute gearing. The value of the integral temperature of mating gear flanks can be expressed by the relation projection of the graphs. One should consider the course of loading and tangential velocity along the meshing line according to Figs. 8 and 9.

Considering Eq. (20), the value of the local flash temperature ϑ_{BlE} at the meshing point E will be determined from Eq. (26) for specific parameters of the end point E, which is in the meshing of the pinion head.

The relation for X_ε is determined to be a part of the area under the course curves of the local flash temperatures along the mating line in Eq. (25).

For calculation of the integral temperature according to Eq. (20), it is necessary to identify the proportionality coefficient C. If we consider the tooth bulk temperature ϑ_O (the surface temperature of the tooth just before contact), the following relation can be applied (13):

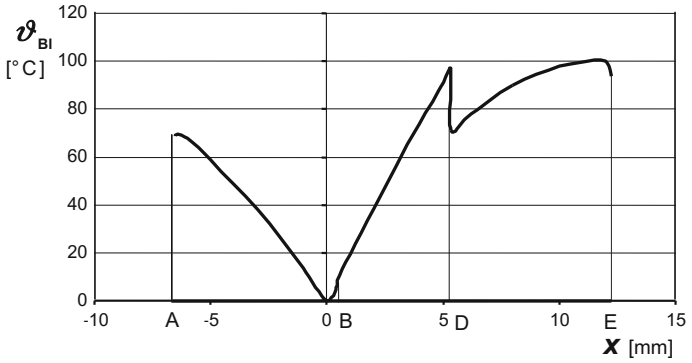

Fig. 10 Flash temperatures along the contact path of external involute gearing with an LCR profile

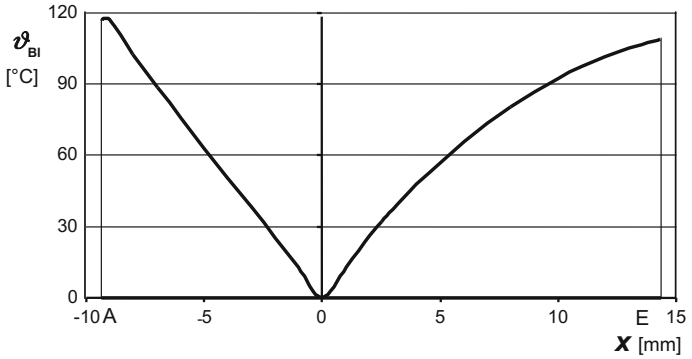

Fig. 11 Flash temperatures along the contact path of external involute gearing with the HCR profile $\varepsilon_\alpha \approx 2$

$$\vartheta_0 = \vartheta_{oil} + A(\vartheta_l - \vartheta_{oil}),$$

and, at the same time, according to Eq. (15), it is

$$\vartheta_i = \vartheta_{oil} + C\vartheta_{Blm}.$$

Comparing and taking into account the relation Eq. (20), the expression can be obtained as

$$C = \frac{\vartheta_0 - \vartheta_{oil}}{A\,\vartheta_{BlE}\,X_\varepsilon}. \tag{33}$$

The size of the coefficient C can be determined from Eq. (33), which is obtained using temperature values ϑ_0 and ϑ_{oil} determined from the measurement values ϑ_{BlE}. The coefficient A expresses the heat transfer from the oil to the gear wheel, and therefore cannot depend on the geometry of the teeth. Its size can be determined from the values of the coefficients B and C for the involute gear, which, according to [8], can be applied as B = 1.5 and C = 2.2. Then, from Eq. (16), it follows that

$$A = 1 - \frac{B}{C} = 0.31818 \quad \text{and} \quad C = \frac{\vartheta_0 - \vartheta_{oil}}{0.3\overline{18}\,\vartheta_{BlE}\,X_\varepsilon}. \tag{34}$$

The goal of the optimization is to obtain HCR involute gearing with a contact ratio factor of $\varepsilon_\alpha = 2$; yet, at the same time, the occurrence of scuffing must be avoided.

If the contact ratio has value two ($\varepsilon_\alpha = 2$), it means that two pairs of gears are always engaged. With this value of the contact ratio, the vibration and gear noise will be reduced, which is very important for the production of transmissions in the

automotive industry. In order to achieve a high contact ratio, the addendum height is made higher in order to obtain a larger line of action. Geometrical and manufacturing constraints are described and their solutions are thoroughly explained in [11, 12]. There are several constraints that should be satisfied (interference during production, meshing interference, minimum thickness of the tooth head circle, slide conditions in HCR involute gearing). According to [11, 12], several constraints are provided, and they come from the limitation condition of the following:

- interference during production:

$$g_{F1} = r_{b1} \tan \alpha_t - \frac{\left(h_{a1}^* - x_1\right) \cdot m_n}{\sin \alpha_t} \geq 0, \tag{35a}$$

$$g_{F2} = r_{b2} \tan \alpha_t - \frac{\left(h_{a2}^* - x_c + x_1\right) \cdot m_n}{\sin \alpha_t} \geq 0; \tag{35b}$$

- meshing interference:

$$B_1 = \sqrt{r_{b1}^2 + \left[a_w \sin \alpha_{wt} - g_{F2}\right]^2} \geq r_{a1}, \tag{36a}$$

$$B_2 = \sqrt{r_{b2}^2 + \left[a_w \sin \alpha_{wt} - g_{F1}\right]^2} \geq r_{a2}; \tag{36b}$$

- minimum thickness of the tooth head circle:

$$s_{a1} = 2r_{a1}\left(\frac{s_{kt1}}{2r_1} + inv\alpha_t - inv\alpha_{at1}\right) \geq 0.4m_n, \tag{37a}$$

$$s_{a2} = 2r_{a2}\left(\frac{s_{kt2}}{2r_2} + inv\alpha_t - inv\alpha_{at2}\right) \geq 0.4m_n. \tag{37b}$$

Furthermore, if the contact ratio should be achieved equal to two, there is an equation for the contact ratio which represents the goal function with the aim that it should have a value of two [23].

$$\varepsilon_\alpha = \frac{z_1}{2\pi}\left[\tan \alpha_{at1} - \tan \alpha_{wt} - i \cdot \tan \alpha_{at2} + i \cdot \tan \alpha_{wt}\right] = 2. \tag{38}$$

Beside the geometric condition, there is another requirement for avoiding the occurrence of scuffing and consequently reducing the rapid damage of tooth flanks. Using the same variable parameters h_{a1}^*, h_{a2}^* and x_1, the flash temperature at the reference point E (Eq. 26) is considered to be the highest temperature at the mating line. Since the occurrence of scuffing depends on the flash temperature, the value $\vartheta_{Bl\ E}$ should be an additional constraint requiring minimization. Since the occurrence of scuffing depends on the factor of load distribution (X_ε) and the factor of

gear geometry (X_G), the product of the coefficients $X_G \cdot X_\varepsilon$, is crucial for assessment of the impact on the flash temperature and thus on the resistance to scuffing of HCR involute gearing. According to Eqs. (27), (30) and (32),

$$\vartheta_{BlE} = \mu_m w^{0.75} v_0^{0.5} a^{-0.25} X_M X_{GE} X_{\varepsilon E} = f(X_{\varepsilon E} \cdot X_{GE}) \Rightarrow \quad f\left(\frac{\left|\sqrt{v_{\rho 1E}} - \sqrt{v_{\rho 2E}}\right|}{\left(\frac{1}{\rho_{rE}}\right)^{0.25}} \cdot \frac{\left|\sqrt{\rho_{1E}} - \sqrt{\rho_{2E}}\right|}{(\rho_{1E}\rho_{2E})^{0.25}} \right) \quad \Rightarrow \quad \min \tag{39}$$

and for both gears made of standard steel (i.e., $B_{M1} = B_{M2} = B_M$), the equation for $\vartheta_{Bl\ E}$ depends on variable parameters only in tangential velocities ($v_{\rho 1E}$ and $v_{\rho 2E}$), reducing the radius of curvature at the reference point E (ρ_{rE}) and the radii of curvature of profiles at the point E (ρ_{1E}, ρ_{2E}). Therefore, additional tooth parameters should be calculated:

- tangential velocity at the reference point E

$$v_{\rho 1E} = \rho_{1E}\,\omega_1, \quad v_{\rho 2E} = \rho_{2E}\,\omega_2, \quad u = \frac{\omega_1}{\omega_2}; \tag{40}$$

- radius of curvature of profiles at the reference point E

$$\rho_{1E} = r_{b1} \cdot \tan \alpha_{at1}; \quad \rho_{2E} = a_w \cdot \sin \alpha_{wt} - r_{b1} \cdot \tan \alpha_{at1} \tag{41}$$

- reduced radius of curvature at the reference point E

$$\frac{1}{\rho_{rE}} = \frac{1}{\rho_{1E}} + \frac{1}{\rho_{2E}}. \tag{42}$$

However, in order to demonstrate this hypothesis regarding the obtainment of a minimal flash temperature at the reference point E, the conditions for achieving a maximal temperature will be found:

$$\vartheta_{BlE} = \mu_m w^{0.75} v_0^{0.5} a^{-0.25} X_M X_{GE} X_{\varepsilon E} = f(X_{\varepsilon E} \cdot X_{GE}) \Rightarrow \quad f\left(\frac{\left|\sqrt{v_{\rho 1E}} - \sqrt{v_{\rho 2E}}\right|}{\left(\frac{1}{\rho_{rE}}\right)^{0.25}} \cdot \frac{\left|\sqrt{\rho_{1E}} - \sqrt{\rho_{2E}}\right|}{(\rho_{1E}\rho_{2E})^{0.25}} \right) \quad \Rightarrow \quad \max \tag{43}$$

The factor of load distribution (X_ε) and the factor of gear geometry (X_G) depend on the variables $v_{\rho 1E}$, $v_{\rho 2E}$, ρ_{1E} and ρ_{2E}, which are also the functions of variable parameters h_{a1}^*, h_{a2}^* and x_1, for the same centre distance a_w. Therefore, it is possible simultaneously to satisfy both of these functions: the objective function which must be equal to two and additional constraints accorded by scuffing. That is the reason for the strong dependence of the temperature ϑ_{Blm} on the shape of the tooth [8].

Obtaining the parameters for HCR involute gearing for maximal temperature at the reference point E, the condition for the occurrence of rapid scuffing on teeth flanks is achieved. Experimentally, it is proven on a test rig according to FZG methodology [12]. In this way, the hypothesis is proven in regard to obtaining minimal flash temperature, and thus obtaining parameters for minimal $\vartheta_{Bl\ E}$ and $\varepsilon_\alpha = 2$ as the solution to this problem.

8 Conclusions

Contact ratio is increased by increasing tooth height. Dynamic loads and noise are reduced by using high contact ratio gears. According to the results of different measurements of gear pairs, the reduction in noise proved to be best using HCR gearing with the contact ratio value $\varepsilon_\alpha = 2$. A decrease in noise is caused by $\varepsilon_\alpha = 2$, because there are always two pairs of teeth in contact, meaning that when one pair of teeth come out of contact, another pair of teeth comes into contact, while the applied force is considerably smaller, since it is divided between two pairs of teeth. Therefore, gearing in the automotive industry should be performed with $\varepsilon_\alpha = 2$ in order to reduce the noise and dynamic forces.

Due to the increased addendum height, there is a larger possibility of some interference or a pointed tooth tip to occur. Consequently, these errors should be prevented by verifying whether all equations and constraints are satisfied. Conditions for the teeth on the pinion and gear wheel are related to the following: conditions for non-occurrence of interference during the production—Eqs. (35a) and (35b), conditions for non-occurrence of meshing interference—Eqs. (36a) and (36b), conditions for minimal thickness of the tooth head circle of both gears—Eqs. (37a) and (37b), and an additional condition related to the balance of specific sliding at the beginning and end of meshing in order to reduce losses during meshing [11, 12].

Also, there is a possibility of the occurrence of scuffing due to higher tangential velocities and high pressure between teeth. Using the criterion of integral temperature, in order to avoid scuffing, the relation (39) must be minimized.

In previous chapters, two optimizations have been processed: geometric and thermal optimization. Combining these two optimization criteria, the problem of HCR gearing is solved, resulting in $\varepsilon_\alpha = 2$ with minimal possibilities of scuffing.

This geometric optimization problem of finding the optimal parameters for gears in order to equalize the contact ratio with two is very real, especially in the automotive industry. However, the analyses presented in this paper cover only external gear pairs. In the future, it would be very interesting to define the method and conditions for an internal gear pair, which is a common kind of gearing in this type of industry.

After researching the external and internal gear pairs and defining the kinematic conditions for obtaining the contact ratio of two, there is still a question as to whether the gears can achieve the expected load-carrying capacity for the defined

interval of time. In other words, will the flanks of teeth sustain loading for a sufficient period of time, without the occurrence of scuffing or pitting, or some other premature damage of the teeth? This requires introduction of new constraints and conditions related to the load carrying ability of and the influence of temperature on the teeth, which are all related to the condition of the high contact ratio of gears. This complicates the existing method for solving tasks and implies defining multiple tasks for achieving the contact ratio equalized by two and loading the torques with no premature damage on tooth flanks.

Therefore, a detailed theoretical analysis of the HCR geometry had to be performed, together with one on the impact of the shape of the involute HCR teeth on its scuffing resistance using the criterion of integral temperature. Besides the theoretical analysis, certain parameters of involute HCR gearing are provided in order to obtain experimental verification of the derived results according to relations of scuffing tests. After evaluating the impact of gearing geometry on its scuffing resistance from the point of integral temperature, it can be concluded that it is possible to achieve a smaller flash temperature, and thus increase the resistance to scuffing. Certainly, besides this condition, the type of transmission oil has a very important influence on the occurrence of scuffing. In other words, scuffing occurrence can be reduced using oils for extra pressure. Experimental verification should confirm if using this type of oil is necessary or not.

This article should contribute to the generalization of the integral temperature criterion for involute HCR gearing. It has been shown that relations for integral temperature criterion for involute HCR gearing need to include a calculation of the factor of load distribution for the case $\varepsilon_\alpha \geq 2$. In the continuation of this research, the criterion for the integral temperature of involute HCR gearing can be optimized and the minimal flash temperature can be obtained. For that case, the factor of load distribution (X_ε) and the factor of gear geometry (X_G) were derived for the case of involute HCR gearing.

This expanded criterion can be used in practice to determine the characteristics of the gears, first and foremost in construction within the automotive industry. In addition, for LCR gears, pitting is the most significant damage for teeth flanks; however, in applying HCR gears, the primary tooth damage is scuffing. Therefore, the calculation of HCR gears must first be performed for scuffing, and after that, for pitting. This procedure can be directly used in designing HCR gears, or as a basis for further theoretical and experimental research of scuffing on gear flanks.

Achieving these results, involute HCR teeth on gear wheels of automotive transmissions will have equal load-carrying capacity during their entire time of operation. Since the load is always distributed on two pairs of teeth, they can resist higher loading with smaller deformation and vibration.

References

1. Bonfiglioli Riduttori, S.P.A. (ed): Gear motor Handbook. Springer (1995)
2. Kuzmanović, S.: Universal Gear Reducers with Cylindrical Gears. University of Novi Sad, Faculty of Technical Sciences, Novi Sad (2009)
3. Muhs, D., Wittel, H., Jannasch, D., Voßiek, J.: Roloff/Matek Maschinenelemente—Normung, Berechnung, Gestaltung. Viewegs Fachbücher der Technik, Wiesbaden (2007)
4. Kuzmanović, S., Vereš, M., Rackov, M.: Product design as the key factor for development in mechanical engineering. In: Proceedings of International Conference Mechanical Engineering in XXI Century, Niš, Serbia, pp. 113–116 (2010)
5. Vereš M.: Odolnost ozubenia voči zadieraniu z hladiska jeho tvaru, Kandidatska dizertačna praca, Slovenska vysoka škola technicka v Bratislave, Strojnicka fakulta, Bratislava (1987)
6. Vereš, M., Bošanský, M., Rackov, M.: Theoretical and experimental research of the HCR gear´s contact strength. Machine Design. **3**(2), 105–108 (2011)
7. Michaelis, K.: Gear Failures—Scuffing (Course at the University of Ljubljana), Forschungsstelle für Zahnräder und Getriebebau Gear Research Centre, FZG TU München
8. Tragfähigkeitsberechnung von Stirnrädern—Berechnung des Freßtragfähigkeit, DIN 3990-4
9. Rackov, M., Milovančević, M., Kanović, Ž., Vereš, M., Rafa, K., Banić, M., Miltenović, A.: Optimization of HCR gearing geometry using generalized particle swarm optimization algorithm. Tehnički vjesnik/Technical Gazette **21**(4), 723–732 (2014)
10. Chao-Hsu, Y.: Automotive Transmissions: Efficiently Transferring Power from Engine to Wheels. Discovery Guides, ProQuest (2008)
11. Rackov, M., Vereš, M., Kanović, Ž., Kuzmanović, S.: HCR gearing and optimization of its geometry. Adv. Mater. Res. **633**, 117–132 (2013)
12. Rackov, M.: Optimization of HCR Gearing Geometry from Scuffing Point of View. Ph.D. thesis (in English), Slovak University of Technology in Bratislava, Faculty of Mechanical Engineering (2014)
13. Hassan, A.R.: Contact stress analysis of spur gear teeth pair. World Acad. Sci. Eng. Techn. 58 (2009)
14. Rameshkumar, M., Sivakumar, P., Sundaresh, S., Gopinath, K.: Load sharing analysis of high-contact-ratio spur gears in military tracked vehicle applications. Geartechnology (2010)
15. Kasuba, R.: Dynamic loads in normal and high contact ratio spur gearing. In: International Symposium on Gearing and Power Transmissions, Tokyo, Japan, pp. 49–55 (1981)
16. Sato, T., Umezawa, K., Ishikawa, J.: Effect of contact ratio and profile correction of spur gears on the rotational vibrations. Bull JSME **26**(221), 2010–2016 (1983)
17. Kahraman, A., Blankenship, G.W.: Effect of involute contact ratio on spur gear dynamics. ASME J. Mech. Des. **121**, 112–118 (1999)
18. Gears—Wears and Damage to Gear Teeth—Terminology, International Organization for Standardization, ISO 10825 (1995)
19. Kuzmanović, S., Vereš, M., Rackov, M.: Possible ways of reducing the number of gears in universal gear units. Trans. FAMENA **38**(1), 77–86 (2014)
20. Miltenović, A., Kuzmanović, S., Miltenović, V., Tica, M., Rackov, M.: Thermal stability of crossed helical gears with wheels made from sintered steel. Therm. Sci. **16**(Suppl. 2), S607–S619 (2012)
21. Blok, H.: Theoretical study of the temperature rise at surfaces of actual contact under oiliness conditions. Inst. Mech. Eng. Gen. Discuss. Lubr. **2**, 222–235 (1937)
22. Winter, H., Michaelis, K.: Scoring Load Capacity of Gears Lubricated With EP-Oils. Technical University of Munich, Gear Technology, October/November (1984)
23. Vereš, M., Bošanský, M., Rackov, M.: Possibility of the HCR gearing geometry optimization from pitting damage point of view. Zesz. Nauk. Politechniky Slaskiej, Transp. z. **76**, 125–128 (2012)

Problems of Developing the Model of Class of Objects in Intelligent CAD of Gearbox Systems

O. Malina

Abstract The paper considers the main principles and methods for development of the model for the class of complex objects through the example of a gearbox. This model allows for applying it as the informational foundation of the design system for samples of the class of objects.

Keywords Complex object · Principle of modularity · Principle of emergency · Principle of sufficiency · Graph model · Methods for development of the generalized model: graph · Table · Graph-table · Matrix · Phantom

1 Introduction

The processing and analysis of complex technical objects are problems with which design engineers are faced. These problems require special solutions in each individual case. As a rule, the initial problems arise when attempting to describe the structure (inner structure of the object) and interaction of individual elements of the complex object, which is not divided into the simplest components at its very first iteration. ***The complex object*** is the object consisting of the set of interacting elements due to which the object acquires unique properties, characteristics, and functions that are directly related to the set of initial elements. The complete representation of the complex object is formed not only through the list of its elements, but also through the description of relations between elements and such characteristics as the layout of elements, the production material, etc.

O. Malina (✉)
Kalashnikov Izhevsk State Technical University, Izhevsk, Russia
e-mail: malina_0705@mail.ru

V. Goldfarb et al. (eds.), *Advanced Gear Engineering*,
Mechanisms and Machine Science 51, DOI 10.1007/978-3-319-60399-5_19

2 Principles of Description for a Complex Object

Elements of the complex object can be complex objects themselves; in such a case, one should talk about the modular organization of the parent complex object. The guarantee of a correct description of any complex object is obedience to the basic rules that allow for formalizing the object, which are stated as principles [1]. As stated above, complex mechanical objects (such as the gearbox) are described through application of the **principle of modularity** when functionally-related parts are grouped into larger unities—nodes. Modular representation of technical objects that are complex systems allows for describing their organization, accounting for participation of one element of the object in the composition of other structures. This is of crucial importance, since, in accordance with **the principle of emergency**, the properties and characteristics of final elements cannot be attributed to "the maternal" structure, as it possesses unique properties that are not inherent to its component objects.

Complex systems differ by the varieties of their inner organization. In accordance with their structure, complex systems are divided into: structured (represented by hierarchic, cluster, mixed-type structures) and non-structured. It is possible to relate the gearbox, or, to be more exact, its layout, to the class of hierarchic systems by applying the principles of decomposition and composition. They allow the design engineer not only to determine the direction of analysis (that is, decomposing the product into units, sub-units, assembled units, assembled sub-units, parts and their surfaces), but also to check the correctness of the performed decomposition.

Formalization of the real object requires determination of the necessary and sufficient degree of specification of description and division into elements. Furthermore, it influences the efficiency of operation of the system of computer-aided design as a whole. The necessary degree of specification for describing the object is determined by **principles of sufficiency and necessity** (**principle of sufficient foundation**).

The principle of sufficient foundation is one of the main principles of the description of complex systems, since it regulates the completeness of information of systems. In accordance with this principle, description of the layout of the object allows for creating such a model of the object of mechanical engineering that accounts for all the features that distinguish the considered object from variations of its layout version.

However, this principle only demonstrates the reasonable description of the object. In our case, this principle should be used with refinement and restrictions on two ends: the maximum description (no greater is needed) and a limiting minimum (no less is allowed). Let us call such a differentiation **the principle of sufficiency from above and the principle of sufficiency from below**.

Meeting the requirement of sufficiency from above allows us to avoid the application of inessential principles of describing the object in regard to features, characteristics, parameters, modules that unreasonably widen the information

database of the classifier. One can relate here the specification of the structure, for example, standard parts (such as bearings or threaded surfaces). Sufficiency from below regulates the minimum volume of information about the object, which allows for identifying it unambiguously among similar objects and obtaining the complete representation of their inner organization. Therefore, due to application of the pointed principles of sufficiency, the optimal balanced state of the system is achieved and its function and productivity are maximized.

3 Order of Description for the Design Solution

It is evident from that stated above that description of the structure of the individual complex technical object is the revelation of features of its division into simpler modules and plotting of the "skeleton" of the layout into a united hierarchical tree-type structure; it is also the establishment of layout features and the characteristics of modules [2].

Plotting the skeleton is the process of step-by-step division of the layout into structure-forming modules in accordance with the practice of design engineering activity. Thus, the spiroid gearbox is decomposed into the gearwheel unit, the worm unit, and the casing unit (Fig. 1).

All elements are inter-related by links that indicate the hierarchy of the elements between each other (Fig. 1).

Therefore, the process of decomposition of the object is advanced from above (from the complex one) downwards (to the simpler one).

The next step in describing the object is the characterization, that is, separation, of specific features, namely characteristics that are inherent to modules of the object. Only an account of the characteristics of modules, along with the structural skeleton, gives us a structurally complete description of the object (Figs. 2, 3 and 4).

Revelation and description of characteristics is a complex process, since it requires analysis of the relevance of each characteristic. Among the whole set of potential characteristics, one should separate only those that are valuable and essential for the design process. Especially valuable characteristics are those that distinguish one object from another. The structure of the characteristic contains two fields: statement of the feature and the value of this feature that is inherent to this version of the module of the object. For example, the characteristic of the gearbox "gear ratio—50" consists of the feature "gear ratio" and the value "50".

During analysis of existing features as components of characteristics, the principle possibility of their uniting into groups has been revealed. Each of the five groups of features describes an independent area of the qualities of the object and its components. The first group involves characteristics of the mutual arrangement of objects with respect to each other. For example, supports of the gearwheel unit are separated. The second group is formed by parameters of manufacturing peculiarities or the manner of operation of functional structure-forming modules. The examples of such characteristics are versions of the assembly of the gearwheel and the shaft

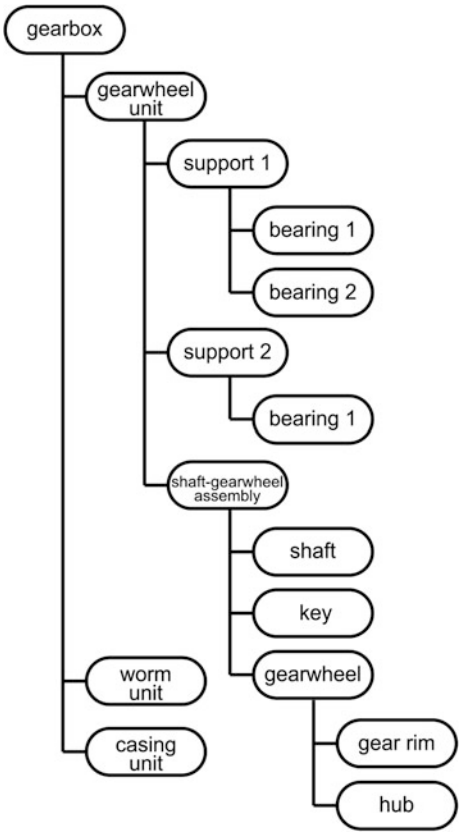

Fig. 1 Version of decomposition of the spiroid gearbox layout (fragment) for structure-forming modules

(press-fit or with the key). The third group describes the material of the module: aluminum, alloys, wood, plastics, etc. The fourth group involves parameters of the shape. The fifth and final group comprises quantitative characteristics: diameter of the gearwheel, 50 mm, gear ratio, 63, etc.

Note here that this classification of features only addresses the design problem. When developing the model of the class of objects to solve other problems, for instance, to implement the complete cycle of product repair, it can be necessary to know the manufacturers, suppliers or testing information for individual parts within the layout analysis.

Both structure-forming modules and their corresponding characteristics are inter-related by unidirectional links. The following types of links are present here: those between structure-forming modules and characteristics and those between characteristics and characteristics. The latter type of relation appears when the value of the characteristic is refined by additional information, for instance: the module is "spiroid gearwheel," the module characteristic is "material—bronze," the description of the characteristic is "temperature of the material melting."

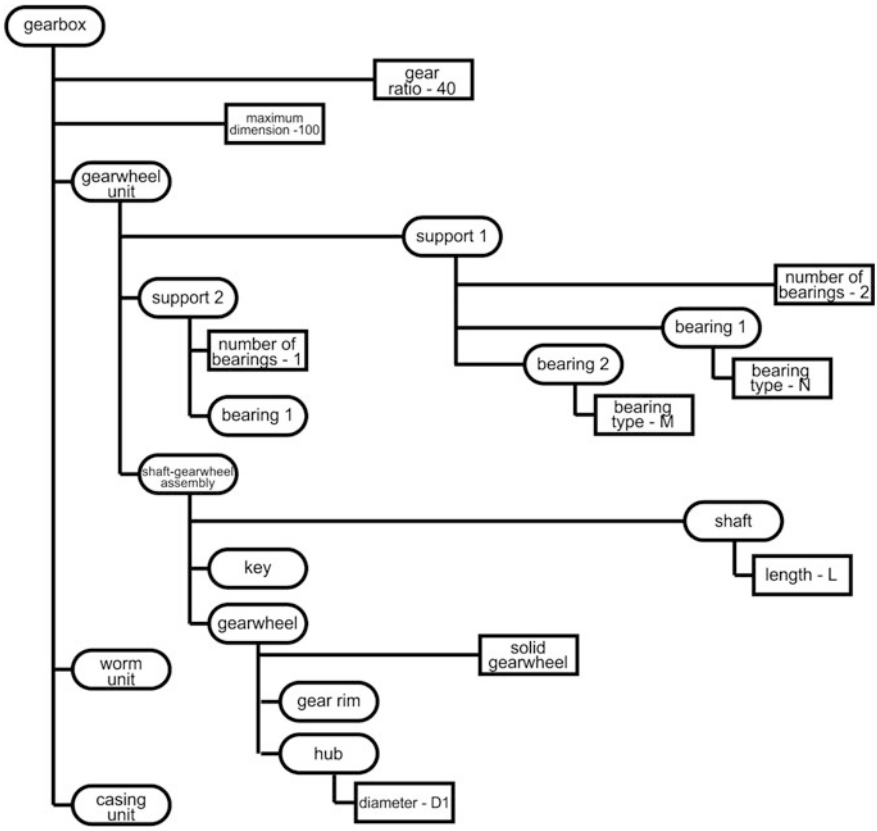

Fig. 2 Graph of decomposition of the 1st version of the spiroid gearbox layout (fragment)

Such a characteristic can be timely if the extreme conditions of the object's operation need to be taken into account.

The obtained models have a hierarchic structure.

4 Basic Background for Development of the Generalized Model

However, the description of individual objects does not have any practical importance without information on the whole class of objects through generalization of the information on its separate representatives. When comparing the description of individual structures that have been previously obtained and when generalizing the information on the structure and its design features and

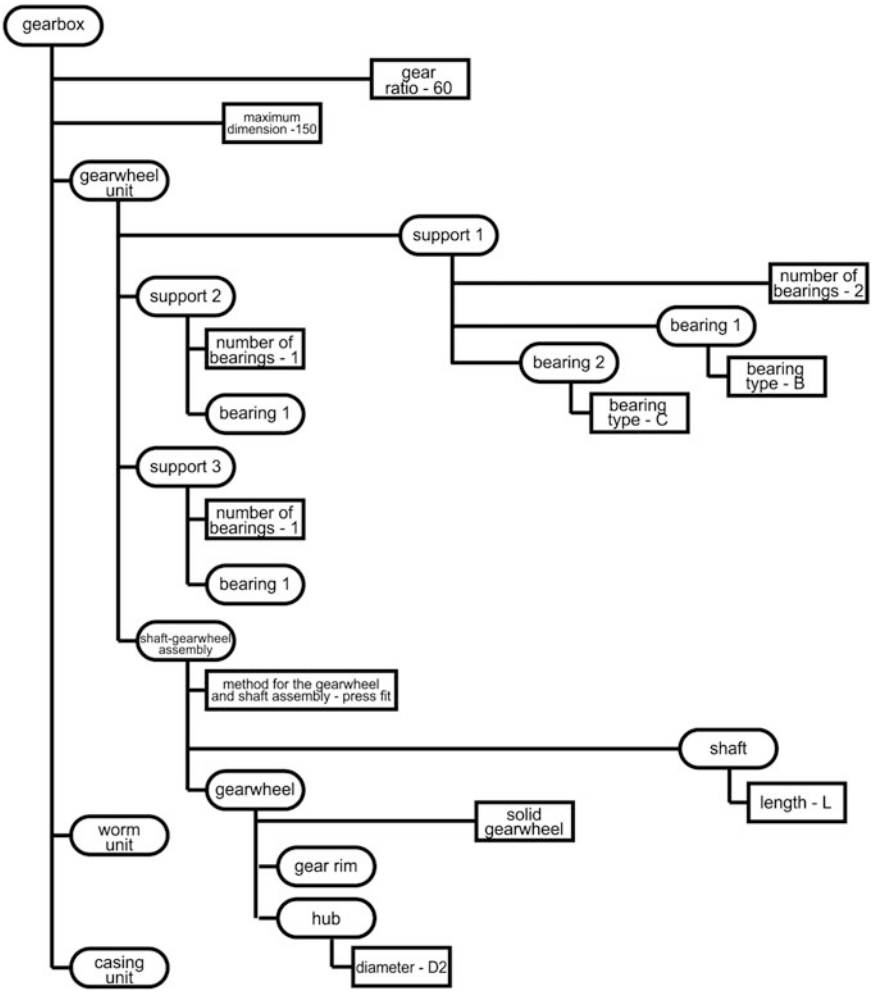

Fig. 3 Graph of decomposition of the 2nd version of the spiroid gearbox layout (fragment)

characteristics, one can obtain representation of essential distinctions between assorted technical solutions for one class of objects.

There are three principle types of distinction:

(a) for the set of structure-forming modules (units, assemblies, parts): presence/absence of a certain module with/without its substitution with the analog;
(b) for the set of characteristics that provide the structural completeness: presence/absence of a characteristic in the part of the feature, different values of characteristics in the part of the value.

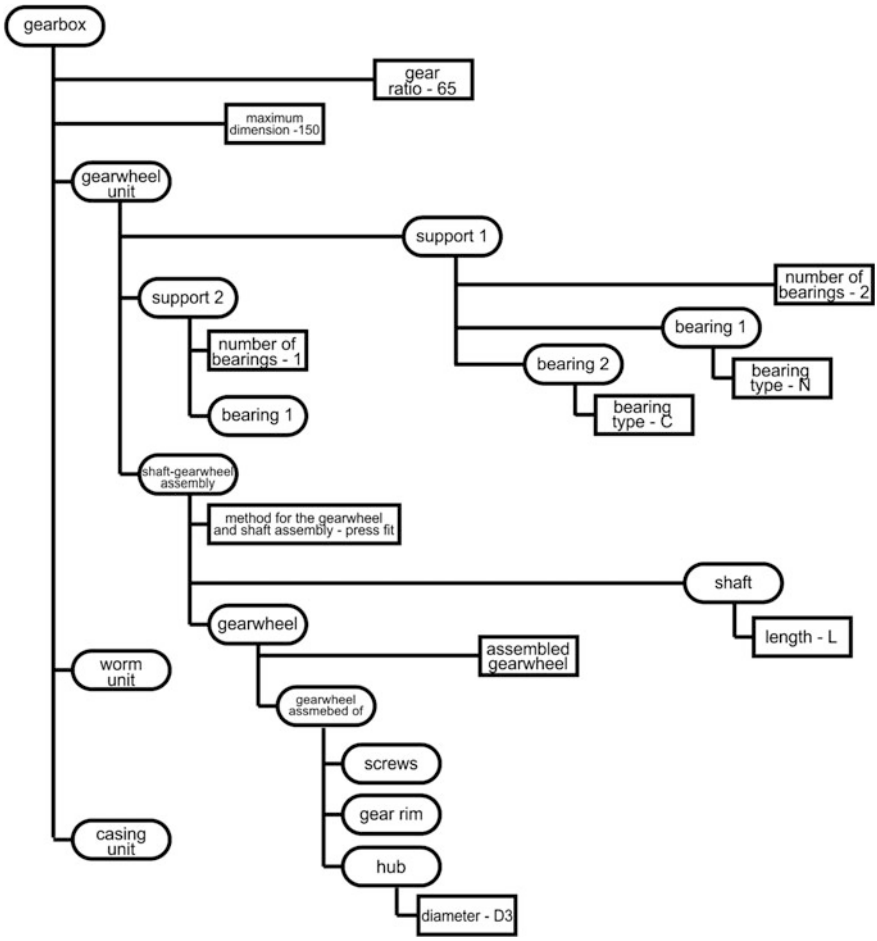

Fig. 4 Graph of decomposition of the 3rd version of the spiroid gearbox layout (fragment)

(c) for the set of links: presence/absence of the link.

The types of distinction considered allow for concluding that the structure of the model comprises both obligatory (always present in any version of the layout) and optional elements, their presence and character determining the different versions of one object within the class.

In accordance with the principle of inheritance of optionality, this optionality, in turn, may have a different character:

– with regard to the model as a whole;
– with regard to the maternal vertex in the hierarchical structure.

Optionality of the element with regard to the model as a whole indicates its alternative character within one class (it can be absent in certain versions of the layout).

Such optionality is passed down from the maternal vertex to its descendants.

Optionality with regards to the maternal vertex indicates that, moving along the model from the root downwards through this vertex within the given module, the change in character from obligatory to optional is possible.

It is important to keep this exact information about these elements in the generalized model of the class of objects. It is desirable here that the generalized model possess a tree-type structure to maintain the principle of inheritance of optionality.

When developing the algorithm of such a generalized model, one should consider that it must allow for solving the following assignments:

1. Generalization of all available information about many objects of the given class;
2. Widening of the existing model without change in the concept of its structure;
3. Generation of new information as the result of analysis of data present in the model (synthesis).

One such algorithm has been proposed in works by Polovinkin [3]. His model is based on representation of information on prototypes or known technical solutions as an "AND-OR" tree ("AND-OR" graph) in which functional modules that are at the same level and components of one functional module of a higher order are united by the operation "AND"; and modules and characteristics that are alternative (interchangeable) with respect to each other are united by means of the vertex "OR," shown in the form of rectangles (Fig. 5).

In order to synthesize a new layout of the object, it is necessary to move from the root vertex along all links united by vertexes "AND" by choosing an alternative version at each vertex "OR." In addition, checking the choice of the correct alternative is also necessary. In practice, implementation of such an algorithm of synthesis is complicated by the necessity to traverse a tree-type structure with an unlimited number of branches. The problem of keeping the tree-type structure also arises in cases when, for different technical solutions, one and the same module is related to different maternal vertexes that can be both hierarchically dependent upon and hierarchically independent of each other.

5 Graph Method for Development of the Generalized Model

To solve the problem of traversing the tree-type structure, an approach to organization of the model for generalization has been changed. It has been proposed by Malina [4, 5] that the "OR" vertex only be applied for uniting characteristics of modules, rather than the modules themselves. In this model, the characteristic has

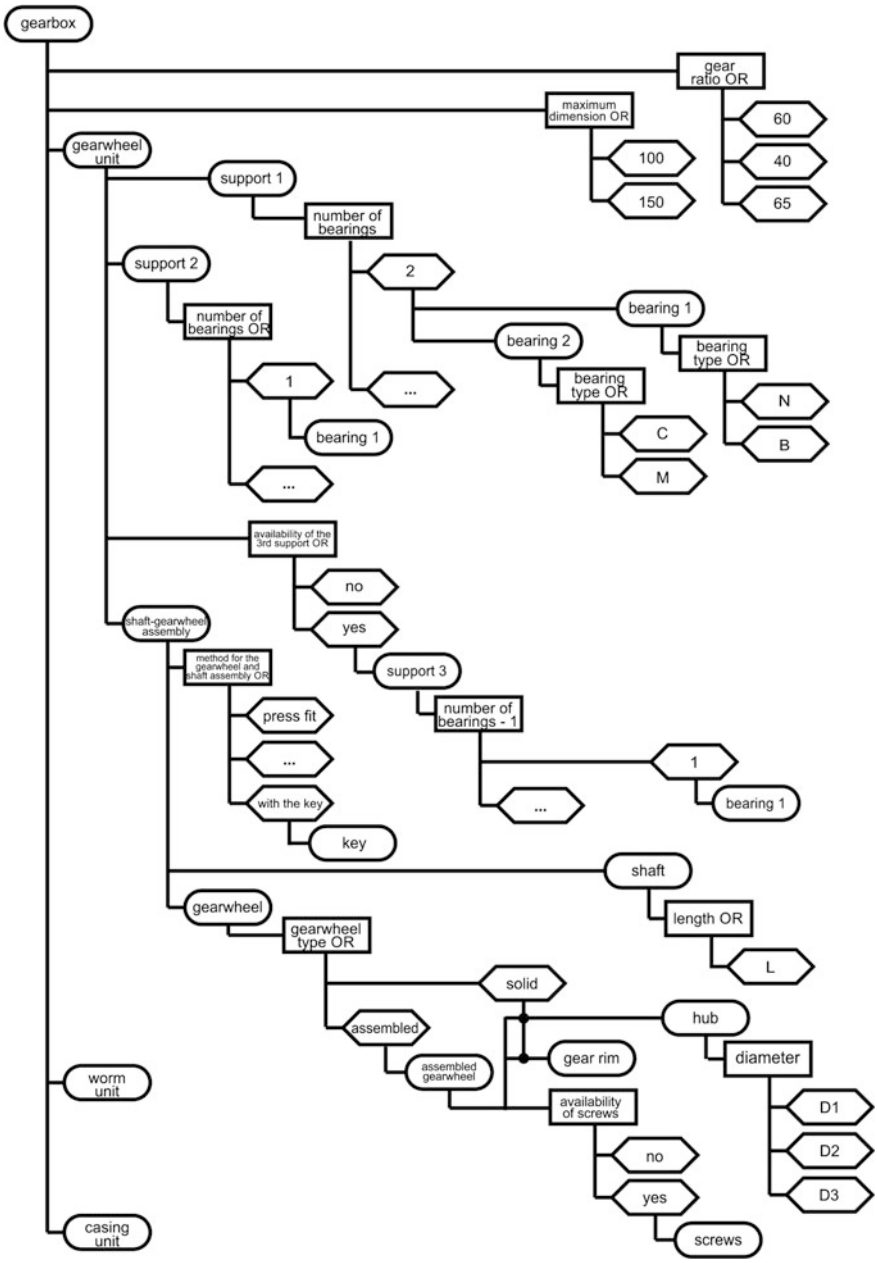

Fig. 5 The generalized "AND-OR" graph designed on the basis of the above-considered versions

been structurally decomposed into individual fields: the "OR" vertex designates the feature to which the values are related.

The proposed graph method for developing the generalized model implies the logical superposition (composition) of graphs of individual decompositions in order to obtain the unified graph that contains all vertexes of graphs and considers all relations between modules that have been called functional vertexes. The algorithm for obtaining the generalized graph is given below:

1. Graphs of individual versions of layouts are united and the graph is obtained having all vertexes and all links of the initial graphs (Fig. 6).
2. All vertexes that conform to characteristics and the corresponding links to these vertexes are eliminated from the obtained graph (Fig. 7).
3. Maintenance of the tree-type structure of the obtained graph is checked. If the tree-type structure is broken, that is, one daughter vertex has several maternal vertexes, the graph is upgraded: phantom structures are introduced. In practice, this means doubling the sub-trees of the daughter vertex in order to recover the tree-type structure (Fig. 8).
4. Each vertex is checked for its presence in all initial graphs. If it is absent, the feature ("OR" vertex) is generated at the maternal vertex with the statement "availability of the daughter vertex" and with two values "yes" and "no"; this daughter vertex is then marked with the attribute "optional—A." The same is done if the vertex that is present in all initial graphs is accepted as being optional by the expert.
5. For each functional vertex, alternative values of characteristics are considered. The feature meeting the corresponding field of the characteristics and values is generated at the functional vertex in this case. If not all initial graphs involved the characteristic with the pointed feature, the number of alternatives of the feature is supplemented with the "NILL" vertex; it designates the presence of the imaginary alternative.
6. "NILL" vertexes are added as values of all features of all functional vertexes accepted as being alternative ones.

"OR" vertexes that unite the alternatives allow for generating the set of features and their values (Fig. 9).

The set of features that are generated in accordance with the graph model will have the following character (Table 1). Features p13 and p14 are in italics, because they are obtained from the part of the graph structure, where the tree-type character is broken.

In this case, the process of synthesis can be considered as a Cartesian multiplication of all features with consequent analysis of the correctness of the sets.

It is possible to widen the scope of information resulting from expert survey by answering the questions stated in regard to features with obtainment of new values. The problem of breaking the tree-type structure does not influence the synthesis process, since the synthesis is not related to traversal of the tree. The drawback of the pointed approach is the complexity of the analysis, the need to account for alternative characteristics, and the presence of doubled features of phantom structures.

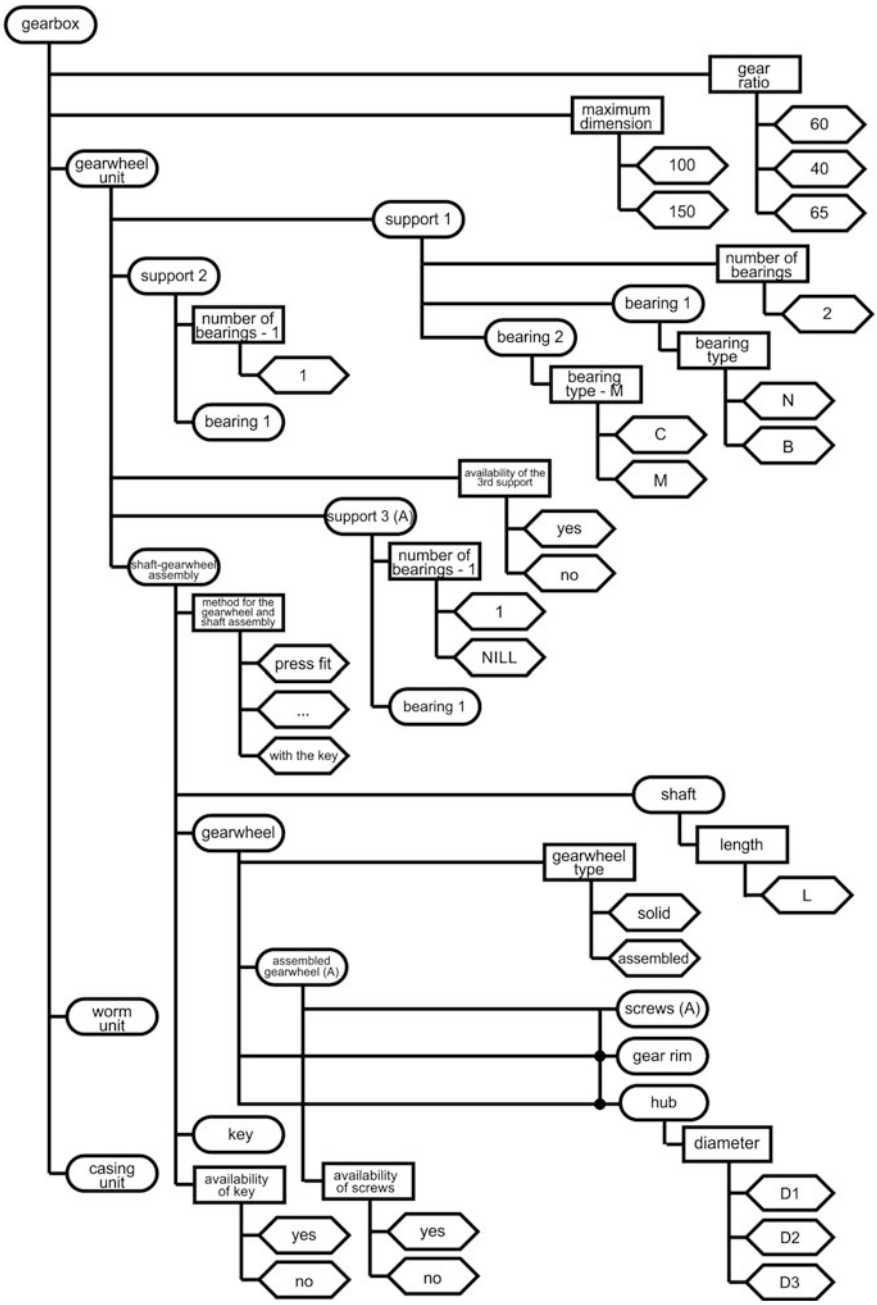

Fig. 6 Result of the 1st step of development of the generalized model

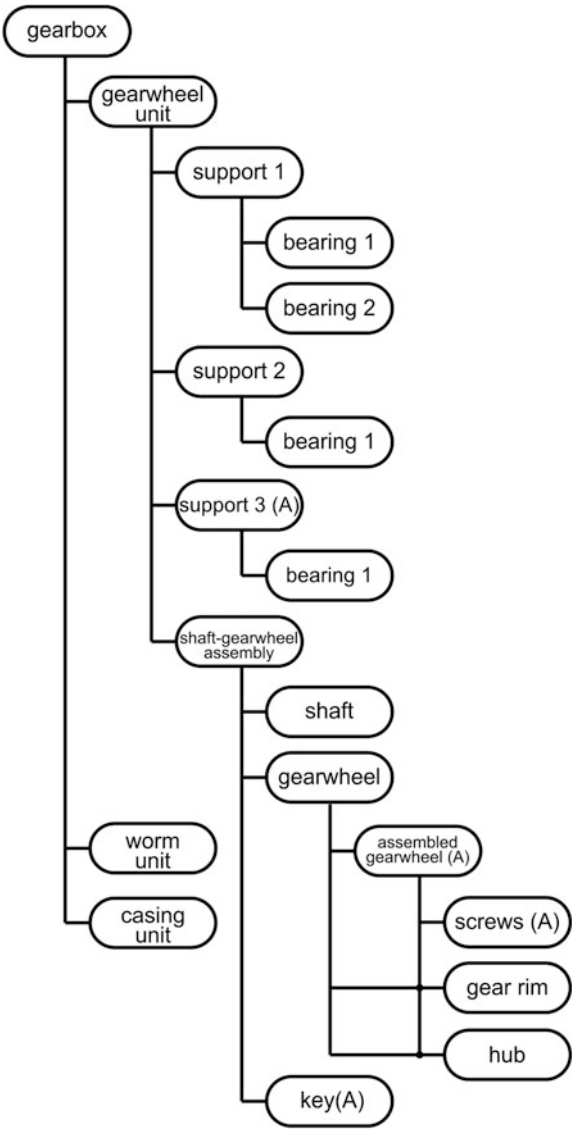

Fig. 7 Result of the 2nd step of development of the generalized model

6 Table Method for Developing the Generalized Model

The table method allows for generalizing the characteristics of the functional vertexes described in decompositions of samples of objects. In this case, the generalized model is represented as a table in which all vertexes of the generalized graph

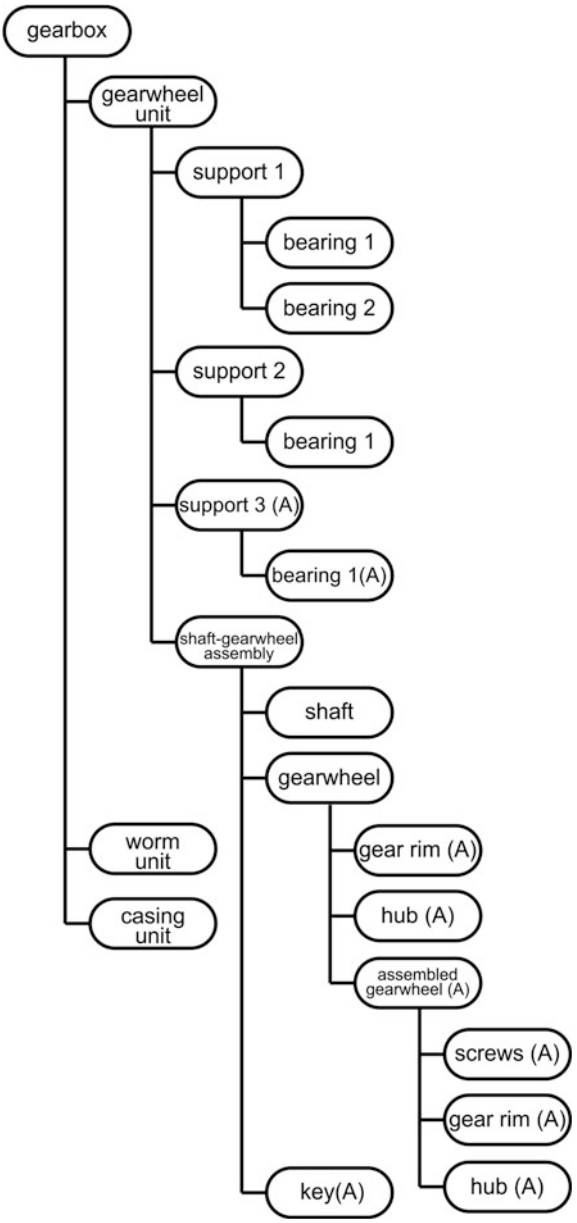

Fig. 8 Result of the 3rd step of development of the generalized model

model and their related characteristics are written down. The complete set of characteristics for each vertex is accumulated here as the result of knowledge of the generalization of this vertex in the graph model and generalization of the sets of characteristics of all decompositions.

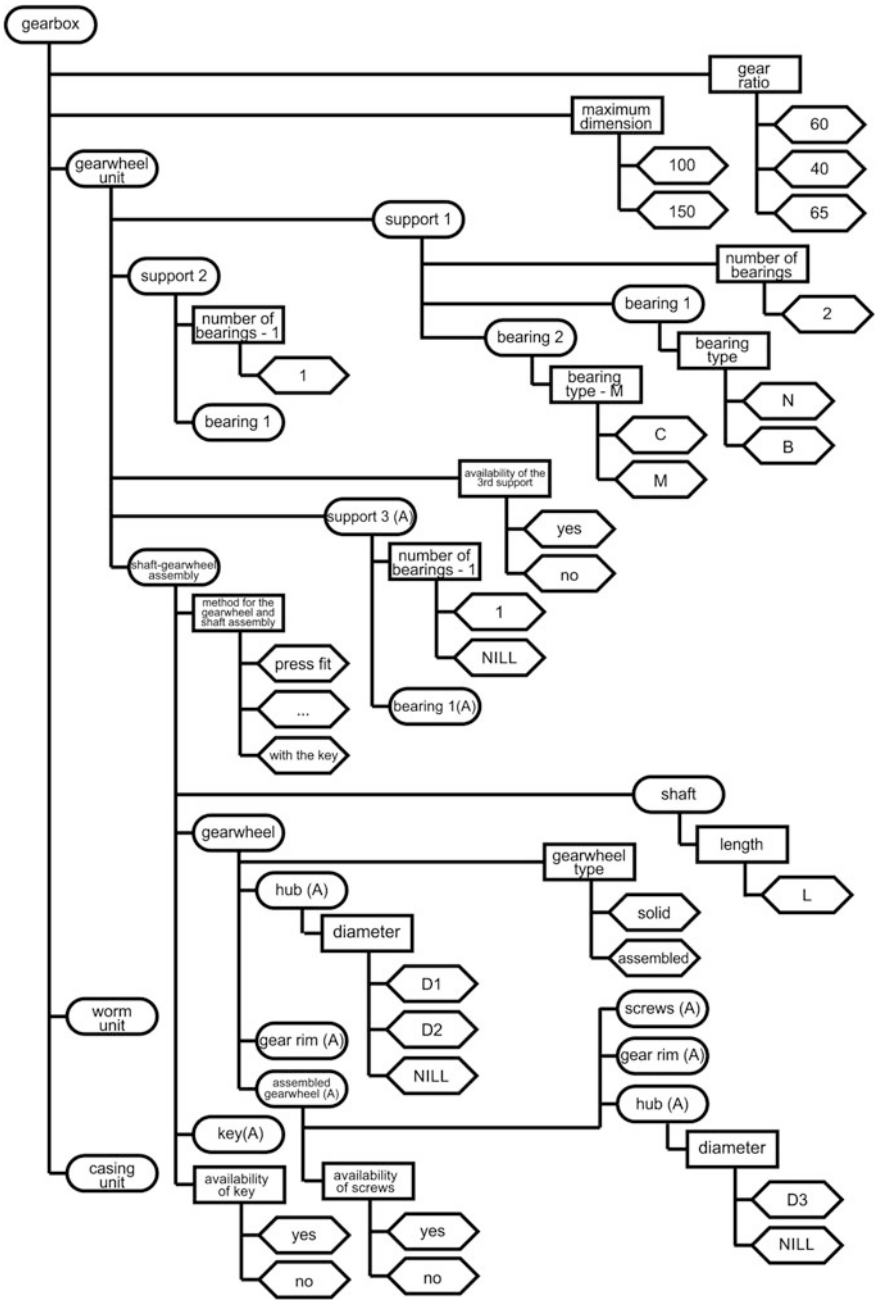

Fig. 9 The generalized graph model of the class of spiroid gearboxes (fragment)

Table 1 The set of features generated by the graph method

Functional vertex	Feature		Values	
Gearbox	Gear ratio	p1	60	a11
			40	a12
			65	a13
			Other	–
	Overall dimension	p2	100	a21
			150	a22
			Other	–
Support 1	Number of bearings	p3	2	a31
			Other	–
Bearing 1	Type of bearing	p4	N	a41
			B	a42
			Other	–
Bearing 2	Type of bearing	p5	M	a51
			C	a52
			Other	–
Support 2	Number of bearings	p6	1	a61
			Other	–
Gearwheel unit	Availability of the 3rd support	p7	Yes	a71
			No	a72
Support 3	Number of bearings	p8	1	a81
			Other	–
			NILL	a82
Shaft-gearwheel assembly	Method for the gearwheel and shaft assembly	p9	Press-fit	a91
			With the key	a92
			Other	–
	Availability of the key	p10	Yes	a101
			No	a102
Shaft of the gearwheel unit	Length	p11	L	a111
			Other	a112
Gearwheel	Type of the gearwheel	p12	Solid	a121
			Assembled	a122
Gearwheel hub	*Diameter*	*p13*	D1	a131
			D2	a132
			NILL	a133
			Other	–
Assembled gearwheel hub	*Diameter*	*p14*	D3	a141
			NILL	a142
			Other	–
Assembled gearwheel	Availability of screws	p15	Yes	a151
			No	a152

The resulting table can be obtained using the following steps:

1. The set of unique functional vertexes of the class of objects is generated by uniting the sets of functional vertexes of individual versions of layouts (decompositions);
2. Each vertex of the set is considered separately, having preliminarily been added to the set of unique functional vertexes. Then, all copies of this vertex are searched for in the set, the copies probably being available in other decompositions, in accordance with the comparability mark, name and functional purpose. After that, the found vertex and the vertex of the search are marked as those considered within this analysis.
3. Each line of the table is correlated with the identifying number and name of the functional vertex of the set; and each column of the table is correlated with the decomposition of the object as its identifying number.
4. For each set of the table, the identifying number and the value of the characteristic are fixed, being correspondent to the version of the layout (decomposition) and to the considered functional vertex. The identifying number of the characteristics is represented by the line «X.Y.Z», where X is the identifying number of the functional vertex, Y is the identifying number of the version of the layout (decomposition), and Z is the number of the group of alternative (correlated) characteristics. The choice of alternative characteristics is made through comparison of categories.
5. In case of the absence of a characteristic of the Z group for the X vertex of any of the graphs Y, the number below «X.Y.Z» should be written as NILL.

The specific value of the feature is chosen according to rules similar to those for developing the graph-generalized model.

Let us consider implementation of the table method with regard to the previously proposed example (Table 2).

After processing the obtained table, the following set of features is obtained (Table 3).

The comparative analysis shows that after applying the table method, features 7, 10, 14 and 15 are excluded from the set of features.

The disappearance of feature 14 has a favorable affect on the generalized model: there is no loss of data. Disappearance of features 7, 10 and 15 complicates the process of studying the obligatory character of vertexes.

7 Graph-Table Method

When analyzing and comparing the graph and table methods, their advantages and drawbacks become evident. The graph method is complicated by the necessity to analyze whether each vertex of the generalized model belongs in each of the individually-considered decompositions in order to reveal the optionality of the

Table 2 Summary table for description of versions of spiroid gearbox layouts (fragment)

No.	Functional vertex	1st graph		2nd graph		3rd graph	
1	Gearbox	1.1.1	Gear ratio—40	1.2.1	Gear ratio—60	1.3.1	Gear ratio—65
		1.1.2	Overall dimension—100	1.2.2	Overall dimension—150	1.3.2	Overall dimension—150
2	Gearwheel unit	2.1.1		2.2.1		2.3.1	
3	Support 1 of the gearwheel unit	3.1.1	Number of bearings—2	3.2.1	Number of bearings—2	3.3.1	Number of bearings—2
4	Bearing 1 of the support 1	4.1.1	Type of bearing—N	4.2.1	Type of bearing—B	4.3.1	Type of bearing—N
5	Bearing 2 of the support 1	5.1.1	Type of bearing—M	5.2.1	Type of bearing—C	5.3.1	Type of bearing—C
6	Support 2 of the gearwheel unit	6.1.1	Number of bearings—1	6.2.1	Number of bearings—1	6.3.1	Number of bearings—1
7	Bearing 1 of the support 2	7.1.1		7.2.1		7.3.1	
8	Support 3 of the gearwheel unit		NILL	8.2.1	Number of bearings—1		NILL
9	Bearing 1 of the support 3			9.2.1			
10	Shaft-gearwheel assembly	10.1.1	Method for assembly—not indicated	10.2.1	Method for assembly—press-fit	10.3.1	Method for assembly—press-fit
11	Shaft	11.1.1	L	11.2.1	L	11.3.1	L
12	Key	12.1.1					
13	Gearwheel	13.1.1	Type of gearwheel—solid	13.2.1	Type of gearwheel—solid	13.3.1	Type of gearwheel—assembled
14	Assembled gearwheel					14.3.1	
15	Screws					15.3.1	
16	Gear rim	16.1.1		16.2.1		16.3.1	
17	Gear hub	17.1.1	Diameter—D1	17.2.1	Diameter—D2	17.3.1	Diameter—D3

Table 3 The set of features generated by the table method

Functional vertex	Feature		Values	
Gearbox	Gear ratio	p1	60	a11
			40	a12
			65	a13
			Other	–
	Overall dimension	p2	100	a21
			150	a22
			Other	–
Support 1	Number of bearings	p3	2	a31
			Other	–
Bearing 1	Type of bearing	p4	N	a41
			B	a42
			Other	–
Bearing 2	Type of bearing	p5	M	a51
			C	a52
			Other	–
Support 2	Number of bearings	p6	1	a61
			Other	–
Support 3	Number of bearings	p8	1	a81
			Other	–
			NILL	a82
Shaft-gearwheel assembly	Method for the gearwheel and shaft assembly	p9	Press-fit	a91
			With the key	a92
			Other	–
Shaft of the gearwheel unit	Length	p11	L	a111
			Other	a112
Gearwheel	Type of gearwheel	p12	Solid	a121
			Assembled	a122
Gearwheel hub	Diameter	p13	D1	a131
			D2	a132
			NILL	a133
			Other	–

vertex and need for use of the NILL mark. The table method easily allows for revealing the necessity of using the optionality NILL marks, but is harder in regard to following the hierarchic links between elements of the generalized graph in order to form the "availability of the optional vertex" feature.

Accounting for the advantages and drawbacks of both methods, a hybrid graph-table method for developing the generalized model has been designed. Application of the graph within this method is stipulated by visualization of representing the structure of the object accounting for all hierarchic links between its

vertexes, revelation of the connection component, the obligatory component of the graph, and vertexes that are alternative to each other. The table method is convenient for processing the characteristics of objects and revealing the necessity to use the optionality NILL mark, the character of which is specified by the graph. The table method does not require analysis of the presence of the functional vertex in each considered decomposition.

The algorithm for developing the generalized model by means of the graph-table method is given below.

1. Graphs of individual versions of layouts are united and the graph is obtained that has all the vertexes and links of the initial graphs.
2. All vertexes corresponding to the characteristics and the correlated links to these vertexes are excluded from the obtained graph.
3. Each vertex is checked for its presence in all initial graphs. If it is absent, the feature ("OR" vertex) is formed at the maternal vertex with the statement "availability of the daughter feature" and with two values "yes" and "no"; this daughter vertex is then marked with the attribute "optional—A." If there are several maternal vertexes, the feature "availability …" is characterized at each maternal vertex. The same is done if the vertex that is present in all initial graphs is accepted as being optional by the expert.
4. For each vertex, an individual table is developed in accordance with the table principle of the model formation.

The pointed approach allows for not losing the features' "availability," thus simplifying the process of inheriting the optionality, as well as simplifying other features due to the ease of the table comparison.

8 Matrix Method

The graph-table method allows for developing the generalized model of the class of objects; however, it is rather bulky from the generalization point of view: graphs need to be visually compared, and at large numbers of decomposition, they require considerable effort for generalization. The table method is also rather bulky and it is not visual without its relation to the graph. The proposed matrix method [6] essentially simplifies the process of generalization of decompositions into a single model, revelation of pseudo-obligatory, non-obligatory components of the generalized graph and, use of the optionality NILL marks.

In order to describe each individual sample of the class of objects, the adjacency matrix is used; it is "… the rectangular matrix, each line of which corresponds to the neighboring node of the net, and each column corresponds to its attributed resource. The record arranged at intersection of the column and the line indicates the type of access to the resource provided by the given node" [7]. In our case, the line corresponds to the maternal vertex and the column corresponds to the daughter;

and the factor "1" is indicated at the intersection, that is, it is the presence of the link between them.

In order to form the matrix, let us use the previously considered example, in which all the functional vertexes have already been revealed and enumerated (Table 4).

On the basis of the obtained matrices (Figs. 10, 11 and 12), the summary matrix (Fig. 13) is developed by imposing the initial matrices.

The result of summation of the columns allows for drawing a conclusion on the optionality of a portion of the vertexes: vertexes with a sum of corresponding columns less than the number of initial versions are optional.

Therefore, the following features have been stated (Table 5). Features p7, p16, p10 and p15 are in italics, since they appeared only as a result of the matrix method, as compared to Table 3.

The necessity of feature "availability" is determined by the maternal vertex, which has the line with a value different from 0 at the corresponding optional vertex.

The matrix method for development of the generalized model as the set of features is the simplest and most visual one.

Table 4 The list of functional vertexes

No.	Functional vertex
1	Gearbox
2	Gearwheel unit
3	Support 1 of the gearwheel unit
4	Bearing 1 of the support 1
5	Bearing 2 of the support 1
6	Support 2 of the gearwheel unit
7	Bearing 1 of the support 2
8	Support 3 of the gearwheel unit
9	Bearing 1 of the support 3
10	Shaft-gearwheel assembly
11	Shaft
12	Key
13	Gearwheel
14	Assembled gearwheel
15	Screws
16	Gear rim
17	Hub
18	Worm unit
19	Casing unit

Matrix	1	2	3	4	5	6	7	8	9	10	11	12	13	14	15	16	17	18	19
1		1																1	1
2			1			1				1									
3				1	1														
4																			
5																			
6							1												
7																			
8																			
9																			
10											1	1	1						
11																			
12																			
13																1	1		
14																			
15																			
16																			
17																			
18																			
19																			
Sum	0	1	1	1	1	1	1	0	0	1	1	1	1	0	0	1	1	1	1

Fig. 10 Matrix of conjugacy of the graph for the 1st version

Matrix	1	2	3	4	5	6	7	8	9	10	11	12	13	14	15	16	17	18	19
1		1																1	1
2			1			1		1		1									
3				1	1														
4																			
5																			
6							1												
7																			
8									1										
9																			
10											1		1						
11																			
12																			
13																1	1		
14																			
15																			
16																			
17																			
18																			
19																			
Sum	0	1	1	1	1	1	1	1	1	1	1	0	1	0	0	1	1	1	1

Fig. 11 Matrix of conjugacy of the graph for the 2nd version

Matrix	1	2	3	4	5	6	7	8	9	10	11	12	13	14	15	16	17	18	19
1		1																1	1
2			1			1				1									
3				1	1														
4																			
5																			
6							1												
7																			
8																			
9																			
10											1		1						
11																			
12																			
13														1					
14															1	1	1		
15																			
16																			
17																			
18																			
19																			
Sum	0	1	1	1	1	1	1	0	0	1	1	0	1	1	1	1	1	1	1

Fig. 12 Matrix of conjugacy of the graph for the 3rd version

Matrix	1	2	3	4	5	6	7	8	9	10	11	12	13	14	15	16	17	18	19
1		3																3	3
2			3			3		1		3									
3				3	3														
4																			
5																			
6							3												
7																			
8									1										
9																			
10											3	1	3						
11																			
12																			
13														1		2	2		
14															1	1	1		
15																			
16																			
17																			
18																			
19																			
Sum	0	3	3	3	3	3	3	1	1	3	3	1	3	1	1	3	3	3	3

Fig. 13 Summary matrix

Table 5 The set of features generated by the matrix method

Functional vertex	Feature		Values	
Gearbox	Gear ratio	p1	60	a11
			40	a12
			65	a13
			Other	–
	Overall dimension	p2	100	a21
			150	a22
			Other	–
Support 1	Number of bearings	p3	2	a31
			Other	–
Bearing 1	Type of bearing	p4	N	a41
			B	a42
			Other	–
Bearing 2	Type of bearing	p5	M	a51
			C	a52
			Other	–
Support 2	Number of bearings	p6	1	a61
			Other	–
Gearwheel unit	*Availability of the 3rd support*	*p7*	*Yes*	*a71*
			No	*a72*
Support 3	Number of bearings	p8	1	a81
			Other	–
			NILL	a82
	Availability of the bearing	*p16*	*Yes*	*a161*
			No	*a162*
Shaft-gearwheel assembly	Method for the gearwheel and shaft assembly	p9	Press-fit	a91
			With the key	a92
			Other	–
	Availability of the key	*p10*	*Yes*	*a101*
			No	*a102*
Shaft of the gearwheel unit	Length	p11	L	a111
			Other	a112
Gearwheel	Type of gearwheel	p12	Solid	a121
			Assembled	a122
Gearwheel shaft	Diameter	p13	D1	a131
			D2	a132
			NILL	a133
			Other	–
Assembled gearwheel hub	Diameter	p14	D3	a141
			NILL	a142
			Other	–
Assembled gearwheel	*Availability of screws*	*p15*	*Yes*	*a151*
			No	*a152*

Investigation of this approach allowed for studying non-standard situations. Let us consider some of them.

9 Optional Vertexes of Group Belonging

Functional vertexes of double necessity are present in the generalized model from the example considered above.

They are the vertexes 16 (gear rim) and 17 (hub). Their double necessity is testified to by the non-empty lines of the matrix in the corresponding columns.

Optionality of the vertex of group necessity is testified to by the presence of several filled lines in the column, the sum value of which is less than the number of initial versions of technical solutions subjected to analysis.

10 Phantoms

A phantom is the vertex of the model that describes the single technical solution with two parent vertexes.

The reason for the appearance of the phantom is the peculiarity of hierarchic decomposition, when one and the same vertex of a lower level is the component of two different modules of a higher level. Thus, in the double-stage gearbox, the shaft of the gearwheel of the first stage is actually the shaft of the worm of the second stage (Fig. 14).

As for the adjacency matrix, the phantom is seen at once; the sum value of its column is greater than 1 (Fig. 15).

The presence of phantoms in the initial version that participates in the synthesis of the generalized model modifies the algorithm for determining the optional elements.

After identification of the phantom in accordance with the matrix, and before uniting this matrix with other matrices to synthesize the generalized model, the initial matrix is modified. Values of 1 in the column corresponding to the phantom are replaced by other positive values different from zero, so that their sum can be equal to 1 (Fig. 16).

11 Conclusions

The considered problems of development of the generalized model and methods for their solution allow for talking about formalization of the stage of preparing the informational support of the structural synthesis of complex objects.

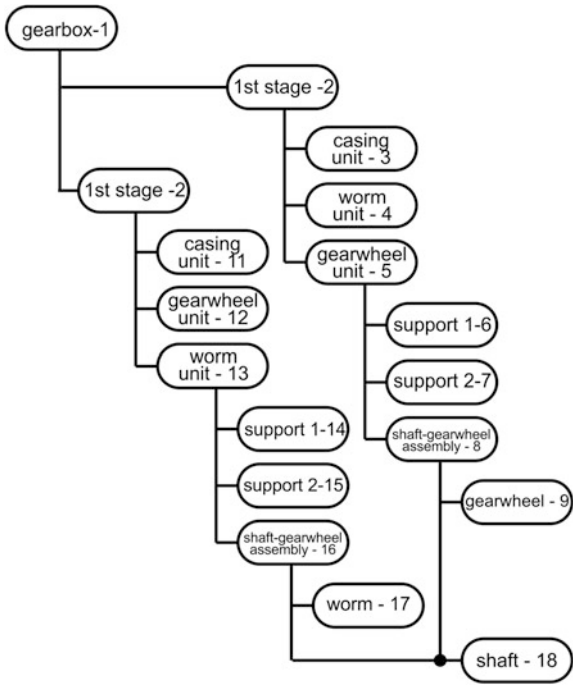

Fig. 14 Graph model of the version that contains the potential phantom

Matrix	1	2	3	4	5	6	7	8	9	10	11	12	13	14	15	16	17	18
1		1								1								
2			1	1	1													
3																		
4																		
5						1	1	1										
6																		
7																		
8									1									1
9																		
10											1	1	1					
11																		
12																		
13														1	1	1		
14																		
15																		
16																	1	1
17																		
18																		
Sum	0	1	1	1	1	1	1	1	1	1	1	1	1	1	1	1	1	2

Fig. 15 The initial matrix of the version that contains the potential phantom

Matrix	1	2	3	4	5	6	7	8	9	10	11	12	13	14	15	16	17	18
1		1								1								
2			1	1	1													
3																		
4																		
5						1	1	1										
6																		
7																		
8									1									1
9																		
10											1	1	1					
11																		
12																		
13														1	1	1		
14																		
15																		
16																	1	1
17																		
18																		
Sum	0	1	1	1	1	1	1	1	1	1	1	1	1	1	1	1	1	1

Fig. 16 Summary matrix of the version that contains the potential phantom

References

1. Malina, O., Urzhumov, N.: Principles of organization and steps of functioning of the module of development of the classifier for spiroid gearboxes. In: Proceedings of the International Conference "Theory and Practice of Gearing", Izhevsk, pp. 316–322 (2004) (in Russian)
2. Malina, O.: Information Models in Problems of Structural Synthesis. Information Mathematics, Moscow, pp. 184–193 (2001) (in Russian)
3. Polovinkin, A.: Theory of Design of New Machines: Trends of Machines and Their Application. Moscow, Informelectro (1991) (in Russian)
4. Goldfarb, V., Malina, O.: Skew axis gearing scheme classifier building technique. In: Proceedings of the Tenth World Congress on the Theory of Machines and Mechanisms, vol. l6, pp. 2227–2232 (1999)
5. Malina, O.: Features of application of tree-type structures in systems of computer-aided design. In: Proceedings of the Symposium "Information Mathematics in Informatiology", Moscow-Izhevsk, ISTU Publishing House, pp. 8–11 (1997) (in Russian)
6. Zarifullina, E., Malina, O.: Matrix approach to formation of the generalized model of the class of designed objects. In: Proceedings of All-Russia Scientific Practical Conference "Innovations in Science and Technology", Izhevsk, USU Publications, pp. 62–64 (2014) (in Russian)
7. Nevdyaev, L: Telecommunication techniques. English-Russian Reference Thesaurus, Moscow. http://www.technical_translator_dictionary.academic.ru/113983/матрица_смежности (2002)

Approximated Rod-Toothed Gears

B. Timofeev and M. Sachkov

Abstract The paper considers approximated rod-toothed gears with parallel and intersecting orthogonal operating axes. Results of mathematical simulation show that even significant errors in manufacture and assembly cause the variation of the transmission function which is one order less than its nominal value.

Keywords Approximated gears · Rod-toothed wheels and gears · Manufacture and assembly errors · Transmission function

1 Introduction

The application of approximated gears is enabled by two essential conditions. First, it is necessary to ensure localization of the bearing contact, that is, elimination of contact running out to any of the tooth edges [1–4]. Second, there is the condition that the cyclic error of the gear should not exceed the preliminary assigned limits at all possible manufacture errors for gearwheels and other elements of the gear, assembly errors and elastic deformations of the drive elements. Another essential condition can be the change in mutual position of the operating axes of the gearwheels during operation, wear of tooth surfaces [5], etc.

In the case of an absence of conjugacy, it is reasonable to apply simple surfaces for the meshing which are not related by the enveloping condition, especially the mutual one [6].

The present paper proposes the application of gears with teeth as cylindrical rods. Such gears, first of all, do not require gear-machining equipment for their manufacture. This can be a significant advantage in the case of a single-part or

B. Timofeev · M. Sachkov (✉)
Department of Mechatronics, ITMO University, Saint Petersburg, Russia
e-mail: Urie2006@yandex.ru

B. Timofeev
e-mail: timofeev@mail.ifmo.ru

V. Goldfarb et al. (eds.), *Advanced Gear Engineering*,
Mechanisms and Machine Science 51, DOI 10.1007/978-3-319-60399-5_20

small-batch production. Repair is enacted through a simple replacement of rods which can be represented by standard products, segments of standard rods of circular cross-section, and so on [7, 8].

2 Rod-Toothed Wheels

Figure 1a shows a rod-toothed gearwheel for which the axes of the rods are the generatrices of the cone. The angle at the apex of the back cone is taken to be α [9]. Arrangement of gearwheel axes on generatrices of a ruled hyperboloid is also possible, but such gears are not considered in this paper. The special case will be for gearwheels with $\alpha = 0$ and $\alpha = \pi$, that is, with the pitch surface made up of a cylinder and a plane (Fig. 1b, c).

An analog of the module for the wheel in Fig. 1a is assigned on the plane perpendicular to the operating axis of the wheel and passing through the reference point of contact in the meshing [10]. The diameter of the circle at the base of an additional cone that passes through the point of reconjugation of the rods (in the case of parallel operating axes) is equal to $D = m_A \cdot z$. It is evident that $2 \cdot d + c' m_A = p = \pi \cdot m_A$, where c' is the backlash factor, d is the diameter of the rod, m_A is the analog of the module, and p is the circular pitch. The backlash factor is determined according to the condition of the absence of interference in the meshing and based on investigations $c' = 0.25$.

Let us determine the addendum and dedendum in a manner similar to that of involute gearing.

Gearwheel parameters are explicitly determined by assigning the values d, z and α. Values of d will be standard here, as opposed to those for m_A.

3 Rod-Toothed Gears

The considered gears are serviceable when they have parallel, intersecting or skewed axes. Gears with parallel and intersecting axes are described in the present paper. Moreover, another restriction has been introduced: the skew angle for axes of interacting rods at the initial position is 90°. These gears are manufactured through the method of quick prototyping (with different numbers of rods and gear ratios) [11]. The gears possess interesting and practically valuable features.

Note that the gears are synthesized according to the following conditions: the geometric overlap ratio is equal to unity, the contact, in theory, is that of the point, re-conjugation takes place due to a knocking out of the pair from the meshing by a consequent pair with a velocity that is, in this instant, greater than that of the previous one.

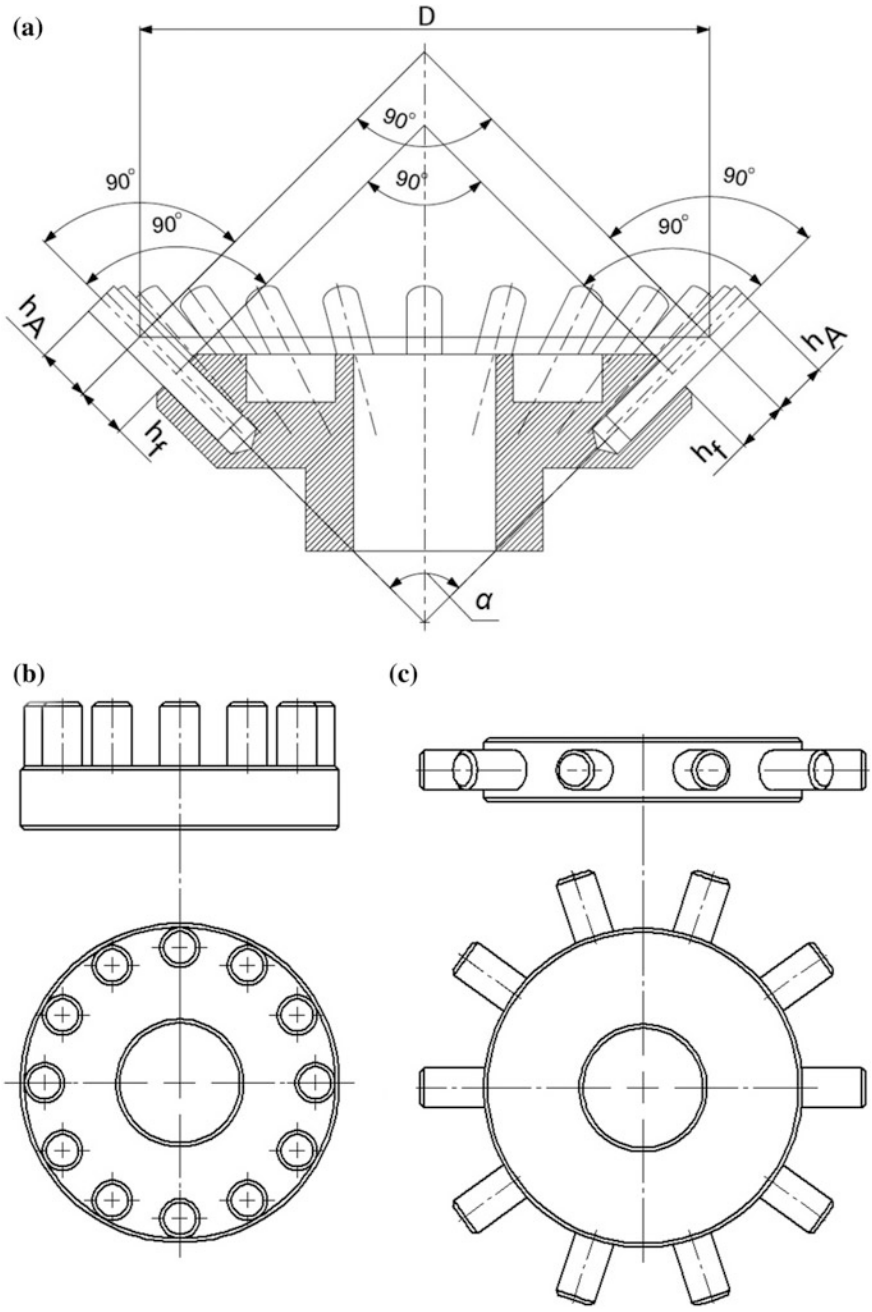

Fig. 1 Rod-toothed gearwheels with the angle at the apex of the back cone: **a** $\alpha = 90°$, **b** $\alpha = 0$, **c** $\alpha = 180°$

The paper also includes investigation of the variation in transmission error as a result of significant errors of manufacture and assembly, that is, greater than for the 8th degree of accuracy as rated in Russian standards GOST 1643-81 and GOST 1758-81.

4 Position Function of Gears with Parallel and Intersecting Orthogonal Axes

The paper summarizes the results of the mathematical simulation of a new approximated gear. The obtained results characterize kinematic parameters of rod-toothed gears with parallel and intersecting orthogonal axes. The investigations were founded on the basic statements of the theory of gearing. The application of matrix methods of spatial meshing analysis provides visualization and validity of the results [12, 13]. Coordinate systems related to the three-link mechanism (driving wheel, driven wheel and fixed stand) are represented in Figs. 2 and 3.

The position functions of the considered gears are obtained through equalities of position vectors and unit normal vectors at points of contact for surfaces of

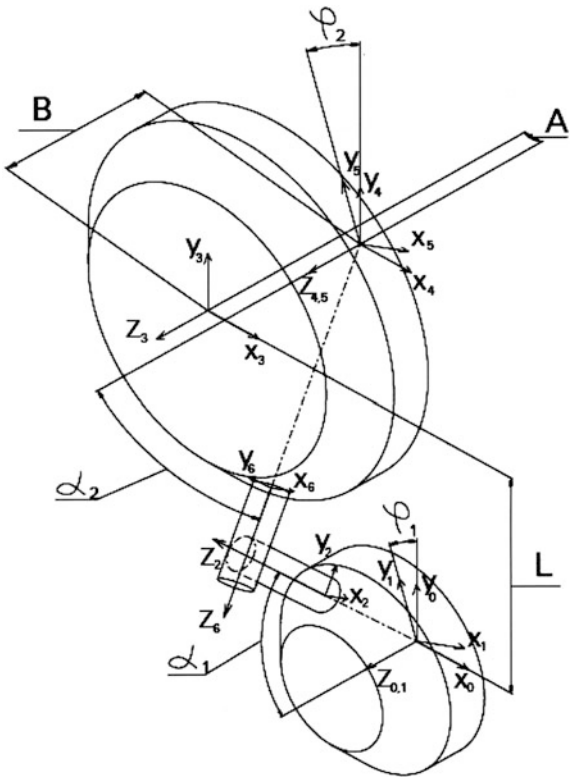

Fig. 2 Mutual arrangement of coordinate systems: a simplified representation of rod-toothed gears with parallel axes

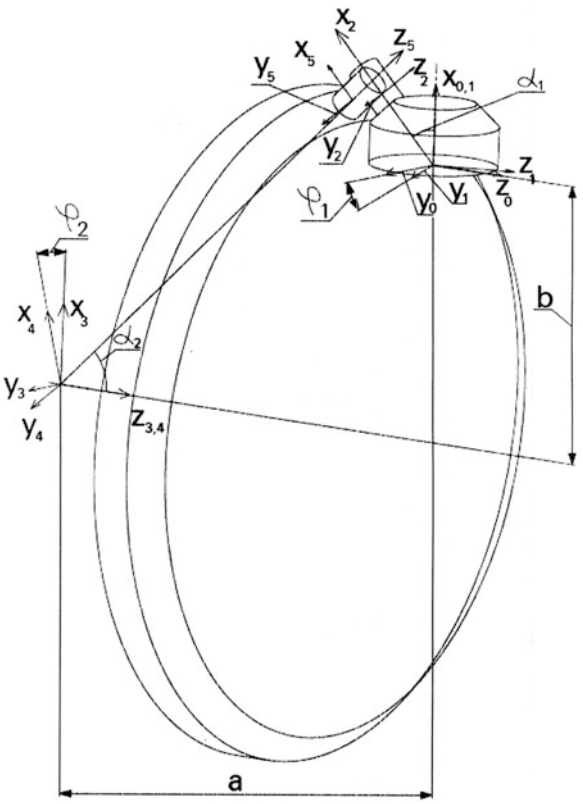

Fig. 3 Mutual arrangement of coordinate systems: a simplified representation of rod-toothed gears with intersected orthogonal axes

cylindrical rods Σ_1 and Σ_2. The equations of surfaces Σ_1 and Σ_2 in coordinate systems S_2 and S_6 (Fig. 1) are represented as follows:

$$x_2 = u_1; \quad y_2 = \rho_1 \cdot \sin\theta_1; \quad z_2 = \rho_1 \cdot \cos\theta_1;$$
$$x_6 = u_2; \quad y_6 = \rho_2 \cdot \sin\theta_2; \quad z_6 = \rho_2 \cdot \cos\theta_2,$$

where ρ_i is the radius of the ith rod. Unit normal vectors of surfaces Σ_1 and Σ_2 are written as

$$e_{x2} = \cos\theta_1; \; e_{y2} = \sin\theta_1; \; e_{z2} = 0; \; e_{x6} = \cos\theta_2; \; , e_{y6} = \sin\theta_2; \; e_{z6} = 0.$$

To transform the coordinates, let us use the following matrix equations: $\mathbf{r}^{(1)} = \mathbf{M}_{01} \cdot \mathbf{M}_{12} \cdot \mathbf{r}_2 = \mathbf{M}_{02} \cdot \mathbf{r}_2$; $\mathbf{r}^{(2)} = \mathbf{M}_{03} \cdot \mathbf{M}_{34} \cdot \mathbf{M}_{45} \cdot \mathbf{M}_{56} \cdot \mathbf{r}_6 = \mathbf{M}_{06} \cdot \mathbf{r}_6$, where M_{ij} is the matrix of transition from the ith coordinate system to the jth one [12].

In the considered equations, $\mathbf{r}_2$, $\mathbf{r}_6$ are column matrices of the position vectors of surfaces Σ_1, Σ_2 in the coordinate system S_2 and S_6. And $\mathbf{r}^{(1)}, \mathbf{r}^{(2)}$ are column matrices of the position vectors of the same surfaces in the fixed coordinate system

S_0. Therefore, the position function of the cylindrical (with parallel axes) rod-toothed gears (Fig. 3) is determined through the system Eq. (1):

$$\begin{cases} \rho_1 \cdot \cos\varphi_1 \cdot \cos\theta_1 - u_1 \cdot \cos\alpha_1 \cdot \sin\varphi_1 - \\ -R_1 \cdot \sin\varphi_1 - \rho_1 \cdot \sin\varphi_1 \cdot \sin\alpha_1 \cdot \sin\theta_1 - \\ -A - R_2 \cdot \sin\varphi_2 - u_2 \cdot \cos\varphi_2 \cdot \sin\alpha_2 - \\ -\rho_2 \cdot \cos\varphi_2 \cdot \cos\theta_2 + \rho_2 \cdot \sin\varphi_2 \cdot \sin\alpha_2 \cdot \sin\theta_2 = 0; \\ R_1 \cdot \cos\varphi_1 + u_1 \cdot \cos\varphi_1 \cdot \cos\alpha_1 + \rho_1 \cdot \cos\theta_1 \cdot \sin\varphi_1 + \\ + \rho_1 \cdot \cos\varphi_1 \cdot \sin\alpha_1 \cdot \sin\theta_1 - \\ -L + R_2 \cdot \cos\varphi_2 + u_2 \cdot \cos\varphi_2 \cdot \cos\alpha_2 - \\ -\rho_2 \cdot \cos\theta_2 \cdot \sin\varphi_2 - \rho_2 \cdot \cos\varphi_2 \cdot \sin\alpha_2 \cdot \sin\theta_2 = 0; \\ R_1 \cdot \tan\alpha_1 + u_1 \cdot \sin\alpha_1 - \rho_1 \cdot \cos\alpha_1 \cdot \sin\theta_1 - \\ -R_2 \cdot \tan\alpha_2 + B - u_2 \cdot \sin\alpha_2 - \rho_2 \cdot \cos\alpha_2 \cdot \sin\theta_2 = 0; \\ \cos\varphi_1 \cdot \cos\theta_1 - \sin\varphi_1 \cdot \sin\alpha_1 \cdot \sin\theta_1 + \\ + \cos\varphi_2 \cdot \cos\theta_2 - \sin\varphi_2 \cdot \sin\alpha_2 \cdot \sin\theta_2 = 0; \\ \cos\theta_1 \cdot \sin\varphi_1 + \cos\varphi_1 \cdot \sin\alpha_1 \cdot \sin\theta_1 + \\ + \cos\theta_2 \cdot \sin\varphi_2 + \cos\varphi_2 \cdot \sin\alpha_2 \cdot \sin\theta_2 = 0; \\ -\cos\alpha_1 \cdot \sin\theta_1 + \cos\alpha_2 \cdot \sin\theta_2 = 0; \end{cases} \quad (1)$$

In system Eq. (1): $R_1 = D_1/2$, $R_2 = D_2/2$, the distance $A = \rho_1 + \rho_2 = 2 \cdot \rho$, $L = (D_1 + D_2)/2$, $B = l_2 \cdot \cos(\alpha) - l_1 \cdot \cos(\alpha)$, and $l_i = (D_i/2 \cdot \sin(\alpha_i))$.

When rod-toothed wheels with intersecting orthogonal axes are operating, the equations of surfaces Σ_1 and Σ_2 in coordinate systems S_2 and S_5 (Fig. 4) are represented as

$$x_2 = u_1;\ y_2 = \rho_1 \cdot \cos\theta_1;\ z_2 = \rho_1 \cdot \sin\theta_1;$$
$$x_5 = \rho_2 \cdot \cos\theta_2;\ y_5 = \rho_2 \cdot \sin\theta_2;\ z_5 = u_2,$$

where ρ_i is the radius of the ith rod.

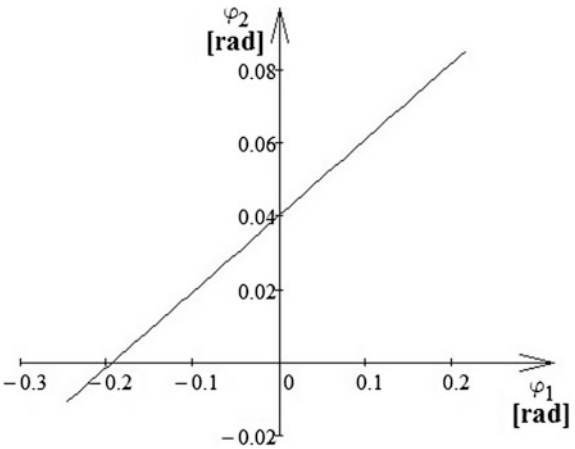

Fig. 4 Transmission function for a cylindrical gear

Unit normal vectors of surfaces Σ_1 and Σ_2 are written as

$$e_{x2} = 0;\ e_{y2} = \cos\theta_1;\ e_{z2} = \sin\theta_1;\ e_{x5} = \cos\theta_2;\ e_{y5} = \sin\theta_2;\ e_{z5} = 0.$$

In order to transform the coordinates, let us use the following matrix equations (Fig. 4): $\mathbf{r}^{(1)} = \mathbf{M}_{01} \cdot \mathbf{M}_{12} \cdot \mathbf{r}_2 = \mathbf{M}_{02} \cdot \mathbf{r}_2$; $\mathbf{r}^{(2)} = \mathbf{M}_{03} \cdot \mathbf{M}_{34} \cdot \mathbf{M}_{45} \cdot \mathbf{r}_5 = \mathbf{M}_{05} \cdot \mathbf{r}_5$[11].

Similar to a cylindrical gear, in these equations, $\mathbf{r}_2$, $\mathbf{r}_5$ are column matrices of the position vectors of surfaces Σ_1, Σ_2. And $\mathbf{r}^{(1)}$, $\mathbf{r}^{(2)}$ are column matrices of the position vectors of the same surfaces in the fixed coordinate system S_0. Therefore, the position function of the bevel (with intersecting orthogonal axes) of the rod-toothed gear (Fig. 3) is determined through the system of Eq. (2).

$$\begin{cases} R_1 \cot\alpha_1 + u_1 \cos\alpha_1 + \rho_1 \sin\alpha_1 \sin\theta_1 - \\ -R_2 \cos\varphi_2 + b - u_2 \cos\varphi_2 \sin\alpha_2 + \rho_2 \sin\varphi_2 \sin\theta_2 - \rho_2 \cos\varphi_2 \cos\alpha_2 \cos\theta_2 = 0; \\ R_1 \sin\varphi_1 + u_1 \sin\varphi_1 \sin\alpha_1 + \rho_1 \cos\varphi_1 \cos\theta_1 - \rho_1 \cos\alpha_1 \sin\varphi_1 \sin\theta_1 - \\ -R_2 \sin\varphi_2 - u_2 \sin\varphi_2 \sin\alpha_2 - \rho_2 \cos\varphi_2 \sin\theta_2 - \rho_2 \cos\alpha_2 \cos\theta_2 \sin\varphi_2 = 0; \\ \rho_1 \sin\varphi_1 \cos\theta_1 - u_1 \cos\varphi_1 \sin\alpha_1 - R_1 \cos\varphi_1 + \rho_1 \cos\varphi_1 \cos\alpha_1 \sin\theta_1 - \\ -R_2 \cot\alpha_2 + a - u_2 \cos\alpha_2 + \rho_2 \sin\alpha_2 \cos\theta_2 = 0; \\ \sin\alpha_1 \sin\theta_1 + \cos\varphi_2 \cos\alpha_2 \cos\theta_2 - \sin\varphi_2 \sin\theta_2 = 0; \\ \cos\varphi_1 \cos\theta_1 - \cos\alpha_1 \sin\varphi_1 \sin\theta_1 + \cos\varphi_2 \sin\theta_2 + \cos\alpha_2 \cos\theta_2 \sin\varphi_2 = 0; \\ \sin\varphi_1 \cos\theta_1 + \cos\varphi_1 \cos\alpha_1 \sin\theta_1 - \cos\theta_2 \sin\alpha_2 = 0; \end{cases} \tag{2}$$

where $R_1 = D_1/2$, $R_2 = D_2/2$. The distance between the axis of the driving wheel and the apex of the back cone of the driven wheel is equal to $a = D_2/2 + D_1/2 \cdot \tan(\alpha_1)$, and the distance between the axis of the driven wheel and the apex of the back cone of the driving wheel is equal to $b = D_2/2 - D_1/2 \cdot \tan(\alpha_1)$ (Fig. 3).

The initial values for mathematical simulation of the meshing are taken to be: $z_1 = 7$, $z_2 = 40$, $\rho_1 = \rho_2 = 1.5$ [mm]. By varying the parameter φ_1 , we obtain the values φ_2, u_1,u_2, θ_1, θ_2 through solving the systems (1) and (2). After application of numerical methods of the program software MathCad, the diagrams are obtained for $\varphi_2 = f_1(\varphi_1)$, $\Delta\varphi_2 = f_2(\varphi_1)$, where $\Delta\varphi_2 = \varphi_{2fact} - \varphi_{2nom} = \varphi_{2fact} - \varphi_1 \cdot i_{12}$ (the index "*fact*" designates the factual value of φ_2, the index "*nom*" is for the nominal one), and $\Delta i_{21} = f_3(\varphi_1) = i_{21fact} - i_{21nom}$. Functions $u_1 = f_4(\theta_1)$, $u_2 = f_5(\theta_2)$ determine the coordinates of the points of contact on surfaces Σ_1, Σ_2. Therefore, the numerical values are obtained for transmission functions, functions i_{21}, $\Delta\varphi_2$ and Δi_{21}. Figures 4, 5, 6 and 7 represent nominal values accounting for the directions of rotation of rod-toothed wheels in gears (we accept that all geometric parameters of wheels and their mutual arrangement are without error).

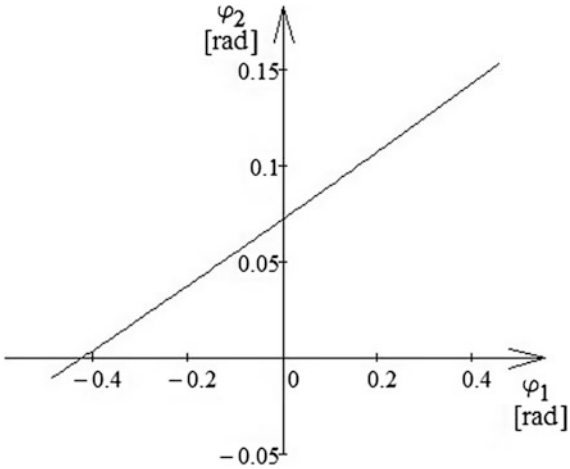

Fig. 5 Transmission function for a bevel gear

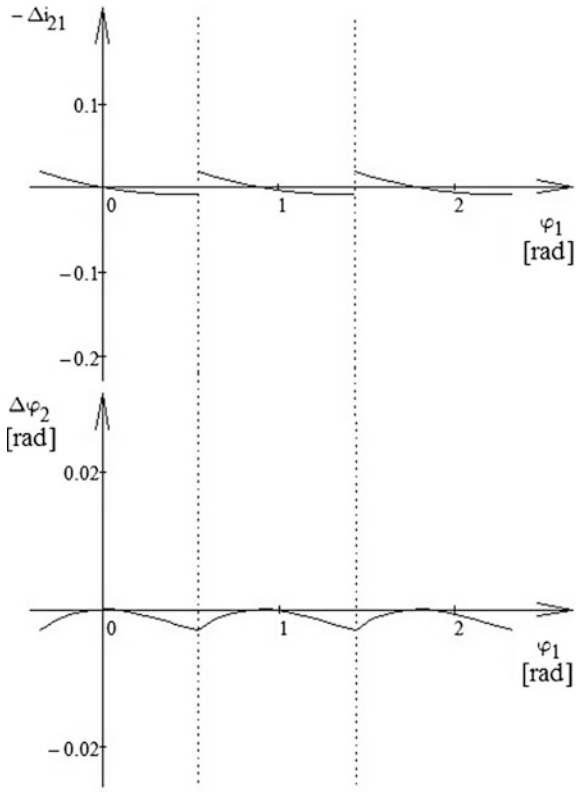

Fig. 6 Error of gear ratio and displacement for a cylindrical rod-toothed gear

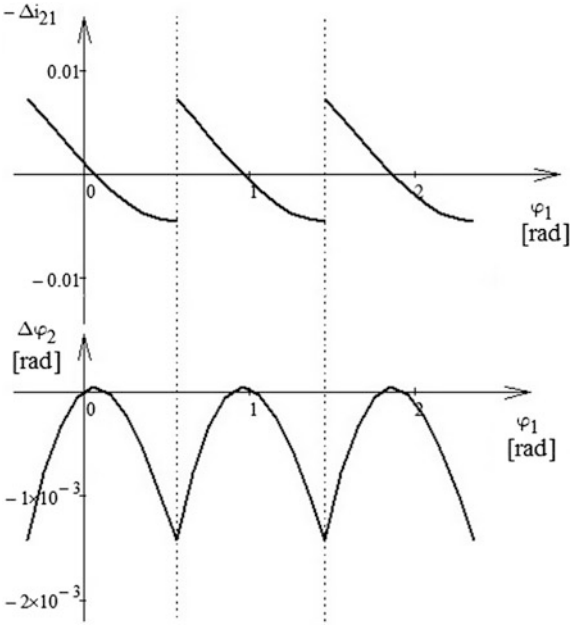

Fig. 7 Error of gear ratio and displacement for a bevel rod-toothed gear

5 Analysis of the Influence of Manufacturing Errors on Motion Parameters

Let us qualitatively assess the errors of the transmission function and "the abrupt change" in the gear ratio by considering errors made while mounting the rod in the hub. Inaccuracy of mounting expressed by the error of the angular pitch characterizes the deviation of the rod axis on a plane passing through the axis of the rod and perpendicular to the plane assigned by the axis of the rod and the operating axis of the gearwheel.

The angular pitch at the circumference of the analog of the diameter of a rod-toothed gearwheel is $\delta = 360^0/z_1$ (angular pitch). The numerical value of the error made while mounting the rod is expressed through the shift in the angular pitch and is taken to be 10% of its nominal value. Let us state the maximum values of the error of the transmission function for different gear ratios and numbers of rods for the driving wheel. Design values of the relation $\Delta\varphi_2 = f_2(\varphi_1)$ for a cylindrical gear are represented in Figs. 8, 9 and 10. Design values of the relation $\Delta\varphi_2 = f_2(\varphi_1)$ for a bevel gear are represented in Figs. 11, 12 and 13.

For the pair considered at moments of entering and leaving the mesh, the error of the transmission function (see Table 1) at points of re-conjugation varies from the

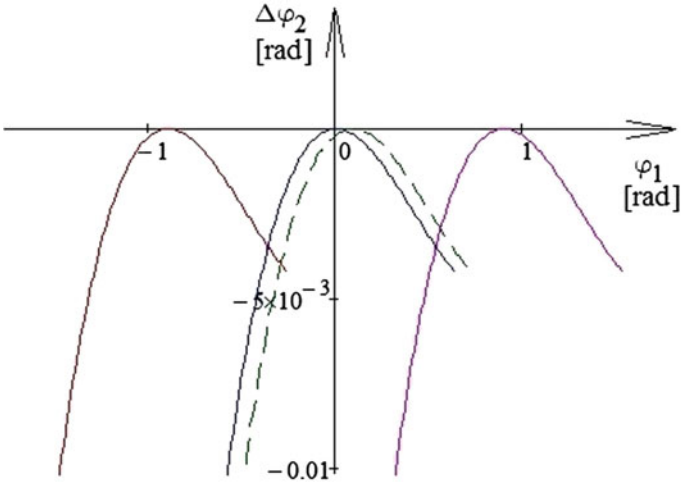

Fig. 8 Variation of the error of the position function for the error of the angular pitch equal to 10% for a cylindrical rod-toothed gear with parameters $z_1 = 7$, $z_2 = 36$

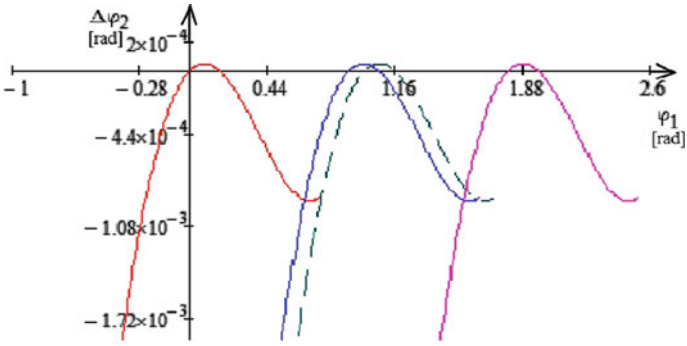

Fig. 9 Variation of the error of the position function for the error of the angular pitch equal to 10% for a bevel rod-toothed gear with parameters $z_1 = 7$, $z_2 = 36$

greater value to the lower one and otherwise (depending on the direction of the error of the circumferential pitch).

The value of deviation of the error of the transmission function is lower by one order than the nominal value for both cylindrical and bevel rod-toothed gears.

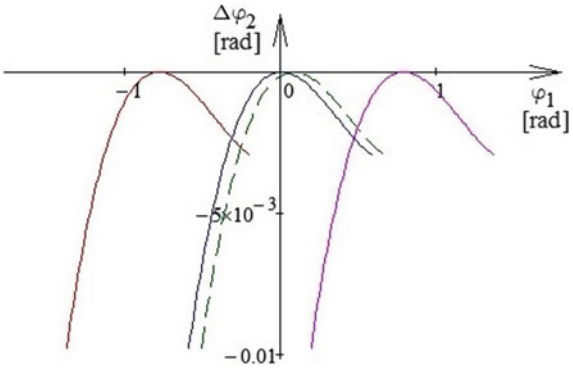

Fig. 10 Variation of the error of the position function for the error of the angular pitch equal to 10% for a cylindrical rod-toothed gear with parameters $z_1 = 8$, $z_2 = 41$

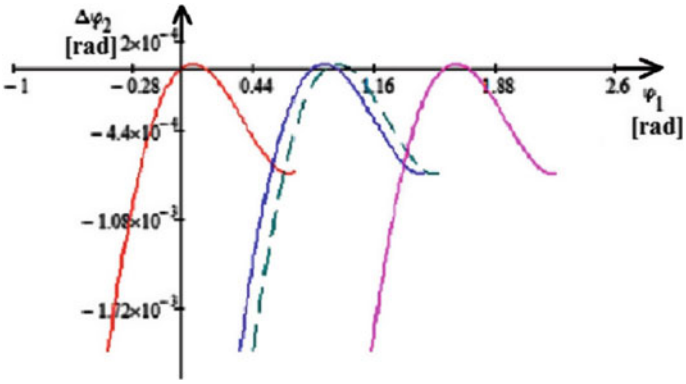

Fig. 11 Variation of the error of the position function for the error of the angular pitch equal to 10% for a bevel rod-toothed gear with parameters $z_1 = 8$, $z_2 = 41$

Fig. 12 Variation of the error of the position function for the error of the angular pitch equal to 10% for a cylindrical rod-toothed gear with parameters $z_1 = 9$, $z_2 = 45$

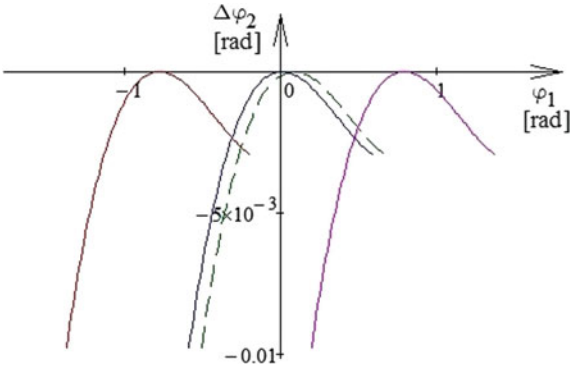

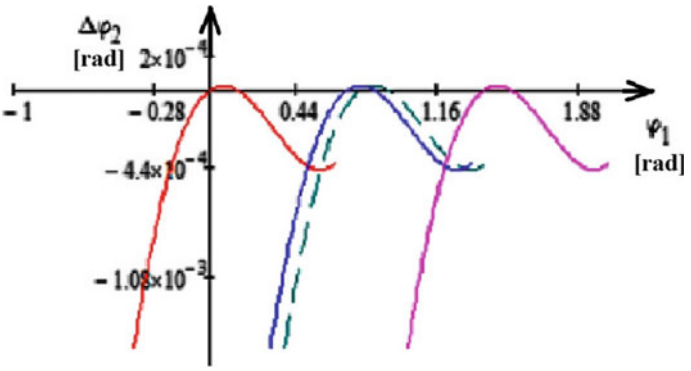

Fig. 13 Variation of the error of the position function for the error of the angular pitch equal to 10% for a bevel rod-toothed gear with parameters $z_1 = 9$, $z_2 = 45$

Table 1 Values of the error of the transmission function

	Nominal value ($\cdot 10^{-4}$ rad)		With account for the error of the angular pitch ($\cdot 10^{-4}$ rad)			
	Cylindrical	Bevel	Cylindrical		Bevel	
			[a]	[b]	[a]	[b]
$z_1 = 7$, $z_2 = 36$	34.73	9.03	36.78	22.10	8.75	8.41
$z_1 = 8$, $z_2 = 41$	23.47	6.96	24.91	15.01	7.63	6.16
$z_1 = 9$, $z_2 = 45$	17.00	4.50	18.08	10.93	4.60	3.95

[a]Entering the mesh, [b]leaving the mesh

6 Analysis of the Influence of Mounting Errors on Motion Parameters

One comparative advantage of cylindrical involute gears is the theoretical insensitivity of the gear ratio to errors of the center distance. Let us analyze the error of the transmission function of the cylindrical rod-toothed gears depending on the error of the center distance when varying the distance L (Fig. 1a) by 10 μm (Figs. 14 and 15).

As is shown in Figs. 14 and 15, the relation remains the same and the error of the transmission function at the point of re-conjugation varies insignificantly (by one order less than the nominal value). In a bevel gear, the mutual arrangement of wheels with respect to the fixed column is characterized by distances «a» and «b» (Fig. 3). Let us consider the influence of variation of the distance "a"

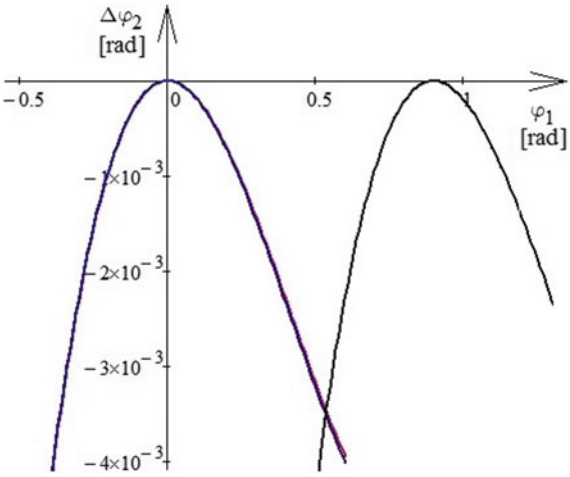

Fig. 14 Variation of the error of the transmission function when decreasing the distance L for the cylindrical rod-toothed gear with parameters $z_1 = 7$, $z_2 = 36$

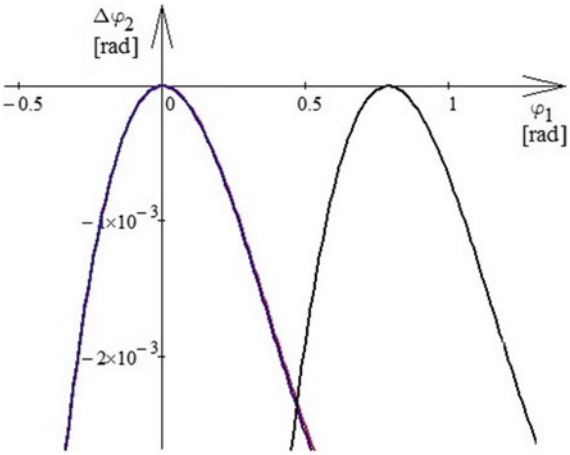

Fig. 15 Variation of the error of the transmission function when decreasing the distance L for the cylindrical rod-toothed gear with parameters $z_1 = 8$, $z_2 = 41$

in the meshing caused by its variation by the value equal to the tolerance for radial error of a ball bearing according to the Russian standard GOST 520-2011 of the sixth degree of accuracy (Tables 2 and 3).

The design values (Tables 2 and 3) characterize the decrease in the displacement error with the increase in the number of rods. Variation of the distance «a» does not cause any variation of the character of kinematic relations. The maximum deviation of the position function (according to the module) from the nominal value is $1.97 \cdot 10^{-4}$ rad, while the deviation of "the abrupt change" of the gear ratio is

Table 2 Values of motion parameters for rod numbers $z_1 = 7$, $z_2 = 36$, $i_{21} = 5.143$

$\varphi_1 \cdot 10^{-1}$ (rad)	$\varphi_2(\varphi_1) \cdot 10^{-1}$ (rad)	$\Delta\varphi_2(\varphi_1) \cdot 10^{-4}$ (rad)	$\Delta i_{12}(\varphi_1) \cdot 10^{-3}$ (rad)	$u_1(\theta_1) \cdot 10^{-1}$ (mm)	$u_2(\theta_2) \cdot 10^{-1}$ (mm)
−3.0	0.23	12.07	−7.07	−4.08	1.86
−2.4	0.35	8.21	−5.81	−3.72	0.93
−1.8	0.46	5.10	−4.57	−3.21	0.19
−1.2	0.57	2.71	−3.38	−2.54	−0.34
−0.6	0.69	1.03	−2.25	−1.73	−0.67
0.0	0.80	0	−1.19	−0.78	−0.78
0.6	0.92	-0.42	−0.23	0.31	−0.67
1.2	1.04	-0.30	0.62	1.55	−0.33
1.8	1.15	0.29	1.33	2.93	0.25
2.4	1.27	1.27	1.90	4.45	1.07
3.0	1.39	2.53	2.30	6.12	2.15

Table 3 Values of motion parameters for rod numbers $z_1 = 8$, $z_2 = 41$, $i_{21} = 5.125$

$\varphi_1 \cdot 10^{-1}$ (rad)	$\varphi_2(\varphi_1) \cdot 10^{-1}$ (rad)	$\Delta\varphi_2(\varphi_1) \cdot 10^{-4}$ (rad)	$\Delta i_{12}(\varphi_1) \cdot 10^{-3}$ (rad)	$u_1(\theta_1) \cdot 10^{-1}$ (mm)	$u_2(\theta_2) \cdot 10^{-1}$ (mm)
−3.0	−3.0	−3.0	−3.0	−3.0	−3.0
−2.4	−2.4	−2.4	−2.4	−2.4	−2.4
−1.8	−1.8	−1.8	−1.8	−1.8	−1.8
−1.2	−1.2	−1.2	−1.2	−1.2	−1.2
−0.6	−0.6	−0.6	−0.6	−0.6	−0.6
0.0	0.0	0.0	0.0	0.0	0.0
0.6	0.6	0.6	0.6	0.6	0.6
1.2	1.2	1.2	1.2	1.2	1.2
1.8	1.8	1.8	1.8	1.8	1.8
2.4	2.4	2.4	2.4	2.4	2.4
3.0	3.0	3.0	3.0	3.0	3.0

$0.17 \cdot 10^{-3}$. Similar to the distance «a», let us consider the influence of variation of the distance «b» (Fig. 1b) at other constant parameters (Tables 4 and 5).

When varying the distance «b», the error of the position function and variation of the gear ratio are different from their nominal values by $0.52 \cdot 10^{-4}$ rad and $0.18 \cdot 10^{-3}$, respectively. Variation of the distance «b» is thus of less influence on motion parameters than variation of the distance «a».

Table 4 Values of motion parameters for rod numbers $z_1 = 7$, $z_2 = 36$, $i_{21} = 5.143$

$\varphi_1 \cdot 10^{-1}$ (rad)	$\varphi_2(\varphi_1) \cdot 10^{-1}$ (rad)	$\Delta\varphi_2(\varphi_1) \cdot 10^{-4}$ (rad)	$\Delta i_{12}(\varphi_1) \cdot 10^{-3}$ (rad)	$u_1(\theta_1) \cdot 10^{-1}$ (mm)	$u_2(\theta_2) \cdot 10^{-1}$ (mm)
−3.0	0.23	12.88	−7.33	−4.22	1.86
−2.4	0.35	8.86	−6.08	−3.86	0.92
−1.8	0.46	5.58	−4.84	−3.35	0.19
−1.2	0.57	3.04	−3.65	−2.69	−0.35
−0.6	0.69	1.19	−2.52	−1.88	−0.67
0.0	0.80	0	−1.46	−0.92	−0.78
0.6	0.92	−0.58	−0.50	0.17	−0.67
1.2	1.04	−0.62	0.35	1.41	−0.33
1.8	1.15	−0.19	1.07	2.79	0.24
2.4	1.27	0.64	1.64	4.31	1.07
3.0	1.39	1.75	2.05	5.98	2.15

Table 5 Values of motion parameters for rod numbers $z_1 = 8$, $z_2 = 41$, $i_{21} = 5.125$

$\varphi_1 \cdot 10^{-1}$ (rad)	$\varphi_2(\varphi_1) \cdot 10^{-1}$ (rad)	$\Delta\varphi_2(\varphi_1) \cdot 10^{-4}$ (rad)	$\Delta i_{12}(\varphi_1) \cdot 10^{-3}$ (rad)	$u_1(\theta_1) \cdot 10^{-1}$ (mm)	$u_2(\theta_2) \cdot 10^{-1}$ (mm)
−3.0	0.13	10.94	−6.37	−3.84	2.36
−2.4	0.24	7.46	−5.23	−3.58	1.28
−1.8	0.36	4.66	−4.13	−3.14	0.43
−1.2	0.47	2.50	−3.07	−2.54	−0.18
−0.6	0.59	0.96	−2.07	−1.76	−0.55
0.0	0.71	0	−1.14	−0.82	−0.68
0.6	0.82	−0.43	−0.31	0.29	−0.55
1.2	0.94	−0.39	0.42	1.56	−0.16
1.8	1.06	0.05	1.03	2.99	0.49
2.4	1.18	0.81	1.49	4.59	1.43
3.0	1.29	1.81	1.80	6.36	2.65

7 Conclusions

According to the results obtained, one can prove that the bevel rod-toothed gears are more sensitive to errors of mounting errors than to those of manufacture. The error of the transmission function of the cylindrical gears is several times greater than that of the bevel at equal numbers of rods and their diameters. The manufacture error implying the variation of the value of the angular pitch can be caused by the set of factors, and it characterizes the deviation of geometrical parameters of wheels correctly enough, thus creating the basis for development of a technique for technical control.

Inevitable mounting errors in regard to the gears are caused by compliance of supports, the presence of clearances in supports, and so on. The design values prove that variation of the error of the transmission function of the cylindrical gears is less than the nominal value by one order. Bevel rod-toothed gears are sensitive only to variation of the distance between the axis of the driven wheel and the apex of the back cone of the driving wheel.

The obtained calculation results prove the serviceability of rod-toothed gears and the presence of minor transmission errors caused by manufacture and mounting errors.

Acknowledgements The authors wish to acknowledge the support received from the Federal Program «U.M.N.I.K.». This investigation was also supported by a grant from Saint-Petersburg in the sphere of scientific and technical activity KNVSh#165 "Analysis of the influence of manufacture and assembly errors on motion parameters of rod toothed gears with intersecting orthogonal axes".

References

1. Medvedev, V.I.: Calculation of settings for gear-machining tools to produce bevel pairs with circular teeth. In: The 3rd International Congress "KTI-96", Moscow (1996) (in Russian)
2. Pavlov, A.M.: Method of auxiliary generating surfaces and contact localization in a bevel gear pair. Gearing Transmissions. **1**, 42–45 (1991) (in Russian)
3. Segal, M.G.: To definition of boundaries of the bearing contact for teeth of bevel and hypoid gears. Mashinovedeniye **4**, 61–68 (1971) (in Russian)
4. Segal, M.G.: Types of localized contact in bevel and hypoid gears. Mashinovedeniye **1**, 56–63 (1970) (in Russian)
5. Dorofeev, V.L., Golovanov, V.V., Gukasyan, S.G.: Modification of aviation gears to decrease the wear of contact surfaces. Advanced mechanical engineering. Science and education **4**, 173–183 (2014) (in Russian)
6. Sheveleva, G.I.: Meshing of approximated bevel gearwheels. In: Theory of Gears in Machines, M., Mashgiz, pp. 38–48 (1966) (in Russian)
7. Lifits, I.M.: Fundamentals of Standardization, Metrology and Certification. Moscow, Yurait, p 345 (2005) (in Russian)
8. Morozov, I.M., Shamin, V.Y.: Fundamentals of assembly technique in mechanical engineering. Study guide, Chelyabinsk, YuUrGU (2006) (in Russian)
9. Patent RU 146159. MPK F16H 55/10 F15H 55/17. Wheel for the transmission of rotary motion. N 2014120175/11; appl. 19.05.2014; publ. 10.10.2014, Bul. N 28 (in Russian)
10. Timofeev, B.P., Sachkov, M.Y.: Synthesis of rod toothed gears according to the absence of edge contact. Theory Mech. Mach. **2**(26, 13), 23–32 (2015) (in Russian)
11. Timofeev, B.P., Sachkov, M.Y.: Prototyping of a rod toothed gear. J. Automobile Eng. **2**(91), 32–33 (2015) (in Russian)
12. Litvin, F.L., Fuentes A. Gear Geometry and Applied Theory, 2nd edn. Cambridge University Press, p. 800 (2004)
13. Litvin, F.L.: Development of Mechanisms and Parts of Devices. L. Mashinostroeniye (1973) (in Russian)

Planetary Rotor Hydraulic Machine with Two Central Gearwheels Having Similar Tooth Number

G. Volkov and D. Kurasov

Abstract The paper is devoted to issues of improving the planetary rotor hydraulic machine (PRHM) applied for pumps and hydraulic motors. It is proposed that the same number of waves (and teeth) for the central gearwheel with internal teeth and the central gearwheel with external teeth be provided. First, the maximum parameters of the effective volume of working spaces are achieved, and, second, there is a possibility of a series type connection of two working sections of the hydraulic machine. The latter circumstance essentially allows for increasing the section of channels for feed and return of the working medium, the channels being made in the stationary central gearwheel. This results in increasing the performance of the hydraulic machine in the pump mode and its specific power in the motor mode.

Keywords Planetary rotor hydraulic machine · Floating satellites · Effective volume · Expanding of channels

1 Introduction

Hydraulic and pneumatic volume displacement machines are commonly used in mechanical engineering. The greatest pressure of the operating medium (100 MPa) is provided by piston hydraulic machines. Their drawbacks are the small payload volume, complexity of the design and high cost. A simpler and cheaper design is provided by rotor pinion hydraulic machines (pumps). They create pressures of 15–25 MPa, they have limited performance and lifetime, and they operate reliably only at operating media with lubricating properties. In order to displace viscous media, including suspensions, screw pumps are applied. They provide high pressure at low

G. Volkov (✉) · D. Kurasov
Kurgan State University, Kurgan, Russia
e-mail: vlkv48@mail.ru

D. Kurasov
e-mail: naukka@mail.ru

V. Goldfarb et al. (eds.), *Advanced Gear Engineering*,
Mechanisms and Machine Science 51, DOI 10.1007/978-3-319-60399-5_21

performance. Sliding-vane pumps and motors have rather high performance at pressures of 15–25 MPa. Possibilities for sliding-vane pumps are limited by the sliding friction in a kinematic pair, generated by a vane with a stationary casing.

2 Structure of Planetary Rotor Hydraulic Machines

Volume hydraulic machines also include rotor pumps and motors, containing a planetary mechanism with variable operating volumes closed between central gearwheels and floating satellites. In this case, the central gearwheels can be both circular and non-circular.

As is known, the first planetary rotor hydraulic machine (PRHM) was patented in 1913 in Germany [3] (Fig. 1). It includes a non-circular central gearwheel 2 with internal teeth, and its centroid has three "waves" (N = 3). The central gearwheel 1 with external teeth is circular, that is, its centroid has one wave (M = 1). The number K of freely mounted satellites 3 is equal to the sum of waves for gearwheels 1 and 2 (K = M + N = 4). Channels 4 of the feed and return of the operating medium are made in the face caps rigidly related to the stationary central gearwheel 2 with internal teeth. The number P of channels is equal to the doubled number of waves N of the stooped central gearwheel 2 (P = 2•N = 6). The ratio of tooth

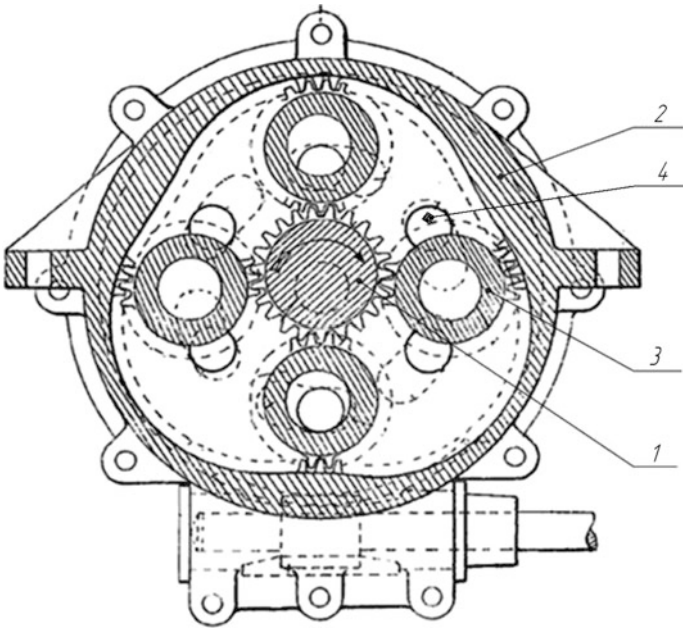

Fig. 1 Rotor hydraulic machine (N = 3; M = 1; K = 4; P = 6) [3]

numbers of central gearwheels is equal to the ratio of corresponding numbers of waves: $Z_2/Z_1 = N/M$.

The basis of the rotor-piston motor [2] shown in Fig. 2 is also a kinematic scheme of the PRHM. In this scheme, N = 2, M = 1, K = 3. Channels 4 of the feed and return of the operating medium are made directly in the central gearwheel 2 with internal teeth.

Similar to many other hydraulic machines, both central gearwheels are non-circular for the PRHM, which is characterized by numbers of waves M = 2, N = 4 (Fig. 3) and which was proposed and investigated by the Russian scientist An-I-Kan [1]. The advantage of this scheme over the planetary rotor hydraulic machines shown in Figs. 1 and 2 is the symmetrical load on the rotor 1 axis. It relieves the rotor supports and even allows for producing a floating rotor.

In all of the PRHM layouts described above, the channels of feed and return of the operating medium are made in parts that are rigidly connected to the fixed epicyclical gearwheel 2. However, similar schemes are known (for example, [1]) with the fixed sun gearwheel and channels related to it.

The principle advantage of planetary rotor hydraulic machines is the automatic compensation of clearances in radial contacts of the rotor and stator independent of tooth wear, thus predetermining the increased lifetime of these machines. Other advantages of PRHM are the great payload volume of working spaces and the absence of loaded sliding pairs. The reason for the rather narrow application of PRHM is the absence of economically-justified techniques for the manufacture of non-circular gearwheels and the absence of optimal layout and design solutions. Nowadays, new manufacturing techniques have appeared for production of the parts of PRHM. There are 2D techniques, in particular, electric discharge treatment,

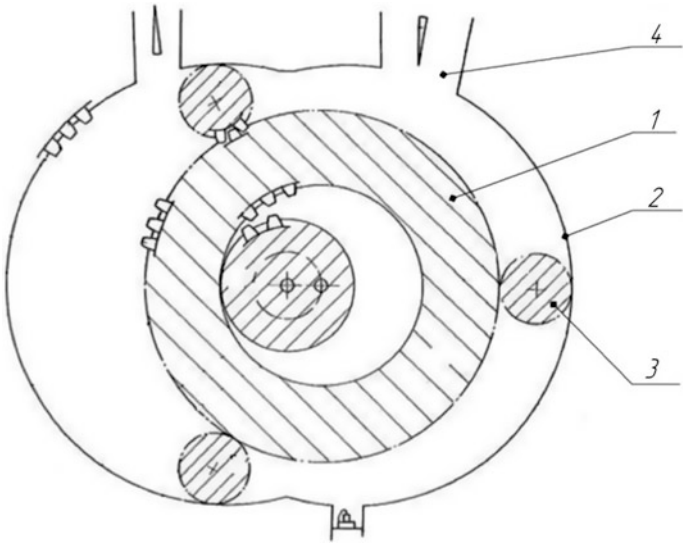

Fig. 2 Rotor-piston motor (N = 2; M = 1; K = 3) [2]

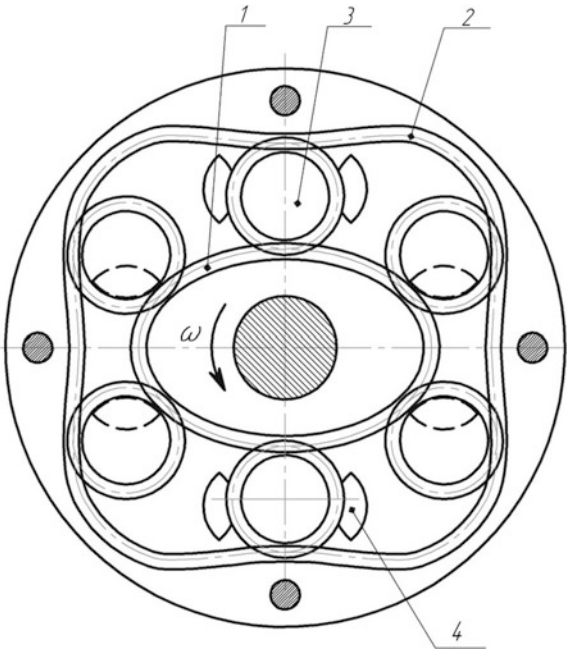

Fig. 3 Planetary rotor hydraulic machine (scheme M = 2; N = 4; K = 6; P = 8) [1]. *1* central gearwheel with external teeth; *2* central gearwheel with internal teeth; *3* satellites; *4* channels of feed and return of the operating medium

Table 1 Combinations of numbers of waves M of the sun gearwheel (with external teeth) and N of the epicyclical gearwheel (with internal teeth)

N	*M*					
	1	2	3	4	5	6
1	[7] + −					
2	[2, 4] ± −	[8] + +				
3	[1] − −	[4, 5] ± −	[8] + +			
4	[4] − −	[3] ± +	[3, 4] + −			
5		[3, 4] − −	[3, 4] ± −	[3, 4] + −		
6		[4] − +	[4] − +	[3, 6] + +	[4] + −	
7		[4] − −	[4] − −	[4] ± −	[4] ± −	[4] + −
8			[4] − −	[4] − +	[4] − −	[4, 6] + +

and laser and hydraulic abrasive cutting of the sheet material. 3D techniques are being actively developed. Therefore, optimization tasks for PRHM layouts became more vital.

The DSc thesis by An-I-Kan [1] included classification of the schemes of planetary rotor hydraulic machines known at that time. The same schemes of PRHM are considered in works by the Chinese researcher Zhang Quan [8]. Varieties of PRHM are demonstrated in Table 1. It presents possible combinations of parameters M (number of waves of the sun gearwheel) and N (number of waves of the epicyclical gearwheels).

3 Features of PRHM with the Same Tooth Number for Both Central Gearwheels

Schemes meeting the condition M = N, that is, with the same tooth number for both central gearwheels, were previously considered to be unrealizable. However, the authors have subsequently proved the availability and feasibility of performing these schemes [4, 5].

The version of PRHM with N = 1, M = 1 [5] is shown in Fig. 4. The rotor hydraulic machine comprises a circular central gearwheel 1 with external teeth, a stationary circular central gearwheel 2 with internal teeth and two floating satellites 3. The axes of mutual rotation of gearwheels 1 and 2 are shifted with respect to the geometrical axes of their centroids by the same distance *e*.

Figure 5 shows schemes of PRHM [4] characterized by numbers of waves N = 2, M = 2; and in Fig. 6, the number of waves are N = 3, M = 3. Arrangement of satellites between central gearwheels with the same numbers of waves (M = N) and, consequently, the same tooth numbers ($Z_1 = Z_2$) becomes possible at definite extreme geometrical parameters of meshing.

Let us compare different schemes of PRHM based on the following criteria:

1. Increase in the payload volume;
2. Absence of shaft support (simplification of the layout);
3. Absence of external casing (simplification of the layout);
4. Dimensions of channels (free flow of liquid).

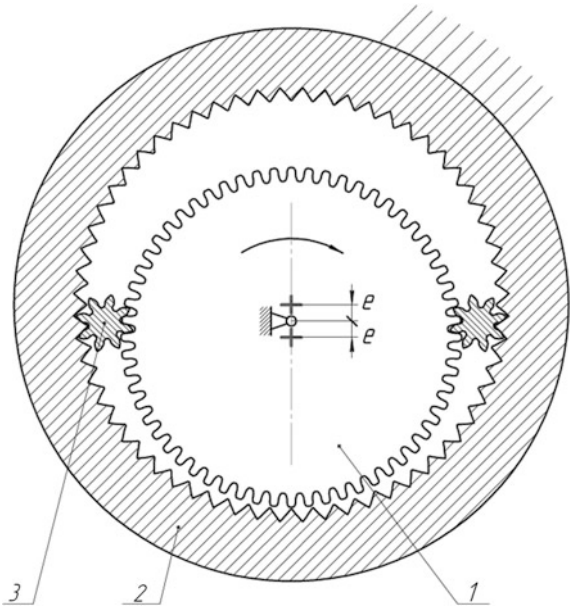

Fig. 4 Rotor hydraulic machine (N = 1; M = 1; K = 2; P = 2) [5]

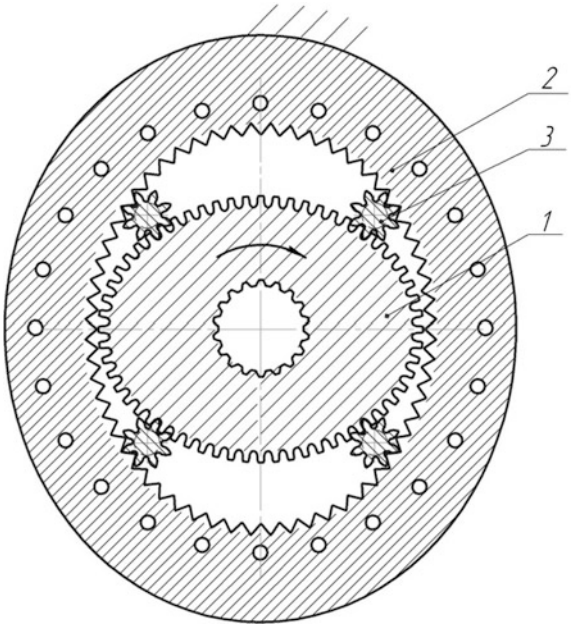

Fig. 5 Rotor hydraulic machine (N = 2; M = 2; K = 4; P = 4) [4]

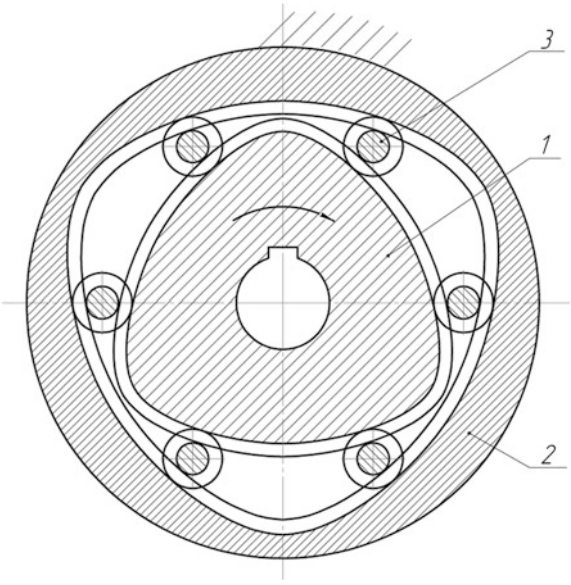

Fig. 6 Rotor hydraulic machine (N = 3; M = 3; K = 6; P = 6) [4]

At a considerable difference between N and M, the satellites become too bulky and occupy too much space in the operating chambers of PRHM. That is why the first criterion is generally met by schemes close to the main diagonal in Table 1.

Supports of the rotor shaft can be excluded in symmetrical schemes, for which *M* and *N* are simultaneously multiple by any number besides «1».

Evaluation results for PRHM in accordance with criteria 1 and 2 are shown in Table 1: «+» means "good", «±» means "so-so", «−» means "bad".

Implementation of the third and forth criteria depends on the fixed central gearwheel. If the epicyclical gearwheel is fixed, the external casing of PRHM is not required; this essentially simplifies the design of the hydraulic machine. However, the greater the difference between M and N, the more limited the sections of the channels become. The pointed limitation is so crucial that schemes (M = 1, N = 2) in Fig. 1 and (M = 1, N = 2) in Fig. 2 cannot be implemented as the simplest design version with channels in stationary caps. That is why schemes (M = 4, N = 6) and (M = 6, N = 8) are applied in practice [7]. Therefore, in accordance with this criterion, the schemes near the main diagonal in Table 1 are once again preferable.

The drastic solution to the problem of increasing the sections of the channels at the fixed epicyclical gearwheel is provided by application of schemes of PRHM with M = N. Let us consider this issue in more detail.

For this purpose, let us draw (Fig. 7) the elements of PRHM made in accordance with the scheme (M = 1, N = 1 (see Fig. 2)) as a number of consequent positions corresponding to rotations of the rotor 1 by 45°. In Fig. 7, the chambers with their volume increasing at the given moment (that is, the instant of intake) are designated by the symbol «−», and the chambers with decreasing volume (that is, the instant of forcing out) are designated by the symbol «#». Operating chambers are designated by Roman numerals I and II. Central points of channels are designated by letters A and B.

Figure 8 shows the diagrams of intensity of variation for the volume of each inter-satellite chamber (that is, consumption from the given chamber), depending on the angle of rotor rotation. The length of the diagram along the abscissa axis corresponds to a complete revolution of the system of satellites (imaginary carrier) or two revolutions of the rotor. The complete cycle of variation of the volume of the inter-satellite chamber (forcing out—intake) also takes place per one revolution of the imaginary carrier or per two revolutions of the rotor. Channels A and B are periodically opened to this chamber. The interval of one opening of each channel corresponds to the time of one inter-satellite interval. For two satellites, it is equal to a period of one revolution of the rotor. When comparing the phases of forcing out and intake in the individual inter-satellite chamber, the following should be noted:

First, each channel is operating by either forcing out or intaking.

Second, transition from the forcing out to the intake, and vice versa, occurs simultaneously in different chambers.

The noted synchronous character of the operation of chambers and channels is specific for PRHM when M = N. This is explained by the fact that in such schemes, the number K of satellites is equal to the number P of channels (K = P). Taking into account that K = M + N and P = 2·N, we get the condition of synchronous operation of chambers: M = N.

For all other relations between M and N, the following is valid:

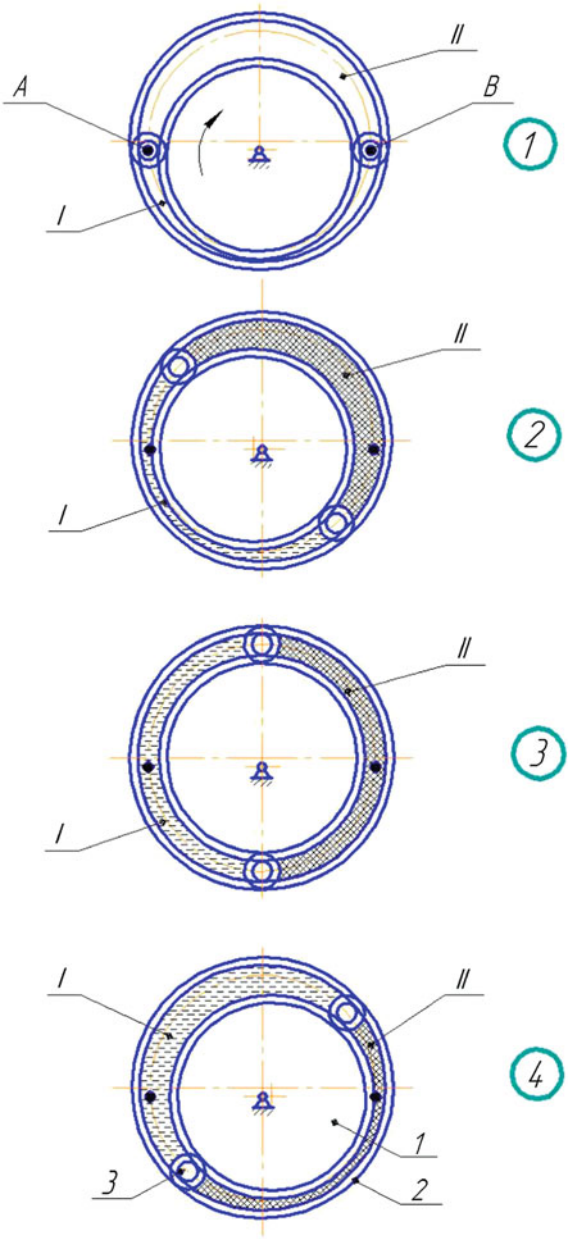

Fig. 7 Change in volume of inter-satellite chambers of the hydraulic machine (M = 1, N = 1) during one cycle

First, there are moments when one chamber tends to join two opposite channels simultaneously. In practice, such moments are excluded due to the rather large dimensions of satellites and the small dimensions of channels.

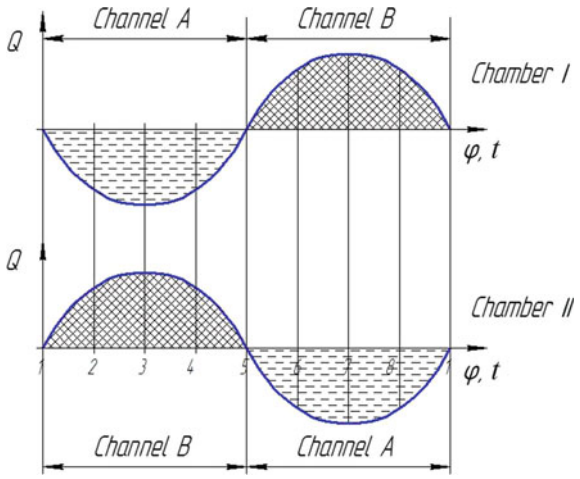

Fig. 8 Output of Q from chambers I and II of the hydraulic machine (M = 1, N = 1) vs. the angle φ of rotor revolution

Second, transition from the forcing out to the intake, and vice versa, is shifted into different chambers with respect to each other by the angle of rotor revolution, that is, it does not coincide in time.

4 Proposed Layout of PRHM

The above-mentioned properties of PRHM with M = N allow for performing the essential increase in the section of channels due to the consequent joining of two sections of PRHM [4, 5], as is shown in Fig. 9. Both sections (left and right) are similar, in this case, M = N = 2. They are separated from each other by the plane dividing plate 7.

Operating chambers of the two sections are consequently connected. Movable (sun) central gearwheels 1 of the left and right sections are fixed at the common central shaft 8 without relative revolution. Stationary (epicyclical) central gearwheels 2 with internal gearwheels are turned with respect to each other by 90°. Two channels 5 for supply of the operating medium are made in the face cap of the left section. Two channels 6 for discharge of the operating medium are made in the face cap of the right section. Two transfer channels 9 shifted relative to the channels of supply and discharge by 90° are made in the plane dividing plate 7. The dimension of all channels in the tangential direction exceeds the external diameter of satellites.

The hydraulic machine operates as follows. When the sun gearwheel 1 is rotating, floating satellites 3 interacting with this gearwheel are rolled over the internal gear rim of the stationary epicyclical gearwheel 2. Since the numbers of teeth Z_1 and Z_2 of the central gearwheels are the same, the angular velocity of the central gearwheel 1 is twice as large as the transportation velocity of the system of satellites (that is, the velocity of the imaginary carrier). One cycle of the change in

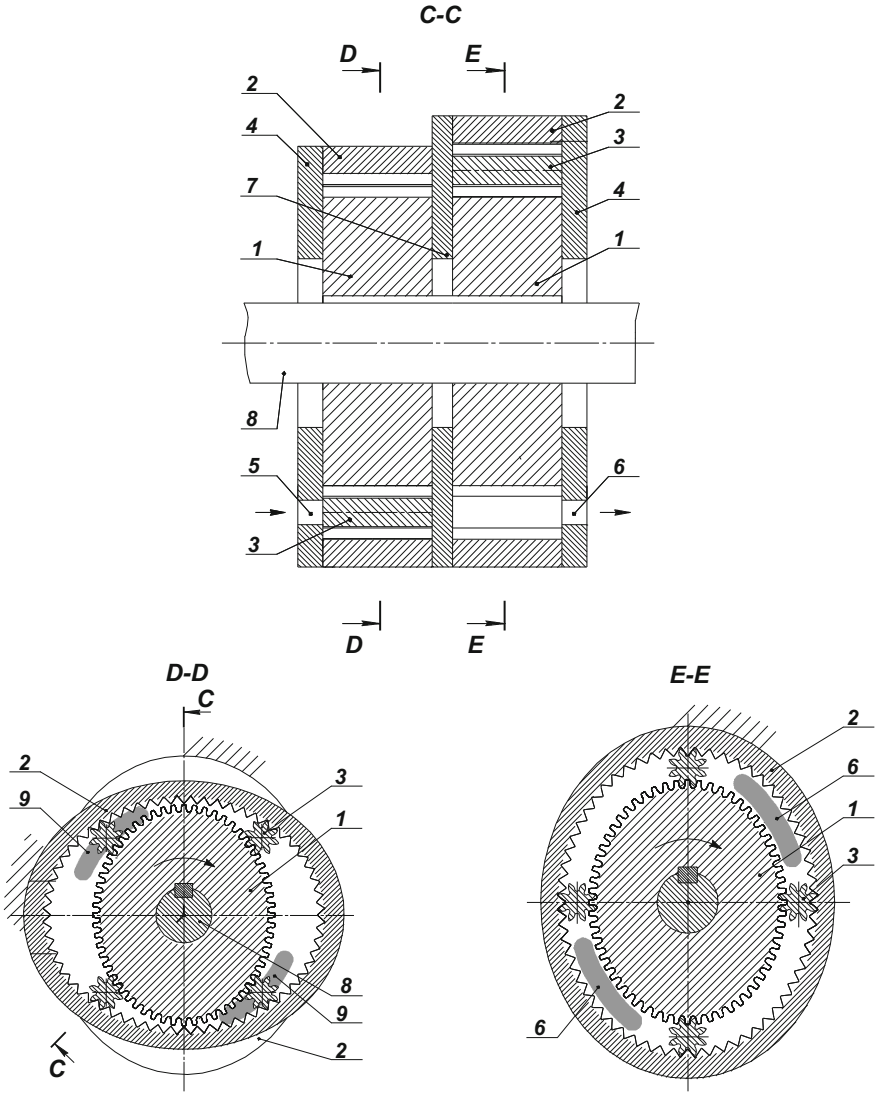

Fig. 9 Planetary rotor hydraulic machine (N = 2; M = 2) with consequent joining of sections [4]

the configuration of the system of satellites 3 corresponds here to one revolution of the central gearwheel 1. As a result of the motion of the elements, the volumes of the operating chambers closed between face caps and surfaces of all gearwheels vary cyclically. During operation, the channels 5, 6, and 9 are not completely closed simultaneously. Here, sections consequently create (or receive) the pressure of the medium. During one period of time, the left section is in the phase of active

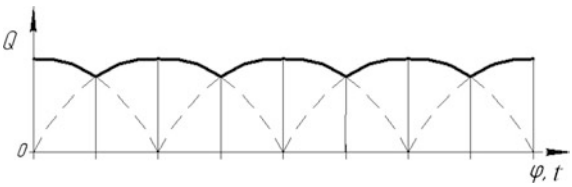

Fig. 10 Output of the operating medium versus time for PRHM with a consequent joining of sections

operation and the pressure of the operating medium acts on its satellites 3. At this moment, the right section is in the passive phase: the operating medium flows freely in channels 9 and 6, bypassing the satellites. In the other period of time, the pressure is perceived by satellites 3 of the right section and the operating medium freely passes through the left section. There is a short instant when both sections are in the active phase and have the same output. Finally, two sections smooth the variation of the output and pressure head when the hydraulic machine is operating in the pump mode (Fig. 10) and they provide the continuous rotation of the rotor in the motor mode. Besides providing the continuous operation of sections, the elongated shape of the sections of channels 5, 6, and 9 reduces the resistance to the medium flow, thus increasing the hydraulic efficiency of the hydraulic machine.

The pressure of the medium is limited by the bending and contact strength of the teeth. In the case of mild steel or even brass being used for the tooth elements, the maximum pressure is 5–10 MPa. Application of hardened steels allows for increasing the pressure up to 15–20 MPa or more.

As compared to the known planetary rotor hydraulic machines, the technical result is an increase in the net volume of operating chambers, relief of the rotor shaft supports, an increase in stability of the output parameters, and a decrease in mechanical and hydraulic losses of the hydraulic machine. As compared to the piston pump applied nowadays, the advantage is the essential simplification of the layout and the reduction of weight and overall dimensions. As compared to pinion hydraulic machines, the advantage is in the significant increase in the specific manufacturability (that is, the decrease in overall dimensions) and in wear resistance. As compared to impeller hydraulic machines, the advantage is in the decrease in mechanical losses and the increase in wear resistance.

The promising applications of the proposed hydraulic machine are as pumps for oil and residuum transfer, pumps for water, including contaminated bodies (drilling and fire pumps), dosing pumps for various liquids, and pumps and motors for hydraulic and pneumatic drives.

5 Conclusions

The authors of the paper proposed a new type of planetary rotor hydraulic machine characterized by the same number of waves for both central gearwheels. Meeting this requirement allowed for increasing the net volume of the hydraulic machine

and enlarging the channels for supply and discharge of the operating medium due to the consequent connection of two sections. This resulted in an essential increase in the manufacturability of the PRHM.

References

1. An I-Kan.: Synthesis, geometrical and strength calculations of planetary mechanisms with non-circuar gears of rotary hydraulic machine. DSc in Engineering Thesis, Tomsk (2001) (in Russian)
2. DE 19621051, МПК F01 C1/08; F01 C1/22; F02 B53/00; F02 B55/02.: Rotary piston engine/Heyne Wolfgang. Filed 24 May 1996; date of patent 18 Dec 1997
3. DE 288340.: Rotary hydraulic machine/Briscoe and dock engineering company. Date of patent. 11 Sept 1913
4. RU 144306.: Rotary hydraulic machine/Volkov G.J., Kurasov D.A.—№ 2014113740; filed 08 Apr 2014; date of patent 20 Oct 2014. Bull. № 23
5. RU 2513057.: Rotary hydraulic machine/Volkov G.J.—№ 2012129487; filed 11 July 2012; date of patent 20 Apr 2014. Bull. № 11
6. SU 484710.: Volume rotor engine/Sieniawski Bohdan.—№ 1854876; filed 01 Dec 1972; date of patent 15 Sept 1975. Bull. № 34
7. US 6230823, МПК E21 B4/02; F03 C2/08; F04 B47/08; F04 C2/14.: Downhole motor/Sieniawski Dariusz.—№ 09/185,420; filed 03 Nov 1998; date of patent 15 May 2001
8. WO 0166948.: A positive-displacement machine of gear type/Zhang Quan. Date of patent. 13 Sept 2001

Aspects of Optimization of the Process of Computer-Aided Design of Complex Objects

O. Malina and O. Valeyev

Abstract The paper presents theoretical fundamentals of the optimization of the process of structural synthesis of objects generated on discrete structures. The pointed model of the process of synthesis can be implemented in computer-aided design systems that are invariant with regard to the design object, when knowledge of the subject field comprises informational support of the system, and the optimized combinatorial search is in the basis of the process of synthesis.

Keywords Structural synthesis of complex objects · Forbidden version · Empiric forbidden figures · Functional forbidden figures · Optimization of the process of synthesis · Family of functions · Model of the process of structural synthesis

1 Introduction

In [1–3], the model of the class of objects has been considered that allows for execution of the synthesis of possible versions of the object by calculating the Cartesian multiplication of classification features of the object with the consequent exclusion of forbidden (unrealizable) versions that contain forbidden figures—the reason for the unrealizability of the design solution:

$$F_{rv} = M_{om} \times \prod_{i=1}^{N} (p_i) \backslash F_z, \tag{1}$$

where F_{rv} is the set of realizable versions of the object, M_{om} is the set of obligatory modules, N is the power of the set of features, p_i is the ith features the set of its values, and F_z is the set of forbidden versions. This method for synthesis of the

O. Malina (✉) · O. Valeyev
Kalashnikov Izhevsk State Technical University, Izhevsk, Russia
e-mail: malina_0705@mail.ru

V. Goldfarb et al. (eds.), *Advanced Gear Engineering*,
Mechanisms and Machine Science 51, DOI 10.1007/978-3-319-60399-5_22

object implies two steps: synthesis of all versions of the object and exclusion of forbidden versions.

In practice, execution of the synthesis of the object of at least medium complexity in accordance with formula (1) for an acceptable time interval is not possible for the following reasons:

1. High demands on memory space for keeping intermediate and final versions of the object.
2. High computational load at synthesis of versions of the object and exclusion of forbidden versions.

High demands on memory space for keeping intermediate and final versions of the object are stipulated first of all by their number. The object of medium complexity is characterized, as a rule, by at least one hundred classification features, a portion of which is represented by the set of values of high power (about 1000), since they reflect, for instance, linear dimensions of a certain design element of the object. For example, if the synthesized object is described by 80 features with the number of values equal to 2, and 20 features with the number of values equal to 100, we will obtain $2^{80} + 1000^{20} \approx 10^{60}$ different versions of the object. High total computational load at the synthesis of versions of the object is first explained by their value.

A high computational load at the step of exclusion of a forbidden version is provided by a great number of both the analyzed versions of the object and the forbidden figures, their presence being necessary so they can be checked for the versions of the object. The computational load is especially increased when analyzing the versions for the presence of functional forbidden figures, implying the necessity of implementing functional relations expressed more often by calculations. The calculation, as a rule, consists of several elementary mathematical operations, that is, it has increased computational complexity in contrast to the operation of comparison of values when checking for the presence of empiric forbidden figures.

Therefore, an attempt to execute the synthesis of the object through a combinatorial search of its features faces the effect of the "curse of dimensionality"; and finally, it requires presently unreachable computational power and memory space. Therefore, the aim of optimization of the process of synthesis is the reduction of memory space and the computational power necessary to execute the process of synthesis. Let us consider further main trends and methods for optimization of the process of synthesis.

2 Trends and Methods for Optimization of the Process of Synthesis

The process of synthesis of the object consisting of steps of synthesis of versions and the exclusion of forbidden versions cannot be executed as it is, due to the "curse of dimensionality" for advanced computers, which is why it needs optimization. Let us consider the main trends of optimization of the process of synthesis.

One of the main trends of optimization of the process of synthesis is minimization of the increment of the number of intermediate versions during synthesis. Minimization of the number of intermediate versions during synthesis (after the next multiplication by the feature) leads to smoother increment of memory consumption for keeping the versions.

Optimization of the process of synthesis is achieved through reduction of the computational load during analysis of the versions for the presence of forbidden figures. The most essential factor influencing the computational load during this analysis is the number of analyzed versions. Therefore, analysis of individual subsets of forbidden figures should be done as early as possible during the process of synthesis, rather than after generation of all versions of the object. It is also evident that analysis of versions for the presence of functional forbidden figures is related to the increased computational load, since, in this case, the analysis is executed through computation of the parameters of the functional relation, during which a sequence of elementary mathematical operations is executed, as a rule.

Therefore, it is assumed that optimization of the process of synthesis is achieved by solving the following problems:

- Minimization of the number of intermediate versions after multiplication by the next feature during synthesis, in particular, due to previously executed analysis of intermediate versions for the presence of forbidden figures;
- Minimization of the computational load during analysis for the presence of functional forbidden figures.

In order to solve the enumerated problems, it is proposed that the following methods be applied:

- Alternation of synthesis and analysis [4]. This method implies dividing the process of synthesis into elementary steps, each of which involves the stage of synthesis as additional multiplication by the next feature with obtainment of intermediate versions and the stage of analysis implying the reduction of the set of intermediate versions by exclusion of versions that contain forbidden figures. Such an approach promotes the solution of the problem of minimization of the number of intermediate versions after multiplication by the next feature.

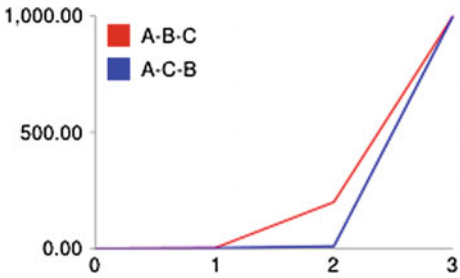

Fig. 1 Number of intermediate versions during synthesis for different orders of the multiplication of features

– Ordering the features for multiplication during synthesis [5]. This method, especially as it relates to the previous one, is a powerful tool for controlling the rate of increasing the number of intermediate versions. For example, if the object is described by features $A = \{a_1, a_2\}, B = \{b_1, \ldots, b_{100}\}, C = \{c_1, \ldots, c_5\}$, then their multiplication in the order A–B–C will lead to a greater average number of intermediate versions after multiplication by the next feature, as compared to multiplication in the order A–C–B (see Fig. 1).

Moreover, ordering the features allows for approaching the check of a greater number of forbidden figures at the beginning of the synthesis, thus subjecting a smaller number of intermediate versions to analysis.

– Classification of functional forbidden figures and their generating functional relations in accordance with the level of computational complexity and obtainment of new relations with lower computational complexity, thus promoting minimization of computational complexity during analysis of intermediate versions for the presence of forbidden figures.
– Prevention of generation of forbidden figures, instead of analysis of the set of versions for the presence of forbidden figures [3]. As far as empiric forbidden figures are concerned, this method implies the application of marks showing that the intermediate version can be the argument for the forbidden figure. Synthesis of the best set of intermediate versions is executed by means of the matrix with columns showing the current intermediate versions and lines showing the values of the next feature. Therefore, during synthesis, the forbidden figures are not generated, thus promoting minimization of the number of intermediate versions.

In order to exclude the analysis of functional forbidden figures, the method is applied as direct generation of allowed versions. Thus, when multiplying the intermediate set of versions with the power N by the feature P that is the result of the function of certain previously multiplied features, in order to obtain the intermediate set of allowed versions with the power (N + 1), it is enough to calculate the value (or values) of the function for each of the initial versions, having substituted the corresponding values-arguments involved into this version; and to check whether these values belong in the set of possible values of the additionally multiplied feature. For example, if after additional multiplication by the feature E for the initial version $(a_i, b_j, \ldots, d_k)$, the result of calculation of the function $f(a_i, d_k)$ is

the values x, y, z (here, x corresponds to the possible value e_1, and z corresponds to the value e_3), then the new set of intermediate versions will involve the versions $(a_i, b_j, \ldots, d_k, e_1)$ and $(a_i, b_j, \ldots, d_k, e_3)$.

Further "analysis for the presence of forbidden figures" will imply such a set of additional operations at the stage of synthesis that allows for preventing the generation of forbidden versions.

– Application of binary logic for coding the version of the object. This method implies the record of the version of the object as a sequence of zeros and units designating the presence or absence of the value of a certain feature in the version of the object. The optimization effect of the application of binary logic is revealed due to peculiarities of data storage in computers. It is supposed that such an approach will reduce the memory space necessary for keeping the versions, since it allows for applying the minimum memory space for data storage. The methods described above for solving the problems of optimization of the process of synthesis give the greatest effect within their combination, which is why their further detailed consideration will be joined rather than the separate one. Let us consider further the factors influencing the order of multiplication of features during synthesis.

3 Factors of Ordering the Features During Multiplication

As was mentioned above, it is supposed that the exact ordering of features for multiplication during synthesis is a powerful tool for optimization of the process of synthesis. Let us consider the factors influencing the order of multiplication of features.

The first factor is the number of values of each feature, since the number of intermediate versions is increased proportionally to this number when multiplying by the corresponding feature. However, one should take into account that certain values can be excluded even before the beginning of synthesis through analysis of the presence of forbidden figures consisting of one value. For this purpose, it is reasonable to classify forbidden figures in accordance with the number of values into atomic (consisting of one value) and complex (consisting of two or more values). Atomic forbidden figures involve, as a rule, the majority of relatively forbidden figures, since the technical assignment in its classical statement is more likely to define the allowable range of values of a certain parameter (feature) of the object than forbidden combinations of values of two or more parameters. The remaining relatively forbidden figures and all empiric and functional relations are complex.

It is evident that analysis of the presence of atomic forbidden figures can be executed even before the beginning of the process of synthesis. Thus, excluding a great number of values of different features from the process of synthesis, a somewhat similar reduction of the feature will take place. The factor of such a reduction of the feature can be determined to be the ratio of the number of forbidden values of the feature to the number of all values of the feature:

$K_p = \frac{F_P}{M_P}$, where F_P is the power of forbidden values of the feature P, and M_P is the power of the set of all values of the feature P.

The increase in the number of intermediate versions during synthesis is influenced only by those values of the feature that participate in the process of synthesis, that is, they are not forbidden. For example, we accept that the class of objects is described by features $A = \{a_1, a_2\}, B = \{b_1, \ldots, b_{100}\}, C = \{c_1, \ldots, c_5\}$, which should be multiplied in the order A–C–B in order to minimize the reduction. Furthermore, we assume that when imposing the technical assignment, the set of relatively forbidden figures is generated. Their application excludes the majority of values of the feature B, thus transforming the pointed features into $A' = \{a_1, a_2\}, B' = \{b_1, \ldots, b_3\}, C' = \{c_1, \ldots, c_5\}$. In this case, it is reasonable to multiply them in the other order A–B–C. Such influence of relatively forbidden figures on the order of multiplication of features allows for assuming that features of the object with the maximum factor of reduction K_p will more often be multiplied first during the process of synthesis.

The second factor of ordering the features for multiplication during synthesis is the sets of forbidden figures; their contents in intermediate versions can be analyzed at the next stage of synthesis after multiplication by the next feature (or during it). For example, we assume that the object is described by features $A = \{a_1, a_2\}$, $B = \{b_1, \ldots, b_{100}\}, C = \{c_1, \ldots, c_5\}$, the set of forbidden figures contains $f_1 = \{a_1, c_2\}, f_1 = \{a_1, c_4\}, f_1 = \{a_2, c_3\}$, and features will be multiplied during synthesis in the order A–C–B in accordance with the previously-considered factor of minimization of the average number of intermediate versions during synthesis. Then, if the analysis for the presence of forbidden figures is executed after multiplication by features A and C, we obtain the dynamics of the number of

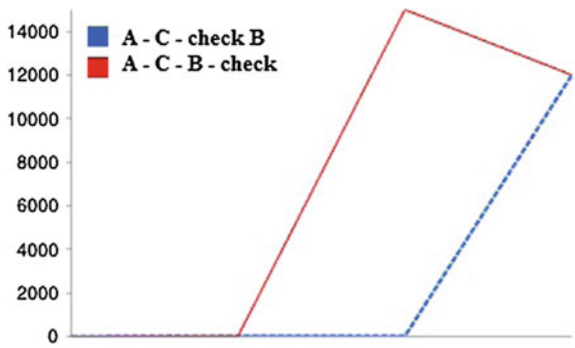

Fig. 2 Dynamics of the number of intermediate versions during the multiplication of features versus the moment of checking for the presence of forbidden figures

intermediate versions shown in Fig. 2 (blue diagram). If the analysis of the presence of forbidden figures is executed after multiplication by the feature B, we obtain another pattern (see Fig. 2, red diagram).

In the first case, the average number of intermediate versions is significantly less than that in the second one. Therefore, the timely analysis of the presence of forbidden figures leads to a decrease in the average number of intermediate versions during synthesis.

Analysis of the presence of the atomic forbidden figure can be executed prior to beginning the process of synthesis. Therefore, relatively forbidden figures that consist of one value do not influence the order of multiplication of features within the considered factor of ordering the features.

Analysis of the presence of the complex forbidden figure can be executed when all features are multiplied, the values of these features generating the given forbidden figure. Therefore, features with values that participate in complex forbidden figures should more often be multiplied earlier than the other features. However, the subset of complex forbidden figures involves the subset of functional forbidden figures, the analysis for their presence having essential peculiarities. In order to minimize the computational load, the analysis is executed not for a separate functional forbidden figure (an impossible combination of values of features that is substantiated by calculation in accordance with the available functional relation), but for the whole subset of forbidden figures caused by the pointed functional relation, this relation being used as the tool for analysis.

Furthermore, the analysis of the presence of functional forbidden figures will imply the exact approach described above, which can be characterized as the "synthesis without analysis." Obviously, the parameters of the functional relation correspond to the features of the class of objects. Therefore, the feature-result and features-arguments of the functional relation can be singled out. Further reduction of the computational load at analysis of the presence of functional forbidden figures depends on the order of multiplication during the synthesis of features that are parameters of the functional relation. Reduction of the computational load at this analysis is achieved at its combination with synthesis of the next set of intermediate versions, provided that the feature—result is participating in multiplication after features-arguments.

Therefore, the first of the considered factors of ordering during multiplication implies early multiplication of features with values defined in the technical assignment; and the second one implies multiplication of features-results of functional relations after features-arguments.

However, the above-described factors of ordering can contradict each other in certain cases. This takes place when the technical assignment exactly determines the value of the feature-result: the first factor implies its multiplication closer to the beginning of synthesis, and the second one implies multiplication after multiplication of features-arguments. Let us consider the example and compare the computational load for the case in which the technical assignment determines the possible values of the feature-result and when this feature determines the possible values of the feature-argument. Thus, having the function $C = f_1(A, B)$, where

A = {a_1, a_2}, B = {b_1, b_2}, and C = {c_1, c_2}, in accordance with the second factor of ordering, the features should be multiplied in the order A–B–C or B–A–C. If the technical assignment states the value of the feature A = a_1, then the value a_2 becomes forbidden; and in the process of synthesis, the calculation of C = f_1(A, B) will be executed once for each set (a_1b_1 and a_1b_2), that is, twice. If the technical assignment determines the value of the feature C = c_1, then in the process of synthesis, it will be necessary to execute the calculation once for each set (a_1b_1, a_1b_2, a_2b_1, a_2b_2), that is, four times, thus increasing the computational load twice.

This example allows for concluding that the computational load at analysis of the presence of forbidden figures can vary significantly, depending on the statement of the technical assignment in the absence of reverse functional relations to the functional relation available in the subject field. In order to minimize the computational load of any contents of the technical assignment for each known calculation relation $P_n = f_1(P_1, P_2, \ldots, P_{n-1})$, it is reasonable to plot the family of functions $F = \{P_n = f_1(P_1, P_2, \ldots, P_{n-1}), \quad P_1 = f_2(P_2, \ldots, P_n), \quad P_2 = f_3(P_1, P_3, \ldots, P_n), P_{n-1} = f_n(P_1, P_2, \ldots, P_{n-2}, P_n)\}$. The problem of choosing the function that is the most effective for analysis of the presence of forbidden figures among the functions of each family will be considered later.

Therefore, it is explored that the order of multiplication of features also influences the choice of the function from each family of functions that will be participating in the analysis of the presence of corresponding functional forbidden figures. In other words, the order of multiplication of features influences the computational load of analysis of versions for the presence of functional forbidden figures, which is the third factor for ordering the features for multiplication.

Since each family of functions initially contains only one (initial) function and, therefore, is incomplete, the obtainment of reverse functions to those relations available in the subject area is an important problem of the optimization of the process of synthesis [6].

4 Determination of the Order of Multiplication of Features at Synthesis

As was shown above, ordering the features for multiplication at synthesis allows for solving the problem of minimizing the number of intermediate versions at the same time, as does approaching the analysis by the maximum possible number of forbidden figures at the beginning of synthesis.

The important factor of ordering the features is the set of functional forbidden figures. The above-described feature of analysis of the presence of functional forbidden figures (obtaining the allowed value when multiplying by the next feature by means of calculating the function) allows for applying the functional relations at synthesis as a tool for direct determination of allowed combinations among the set of all combinations. It requires an essentially lower number of computational

operations, as compared to analysis of each combination for the presence of each forbidden figure generated by the functional relation. Moreover, multiplication by the feature that is the result of the functional relation leads to the minimum increase in the power of the set of intermediate versions, since the result of calculation of the function represents, as a rule, the only value (and on seldom occasions, two or more values). Therefore, in order to minimize the computational load and the number of intermediate versions at synthesis, it is necessary, first of all, to multiply the features that participate in families of functions.

The set of complex forbidden figures (excluding functional ones) should be considered as the secondary factor of ordering the features. The exclusion of versions containing such forbidden figures also influences the reduction of the power increment for the set of intermediate versions at synthesis. Analysis of the presence of atomic forbidden figures does not influence the order of multiplication of features at synthesis.

Thus, solving the problem of minimization of the number of intermediate versions at synthesis implies the following order of multiplication of features:

1. Features, participating in families of functions, that is, inter-linked by the functional relation.
2. Features with values participating in certain complex forbidden figures besides the functional ones.
3. Features with values not participating in complex forbidden figures.

Let us consider the contents of each step of the above-presented order of multiplication of features.

Obviously, it is unreasonable to alternate the multiplication of features involved in one family of functions with features of the other family of functions, since the instance of analysis of the presence of forbidden figures is moved away from the beginning of multiplication. It leads both to an increase in the average number of intermediate versions at synthesis and an increase in the power of the set of versions subject to analysis of the presence of forbidden figures. For instance, accept that the family of functions S_1 consists of features A = {1, 5, 6}, B = {2, 4}, C = {0, …, 100} and is based on calculation of $C = f_1(A, B) = A + B$; and that the family of functions S_2 consists of features D = {1, 5, 6}, E = {2, 4}, F = {0, …, 100} and is based on calculation of $F = f_2(D, E) = D * E$. Then, considering that calculations of $C = f_1(A, B)$ and $F = f_2(D, E)$ give the only resulting value, let us consider two alternative orders of multiplication of features: in the first case, let us primarily multiply the features-arguments and then the features-values of functions; in the second case, let us primarily multiply the features of one calculation and then of the other one. The process of increasing the power of intermediate versions will be subjected to analysis. When multiplying the features in the order A–B–D–E–C–F after each step of synthesis, we have the following number of intermediate versions: K_A, $K_A * K_B$, $K_A * K_B * K_D$, $K_A * K_B * K_D * K_E$, $K_A * K_B * K_D * K_E$, $K_A * K_B * K_D * K_E$, where K_P is the power of the set of values for the feature P. The absence of the change in the number of intermediate versions at multiplication by features C

and F is substantiated by the executed analysis of the presence of forbidden figures. Indeed, when multiplying by the feature C for each pair of values A and B (which is involved in the additionally multiplied intermediate version), this will be determined by calculating the only allowed value of the feature C; and therefore, each intermediate version is projected onto the only intermediate version at the next step of synthesis, that is why the power of the set of intermediate versions after the additional multiplication by the feature C will not exceed the power of the set at the previous step of synthesis. When multiplying the features in the order A–B–C–D–E–F, we obtain the following number of intermediate versions after the corresponding step of the synthesis: K_A, $K_A * K_B$, $K_A * K_B$, $K_A * K_B * K_D$, $K_A * K_B * K_D * K_E$, $K_A * K_B * K_D * K_E$. Obviously, in the second step, the power of the set of intermediate versions is increased slower than at synthesis; and analysis of the presence of forbidden figures at an additional multiplication by the feature C is executed, in this case, for a smaller number of versions: $K_A * K_B$ instead of $K_A * K_B * K_D * K_E$.

Therefore, it is reasonable first to multiply all features involved in one family of functions, and only after that to move to multiplication of features involved in another family of functions. Furthermore, it is necessary to determine the order of multiplication of features within each family of functions.

As was shown previously, the reduction of the computational load as an analysis of the presence of functional forbidden figures is stipulated by multiplication of the intermediate set of versions by the feature-result of the function after features-arguments. Therefore, in order to determine the feature multiplied last, it is necessary to choose the most effective function of the family for participation in the process of synthesis. Computational complexity of analysis of an intermediate version for the presence of the subset of forbidden figures generated by the family of functions depends on the following factors:

- Computational complexity of the function chosen for the analysis of the presence of forbidden figures;
- Power of the set of versions to which the chosen function will be implemented.

In order to analyze the computational load further, let us introduce the concept of an integrated assessment of computational complexity (IACC) of the analysis of intermediate versions for the presence of the set of forbidden figures equal to the product of computational complexity of the function applied for analysis and the power of the set of analyzed versions.

The computational complexity of the function can be determined by the number of its component operations, and the power of the set of arguments can be calculated as follows: $\prod_i |p_i| - |V_z|$, where p_i is the ith feature-argument of the given function, and V_z is the set of forbidden versions generated at the set of features-arguments P. The set of forbidden versions V_z can even be assessed prior to

the synthesis through analysis of the set of empiric forbidden figures (EFF) consisting of values of features of the set of functions.

Let us consider the power of the set of forbidden figures as the factor of ordering the remaining features of the family of functions. Analysis of the presence of these forbidden figures is possible at the multiplication of certain features-arguments of the module for generation of allowed versions chosen as a part of synthesis. Such a set involves the component non-functional forbidden figures that consist of values of multiplied features; and in order to determine them, it is necessary to classify the forbidden figures by features possessing the values that are components of the forbidden figure, and by the power, that is, by the number of values that are components of the forbidden figure. The set of forbidden figures F_P of the feature P comprise all forbidden figures having one of the values that is the value of the feature P: $F_P = \{z_P\}$, where for $z_P = \{a_k\}$ $\exists a_k : a_k \in P$, and where a_k is the kth value of the forbidden figure z_P.

Then, the set of forbidden figures (analysis of their presence is possible at the multiplication of two or more features) can be determined as the intersection of sets of forbidden figures related to these features and with the united set of forbidden figures having a power no greater than the number of multiplied features.

Therefore, in order to determine the order of multiplication of features P_1, P_2, …, P_N that are not inter-linked by the functional relation, it is necessary to take the following steps:

1. For each pair of features (P_i, P_j), the set of forbidden figures Z_{ij}, is determined (analysis of their presence is possible for intermediate versions obtained at multiplication of these features).
2. The first pair of multiplied features (P_a, P_b) is chosen so that $|Z_{ab}| = \max(|Z_{ij}|)$.
3. For each un-ordered feature P_k, the set of forbidden figures Z_{abk} is determined.
4. Among un-ordered features, the next feature P_c is chosen for multiplication so that $|Z_{abc}| = \max(|Z_{abk}|)$.
5. If all the features are ordered, the desired order of multiplication has been determined; otherwise, the step from p.3 should be repeated.

Therefore, the order of feature multiplication has been determined for each family of functions. Ordering all features that participate in families of functions can be done by determining the order of multiplication of those families.

It has previously been concluded that it is reasonable to multiply features of families of functions in sequence one after another, if possible. However, one and the same feature often participates in two or more families of functions, which is why, after multiplication of the features of the family of functions that contain the feature P, it is reasonable to multiply the features of other families of functions that contain the feature P.

The presence of dependence between families of functional relations as common features allows for reducing the computational load, since its volume at the multiplication of features of the family of functions depends on the number of intermediate versions after multiplication by the next feature that, in turn, depends on

the number of allowed values of each feature. The number of allowed values of each feature can be reduced not only through application of simple forbidden figures, but also within analysis of the presence of forbidden figures when multiplying by the next feature within the previous functional relation. For example, accept that the family of functions is determined for features A, B and C; and that the power of feature A is equal to 10, for feature B, it is equal to 20, and for feature C, it is equal to 1000. For analysis of the presence of functional forbidden figures, the function $C = f(A, B)$ is chosen, giving the only value-result for each array of arguments. In this case, the result of the multiplication of features of the family of functions will be the power of the obtained set of intermediate versions that is no greater than $|A| * |B| = 10 * 20 = 200$, since each pair of values (a_i, b_j) is only correlated to one allowed value of c_k. Therefore, no less than 800 values of the feature C will be excluded from the process of synthesis, since they do not participate in any of the intermediate versions.

The exclusion of values from the process of synthesis obviously leads to, firstly, elimination of already-generated versions that contain such values, and secondly, reduction of the set of possible values of features. This, as was stated above, influences the computational load of generation of a certain set of intermediate versions. Therefore, it is necessary to determine the order of generation of sets of intermediate versions for which minimization of the computational load during the process of their synthesis is achieved.

In order to minimize the computational load at synthesis of sets of intermediate versions, it is proposed that we start the synthesis of intermediate versions from the family of functions S with the maximum factor of reduction of sets of possible values of features R_S, which is determined as follows:

$R_S = \prod_i \frac{|M_{P_i}|}{|M'_{P_i}|}$, where M_{P_i} is the set of all values of the feature P_i, and M'_{P_i} is the set of possible values of the feature P_i; $P_i \in \Omega$, where Ω is the set of features for which the family of functions is determined.

After generation of the set of intermediate versions for the given family of functions, it is necessary once again to determine the set of allowed values for each feature that is a component of the family of functions. The value is considered to be allowed if it participates in at least one of the versions of the obtained set of intermediate versions; otherwise, it is forbidden. Furthermore, synthesis of intermediate families of functions will probably be done, the functions including one of features that have been processed during the previous step, since the set of its possible values can be reduced. Therefore, by sequentially choosing the family of functions with the maximum factor of the reduction of sets of possible values of the features R, we obtain sets of intermediate versions for all families of functions. In this case, each set consists of versions that contain values of features of the corresponding family of functions; and it is reduced to a maximum due to two factors:

– Analysis of the presence of forbidden figures determined for the set of values of the given family;

– Exclusion of values of features in accordance with results of the generation of sets of intermediate versions for other families of functions.

It is further necessary to determine the order of multiplication of sets of intermediate versions generated within families of functions. To solve this problem, one can use the same principle as for the solution of the problem of ordering the multiplication of features-arguments of the function, to be exact, by the principle of minimization of the number of intermediate versions at multiplication due to the earliest possible analysis of the presence of the greater number of forbidden figures. In accordance with this principle, a pair of sets of intermediate versions (multiplied at the next step) should be chosen to perform the analysis of the presence of the maximum possible number of forbidden figures. Since analysis of the presence of all simple and complex functional forbidden figures has already been executed, it is now required that we analyze the set of complex non-functional forbidden figures. In order to determine the set of forbidden figures that can be analyzed when multiplying sets of intermediate versions, it is necessary to correlate the set of potential analyzed forbidden figures Ψ_i with each set of intermediate versions Π_i, the first set consisting of forbidden figures that contain at least one value a_k. In this case, a_k should be such a value of the feature A that $A \in \Omega_i$, where Ω_i is the set of features consisting of values that are components of versions of the set Π_i; and at least one value b_m should prove that b_m is the value of the feature B with $B \in \Omega_h, h \neq i$. Let us consider peculiarities of the composition of the set of potentially analyzed forbidden figures Ψ_i. The set Ψ_i does not involve:

– Simple and functional forbidden figures, since their analysis has already been performed;
– Complex non-functional forbidden figures with at least one value corresponding to the feature that is not participating in functional forbidden figures, since it is evident that at the step of multiplication of sets of intermediate versions, analysis of the presence of such forbidden figures will not be performed. That is why their exclusion from consideration in the current step allows for minimizing the memory space for storage of sets of forbidden figures Ψ_i related to the set of intermediate versions Π_i.

Therefore, the set Ψ_i involves only complex non-functional forbidden figures determined for values of features that participate in families of functions. Then, the set of forbidden figures Z_{ij} analyzed at multiplication of sets of intermediate versions Π_i and Π_j can be determined as the result of the intersection of sets of potentially analyzed figures Ψ_i and Ψ_j and the set Y_{ij} consisting of forbidden figures with at least one value that is not related to uniting the sets of values of features for which families Π_i and Π_j are determined:

$Z_{ij} = (\Psi_i \cap \Psi_j) \backslash \mathrm{Y}_{ij}$, where Z_{ij} is the set of forbidden figures that can be analyzed at the multiplication of sets of intermediate versions Π_i and Π_j, and Ψ_i and Ψ_j are

sets of forbidden figures related to sets of intermediate versions Π_i and Π_j, respectively;

$Y_{ij} = \{\upsilon_{ij}\}$, where for $\upsilon_{ij} = \{a_k\}$ $\exists a_k : a_k \notin (V_i \cup V_j)$, where a_k is the kth value of the forbidden figure υ_{ij}, and V_i, V_j are sets of values characterizing the sets of intermediate versions Π_i and Π_j, respectively.

With an opportunity to determine the set of forbidden figures analyzed at multiplication of a pair of sets of intermediate versions, minimization of the number of intermediate versions at multiplication can be achieved in accordance with the following algorithm:

1. Begin.
2. Such a pair of sets of intermediate versions Π_i and Π_j is chosen from the current array of sets of intermediate versions $\Pi = \{\Pi_1, \Pi_2, \ldots, \Pi_n\}$, so that their multiplication could lead to the possibility of checking the maximum possible number of forbidden figures. The number of such forbidden figures K_{ij} is equal to the power of the set Z_{ij}.
3. After multiplication of a pair of chosen intermediate versions Π_i and Π_j, a new set of intermediate versions Π_{ij} is obtained that is correlated to the set of forbidden figures $\Psi_{ij} = (\Psi_i \cup \Psi_j) \backslash Z_{ij})$. For example, accept that there is a set of intermediate versions $\Pi_1 = \{a_1b_1c_2, a_1b_2c_1, a_2b_1c_3, a_3b_2c_1\}$ and $\Pi_2 = \{c_1d_2e_1, c_1d_3e_1, c_3d_1e_2, c_3d_3e_3\}$ as arguments of multiplication. Then, the matrix of synthesis (Fig. 3) is written with the lines and columns containing intermediate versions of sets Π_1 and Π_2; and their intersections are equal to 1 if the synthesized version is implementable, otherwise they are equal to 0. The synthesized version is accepted as being un-implementable if its generating versions contain different values of a certain feature (in this case, they are the values of the feature C).

   Therefore, the result of the multiplication of sets of intermediate versions Π_1 and Π_2 will be the following set:

$$\Pi_{12} = a_1b_2c_1d_2e_1, a_1b_2c_1d_3e_1, a_3b_2c_1d_2e_1, a_3b_2c_1d_2e_1, a_2b_1c_3d_1e_2, a_2b_1c_3d_3e_3,$$

			a_1 b_1 c_2	a_1 b_2 c_1	a_2 b_1 c_3	a_3 b_2 c_1
c_1	d_2	e_1	0	1	0	1
c_1	d_3	e_1	0	1	0	1
c_3	d_1	e_2	0	0	1	0
c_3	d_3	e_3	0	0	1	0

Fig. 3 Matrix of synthesis when multiplying the sets of intermediate versions

with its versions to be analyzed for the presence of forbidden figures of the set Z_{12}.

4. Sets of intermediate versions Π_i and Π_j are excluded from the set Π; and the obtained set of intermediate versions Π_{ij} is added to it and, equal to other sets of intermediate versions, this set participates in the choice of the next pair of multiplied sets.
5. If there is only one remaining element in the set Π, then it is the desired result of the multiplication of sets of intermediate versions. Otherwise, return to p.2.
6. End.

Therefore, all the features that participate in functionally forbidden figures are multiplied and the set of intermediate versions is obtained. The obtained set should be further multiplied by features that participate in complex non-functional forbidden figures. In accordance with the same principle of minimization of the number of intermediate versions at multiplication due to the earliest possible analysis of the greater number of forbidden figures, the next feature to be multiplied should be chosen in order to execute the analysis of the maximum possible number of forbidden figures. The pointed set is determined as follows: $Z_{\Pi P} = (\Psi_\Pi \cap \Psi_P) \backslash Y_{\Pi P}$, where $Z_{\Pi P}$ is the set of forbidden figures that can be analyzed at multiplication of the current set of intermediate versions Π by the feature p, Ψ_Π is the set of forbidden figures correlated to the current set of intermediate versions Π; and Ψ_P is the set of forbidden figures with one of the values being the value of the feature P; $Y_{\Pi P} = \{\upsilon_{\Pi P}\}$, where for $\upsilon_{\Pi P} = \{a_k\}$ $\exists a_k : a_k \notin (V_\Pi \cup V_P)$, where a_k is the kth value of the forbidden figure $\upsilon_{\Pi P}$, V_Π is the set of values characterizing the set of intermediate versions Π; and V_P is the set of values of the feature P.

Therefore, sequentially multiplying the set of intermediate versions Π by the feature P with the maximum power of the set of forbidden figures $Z_{\Pi P}$, we obtain the set of allowed intermediate versions consisting of values of features participating in complex forbidden figures.

In order to finalize the synthesis, it is necessary additionally to multiply the obtained set of intermediate versions by features that are not participating in complex forbidden figures. However, there is no necessity to it in practice, since first of all, the analysis of the presence of forbidden figures is not implied at this step of synthesis and, second of all, it will be more convenient for a user to have such a representation of versions of the object as the result of synthesis, for which the values of features that are not participating in complex forbidden figures correspond to "any value of the feature besides those forbidden undoubtedly by the technical assignment."

Thus, answers to the stated issues allow for developing the model of the process of synthesis that allows for significantly reducing the possibility of achieving the limiting values of the computational process at synthesis due to minimization of the number of intermediate versions and computational load at executing the

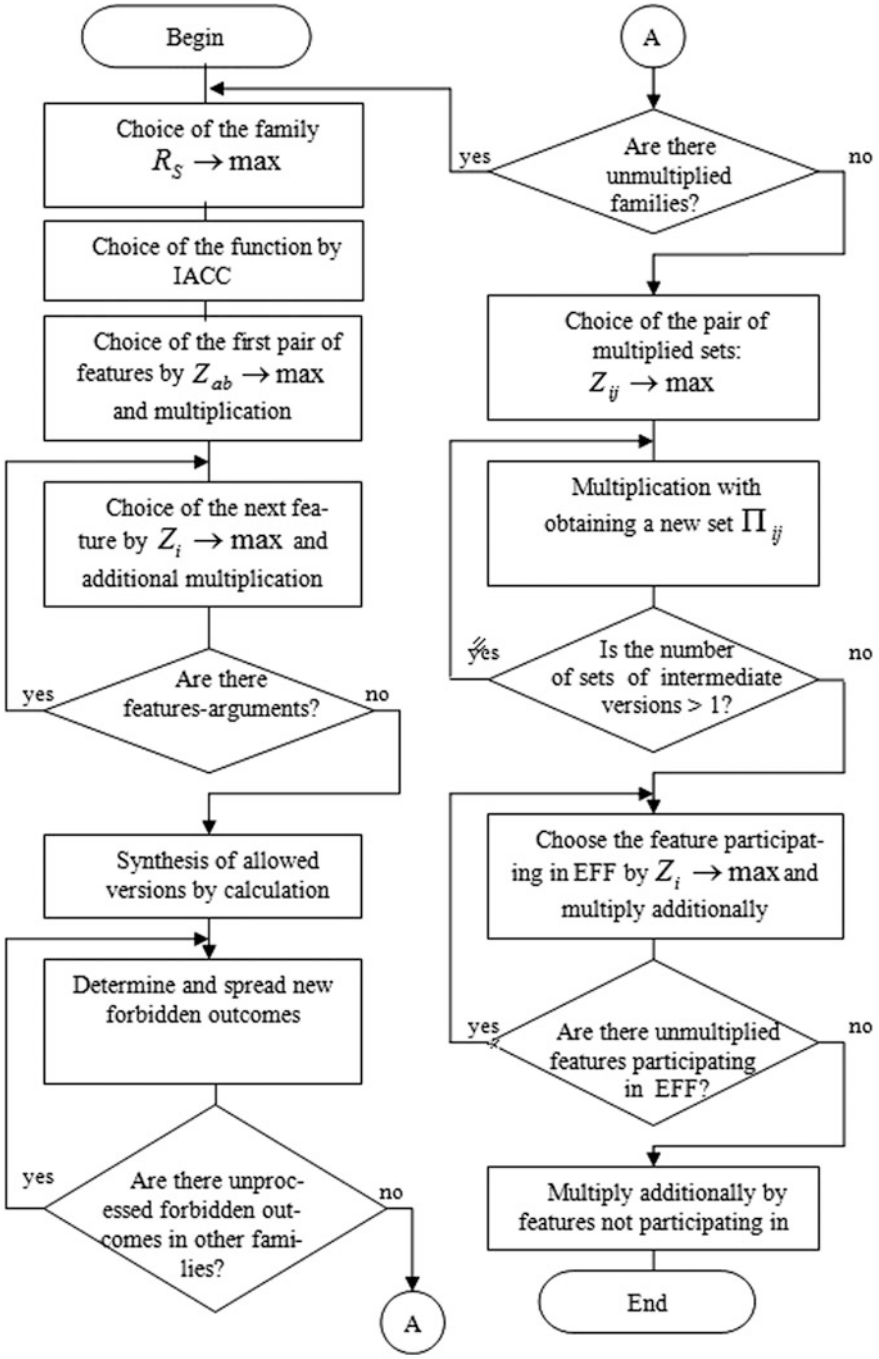
Begin
Choice of the family $R_S \to \max$
Choice of the function by IACC
Choice of the first pair of features by $Z_{ab} \to \max$ and multiplication
Choice of the next feature by $Z_i \to \max$ and additional multiplication
Are there features-arguments?
yes
no
Synthesis of allowed versions by calculation
Determine and spread new forbidden outcomes
Are there unprocessed forbidden outcomes in other families?
yes
no
A
A
Are there unmultiplied families?
yes
no
Choice of the pair of multiplied sets: $Z_{ij} \to \max$
Multiplication with obtaining a new set Π_{ij}
Is the number of sets of intermediate versions > 1?
yes
no
Choose the feature participating in EFF by $Z_i \to \max$ and multiply additionally
Are there unmultiplied features participating in EFF?
yes
no
Multiply additionally by features not participating in
End

◂**Fig. 4** Algorithm of the process of synthesis. *IACC* Integrated Assessment of Computational Complexity, *EFF* Empiric Forbidden Figure, *FF* Forbidden Figure

process of synthesis. The algorithm of the process of synthesis is demonstrated by the flowchart in Fig. 4.

5 Conclusions

When developing the model and methods for optimization of the process of synthesis, the following classifications of forbidden figures have been used:

1. With regard to the origin source: empiric and functional.
2. With regard to application for processes of synthesis: absolute and relative.
3. With regard to the number of values: atomic (one value) and complex (more than one value).

The enumerated classifications are the basis of the model, the methods for optimization and the algorithm of the process of synthesis; together with the model of the class of object, they allow for developing the apparatus for development of a CAD system for specific products.

References

1. Goldfarb, V., Malina, O., Bazhin, A.: Module synthesis of spiroid gearbox layouts. In: Proceedings of the 16th Sympozion Podstaw Konstrukcji Maszyn, Warszawa, Polska, pp. 102–109 (1993)
2. Malina, O., Urzhumov, N.: Mathematical model of the process of structural synthesis of objects developed by discrete structures, eliminating the origin of forbidden versions. In: Information Mathematics, vol. 1, no. 5, pp. 114–120, Moscow (2005) (in Russian)
3. Malina, O., Valeyev, O.: Model of the process of structural synthesis of objects developed by discrete structures and features of their implementation. In: Vestnik of ISTU, vol. 2, no. 57, pp. 24–26. ISTU Publications, Izhevsk (2013) (in Russian)
4. Malina, O., Urzhumov, N.: Optimization of the process of structural synthesis of objects of the medium degree of complexity. In: Vestnik of ISTU, vol. 1, no. 33, pp. 144–150. ISTU Publications, Izhevsk (2007) (in Russian)
5. Malina, O., Valeyev, O.: Approaches to minimization of computer resources necessary for implementation of the process of structural synthesis of objects developed by discrete structures. In: Intelligent Systems in Manufacturing, vol. 1, no. 18, pp. 29–34 (2013) (in Russian)
6. Malina, O., Valeyev, O.: Mathematical model of the design process in CAD systems. Intell. Syst. Manuf. **1**, 67–69 (2014) (in Russian)

Efficient Schemes and Methods for Gear Machining of Spiroid Gearwheels and Worms

E. Trubachev, S. Loginov, K. Bogdanov, D. Khvatov and A. Shutkina

Abstract The paper considers the issues of improving the efficiency of gear machining of spiroid gearwheels and worms, including new schemes for machining on common equipment subjected to moderate and low-cost modification. Basic requirements for modification of equipment and tools are stated; basic relations for the calculation of generation parameters are presented and certain results of calculations and practical machining are shown.

Keywords Spiroid gear · Tooth cutting

1 Introduction

Low-series production is characterized by relatively small batches of products, which often change each other, as well as changing the time it takes for order implementation. There are efficient, relatively cheap and, therefore, common solutions related to both improving efficiency and reducing the time of manufacturing preparation for many types of machining (turning, milling). Unfortunately, this situation has nevertheless remained unchanged in the case of the production of worms, spiroid and worm gearwheels. Apart from the obvious relatively high cost of gear machining, it leads to asynchronous operations within the manufacturing processes: gear machining limits the output cycle time and, consequently, leads to excessive backlogs or the shutting down of equipment. In the present paper, we consider several ideas for improving the efficiency of gear machining in low-series multiproduct manufacturing of spiroid gears at the Innovation Scientific and Production Enterprise "Mechanik" with the application of non-specialized equipment and versatile techniques for machine-tool setting.

E. Trubachev (✉) · S. Loginov · K. Bogdanov · D. Khvatov · A. Shutkina
Kalashnikov Izhevsk State Technical University, Izhevsk, Russia
e-mail: truba@istu.ru

V. Goldfarb et al. (eds.), *Advanced Gear Engineering*,
Mechanisms and Machine Science 51, DOI 10.1007/978-3-319-60399-5_23

2 Conventional Methods for the Machining of Gearwheel Teeth and Worm Threads

Though the conventional method for cutting spiroid gearwheels with a spiroid hob does not have a high efficiency as compared to, for instance, methods of machining bevel and hypoid gearwheels by means of cutting heads, it is usually considered to have a number of advantages within low-series and medium series multiproduct manufacturing: flexibility, versatility, simple setting procedure, and the application of universal and common equipment. The versatility and convenience of gear machining for spiroid and worm gearwheels improved significantly over the last decade due to advanced methods for design and production in accordance with the unification of expensive gear cutting tools (in particular, provision of application of available tools and an abrupt decrease in the range of the required tools) [1, 2, 6, 8, 11].

The edge cutting machining of worm threads and other responsible threads is, in many cases, preliminary, and it is carried out prior to the hardening heat treatment. There is a wide choice of methods for such machining, and it can be implemented by means of:

- a single cutter that can effect multiple cutting of the inter-thread space;
- a whirling head at a lathe, with the worm to be cut arranged either inside the tool or outside of it;
- a disc, face or end-type mill at a specialized thread-milling machine or versatile milling machine.

The first of the methods is more versatile and simple to be implemented on a CNC lathe; it is specific to single and low-series production and is of low efficiency: the machining time for medium-sized worms (with the axial module 3–5 mm) comprises 15–55 min (and even more for multi-thread worms). The second and third methods imply application of multi-cutter tools, and are consequently more efficient; however, for the same reason, they are more specialized, and their application within low-series production is accompanied by an increased change-over time.

3 Machining of Spiroid Gearwheel Teeth by a Plane Cutting Head on a CNC Lathe

The plane shape of a gearwheel, in our opinion, itself ensures the development and implementation of new methods for gear machining. One of these methods, which implements tooth generation through a two-parametric family of generating lines [12], was first proposed in [10]. The cutting scheme is shown in Fig. 1.

In the case of this scheme, the tooth flanks are generated by a two-parametric family of generating lines—the cutting edges of the head cutters. Two independent parameters (the angle of the cutting head rotation and its coordinate at the feed) are

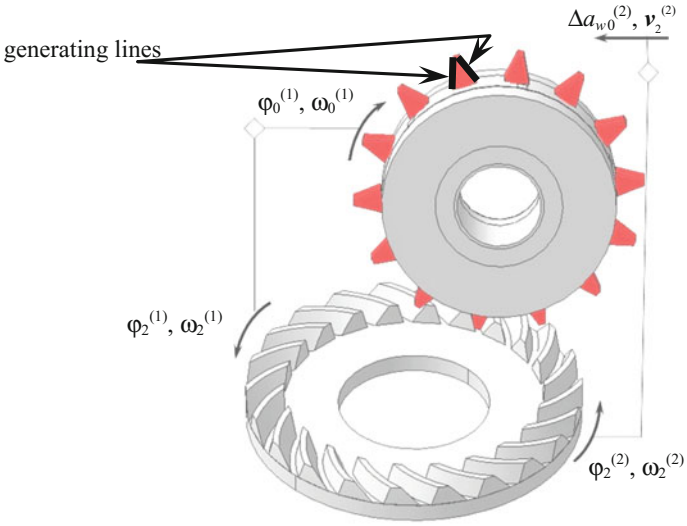

Fig. 1 Scheme of spiroid gearwheel tooth generation by means of a plane cutting head

linearly related to the rotation angles of the gearwheel to be cut—the main angle that provides partition to the teeth $\left(\varphi_2{}^{(1)}\right)$ and the additional one $\left(\varphi_2{}^{(2)}\right)$. In order to determine the coordinates of the points on the surface to be generated, it is necessary to solve the equation of the machine-tool meshing that reflects the complanarity condition for three vectors—the tangential vector to the cutting edge of the cutter (f_2) and two speeds at independent relative motions $\left(v_{s2}{}^{(1)} \text{ and } v_{s2}{}^{(2)}\right)$:

$$\mathbf{f}_2 \cdot \left(\mathbf{v}_{s2}{}^{(1)} \cdot \mathbf{v}_{s2}{}^{(2)}\right) = 0. \tag{1}$$

Analysis has shown that application of the proposed scheme and implementation of cutting the opposite surfaces per one cutting pass of the tool (similar to the double-sided method) allows for obtaining a good approximation of the conjugated surface of the tooth [9, 10]. The profile modification of the tooth can be controlled, in this case, by applying the straight profile of the cutters and varying the diameter of the cutting head and gear ratio at machining.

In order to control the longitudinal modification effectively, it is necessary:

- to arrange the cutters (that generate the opposite tooth flanks) on two different planes;
- to carry out the tool feed along the arc of the circle.

Therefore, the cutting head should contain two groups of cutters, each of them being arranged on its own face plane and serving to cut two opposite tooth flanks.

This scheme is implemented on a CNC lathe with a straight bedplate as its relatively simple modification.

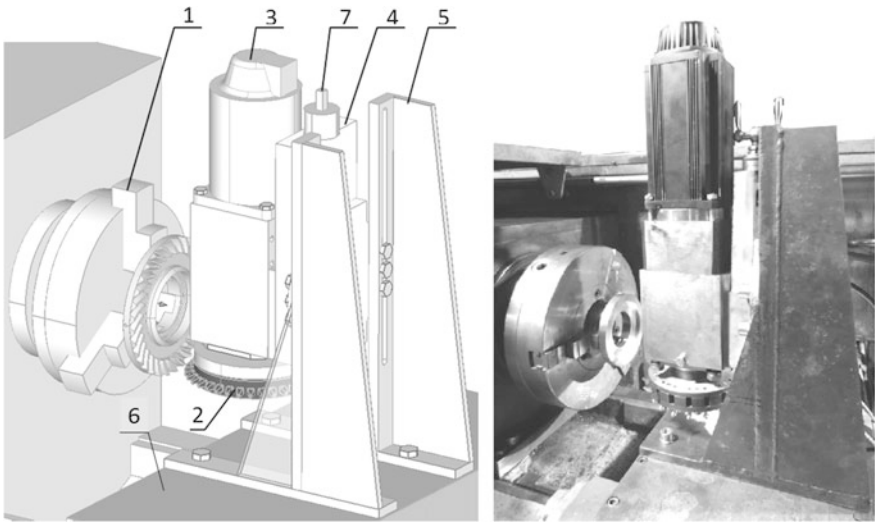

Fig. 2 Modification of the mechanical part of the CNC lathe

The mechanical part of modification implies replacement of the turret head (or a tool holder) by a mechanism that provides the mounting and motion of the cutting head (Fig. 2). The gearwheel blank is mounted in the spindle stock 1. The cutting head 2 with the drive 3 and the vertical support 4 is mounted on the cross feed support 6 of the lathe by means of the support arm 5 after preliminary removal of the tooth holder.

The main requirements for the mechanism are related to providing the adjustment and maintenance of the setting parameters at machining, including:

- the distance B_0 from the plane of the head cutters to the axis of the blank (axis of lathe centers) is adjusted by rotation of the screw 7 of the vertical support 4;
- the machine-tool interaxial angle $\sum_0$ (the angle between the axes of the blank and the cutting head; in the most common case, this angle is equal to 90°) is provided by adjustment, at mounting, of the support arm 5 onto the cross feed support 6.

The position of the center x_c, z_c and the radius ρ of the arched trajectory of the cutting head feeding, and the initial and final machine-tool center distance a_{w0} are assigned in the control program.

Cutters of the head are subjected to loading mainly perpendicular to their front planes, that is, the axial component of the cutting force acting on the cutting head (CH) is the dominant one; this requires application of the corresponding bearings of the CH spindle. In this case, four versions of arrangement of the cutting head and its cutters correspond to one and the same set of design-setting parameters, these four versions having the following two pairs of alternatives in Fig. 3: the planes of the cutters are higher (a) or lower (b) than the axis of the centers, and the front planes of

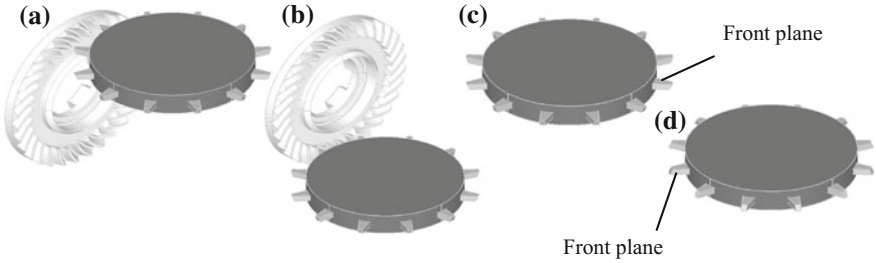

Fig. 3 Versions of arrangement of the cutting head and cutters

the cutters are facing upwards (c) and downwards (d). The version in which the front surfaces of the cutters are facing upwards at an arrangement of the cutting head lower than the axis of the centers is the main version providing a high rigidity and reliable pressing to guideways of the machine-tool bedplate by forces of cutting.

The tool applied for the method (a cutting head, see Fig. 4) differs from similar ones applied for production of spiral bevel and hypoid gears. Its cutters are mounted in precisely positioned radial slots so that their front planes can form a single face plane (to be more exact, two planes generated by groups of cutters for opposite surfaces of teeth), thus greatly simplifying the setting of the head. Adjustment of cutters along the radial and axial position and compensation for changes in their size during re-sharpening are provided.

Upgrading of the numerical control system of the lathe implies coordination of three pairs of motion (Fig. 5):

i. rotation of the gearwheel (φ_{sp}) and feed of the cutting head (Δp_{arc});
ii. longitudinal Δp_z and lateral Δp_x feed;
iii. rotation of the cutting head (φ_{CH}) and rotation of the gearwheel (φ_{sp}).

As was stated above, it is possible to obtain the necessary longitudinal tooth modification when performing the feed along the circle arc, that is, with a variable relation of feeds Δp_z and Δp_x (Fig. 5). In order to overcome this difficulty, it is proposed that we divide the circular trajectory of the tool feed into a number of rather small linear segments. Coordination of motions i and ii at each of the segments is provided within the mode of cutting the tapered thread.

In order to align the rotations of the head-cutter and the blank (condition iii), one must set the servo-drive, which will provide an additional link between them, and specify the NC control block, that is, to switch the mode of NC control block operation from the lathe (control of two or three coordinates) to the milling one (control of four coordinates). In this case, the correspondence between the control signals of the CNC block and the displacements processed to implement the proposed scheme of gear machining is established.

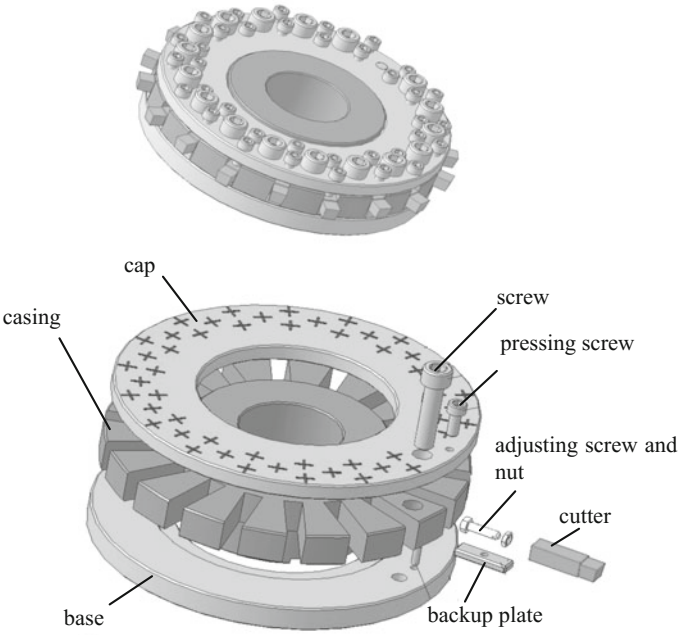

Fig. 4 Plane cutting head for machining the spiroid gearwheel teeth

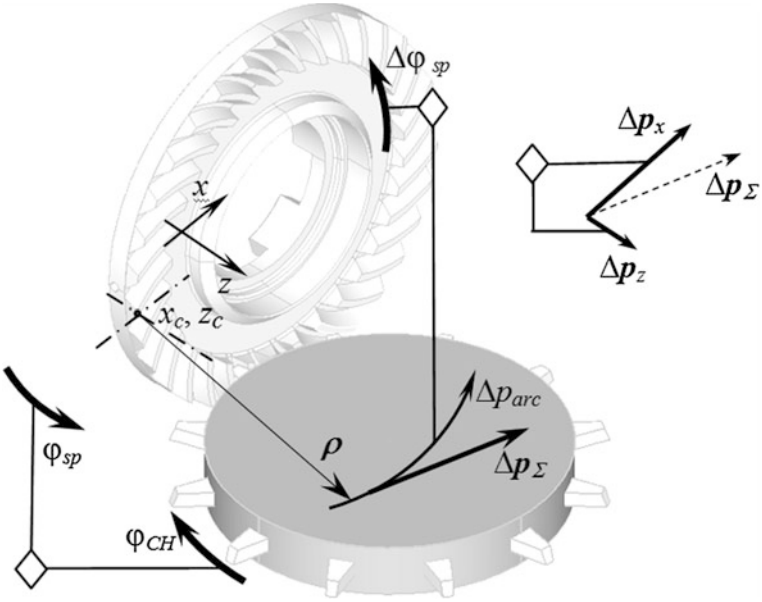

Fig. 5 Agreement of motions implemented at gear machining

The accuracy of the agreed-upon motions made at gear cutting is provided by mounting the corresponding encoders (feedback sensors—FS) onto the spindle, the servo-drive of the cutting head and the longitudinal and cross actuator screws.

The authors have modernized the lathe 16K30Ф3 with the Balt-System NC-210, according to the described requirements (Fig. 2). The results of the first cuttings of spiral teeth by a plane cutting head showed the following:

1. A harmful influence of vibrations due to the shock input of cutters can be reduced by:
   - mounting the inertial masses onto the machine-tool spindle and the cutting head;
   - manufacturing the column out of cast iron.
2. As was expected, the axial components of the cutting force acting on the CH is the dominant one, however, the angular component of the cutting force can also be significant.
3. The discrepancy of angular FS on the machine-tool spindles and of the CH drive by the value of 16,000–32,000 pulses per one revolution provides the appropriate accuracy of agreement for motions of division (it influences the error of the tooth pitch) and feed (the error of the longitudinal tooth line).

4 Machining of Worm Threads by a Face Cutting Head on a CNC Lathe

The possibility of worm thread machining with a face (cup-type) tool (Fig. 6) is not new in its essence. It is applied to form cylindrical worms with the flank profiles ZK3 generated by the cone and ZCT3 generated by the torus (designations in accordance with Russian standards [4, 5]). In both cases, the worm threads are manufactured by the cup tool with the axis crossing the axis of the worm at a right angle. Thus, strictly speaking, the orthogonality of the pointed axes is of no critical limitation.

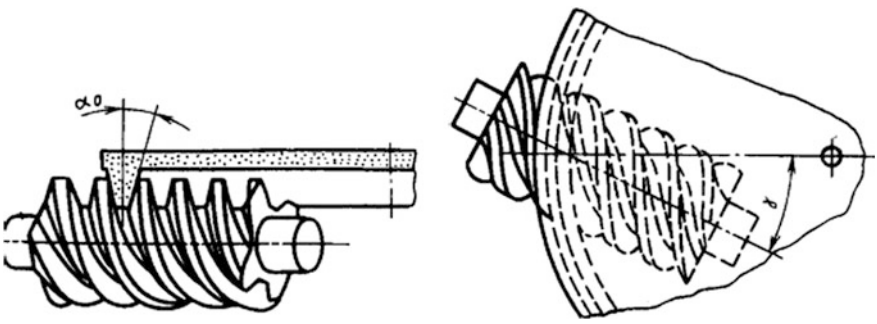

Fig. 6 Scheme of generation of ZK3 [4] and SZK3 [5] worms

In accordance with Fig. 6 (taken from the standard [4, 5]), the grinding of threads for the above-mentioned types is first implied. Indeed, in this case, unlike worms ZK (ZK1 in Russian terminology) and ZCT (ZCT1), dressing of the grinding wheel and corresponding variation of its dimensions does not theoretically influence the geometry of the generated thread. Premises for achieving high efficiency of the machining process are maintained in this case, that is, relatively large dimensions and tool rigidity. However, in this case of the preliminary cutting of threads, implementation of the scheme shown in Fig. 6 is not only possible, but, in our opinion, is rather justified, since it possesses the following advantages as compared to the scheme of thread generation for worms ZK (ZK1) and ZCT (ZCT1):

- the above-mentioned theoretical insensitivity of the geometry of the threads to be cut to variation in the overhang of the head cutters;
- the possibility of application of a wide spectrum of common (and, therefore, relatively cheap) cutting heads for circular tooth cutting;
- the possibility of performing the setting (re-setting) by means of easily implemented linear displacements;
- a structurally simple modification of the thread-cutting lathe to be implemented.

In the scheme considered, the flanks of the worm threads are formed by an enveloping of the generating surface of the tool (cone or torus). The coordinates of the points of the thread flanks can be obtained, as usual, by solving the equation of the machine-tool meshing:

$$\mathbf{n} \cdot \mathbf{v}_{s1} = 0, \tag{2}$$

where $\mathbf{n}$ is the normal vector to the generating surface, and $\mathbf{v}_{s1}$ is the vector of the relative velocity in the machine-tool meshing, which, in its essence, is the velocity of the screw motion of the tool with respect to the cut worm.

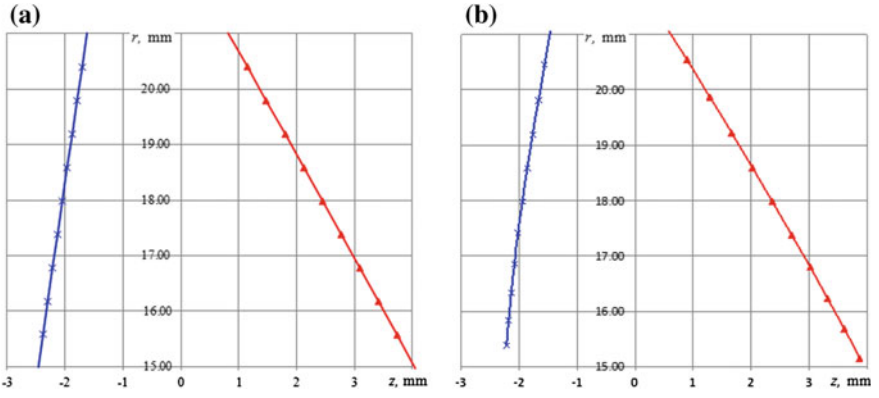

Fig. 7 Axial profile of threads for SZK3 worms (m_{x1} = 2.75 mm, d_1 = 36.5 mm, $\alpha_{0R} = 10°$, $\alpha_{0L} = 28°$): **a** $z_1 = 1$, $\gamma_1 = 4.31°$, **b** $z_1 = 4$, $\gamma_1 = 16.77°$

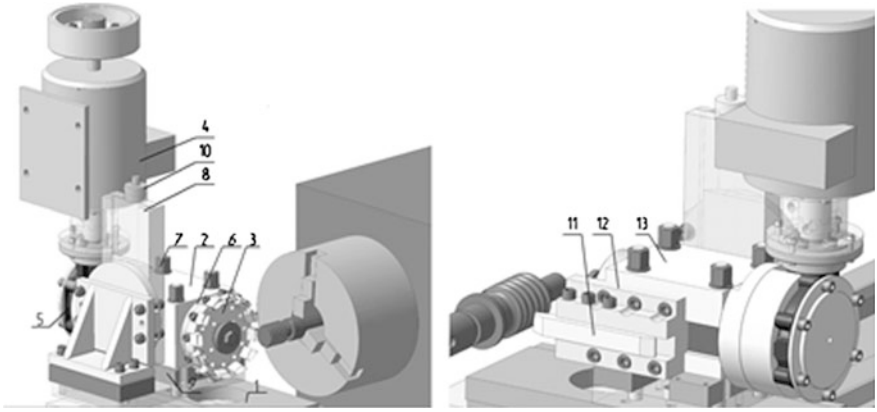

Fig. 8 The lathe 16A20Φ3 modified for cutting worm threads with the face cutting head

Application of (2) in the analysis shows that the axial profile of threads for the worms ZK3 and SZK3 turns out to be convex; additionally, the greater the helix angle γ_1 and the lower the pressure angle α_0 (Fig. 7), the greater the value of convexity.

In the USSR, the development of the method for cutting SZK3 and SZCT3 spiroid worms was focused on the specialized equipment in terms a large-series and mass production [3]. In terms of flexible low-series production, we made an attempt to modify the common CNC lathe for worm cutting in accordance with the scheme in Fig. 8.

As can be seen, the tool turret is demounted from the slide 1, and the mechanism 2 is put in its place, intended for alignment, fixation and driving of the face cutting head 3. In this case, there is no need for this in motions that are additional to those implemented at the machine-tool at thread cutting. The main feature is the frequency of the spindle rotation—0.4 to 7 rpm, which is low for the usual terms of turning.

The mechanism is driven by means of the induction motor 4 and the auxiliary gearbox 5. Common head-cutters for spiral bevel gears are applied here. The head is mounted, in this case, so that the cutting forces can press it to the guideways of the machine bed. In order to ensure a greater versatility, the possibility is provided in this layout for mounting a single cutter 11 (Fig. 8) in the tool holder 12 mounted on the casing of the mechanism 13.

The gear cutting head is provided by cutters 2 with standard replaceable cutting carbide plates 1; their application allowed for increasing the cutting speed from 25 to 40 up to 100 to 125 m/min.

When choosing the dimension of the cutting head, it is necessary to follow the term of preventing the thread cut-off by the concave flank of the generating surface (Fig. 9). We apply two rather simple methods for calculation of the minimum tool diameter $d_{0\ min}$.

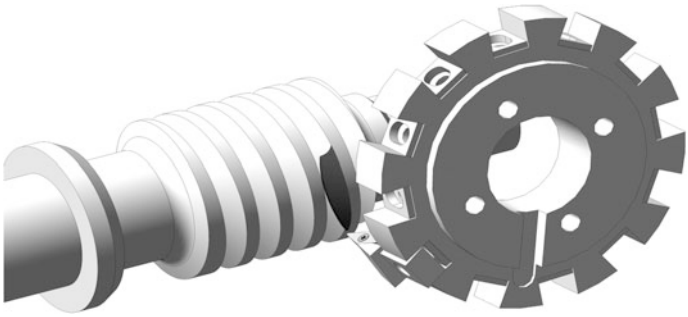

Fig. 9 Thread cutoff by the concave flank of the generating surface

1. The differential method is based on analysis of the radius of curvature of the worm thread in the plane section parallel to its axis and located away from it by the value of the radius $d/2$. The pointed section is inclined (not normal) to a helical surface, which is why, in order to transfer away from the normal curvature, Meusnier's formula should be applied. Omitting the calculations, let us give the final formula for obtaining $d_{0\ min}$:

$$d_{0\,\min} = d\,\cos\phi\ \sec^2\gamma\sqrt{1+\sec^2\gamma\cot^2\alpha_x}, \tag{3}$$

   where γ is the lead thread angle, α_x is the axial pressure angle of the thread, and ϕ is the angle of inclination of the normal section of the thread to the considered cutting plane (all parameters should be taken for the point of the profile located on the cylinder with the diameter d).
2. The graphic method consists in direct visual comparison within the available CAD-system of the pointed section of the worm with the circumference of the chosen diameter in Fig. 10. Despite its approximate and, seemingly, archaic character, this method is often more available, demonstrative and convenient for a design engineer. Moreover, it allows for checking the absence of interference of the generating and generated surfaces along their whole length, and not only in the local vicinity of the point of their contact.

In practice, we combine both methods, which mutually check each other. Table 1 presents the results and comparison of calculation of the diameter $d_{0\ min}$ for different numbers of threads and pressure angles of the worm with an axial module of 2.75 mm and a pitch diameter of 36 mm.

The distance between the axis of rotation of the worm to be cut and the axis of rotation of the CH at machining are chosen to be equal or close to the value (Fig. 10)

$$a_{w0} = 0.5d_0\sin\gamma_1, \tag{4}$$

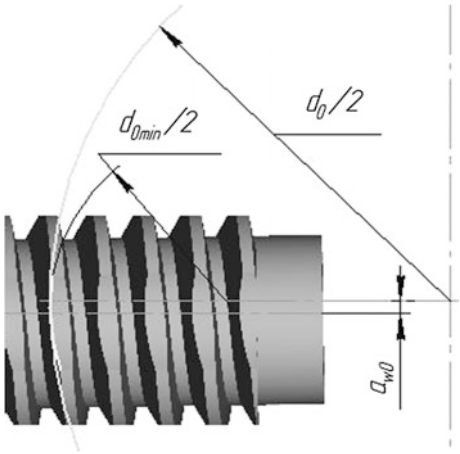

Fig. 10 Graphic method for determining $d_{0\ min}$

Table 1 Minimum diameter of the face cutting head

No	z_1	α_x (°)	$d_{0\ min}$ (mm)	
			Differential method	Graphical method
1.	1	12	170.8	168.2
2.		30	62.9	60.6
3.	4	12	193.6	191.4
4.		30	71.3	70.5

where γ_1 is the pitch lead angle of the worm, and d_0 is the diameter of the cutting head. Adjustment of the center distance is performed by vertical displacement of the slide along the guideways of the support arm with the consequent fixation.

Cutting the worm threads on the pointed modified machine allowed for reducing the time of the provisional machining of threads by a factor of 3–4, as compared to machining by the single cutter on the same machine-tool.

5 Continuous Machining of Multi-thread Worms by a Face Cutting Head at CNC Lathe

One can state that worms with a relatively high number of threads (greater than 3–4) are considerably similar to helical gears with big helix angles. Obviously, the separate cutting of each space between the teeth has drawbacks known from similar methods for helical gears. Continuous indexing for cutting multi-thread worms can be implemented on the gear-hobbing machine by means of a hob. In this case, significant correction of the profile parameters for the worm to be cut relates to the necessity re-profiling of the hob; it is a rather consuming and expensive operation that is not implemented for each enterprise. In this regard, this method is not

featured on account of the flexibility necessary within low-series production. Moreover, as was already stated above, machining by a hob does not provide the high efficiency of the method.

For these reasons, we proposed, in [11], a new method for worm cutting with a face cutting head at continuous partition into threads, thus giving premises for providing both high efficiency and flexibility of production. Although this method can also be applied for single-thread worms, in our opinion, it creates great advantages precisely for those of multi-thread by ensuring cutting in one stroke of the tool.

The scheme of thread generation is shown in Fig. 11. The cutting head and the generated worm are concurrently rotated by angular velocities ω_0 and ω_1, respectively, with the gear ratio i_{01} equal to the ratio of the threads to be cut z_1 to the number of cutters z_0 (or pairs of cutters with one cutter for the left flanks of threads and the other for the right ones) of the head. When meeting this requirement, each next cutter (or the next pair) enters each next space between the threads. Besides, the feed p_0 of the cutting head is provided along the worm axis. The feed agrees with the angular velocity $\Delta\omega_1$ of the additional rotation of the worm with the ratio $p_0/\Delta\omega_1 = p_{\gamma 1}$, where $p_{\gamma 1}$ is the helical parameter of the generated worm.

Flanks of threads in such a scheme are generated by a double-parametric family of generatrices—cutting edges of the cutting head. The first parameter of the family is the angle φ_0 of the cutting head rotation; the second one is the coordinate z characterizing its location along the worm axis. The relation between rates of variation of these parameters within a wide range (at least, at meeting the requirement $\omega_0 \ll \Delta\omega_0$) does not practically influence the obtained geometry of the threads, thus indicating the independence of their influence. For this reason, flanks of threads generated in accordance with the scheme in Fig. 11 can be determined by the relation that coincides, in its essence, with (1) [12]:

$$\mathbf{f}_2 \cdot \left(\mathbf{v}_{s2}{}^{(1)} \cdot \mathbf{v}_{s2}{}^{(2)} \right) = 0. \tag{5}$$

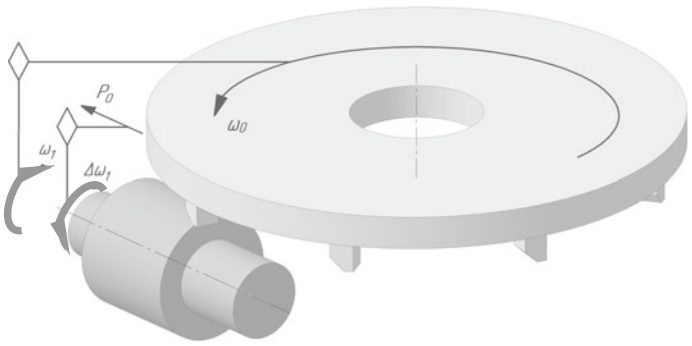

Fig. 11 Scheme of generation of worm threads with a plane cutting head at continuous partition

The subscript $_1$ is used here instead of $_2$ in Eq. (1) in order to emphasize the difference: the relation and method for machining is applied to generate the first element of the gear—a worm.

It is reasonable to choose a gear ratio for rotations of the worm and the cutting head equal or close to the value [11]:

$$i_{10} = \frac{\omega_1}{\omega_0} = \frac{z_0}{z_1} = \frac{a_{w01}}{p_{\gamma 1}} - \frac{\sqrt{d_0^2 - 4a_{w01}^2}}{d_1}, \tag{6}$$

where a_{w0} is the machine-tool center distance, and d_1 is the pitch diameter of the worm.

The front planes of the head cutters should be arranged perpendicular to the first relative motion (the main cutting motion) of the cutters, that is, inclined at the angle γ_0 with respect to the axial plane of the head:

$$\cos\gamma_0 = \frac{\boldsymbol{v}_{01}^{(1)}\boldsymbol{v}_0^{(1)}}{\boldsymbol{v}_{01}^{(1)}\boldsymbol{v}_0^{(1)}} \tag{7}$$

$$\text{or} \quad \gamma_0 \approx \arcsin\left(\frac{2a_{w0}}{d_0}\right) - \gamma_1. \tag{8}$$

There is much in common between the continuous cutting of the threads with a face cutting head and the above-considered method for cutting ZK3 and SZK3 worms. In particular, when choosing the diameter of the cutting head, one can apply relations (6). In the case of a rectilinear profile of the cutters, the axial profile of the generated thread turns out to be slightly convex; and the value of convexity is increased with an increase in the lead thread angle γ_1 and a decrease in the pressure angle α_0 (Fig. 12).

The manner of implementing the methods can also be rather common: on a thread-cutting lathe with practically the same manufacturing tooling (Fig. 7). The essential differences are:

- a considerably greater rotational velocity of the worm to be cut. This makes the scheme less sensitive to dynamic processes at cutting;
- the necessity of organizing an additional program control of the rotation of the cutting head, agreeing with the worm rotation. For this purpose, it is necessary here to apply a servo-drive and incorporate the control of the corresponding additional coordinate into the NC control block.

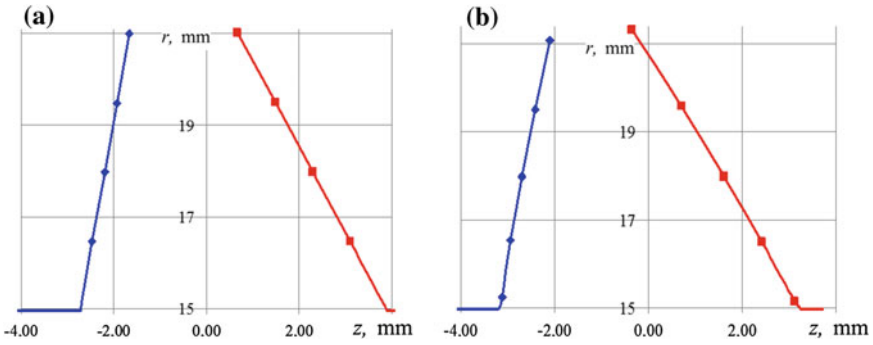

Fig. 12 Axial profile of worm threads machined at continuous partition by the face cutting head (m_{x1} = 2.75 mm, d_1 = 36.5 mm, $\alpha_{0R} = 10°$, $\alpha_{0L} = 28°$): **a** $z_1 = 1$, $\gamma_1 = 4.31°$, **b** $z_1 = 4$, $\gamma_1 = 16.77°$

6 Other Progressive Schemes of Efficient Machining

The increased efficiency of gear machining is usually related to application of the rigidly assembled multi-cutter tool provided with carbide plates—a cutting head. Disc-type (in other words, assembled disc cutters) and face-type heads are widely known. Earlier, we considered new promises for applying the face cutting head on the thread cutting lathe for single and continuous indexing into teeth/threads. Note that these two methods for machining are quite similar to two methods for gear machining of bevel and face gearwheels—*face milling* and *face hobbing* [7]. The version of applying the plane cutting head for machining at continuous indexing is also considered. The exact continuous corresponding motion of the blank and the tool provide the possibility of machining by cutters with their front surfaces forming a united plane. It seems this version of the arrangement of the front plane is inconvenient for providing the cutting motion; in this case, cutters move along their front planes within the tool rotation. However, it is possible both for gearwheels (as was shown above) and for worms (as is shown in Fig. 13) if the corresponding motion of the tool and the worm to be cut is implemented so that the main relative motion at the area of machining can be orthogonal (or almost orthogonal) to the plane of locations of the cutters. The advantages of the latter scheme are:

- the simplicity of mounting the cutters (on a united plane), both at cutting and at sharpening;
- the almost complete absence of the angular component of the cutting force. This allows for concentrating the cutting process mainly at the primary drive of the lathe.

Another version of the cutter arrangement can be a cylindrical or a bevel cutting head [12] (Fig. 14). Such an arrangement, at first glance, is also inconvenient for implementing the cutting process: at rotation of the cutting head, the cutters move

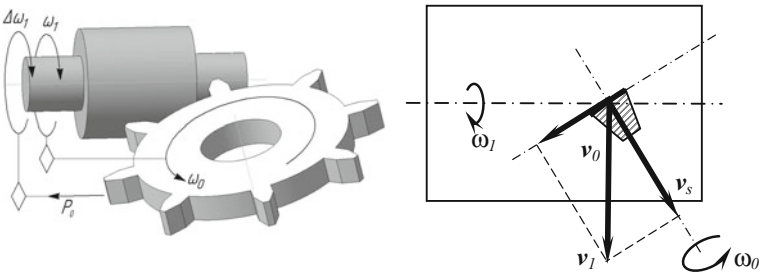

Fig. 13 Scheme of cutting the worm threads with a plane cutting head

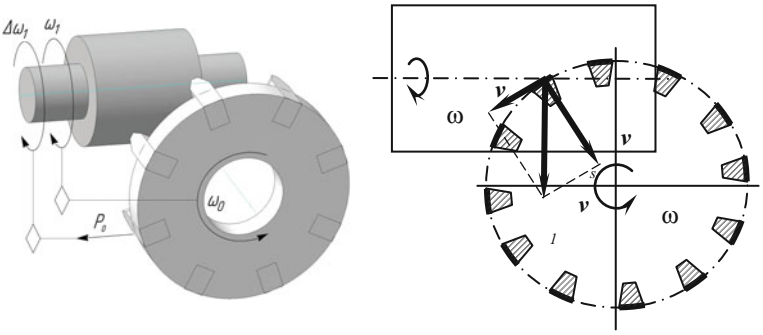

Fig. 14 Scheme of cutting worm threads with a cylindrical cutting head

along the front surfaces. However, similar to the previous case, this inconvenience can be eliminated simply by implementing the main relative motion of the tool and the cut worm perpendicular to the cylinder or cone on which the front surfaces of the cutters are located. This scheme also has premises for a high rigidity of the tool and efficiency, convenience of re-sharpening and control of the cutter arrangement, and a relatively low power of the tool drive.

7 Conclusions

Recently, more and more information has become available on new possibilities for the blade machining of teeth at advanced, multi-coordinate (multi-axes), universal CNC machine-tools by means of versatile face and disc tools. These possibilities are competitive with traditional methods for gear machining implemented on specialized machine-tools. This technique is attractive for a manufacturer, in no small measure, owing to the widespread availability of the equipment and tooling. New schemes and methods for gear machining considered in this paper, and partially implemented in practice, occupy a somewhat intermediate position between

competing techniques: they provide high efficiency, flexibility and the possibility of applying the common equipment. For this reason, they deserve, in our opinion, further study and approbation, especially for multi-range low-series production.

References

1. Goldfarb, V., Trubachev, E., Lunin, S.: System of hobs unification for gear-wheel cutting of worm-type gears. In: 10th International ASME Power Transmission and Gearing Conference, Las-Vegas, USA, DETC2007-34916 (2007)
2. Lagutin, S.A., Verhovski, A.V., Dolotov, S.V.: Technological design of worm gears with a localized contact. In: Proceedings of 2nd International Conference "Power Transmissions 2006", Novi Sad, Serbia, pp. 177–182 (2006)
3. Long, V.: Development and investigation of issues of the technique for applying the face tool for cutting the worms of spiroid gears of special and general-purpose mechanisms and devices. Ph.D. thesis, p. 22. Izhevsk (1984) (in Russian)
4. Russian Standard GOST 18498-89. Worm gears. Terms, definitions and designations
5. Russian Standard GOST 22850-77. Spiroid gears. Terms, definitions and designations
6. Sandler, A.I., Lagutin, S.A., Verhovski, A.V.: In: Lagutin, S.A. (eds.) Manufacturing of Worm Gears, p. 272. Mashinostroenie, Moscow (2008) (in Russian)
7. Stadtfeld, H.J. Gleason Bevel Gear Technology. Manufacturing, Inspections and Optimization: Collected Publications 1994/95, p. 202. The Gleason Works, Rochester, New York, USA (1995)
8. Trubachev, E., Glazyrin, A., Savelyeva, T.: New solution of the problem of unification of hobs at design and production of cylindrical worm gears. In: Proceedings of the Scientific Conference on Gears, Izhevsk, pp. 298–301 (2008) (in Russian)
9. Trubachev, E., Loginov, S.: New method for cutting the teeth of spiroid gearwheels. In: Proceedings of the International Symposium "Theory and Practice of Gearing", Russia, Izhevsk, pp. 232–237 (2014) (in Russian)
10. Trubachev, E., Zlobina, P., Loginov, S.: New Scheme of Spiroid Gearwheel Tooth Generation. Intelligent Systems in Manufacturing, vol. 3, pp. 178–184. ISTU Publ., Izhevsk (2011) (in Russian)
11. Trubachev, E., Zubkova, A.: Method for cutting the threads of multi-thread cylindrical worms. In: Proceedings of the International Symposium "Theory and Practice of Gearing", Russia, Izhevsk, pp. 238–243 (2014) (in Russian)
12. Trubachev, E.: Several issues of tooth generating process by two-parametric families of generating lines. In: Honor of Professor Litvin, F.L., Goldfarb, V., Barmina, N. (eds.) Theory and Practice of Gearing and Transmissions, vol. IX, pp. 97–116, 450 (2016)

Influence of Layout Features and Parameters of a Planetary Gear on Its Dynamics and Strength Characteristics

F. Plekhanov, A. Pushkarev and I. Pushkarev

Abstract Problems of dynamics of multi-satellite and eccentric planetary gears are considered in the paper. The influence of dynamic loads on meshing strength at transient operating modes of a drive, taking into account gear layout features and the flexibility of mechanism elements, is investigated. The dependence between multi-satellite planetary gear parameters and the limiting angular speed of a sun gearwheel, taking into account meshing strength characteristics, is established. The influence of inertial force at steady motion on the support reaction value of the eccentric gear satellite with a roller mechanism of torque absorption from the satellites is considered.

Keywords Planetary gear · Dynamics · Inertial force · Strength

1 Introduction

Planetary gears are widely applied in many areas of mechanical engineering, due to their positive mass-dimensional performances and certain other favorable characteristics. The most widespread of these are the multi-satellite gears consisting of a sun gearwheel, satellites, a fixed central gearwheel and a planetary carrier, as well as gears containing a high-speed eccentric planetary carrier, one or several satellites, a fixed gearwheel and a mechanism of torque absorption from the satellites. In the researches of machines and mechanisms, including planetary gears, great attention has been paid to their dynamics [2, 4–6, 8, 23–26]. This is especially urgent for high-loaded planetary mechanisms working at high angular speeds.

The problems of planetary gears dynamics can be divided into several types.

The first type is connected to the research into load ability and strength at transient modes, during running-up or running-out that is specific to repeated and short-term action gears.

F. Plekhanov (✉) · A. Pushkarev · I. Pushkarev
Kalashnikov Izhevsk State Technical University, Izhevsk, Russia
e-mail: fplehanov@list.ru

V. Goldfarb et al. (eds.), *Advanced Gear Engineering*,
Mechanisms and Machine Science 51, DOI 10.1007/978-3-319-60399-5_24

The second type concerns their application at steady operation, at the maximum angular speed.

The third type is related to the oscillatory processes in planetary mechanisms.

2 Dynamic Loads of Planetary Gears in Transient Modes

Great influence is exerted on planetary transmission meshing strength by dynamic loads which, in turn, depend on the flexibility of mechanism elements [15, 16, 19, 20].

Let us consider the multi-satellite planetary gear (Fig. 1) at the running start.

For determination of the relation between power factors and mechanical drive parameters, we use the theorem on kinetic energy variation:

$$\Delta W = W - W_0 = \int_0^{\varphi_1} T_h(\varphi_h)\, d\varphi_h, \tag{1}$$

where W_0 is the kinetic energy of a mechanism at the initial time instant, $W_0 = 0$; $T_h(\varphi)$ is the dependence of the torque of a planetary carrier shaft on the rotation angle φ; and φ_1 is the rotation angle during the running start caused by flexibility of the gear elements.

The planetary mechanism kinetic energy is

$$W = n_w \frac{M_g V_C^2}{2} + n_w \frac{I_g \omega_g^2}{2} + \frac{I_h \omega_h^2}{2} + \frac{I_a \omega_a^2}{2},$$

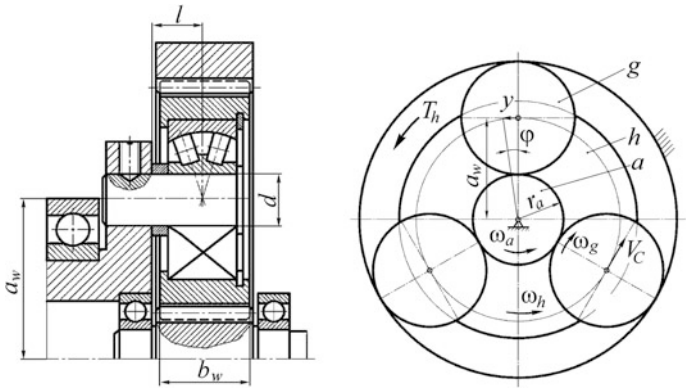

Fig. 1 A planetary mechanism with console satellite axles

where n_w is the number of satellites; M_g is the satellite mass; V_C is the speed of the satellite's center of mass; I_i are moments of inertia of the parts; ω_i are angular speeds; and indexes g, h, a relate to the satellite, the planetary carrier and the sun gearwheel, respectively.

Considering the relation between the geometrical and kinematic parameters of a gear, we will express the weight and the moments of inertia of its parts through the sun gearwheel mass M_a:

$$
\begin{aligned}
M_g &= k_g \pi \rho r_g^2 b_w = k_g M_a r_g^2 / r_a^2 = k_g M_a (0.5i - 1)^2; \\
M_h &\approx \pi \rho (1.2 a_w)^2 b_h = 0.36 M_a i^2 b_h / b_w; \\
I_h &= \frac{M_h (1.2 a_w)^2}{2} = \frac{0.065 M_a^2 i^4 b_h}{\pi \rho b_w^2}; \\
I_a &= \frac{M_a r_a^2}{2} = \frac{M_a^2}{2\pi \rho b_w}; \\
I_g &= \frac{k_g M_g r_g^2}{2} = \frac{k_g M_g^2}{2\pi \rho b_w} = k_g M_a^2 \frac{(0.5i - 1)^4}{2\pi \rho b_w}; \\
M_a &= \pi \rho r_a^2 b_w.
\end{aligned}
$$

Here, ρ is the material density of the gear part; b_w is the face width of the gearwheel; b_h is the web width of the planetary carrier; k_g is the satellite filling coefficient (the filling coefficient of a sun gearwheel is accepted as being equal to one); i is the gear ratio; r are the gearwheel radii; and a_w is the inter-axial distance.

The angular speeds of the parts and the speed of the satellite's center of mass can be presented in the form of functions of the planetary carrier's angular speed and gear ratio:

$$
\begin{aligned}
\omega_g &= \omega_h \frac{i}{0.5i - 1}; \\
V_C^2 &= (\omega_h a_w)^2 = (\omega_h 0.5 i\, r_a)^2 = \omega_h^2 \frac{i^2 r_a^2 \pi\, \rho b_w}{4\pi \rho b_w} = \omega_h^2 \frac{M_a}{4} \cdot \frac{i^2}{\pi \rho b_w}.
\end{aligned}
$$

Then, the kinetic energy of a mechanism with a double-web planetary carrier which is rigidly fixed to the driven shaft will be as follows:

$$
W = \frac{M_a^2 \omega_h^2}{2\pi \rho b_w} \left[n_w \frac{k_g (0.5i - 1)^2 i^2}{2} + n_w \frac{k_g (0.5i - 1)^2 i^2}{4} + 0.065 \frac{b_h}{b_w} i^4 + \frac{i^2}{2} \right].
$$

The infinitesimal rotation angle is $d\varphi = \frac{dy}{a_w} = \frac{2dy}{ir_a}$, where y is the tangential displacement of points of the driven part on a circle having the radius a_w which consists of bending y_1 and shearing y_2 strains of satellite axles, taking into account the influence of stiffness on the jumper jointing planetary carrier webs with two-point axles of satellites; the gearwheel teeth strains y_3 [1, 7], displacements

caused by flexibility in the satellite bearing y_4 [3] and the sun gearwheel twisting strain y_5 [17]:

$$y = y_1 + y_2 + y_3 + y_4 + y_5.$$

The tangential displacement components for the simplest technological planetary gear layout with console satellite axles (see Fig. 1) are defined as follows:

$$y_1 = F_0(y)\frac{l^3}{3I_xE} = \frac{T_h(y)}{a_w n_w} \cdot \frac{l^3}{3I_xE},$$

where F_0 is the force acting on the axle of one satellite, l is the distance between a planetary carrier web and the concentrated force acting on a satellite axle from the bearing (see Fig. 1), and I_x is the moment of inertia of the satellite axle cross-section, and E is the Young modulus

$$y_2 = F_0(y)\frac{1.1l}{SG} = \frac{T_h(y)}{a_w n_w} \cdot \frac{1.1l}{SG} = \frac{2.2(1+\mu)T_h(y)l}{a_w n_w SE},$$

where S is the cross-sectional area of the satellite axle, G is the shear module, and μ is the Poisson coefficient (flexibility of the axle is determined by the given expressions, approximately; for a more exact definition, it is necessary to use the technique given in [12]);

$$y_3 = \frac{F_t(y)}{b_w C} = \frac{T_h(y)}{a_w n_w 2b_w C},$$

where $C = 0.075E$ is the meshing rigidity [1], F_t is the tangential force acting on the tooth;

$$y_4 \approx \frac{T_h(y)}{b_w a_w n_w (0.2E)}$$

(this approximate expression corresponds to the average series bearings, which are often used in practice);

$$y_5 = 0.5r_a\varphi_a = 0.5r_a\left[\frac{0.5T_h(y)b_w}{2iGI_{pa}} + \int_0^{0,5b_w} \frac{T_h(y)(0.5b_w - z)dz}{ib_w I_{pa} G}\right]$$
$$= \frac{0.375T_h(y)(1+\mu)b_w r_a}{iEI_{pa}},$$

where I_{pa} is the polar moment of inertia of the sun gearwheel cross-section.

As a result,

$$dy = \frac{dT_h}{Ea_w n_w}\left[\frac{l^3}{3I_x} + \frac{2.2(1+\mu)l}{S} + \frac{1}{0.15b_w} + \frac{1}{0,2b_w} + \frac{0.375a_w n_w(1+\mu)b_w r_a}{iI_{pa}}\right],$$

$$d\varphi_h = \frac{2dy}{ir_a} = \frac{2dT_h}{ir_a Ea_w n_w}\left(\frac{l^3}{3I_x} + \frac{2.8l}{S} + \frac{6.7}{b_w} + \frac{5}{b_w} + \frac{0.47n_w b_w r_a^2}{2I_{pa}}\right).$$

Taking into account the obtained formulas, the work of the torque is

$$\int_0^{\varphi_1} T_h(\varphi_h)d\varphi_h = \int_0^{T_M} \frac{4T_h}{i^2 r_a^2 En_w}\left(\frac{64l^3}{3\pi d^4} + \frac{11.2l}{\pi d^2} + \frac{11.7}{b_w} + \frac{0.47n_w b_w}{\pi r_a^2}\right)dT_h = A\frac{T_M^2}{2}, \tag{2}$$

where the constant $A = \frac{4}{i^2 r_a^2 En_w}\left(\frac{64l^3}{3\pi d^4} + \frac{11.2l}{\pi d^2} + \frac{11.7}{b_w} + \frac{0.47n_w b_w}{\pi r_a^2}\right)$.

In accordance with the known dependence on calculation of teeth bending strength, the allowed torque is

$$[T_h] = T_M = \frac{2[\sigma_F]a_w n_w b_w m}{Y_F K_F} = \frac{2i[\sigma_F]n_w M_a}{Y_F K_F z_a \pi\rho}, \tag{3}$$

where Y_F is the tooth shape coefficient; K_F is the non-uniformity loading distribution coefficient in gearwheel meshing [18]; m is the gearing module; $[\sigma_F]$ is the allowed tooth bending strength; and z_a is the sun gearwheel tooth number.

After substitution of expression (2) into Eq. (1), and taking into account the equality in (3) for a gear with console satellite axles, we get

$$\frac{i^2 M_a^2 \omega_h^2}{2\pi\rho b_w}\left[0.75n_w k_g(0.5i-1)^2 + 0.5\right] = \frac{4}{i^2 r_a^2 En_w}\left(\frac{64l^3}{3\pi d^4} + \frac{11.2l}{\pi d^2} + \frac{11.7}{b_w} + \frac{0.47n_w b_w}{\pi r_a^2}\right)\cdot 2\left(\frac{i[\sigma_F]n_w M_a}{Y_F K_F z_a \pi\rho}\right)^2.$$

From here, considering that $\omega_a = \omega_h i$,

$$\omega_a^2 = \frac{\frac{4}{i^2 r_a^2 En_w}\left(\frac{64l^3}{3\pi d^4} + \frac{11.2l}{\pi d^2} + \frac{11.7}{b_w} + \frac{0.47n_w b_w}{\pi r_a^2}\right)\cdot 2\left(\frac{i[\sigma_F]n_w}{Y_F K_F z_a \pi\rho}\right)^2 2\pi\rho b_w}{(0.5z_a m)^2 i^2\left[0.75n_w k_g(0.5i-1)^2 + 0.5\right]}$$

$$= \frac{16n_w[\sigma_F]^2\left(\frac{64}{3\pi}\bar{b}_w\bar{l}^4 + \frac{11.2}{\pi}\bar{b}_w\bar{l}^2 + 11.7 + \frac{0.47n_w}{\pi r_a^2}\cdot\left(\frac{b_w}{d_a}\right)^2\right)}{(0.5z_a m)^2\pi\rho E(Y_F K_F z_a)^2(0.75n_w k_g(0.5i-1)^2 + 0.5)},$$

$$\omega_a = \frac{4[\sigma_F]}{0.5\pi Y_F K_F z_a m}\sqrt{\frac{n_w[21.3\bar{b}_w\bar{l}^4 + 11.2\bar{b}_w\bar{l}^2 + 11.7\pi + 1.5(1+\mu)n_w(b_w/d_a)^2]}{\rho E[0.75n_w k_g(0.5i-1)^2 + 0.5]}},$$

where $\bar{b}_w = b_w/l$, $\bar{l} = l/d$.

Figures 2 and 3 show the relations for the angular speed of the sun gearwheel versus the gearing module and the gear ratio for which the maximum starting moment does not exceed its allowed value. The diagrams correspond to the following values entering the above-stated equations: $[\sigma_F] = 550$ MPa, $n_w = 3$, $K_F = 1$, $\bar{b}_w = 2$, $z_a = 18$, $Y_F = 3.75$, $E = 2.1 \cdot 10^{11}$ Pa, $\rho = 7800$ kg/m^3, $k_g = 0.8$, $4 \le i \le 11$.

It follows from the calculations and the diagrams that are plotted on their base that the variation of the satellite number within the range $n_w = 3...5$ and the relative width of the sun gearwheel within the range $\bar{b}_w = 1...3$ do not practically influence the ratio between ω_a and m. An increase in the flexibility of the gear elements reduces the dynamic load in the transient mode of the drive operation; and it gives the possibility of using the drive at high angular speeds without the necessity of additional means to reduce the starting torque. At the increase of the gearing module, and, therefore, the increase in gearwheel diameters, the value of the angular speed of the sun gearwheel that is allowable in accordance with the tooth bending strength is reduced. In this regard, it is expedient to carry out high-speed gears with a big width relation to the diameter and a multi-set arrangement of satellites (Fig. 4) [18, 21].

In the planetary gear with two-point axles of satellites, it is possible to reduce the stiffness of the mechanism and to improve its dynamics by manufacturing the planetary carrier web with grooves (Fig. 5) [12].

In order to determine the displacement of the satellite axle of such a gear, let us single out the planetary carrier web element (Fig. 6) and determine the influence of the force acting on it from the axle $F = T_h(y) / (2n_w a_w)$.

We will find the torque in the lower part of the singled out web element M_0, using Mohr's integral (the angular displacement is equal to zero in this cross-section). Then,

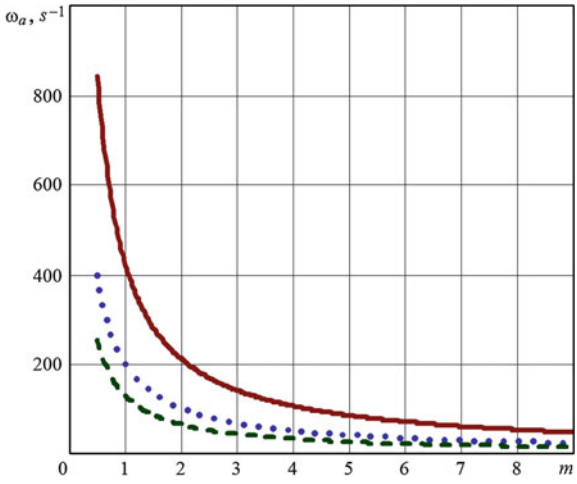

Fig. 2 Multi-satellite planetary gear sun gearwheel angular speed ω_a versus the gearing module m and the gear ratio i at l/d = 1.2: (*brown solid lines*) i = 4; (*blue dashed lines*) i = 7; (*green dotted lines*) i = 10 (Color figure online)

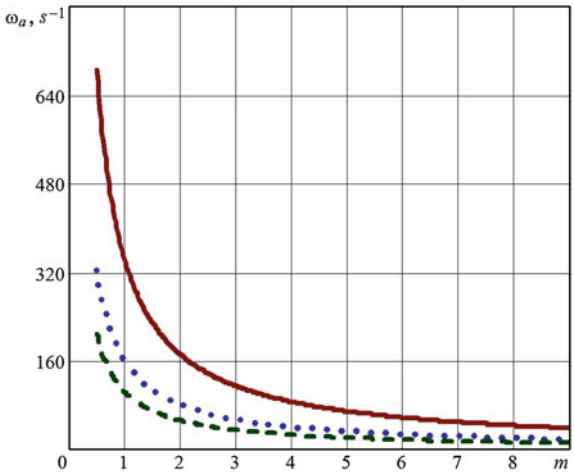

Fig. 3 Multi-satellite planetary gear sun gearwheel angular speed ω_a versus the gearing module m and the gear ratio i at $l/d = 1$: (*brown solid lines*) $i = 4$; (*blue dashed lines*) $i = 7$; (*green dotted lines*) $i = 10$ (Color figure online)

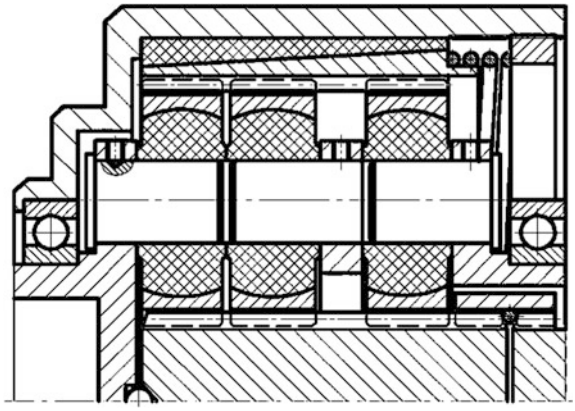

Fig. 4 Planetary gear with a limited radial size and flexible satellite axles

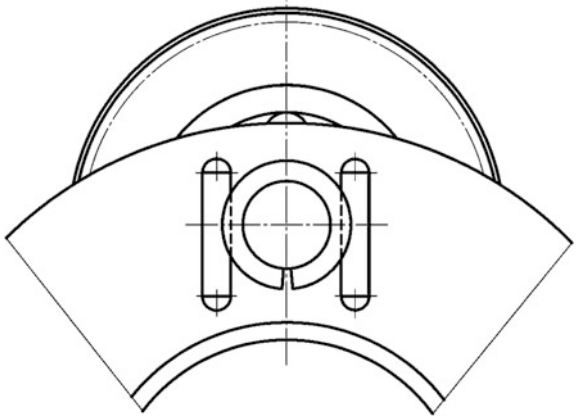

Fig. 5 Satellite unit of the planetary gear with a flexible planetary carrier

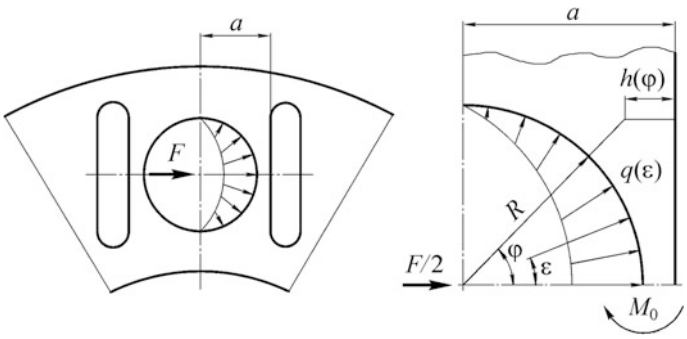

Fig. 6 Element of the flexible planetary carrier web

$$M_0 = \frac{F}{\pi}\left\{\int_0^{\pi/2} \varphi\left[\frac{1}{h(\varphi)}\right]^3 \frac{R+a}{1+\cos\varphi}\sin\varphi\, d\varphi\right\} \Big/ \int_0^{\pi/2}\left[\frac{1}{h(\varphi)}\right]^3 d\varphi,$$

$$M(\varphi) = \int_0^{\varphi} q(\varepsilon)[R+h(\varphi)]\sin(\varphi-\varepsilon)Rd\varepsilon - M_0 = \frac{F(R+a)}{\pi(1+\cos\varphi)}\varphi\sin\varphi - M_0.$$

Here, $R = 0.5d$ is the satellite axle radius; $h(\varphi) = \frac{a - R\cos\varphi}{1+\cos\varphi}$ is half of the broken cross-section's total length; and $q(\varepsilon) = q_0\cos\varepsilon = 2F\cos\varepsilon\,/\,(\pi R)$ is the distributed load.

The axle displacement in the direction of the force F is caused by the action of the bending torque and transverse force on the web element

$$y_h = \frac{R}{b}\left\{\frac{1.5}{E}\int_0^{\pi/2}\frac{M(\varphi)[R+h(\varphi)]\sin\varphi}{h^3(\varphi)}d\varphi + \frac{1.2}{G}\int_0^{\pi/2}\frac{Q(\varphi)}{a - R\cos\varphi}d\varphi\right\},$$

where

$$Q(\varphi) = R\int_0^{\varphi} q(\varepsilon)\cos\varepsilon\, d\varepsilon = \frac{F}{\pi}(\varphi + 0.5\sin 2\varphi).$$

Solving the mentioned equations, we will define the flexibility of a planetary carrier web (the strain caused by the action of a longitudinal force is discounted due to its smallness). The dependence of the relative specific flexibility on the relative parameter $\bar{a} = a/2R = a/d$ at $0.55 \le \bar{a} \le 0.7$ can be presented through the following approximation:

$$\bar{\delta}_h = Eb_h y_h / F \cong \left(\frac{120}{\bar{a}} + 228\bar{a} - 325 \right).$$

Then,

$$y_h = \frac{T_h(y)}{2\bar{b}_h b_w E a_w n_w} \left(\frac{120}{\bar{a}} + 228\bar{a} - 325 \right).$$

The deflection of the two-point satellite axle for such a gear can be found through the technique presented in [20].

Therefore, the calculation of the ratio between the angular speed of the sun gearwheel and the gear module has shown that, for $\bar{a} = 0.55$ and earlier accepted values of gear parameters, the decrease in flexibility of the two-point axle (as compared to the console one) is compensated for by the increase in flexibility of the planetary carrier web; and dependences $\omega_a = f(m)$ are approximately similar to those shown in Figs. 2 and 3.

3 Dynamic Load at Steady Operation

The dynamic loads in steady operation can be considered as a first approximation by means of inertial forces which have a significant effect on the loaded state of the satellite bearings [23, 24].

The value of the main vector of inertial forces acts on the satellite $F_{in} = M_g a_C$, where $a_C = \omega_h^2 a_w$ is the mass center acceleration.

With the self-adjusting satellites (see Fig. 1), the satellite bearing load F_g can be significantly increased in the high-speed multi-satellite planetary gear due to inertial forces. Having expressed the satellite mass through the gear parameters and the torque on the planetary carrier shaft, corresponding to the bending strength of external gearing that limits the gear's bearing ability, we will obtain the following dependences:

$$F_g / F_t = \frac{1}{F_t} \sqrt{\left(M_g a_w \omega_h^2\right)^2 + \left(\frac{T_h}{n_w a_w}\right)^2},$$

or

$$F_g / F_t = \sqrt{\left\{ \frac{V^2 Y_F K_F \pi \rho z_a K_g (0.5i - 1)^2}{8i[\sigma_F]} \right\}^2 + 1}, \tag{4}$$

where F_t is the tangential component of the force acting on a satellite axle, and V is the peripheral speed in meshing of a sun gearwheel with the satellite.

Figure 7 presents the dependence of the satellite bearing load relation to its tangential component on the peripheral speed. This dependence was plotted in accordance with (4) for the earlier accepted values of gear parameters.

Considering that the load ability of the multi-satellite planetary gear of the type being studied is most often limited by the external gearing contact strength, the relation of forces will be

$$F_g/F_t = \sqrt{\left[\frac{0.175V^2\pi\rho K_H E K_g(0.5i-1)}{8[\sigma_H]^2\cos\alpha_w \sin\alpha_w}\right]^2 + 1}. \quad (5)$$

The relation of forces calculated by the formula (5) is presented in Fig. 8. The diagram corresponds to the allowed normal contact strength $[\sigma_H] = 700$ MPa, $E = 2.1 \cdot 10^5$ MPa, $\alpha_w = 20°$, $K_H = 1$.

In the planetary gears consisting of a driver eccentric planetary carrier, one or several satellites, and the mechanism of torque absorption from the satellites (Fig. 9), big support loads take place [9–11, 13]. The satellite-loading layout of such a gear with a four-roller torque absorption mechanism is shown in Fig. 10.

The satellite support reaction is:

$$R_C = \sqrt{X_C^2 + Y_C^2} = \sqrt{(F_n\cos\alpha_w)^2 + (F_R + F_n\sin\alpha_w - F_{in})^2}.$$

Here, F_n is the normal force in meshing of gearwheels, F_R is the force acting on the satellite from the roller of the torque absorption mechanism, and α_w is the gearwheel pressure angle (for the difference between gearwheel and satellite tooth numbers $\Delta Z \leq 2$, the pressure angle is $\alpha_w = 50° \div 60°$ [14, 19, 22]).

Using the formula for the calculation of tooth bending strength to express the satellite mass through the power factors and the gear parameters, and also

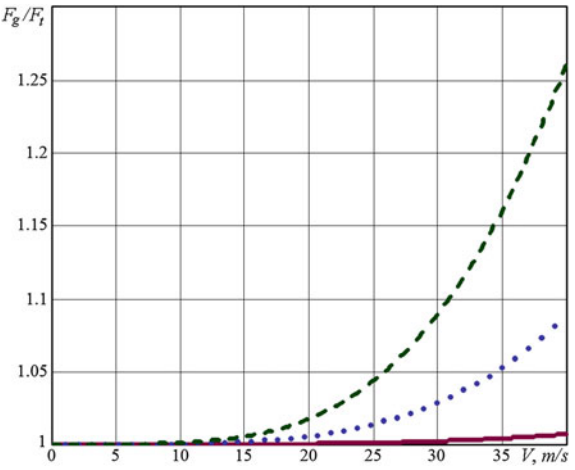

Fig. 7 Relation of the satellite bearing load F_g to its tangential component F_t versus the peripheral speed V in external gearing and the gear ratio i of multi-satellite planetary gear, the load ability of which is limited by the tooth bending strength: (*brown solid lines*) $i = 4$; (*blue dashed lines*) $i = 7$; (*green dotted lines*) $i = 10$ (Color figure online)

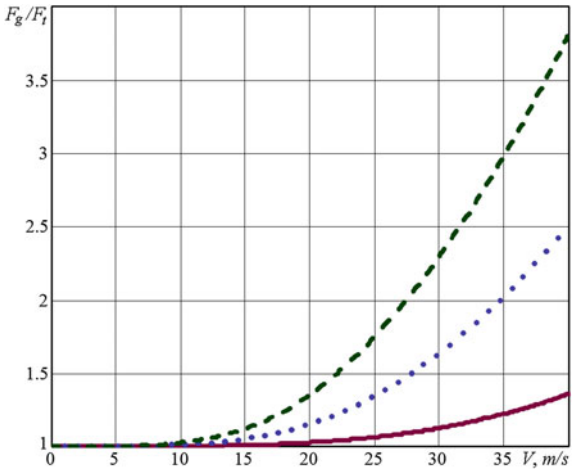

Fig. 8 Relation of the satellite bearing load F_g to its tangential component F_t versus the peripheral speed V in external gearing and the gear ratio i of multi-satellite planetary gearthe load ability of which is limited by the tooth contact strength: (*brown solid lines*) $i = 4$; (*blue dashed lines*) $i = 7$; (*green dotted lines*) $i = 10$ (Color figure online)

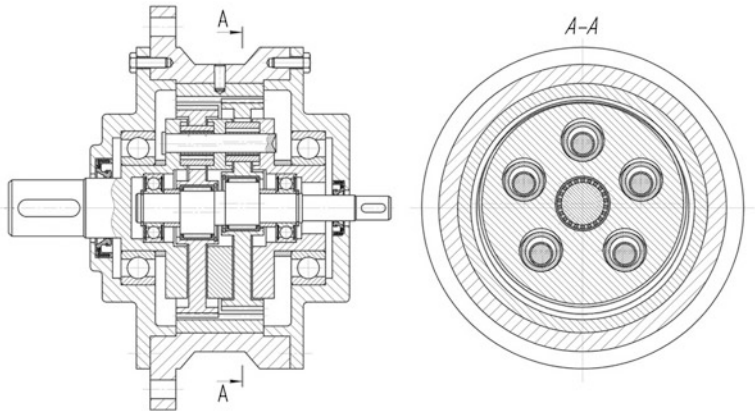

Fig. 9 Planetary gear with the roller mechanism of the torque absorption from satellites

considering equalities $i = -\frac{z_g}{\Delta Z}$, $a_w = \frac{r_g \cos\alpha}{\cos\alpha_w |i|}$ (α is the angle of the basic rack profile), we obtain

$$R_C/F_n = \sqrt{\cos^2\alpha_w + \left\{\sin\alpha_w + \frac{\cos\alpha}{\bar{e}} - V^2 \frac{i^2 \pi \rho \Delta Z Y_F K_\varepsilon K_g \cos^2\alpha}{2[\sigma_F]\cos\alpha_w}\right\}^2},$$

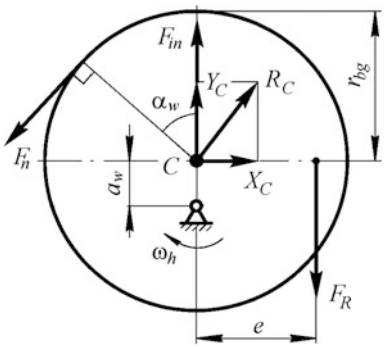

Fig. 10 The satellite loading layout of a planetary gear with the four-roller torque absorption mechanism

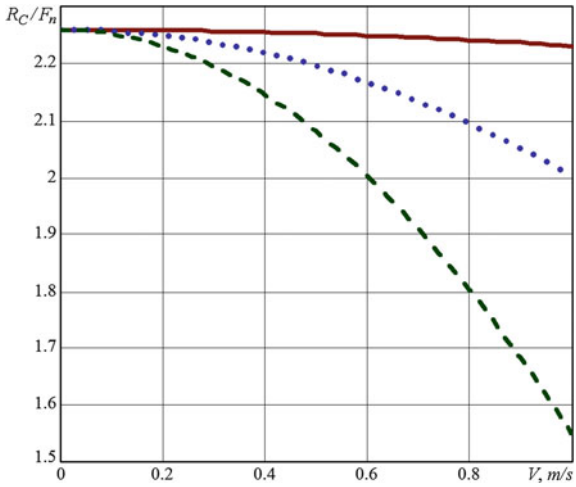

Fig. 11 Relation R_C of the satellite support reaction to the normal force F_n in meshing versus the peripheral speed of the satellite V and the gear ratio i of eccentric planetary gear: (*brown solid lines*) i = 20; (*blue dashed lines*) i = 60; (*green dotted lines*) i = 100 (Color figure online)

where $\bar{e} = e/r_g$, V is the satellite peripheral speed, and K_ε is the coefficient considering a multi-paired relationship of the meshing of the satellite with a fixed gearwheel.

The satellite support reaction dependence on the peripheral speed and the planetary mechanism gear ratio is given in Fig. 11 for $\Delta Z = 1, K_\varepsilon = 0.5$, $\bar{e} = 0.7$, $K_g = 1$, $Y_F = 3.75$, $\alpha_w = 60°$, $\alpha = 20°$.

It follows from the calculations and the diagram provided in Fig. 11 that the inertial force promotes the decrease in satellite support reaction, and this decrease is amplified with the increase in peripheral speed in the external gearing and the increase in the gear ratio.

4 Conclusions

Dynamic loads in planetary gears ambiguously affect the meshing strength. Their influence is defined by the gear layout features; and it depends on the operating modes.

In gears that have repeated and short-term action, the flexibility of multi-satellite planetary gear elements positively affects their dynamics. This gives us the possibility of using the drive at high rotary speeds without the additional resources intended to decrease the starting torque. It is expedient to implement a multi-row version for high-speed multi-satellite planetary gears with a big relation of the width to the diameter. The additional reduction of dynamic loads is reached by decreasing the rigidity by means of grooves in the webs of the planetary carrier.

In a high-speed planetary gear that contains an eccentric planetary carrier, one or several satellites, and the torque absorption mechanism, the satellite's inertial force significantly reduces the support reaction. This effect amplifies at the increase in the peripheral speed in external gearing and at the increase in the gear ratio.

The received dependences between the meshing strength characteristics and the planetary gear characteristics allow for picking up the rational values of planetary gear parameters providing its maximum load ability at the improved mass-dimensional characteristics.

References

1. Airapetov, E., Genkin, M.: Deformability of planetary mechanisms. Moscow, Nauka Publ., p. 212 (1973) (in Russian)
2. Airapetov, E., Genkin, M.: Dynamics of Planetary Mechanisms. Moscow, Nauka Publ., p. 256 (1980) (in Russian)
3. Chermensky, O., Fedotov, N.: Rolling bearings. Reference book catalog. Moscow, Mashinostroenie Publ., p. 575 (2003) (in Russian)
4. Grinberg, V., Pushkarev, A.: Structure and dynamics of folding aerodynamic surfaces of aircraft. J. Mach. Manuf. Reliab. **1**, 34–41 (2001) (in Russian)
5. Inalpolat, M., Kahraman, A.: A dynamic regime to predict modulation sidebands of a planetary gear set having manufacturing errors. J. Sound Vib. **329**, 371–393 (2010)
6. Kahraman, A., Ding, H.: A methodology to predict surface wear of planetary gears under dynamic conditions. Mech Based Constr Struct Mach **38**, 493–515 (2010)
7. Kudryavtsev, V.: Planetary gears. Moscow-Leningrad, Mashinostroenie Publ., p. 307 (1966) (in Russian)
8. Li, S., Kahraman, A.: A tribo-dynamic regime of a spur gear pair. J. Sound Vib. **332**, 4963–4978 (2013)
9. Plekhanov, F.I., Goldfarb, V.I.: Patent RF for invention 2460916. Planetary gear. Declared 13.04.2011. Published 10 Sept 2012 (in Russian)
10. Plekhanov, F.I., Perminov, L.P.: Patent RF for invention 2462631. Planetary gear. Declared 16.05.2011. Published 27 Sept 2012 (in Russian)
11. Plekhanov, F.I., Lopatin, B.A.: Patent RF for invention 2550598. Planetary gear. Declared 11.02.2014. Published 10 May 2015 (in Russian)

12. Plekhanov, F.I., Senyutkin, P.A., Plekhanov, A.D.: Patent RF for invention 2567973. Tooth planetary gear. Declared 28.07.2014. Published 10 Nov 2015 (in Russian)
13. Plekhanov, F.I., Veretennikov I.N., Maximov, A.N., Chupin, I.B.: Patent RF for invention 2589765. Planetary gear. Declared 22.06.2015. Published 10 July 2016 (in Russian)
14. Plekhanov, F., Goldfarb, V.: Development and research of heavy-loaded planetary gears with roll-type mechanism of motion transmission from satellites. In: Proceedings of the International Symposium "Theory and practice of gearing", pp. 330–337 (2014) (in Russian)
15. Plekhanov, F.: Investigation of the stress-strain state of a satellite axle-carrier joint in a planetary gear. News of higher education institutions. Mech. Eng. **2**, 36–41 (2015) (in Russian)
16. Plekhanov, F.: Deformability of units of a planetary gear and its effect on load distribution in gear meshes. J. Mach. Manuf. Reliab. **44**(3), 227–231 (2015)
17. Plekhanov, F.: Influence of deformability of sun gear and axles of satellites of planetary gear on load distribution in gearings. Bull. Mech. Eng. **4**, 16–19 (2015) (in Russian)
18. Plekhanov, F., Tonkikh, A., Vychuzhanina, E.: Planetary gear rigs: design features and technical-economic indicators. Oil Ind. **6**, 44–46 (2015) (in Russian)
19. Plekhanov, F.: Influence of gear deformability in a planetary gear on the load distribution in tooth engagement. Russ. Eng. Res. **35**(7), 485–488 (2015)
20. Plekhanov, F., Suntsov, A.: The influence of stiffness of the planet shafts and bearings on load distribution among the planets in a planetary gear. News of higher education institutions. Mech. Eng. **3**, 10–16 (2016) (in Russian)
21. Plekhanov, F., Grakhov, V., Suntsov, A.: Planetary gear transmissions of build and travelling machines: rational design, cost and performance data. Build. Mech. **4**, 22–25 (2016) (in Russian)
22. Plekhanov, F., Goldfarb, V.: Rational designs of planetary gear, geometry of gearing and strength parameters. In: Mechanisms and Machine Science, vol. 34, pp. 285–300, Springer (2016)
23. Pushkarev, A., Morozov, D., Pushkareva, L.: Dynamic reactions in bearings of wind turbine. In: Proceedings of the All-Russian Scientific and Practical Conference Devoted to the 90 Anniversary of Udmurt Republic "Scientific Ensuring Innovative Development of Agrarian and Industrial Complex", vol. 3, pp. 226–230. Izhevsk State Agricultural Academy, Izhevsk (2010) (in Russian)
24. Pushkarev, A., Pushkareva, L.: Dynamic synthesis of the wind turbine working in the field of small high-speed streams. Mod. Mech. Eng. Sci. Educ. **1**, 343–347 (2011) (in Russian)
25. Pushkarev, A., Pushkarev, I.: Structure of construction systems with mobile loadings and elements of protection against vibration. Electron Sci J **2**(2), 235–238 (2015) (in Russian)
26. Sondkar, P., Kahraman, A.: A dynamic regime of a double-helical planetary gear set. Mech. Mach. Theory **70**, 157–174 (2013)

Index

V. Goldfarb et al. (eds.), *Advanced Gear Engineering*,
Mechanisms and Machine Science 51, DOI 10.1007/978-3-319-60399-5